Fundamentals of Plasma Physics and Controlled Fusion

The Third Edition

Kenro Miyamoto

The first edition of 'Fundamentals of Plasma Physics and Controlled Fusion' was published in 1997 by Iwanami Book Service Center. (ISBN 4-900491-11)
The second edition was published in 2000 as NIFS-PROC-48 by National Institute of Fusion Science (NIFS) in Toki

This new book (NIFS-PROC-88) is the revised edition of the former English publication NIFS-PROC-48 “Fundamentals of Plasma Physics and Controlled Nuclear Fusion” (2000) by Kenro Miyamoto. A new age of fusion research has been opened in the last decade. The ITER Project has officially started. Intensive research into Zonal Flows has improved the understanding of confinement physics. This new book includes those new understandings.

The famous textbook “Plasma Physics for Controlled Nuclear Fusion” by K. Miyamoto was first published in 1976 in Japanese and then translated into English. It was the first comprehensive textbook on fusion plasma physics. Many scientists and engineers in fusion research were educated by studying this textbook over the following 20 years. In the meantime, plasma physics has been continuously refined through experimental and theoretical research. The National Institute for Fusion Science (NIFS), which has a graduate course as a part of the Graduate University for Advanced Studies (Sokendai), had asked Professor Miyamoto to publish his revised textbook from NIFS, and he accepted the proposal. It was NIFS-PROC-48, which has gained a good reputation from all over the world. In 2010 “Plasma Physics for Nuclear Fusion” by K. Miyamoto (NIFS-PROC-80 in Japanese) was published including new understandings in recent years. This new book (NIFS-PROC-88) is the English translation of NIFS-PROC-80 as well as the revised edition of NIFS-PROC-48.

We hope that this new textbook will be widely used for education and research in plasma physics and controlled nuclear fusion all over the world.

June 2011

Harukazu Iguchi
Chairperson of Book & Publication Committee
National Institute for Fusion Science

この本は 2000 年に出版された NIFS-PROC-48「Fundamentals of Plasma Physics and Controlled Nuclear Fusion」の改訂版です。この 10 年あまりの間に ITER 計画が正式にスタートするなど核融合研究は新しい時代に入り、またゾーナルフローに関する物理理解ほか新たな進展もありました。今回の改訂ではこれら最新の内容が取り込まれています。

1976 年に日本語で出版され、その後英訳もされた宮本先生のプラズマ物理の教科書は、初めての本格的な核融合プラズマ物理の教科書として国内外で高い評価を受け、多くの核融合研究者がこの教科書を使って育ってきました。その後、高温プラズマの閉じ込め研究を通じてプラズマ物理学は理論、実験の両面からさらに精密化されていきました。総合研究大学院大学核融合科学専攻を併設する核融合科学研究所が宮本先生にお願いして、初版以降 20 余年の進展を取り込んで改訂した新しい教科書が NIFS-PROC-48 でした。これに対して、世界中から問い合わせが寄せられ、大きな評判を呼びました。その後宮本先生は、最近の進展、成果を取り入れた「核融合のためのプラズマ物理」（日本語版）を、2010 年に NIFS-PROC-80 として刊行されました。本稿は、NIFS-PROC-48 の改訂版であると同時に、NIFS-PROC-80 の英語版ともいえるものです。

この最新の教科書が日本国内に限らず、広く世界中でプラズマ・核融合の研究と教育に利用されることを期待致します。

2011 年 6 月

核融合科学研究所　図書・出版委員長
井口　春和

Fundamentals of Plasma Physics and Controlled Fusion (The Third Edition)

Contents

Preface

Primary objective of this lecture note is to provide a basic text for the students to study plasma physics and controlled fusion researches. Secondary objective is to offer a reference book describing analytical methods of plasma physics for the researchers. This was written based on lecture notes for a graduate course and an advanced undergraduate course those have been offered at Department of Physics, Faculty of Science, University of Tokyo.

In ch.1 and 2, basic concept of plasma and its characteristics are explained. In ch.3, orbits of ion and electron are described in several magnetic field configurations. Chapter 4 formulates Boltzmann equation of velocity space distribution function, which is the basic relation of plasma physics.

From ch.5 to ch.9, plasmas are described as magnetohydrodynamic (MHD) fluid. MHD equation of motion (ch.5), equilibrium (ch.6) and diffusion and confinement time of plasma (ch.7) are described by the fluid model. Chapters 8 and 9 discuss problems of MHD instabilities whether a small perturbation will grow to disrupt the plasma or will damp to a stable state. The basic MHD equation of motion can be derived by taking an appropriate average of Boltzmann equation. This mathematical process is described in appendix A. The derivation of useful energy integral formula of axisymmetric toroidal system and the analysis of high n ballooning mode are described in app. B.

From ch.10 to ch.14, plasmas are treated by kinetic theory. This medium, in which waves and perturbations propagate, is generally inhomogeneous and anisotropic. It may absorb or even amplify the wave. Cold plasma model described in ch.10 is applicable when the thermal velocity of plasma particles is much smaller than the phase velocity of wave. Because of its simplicity, the dielectric tensor of cold plasma can be easily derived and the properties of various wave can be discussed in the case of cold plasma. If the refractive index becomes large and the phase velocity of the wave becomes comparable to the thermal velocity of the plasma particles, then the particles and the wave interact with each other. In ch.11, Landau damping, which is the most characteristic collective phenomenon of plasma, as well as cyclotron damping are described. Chapter 12 discusses wave heating (wave absorption) in hot plasma, in which the thermal velocity of particles is comparable to the wave phase velocity, by use of the dielectric tensor of hot plasma. In ch.13 the amplification of wave, that is, the growth of perturbation and instabilities, is described. Since long mathematical process is necessary for the derivation of dielectric tensor of hot plasma, its processes are described in app.C. In ch.14 instabilities driven by energetic particles, that is, fishbone instability and toroidal Alfvén eigenmodes are described.

In ch.15, confinement researches toward fusion grade plasmas are reviewed. During the last decade, tokamak experiments have made remarkable progresses. Now construction stage of "International Tokamak Experimental Reactor", called ITER, has already started. In ch.16, research works of critical subjects on tokamak plasmas and reactors are explained. As non-tokamak confinement systems, reversed field pinch, stellarator, tandem mirror are described in ch.17. Elementary introduction of inertial confinement is added in ch.18. New topics, zonal flow, is described in app. E

Readers may have impression that there is too much mathematics in this lecture note. However there is a reason for that. If a graduate student tries to read and understand, for examples, two of frequently cited short papers on the analysis of high n ballooning mode by Connor, Hastie, Taylor, fishbone instability by L.Chen, White, Rosenbluth, without preparative knowledge, he must read and understand several tens of cited references and references of references. I would guess from my experience that he would be obliged to work hard for a few months. It is one of motivation to write this lecture note to save his time to struggle with mathematical derivation so that he could spend more time to think physics and experimental results.

This lecture note has been attempted to present the basic physics and analytical methods which are necessary for understanding and predicting plasma behavior and to provide the recent status of fusion researches for graduate and senior undergraduate students. I also hope that it will be a useful reference for scientists and engineers working in the relevant fields.

May 2011

Kenro Miyamoto
Professor Emeritus Unversity of Tokyo

Ch.1 Nature of Plasma

1.1 Introduction

As the temperature of a material is raised, its state changes from solid to liquid and then to gas. If the temperature is elevated further, an appreciable number of the gas atoms are ionized and become the high temperature gaseous state in which the charge numbers of ions and electrons are almost the same and charge neutrality is satisfied in a macroscopic scale.

When the ions and electrons move collectively, these charged particles interact with coulomb force which is long range force and decays only in inverse square of the distance r between the charged particles. The resultant current flows due to the motion of the charged particles and Lorentz interaction takes place. Therefore many charged particles interact with each other by long range forces and various collective movements occur in the gaseous state. The typical cases are many kinds of instabilities and wave phenomena. The word "plasma" is used in physics to designate the high temperature ionized gaseous state with charge neutrality and collective interaction between the charged particles and waves.

When the temperature of a gas is T(K), the average velocity of the thermal motion, that is, thermal velocity v_{T} is given by

$$mv_{\mathrm{T}}^2/2 = \kappa T/2 \tag{1.1}$$

where κ is Boltzmann constant $\kappa = 1.380658(12)\times 10^{-23}$ J/K and κT indicates the thermal energy. Therefore the unit of κT is Joule (J) in MKSA unit. In many fields of physics, one electron volt (eV) is frequently used as a unit of energy. This is the energy necessary to move an electron, charge $e = 1.60217733(49) \times 10^{-19}$ Coulomb, against a potential difference of 1 volt:

$$1\mathrm{eV} = 1.60217733(49) \times 10^{-19}\,\mathrm{J}.$$

The temperature corresponding to the thermal energy of 1eV is 1.16×10^4 K$(= e/\kappa)$. The ionization energy of hydrogen atom is 13.6 eV. Even if the thermal energy (average energy) of hydrogen gas is 1 eV, that is $T \sim 10^4$ K, small amount of electrons with energy higher than 13.6 eV exist and ionize the gas to a hydrogen plasma. Plasmas are found in nature in various forms (see fig.1.1). There exits the ionosphere in the heights of 70∼500 km (density $n \sim 10^{12}\,\mathrm{m}^{-3}$, $\kappa T \sim 0.2$ eV). Solar wind is the plasma flow originated from the sun with $n \sim 10^{6\sim 7}\,\mathrm{m}^{-3}$, $\kappa T \sim 10$ eV. Corona extends around the sun and the density is $\sim 10^{14}\,\mathrm{m}^{-3}$ and the electron temperature is ~ 100 eV although these values depend on the different positions. White dwarf, the final state of stellar evolution, has the electron density of $10^{35\sim 36}\,\mathrm{m}^{-3}$. Various plasma domains in the diagram of electron density $n(\mathrm{m}^{-3})$ and electron temperature κT (eV) are shown in fig.1.1. Active researches in plasma physics have been motivated by the aim to create and confine hot plasmas in fusion researches. Plasmas play important roles in the studies of pulsars radiating microwave or solar X ray sources observed in space physics and astrophysics. The other application of plasma physics is the study of the earth's environment in space. Practical applications of plasma physics are MHD (magnetohydrodynamic) energy conversion for electric power generation, ion rocket engines for space crafts, and plasma processing which attracts much attention recently.

1.2 Charge Neutrality and Landau Damping

One of the fundamental property of plasma is the shielding of the electric potential applied to the plasma. When a probe is inserted into a plasma and positive (negative) potential is applied, the probe attracts (repulses) electrons and the plasma tends to shield the electric disturbance. Let us estimate the shielding length. Assume that the ions are in uniform density ($n_{\mathrm{i}} = n_0$) and there is small perturbation in electron density n_{e} or potential ϕ. Since the electrons are in Boltzmann distribution usually, the electron density n_{e} becomes

$$n_{\mathrm{e}} = n_0\ \exp(e\phi/\kappa T_{\mathrm{e}}) \simeq n_0(1 + e\phi/\kappa T_{\mathrm{e}}).$$

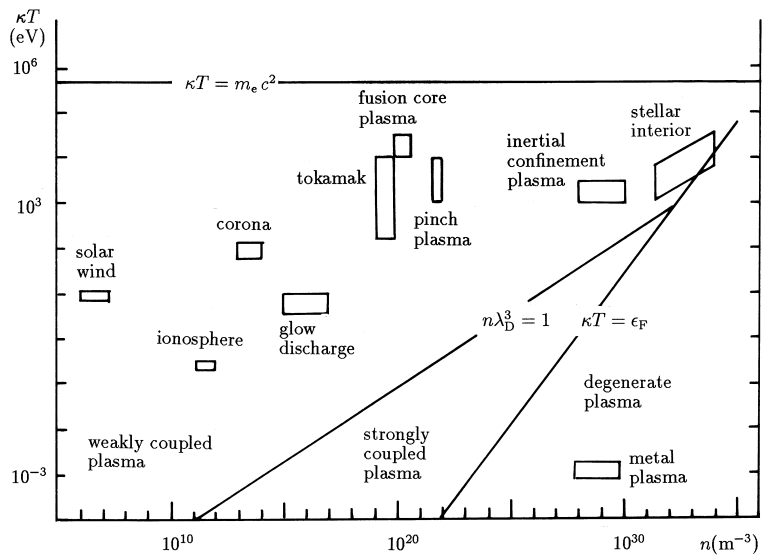

Fig.1.1 Various plasma domain in n-κT diagram.

Poisson's eqation is

$$\boldsymbol{E} = -\nabla\phi, \qquad \nabla(\epsilon_0 \boldsymbol{E}) = -\epsilon_0 \nabla^2\phi = \rho = -e(n_\mathrm{e} - n_0) = -\frac{e^2 n_0}{\kappa T_\mathrm{e}}\phi$$

and

$$\nabla^2\phi = \frac{\phi}{\lambda_\mathrm{D}^2}, \qquad \lambda_\mathrm{D} = \left(\frac{\epsilon_0 \kappa T_\mathrm{e}}{n_\mathrm{e} e^2}\right)^{1/2} = 7.45 \times 10^3 \left(\frac{1}{n_\mathrm{e}}\frac{\kappa T_\mathrm{e}}{e}\right)^{1/2} \ (\mathrm{m}) \tag{1.2}$$

where n_e is in m^{-3} and $\kappa T_\mathrm{e}/e$ is in eV. When $n_\mathrm{e} \sim 10^{20}\mathrm{cm}^{-3}$, $\kappa T_\mathrm{e}/e \sim 10\mathrm{keV}$, then $\lambda_\mathrm{D} \sim 75\mu\mathrm{m}$. In spherically symmetric case, Laplacian ∇^2 becomes $\nabla^2\phi = (1/r^2)(\partial/\partial r)(r^2 \partial\phi/\partial r)$ and the solution is

$$\phi = \frac{q}{4\pi\epsilon_0}\frac{\exp(-r/\lambda_\mathrm{D})}{r}.$$

It is clear from the foregoing formula that Coulomb potential $q/4\pi\epsilon_0 r$ of point charge is shielded out to a distance λ_D. This distance λ_D is called the *Debye length*. When the plasma size is a and $a \gg \lambda_\mathrm{D}$ is satisfied, then plasma is considered neutral in charge. If $a < \lambda_\mathrm{D}$ in contrary, individual particle is not shielded electrostatically and this state is no longer plasma but an assembly of independent charged particles. The number of electrons included in the sphere of radius λ_D is called *plasma parameter* and is given by

$$n\lambda_\mathrm{D}^3 = \left(\frac{\epsilon_0}{e}\frac{\kappa T_\mathrm{e}}{e}\right)^{3/2}\frac{1}{n_\mathrm{e}^{1/2}}. \tag{1.3}$$

When the density is increased while keeping the temperature constant, this value becomes small. If the plasma parameter is less than say $\sim$1, the concept of Debye shielding is not applicable since the continuity of charge density breaks down in the scale of Debye length. Plasmas in the region of $n\lambda^3 > 1$ are called classical plasma or *weakly coupled plasma*, since the ratio of electron thermal energy κT_e and coulomb energy between electrons $E_\mathrm{coulomb} = e^2/4\pi\epsilon_0 d$ ($d \simeq n^{-1/3}$ is the average distance between electrons with the density n) is given by

$$\frac{\kappa T_\mathrm{e}}{E_\mathrm{coulomb}} = 4\pi(n\lambda_\mathrm{D}^3)^{2/3} \tag{1.4}$$

and $n\lambda^3 > 1$ means that coulomb energy is smaller than the thermal energy. The case of $n\lambda_D^3 < 1$ is called *strongly coupled plasma* (see fig.1.1). Fermi energy of degenerated electron gas is given by $\epsilon_F = (h^2/2m_e)(3\pi^2 n)^{2/3}$. When the density becomes very high, it is possible to become $\epsilon_F \geq \kappa T_e$. In this case quantum effect is more dominant than thermal effect. This case is called *degenerated electron plasma*. One of this example is the electron plasma in metal. Most of plasmas in experiments are classical weakly coupled plasma.

The other fundamental process of plasma is collective phenomena of charged particles. Waves are associated with coherent motions of charged particles. When the phase velocity v_{ph} of wave or perturbation is much larger than the thermal velocity v_T of charged particles, the wave propagates through the plasma media without damping or amplification. However when the refractive index N of plasma media becomes large and plasma becomes hot, the phase velocity $v_{ph} = c/N$ (c is light velocity) of the wave and the thermal velocity v_T become comparable ($v_{ph} = c/N \sim v_T$), then the exchange of energy between the wave and the thermal energy of plasma is possible. The existence of a damping mechanism of wave was found by L.D. Landau. The process of Landau damping involves a direct wave-particle interaction in collisionless plasma without necessity of randamizing collision. This process is fundamental mechanism in wave heatings of plasma (wave damping) and instabilities (inverse damping of perturbations). Landau damping will be described in ch.11, ch.12 and appendix C.

1.3 Fusion Core Plasma

Progress in plasma physics has been motivated by how to realize fusion core plasma. Necessary condition for fusion core plasma is discussed in this section. Nuclear fusion reactions are the fused reactions of light nuclides to heavier one. When the sum of the masses of nuclides after a nuclear fusion is smaller than the sum before the reaction by Δm, we call it mass defect. According to theory of relativity, amount of energy $(\Delta m)c^2$ (c is light speed) is released by the nuclear fusion.

Nuclear reactions of interest for fusion reactors are as follows (D; deuteron, T; triton, He^3; helium-3, Li; lithium):

(1) D+D→T(1.01 MeV)+p(3.03 MeV)
(2) D+D→ He^3(0.82 MeV)+n(2.45 MeV)
(3) T+D→ He^4(3.52 MeV)+n(14.06 MeV)
(4) D+He^3 → He^4(3.67 MeV) +p(14.67 MeV)
(5) Li^6+n→T+He^4+4.8 MeV
(6) Li^7+n(2.5 MeV)→T+He^4+n

where p and n are proton (hydrogen ion) and neutron respectively (1 MV=10^6 eV). Since the energy released by chemical reaction of $H_2 + (1/2)O_2 \rightarrow H_2O$ is 2.96 eV, fusion energy released is about million times as large as chemical one. A binding energy per nucleon is smaller in very light or very heavy nuclides and largest in the nuclides with atomic mass numbers around 60. Therefore, large amount of the energy can be released when the light nuclides are fused. Deuterium exists aboundantly in nature; for example, it comprises 0.015 atom percent of the hydrogen in sea water with the volume of about 1.35×10^9 km^3 .

Although fusion energy was released in an explosive manner by the hydrogen bomb in 1951, controlled fusion is still in the stage of research development. Nuclear fusion reactions were found in 1920's. When proton or deuteron beams collide with target of light nuclide, beam loses its energy by the ionization or elastic collisions with target nuclides and the probability of nuclear fusion is negligible. Nuclear fusion researches have been most actively pursued by use of hot plasma. In fully ionized hydrogen, deuterium and tritium plasmas, the process of ionization does not occur. If the plasma is confined in some specified region adiabatically, the average energy does not decrease by the processes of elastic collisions. Therefore if the very hot D-T plasmas or D-D plasmas are confined, the ions have velocities large enough to overcome their mutual coulomb repulsion, so that collision and fusion take place.

Let us consider the nuclear reaction that D collides with T. The effective *cross section* of T nucleous is denoted by σ. This cross section is a function of the kinetic energy E of D. The cross section of D-T reaction at $E = 100$ keV is 5×10^{-24} cm^2 . The cross sections σ of D-T, D-D, D-He^3 reaction versus the kinetic energy of colliding nucleous are shown in fig.1.2(a) (ref.[1],[2]). The

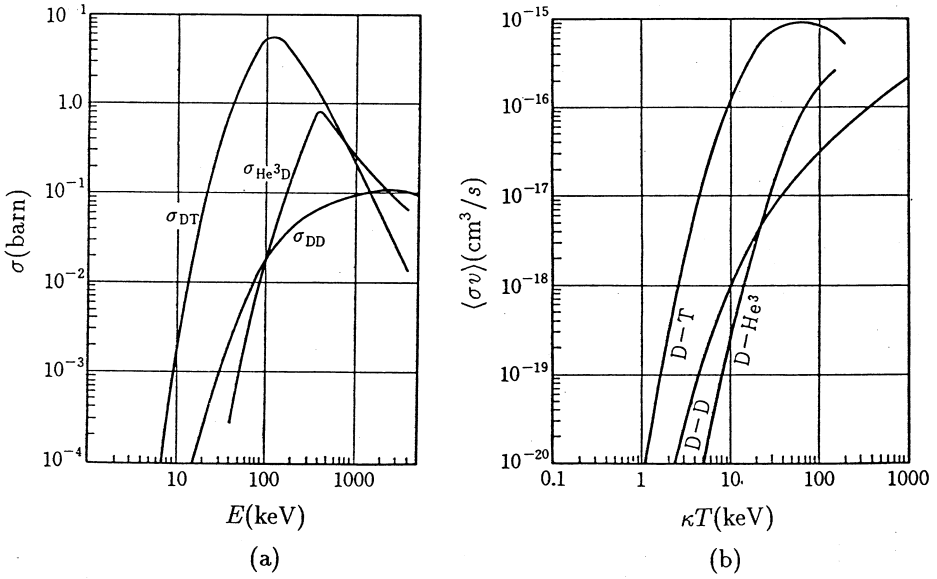

Fig.1.2 (a) The dependence of fusion cross section σ on the kinetic energy E of colliding nucleous. $\sigma_{\rm DD}$ is the sum of the cross sections of D-D reactions (1) (2). 1 barn=10^{-24} cm^2.
(b) The dependence of fusion rate $\langle\sigma v\rangle$ on the ion temperature $T_{\rm i}$.

probability of fusion reaction per unit time in the case that a D ion with the velocity v collides with T ions with the density of $n_{\rm T}$ is given by $n_{\rm T}\sigma v$ (we will discuss the collision probability in more details in sec.2.7). When a plasma is Maxwellian with the ion temperature of $T_{\rm i}$, it is necessary to calculate the average value $\langle\sigma v\rangle$ of σv over the velocity space. The dependence of $\langle\sigma v\rangle$ on ion temperature $T_{\rm i}$ is shown in fig.1.2(b) (ref.[3]). A fitting equation of $\langle\sigma v\rangle$ of D-T reaction as a function of κT in unit of keV is (ref.[4])

$$\langle\sigma v\rangle({\rm m}^{-3}) = \frac{3.7\times10^{-18}}{H(\kappa T)\times(\kappa T)^{2/3}}\exp\left(-\frac{20}{(\kappa T)^{1/3}}\right), \qquad H(\kappa T)\equiv\frac{\kappa T}{37}+\frac{5.45}{3+\kappa T(1+\kappa T/37.5)^{2.8}} \tag{1.5}$$

Figure 1.3 shows an example of electric power plant based on D-T fusion reactor. Fast neutrons produced in fusion core plasma penetrate the first wall and a lithium blanket surrounding the plasma moderates the fast neutrons, converting their kinetic energy to heat. Furthermore the lithium blanket breeds tritium due to reaction (5),(6). Lithium blanket gives up its heat to generate the steam by a heat exchanger; steam turbine generates electric power. A part of the generated electric power is used to operate heating system of plasma to compensate the energy losses from the plasma to keep the plasma hot. The fusion output power must be larger than the necessary heating input power taking account the conversion efficiency. Since the necessary heating input power is equal to the energy loss rate of fusion core plasma, good energy confinement of hot plasma is key issue.

The thermal energy of plasma per unit volume is given by $(3/2)n\kappa(T_{\rm i}+T_{\rm e})$. This thermal energy is lost by thermal conduction and convective losses. The notation $P_{\rm L}$ denotes these energy losses of the plasma per unit volume per unit time (power loss per unit volume). There is radiation loss R due to bremsstrahlung of electrons and impurity ion radiation in addition to $P_{\rm L}$. The total energy confinement time $\tau_{\rm E}$ is defined by

$$\tau_{\rm E}\equiv\frac{(3/2)n\kappa(T_{\rm e}+T_{\rm i})}{P_{\rm L}+R}\simeq\frac{3n\kappa T}{P_{\rm L}+R}. \tag{1.6}$$

The necessary heating input power $P_{\rm heat}$ is equal to $P_{\rm L}+R$. In the case of D-T reaction, the sum of kinetic energies $Q_\alpha = 3.52\,{\rm MeV}$ of α particle (He^4 ion) and $Q_{\rm n} = 14.06\,{\rm MeV}$ of neutron is

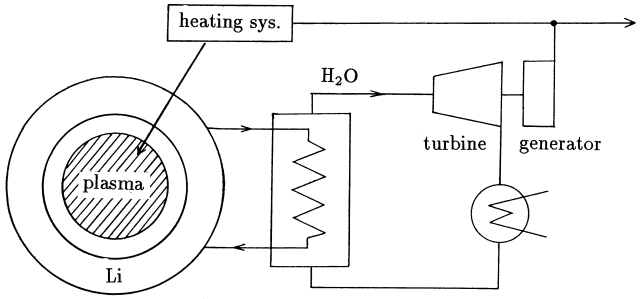

Fig.1.3 An electric power plant based on a D-T fusion reactor

$Q_{\rm NF}$=17.58 MeV per 1 reaction. Since the densities of D ions and T ions of equally mixed plasma are $n/2$, number of D-T reaction per unit time per unit volume is $(n/2)(n/2)\langle\sigma v\rangle$, so that fusion output power per unit volume $P_{\rm NF}$ is given by

$$P_{\rm NF} = (n/2)(n/2)\langle\sigma v\rangle Q_{\rm NF}. \tag{1.7}$$

Denote the thermal-to-electric conversion efficiency by $\eta_{\rm el}$ and heating efficiency (ratio of the deposit power into the plasma to the electric input power of heating device) by $\eta_{\rm heat}$. Then the condition of power generation is

$$P_{\rm heat} = P_{\rm L} + R = \frac{3n\kappa T}{\tau_{\rm E}} < (\eta_{\rm el})(\eta_{\rm heat})P_{\rm NF} \tag{1.8}$$

that is

$$\begin{aligned} &\frac{3n\kappa T}{\tau_{\rm E}} < (\eta_{\rm heat})(\eta_{\rm el})\frac{Q_{\rm NF}}{4}n^2\langle\sigma v\rangle, \\ &n\tau_{\rm E} > \frac{12\kappa T}{\eta Q_{\rm NF}\langle\sigma v\rangle} \end{aligned} \tag{1.9}$$

where η is the product of two efficiencies. The right-hand side of the last foregoing equation is the function of temperature T only. When $\kappa T = 10^4$ eV and $\eta \sim 0.3$ ($\eta_{\rm el} \sim 0.4$, $\eta_{\rm heat} \sim 0.75$), the necessary condition is $n\tau_{\rm E} > 1.7 \times 10^{20}\,{\rm ms}^{-3} \cdot {\rm sec}$. The condition of D-T fusion plasma in the case of $\eta \sim 0.3$ is shown in fig.1.4. In reality the plasma is hot in the core and is cold in the edge. For the more accurate discussion, we must take account of the profile effect of temperature and density and will be analyzed in sec.16.12.

The condition $P_{\rm heat} = P_{\rm NF}$ is called *break even condition*. This corresponds to the case of $\eta = 1$ in the condition of fusion core plasma. The ratio of the fusion output power due to α particles to the total is $Q_\alpha/Q_{\rm NF} = 0.2$. Since α particles are charged particles, α particles can heat the plasma by coulomb collision (see sec.2.8). If the total kinetic energy (output energy) of α particles contributes to heat the plasma, the condition $P_{\rm heat} = 0.2P_{\rm NF}$ can sustain the necessary high temperature of the plasma without heating from outside. This condition is called *ignition condition*, which corresponds the case of $\eta = 0.2$.

References

[1] W. R. Arnold, J. A. Phillips, G. A. Sawyer, E. J. Stovall, Jr. and J. C. Tuck: Phys. Rev. **93**, 483 (1954).
[2] C. F. Wandel, T. Hesselberg Jensen and O. Kofoed-Hansen: Nucl. Instr. and Methods **4**, 249 (1959).
[3] J. L. Tuck: Nucl. Fusion **1**, 201 (1961)
[4] T. Takizuka and M. Yamagiwa: JAERI-M 87-066 (1987) Japan Atomic Energy Research Institute.

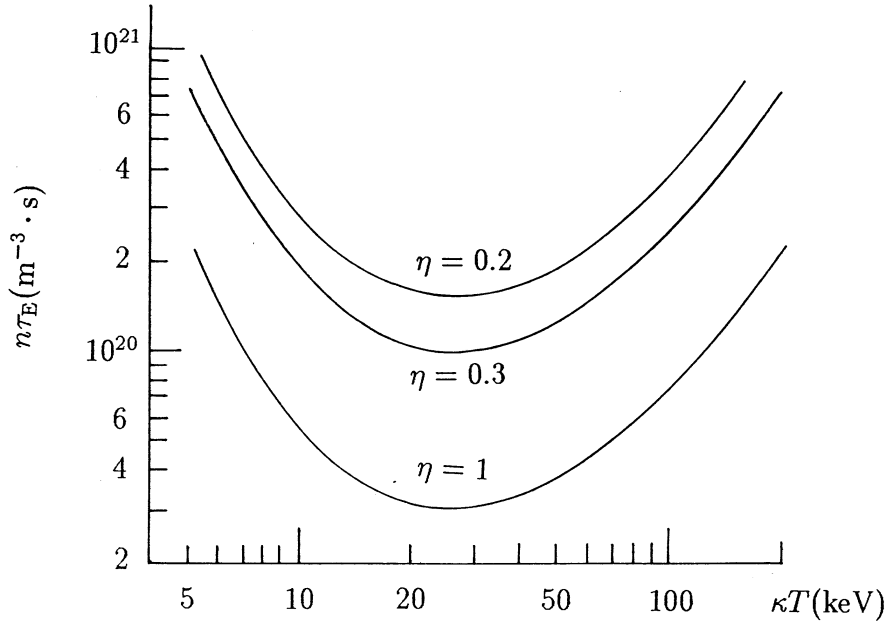

Fig.1.4 Condition of D-T fusion core plasma in $n\tau_E$ - κT diagram in the case of $\eta = 0.3$, critical condition ($\eta = 1$) and ignition condition ($\eta = 0.2$).

Ch.2 Plasma Characteristics

2.1 Velocity Space Distribution Function, Electron and Ion Temperatures

Electrons as well as ions in a plasma move with various velocities. The number of electrons in a unit volume is the electron density n_e and the number of electrons $\mathrm{d}n_\mathrm{e}(v_x)$ with the x component of velocity between v_x and $v_x + \mathrm{d}v_x$ is given by

$$\mathrm{d}n_\mathrm{e}(v_x) = f_\mathrm{e}(v_x)\mathrm{d}v_x.$$

Then $f_\mathrm{e}(v_x)$ is called electron's *velocity space distribution function*. When electrons are in thermally equilibrium state with the electron temperature T_e, the velocity space distribution function becomes following Maxwell distribution:

$$f_\mathrm{e}(v_x) = n_\mathrm{e}\left(\frac{\beta}{2\pi}\right)^{1/2}\exp\left(-\frac{\beta v_x^2}{2}\right), \qquad \beta = \frac{m_\mathrm{e}}{\kappa T_\mathrm{e}}.$$

By the definition the velocity space distribution function satisfies following relation:

$$\int_{-\infty}^{\infty} f_\mathrm{e}(v_x)\mathrm{d}v_x = n_\mathrm{e}.$$

Maxwell distribution function in three dimensional velocity space is given by

$$f_\mathrm{e}(v_x, v_y, v_z) = n_\mathrm{e}\left(\frac{m_\mathrm{e}}{2\pi\kappa T_\mathrm{e}}\right)^{3/2}\exp\left(-\frac{m_\mathrm{e}(v_x^2 + v_y^2 + v_z^2)}{2\kappa T_\mathrm{e}}\right). \tag{2.1}$$

Ion distribution function is also defined by the same way as the electron's case. The mean square of velocity v_x^2 is given by

$$v_\mathrm{T}^2 = \frac{1}{n}\int_{-\infty}^{\infty} v_x^2 f(v_x)\mathrm{d}v_x = \frac{\kappa T}{m}. \tag{2.2}$$

The pressure p is

$$p = n\kappa T.$$

Particle flux in the x direction per unit area $\mathit{\Gamma}_{+,x}$ is given by

$$\mathit{\Gamma}_{+,x} = \int_0^{\infty} v_x f(v_x)\mathrm{d}v_x = n\left(\frac{\kappa T}{2\pi m}\right)^{1/2}.$$

When an electron beam with the average velocity v_b is injected into a plasma with a Maxwell distribution, the distribution function becomes humped profile as is shown in fig.2.1(b). Following expression can be used for the modeling of the distribution function of a plasma with an electron beam:

$$f_\mathrm{e}(v_z) = n_\mathrm{e}\left(\frac{m_\mathrm{e}}{2\pi\kappa T_\mathrm{e}}\right)^{1/2}\exp\left(-\frac{m_\mathrm{e}v_z^2}{2\kappa T_\mathrm{e}}\right) + \ n_\mathrm{b}\left(\frac{m_\mathrm{e}}{2\pi\kappa T_\mathrm{b}}\right)^{1/2}\exp\left(-\frac{m_\mathrm{e}(v_z - v_\mathrm{b})^2}{2\kappa T_\mathrm{b}}\right).$$

2.2 Plasma Frequency, Debye Length

Let us consider the case where a small perturbation occurs in a uniform plasma and the electrons

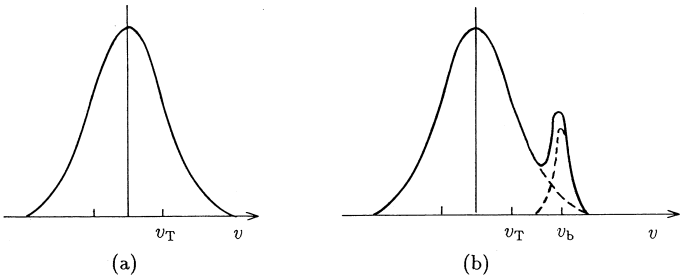

Fig.2.1 (a) Velocity space distribution function of Maxwellian with electron temperature T_e. (b) velocity space distribution function of Maxwellian plasma with electron temterature T_e and injected electron beam with the average velocity v_b.

in the plasma move by the perturbation. It is assumed that ions do not move because the ion's mass is much more heavy than electron's. Due to the displacement of electrons, electric charges appear and an electric field is induced. The electric field is given by Poisson's equation:

$$\epsilon_0 \nabla \cdot \boldsymbol{E} = -e(n_e - n_0).$$

Electrons are accelerated by the electric field:

$$m_e \frac{d\boldsymbol{v}}{dt} = -e\boldsymbol{E}.$$

Due to the movement of electrons, the electron density changes:

$$\frac{\partial n_e}{\partial t} + \nabla \cdot (n_e \boldsymbol{v}) = 0.$$

Denote $n_e - n_0 = n_1$ and assume $|n_1| \ll n_0$, then we find

$$\epsilon_0 \nabla \cdot \boldsymbol{E} = -en_1, \quad m_e \frac{\partial \boldsymbol{v}}{\partial t} = -e\boldsymbol{E}, \quad \frac{\partial n_1}{\partial t} + n_0 \nabla \cdot \boldsymbol{v} = 0.$$

For simplicity the displacement is assumed only in the x direction and is sinusoidal:

$$n_1(x,t) = n_1 \exp(ikx - i\omega t).$$

Time differential $\partial/\partial t$ is replaced by $-i\omega$ and $\partial/\partial x$ is replaced by ik, then

$$ik\epsilon_0 E = -en_1, \quad -i\omega m_e v = -eE, \quad -i\omega n_1 = -ikn_0 v$$

so that we find

$$\omega^2 = \frac{n_0 e^2}{\epsilon_0 m_e}. \tag{2.3}$$

This wave is called *electron plasma wave* or *Langmuir wave* and its frequency is called *electron plasma frequency* Π_e:

$$\Pi_e = \left(\frac{n_e e^2}{\epsilon_0 m_e}\right)^{1/2} = 5.64 \times 10^{11} \left(\frac{n_e}{10^{20}}\right)^{1/2} \quad \text{rad/sec.}$$

There is following relation between the plasma frequency and Debye length λ_D:

$$\lambda_D \Pi_e = \left(\frac{\kappa T_e}{m_e}\right)^{1/2} = v_{Te}.$$

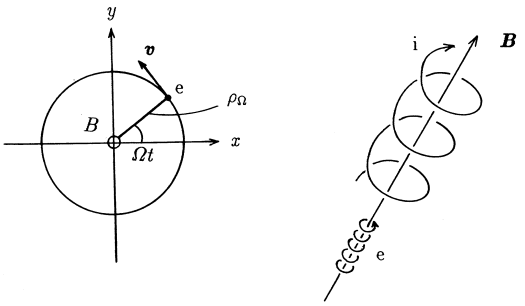

Fig.2.2 Larmor motion of charged particle in magnetic field

2.3 Cyclotron Frequency, Larmor Radius

The equation of motion of charged particle with the mass m and the charge q in an electric and magnetic field $\boldsymbol{E}$, $\boldsymbol{B}$ is given by

$$m\frac{\mathrm{d}\boldsymbol{v}}{\mathrm{d}t} = q(\boldsymbol{E} + \boldsymbol{v} \times \boldsymbol{B}). \tag{2.4}$$

When the magnetic field is homogenous and is in the z direction and the electric field is zero, the equation of motion becomes $\dot{\boldsymbol{v}} = (qB/m)(\boldsymbol{v} \times \boldsymbol{b})$ $(\boldsymbol{b} = \boldsymbol{B}/B)$ and

$$v_x = -v_\perp \sin(\Omega t + \delta),$$

$$v_y = v_\perp \cos(\Omega t + \delta),$$

$$v_z = v_{z0},$$

$$\Omega = -\frac{qB}{m}. \tag{2.5}$$

The solution of these equation is a spiral motion around the magnetic line of force with the angular velocity of Ω (see fig.2.2). This motion is called *Larmor motion*. The angular frequency Ω is called *cyclotron (angular) frequency*. Denote the radius of the orbit by ρ_Ω, then the centrifugal force is $mv_\perp^2/\rho_\Omega$ and Lorentz force is $qv_\perp B$. Since both forces must be balanced, we find

$$\rho_\Omega = \frac{mv_\perp}{\mid q \mid B}. \tag{2.6}$$

This radius is called *Larmor radius*. The center of Larmor motion is called *guiding center*. Electron's Larmor motion is right-hand sence $(\Omega_\mathrm{e} > 0)$, and ion's Larmor motion is left-hand sence $(\Omega_\mathrm{i} < 0)$ (see fig.2.2). When $B = 1\,\mathrm{T}$, $\kappa T = 100\,\mathrm{eV}$, the values of Larmor radius and cyclotron freqency are given in the following table:

B=1T, κT=100eV	electron	proton
thermal velocity $v_\mathrm{T} = (\kappa T/m)^{1/2}$	$4.2 \times 10^6\,\mathrm{m/s}$	$9.8 \times 10^4\,\mathrm{m/s}$
Larmor radius ρ_Ω	$23.8\,\mu\mathrm{m}$	$1.02\,\mathrm{mm}$
(angular) cyclotron frequency Ω	$1.76 \times 10^{11}/\mathrm{s}$	$-9.58 \times 10^7/\mathrm{s}$
cyclotron freqeuncy $\Omega/2\pi$	$28\,\mathrm{GHz}$	$-15.2\,\mathrm{MHz}$

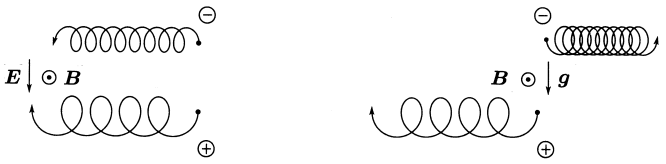

Fig.2.3 Drift motion of guiding center in electric and gravitational field (conceptional drawing).

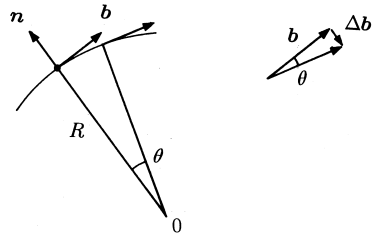

Fig.2.4 Radius of curvature of line of magnetic force

2.4 Drift Velocity of Guiding Center

When a uniform electric field $\boldsymbol{E}$ perpendicular to the uniform magnetic field is superposed, the equation of motion is reduced to

$$m\frac{\mathrm{d}\boldsymbol{u}}{\mathrm{d}t} = q(\boldsymbol{u}\times\boldsymbol{B})$$

by use of

$$\boldsymbol{v} = \boldsymbol{u}_{\mathrm{E}} + \boldsymbol{u}, \qquad \boldsymbol{u}_{\mathrm{E}} = \frac{\boldsymbol{E}\times\boldsymbol{b}}{B}. \tag{2.7}$$

Therefore the motion of charged particle is superposition of Larmor motion and drift motion $\boldsymbol{u}_{\mathrm{E}}$ of its guiding center. The direction of guiding center drift by $\boldsymbol{E}$ is the same for both ion and electron (fig.2.3). When a gravitational field $\boldsymbol{g}$ is superposed, the force is $m\boldsymbol{g}$, which corresponds to $q\boldsymbol{E}$ in the case of electric field. Therefore *the drift velocity of the guiding center* due to the gravitation is given by

$$\boldsymbol{u}_{\mathrm{g}} = \frac{m}{qB}(\boldsymbol{g}\times\boldsymbol{b}) = -\frac{\boldsymbol{g}\times\boldsymbol{b}}{\Omega}. \tag{2.8}$$

The directions of ion's drift and electron's drift due to the gravitation are opposite with each other and the drift velocity of ion guiding center is much larger than electron's one (see fig.2.3). When the magnetic and electric fields change slowly and gradually in time and in space ($|\omega/\Omega| \ll 1, \rho_\Omega/R \ll 1$), the formulas of drift velocity are valid as they are. However because of the curvature of field line of magnetic force, centrifugal force acts on the particle which runs along a field line with the velocity of $v_\parallel$. The acceleration of centrifugal force is

$$\boldsymbol{g}_{\mathrm{curv}} = \frac{v_\parallel^2}{R}\boldsymbol{n}$$

where R is the radius of curvature of field line and $\boldsymbol{n}$ is the unit vector with the direction from the center of the curvature to the field line (fig.2.4).

Furthermore, as is described later, the resultant effect of Larmor motion in an inhomogeneous magnetic field is reduced to the acceleration of

$$\boldsymbol{g}_{\nabla B} = -\frac{v_\perp^2/2}{B}\nabla B.$$

Therefore drift velocity of the guiding center due to inhomogenous curved magnetic field is given by the *drift approximation* as follows:

$$\boldsymbol{u}_{\mathrm{g}} = -\frac{1}{\Omega}\left(\frac{v_{\parallel}^2}{R}\boldsymbol{n} - \frac{v_{\perp}^2}{2}\frac{\nabla B}{B}\right) \times \boldsymbol{b}. \tag{2.9}$$

The first term is called *curvature drift* and the second term is called ∇B *drift*. Since $\nabla \times \boldsymbol{B} = \mu_0 \boldsymbol{j}$, the vector formula reduces

$$\frac{1}{2B}\nabla(\boldsymbol{B}\cdot\boldsymbol{B}) = (\boldsymbol{b}\cdot\nabla)\boldsymbol{B} + \boldsymbol{b}\times(\nabla\times\boldsymbol{B}) = \frac{\partial}{\partial l}(B\boldsymbol{b}) + \boldsymbol{b}\times\mu_0\boldsymbol{j}$$

$$= \frac{\partial B}{\partial l}\boldsymbol{b} + B\frac{\partial \boldsymbol{b}}{\partial l} - \mu_0\frac{\nabla p}{B} = \frac{\partial B}{\partial l}\boldsymbol{b} - B\frac{\boldsymbol{n}}{R} - \mu_0\frac{\nabla p}{B}.$$

We used the following relation (see fig.2.4)

$$\frac{\partial \boldsymbol{b}}{\partial l} = -\frac{\boldsymbol{n}}{R}.$$

Then we have

$$\frac{\boldsymbol{n}\times\boldsymbol{b}}{R} = -\left(\frac{\nabla B}{B} + \mu_0\frac{\nabla p}{B^2}\right)\times\boldsymbol{b}.$$

If ∇p is much smaller than $\nabla B^2/(2\mu_0)$, we find

$$\boldsymbol{u}_{\mathrm{g}} = -\frac{1}{\Omega}\frac{v_{\parallel}^2 + v_{\perp}^2/2}{R}(\boldsymbol{n}\times\boldsymbol{b}).$$

The parallel motion along the magnetic field is given by

$$m\frac{\mathrm{d}v_{\parallel}}{\mathrm{d}t} = qE_{\parallel} + mg_{\parallel} - \frac{mv_{\perp}^2/2}{B}\nabla_{\parallel}B$$

where l is the length along the field line.

Let us consider the effect of inhomogeneity of magnetic field on gyrating charged particle. The x component of Lorentz force $\boldsymbol{F}_{\mathrm{L}} = q\boldsymbol{v}\times\boldsymbol{B}$ perpendicular to the magnetic field (z direction) and the magnitude B of the magnetic field near the guiding center are

$$F_{\mathrm{L}x} = qv_yB = -|q|v_{\perp}\cos\theta B$$

$$B = B_0 + \frac{\partial B}{\partial x}\rho_{\Omega}\cos\theta + \frac{\partial B}{\partial y}\rho_{\Omega}\sin\theta.$$

The time average of x component of Lorentz force is given by $\langle F_{\mathrm{L}x}\rangle = \frac{1}{2}(\partial B/\partial x)(-|q|)v_{\perp}\rho_{\Omega}$ and the y component is also given by the same way, and we find (see fig.2.5)

$$\langle \boldsymbol{F}_{\mathrm{L}}\rangle_{\perp} = -\frac{mv_{\perp}^2/2}{B}\nabla_{\perp}B.$$

Next it is necessary to estimate the time average of z component of Lorentz force. The equation $\nabla\cdot\boldsymbol{B} = 0$ near the guiding center in fig.2.5 becomes $B_r/r + \partial B_r/\partial r + \partial B_z/\partial z = 0$ and we find

$$\langle F_{\mathrm{L}z}\rangle = -\langle qv_{\theta}B_r\rangle = |q|v_{\perp}\rho_{\Omega}\frac{\partial B_r}{\partial r} = -\frac{mv_{\perp}^2/2}{B}\frac{\partial B}{\partial z},$$

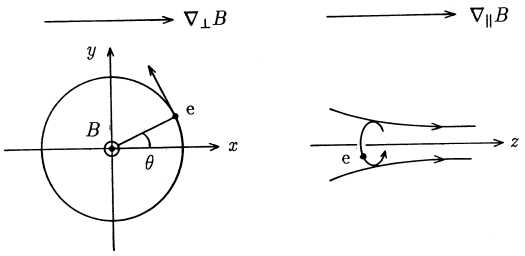

Fig.2.5 Larmor motion in inhomogeneous magnetic field.

since r is very small. Thus the necessary expression of $\boldsymbol{g}_{\nabla B}$ is derived.

2.5 Magnetic Moment, Mirror Confinement, Longitudinal Adiabatic Constant

A current loop with the current I encircling the area S has the magnetic moment of $\mu_{\rm m} = IS$. Since the current and encircling area of gyrating Larmor motion are $I = q\Omega/2\pi,\ S = \pi\rho_\Omega^2$ respectively, it has the *magnetic moment* of

$$\mu_{\rm m} = \frac{q\Omega}{2\pi}\pi\rho_\Omega^2 = \frac{mv_\perp^2}{2B}. \tag{2.10}$$

This physical quantity is adiabatically invariant as is shown later in this section. When the magnetic field changes slowly, the magnetic moment is conserved. Therefore if B is increased, $mv_\perp^2 = \mu_{\rm m}B$ is also increased and the particles are heated. This kind of heating is called *adiabatic heating*.

Let us consider a mirror field as is shown in fig.2.6, in which magnetic field is weak at the center and is strong at both ends of mirror field. For simplicity the electric field is assumed to be zero. Since Lorentz force is perpendicular to the velocity, the magnetic field does not contribute the change of kinetic energy and

$$\frac{mv_\parallel^2}{2} + \frac{mv_\perp^2}{2} = \frac{mv^2}{2} = E = \text{const.} \tag{2.11}$$

Since the magnetic moment is conserved, we find

$$v_\parallel = \pm\left(\frac{2}{m}E - v_\perp^2\right)^{1/2} = \pm\left(v^2 - \frac{2}{m}\mu_{\rm m}B\right)^{1/2}.$$

When the particle moves toward the open ends, the magnetic field becomes large and $v_\parallel$ becomes small or even zero. Since the force along the parallel direction to the magnetic field is $-\mu_{\rm m}\nabla_\parallel B$, the both ends of the mirror field repulse charged particles as a mirror reflects light. The ratio of magnitude of magnetic field at open end to the central value is called *mirror ratio*:

$$R_{\rm M} = \frac{B_{\rm M}}{B_0}.$$

Let us denote the parallel and perpendicular components of the velocity at the mirror center by $v_{\parallel 0}$ and $v_{\perp 0}$ respectively. The value $v_\perp^2$ at the position of maximum magnetic field $B_{\rm M}$ is given by

$$v_{\perp{\rm M}}^2 = \frac{B_{\rm M}}{B_0}v_{\perp 0}^2.$$

If this value is larger than $v^2 = v_0^2$, this particle can not pass through the open end, so that the particle satisfying the following condition is reflected and is trapped in the mirror field:

$$\left(\frac{v_{\perp 0}}{v_0}\right)^2 > \frac{B_0}{B_{\rm M}} = \frac{1}{R_{\rm M}}. \tag{2.12}$$

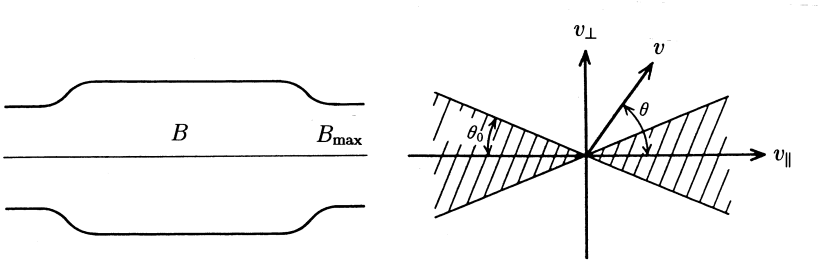

Fig.2.6 Mirror field and loss cone in $v_\parallel$ - $v_\perp$ space.

Particles in the region where $\sin\theta \equiv v_{\perp 0}/v_0$ satisfies

$$\sin^2\theta \leq \frac{1}{R_{\rm M}}$$

are not trapped and the region is called *loss cone* in $v_\parallel$ - $v_\perp$ space (see Fig.2.6).

Let us check the invariance of $\mu_{\rm m}$ in the presence of a slowly changing magnetic field ($|\partial B/\partial t| \ll |\Omega B|$). Scalar product of $\boldsymbol{v}_\perp$ and the equation of motion is

$$m\boldsymbol{v}_\perp \cdot \frac{{\rm d}\boldsymbol{v}_\perp}{{\rm d}t} = \frac{\rm d}{{\rm d}t}\left(\frac{mv_\perp^2}{2}\right) = q(\boldsymbol{v}_\perp \cdot \boldsymbol{E}_\perp).$$

During one period $2\pi/|\Omega|$ of Larmor motion, the change $\Delta W_\perp$ of the kinetic energy $W_\perp = mv_\perp^2/2$ is

$$\Delta W_\perp = q\int (\boldsymbol{v}_\perp \cdot \boldsymbol{E}_\perp){\rm d}t = q\oint \boldsymbol{E}_\perp \cdot {\rm d}\boldsymbol{s} = q\int (\nabla \times \boldsymbol{E}\cdot \boldsymbol{n}){\rm d}S$$

where $\oint {\rm d}s$ is the closed line integral along Larmor orbit and $\int {\rm d}S$ is surface integral over the encircled area of Larmor orbit. Since $\nabla \times \boldsymbol{E} = -\partial \boldsymbol{B}/\partial t$, $\Delta W_\perp$ is

$$\Delta W_\perp = -q\int \frac{\partial \boldsymbol{B}}{\partial t}\cdot \boldsymbol{n}{\rm d}S = |q|\pi\rho_\Omega^2 \frac{\partial B}{\partial t}.$$

The change of magnetic field ΔB during one period of Larmor motion is $\Delta B = (\partial B/\partial t)(2\pi/|\Omega|)$, we find

$$\Delta W_\perp = \frac{mv_\perp^2}{2}\frac{\Delta B}{B} = W_\perp \frac{\Delta B}{B}$$

and

$$\mu_{\rm m} = \frac{W_\perp}{B} = {\rm const.}$$

When a system is periodic in time, the action integral $\oint p{\rm d}q$, in terms of the canonical variables p, q, is an adiabatic invariant in general. The action integral of Larmor motion is $J_\perp = (-m\rho_\Omega\Omega)2\pi\rho_\Omega = -(4\pi m/q)\mu_{\rm m}$. $J_\perp$ is called *transversal adiabatic invariant*.

A particle trapped in a mirror field moves back and forth along the field line between both ends. The second action integral of this periodic motion

$$J_\parallel = m\oint v_\parallel {\rm d}l \tag{2.13}$$

is also another adiabatic invariant. $J_\parallel$ is called *longitudinal adiabatic invariant*. As one makes the mirror length l shorter, $\langle v_\parallel\rangle$ increases (for $J_\parallel = 2m\langle v_\parallel\rangle l$ is conserved), and the particles are accelerated. This phenomena is called *Fermi acceleration*.

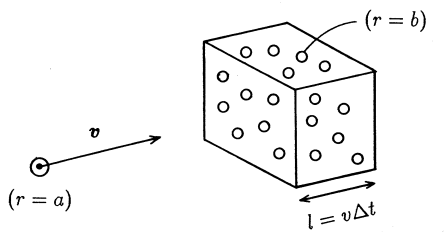

Fig.2.7 Probability of collision of a sphere a with spheres b.

The line of magnetic force of mirror is convex toward outside. The particles trapped by the mirror are subjected to curvature drift and gradient B drift, so that the trapped particles move back and forth, while drifting in θ direction. The orbit $(r,\ \theta)$ of the crossing point at $z = 0$ plane of back and forth movement is given by $J_{\parallel}(r, \theta, \mu_{\rm m}, E) = \text{const.}$

2.6 Coulomb Collision Time, Fast Neutral Beam Injection

The motions of charged particles were analyzed in the previous section without considering the effects of collisions between particles. In this section, phenomena associated with *Coulomb collisions* will be discussed. Let us start from a simple model. Assume that a sphere with the radius a moves with the velocity v in the region where spheres with the radius b are filled with the number density n (see fig.2.7). When the distance between the two particles becomes less than $a + b$, collision takes place. The cross section σ of this collision is $\sigma = \pi(a + b)^2$. Since the sphere a moves by the distance $l = v\delta t$ during δt, the probability of collision with the sphere b is

$$nl\sigma = n\sigma v\delta t$$

since nl is the possible number of the sphere b, with which the sphere a within a unit area of incidence may collides, and $nl\sigma$ is the total cross section per unit area of incidence during the period of δt. Therefore the inverse of collision time $t_{\rm coll}$ is

$$(t_{\rm coll})^{-1} = n\sigma v.$$

In this simple case the cross section σ of the collision is independent of the velocity of the incident sphere a. However the cross section is dependent on the incident velocity in general.

Let us consider strong Coulomb collision of an incident electron with ions (see fig.2.8) in which the electron is deflected strongly after the collision. Such a collision can take place when the magnitude of electrostatic potential of the electron at the closest distance b is the order of the kinetic energy of incident electron, that is,

$$\frac{Ze^2}{4\pi\epsilon_0 b} = \frac{m_{\rm e}v_{\rm e}^2}{2}.$$

The cross section of the strong Coulomb collision is $\sigma = \pi b^2$. The inverse of the collision time of

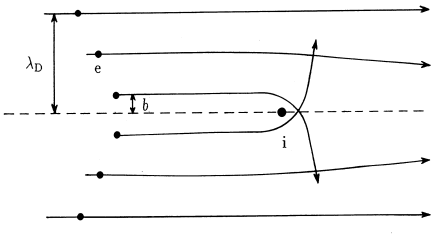

Fig.2.8 Coulomb collision of electron with ion.

the strong Coulomb collision is

$$\frac{1}{t_{\rm coll}} = n_{\rm i}\sigma v_{\rm e} = n_{\rm i} v_{\rm e}\pi b^2 = \frac{n_{\rm i}\pi (Ze^2)^2 v_{\rm e}}{(4\pi\epsilon_0 m_{\rm e} v_{\rm e}^2/2)^2} = \frac{Z^2 e^4 n_{\rm i}}{4\pi\epsilon_0^2 m_{\rm e}^2 v_{\rm e}^3}.$$

Since Coulomb force is long range interaction, a test particle is deflected by small angle even by a distant field particle, which the test particle does not become very close to. As is described in sec.1.2, the Coulomb field of a field particle is not shielded inside the Debye sphere with the radius of Debye length $\lambda_{\rm D}$ and there are many field particles inside the Debye sphere in the usual laboratory plasmas (weakly coupled plasmas). Accumulation of many collisions with small angle deflection results in large effect. When the effect of the small angle deflection is taken into account, the total Coulomb cross section increases by the factor of *Coulomb logarithm*

$$\ln \Lambda \simeq \ln\left(\frac{2\lambda_{\rm D}}{b}\right) \simeq \int_{b/2}^{\lambda_{\rm D}} \frac{1}{r}{\rm d}r \simeq 15 \sim 20.$$

The time derivative of the momentum $p_\parallel$ parallel to the incident direction of the electron is given by use of the *collision time* $\tau_{{\rm ei}\parallel}$ as follows: (ref.[1])

$$\frac{{\rm d}p_\parallel}{{\rm d}t} = -\frac{p_\parallel}{\tau_{{\rm ei}\parallel}},$$

$$\frac{1}{\tau_{{\rm ei}\parallel}} = \frac{Z^2 e^4 n_{\rm i} \ln \Lambda}{4\pi\epsilon_0^2 m_{\rm e}^2 v_{\rm e}^3} \tag{2.14}$$

where $\tau_{{\rm ei}\parallel}$ indicates the deceleration time of an electron by ions.

When a test particle with the charge q, the mass m and the velocity v collides with the field particles with the charge q^*, the mass m^* and the thermal velocity $v_{\rm T}^* = (T^*/m^*)^{1/2}$ in general, the collision time of the test particle is given by (ref.[1])

$$\frac{1}{\tau_\parallel} = \frac{q^2 q^{*2} n^* \ln \Lambda}{4\pi\epsilon_0^2 m m_{\rm r} v^3} = \left(\frac{qq^* n^*}{\epsilon_0 m}\right)^2 \frac{\ln \Lambda}{4\pi (m_{\rm r}/m) v^3 n^*} \tag{2.15}$$

under the assumption of $v > v_{\rm T}^*$. $m_{\rm r}$ is the reduced mass $m_{\rm r} = mm^*/(m+m^*)$. Taking the average of $(m/2)v^2 = (3/2)\kappa T$, $1/\tau_\parallel$ becomes

$$\frac{1}{\tau_\parallel} = \frac{q^2 q^{*2} n^* \ln \Lambda}{3^{1/2} 12\pi\epsilon_0^2 (m_{\rm r}/m^{1/2})(\kappa T)^{3/2}}. \tag{2.16}$$

This collision time in the case of electron with ions is

$$\frac{1}{\tau_{{\rm ei}\parallel}} = \frac{Z^2 e^4 n_{\rm i} \ln \Lambda}{3^{1/2} 12\pi\epsilon_0^2 m_{\rm e}^{1/2} (\kappa T)^{3/2}}. \tag{2.17}$$

This collision time of electron with ions is within 20% of Spitzer's result (ref.[2])

$$\frac{1}{\tau_{{\rm ei}\parallel\ {\rm Spitzer}}} = \frac{Z^2 e^4 n_{\rm i} \ln \Lambda}{51.6\pi^{1/2}\epsilon_0^2 m_{\rm e}^{1/2} (\kappa T_{\rm e})^{3/2}}. \tag{2.18}$$

When an ion with the charge Z and the mass $m_{\rm i}$ collides with the same ions, the ion-ion collision time is given by

$$\frac{1}{\tau_{{\rm ii}\parallel}} = \frac{Z^4 e^4 n_{\rm i} \ln \Lambda}{3^{1/2} 6\pi\epsilon_0^2 m_{\rm i}^{1/2} (\kappa T_{\rm i})^{3/2}}. \tag{2.19}$$

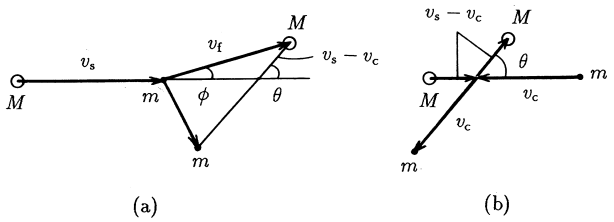

Fig.2.9 Elastic collision of test particle M and field particle m in laboratory system (a) and center-of-mass system (b).

Electron-electron Coulomb collision time can be derived by substitution of $m_\mathrm{i} \to m_\mathrm{e}$ and $Z \to 1$ into the formula of $\tau_{\mathrm{ii}\parallel}$.

$$\frac{1}{\tau_{\mathrm{ee}\parallel}} = \frac{n_\mathrm{e} e^4 \ln \Lambda}{3^{1/2} 6\pi\epsilon_0^2 m_\mathrm{e}^{1/2} (\kappa T_\mathrm{e})^{3/2}}. \tag{2.20}$$

However the case of ion to electron Coulomb collision is more complicated to treat because the assumption $v_\mathrm{i} > v_\mathrm{T}^*$ is no longer hold. Let us consider the case that a test particle with the mass M and the velocity v_s collides with a field particle with the mass m. In center-of-mass system where the center of mass is rest, the field particle m moves with the velocity of $v_\mathrm{c} = -Mv_\mathrm{s}/(M+m)$ and the test particle M moves with the velocity of $v_\mathrm{s} - v_\mathrm{c} = mv_\mathrm{s}/(M+m)$ (see fig.2.9). Since the total momentum and total kinetic energy of two particles are conserved in the process of elastic collision, the velocities of the test particle and the field particle do not change and two particles only deflect their direction by the angle of θ in center-of -mass system. The velocity v_f and scattering angle ϕ of the test particle after the collision in laboratory system are given by (see fig.2.9)

$$v_\mathrm{f}^2 = (v_\mathrm{s} - v_\mathrm{c})^2 + {v_\mathrm{c}}^2 + 2(v_\mathrm{s} - v_\mathrm{c}) v_\mathrm{c} \cos\theta = v_\mathrm{s}^2 \frac{(M^2 + 2Mm\cos\theta + m^2)}{(M+m)^2},$$

$$\sin\phi = \frac{m \sin\theta}{(M^2 + 2Mm\cos\theta + m^2)^{1/2}}.$$

Denote the momentum and the kinetic energy of the test particle before and after the collision by p_s, E_s, and p_f, E_f respectively, then we find

$$\frac{\Delta E}{E_\mathrm{s}} \equiv \frac{E_\mathrm{f} - E_\mathrm{s}}{E_\mathrm{s}} = -\frac{2Mm}{(M+m)^2}(1 - \cos\theta).$$

When the average is taken by θ, we obtain the following relations in the case of $m/M \ll 1$:

$$\langle \frac{\Delta E}{E_\mathrm{s}} \rangle \simeq -\frac{2m}{M}, \qquad \langle \frac{\Delta p_\parallel}{p_\mathrm{s}} \rangle \simeq -\frac{m}{M}.$$

From the foregoing discussion, the inverse of collision time $1/\tau_{\mathrm{ie}\parallel}$ where a heavy ion collides with light electrons is about $m_\mathrm{e}/m_\mathrm{i}$ times the value of $1/\tau_{\mathrm{ei}\parallel}$ and is given by (ref.[1],[2])

$$\frac{1}{\tau_{\mathrm{ie}\parallel}} = \frac{m_\mathrm{e}}{m_\mathrm{i}} \frac{Z^2 e^4 n_\mathrm{e} \ln \Lambda}{(2\pi)^{1/2} 3\pi\epsilon_0^2 m_\mathrm{e}^{1/2} (\kappa T_\mathrm{e})^{3/2}}. \tag{2.21}$$

When the parallel and perpendicular components of the momentum of a test particle are denoted by $p_\parallel$ and $p_\perp$ respectively and the energy by E, there are following relations

$$E = \frac{p_\parallel^2 + p_\perp^2}{2m},$$

$$\frac{\mathrm{d}p_\perp^2}{\mathrm{d}t} = 2m\frac{\mathrm{d}E}{\mathrm{d}t} - 2p_\parallel\frac{\mathrm{d}p_\parallel}{\mathrm{d}t}.$$

We define the *velocity diffusion time* $\tau_\perp$ in the perpendicular direction to the initial momentum and the *energy relaxation time* τ^ϵ by

$$\frac{\mathrm{d}p_\perp^2}{\mathrm{d}t} \equiv \frac{p_\perp^2}{\tau_\perp},$$

$$\frac{\mathrm{d}E}{\mathrm{d}t} \equiv -\frac{E}{\tau^\epsilon}$$

respectively. $1/\tau_\perp$ and $1/\tau^\epsilon$ are given by (ref.[1])

$$\frac{1}{\tau_\perp} = \frac{q^2q^{*2}n^*\ln\Lambda}{2\pi\epsilon_0^2 v(mv)^2} = \frac{q^2q^{*2}n^*\ln\Lambda}{2\pi\epsilon_0^2 m^2v^3}, \tag{2.22}$$

$$\frac{1}{\tau^\epsilon} = \frac{q^2q^{*2}n^*\ln\Lambda}{4\pi\epsilon_0^2 m^*v(mv^2/2)} = \frac{q^2q^{*2}n^*\ln\Lambda}{2\pi\epsilon_0^2 mm^*v^3} \tag{2.23}$$

respectively under the assumption $v > v_{\mathrm{T}}^*$.

In the case of electron to ion collision, we find

$$\frac{1}{\tau_{\mathrm{ei}\perp}} \simeq \frac{2}{\tau_{\mathrm{ei}\parallel}}, \tag{2.24}$$

$$\frac{1}{\tau_{\mathrm{ei}}^\epsilon} \simeq \frac{m_\mathrm{e}}{m_\mathrm{i}}\frac{2}{\tau_{\mathrm{ei}\parallel}}. \tag{2.25}$$

In the case of electron to electron collision, and ion to ion collision, we find

$$\frac{1}{\tau_{\mathrm{ee}\perp}} \simeq \frac{1}{\tau_{\mathrm{ee}\parallel}}, \qquad \left(\frac{1}{\tau_{\mathrm{ee}\parallel}} \simeq \frac{2}{Z}\frac{1}{\tau_{\mathrm{ei}\parallel}}\right), \tag{2.26}$$

$$\frac{1}{\tau_{\mathrm{ee}}^\epsilon} \simeq \frac{1}{\tau_{\mathrm{ee}\parallel}} \tag{2.27}$$

and

$$\frac{1}{\tau_{\mathrm{ii}\perp}} \simeq \frac{1}{\tau_{\mathrm{ii}\parallel}}, \tag{2.28}$$

$$\frac{1}{\tau_{\mathrm{ii}}{}^\epsilon} \simeq \frac{1}{\tau_{\mathrm{ii}\parallel}} \tag{2.29}$$

respectively.

In the case of ion to electron collision we have following relations: (ref.[1])

$$\frac{1}{\tau_{\mathrm{ie}\perp}} \simeq \frac{Z^2e^4n_\mathrm{e}\ln\Lambda}{(2\pi)^{3/2}\epsilon_0^2 m_\mathrm{e}^{1/2}E_\mathrm{i}(\kappa T_\mathrm{e})^{1/2}}\frac{m_\mathrm{e}}{m_\mathrm{i}}, \tag{2.30}$$

$$\frac{1}{\tau_{\mathrm{ie}}{}^\epsilon} \simeq \frac{Z^2e^4n_\mathrm{e}\ln\Lambda}{4\pi\epsilon_0^2 m_\mathrm{e}^{1/2}(\kappa T_\mathrm{e})^{3/2}}\frac{4}{3(2\pi)^{1/2}}\frac{m_\mathrm{e}}{m_\mathrm{i}} \simeq \frac{1}{\tau_{\mathrm{ie}\parallel}} \simeq \frac{m_\mathrm{e}}{m_\mathrm{i}}\frac{2.77}{\tau_{\mathrm{ei}\parallel}} \tag{2.31}$$

where $E_\mathrm{i} = (3/2)\kappa T_\mathrm{i}$ is the kinetic energy of the ion. The inverse of collision time is called *collisional frequency* and is denoted by ν. The *mean free path* is given by $\lambda = 3^{1/2}v_\mathrm{T}\,\tau$.

High energy neutral particle beams can be injected into plasmas across strong magnetic fields. The neutral particles are converted to high-energy ions by means of charge exchange with plasma ions or ionization. The high energy ions (mass m_b, electric charge Z_be, energy E_b) running through the plasma slow down by Coulomb collisions with the plasma ions $(m_\mathrm{i}, Z_\mathrm{i})$ and electrons $(m_\mathrm{e}, -e)$ and the beam energy is thus transferred to the plasma. This method is called heating by *neutral beam injection* (NBI). The rate of change of the fast ion's energy, that is, the heating rate of plasma is

$$\frac{\mathrm{d}E_\mathrm{b}}{\mathrm{d}t} = -\frac{E_\mathrm{b}}{\tau^\epsilon_\mathrm{bi}} - \frac{E_\mathrm{b}}{\tau^\epsilon_\mathrm{be}},$$

$$\frac{1}{\tau^\epsilon_\mathrm{bi}} = \frac{(Z_\mathrm{b}e)^2(Z_\mathrm{i}e)^2 \ln \Lambda n_\mathrm{i}}{2\pi\epsilon_0^2 m_\mathrm{i} m_\mathrm{b} v_\mathrm{bi}^3}$$

and

$$\frac{\mathrm{d}E_\mathrm{b}}{\mathrm{d}t} = -\frac{Z_\mathrm{b}^2 e^4 \ln \Lambda n_\mathrm{e}}{4\pi\epsilon_0^2 m_\mathrm{e} v_\mathrm{bi}} \left(\sum \frac{m_\mathrm{e}}{m_\mathrm{i}} \frac{n_\mathrm{i} Z_\mathrm{i}^2}{n_\mathrm{e}} + \frac{4}{3\pi^{1/2}} \left(\frac{m_\mathrm{e} E_\mathrm{b}}{m_\mathrm{b} \kappa T_e} \right)^{3/2} \right) \tag{2.32}$$

when beam ion's velocity v_b is much less (say 1/3) than the plasma electron thermal velocity and much larger (say 2 times) than the plasma ion thermal velocity (ref.[3]). The first term in the right-hand side is due to beam-ion collisions and the second term is due to beam-electron collisions respectively. A critical energy E_cr of the beam ion, at which the plasma ions and electrons are heated at equal rates is given by

$$\frac{m v_\mathrm{cr}^2}{2} = E_\mathrm{cr} = 14.8 \kappa T_\mathrm{e} A_\mathrm{b} \left(\frac{1}{n_\mathrm{e}} \sum \frac{n_\mathrm{i} Z_\mathrm{i}^2}{A_\mathrm{i}} \right)^{2/3} \tag{2.33}$$

where A_b, A_i are atomic weights of the injected ion and plasma ion respectively. When the energy of the injected ion is larger than E_cr, the contribution to the electron heating is dominant. The slowing down time of the ion beam is given by

$$\tau_\mathrm{slowdown} = \int_{E_\mathrm{cr}}^{E_\mathrm{b}} \frac{-\mathrm{d}E_\mathrm{b}}{(\mathrm{d}E_\mathrm{b}/\mathrm{d}t)} = \frac{\tau^\epsilon_\mathrm{be}}{1.5} \ln \left(1 + \left(\frac{E}{E_\mathrm{cr}} \right)^{3/2} \right),$$

$$\frac{1}{\tau^\epsilon_\mathrm{be}} = \frac{Z^2 n_\mathrm{e} e^4 \ln \Lambda}{(2\pi)^{1/2} 3\pi\epsilon_0^2 m_\mathrm{e}^{1/2} (\kappa T_\mathrm{e})^{3/2}} \frac{m_\mathrm{e}}{m_\mathrm{b}}, \tag{2.34}$$

where $\tau^\epsilon_\mathrm{be}$ is the energy relaxation time of beam ion with electrons.

2.7 Runaway Electron, Dreicer Field

When a uniform electric field $\boldsymbol{E}$ is applied to a plasma, the motion of a test electron is

$$m_\mathrm{e} \frac{\mathrm{d}\boldsymbol{v}}{\mathrm{d}t} = -e\boldsymbol{E} - \frac{1}{\tau_\mathrm{ee}(v)} m_\mathrm{e} \boldsymbol{v},$$

$$\frac{1}{\tau_\mathrm{ee}} = n_\mathrm{e} \sigma v = \frac{e^4 \ln \Lambda}{2\pi\epsilon_0^2 m_\mathrm{e}^2 v^3}.$$

The deceleration term decreases as v increases and its magnitude becomes smaller than the acceleration term $|-e\boldsymbol{E}|$ at a critical value v_cr. When $v > v_\mathrm{cr}$, the test particle is accelerated. The deceleration term becomes smaller and the velocity starts to increase without limit. Such an electron is called a *runaway electron*. The critical velocity is given by

$$\frac{m_\mathrm{e} v_\mathrm{cr}^2}{2e} = \frac{e^2 n \ln \Lambda}{4\pi\epsilon_0^2 E}. \tag{2.35}$$

The necessary electric field for a given electron velocity to be $v_{\rm cr}$ is called *Dreicer field*. Taking $\ln\Lambda = 20$, we find

$$\frac{m_{\rm e}v_{\rm cr}^2}{2e} = 5\times10^{-16}\frac{n}{E}. \qquad \text{(SI units)}$$

When $n = 10^{19}\,{\rm m}^{-3}$, $E = 1\,{\rm V/m}$, electrons with energy larger than 5keV become runaway electrons.

2.8 Electric Resistivity, Ohmic Heating

When an electric field less than Dreicer field is applied to a plasma, electrons are accelerated and are decelerated by collisions with ions to be an equilibrium state as follows:

$$\frac{m_{\rm e}(v_{\rm e}-v_{\rm i})}{\tau_{\rm ei}} = -eE.$$

The current density j induced by the electric field becomes

$$j = -en_{\rm e}(v_{\rm e}-v_{\rm i}) = \frac{e^2n_{\rm e}\tau_{\rm ei}}{m_{\rm e}}E.$$

The *specific electric resistivity* defined by $\eta j = E$ is (ref.[2])

$$\eta = \frac{m_{\rm e}\nu_{\rm ei\|}}{n_{\rm e}e^2} = \frac{(m_{\rm e})^{1/2}Ze^2\ln\Lambda}{51.6\pi^{1/2}\epsilon_0^2}\,(\kappa T_{\rm e})^{-3/2} \tag{2.36}$$

$$= 5.2\times10^{-5}Z\ \ln\Lambda\ \left(\frac{\kappa T_{\rm e}}{e}\right)^{-3/2}. \ (\Omega{\rm m})$$

The specific resistivity of a plasma with $T_{\rm e} = 1\,{\rm keV},\ Z = 1$ is $\eta = 3.3\times10^{-8}\,\Omega{\rm m}$ and is slightly larger than the specific resistivity of copper at 20°C, $1.8\times10^{-8}\,\Omega{\rm m}$. When a current density of j is induced, the power ηj^2 per unit volume contributes to electron heating. This heating mechanism of electron is called *Ohmic heating*.

2.9 Variety of Time and Space Scales in Plasmas

Various kinds of plasma characteristics have been described in this chapter. Characteristic time scales are a period of electron plasma frequency $2\pi/\Pi_{\rm e}$, an electron cyclotron period $2\pi/\Omega_{\rm e}$, an ion cyclotron period $2\pi/|\Omega_{\rm i}|$, electron to ion collision time $\tau_{\rm ei}$, ion to ion collision time $\tau_{\rm ii}$ and electron-ion thermal energy relaxation time $\tau_{\rm ei}^{\epsilon}$. Alfv́en velocity $v_{\rm A}$, which is a propagation velocity of magnetic perturbation, is $v_{\rm A}^2 = B^2/(2\mu_0\rho_{\rm m})$ ($\rho_{\rm m}$ is mass density)(see chs.5,10). Alfv́en transit time $\tau_{\rm H} = L/v_{\rm A}$ is a typical magnetohydrodynamic time scale, where L is a plasma size. In a medium with the specific resistivity η, electric field diffuses with the time scale of $\tau_{\rm R} = \mu_0L^2/\eta$ (see ch.5). This time scale is called resistive diffusion time.

Characteristic scales in length are Debye length $\lambda_{\rm D}$, electron Larmor radius $\rho_{\Omega{\rm e}}$, ion Larmor radius $\rho_{\Omega{\rm i}}$, electron-ion collision mean free path $\lambda_{\rm ei}$ and a plasma size L.

The relations between space and time scales are $\lambda_{\rm D}\Pi_{\rm e} = v_{\rm Te}, \rho_{\Omega e}\Omega_{\rm e} = v_{\rm Te},\ \rho_{\Omega{\rm i}}|\Omega_{\rm i}| = v_{\rm Ti}$, $\lambda_{\rm ei}/\tau_{\rm ei} \simeq 3^{1/2}v_{\rm Te},\ \ \lambda_{\rm ii}/\tau_{\rm ii} \simeq 3^{1/2}v_{\rm Ti},\ L/\tau_{\rm H} = v_{\rm A}$, where $v_{\rm Te}$, $v_{\rm Ti}$ are the thermal velocities $v_{\rm Te}^2 = \kappa T_{\rm e}/m_{\rm e},\ v_{\rm Ti}^2 = \kappa T_{\rm i}/m_{\rm i}$. The drift velocity of guiding center is $v_{\rm drift} \sim \kappa T/eBL = v_{\rm T}(\rho_\Omega/L)$. Parameters of a typical D-T fusion plasma with $n_{\rm e} = 10^{20}\,{\rm m}^{-3}$, $\kappa T_{\rm e} = \kappa T_{\rm i} = 10\,{\rm keV},\ B = 5\,{\rm T},\ L = 1\,{\rm m}$ are followings:

$2\pi/\Pi_{\rm e} = 11.1\,{\rm ps}\quad (\Pi_{\rm e}/2\pi = 89.8\,{\rm GHz})$
$2\pi/\Omega_{\rm e} = \ 7.1\,{\rm ps}\quad (\Omega_{\rm e}/2\pi = 140\,{\rm GHz})$
$2\pi/|\Omega_{\rm i}| = 26\,{\rm ns}\quad (|\Omega_{\rm i}|/2\pi = 38\,{\rm MHz})$
$\tau_{\rm ei} = 0.34\,{\rm ms}$
$\tau_{\rm ii} = 5.6\,{\rm ms}$
$\tau_{\rm ei}^{\epsilon} = 0.3\,{\rm s}$

$\lambda_{\rm D} = 74.5\,\mu{\rm m}$
$\rho_{\Omega{\rm e}} = 47.6\,\mu{\rm m}$
$\rho_{\Omega{\rm i}} = 2.88\,{\rm mm}$
$\lambda_{\rm ei} = 25\,{\rm km}$
$\lambda_{\rm ii} = 9.5\,{\rm km}$

$\tau_{\mathrm{H}} = 0.13\,\mu\mathrm{s}$
$\tau_{\mathrm{R}} = 1.2 \times 10^{3}\,\mathrm{s}$.
The ranges of scales in time and space extend to $\tau_{\mathrm{R}}\Pi_{\mathrm{e}} \sim 10^{14}$, $\lambda_{\mathrm{ei}}/\lambda_{\mathrm{D}} \sim 1.6 \times 10^{8}$ and the wide range of scales suggests the variety and complexity of plasma phenomena.

References

[1] D. V. Sivukhin: *Reviews of Plasma Physics* **4** p.93 (ed. by M. A. Leontovich) Consultant Bureau, New York 1966.
[2] L. Spitzer, Jr.: *Physics of Fully Ionized Gases*, Interscience, New York 1962.
[3] T. H. Stix: Plasma Phys. **14**, 367 (1972).

Ch.3 Magnetic Configuration and Particle Orbit

In this chapter, the motion of individual charged particles in a more general magnetic fields is studied in detail. There are a large number of charged particles in a plasma, thus movements do affect the magnetic field. But this effect is neglected here.

3.1 Maxwell Equations

Let us denote the *electric intensity,* the *magnetic induction*, the *electric displacement* and the *magnetic intensity* by $\boldsymbol{E}$, $\boldsymbol{B}$, $\boldsymbol{D}$, and $\boldsymbol{H}$, respectively. When the *charge density* and *current density* are denoted by ρ, and $\boldsymbol{j}$, respectively, Maxwell equations are

$$\nabla \times \boldsymbol{E} + \frac{\partial \boldsymbol{B}}{\partial t} = 0, \tag{3.1}$$

$$\nabla \times \boldsymbol{H} - \frac{\partial \boldsymbol{D}}{\partial t} = \boldsymbol{j}, \tag{3.2}$$

$$\nabla \cdot \boldsymbol{B} = 0, \tag{3.3}$$

$$\nabla \cdot \boldsymbol{D} = \rho. \tag{3.4}$$

ρ and $\boldsymbol{j}$ satisfy the relation

$$\nabla \cdot \boldsymbol{j} + \frac{\partial \rho}{\partial t} = 0. \tag{3.5}$$

Eq.(3.2),(3.4) and (3.5) are consistent with each other due to the Maxwell displacement current $\partial \boldsymbol{D}/\partial t$. From (3.3) the vector $\boldsymbol{B}$ can be expressed by the rotation of the vector $\boldsymbol{A}$:

$$\boldsymbol{B} = \nabla \times \boldsymbol{A}. \tag{3.6}$$

$\boldsymbol{A}$ is called *vector potential*. If (3.6) is substituted into (3.1), we obtain

$$\nabla \times \left(\boldsymbol{E} + \frac{\partial \boldsymbol{A}}{\partial t} \right) = 0. \tag{3.7}$$

The quantity in parenthesis can be expressed by a *scalar potential* ϕ and

$$\boldsymbol{E} = -\nabla \phi - \frac{\partial \boldsymbol{A}}{\partial t}. \tag{3.8}$$

Since any other set of ϕ' and $\boldsymbol{A'}$,

$$\boldsymbol{A'} = \boldsymbol{A} - \nabla \psi, \tag{3.9}$$

$$\phi' = \phi + \frac{\partial \psi}{\partial t} \tag{3.10}$$

can also satisfy (3.6),(3.8) with an arbitrary ψ, ϕ' and $\boldsymbol{A'}$ are not uniquely determined.

When the medium is uniform and isotropic, $\boldsymbol{B}$ and $\boldsymbol{D}$ are expressed by

$$\boldsymbol{D} = \epsilon \boldsymbol{E}, \qquad \boldsymbol{B} = \mu \boldsymbol{H}.$$

ϵ and μ are called *dielectric constant* and *permeability* respectively. The value of ϵ_0 and μ_0 in vacuum are

$$\epsilon_0 = \frac{10^7}{4\pi c^2}\ \mathrm{C}^2\cdot\mathrm{s}^2/\mathrm{kg}\cdot\mathrm{m}^3 = 8.854\times10^{-12}\,\mathrm{F/m}$$

$$\mu_0 = 4\pi\times10^{-7}\,\mathrm{kg}\cdot\mathrm{m/C}^2 = 1.257\times10^{-6}\,\mathrm{H/m}$$

$$\frac{1}{\epsilon_0\mu_0} = \mathrm{c}^2$$

where c is the light speed in vacuum (C is Coulomb). Plasmas in magnetic field are anisotropic and ϵ and μ are generally in tensor form. In vacuum, (3.2) and (3.3) are reduced to

$$\nabla\times\nabla\times\boldsymbol{A} + \frac{1}{\mathrm{c}^2}\nabla\frac{\partial\phi}{\partial t} + \frac{1}{\mathrm{c}^2}\frac{\partial^2\boldsymbol{A}}{\partial t^2} = \mu_0\boldsymbol{j}, \tag{3.11}$$

$$\nabla^2\phi + \nabla\frac{\partial\boldsymbol{A}}{\partial t} = -\frac{1}{\epsilon_0}\rho. \tag{3.12}$$

As ϕ and $\boldsymbol{A}$ have arbitrariness of ψ as shown in (3.9),(3.10), we impose the supplementary condition (Lorentz condition)

$$\nabla\cdot\boldsymbol{A} + \frac{1}{c}\frac{\partial\phi}{\partial t} = 0. \tag{3.13}$$

Then (3.11),(3.12) are reduced to the wave equations

$$\nabla^2\phi - \frac{1}{c^2}\frac{\partial^2\phi}{\partial t^2} = -\frac{1}{\varepsilon_0}\rho, \tag{3.14}$$

$$\nabla^2\boldsymbol{A} - \frac{1}{c^2}\frac{\partial^2\boldsymbol{A}}{\partial t^2} = -\mu_0\boldsymbol{j}. \tag{3.15}$$

In derivation of (3.15), a vector relation

$$\nabla\times(\nabla\times\boldsymbol{a}) - \nabla(\nabla\cdot\boldsymbol{a}) = -\nabla^2\boldsymbol{a}$$

is used, which is valid only in (x, y, z) coordinates. The propagation velocity of electromagnetic field is $1/(\mu_0\epsilon_0)^{1/2} = c$ in vacuum.

When the fields do not change in time, the field equations reduce to

$$\boldsymbol{E} = -\nabla\phi, \qquad \boldsymbol{B} = \nabla\times\boldsymbol{A},$$

$$\nabla^2\phi = -\frac{1}{\varepsilon_0}\rho, \qquad \nabla^2\boldsymbol{A} = -\mu\boldsymbol{j}, \qquad \nabla\cdot\boldsymbol{A} = 0, \qquad \nabla\cdot\boldsymbol{j} = 0.$$

The scalar and vector potentials ϕ and $\boldsymbol{A}$ at an observation point P (given by the position vector $\boldsymbol{r}$) are expressed in terms of the charge and current densities at the point Q (given by $\boldsymbol{r}'$) by (see fig.3.1)

$$\phi(\boldsymbol{r}) = \frac{1}{4\pi\epsilon_0}\int\frac{\rho(\boldsymbol{r}')}{R}\mathrm{d}\boldsymbol{r}', \tag{3.16}$$

$$\boldsymbol{A}(\boldsymbol{r}) = \frac{\mu_0}{4\pi}\int\frac{\boldsymbol{j}(\boldsymbol{r}')}{R}\mathrm{d}\boldsymbol{r}' \tag{3.17}$$

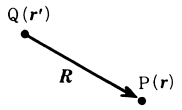

Fig.3.1 Observation point P and the location Q of charge or current.

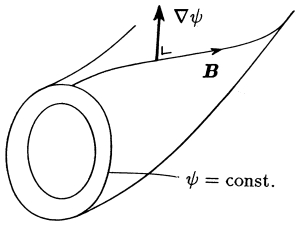

Fig.3.2 Magnetic surface $\psi = \text{const.}$, the normal $\nabla\psi$ and line of magnetic force.

where $\boldsymbol{R} \equiv \boldsymbol{r} - \boldsymbol{r}'$, $R = |\boldsymbol{R}|$ and $\mathrm{d}\boldsymbol{r}' \equiv \mathrm{d}x'\mathrm{d}'\mathrm{d}z'$. Accordingly $\boldsymbol{E}$ and $\boldsymbol{B}$ are expressed by

$$\boldsymbol{E} = \frac{1}{4\pi\epsilon_0}\int \frac{\boldsymbol{R}}{R^3}\rho \mathrm{d}\boldsymbol{r}', \tag{3.18}$$

$$\boldsymbol{B} = \frac{\mu_0}{4\pi}\int \frac{\boldsymbol{j}\times\boldsymbol{R}}{R^3}\mathrm{d}\boldsymbol{r}'. \tag{3.19}$$

When the current distribution is given by a current I flowing in closed loops C, magnetic intensity is described by *Biot-Savart equation*

$$\boldsymbol{H} = \frac{\boldsymbol{B}}{\mu_0} = \frac{I}{4\pi}\oint_{\mathrm{c}} \frac{\boldsymbol{s}\times\boldsymbol{n}}{R^2}\mathrm{d}s \tag{3.20}$$

where $\boldsymbol{s}$ and $\boldsymbol{n}$ are the unit vectors in the directions of $\mathrm{d}s$ and $\boldsymbol{R}$, respectively.

3.2 Magnetic Surface

A *magnetic line of force* satisfies the equations

$$\frac{\mathrm{d}x}{B_x} = \frac{\mathrm{d}y}{B_y} = \frac{\mathrm{d}z}{B_z} = \frac{\mathrm{d}l}{B} \tag{3.21}$$

where l is the length along a magnetic line of force $(\mathrm{d}l)^2 = (\mathrm{d}x)^2 + (\mathrm{d}y)^2 + (\mathrm{d}z)^2$. The *magnetic surface* $\psi(\boldsymbol{r}) = \text{const.}$ is such that all magnetic lines of force lie upon on that surface which satisfies the condition

$$(\nabla\psi(\boldsymbol{r}))\cdot\boldsymbol{B} = 0. \tag{3.22}$$

The vector $\nabla\psi(\boldsymbol{r})$ is normal to the magnetic surface and must be orthogonal to $\boldsymbol{B}$ (see fig.3.2).

In terms of cylindrical coordinates (r, θ, z) the magnetic field $\boldsymbol{B}$ is given by

$$B_r = \frac{1}{r}\frac{\partial A_z}{\partial\theta} - \frac{\partial A_\theta}{\partial z}, \quad B_\theta = \frac{\partial A_r}{\partial z} - \frac{\partial A_z}{\partial r}, \quad B_z = \frac{1}{r}\frac{\partial}{\partial r}(rA_\theta) - \frac{1}{r}\frac{\partial A_r}{\partial\theta}. \tag{3.23}$$

In the case of *axi-symmetric configuration* $(\partial/\partial\theta = 0)$,

$$\psi(r, z) = rA_\theta(r, z) \tag{3.24}$$

satisfies the condition (3.22) of magnetic surface; $B_r\partial(rA_\theta)/\partial r + B_\theta \cdot 0 + B_z\partial(rA_\theta)/\partial z = 0$.

The magnetic surface in the case of translational symmetry ($\partial/\partial z = 0$) is given by

$$\psi(r,\theta) = A_z(r,\theta) \tag{3.25}$$

and the magnetic surface in the case of helical symmetry, in which ψ is the function of r and $\theta - \alpha z$ only, is given by

$$\psi(r,\theta-\alpha z) = A_z(r,\theta-\alpha z) + \alpha r A_\theta(r,\theta-\alpha z) \tag{3.26}$$

where α is helical pitch parameter.

3.3 Equation of Motion of a Charged Particle

The equation of motion of a particle with the mass m and the charge q in an electromagnetic field $\boldsymbol{E}$, $\boldsymbol{B}$ is

$$m\frac{\mathrm{d}^2\boldsymbol{r}}{\mathrm{d}t^2} = \boldsymbol{F} = q\left(\boldsymbol{E} + \frac{\mathrm{d}\boldsymbol{r}}{\mathrm{d}t} \times \boldsymbol{B}\right). \tag{3.27}$$

Since Lorentz force of the second term in the right-hand side of (3.27) is orthogonal to the velocity $\boldsymbol{v}$, the scalar product of Lorentz force and $\boldsymbol{v}$ is zero. The kinetic energy is given by

$$\frac{mv^2}{2} - \frac{m{v_0}^2}{2} = q\int_{t=t_0}^{t} \boldsymbol{E}\cdot\boldsymbol{v}\mathrm{d}t.$$

When the electric field is zero, the kinetic energy of charged particle is conserved. The x component of (3.27) in the orthogonal coordinates (x,y,z) is written by $m\mathrm{d}^2x/\mathrm{d}t^2 = q(E_x + (\mathrm{d}y/\mathrm{d}t)B_z - (\mathrm{d}z/\mathrm{d}t)B_y)$, However the radial component of (3.27) in the cylindrical coordinates (r,θ,z) is $m\mathrm{d}^2r/\mathrm{d}t^2 \neq q(E_r + r(\mathrm{d}\theta/\mathrm{d}t)B_z - (\mathrm{d}z/\mathrm{d}t)B_\theta)$. This indicates that form of (3.27) is not conserved by the coordinates transformation. When generalized coordinates q_i $(i = 1,2,3)$ are used, it is necessary to utilize the Lagrangian formulation. Lagrangian of a charged particle in the field with scalar and vector potentials ϕ, $\boldsymbol{A}$ is given by

$$L(q_i,\dot{q}_i,t) = \frac{mv^2}{2} + q\boldsymbol{v}\cdot\boldsymbol{A} - q\phi. \tag{3.28}$$

Lagrangians in the orthogonal and cylindrical coordinates are given by

$$L(x,y,z,\dot{x},\dot{y},\dot{z},t) = \frac{m}{2}(\dot{x}^2+\dot{y}^2+\dot{z}^2) + q(\dot{x}A_x + \dot{y}A_y + \dot{z}A_z) - q\phi,$$

$$L(r,\theta,z,\dot{r},\dot{\theta},\dot{z},t) = \frac{m}{2}(\dot{r}^2 + (r\dot{\theta})^2 + \dot{z}^2) + q(\dot{r}A_r + r\dot{\theta}A_\theta + \dot{z}A_z) - q\phi$$

respectively. The equation of motion in Lagrangian formulation is

$$\frac{\mathrm{d}}{\mathrm{d}t}\left(\frac{\partial L}{\partial \dot{q}_i}\right) - \frac{\partial L}{\partial q_i} = 0. \tag{3.29}$$

The substitution of (3.28) into (3.29) in the case of the orthogonal coordinates yields

$$\frac{\mathrm{d}}{\mathrm{d}t}(mv_x + qA_x) - q\left(\boldsymbol{v}\cdot\frac{\partial\boldsymbol{A}}{\partial x} - \frac{\partial\phi}{\partial x}\right) = 0,$$

$$m\ddot{x} = q\left(-\frac{\partial A_x}{\partial t} - \left(\frac{\mathrm{d}x}{\mathrm{d}t}\frac{\partial}{\partial x} + \frac{\mathrm{d}y}{\mathrm{d}t}\frac{\partial}{\partial y} + \frac{\mathrm{d}z}{\mathrm{d}t}\frac{\partial}{\partial z}\right)A_x + \boldsymbol{v}\cdot\frac{\partial\boldsymbol{A}}{\partial x} - \frac{\partial\phi}{\partial x}\right)$$

$$= q(\boldsymbol{E} + \boldsymbol{v}\times\boldsymbol{B})_x,$$

and this equation is equivalent to (3.27). Lagrangian equation of motion with respect to the cylindrical coordinates is $m\ddot{r} = q(\boldsymbol{E}+\boldsymbol{v}\times\boldsymbol{B})_r + m(r\dot{\theta})^2/r$ and the term of centrifugal force appears.

Canonical transformation is more general than the coordinates transformation. Hamiltonian equation of motion is conserved with respect to canonical transformation. In this formulation we introduce momentum coordinates (p_i), in addition to the space coordinates (q_i), defined by

$$p_i \equiv \frac{\partial L}{\partial \dot{q}_i} \tag{3.30}$$

and treat p_i as independent variables. Then we can express $\dot{q}_i$ as a function of (q_j, p_j, t) from (3.30) as follows:

$$\dot{q}_i = \dot{q}_i(q_j, p_j, t). \tag{3.31}$$

The Hamiltonian $H(q_i, p_i, t)$ is given by

$$H(q_i, p_i, t) \equiv -L(q_i, \dot{q}_i(q_j, p_j, t), t) + \sum_i p_i \dot{q}_i(q_j, p_j, t). \tag{3.32}$$

The x component of momentum p_x in the orthogonal coordinates and θ component p_θ in the cylindrical coordinates are written as examples as follows:

$$p_x = m\dot{x} + qA_x, \qquad \dot{x} = (p_x - qA_x)/m,$$

$$p_\theta = mr^2\dot{\theta} + qrA_\theta, \qquad \dot{\theta} = (p_\theta - qrA_\theta)/(mr^2).$$

Hamiltonian in the orthogonal coordinates is

$$H = \frac{1}{2m}\Big((p_x - qA_x)^2 + (p_y - qA_y)^2 + (p_z - qA_z)^2\Big) + q\phi(x, y, z, t)),$$

and Hamiltonian in the cylindrical coordinates is

$$H = \frac{1}{2m}\left((p_r - qA_r)^2 + \frac{(p_\theta - qrA_\theta)^2}{r^2} + (p_z - qA_z)^2\right) + q\phi(r, \theta, z, t).$$

The variation of Lagrangian L is given by

$$\delta L = \sum_i \left(\frac{\partial L}{\partial q_i}\delta q_i + \frac{\partial L}{\partial \dot{q}_i}\delta\dot{q}_i\right) = \sum_i (\dot{p}_i \delta q_i + p_i \delta\dot{q}_i) = \delta\left(\sum_i p_i\dot{q}_i\right) + \sum_i (\dot{p}_i\delta q_i - \dot{q}_i\delta p_i)$$

and

$$\delta(-L + \sum_i p_i\dot{q}_i) = \sum_i (\dot{q}_i\delta p_i - \dot{p}_i\delta q_i), \qquad \delta H(q_i, p_i, t) = \sum_i (\dot{q}_i\delta p_i - \dot{p}_i\delta q_i).$$

Accordingly Hamiltonian equation of motion is reduced to

$$\frac{\mathrm{d}q_i}{\mathrm{d}t} = \frac{\partial H}{\partial p_i}, \qquad \frac{\mathrm{d}p_i}{\mathrm{d}t} = -\frac{\partial H}{\partial q_i}. \tag{3.33}$$

Equation (3.33) in the orthogonal coordinates is

$$\frac{\mathrm{d}x}{\mathrm{d}t} = \frac{p_x - qA_x}{m}, \qquad \frac{\mathrm{d}p_x}{\mathrm{d}t} = \frac{q}{m}\frac{\partial \boldsymbol{A}}{\partial x}\cdot(\boldsymbol{p} - q\boldsymbol{A}) - q\frac{\partial\phi}{\partial x},$$

$$m\frac{\mathrm{d}^2x}{\mathrm{d}t^2} = \frac{\mathrm{d}p_x}{\mathrm{d}t} - q\frac{\mathrm{d}A_x}{\mathrm{d}t} = q\left[\left(\boldsymbol{v}\cdot\frac{\partial\boldsymbol{A}}{\partial x}\right) - \frac{\partial\phi}{\partial x} - \left(\frac{\partial A_x}{\partial t} + (\boldsymbol{v}\cdot\nabla)A_x\right)\right]$$

$$= q(\boldsymbol{E} + \boldsymbol{v} \times \boldsymbol{B})_x$$

and it was shown that (3.33) is equivalent to (3.27).

When H does not depend on t explicitly (when ϕ , $\boldsymbol{A}$ do not depend on t),

$$\frac{\mathrm{d}H(q_i, p_i)}{\mathrm{d}t} = \sum_i \left(\frac{\partial H}{\partial q_i} \frac{\mathrm{d}q_i}{\mathrm{d}t} + \frac{\partial H}{\partial p_i} \frac{\mathrm{d}p_i}{\mathrm{d}t} \right) = 0,$$

$$H(q_i, p_i) = \text{const.} \tag{3.34}$$

is one integral of Hamiltonian equations. This integral expresses the conservation of energy.

When the electromagnetic field is axially symmetric, p_θ is constant due to $\partial H/\partial\theta = 0$ as is seen in (3.33) and

$$p_\theta = mr^2\dot{\theta} + qrA_\theta = \text{const.} \tag{3.35}$$

This indicates conservation of the angular momentum. In the case of translational symmetry $(\partial/\partial z = 0)$, we have

$$p_z = m\dot{z} + qA_z = \text{const.} \tag{3.36}$$

3.4 Particle Orbit in Axially Symmetric System

The coordinates (r^*, θ^*, z^*) on a magnetic surface of an axially symmetric field satisfy

$$\psi = r^* A_\theta(r^*, z^*) = c_\mathrm{M}.$$

On the other hand the coordinates (r, θ, z) of a particle orbit are given by the conservation of the angular momentum (3.35) as follows;

$$rA_\theta(r, z) + \frac{m}{q} r^2\dot{\theta} = \frac{p_\theta}{q} = \text{const.}.$$

If c_M is chosen to be $c_\mathrm{M} = p_\theta/q$, the relation between the magnetic surface and the particle orbit is reduced to

$$rA_\theta(r, z) - r^* A_\theta(r^*, z^*) = -\frac{m}{q} r^2\dot{\theta}.$$

The distance $\boldsymbol{\delta}$ (fig.3.3) between the magnetic surface and the orbit is given by

$$\boldsymbol{\delta} = (r - r^*)\boldsymbol{e}_r + (z - z^*)\boldsymbol{e}_z,$$

$$\boldsymbol{\delta} \cdot \nabla(rA_\theta) = -\frac{m}{q} r^2\dot{\theta}.$$

From the relations $rB_r = -\partial(rA_\theta)/\partial z$, $rB_z = \partial(rA_\theta)/\partial r$, we find

$$[-(z - z^*)B_r + (r - r^*)B_z] = -\frac{m}{q} r\dot{\theta}.$$

This expression in the left-hand side is the θ component of the vector product of $\boldsymbol{B}_\mathrm{p} = (B_r, 0, B_z)$ and $\boldsymbol{\delta} = (r - r^*, 0, z - z*)$. Then this is reduced to

$$(\boldsymbol{B}_\mathrm{p} \times \boldsymbol{\delta})_\theta = -\frac{m}{q} r\dot{\theta}.$$

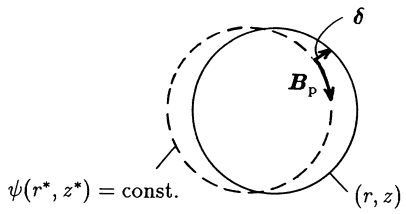

Fig.3.3 Magnetic surface (dotted line) and particle orbit (solid line).

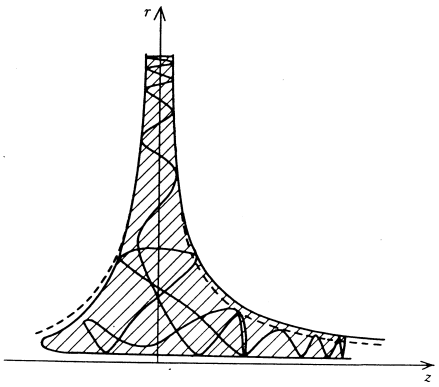

Fig.3.4 The dotted lines are lines of magnetic force and the solid lines are particle orbit in cusp field.

Denote the magnitude of poloidal component $\boldsymbol{B}_{\rm p}$ (component within (rz) plane) of $\boldsymbol{B}$ by $B_{\rm p}$. Then we find the relation $-B_{\rm p}\delta = -(m/q)v_\theta$ $(v_\theta = r\dot{\theta})$ and

$$\delta = \frac{mv_\theta}{qB_{\rm p}} = \rho_{\Omega{\rm p}}.$$

This value is equal to the Larmor radius corresponding to the magnetic field $B_{\rm p}$ and the tangential velocity v_θ. If $c_{\rm M}$ is chosen to be $c_{\rm M} = (p_\theta - m\langle rv_\theta\rangle)/q$ ($\langle rv_\theta\rangle$ is the average of rv_θ), we find

$$\delta = \frac{m}{qB_{\rm p}}\left(v_\theta - \frac{\langle rv_\theta\rangle}{r}\right). \tag{3.37}$$

Let us consider a cusp field as a simple example of axi-symmetric system. Cusp field is given by

$$A_r = 0, \qquad A_\theta = arz, \qquad A_z = 0, \tag{3.38}$$

$$B_r = -ar, \qquad B_\theta = 0, \qquad B_z = 2az. \tag{3.39}$$

From (3.34) of energy conservation and (3.35) of angular momentum conservation, we find

$$mr\dot{\theta} = \frac{p_\theta}{r} - qazr,$$

$$\frac{m}{2}(\dot{r}^2 + \dot{z}^2) + \frac{(p_\theta - qar^2z)^2}{2mr^2} = W\left(= \frac{m}{2}v_0^2\right).$$

These equations correspond to the motion of particle in a potential of $X = (p_\theta - qar^2z)^2/(2mr^2)$. When the electric field is zero, the kinetic energy of the particle is conserved, the region containing orbits of the particle with the energy of $mv_0^2/2$ is limited by (see fig.3.4)

$$X = \frac{1}{2m}\left(\frac{p_\theta}{r} - qarz\right)^2 < \frac{mv_0^2}{2}.$$

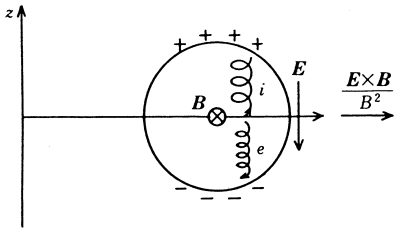

Fig.3.5 Toroidal drift.

3.5 Drift of Guiding Center in Toroidal Field

Let us consider the drift of guiding center of a charged particle in a simple toroidal field ($B_r = 0,\ B_\varphi = B_0R_0/R,\ B_z = 0$) in terms of cylindrical coordinates (R, φ, z). The φ component B_φ is called toroidal field and B_φ decreases in the form of $1/R$ outward. The magnetic lines of force are circles around z axis. The z axis is called the *major axis* of the torus. As was described in sec.2.4, the drift velocity of the guiding center is given by

$$\boldsymbol{v}_{\rm G} = v_\parallel \boldsymbol{e}_\varphi + \frac{m}{qB_\varphi R}\left(v_\parallel^2 + \frac{v_\perp^2}{2}\right)\boldsymbol{e}_z.$$

Particles in this simple torus run fast in the toroidal direction and drift slowly in the z direction with the velocity of

$$v_{\rm dr} = \frac{m}{qB_0R_0}\left(v_\parallel^2 + \frac{v_\perp^2}{2}\right) \sim \left(\frac{\rho_\Omega}{R_0}\right)v. \tag{3.40}$$

This drift is called *toroidal drift*. Ions and electrons drift in opposite direction along z axis. As a consequence of the resultant charge separation, an electric field $\boldsymbol{E}$ is induced and both ions and electrons drift outward by $\boldsymbol{E}\times\boldsymbol{B}/B^2$ drift. Consequently, a simple toroidal field cannot confine a plasma (fig.3.5), unless the separated charges are cancelled or short-circuited by an appropriate method. If lines of magnetic force connect the upper and lower regions as is shown in fig.3.6, the separated charges can be short-circuited, as the charged particles can move freely along the lines of force. If a current is induced in a toroidal plasma, the component of magnetic field around the *magnetic axis* (which is also called *minor axis*) is introduced as is shown in fig.3.6. This component $\boldsymbol{B}_{\rm p}$ is called *poloidal magnetic field*. The radius R of the magnetic axis is called *major radius* of torus and the radius a of the plasma cross section is called *minor radius*. Denote the radial coordinate in plasma cross section by r. When a line of magnetic force circles the major axis of torus and come back to cross the plane P, the cross point rotates around the minor axis O by an angle ι in P, there is following relation:

$$\frac{r\iota}{2\pi R} = \frac{B_{\rm p}}{B_\varphi}.$$

The angle ι is called *rotational transform angle* and is given by

$$\frac{\iota}{2\pi} = \frac{R}{r}\frac{B_{\rm p}}{B_\varphi}. \tag{3.41}$$

$A \equiv R/a$ is called *aspect ratio*.

3.5a Guiding Center of Circulating Particles

When a particle circulates torus with the velocity of $v_\parallel$, it takes $T = 2\pi R_0/v_\parallel$. Accordingly the particle rotates around the minor axis with angular velocity of

$$\omega = \frac{\iota}{T} = \frac{\iota v_\parallel}{2\pi R_0}$$

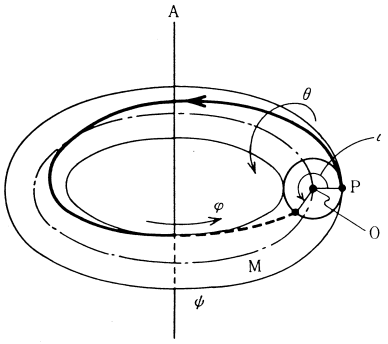

Fig.3.6 The major axis A, the minor axis M of toroidal field and rotational transform angle ι.

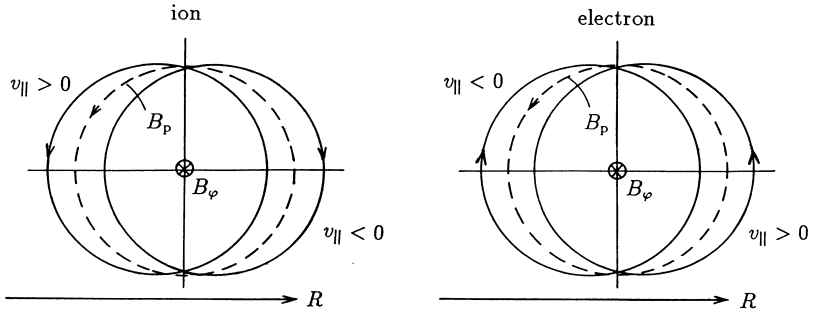

Fig.3.7 Orbits (solid lines) of guiding center of circulating ions and electrons and magnetic surfaces (dotted lines).

and drifts in z direction with the velocity of $v_{\rm dr}$. Introducing $x = R - R_0$ coordinate, the orbit of the guiding center of the particle is given by

$$\frac{{\rm d}x}{{\rm d}t} = -\omega z, \qquad \frac{{\rm d}z}{{\rm d}t} = \omega x + v_{\rm dr}.$$

The solution is

$$\left(x + \frac{v_{\rm dr}}{\omega}\right)^2 + z^2 = r^2.$$

If a rotational transform angle is introduced, the orbit becomes a closed circle and the center of orbit circle deviates from the center of magnetic surface by the amount of

$$\Delta = -\frac{v_{\rm dr}}{\omega} = -\frac{mv_\parallel}{qB_0}\frac{2\pi}{\iota}\left(1 + \frac{v_\perp^2}{2v_\parallel^2}\right), \tag{3.42}$$

$$|\Delta| \sim \rho_\Omega \left(\frac{2\pi}{\iota}\right)$$

where ρ_Ω is Larmor radius. As is seen in fig.3.7, the sign of the deviation is $\Delta < 0$ for the case of $v_\parallel > 0,\ q > 0$ (ion) since $v_{\rm dr} > 0,\ \omega > 0$ and the sign becomes $\Delta > 0$ for the case of $v_\parallel < 0$ (opposit to $v_\parallel > 0$) $q > 0$ (ion).

3.5b Guiding Center of Banana Particles

In the case of $|B_\varphi| \gg |B_{\rm p}|$, the magnitude of toroidal field is nearly equal to B_φ and

$$B = \frac{B_0 R_0}{R} = \frac{B_0}{1 + (r/R)\cos\theta} \simeq B_0\left(1 - \frac{r}{R_0}\cos\theta\right).$$

Denote the length along magnetic line of force by l, and denote the projection of a location on the magnetic line of force to (R, z) plane by the coordinates (r, θ) as is shown in fig.3.8. Since the following relations

$$\frac{r\theta}{l} = \frac{B_\mathrm{p}}{B_0}, \qquad \theta = \frac{l}{r}\frac{B_\mathrm{p}}{B_0} = \kappa l$$

holds, we find

$$B = B_0\left(1 - \frac{r}{R_0}\cos(\kappa l)\right).$$

If $v_\parallel$ (parallel component to magnetic field) is much smaller than $v_\perp$ component and satisfies the condition;

$$\frac{v_\perp^2}{v^2} > 1 - \frac{r}{R}, \qquad \frac{v_\parallel^2}{v^2} < \frac{r}{R} \tag{3.43}$$

the particle is trapped outside in the weak region of magnetic field due to the mirror effect as is described in sec.2.5 (The mirror ratio is $(1/R)/(1/(R+r))$). This particle is called *trapped particle*. Circulating particle without trapped is called untrapped particles. Since $v_\parallel^2 \ll v_\perp^2$ for the trapped particle, the r component of the toroidal drift v_dr of trapped particle is given by

$$\dot{r} = v_\mathrm{dr}\sin\theta = \frac{m}{qB_0}\frac{v_\perp^2}{2R}\sin\theta.$$

The parallel motion of the guiding center is given by (see sec.2.4)

$$\frac{\mathrm{d}v_\parallel}{\mathrm{d}t} = -\frac{\mu_\mathrm{m}}{m}\frac{\partial B}{\partial l},$$
$$\dot{v}_\parallel = -\frac{\mu_\mathrm{m}}{m}\frac{r}{R}\kappa B_0\sin\kappa l = -\frac{v_\perp^2}{2R}\frac{B_\mathrm{p}}{B_0}\sin\theta.$$

The solution is

$$\frac{\mathrm{d}}{\mathrm{d}t}\left(r + \frac{m}{qB_\mathrm{p}}v_\parallel\right) = 0,$$
$$r - r_0 = -\frac{m}{qB_\mathrm{p}}v_\parallel. \tag{3.44}$$

Here $r = r_0$ indicates the radial coordinate of turning point by mirror effect. Since the orbit is of banana shape, the trapped particle is also called *banana particle* (see fig.3.9). The width of banana Δ_b is given by

$$\Delta_\mathrm{b} = \frac{m}{qB_\mathrm{p}}v_\parallel \sim \frac{mv}{qB_0}\frac{v_\parallel}{v}\frac{B_0}{B_\mathrm{p}} \sim \frac{B_0}{B_\mathrm{p}}\left(\frac{r}{R}\right)^{1/2}\rho_\Omega \sim \left(\frac{R}{r}\right)^{1/2}\left(\frac{2\pi}{\iota}\right)\rho_\Omega. \tag{3.45}$$

3.6 Orbit of Guiding Center and Magnetic Surface

The velocity of guiding center was derived in sec.2.4 as follows:

$$\boldsymbol{v}_\mathrm{G} = v_\parallel\boldsymbol{b} + \frac{1}{B}(\boldsymbol{E}\times\boldsymbol{b}) + \frac{mv_\perp^2/2}{qB^2}(\boldsymbol{b}\times\nabla B) + \frac{mv_\parallel^2}{qB^2}(\boldsymbol{b}\times(\boldsymbol{b}\cdot\nabla)\boldsymbol{B}) \tag{3.46}$$

and

$$\mu_\mathrm{m} = mv_\perp^2/(2B) = \text{const.}$$

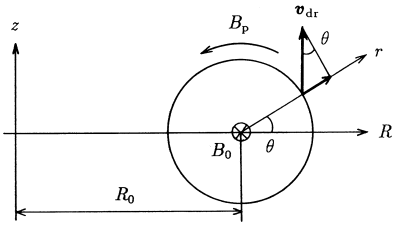

Fig.3.8 (r, θ) coordinates

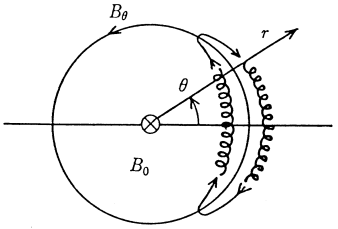

Fig.3.9 Banana orbit of ion

When the electric field $\boldsymbol{E}$ is static and is expressed by $\boldsymbol{E} = -\nabla\phi$, the conservation of energy

$$\frac{m}{2}(v_\parallel^2 + v_\perp^2) + q\phi = W$$

holds. Then $v_\parallel$ is expressed by

$$v_\parallel = \pm\left(\frac{2}{m}\right)^{1/2}(W - q\phi - \mu_{\rm m}B)^{1/2}.$$

Noting that $v_\parallel$ is a function of the coodinates, we can write

$$\nabla \times (mv_\parallel \boldsymbol{b}) = mv_\parallel \nabla \times \boldsymbol{b} + \nabla(mv_\parallel) \times \boldsymbol{b}$$

$$= mv_\parallel \nabla \times \boldsymbol{b} + \frac{1}{v_\parallel}(-q\nabla\phi - \mu_{\rm m}\nabla B) \times \boldsymbol{b}$$

and

$$\frac{v_\parallel}{qB}\nabla \times (mv_\parallel \boldsymbol{b}) = \frac{mv_\parallel^2}{qB}\nabla \times \boldsymbol{b} + \frac{1}{B}(\boldsymbol{E} \times \boldsymbol{b}) + \frac{mv_\perp^2/2}{qB^2}(\boldsymbol{b} \times \nabla B).$$

Then (3.46) for $\boldsymbol{v}_{\rm G}$ is reduced to

$$\boldsymbol{v}_{\rm G} = v_\parallel \boldsymbol{b} + \left(\frac{v_\parallel}{qB}\nabla \times (mv_\parallel \boldsymbol{b}) - \frac{mv_\parallel^2}{qB}\nabla \times \boldsymbol{b}\right) + \frac{mv_\parallel^2}{qB^2}(\boldsymbol{b} \times (\boldsymbol{b} \cdot \nabla)\boldsymbol{B})$$

$$= v_\parallel \boldsymbol{b} + \frac{v_\parallel}{qB}\nabla \times (mv_\parallel \boldsymbol{b}) - \frac{mv_\parallel^2}{qB}(\nabla \times \boldsymbol{b} - \boldsymbol{b} \times (\boldsymbol{b} \cdot \nabla)\boldsymbol{b}).$$

As the relation $\nabla(\boldsymbol{b}\cdot\boldsymbol{b}) = 2(\boldsymbol{b}\cdot\nabla)\boldsymbol{b} + 2\boldsymbol{b}\times(\nabla\times\boldsymbol{b}) = 0$ ($(\boldsymbol{b}\cdot\boldsymbol{b}) = 1$) holds (see appendix Mathematical Formula), the third term in right-hand side of the equation for $\boldsymbol{v}_{\rm G}$ becomes $(\nabla\times\boldsymbol{b} - \boldsymbol{b}\times(\boldsymbol{b}\cdot\nabla)\boldsymbol{b}) = (\nabla\times\boldsymbol{b}) - (\nabla\times\boldsymbol{b})_\perp = (\nabla\times\boldsymbol{b})_\parallel = (\boldsymbol{b}\cdot(\nabla\times\boldsymbol{b}))\boldsymbol{b}$. Accordingly, within accuracy of the 1st order of the Larmor radius/characteristic length of $\boldsymbol{b}$ (radius of curvature), the velocity of the guiding center is reduced to

$$\boldsymbol{v}_{\rm G} = \left(v_\parallel - \frac{mv_\parallel^2}{qB}(\boldsymbol{b} \cdot \nabla \times \boldsymbol{b})\right)\boldsymbol{b} + \frac{mv_\parallel}{qB}\nabla \times (v_\parallel \boldsymbol{b})$$

$$= \frac{1}{1 + (mv_\parallel/qB)\boldsymbol{b}\cdot\nabla\times\boldsymbol{b}} \left(v_\parallel \boldsymbol{b} + \frac{mv_\parallel}{qB}\nabla\times(v_\parallel\boldsymbol{b}) \right). \tag{3.47}$$

The first factor in the right-hand side of (3.47) is necessary in order to conserve the phase space volume in the Lagrange-Hamiltonian formulation of the guiding center motion (ref.[1]). Since $\nabla\times\boldsymbol{B} = B\nabla\times\boldsymbol{b} + \nabla B\times\boldsymbol{b} = \mu_0\boldsymbol{j}$, we have $\boldsymbol{b}\cdot\nabla\times\boldsymbol{b} = \mu_0 j_\parallel/B$. The second term of the denominator is usually very small compared with 1 (zero in the case of $j_\parallel = 0$). If the second term of the denominator can be neglected, (3.47) for $\boldsymbol{v}_\mathrm{G}$ is reduced to (ref.[2]).

$$\frac{\mathrm{d}\boldsymbol{r}_\mathrm{G}}{\mathrm{d}t} = \frac{v_\parallel}{B}\nabla\times\left(\boldsymbol{A} + \frac{mv_\parallel}{qB}\boldsymbol{B}\right). \tag{3.48}$$

The orbit of guiding center is equal to the line of magnetic field $\boldsymbol{B}^* = \nabla\times\boldsymbol{A}^*$ with the vector potential

$$\boldsymbol{A}^* \equiv \boldsymbol{A} + \frac{mv_\parallel}{qB}\boldsymbol{B}.$$

By reason analogous to that in sec.3.2, the *orbit surface of drift motion* of guiding center is given by

$$rA^*_\theta(r,z) = \text{const.} \tag{3.49}$$

in the case of axi-symmetric configuration.

3.7 Effect of Longitudinal Electric Field on Banana Orbit

In the tokamak configuration, a toroidal electric field is applied in order to induce the plasma current. The guiding center of a particle drifts by $\boldsymbol{E}\times\boldsymbol{B}/B^2$, but the banana center moves in different way. The toroidal electric field can be described by

$$E_\varphi = -\frac{\partial A_\varphi}{\partial t}$$

in (R,φ,z) coordinates. Since angular momentum is conserved, we can write

$$R(mR\dot{\varphi} + qA_\varphi) = \text{const.}$$

Taking the average of foregoing equation over a Larmor period, and using the relation

$$\langle R\dot{\varphi}\rangle = \frac{B_\varphi}{B}v_\parallel$$

we find

$$R\left(mv_\parallel\frac{B_\varphi}{B} + qA_\varphi\right) = \text{const.} \tag{3.50}$$

For particles in banana motion ($v_\parallel \ll v_\perp$), $v_\parallel$ becomes 0 at the turning points of the banana orbit. The displacement of a turning point (R,Z) per period Δt is obtained from

$$0 = \Delta(RA_\varphi(R,Z)) = \Delta r\frac{\partial}{\partial r}RA_\varphi + \Delta t\frac{\partial}{\partial t}RA_\varphi$$

where r is the radial coordinate of the magnetic surface. The differentiations of $RA_\varphi = \text{const.}$ with respect to φ and θ are zero, since $RA_\varphi = \text{const.}$ is the magnetic surface. By means of the relation

$$\frac{1}{R}\frac{\partial}{\partial r}(RA_\varphi) = \frac{1}{R}\left(\frac{\partial R}{\partial r}\frac{\partial(RA_\varphi)}{\partial R} + \frac{\partial Z}{\partial r}\frac{\partial(RA_\varphi)}{\partial Z}\right)$$

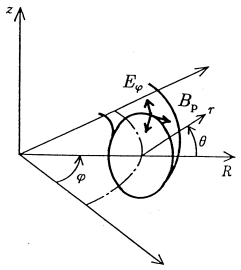

Fig.3.10 Coordinate system for explanation of Ware's pinch.

$$= \cos\theta B_Z - \sin\theta B_R = B_\mathrm{p},$$

we obtaine the drift velocity

$$\frac{\Delta r}{\Delta t} = \frac{E_\theta}{B_\mathrm{p}}. \tag{3.51}$$

When the sign of B_p produced by the current induced by the electric field E_φ is taken account (see fig.3.10), the sign of $\Delta r/\Delta t$ is negative and the banana center moves inward. Since $|B_\mathrm{p}| \ll |B_\varphi| \simeq B$, the drift velocity of banana center is $(B/B_\mathrm{p})^2$ times as fast as the the drift velocity $E_\varphi B_\mathrm{p}/B^2$ of guiding center of particle. This phenomena is called *Ware's pinch.*

3.8 Pressesion of Trapped Particle

The center of banana orbit of the trapped particle in the region of weak magnetic field outside of tokamak drifts in the toroidal direction. For the general orbit analysis on the precession of a trapped particle, we use general coordinates (u^1, u^2, u^3) shown in fig.3.11, that is

$$u^1 = u^1(x, y, z), \quad u^2 = u^2(x, y, z), \quad u^3 = u^3(x, y, z).$$

A vector $\boldsymbol{F}$ is expressed by $\boldsymbol{F} = \sum f^i \boldsymbol{a}_i$ where $f^i \equiv \boldsymbol{F} \cdot \boldsymbol{a}^i$ is contravariant and $\boldsymbol{a}^i \equiv \nabla u^i$. $\boldsymbol{F}$ is

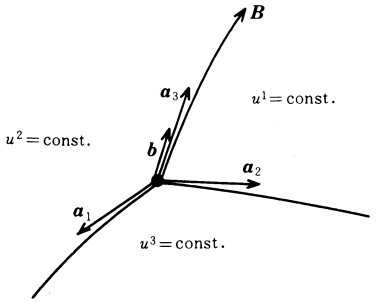

Fig.3.11 General coordinate (u^1, u^2, u^3) for the analysis of presession of trapped particle.

also exressed by $\boldsymbol{F} = \sum f_i \boldsymbol{a}^i$ where $f_i = \boldsymbol{F} \cdot \boldsymbol{a}_i$ is covariant and $\boldsymbol{a}_i \equiv \partial \boldsymbol{r}/\partial u^i$ (refer to fig.3.11 and Table D.1 in appendix D). General coordinates (u^1, u^2, u^3) are chosen so that the cross line of the surface $u^1(x, y, z) = \text{const}$ and $u^2(x, y, z) = \text{const}$ is the line of magnetic force. The unit vector along the line of magnetic force $\boldsymbol{b}$ is expressed by $\boldsymbol{b} = b^3 \boldsymbol{a}_3 = (\boldsymbol{a}_3 \cdot \boldsymbol{a}_3)^{-1/2} \boldsymbol{a}_3$. The center of the orbit of trapped particle with the total energy W, magnetic moment μ_m is given by the longitudinal adiabatic invariant

$$J_\parallel(u^1, u^2, \mu_\mathrm{m}, W) = m \oint v_\parallel \mathrm{d}l = \text{const.} \tag{3.52}$$

where $v_\parallel$ is

$$v_\parallel = \pm((2/m)(W - \mu_\mathrm{m}B - q\phi))^{1/2}. \tag{3.53}$$

The orbit of trapped particle is given by

$$\boldsymbol{v} = \left(v_\parallel - \frac{mv_\parallel^2}{qB}(\boldsymbol{b}\cdot\nabla\times\boldsymbol{b})\right)\boldsymbol{b} + \frac{v_\parallel}{qB}\nabla\times(mv_\parallel\boldsymbol{b}). \tag{3.54}$$

Time variation of (u^1, u^2) becomes from (3.54) as follows (refer to Table D.1),

$$\frac{\mathrm{d}u^1}{\mathrm{d}t} = \frac{v_\parallel}{qBg^{1/2}}\left(\frac{\partial}{\partial u^2}(mv_\parallel b_3) - \frac{\partial}{\partial u^3}(mv_\parallel b_2)\right),$$

$$\frac{\mathrm{d}u^2}{\mathrm{d}t} = \frac{v_\parallel}{qBg^{1/2}}\left(\frac{\partial}{\partial u^3}(mv_\parallel b_1) - \frac{\partial}{\partial u^1}(mv_\parallel b_3)\right).$$

The variation of u^1 and u^2 during one period is

$$\begin{aligned}\Delta u^1 &= \oint \frac{1}{qB}\left(\frac{g_{33}}{g}\right)^{1/2}\left(\frac{\partial}{\partial u^2}(mv_\parallel b_3) - \frac{\partial}{\partial u^3}(mv_\parallel b_2)\right)\mathrm{d}u_3 \\ &= \left(\frac{1}{qB}\left(\frac{g_{33}}{g}\right)^{1/2}\right)_\mathrm{m}\frac{\partial J_\parallel}{\partial u^2}, \\ \Delta u^2 &= -\left(\frac{1}{qB}\left(\frac{g_{33}}{g}\right)^{1/2}\right)_\mathrm{m}\frac{\partial J_\parallel}{\partial u^1},\end{aligned}$$

where $J_\parallel = \oint(mv_\parallel b_3)\mathrm{d}u^3 = \oint(mv_\parallel)\mathrm{d}l$ $(\mathrm{d}l = (\boldsymbol{v}\cdot\boldsymbol{b})\mathrm{d}t = \mathrm{d}u^3(\boldsymbol{a}_3\cdot\boldsymbol{b}) = \mathrm{d}u^3 g_{33}^{1/2}$. The definition of g, g_{ij} are given in Table D.1). The notion of $(f)_\mathrm{m}$ means the value of f at a point within the orbit (mean value theorem). The period of one cycle τ is

$$\tau = \oint\frac{\mathrm{d}l}{v_\parallel} = m\frac{\partial}{\partial W}\oint v_\parallel\mathrm{d}l = \frac{\partial J_\parallel}{\partial W}. \tag{3.55}$$

Consequently, the drift velocity of precession of the trapeed particle is given by

$$\frac{\mathrm{d}u^1}{\mathrm{d}t} = \frac{\Delta u^1}{\tau} = \left(\frac{1}{qB}\left(\frac{g_{33}}{g}\right)^{1/2}\right)_\mathrm{m}\frac{\partial J_\parallel/\partial u^2}{\partial J_\parallel/\partial W}, \tag{3.56}$$

$$\frac{\mathrm{d}u^2}{\mathrm{d}t} = \frac{\Delta u^2}{\tau} = -\left(\frac{1}{qB}\left(\frac{g_{33}}{g}\right)^{1/2}\right)_\mathrm{m}\frac{\partial J_\parallel/\partial u^1}{\partial J_\parallel/\partial W}, \tag{3.57}$$

provided the period τ is much smaller than the time scale of the precession.

Let us take the example of the precession of banana in tokamak. The magnitude of magnetic field of tokamak is

$$B = B_0(1 - \epsilon\cos\theta),$$

where ϵ is inverse aspect ratio $\epsilon = r/R$. We choose the following general coordinates

$$u^1 = r, \quad u^2 = \theta - \frac{1}{q_\mathrm{s}}\varphi, \quad u^3 = R\varphi.$$

Longitudinal adiabatic invariant $J_\parallel$ is

$$J_\parallel = m\oint((2/m)(W - q\phi - \mu_\mathrm{m}B(1 - \epsilon\cos\theta))^{1/2}\,\mathrm{d}l$$

Table 3.1 $K(\kappa)$ and $E(\kappa)$

κ	0.0	0.2	0.4	0.5	0.6	0.7	0.8	0.9	1.0
$K(\kappa)$	$\pi/2$	1.660	1.778	1.854	1.950	2.075	2.257	2.578	∞
$E(\kappa)$	$\pi/2$	1.489	1.339	1.351	1.298	1.242	1.178	1.105	1

$$\approx (2m\mu_{\rm m}B\epsilon)^{1/2}(Rq_{\rm s})\oint(2\kappa^2+\cos\theta-1)^{1/2}{\rm d}\theta$$

$$= 4\cdot 4(m\mu_{\rm m}B\epsilon)^{1/2}(Rq_{\rm s})\int_0^{\theta_0/2}(\kappa^2-\sin^2(\theta/2))^{1/2}{\rm d}(\theta/2)$$

$$= 16(m\mu_{\rm m}B\epsilon)^{1/2}(Rq_{\rm s})(E(\kappa)-(1-\kappa^2)K(\kappa)), \tag{3.58}$$

where

$$\kappa^2\equiv\frac{W-\mu_{\rm m}B(1-\epsilon)-q\phi}{2\epsilon\mu_{\rm m}B}<1 \qquad \sin^2(\theta_0/2)=\kappa^2.$$

and $r{\rm d}\theta/{\rm d}l=B_\theta/B=r/Rq_{\rm s}$, ${\rm d}l=Rq_{\rm s}{\rm d}\theta$. $K(\kappa)$ and $E(\kappa)$ are complete elliptic integral of the first kind and the second kind respectively.

$$K(\kappa)=\int_0^{\pi/2}\frac{{\rm d}\phi}{(1-\kappa^2\sin^2\phi)^{1/2}}=\int_0^1\frac{{\rm d}x}{((1-x^2)(1-\kappa^2x^2))^{-1/2}},$$

$$E(\kappa)=\int_0^{\pi/2}(1-\kappa^2\sin^2\phi)^{1/2}{\rm d}\phi=\int_0^1\left(\frac{1-\kappa^2x^2}{1-x^2}\right)^{1/2}{\rm d}x,$$

$$\frac{\partial K}{\partial\kappa}=\frac{1}{\kappa}\left(\frac{E}{1-\kappa^2}-K\right),\quad \frac{\partial E}{\partial\kappa}=\frac{1}{\kappa}(E-K).$$

The values of conplete elliptic integrals are given in Table 3.1.

Since

$$\frac{\partial\kappa^2}{\partial r}=-\frac{1}{r}(\kappa^2-1/2)-\frac{q\partial\phi/\partial r}{2\epsilon\mu_m B},$$

we have

$$\frac{\partial J_\parallel}{\partial r}=16(m\mu_m B\epsilon)^{1/2}Rq_{\rm s}\left((E(\kappa)-(1-\kappa^2)K(\kappa))\frac{1}{2r}+\kappa K(\kappa)\frac{1}{2\kappa}\frac{\partial\kappa^2}{\partial r}\right)$$

$$=16(m\mu_m B\epsilon)^{1/2}Rq_{\rm s}\left((E-K/2)\frac{1}{2r}+\frac{K}{2}\left(-\frac{q\partial\phi/\partial r}{2\epsilon\mu_m B}\right)\right),$$

$$\frac{\partial J_\parallel}{\partial u^2}=0,$$

$$\frac{\partial J_\parallel}{\partial W}=16(m\mu_m B\epsilon)^{1/2}Rq_{\rm s}\frac{K}{2}\frac{1}{2\mu_m B\epsilon}.$$

The motion of precession is given by

$$\frac{{\rm d}u^2}{{\rm d}t}=\frac{{\rm d}(\theta-\varphi/q_{\rm s})}{{\rm d}t}=-\frac{2\mu_m B\epsilon}{qBr^2}(E/K-1/2)-\Big(-\frac{q\partial\phi/\partial r}{rqB}\Big)$$

$$=-\frac{2\mu_m B}{qBrR}(E/K-1/2)-\frac{E_r}{rB},$$

$$\frac{{\rm d}u^1}{{\rm d}t}=\frac{{\rm d}r}{{\rm d}t}=0.$$

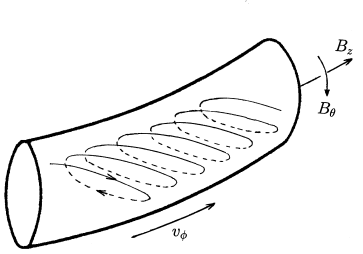

Fig.3.12 Precession of ion banana of tokamak.

The banana of tokamak is trapped at $\theta = 0$ and

$$R\frac{\mathrm{d}\varphi}{\mathrm{d}t} = \frac{mv_\perp^2}{qBr}q_\mathrm{s}\left(\frac{E}{K} - \frac{1}{2}\right) + \frac{E_r}{B}\frac{q_s R}{r} \tag{3.59}.$$

(Refer to fig.3.12)

3.9 Polarization Drift

Let us consider the case that $\boldsymbol{E} = E_0 \exp(-i\omega t)\hat{\boldsymbol{x}}$ in the x direction is time dependent but $\boldsymbol{B}$ is stationary and constant in the z direction. Then the equation of motion is

$$\ddot{v}_x = \frac{q}{m}\dot{E}_x + \frac{q}{m}\dot{v}_y B = i\omega\Omega\frac{E_x}{B} - \Omega^2 v_x$$

$$\ddot{v}_y = -\frac{q}{m}\dot{v}_x B = -\Omega^2\frac{E_x}{B} - \Omega^2 v_y.$$

When we define

$$v_\mathrm{E} \equiv -\frac{E_x}{B}, \quad v_\mathrm{p} = i\frac{\omega}{\Omega}\frac{E_x}{B}$$

then the equation of motion is reduced to

$$\ddot{v}_x = -\Omega^2(v_x - v_\mathrm{p}), \quad \ddot{v}_y = -\Omega^2(v_y - v_\mathrm{E}).$$

When $\Omega^2 \gg \omega^2$, the solution is

$$v_x = -iv_\perp \exp(-i\Omega t) + v_\mathrm{p}, \quad v_y = v_\perp \exp(-i\Omega t) + v_\mathrm{E}.$$

This solution shows that the guiding center motion consists of the usual $\boldsymbol{E}\times\boldsymbol{B}$ drift (but slowly oscillating) and the new drift along $\boldsymbol{E}$. This new term is called *the polarization drift* and is expressed by

$$\boldsymbol{v}_\mathrm{p} = -\frac{1}{\Omega B}\frac{\partial \boldsymbol{E}}{\partial t}. \tag{3.60}$$

Since $\boldsymbol{v}_\mathrm{p}$ is in opposite directions for ions and electrons, there is a *polarization current*

$$\boldsymbol{j}_\mathrm{p} = en_\mathrm{e}(\boldsymbol{v}_\mathrm{pi} - \boldsymbol{v}_\mathrm{pe}) = \frac{n_\mathrm{e}(m_\mathrm{i} + m_\mathrm{e})}{B^2}\frac{\partial \boldsymbol{E}}{\partial t} = \frac{\rho_\mathrm{m}}{B^2}\frac{\partial \boldsymbol{E}}{\partial t} \tag{3.61}$$

where ρ_m is the mass density.

3.10 Pondromotive Force

The equation of motion of an electron in the electromagnetic wave $\boldsymbol{E}(\boldsymbol{r},t)=\widehat{\boldsymbol{E}}(\boldsymbol{r})\cos(\boldsymbol{k}\cdot\boldsymbol{r}-\omega t)$ is

$$m\frac{\mathrm{d}\boldsymbol{v}}{\mathrm{d}t}=-e(\boldsymbol{E}+\boldsymbol{v}\times\boldsymbol{B}).$$

Here we assume that $\widehat{\boldsymbol{E}}(\boldsymbol{r})$ varies slowly in the scale of the wavelength. Using the notation $\alpha\equiv\boldsymbol{k}\cdot\boldsymbol{r}-\omega t$, the magnetic field $\boldsymbol{B}$ is given as follows:

$$\frac{\partial\boldsymbol{B}}{\partial t}=-\nabla\times\boldsymbol{E}=\nabla\times\widehat{\boldsymbol{E}}\cos\alpha+\boldsymbol{k}\times\widehat{\boldsymbol{E}}\sin\alpha,$$

$$\boldsymbol{B}=\frac{\nabla\times\widehat{\boldsymbol{E}}}{\omega}\sin\alpha+\frac{\boldsymbol{k}\times\widehat{\boldsymbol{E}}}{\omega}\cos\alpha.$$

In the first order equations, we neglect the second order term $\boldsymbol{v}\times\boldsymbol{B}$ and we have

$$m\frac{\mathrm{d}\boldsymbol{v}_1}{\mathrm{d}t}=-e\boldsymbol{E}(\boldsymbol{r}_0,t)=-e\widehat{\boldsymbol{E}}(\boldsymbol{r}_0)\cos(\boldsymbol{k}\cdot\boldsymbol{r}_0-\omega t),$$

$$\boldsymbol{v}_1=\frac{e\widehat{\boldsymbol{E}}(\boldsymbol{r}_0)}{m\omega}\sin(\boldsymbol{k}\cdot\boldsymbol{r}_0-\omega t),$$

$$\boldsymbol{r}_1=\frac{e\widehat{\boldsymbol{E}}(\boldsymbol{r}_0)}{m\omega^2}\cos(\boldsymbol{k}\cdot\boldsymbol{r}_0-\omega t),$$

where $\boldsymbol{r}_0$ is the initial position. We expand $\boldsymbol{E}(\boldsymbol{r},t)$ about $\boldsymbol{r}_0$:

$$\boldsymbol{E}(\boldsymbol{r},t)=\boldsymbol{E}(\boldsymbol{r}_0,t)+(\boldsymbol{r}_1\cdot\nabla)\boldsymbol{E}(\boldsymbol{r},t)|_{\boldsymbol{r}_0}$$

$$=\boldsymbol{E}(\boldsymbol{r}_0,t)+(\boldsymbol{r}_1\cdot\nabla)\widehat{\boldsymbol{E}}\cos\alpha_0-\widehat{\boldsymbol{E}}\,(\boldsymbol{r}_1\cdot\boldsymbol{k})\sin\alpha_0$$

where $\alpha_0\equiv\boldsymbol{k}\cdot\boldsymbol{r}_0-\omega t$.
In the second order, we must add the term $\boldsymbol{v}_1\times\boldsymbol{B}$:

$$m\frac{\mathrm{d}\boldsymbol{v}_2}{\mathrm{d}t}=-e((\boldsymbol{r}_1\cdot\nabla)\widehat{\boldsymbol{E}}\cos\alpha_0-\widehat{\boldsymbol{E}}\,(\boldsymbol{r}_1\cdot\boldsymbol{k})\sin\alpha_0)$$

$$-e\boldsymbol{v}_1\times\left(\nabla\times\widehat{\boldsymbol{E}}\sin\alpha_0+\frac{\boldsymbol{k}\times\widehat{\boldsymbol{E}}}{\omega}\cos\alpha_0\right)$$

$$=-\frac{e^2}{m\omega^2}\left((\widehat{\boldsymbol{E}}\cdot\nabla)\widehat{\boldsymbol{E}}\cos^2\alpha_0+\widehat{\boldsymbol{E}}\times\nabla\times\widehat{\boldsymbol{E}}\sin^2\alpha_0\right)$$

$$-\frac{e^2}{m\omega^2}\left(-(\widehat{\boldsymbol{E}}\cdot\boldsymbol{k})\widehat{\boldsymbol{E}}+\widehat{\boldsymbol{E}}\times\boldsymbol{k}\times\widehat{\boldsymbol{E}}\right)\sin\alpha_0\cos\alpha_0$$

$$=-\frac{e^2}{2m\omega^2}\Big(\nabla\frac{\widehat{\boldsymbol{E}}^2}{2}(1-\cos2(\boldsymbol{k}\cdot\boldsymbol{r}_0-\omega t))+2(\widehat{\boldsymbol{E}}\cdot\nabla)\widehat{\boldsymbol{E}}\cos2(\boldsymbol{k}\cdot\boldsymbol{r}_0-\omega t)$$

$$+\boldsymbol{k}\widehat{\boldsymbol{E}}^2\sin2(\boldsymbol{k}\cdot\boldsymbol{r}_0-\omega t)-2(\boldsymbol{k}\cdot\widehat{\boldsymbol{E}})\widehat{\boldsymbol{E}}\sin2(\boldsymbol{k}\cdot\boldsymbol{r}_0-\omega t)\Big). \tag{3.62}$$

We used the formula $\widehat{\boldsymbol{E}}\times(\nabla\times\widehat{\boldsymbol{E}})=\nabla(\widehat{\boldsymbol{E}}\cdot\widehat{\boldsymbol{E}})/2-(\widehat{\boldsymbol{E}}\cdot\nabla)\widehat{\boldsymbol{E}}$, $\widehat{\boldsymbol{E}}\times(\boldsymbol{k}\times\widehat{\boldsymbol{E}})=\boldsymbol{k}\widehat{\boldsymbol{E}}^2-(\boldsymbol{k}\cdot\widehat{\boldsymbol{E}})\widehat{\boldsymbol{E}}$. In the case of transverse electromagnetic wave, the terms $(\widehat{\boldsymbol{E}}\cdot\nabla)\widehat{\boldsymbol{E}}$ and $(\boldsymbol{k}\cdot\widehat{\boldsymbol{E}})\widehat{\boldsymbol{E}}$ are negligible and the terms due to Lorentz force are dominant. The time average of $m\mathrm{d}\boldsymbol{v}_2/\mathrm{d}t$ becomes

$$m\left\langle\frac{\mathrm{d}\boldsymbol{v}_2}{\mathrm{d}t}\right\rangle=-\frac{e^2}{4m\omega^2}\nabla\widehat{\boldsymbol{E}}^2.$$

This is the effective nonlinear force on a single electron. This nonlinear force on plasma per unit volume is

$$nm\left\langle \frac{\mathrm{d}\boldsymbol{v}_2}{\mathrm{d}t} \right\rangle = -\frac{\omega_\mathrm{p}^2}{\omega^2}\nabla\frac{\epsilon_0\widehat{\boldsymbol{E}}^2}{4} = -\frac{\omega_\mathrm{p}^2}{\omega^2}\nabla\frac{\epsilon_0\langle\boldsymbol{E}^2\rangle}{2} \tag{3.63}$$

where ω_p is electron plasma frequency. This force is called *ponderomotive force*. This force moves plasma out of the beam, so that electron plasma frequency $\mathit{\Pi}_\mathrm{e}$ is lower and the dielectric constant $\epsilon = (1-\mathit{\Pi}_\mathrm{e}^2/\omega^2)$ (refer to Section 11.1) is higher inside the beam than outside; that is, the refractive index $N = \epsilon^{1/2}$ is larger inside the beam than outside. Then, the plasma acts as an optical fiber, focusing the beam to a small diameter. By the ponderomotive force, intense laser beam with Peta Watt (10^{15}W) can bore a hole and reach to the core of high density fuel pellet in inertial confinement and heat electrons by the oscillating components in (3.62). This concept is called *fast ignition* (refer to section 18.3).

References

[1] R. G. Littlejohn: Hamiltonian Formulation of Guiding Center Motion. *Phys. Fluids* **24**, 1730 (1981). R. G. Littlejohn: Variational Principles of Guiding Center Motion. J. Plasma Phys. **29**, 111 (1983).

[2] A. I. Morozov and L. S. Solovev: *Rev. of Plasma Physics* **2**, 201, (edited by M. A. Leontovich), Consultant Bureau, New York (1966).

Ch.4 Velocity Space Distribution Function and Boltzmann's Equation

A plasma consists of many ions and electrons, but the individual behavior of each particle can hardly be observed. What can be observed instead are statistical averages. In order to describe the properties of a plasma, it is necessary to define a distribution function that indicates particle number density in the phase space whose ordinates are the particle positions and velocities. The distribution function is not necessarily stationary with respect to time. In sec.4.1, the equation governing the distribution function $f(q_i, p_i, t)$ is derived by means of Liouville's theorem. Boltzmann's equation for the distribution function $f(\boldsymbol{x}, \boldsymbol{v}, t)$ is formulated in sec.4.2. When the collision term is neglected, Boltzmann's equation is called Vlasov's equation.

4.1 Phase Space and Distribution Function

A particle can be specified by its coordinates (x, y, z), velocity (v_x, v_y, v_z), and time t. More generally, the particle can be specified by *canonical variables* $q_1, q_2, q_3, p_1, p_2, p_3$ and t in phase space. The motion of a particle in phase space is described by Hamilton's equations

$$\frac{\mathrm{d}q_i}{\mathrm{d}t} = \frac{\partial H(q_j, p_j, t)}{\partial p_i}, \qquad \frac{\mathrm{d}p_i}{\mathrm{d}t} = -\frac{\partial H(q_j, p_j, t)}{\partial q_i}. \tag{4.1}$$

When canonical variables are used, an infinitesimal volume in phase space $\Delta = \delta q_1 \delta q_2 \delta q_3 \delta p_1 \delta p_2 \delta p_3$ is conserved according to Liouville's theorem, that is,

$$\Delta = \delta q_1 \delta q_2 \delta q_3 \delta p_1 \delta p_2 \delta p_3 = \text{const.} \tag{4.2}$$

Let the number of particles in a small volume of phase space be δN

$$\delta N = F(q_i, p_i, t) \delta \boldsymbol{q} \delta \boldsymbol{p} \tag{4.3}$$

where $\delta \boldsymbol{q} = \delta q_1 \delta q_2 \delta q_3$, $\delta \boldsymbol{p} = \delta p_1 \delta p_2 \delta p_3$, and $F(q_i, p_i, t)$ is the *distribution function in phase space*. If the particles move according to the equation of motion and are not scattered by collisions, the small volume in phase space is conserved. As the particle number δN within the small phase space is conserved, the distribution function ($F = \delta N / \Delta$) is also constant, i.e.,

$$\frac{\mathrm{d}F}{\mathrm{d}t} = \frac{\partial F}{\partial t} + \sum_{i=1}^{3} \left(\frac{\partial F}{\partial q_i} \frac{\mathrm{d}q_i}{\mathrm{d}t} + \frac{\partial F}{\partial p_i} \frac{\mathrm{d}p_i}{\mathrm{d}t} \right) = \frac{\partial F}{\partial t} + \sum_{i=1}^{3} \left(\frac{\partial H}{\partial p_i} \frac{\partial F}{\partial q_i} - \frac{\partial H}{\partial q_i} \frac{\partial F}{\partial p_i} \right) = 0. \tag{4.4}$$

In the foregoing discussion we did not take collisions into account. If we denote the variation of F due to the collisions by $(\delta F / \delta t)_{\text{coll}}$, (4.4) becomes

$$\frac{\partial F}{\partial t} + \sum_{i=1}^{3} \left(\frac{\partial H}{\partial p_i} \frac{\partial F}{\partial q_i} - \frac{\partial H}{\partial q_i} \frac{\partial F}{\partial p_i} \right) = \left(\frac{\delta F}{\delta t} \right)_{\text{coll}}. \tag{4.5}$$

4.2 Boltzmann's Equation and Vlasov's Equation

Let us use the space and velocity-space coordinates x_1, x_2, x_3, v_1, v_2, v_3 instead of the canonical coordinates. The Hamiltonian is

$$H = \frac{1}{2m} (\boldsymbol{p} - q\boldsymbol{A})^2 + q\phi, \tag{4.6}$$

$$p_i = m v_i + q A_i, \tag{4.7}$$

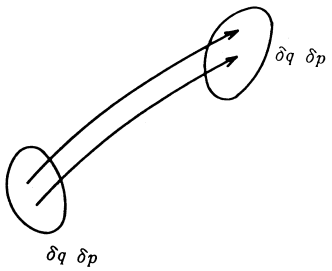

Fig.4.1 Movement of particles in phase space.

$$q_i = x_i \tag{4.8}$$

and

$$\frac{\mathrm{d}x_i}{\mathrm{d}t} = \frac{\partial H}{\partial p_i} = v_i, \tag{4.9}$$

$$\frac{\mathrm{d}p_i}{\mathrm{d}t} = -\frac{\partial H}{\partial x_i} = \sum_k \frac{(p_k - qA_k)}{m} q\frac{\partial A_k}{\partial x_i} - q\frac{\partial \phi}{\partial x_i}. \tag{4.10}$$

Consequently (4.5) becomes

$$\frac{\partial F}{\partial t} + \sum_{i=k}^{3} v_k \frac{\partial F}{\partial x_k} + q\sum_{i=1}^{3}\left(\sum_{k=1}^{3} v_k \frac{\partial A_k}{\partial x_i} - \frac{\partial \phi}{\partial x_i}\right)\frac{\partial F}{\partial p_i} = \left(\frac{\delta F}{\delta t}\right)_{\mathrm{coll}}. \tag{4.11}$$

By use of (4.7) (4.8), independent variables are transformed from (q_i, p_i, t) to (x_j, v_j, t) and

$$\frac{\partial v_j(x_k, p_k, t)}{\partial p_i} = \frac{1}{m}\delta_{ij},$$

$$\frac{\partial v_j(x_k, p_k, t)}{\partial x_i} = -\frac{q}{m}\frac{\partial A_j}{\partial x_i},$$

$$\frac{\partial v_j(x_k, p_k, t)}{\partial t} = -\frac{q}{m}\frac{\partial A_j}{\partial t}.$$

We denote $F(x_i, p_i, t) = F(x_i, p_i(x_j, v_j, t), t) \equiv f(x_j, v_j, t)/m^3$. Then we have $m^3 F(x_i, p_i, t) = f(x_j, v_j(x_i, p_i, t), t)$ and

$$m^3\frac{\partial}{\partial p_i}F(x_h, p_h, t) = \frac{\partial}{\partial p_i}f(x_j, v_j(x_h, p_h, t), t) = \sum_j \frac{\partial f}{\partial v_j}\frac{\partial v_j}{\partial p_i} = \frac{\partial f}{\partial v_i}\frac{1}{m},$$

$$m^3\frac{\partial}{\partial x_k}F(x_h, p_h, t) = \frac{\partial}{\partial x_k}f(x_i, v_i(x_h, p_h, t), t) = \frac{\partial f}{\partial x_k} + \sum_i \frac{\partial f}{\partial v_i}\frac{\partial v_i}{\partial x_k}$$

$$= \frac{\partial f}{\partial x_k} + \sum_i \frac{\partial f}{\partial v_i}\left(\frac{-q}{m}\right)\frac{\partial A_i}{\partial x_k}$$

$$m^3\frac{\partial}{\partial t}F(x_h, p_h, t) = \frac{\partial}{\partial t}f(x_i, v_i(x_h, p_h, t), t) = \frac{\partial f}{\partial t} + \sum_i \frac{\partial f}{\partial v_i}\left(\frac{-q}{m}\right)\frac{\partial A_i}{\partial t}.$$

Accordingly (4.11) is reduced to

$$\frac{\partial f}{\partial t}+\sum_i \frac{\partial f}{\partial v_i}\left(\frac{-q}{m}\right)\frac{\partial A_i}{\partial t}+\sum_k v_k\left(\frac{\partial f}{\partial x_k}+\sum_i \frac{\partial f}{\partial v_i}\left(\frac{-q}{m}\right)\frac{\partial A_i}{\partial x_k}\right)$$

$$+\sum_i\left(\sum_k v_k\frac{\partial A_k}{\partial x_i}-\frac{\partial \phi}{\partial x_i}\right)\frac{q}{m}\frac{\partial f}{\partial v_i}=\left(\frac{\delta f}{\delta t}\right)_{\text{coll}},$$

$$\frac{\partial f}{\partial t}+\sum_k v_k\frac{\partial f}{\partial x_k}+\sum_i\left(-\frac{\partial A_i}{\partial t}-\sum_k v_k\frac{\partial A_i}{\partial x_k}+\sum_k v_k\frac{\partial A_k}{\partial x_i}-\frac{\partial \phi}{\partial x_i}\right)\frac{q}{m}\frac{\partial f}{\partial v_i}=\left(\frac{\delta f}{\delta t}\right)_{\text{coll}}.$$

Since the following relation is hold

$$\sum_k v_k\frac{\partial A_k}{\partial x_i}=\sum_k v_k\frac{\partial A_i}{\partial x_k}+(\boldsymbol{v}\times(\nabla\times\boldsymbol{A}))_i=\sum_k v_k\frac{\partial A_i}{\partial x_k}+(\boldsymbol{v}\times\boldsymbol{B})_i.$$

we have

$$\frac{\partial f}{\partial t}+\sum_i v_i\frac{\partial f}{\partial x_i}+\sum_i\frac{q}{m}(\boldsymbol{E}+\boldsymbol{v}\times\boldsymbol{B})_i\frac{\partial f}{\partial v_i}=\left(\frac{\delta f}{\delta t}\right)_{\text{coll}}. \tag{4.12}$$

This equation is called *Boltzmann's equation*. The electric charge density ρ and the electric current $\boldsymbol{j}$ are expressed by

$$\rho=\sum_{\text{i,e}} q\int f\mathrm{d}v_1\mathrm{d}v_2\mathrm{d}v_3, \tag{4.13}$$

$$\boldsymbol{j}=\sum_{\text{i,e}} q\int \boldsymbol{v}f\mathrm{d}v_1\mathrm{d}v_2\mathrm{d}v_3. \tag{4.14}$$

Accordingly Maxwell equations are given by

$$\nabla\cdot\boldsymbol{E}=\frac{1}{\epsilon_0}\sum q\int f\mathrm{d}\boldsymbol{v}, \tag{4.15}$$

$$\frac{1}{\mu_0}\nabla\times\boldsymbol{B}=\epsilon_0\frac{\partial \boldsymbol{E}}{\partial t}+\sum q\int \boldsymbol{v}f\mathrm{d}\boldsymbol{v}, \tag{4.16}$$

$$\nabla\times\boldsymbol{E}=-\frac{\partial \boldsymbol{B}}{\partial t}, \tag{4.17}$$

$$\nabla\cdot\boldsymbol{B}=0. \tag{4.18}$$

When the plasma is rarefied, the collision term $(\delta f/\delta t)_{\text{coll}}$ may be neglected. However, the interactions of the charged particles are still included through the internal electric and magnetic field which are calculated from the charge and current densities by means of Maxwell equations. The charge and current densities are expressed by the distribution functions for the electron and the ion. This equation is called *collisionless Boltzmann's equation* or *Vlasov's equation*.

4.3 Fokker-Planck Collision Term

When Fokker-Planck collision term is adopted as the collision term of Boltzmann's equation, this equation is called Fokker Planck equation. In the case of Coulomb collision, scattering into small angles has a large cross-section and a test particle interacts with many field particles at the same time, since the Coulomb force is a long-range interaction. Consequently it is appropriate to treat Coulomb collision statistically. Assume that the velocity $\boldsymbol{v}$ of a particle is changed to $\boldsymbol{v}+\Delta\boldsymbol{v}$

after the time Δt by Coulomb collisions; denote the probability of this process by $W(\boldsymbol{v}, \Delta\boldsymbol{v})$. Then the distribution function $f(\boldsymbol{r}, \boldsymbol{v}, t)$ satisfies

$$f(\boldsymbol{r}, \boldsymbol{v}, t + \Delta t) = \int f(\boldsymbol{r}, \boldsymbol{v} - \Delta\boldsymbol{v}, t) W(\boldsymbol{v} - \Delta\boldsymbol{v}, \Delta\boldsymbol{v}) \mathrm{d}(\Delta\boldsymbol{v}). \tag{4.19}$$

In this process the state at $t+\Delta t$ depends only on the state at t. Such a process (i.e., one independent of the history of the process) is called the *Markoff process*. The change of the distribution function by virtue of Coulomb collision is

$$\left(\frac{\delta f}{\delta t}\right)_{\mathrm{coll}} \Delta t = f(\boldsymbol{r}, \boldsymbol{v}, t + \Delta t) - f(\boldsymbol{r}, \boldsymbol{v}, t).$$

Taylor expansion of the integrand of (4.19) gives

$$\begin{aligned} & f(\boldsymbol{r}, \boldsymbol{v} - \Delta\boldsymbol{v}, t) W(\boldsymbol{v} - \Delta\boldsymbol{v}, \Delta\boldsymbol{v}) \\ & = f(\boldsymbol{r}, \boldsymbol{v}, t) W(\boldsymbol{v}, \Delta\boldsymbol{v}) - \sum_r \frac{\partial (fW)}{\partial v_r} \Delta v_r + \sum_{r\,s} \frac{1}{2} \frac{\partial^2 (fW)}{\partial v_r \partial v_s} \Delta v_r \Delta v_s + \cdots . \end{aligned} \tag{4.20}$$

From the definition of $W(\boldsymbol{v}, \Delta\boldsymbol{v})$, the intgral of W is

$$\int W \mathrm{d}(\Delta\boldsymbol{v}) = 1.$$

Introducing the quantities

$$\int W \Delta\boldsymbol{v} \mathrm{d}(\Delta\boldsymbol{v}) = \langle \Delta\boldsymbol{v} \rangle_t \Delta t, \qquad \int W \Delta v_r \Delta v_s \mathrm{d}(\Delta\boldsymbol{v}) = \langle \Delta v_r \Delta v_s \rangle_t \Delta t,$$

we find

$$\left(\frac{\delta f}{\delta t}\right)_{\mathrm{coll}} = -\nabla_v (\langle \Delta\boldsymbol{v} \rangle_t f) + \sum \frac{1}{2} \frac{\partial^2}{\partial v_r \partial v_s} (\langle \Delta v_r \Delta v_s \rangle_t f). \tag{4.21}$$

This term is called the *Fokker-Planck collision term* and $\langle \Delta\boldsymbol{v} \rangle_t$, $\langle \Delta v_r \Delta v_s \rangle_t$ are called *Fokker-Planck coefficients*. $\int W \Delta v_r \Delta v_s \mathrm{d}(\Delta\boldsymbol{v})$ is proportional to Δt. Δv_r is the sum of Δv_r^i, which is, the change of v_r due to the i-th collisons during Δt, i.e., $\Delta v_r = \sum_i \Delta v_r^i$, so that $\Delta v_r \Delta v_s = \sum_i \sum_j \Delta v_r^i \Delta v_s^j$. When the collisions are statistically independent, statistical average of $\langle \Delta v_r^i \Delta v_s^j \rangle_t$ $(i \neq j)$ is zero and

$$\int W \Delta v_r \Delta v_s \mathrm{d}(\Delta\boldsymbol{v}) = \sum_i \int \Delta v_r^i \Delta v_s^i \mathrm{d}(\Delta\boldsymbol{v}).$$

This expression is proportinal to Δt.

The Fokker-Planck equation can be expressed in the form (ref.[1])

$$\frac{\partial f}{\partial t} + \boldsymbol{v} \cdot \nabla_r f + \frac{\boldsymbol{F}}{m} \nabla_v f + \nabla_v \cdot \boldsymbol{J} = 0, \tag{4.22}$$

where

$$J_i = A_i f - \sum_j D_{i\,j} \frac{\partial f}{\partial v_j},$$

$$A_i = \langle \Delta v_i \rangle_t - \frac{1}{2} \sum_j \frac{\partial}{\partial v_j} \langle \Delta v_i \Delta v_j \rangle_t,$$

$$D_{i\,j} = \frac{1}{2} \langle \Delta v_i \Delta v_j \rangle_t.$$

The tensor D is called the *diffusion tensor* in the velosity space and $\boldsymbol{A}$ is called the *coefficient of dynamic friction*. For convenience we consider the components of $\boldsymbol{J}$ parallel and perpendicular to

the velocity $\boldsymbol{v}$ of the test particle. When the distribution function of field particles is isotropic, we find

$$\left.\begin{aligned} \boldsymbol{J}_{\parallel} &= -D_{\parallel}\nabla_{\parallel} f + \boldsymbol{A} f, \\ \boldsymbol{J}_{\perp} &= -D_{\perp}\nabla_{\perp} f. \end{aligned}\right\} \tag{4.23}$$

$\boldsymbol{A}$ is parallel to $\boldsymbol{v}$ and the diffusion tensor becomes diagonal. When the distribution function of field particles is Maxwellian, $\boldsymbol{A}$ and D are given by (ref.[1])

$$mvD_{\parallel} = -T^{*}A, \tag{4.24}$$

$$D_{\parallel} = \frac{(qq^{*})^{2} n^{*} \ln \Lambda}{8\pi\varepsilon_{0}^{2} v m^{2}} \frac{\Phi_{1}(b^{*})}{b^{*2} v^{2}}, \tag{4.25}$$

$$D_{\perp} = \frac{(qq^{*})^{2} n^{*} \ln \Lambda}{8\pi\varepsilon_{0}^{2} v m^{2}} \left(\Phi(b^{*}v) - \frac{\Phi_{1}(b^{*}v)}{2b^{*2}v^{2}} \right). \tag{4.26}$$

q^{*}, n^{*}, b^{*}, and T^{*} are those of field particles and q, m, and v are those of test particles. $\Phi(x)$ and $\Phi_{1}(x)$ are

$$\Phi(x) = \frac{2}{\pi^{1/2}} \int_{0}^{x} \exp(-\xi^{2} \mathrm{d}\xi),$$

$$\Phi_{1}(x) = \Phi(x) - \frac{2x}{\pi^{1/2}} \exp(-x^{2}).$$

When $x > 2$, then $\Phi(x) \approx \Phi_{1}(x) \approx 1$.

References

[1] D. V. Sivukhin: *Reviews of Plasma Physics* **4** p.93 (ed. by M. A. Leontovich) Consultant Bureau, New York 1966.

Ch.5 Plasma as Magnetohydrodynamic Fluid

5.1 Magnetohydrodynamic Equations for Two Fluids

Plasmas can be described as magnetohydrodynamic two fluids of ions and electrons with mass densities $\rho_{\rm mi}$, $\rho_{\rm me}$, charge density ρ, current density $\boldsymbol{j}$, flow velocities $\boldsymbol{V}_{\rm i}$, $\boldsymbol{V}_{\rm e}$, and pressures $p_{\rm i}$, $p_{\rm e}$. These physical quantities can be expressed by appropriate averages in velocity space by use of the velocity space distribution functions $f_i(\boldsymbol{r},\boldsymbol{v},t)$ of ions and electrons, which were introduced in ch.4. The number density of ion $n_{\rm i}$, the ion mass density $\rho_{\rm m,i}$, and the ion flow velocity $\boldsymbol{V}_{\rm i}(\boldsymbol{r},t)$ are expressed as follows:

$$n_{\rm i}(\boldsymbol{r},t) = \int f_{\rm i}(\boldsymbol{r},\boldsymbol{v},t){\rm d}\boldsymbol{v}, \tag{5.1}$$

$$\rho_{\rm mi}(\boldsymbol{r},t) = m_{\rm i}n_{\rm i}(\boldsymbol{r},t), \tag{5.2}$$

$$\boldsymbol{V}(\boldsymbol{r},t) = \frac{\int \boldsymbol{v}f_{\rm i}(\boldsymbol{r},\boldsymbol{v},t){\rm d}\boldsymbol{v}}{\int f_{\rm i}(\boldsymbol{r},\boldsymbol{v},t){\rm d}\boldsymbol{v}} = \frac{1}{n_{\rm i}(\boldsymbol{r},t)}\int \boldsymbol{v}f_{\rm i}(\boldsymbol{r},\boldsymbol{v},t){\rm d}\boldsymbol{v}. \tag{5.3}$$

We have the same expressions for electrons as those of ions. Since magnetohydrodynamics will treat average quantities in the velocity space, phenomena associated with the shape of the velocity space distribution function (ch.11) will be neglected. However the independent variables are $\boldsymbol{r},t$ only and it is possible to analyze geometrically complicated configurations.

Equations of magnetohydrodynamics are followings:

$$\frac{\partial n_{\rm e}}{\partial t} + \nabla\cdot(n_{\rm e}\boldsymbol{V}_{\rm e}) = 0, \tag{5.4}$$

$$\frac{\partial n_{\rm i}}{\partial t} + \nabla\cdot(n_{\rm i}\boldsymbol{V}_{\rm i}) = 0, \tag{5.5}$$

$$n_{\rm e}m_{\rm e}\frac{{\rm d}\boldsymbol{V}_{\rm e}}{{\rm d}t} = -\nabla p_{\rm e} - en_{\rm e}(\boldsymbol{E}+\boldsymbol{V}_{\rm e}\times\boldsymbol{B}) + \boldsymbol{R}, \tag{5.6}$$

$$n_{\rm i}m_{\rm i}\frac{{\rm d}\boldsymbol{V}_{\rm i}}{{\rm d}t} = -\nabla p_{\rm i} + Zen_{\rm i}(\boldsymbol{E}+\boldsymbol{V}_{\rm i}\times\boldsymbol{B}) - \boldsymbol{R}. \tag{5.7}$$

Here $\boldsymbol{R}$ denotes the rate of momentum (density) change of the electron fluid by the collision with the ion fluid. The rate of momentum change of the ion fluid due to the collision with electron fluid is $-\boldsymbol{R}$. The change of the number $n(x,y,z,t)\Delta x\Delta y\Delta z$ of particles within the region of $\Delta x\Delta y\Delta z$ is the difference between the incident particle flux $n(x,y,z,t)V_x(x,y,z,t)\Delta y\Delta z$ into the surface A in fig.5.1 and outgoing particle flux $n(x+\Delta x,y,z,t)V_x(x+\Delta x,y,z,t)\Delta y\Delta z$ from the surface A$'$, that is,

$$(n(x,y,z,t)V_x(x,y,z,t) - n(x+\Delta x,y,z,t)V_x(x+\Delta x,y,z,t))\Delta y\Delta z$$

$$= -\frac{\partial(nV_x)}{\partial x}\Delta x\Delta y\Delta z.$$

When the particle fluxes of the other surfaces are taken into accout, we find (5.4), that is

$$\frac{\partial n}{\partial t}\Delta x\Delta y\Delta z = -\left(\frac{\partial(nV_x)}{\partial x} + \frac{\partial(nV_y)}{\partial y} + \frac{\partial(nV_z)}{\partial z}\right)\Delta x\Delta y\Delta z.$$

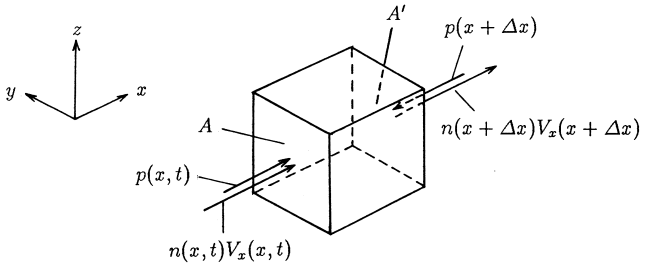

Fig.5.1 Particle flux and force due to pressure

The term $-\nabla p$ in eqs.(5.6),(5.7) is the force per unit volume of plasma due to the pressure p by the following reason. The force applied to the surface A in fig.5.1 is $p(x,y,z,t)\Delta y\Delta z$ and the force on the surface A$'$ is $-p(x+\Delta x,y,z,t)\Delta y\Delta z$. Therefore the sum of these two forces is

$$(-p(x+\Delta x,y,z,t)+p(x,y,z,t))\Delta y\Delta z=-\frac{\partial p}{\partial x}\Delta x\Delta y\Delta z$$

in the x direction. When the effects of the pressure on the other surfaces are taken account, the resultant force due to the pressure per unit volume is

$$-\left(\frac{\partial p}{\partial x}\hat{\boldsymbol{x}}+\frac{\partial p}{\partial y}\hat{\boldsymbol{y}}+\frac{\partial p}{\partial z}\hat{\boldsymbol{z}}\right)=-\nabla p$$

where $\hat{\boldsymbol{x}},\hat{\boldsymbol{y}},\hat{\boldsymbol{z}}$ are the unit vector in x,y,z directions respectively. The second term in right-hand side of (5.6),(5.7) is Lorentz force per unit volume. The third term is the collision term of electron-ion collision as is mentioned in sec.2.8 and is given by

$$\boldsymbol{R}=-n_{\mathrm{e}}m_{\mathrm{e}}(\boldsymbol{V}_{\mathrm{e}}-\boldsymbol{V}_{\mathrm{i}})\nu_{\mathrm{ei}} \tag{5.8}$$

where ν_{ei} is coulomb collision frequency of electron with ion.

Let us consider the total time differential in the left-hand side of equation of motion. The flow velocity $\boldsymbol{V}$ is a function of space coordinates $\boldsymbol{r}$ and time t. Then the acceleration of a small volume of fluid is given by

$$\frac{\mathrm{d}\boldsymbol{V}(\boldsymbol{r},t)}{\mathrm{d}t}=\frac{\partial\boldsymbol{V}(\boldsymbol{r},t)}{\partial t}+\left(\frac{\mathrm{d}\boldsymbol{r}}{\mathrm{d}t}\cdot\nabla\right)\boldsymbol{V}(\boldsymbol{r},t)=\frac{\partial\boldsymbol{V}(\boldsymbol{r},t)}{\partial t}+(\boldsymbol{V}(\boldsymbol{r},t)\cdot\nabla)\boldsymbol{V}(\boldsymbol{r},t).$$

Therefore the equations of motion (5.6),(5.7) are reduced to

$$n_{\mathrm{e}}m_{\mathrm{e}}\left(\frac{\partial\boldsymbol{V}_{\mathrm{e}}}{\partial t}+(\boldsymbol{V}_{\mathrm{e}}\cdot\nabla)\boldsymbol{V}_{\mathrm{e}}\right)=-\nabla p_{\mathrm{e}}-en_{\mathrm{e}}(\boldsymbol{E}+\boldsymbol{V}_{\mathrm{e}}\times\boldsymbol{B})+\boldsymbol{R} \tag{5.9}$$

$$n_{\mathrm{i}}m_{\mathrm{i}}\left(\frac{\partial\boldsymbol{V}_{\mathrm{i}}}{\partial t}+(\boldsymbol{V}_{\mathrm{i}}\cdot\nabla)\boldsymbol{V}_{\mathrm{i}}\right)=-\nabla p_{\mathrm{i}}+Zen_{\mathrm{i}}(\boldsymbol{E}+\boldsymbol{V}_{\mathrm{i}}\times\boldsymbol{B})-\boldsymbol{R}. \tag{5.10}$$

Conservation of particle (5.4),(5.5), the equations of motion (5.9), (5.10) can be derived from Boltzmann equation (4.12). Integration of Boltzmann equation over velocity space yields (5.4), (5.5). Integration of Boltzmann equation multiplied by $m\boldsymbol{v}$ yields (5.9),(5.10). The process of the mathematical derivation is described in Appendix A.

5.2 Magnetohydrodynamic Equations for One Fluid

Since the ion-to-electron mass ratio is $m_{\mathrm{i}}/m_{\mathrm{e}}=1836A$ (A is atomic weight of the ion), the contribution of ions to the mass density of plasma is dominant. In many cases it is more convenient to reorganize the equations of motion for two fluids to the equation of motion for one fluid and Ohm's law.

The total mass density of plasma ρ_{m}, the flow velocity of plasma $\boldsymbol{V}$, the electric charge density ρ and the current density $\boldsymbol{j}$ are defined as follows:

$$\rho_{\rm m} = n_{\rm e} m_{\rm e} + n_{\rm i} m_{\rm i}, \tag{5.11}$$

$$\boldsymbol{V} = \frac{n_{\rm e} m_{\rm e} \boldsymbol{V}_{\rm e} + n_{\rm i} m_{\rm i} \boldsymbol{V}_{\rm i}}{\rho_{\rm m}}, \tag{5.12}$$

$$\rho = -e n_{\rm e} + Z e n_{\rm i}, \tag{5.13}$$

$$\boldsymbol{j} = -e n_{\rm e} \boldsymbol{V}_{\rm e} + Z e n_{\rm i} \boldsymbol{V}_{\rm i}. \tag{5.14}$$

From (5.4),(5.5), it follows that

$$\frac{\partial \rho_{\rm m}}{\partial t} + \nabla \cdot (\rho_{\rm m} \boldsymbol{V}) = 0, \tag{5.15}$$

$$\frac{\partial \rho}{\partial t} + \nabla \cdot \boldsymbol{j} = 0. \tag{5.16}$$

From (5.9) (5.10), we find

$$\rho_{\rm m} \frac{\partial \boldsymbol{V}}{\partial t} + n_{\rm e} m_{\rm e} (\boldsymbol{V}_{\rm e} \cdot \nabla) \boldsymbol{V}_{\rm e} + n_{\rm i} m_{\rm i} (\boldsymbol{V}_{\rm i} \cdot \nabla) \boldsymbol{V}_{\rm i}$$

$$= -\nabla (p_{\rm e} + p_{\rm i}) + \rho \boldsymbol{E} + \boldsymbol{j} \times \boldsymbol{B}. \tag{5.17}$$

The charge neutrality of the plasma allows us to write $n_{\rm e} \simeq Z n_{\rm i}$. Denote $\Delta n_{\rm e} = n_{\rm e} - Z n_{\rm i}$, we have

$$\rho_{\rm m} = n_{\rm i} m_{\rm i} \left(1 + \frac{m_{\rm e}}{m_{\rm i}} Z\right), \quad p = p_{\rm i} + p_{\rm e}, \quad \boldsymbol{V} = \boldsymbol{V}_{\rm i} + \frac{m_{\rm e} Z}{m_{\rm i}} (\boldsymbol{V}_{\rm e} - \boldsymbol{V}_{\rm i}),$$

$$\rho = -e \Delta n_{\rm e}, \quad \boldsymbol{j} = -e n_{\rm e} (\boldsymbol{V}_{\rm e} - \boldsymbol{V}_{\rm i}).$$

Since $m_{\rm e}/m_{\rm i} \ll 1$, the second and third terms in left-hand side of (5.17) can be written to be $(\boldsymbol{V} \cdot \Delta)\boldsymbol{V}$. Since $\boldsymbol{V}_{\rm e} = \boldsymbol{V}_{\rm i} - \boldsymbol{j}/e n_{\rm e} \simeq \boldsymbol{V} - \boldsymbol{j}/e n_{\rm e}$, (5.9) reduces to

$$\boldsymbol{E} + \left(\boldsymbol{V} - \frac{\boldsymbol{j}}{e n_{\rm e}}\right) \times \boldsymbol{B} + \frac{1}{e n_{\rm e}} \nabla p_{\rm e} - \frac{\boldsymbol{R}}{e n_{\rm e}} = \frac{m_{\rm e}}{e^2 n_{\rm e}} \frac{\partial \boldsymbol{j}}{\partial t} - \frac{m_{\rm e}}{e} \frac{\partial \boldsymbol{V}}{\partial t}. \tag{5.18}$$

By use of the expression of specific resistivity η, (see sec.2.8) the collision term $\boldsymbol{R}$ is reduced to

$$\boldsymbol{R} = n_{\rm e} \left(\frac{m_{\rm e} \nu_{\rm ei}}{n_{\rm e} e^2}\right) (-e n_{\rm e})(\boldsymbol{V}_{\rm e} - \boldsymbol{V}_{\rm i}) = n_{\rm e} e \eta \boldsymbol{j}. \tag{5.19}$$

Equation (5.18) corresponds a generalized Ohm's law. Finally the equation of motion for one fluid model and a generalized Ohm's law are give by

$$\rho_{\rm m} \left(\frac{\partial \boldsymbol{V}}{\partial t} + (\boldsymbol{V} \cdot \nabla)\boldsymbol{V}\right) = -\nabla p + \rho \boldsymbol{E} + \boldsymbol{j} \times \boldsymbol{B}, \tag{5.20}$$

$$\boldsymbol{E} + \left(\boldsymbol{V} - \frac{\boldsymbol{j}}{e n_{\rm e}}\right) \times \boldsymbol{B} + \frac{1}{e n_{\rm e}} \nabla p_{\rm e} - \eta \boldsymbol{j} = \frac{m_{\rm e}}{e^2 n_{\rm e}} \frac{\partial \boldsymbol{j}}{\partial t} - \frac{m_{\rm e}}{e} \frac{\partial \boldsymbol{V}}{\partial t} \simeq 0.$$

$$(|\omega/\Omega_{\rm e}| \ll 1) \tag{5.21}$$

The equation of continuity and Maxwell equations are

$$\frac{\partial \rho_{\rm m}}{\partial t} + \nabla \cdot (\rho_{\rm m} \boldsymbol{V}) = 0, \tag{5.22}$$

$$\frac{\partial \rho}{\partial t} + \nabla \cdot \boldsymbol{j} = 0, \tag{5.23}$$

$$\nabla \times \boldsymbol{E} = -\frac{\partial \boldsymbol{B}}{\partial t}, \tag{5.24}$$

$$\frac{1}{\mu_0} \nabla \times \boldsymbol{B} = \boldsymbol{j} + \frac{\partial \boldsymbol{D}}{\partial t}, \tag{5.25}$$

$$\nabla \cdot \boldsymbol{D} = \rho, \tag{5.26}$$

$$\nabla \cdot \boldsymbol{B} = 0. \tag{5.27}$$

From (5.25),(5.24), it follows $\nabla \times \nabla \times \boldsymbol{E} = -\mu_0 \partial \boldsymbol{j}/\partial t - \mu_0 \epsilon_0 \partial^2 \boldsymbol{E}/\partial t^2$. A typical propagation velocity of magnetohydrodynamic wave or perturbation is Alfven velocity $v_{\rm A} = B/(\mu_0 \rho_{\rm m})^{1/2}$ as is described in sec.5.4 and is much smaller than light speed c and $\omega^2/k^2 \sim v_{\rm A}^2 \ll c^2$. Since $|\nabla \times (\partial \boldsymbol{B}/\partial t)| = |\nabla \times \nabla \times \boldsymbol{E}| \sim k^2 |\boldsymbol{E}|$, and $\mu_0 \epsilon_0 |\partial^2 \boldsymbol{E}/\partial t^2| \sim \omega^2 |\boldsymbol{E}|/c^2$, the displacement current, $\partial \boldsymbol{D}/\partial t$ in (5.25) is negligible. Since the ratio of the first term $(m_{\rm e}/e)\partial \boldsymbol{j}/\partial t$ in right-hand side of (5.21) to the term $(\boldsymbol{j} \times \boldsymbol{B})$ in left-hand side is $\omega/\Omega_{\rm e}$, the first term can be neglected, if $|\omega/\Omega_{\rm e}| \ll 1$. The second term $(m_{\rm e}/e)\partial \boldsymbol{V}/\partial t$ in the right-hand side of (5.21) is of the order of $\omega/\Omega_{\rm e}$ times as large as the term $\boldsymbol{V} \times \boldsymbol{B}$ in the left-hand side. Therefore we may set the right-hand side of (5.21) nearly zero. When the term $\boldsymbol{j} \times \boldsymbol{B}$ is eliminated by the use of (5.20), we find

$$\boldsymbol{E} + \boldsymbol{V} \times \boldsymbol{B} - \frac{1}{en} \nabla p_{\rm i} - \eta \boldsymbol{j} = \frac{\Delta n_{\rm e}}{n_{\rm e}} \boldsymbol{E} + \frac{m_{\rm i}}{e} \frac{{\rm d}\boldsymbol{V}}{{\rm d}t}.$$

The ratio of $(m_{\rm i}/e){\rm d}\boldsymbol{V}/{\rm d}t$ to $\boldsymbol{V} \times \boldsymbol{B}$ is around $|\omega/\Omega_{\rm i}|$, and $\Delta n_{\rm e}/n_{\rm e} \ll 1$. When $|\omega/\Omega_{\rm i}| \ll 1$, we find

$$\boldsymbol{E} + \boldsymbol{V} \times \boldsymbol{B} - \frac{1}{en} \nabla p_{\rm i} = \eta \boldsymbol{j}. \quad (\ |\omega/\Omega_{\rm i}| \ll 1) \tag{5.28}$$

5.3 Simplified Magnetohydrodynamic Equations

When $|\omega/\Omega_{\rm i}| \ll 1$, $|\omega/k| \ll c$, and the ion pressure term $\nabla p_{\rm i}$ can be neglected in Ohm's law, magnetohydrodynamic equations are simplified as follows:

$$\boldsymbol{E} + \boldsymbol{V} \times \boldsymbol{B} = \eta \boldsymbol{j}, \tag{5.29}$$

$$\rho_{\rm m} \left(\frac{\partial \boldsymbol{V}}{\partial t} + (\boldsymbol{V} \cdot \nabla) \boldsymbol{V} \right) = -\nabla p + \boldsymbol{j} \times \boldsymbol{B}, \tag{5.30}$$

$$\nabla \times \boldsymbol{B} = \mu_0 \boldsymbol{j}, \tag{5.31}$$

$$\nabla \times \boldsymbol{E} = -\frac{\partial \boldsymbol{B}}{\partial t}, \tag{5.32}$$

$$\nabla \cdot \boldsymbol{B} = 0, \tag{5.33}$$

$$\frac{\partial \rho_{\rm m}}{\partial t} + (\boldsymbol{V} \cdot \nabla) \rho_{\rm m} + \rho_{\rm m} \nabla \cdot \boldsymbol{V} = 0. \tag{5.34}$$

We may add the adiabatic equation as an equation of state;

$$\frac{\mathrm{d}}{\mathrm{d}t}(p\rho_{\mathrm{m}}^{-\gamma}) = 0,$$

where the quantity γ is the ratio of specific heats and $\gamma = (2+\delta)/\delta$ (δ is the number of degrees of freedom) is 5/3 in the three dimensional case $\delta = 3$. Combined with (5.34), the adiabatic equation becomes

$$\frac{\partial p}{\partial t} + (\boldsymbol{V}\cdot\nabla)p + \gamma p\nabla\cdot\boldsymbol{V} = 0. \tag{5.35}$$

In stead of this relation, we may use the more simple relation of incompressibility

$$\nabla\cdot\boldsymbol{V} = 0. \tag{5.36}$$

if $|(\mathrm{d}\rho/\mathrm{d}t)/\rho)| \ll |\nabla\cdot V|$. From (5.31),(5.32), the energy conservation law is given by

$$\frac{1}{\mu_0}\nabla\cdot(\boldsymbol{E}\times\boldsymbol{B}) + \frac{\partial}{\partial t}\left(\frac{B^2}{2\mu_0}\right) + \boldsymbol{E}\cdot\boldsymbol{j} = 0. \tag{5.37}$$

From (5.29), the third term in the left-hand side of (5.37) becomes

$$\boldsymbol{E}\cdot\boldsymbol{j} = \eta j^2 + (\boldsymbol{j}\times\boldsymbol{B})\cdot\boldsymbol{V}. \tag{5.38}$$

By use of (5.30),(5.34), Lorentz term in (5.38) is expressed by

$$(\boldsymbol{j}\times\boldsymbol{B})\cdot\boldsymbol{V} = \frac{\partial}{\partial t}(\frac{\rho_{\mathrm{m}}V^2}{2}) + \nabla\cdot(\frac{\rho_{\mathrm{m}}V^2}{2}\boldsymbol{V}) + \boldsymbol{V}\cdot\nabla p.$$

From (5.35), it follows that

$$-\nabla\cdot(p\boldsymbol{V}) = \frac{\partial p}{\partial t} + (\gamma-1)p\nabla\cdot\boldsymbol{V}$$

and

$$\boldsymbol{V}\cdot\nabla p = \frac{\partial}{\partial t}\left(\frac{p}{\gamma-1}\right) + \nabla\cdot\left(\frac{p}{\gamma-1}+p\right)\boldsymbol{V}.$$

Therefore the energy conservation law (5.37) is reduced to

$$\nabla\cdot(\boldsymbol{E}\times\boldsymbol{H}) + \frac{\partial}{\partial t}\left(\frac{\rho_{\mathrm{m}}V^2}{2} + \frac{p}{\gamma-1} + \frac{B^2}{2\mu_0}\right) + \eta j^2 + \nabla\cdot\left(\frac{\rho_{\mathrm{m}}V^2}{2} + \frac{p}{\gamma-1} + p\right)\boldsymbol{V} = 0. \tag{5.39}$$

The substitution of (5.29) into (5.32) yields

$$\frac{\partial\boldsymbol{B}}{\partial t} = \nabla\times(\boldsymbol{V}\times\boldsymbol{B}) - \eta\nabla\times\boldsymbol{j} = \nabla\times(\boldsymbol{V}\times\boldsymbol{B}) + \frac{\eta}{\mu_0}\Delta\boldsymbol{B} \tag{5.40}$$

$$\frac{\partial\boldsymbol{B}}{\partial t} = -(\boldsymbol{V}\cdot\nabla)\boldsymbol{B} - \boldsymbol{B}(\nabla\cdot\boldsymbol{V}) + (\boldsymbol{B}\cdot\nabla)\boldsymbol{V} + \frac{\eta}{\mu_0}\Delta\boldsymbol{B}. \tag{5.41}$$

Here we used vector formula for $\nabla\times(\boldsymbol{V}\times\boldsymbol{B})$ (see appendix) and $\nabla\times(\nabla\times\boldsymbol{B}) = -\Delta\boldsymbol{B}$ (valid only in the case of orthogonal coordinates). The quantity $\eta/\mu_0 = \nu_{\mathrm{m}}$ is called *magnetic viscosity*. The substitution of (5.31) into (5.30) yields

$$\rho_{\mathrm{m}}\frac{\mathrm{d}\boldsymbol{V}}{\mathrm{d}t} = -\nabla\left(p + \frac{B^2}{2\mu_0}\right) + \frac{1}{\mu_0}(\boldsymbol{B}\cdot\nabla)\boldsymbol{B}. \tag{5.42}$$

The equation of motion (5.42) and the equation of magnetic diffusion (5.41) are fundamental equations of magnetohydrodynamics. Equation (5.33) $\nabla \cdot \boldsymbol{B} = 0$, equation of continuity (5.34) and equation of state (5.35) or (5.36) are additional equations.

The ratio of the first term to the second term of the right-hand side in (5.40), $R_{\rm m}$, defined by

$$\frac{|\nabla \times (\boldsymbol{V} \times \boldsymbol{B})|}{|\Delta \boldsymbol{B}(\eta/\mu_0)|} \approx \frac{VB/L}{(B/L^2)(\eta/\mu_0)} = \frac{\mu_0 VL}{\eta} \equiv R_{\rm m} \tag{5.43}$$

is called *magnetic Reynolds number*. The notation L is a typical plasma size. Magnetic Reynolds number is equal to the ratio of magnetic diffusion time $\tau_{\rm R} = \mu_0 L^2/\eta$ to Alfven transit time $\tau_{\rm H} = L/v_{\rm A}$ (it is assumed that $v \approx v_{\rm A}$), that is, $R_{\rm m} = \tau_{\rm R}/\tau_{\rm H}$. When $R_{\rm m} \ll 1$, the magnetic field in a plasma changes according to diffusion equation. When $R_{\rm m} \gg 1$, it can be shown that the lines of magnetic force are frozen in the plasma. Let the magnetic flux within the surface element ΔS be $\Delta\Phi$, and take the z axis in the $\boldsymbol{B}$ direction. Then $\Delta\Phi$ is

$$\Delta\Phi = \boldsymbol{B} \cdot \boldsymbol{n}\Delta S = B\Delta x \Delta y.$$

As the boundary of ΔS moves, the rate of change of ΔS is

$$\frac{\mathrm{d}}{\mathrm{d}t}(\Delta x) = \frac{\mathrm{d}}{\mathrm{d}t}(x + \Delta x - x) = V_x(x + \Delta x) - V_x(x) = \frac{\partial V_x}{\partial x}\Delta x,$$

$$\frac{\mathrm{d}}{\mathrm{d}t}(\Delta S) = \left(\frac{\partial V_x}{\partial x} + \frac{\partial V_y}{\partial y}\right)\Delta x \Delta y.$$

The rate of change of the flux $\Delta\Phi$ is

$$\frac{\mathrm{d}}{\mathrm{d}t}(\Delta\Phi) = \frac{\mathrm{d}B}{\mathrm{d}t}\Delta S + B\frac{\mathrm{d}}{\mathrm{d}t}(\Delta S) = \left(\frac{\mathrm{d}\boldsymbol{B}}{\mathrm{d}t} + \boldsymbol{B}(\nabla \cdot \boldsymbol{V}) - (\boldsymbol{B} \cdot \nabla)\boldsymbol{V}\right)_z \Delta S = \frac{\eta}{\mu_{\rm o}}\Delta B_z(\Delta S). \tag{5.44}$$

(see (5.41)). When $R_{\rm m} \to \infty,\ \eta \to 0$, the rate of change of the flux becomes zero, i.e., $\mathrm{d}(\Delta\Phi)/\mathrm{d}t \to 0$. This means the magnetic flux is frozen in the plasma.

5.4 Magnetoacoustic Wave

As usual, we indicate zeroth-order quantities (in equilibrium state) by a subscript 0 and 1st-order perturbation terms by a subscript 1, that is, $\rho_{\rm m} = \rho_{\rm m0} + \rho_{\rm m1}$, $p = p_0 + p_1$, $\boldsymbol{V} = 0 + \boldsymbol{V}$, $\boldsymbol{B} = \boldsymbol{B}_0 + \boldsymbol{B}_1$. The case of $\eta = 0$ will be considered here. Then we find the 1st-order equations as follows:

$$\frac{\partial \rho_{\rm m1}}{\partial t} + \nabla \cdot (\rho_{\rm m0}\boldsymbol{V}) = 0, \tag{5.45}$$

$$\rho_{\rm m0}\frac{\partial \boldsymbol{V}}{\partial t} + \nabla p_1 = \boldsymbol{j}_0 \times \boldsymbol{B}_1 + \boldsymbol{j}_1 \times \boldsymbol{B}_0, \tag{5.46}$$

$$\frac{\partial p_1}{\partial t} + (\boldsymbol{V} \cdot \nabla)p_0 + \gamma p_0 \nabla \cdot \boldsymbol{V} = 0, \tag{5.47}$$

$$\frac{\partial \boldsymbol{B}_1}{\partial t} = \nabla \times (\boldsymbol{V} \times \boldsymbol{B}_0). \tag{5.48}$$

If displacement of the plasma from the equilibrium position $\boldsymbol{r}_0$ is denoted by $\boldsymbol{\xi}(\boldsymbol{r}_0, t)$, it follows that

$$\boldsymbol{\xi}(\boldsymbol{r}_0, t) = \boldsymbol{r} - \boldsymbol{r}_0,$$

$$\boldsymbol{V} = \frac{\mathrm{d}\boldsymbol{\xi}}{\mathrm{d}t} \approx \frac{\partial \boldsymbol{\xi}}{\partial t}. \tag{5.49}$$

The substitution of (5.49) into eqs.(5.48),(5.45),(5.47) yields

$$\boldsymbol{B}_1 = \nabla \times (\boldsymbol{\xi} \times \boldsymbol{B}_0), \tag{5.50}$$

$$\mu_0 \boldsymbol{j}_1 = \nabla \times \boldsymbol{B}_1, \tag{5.51}$$

$$\rho_{\mathrm{m}1} = -\nabla \cdot (\rho_{\mathrm{m}0} \boldsymbol{\xi}), \tag{5.52}$$

$$p_1 = -\boldsymbol{\xi} \cdot \nabla p_0 - \gamma p_0 \nabla \cdot \boldsymbol{\xi}. \tag{5.53}$$

Then equation (5.46) is reduced to

$$\rho_{\mathrm{m}0} \frac{\partial^2 \boldsymbol{\xi}}{\partial t^2} = \nabla(\boldsymbol{\xi} \cdot \nabla p_0 + \gamma p_0 \nabla \cdot \boldsymbol{\xi}) + \frac{1}{\mu_0}(\nabla \times \boldsymbol{B}_0) \times \boldsymbol{B}_1 + \frac{1}{\mu_0}(\nabla \times \boldsymbol{B}_1) \times \boldsymbol{B}_0. \tag{5.54}$$

Let us consider the case where $\boldsymbol{B}_0 = \text{const.}$ $p_0 = \text{const.}$, and the displacement is expressed by $\boldsymbol{\xi}(\boldsymbol{r}, t) = \boldsymbol{\xi}_1 \exp i(\boldsymbol{k} \cdot \boldsymbol{r} - \omega t)$, then (5.54) is reduced to

$$-\rho_{\mathrm{m}0}\omega^2 \boldsymbol{\xi}_1 = -\gamma p_0 (\boldsymbol{k} \cdot \boldsymbol{\xi}_1)\boldsymbol{k} - \mu_0^{-1} (\boldsymbol{k} \times (\boldsymbol{k} \times (\boldsymbol{\xi}_1 \times \boldsymbol{B}_0))) \times \boldsymbol{B}_0. \tag{5.55}$$

Using the vector formula $\boldsymbol{a} \times (\boldsymbol{b} \times \boldsymbol{c}) = \boldsymbol{b}\,(\boldsymbol{a} \cdot \boldsymbol{c}) - \boldsymbol{c}\,(\boldsymbol{a} \cdot \boldsymbol{b})$, we can write (5.55) as

$$\Big((\boldsymbol{k} \cdot \boldsymbol{B}_0)^2 - \mu_0 \omega^2 \rho_{\mathrm{m}0}\Big)\boldsymbol{\xi}_1 + \Big((B_0^2 + \mu_0 \gamma p_0)\boldsymbol{k} - (\boldsymbol{k} \cdot \boldsymbol{B}_0)\boldsymbol{B}_0\Big)(\boldsymbol{k} \cdot \boldsymbol{\xi}_1) - (\boldsymbol{k} \cdot \boldsymbol{B}_0)(\boldsymbol{B}_0 \cdot \boldsymbol{\xi}_1)\boldsymbol{k} = 0.$$

If the unit vectors of $\boldsymbol{k}$, $\boldsymbol{B}_0$ are denoted by $\widehat{\boldsymbol{k}} \equiv \boldsymbol{k}/k$, $\boldsymbol{b} \equiv \boldsymbol{B}_0/B_0$, and the notations $V \equiv \omega/k$, $v_{\mathrm{A}}^2 \equiv B_0^2/(\mu_0 \rho_{\mathrm{m}0})$, $\beta \equiv p_0/(B_0^2/2\mu_0)$, $\cos\theta \equiv (\widehat{\boldsymbol{k}} \cdot \widehat{\boldsymbol{b}})$ are introduced, we find

$$(\cos^2\theta - \frac{V^2}{v_{\mathrm{A}}^2})\boldsymbol{\xi}_1 + \left((1 + \frac{\gamma\beta}{2})\widehat{\boldsymbol{k}} - \cos\theta \boldsymbol{b}\right)(\widehat{\boldsymbol{k}} \cdot \boldsymbol{\xi}_1) - \cos\theta(\boldsymbol{b} \cdot \boldsymbol{\xi}_1)\widehat{\boldsymbol{k}} = 0. \tag{5.56}$$

The scalar product of (5.56) with $\widehat{\boldsymbol{k}}$ and $\boldsymbol{b}$, and the vector product of $\widehat{\boldsymbol{k}}$ with (5.56), yield

$$(1 + \frac{\gamma\beta}{2} - \frac{V^2}{v_{\mathrm{A}}^2})(\widehat{\boldsymbol{k}} \cdot \boldsymbol{\xi}_1) - \cos\theta(\boldsymbol{b} \cdot \boldsymbol{\xi}_1) = 0,$$

$$\frac{\gamma\beta}{2}\cos\theta(\widehat{\boldsymbol{k}} \cdot \boldsymbol{\xi}_1) - \frac{V^2}{v_{\mathrm{A}}^2}(\boldsymbol{b} \cdot \boldsymbol{\xi}_1) = 0,$$

$$(\cos^2\theta - \frac{V^2}{v_{\mathrm{A}}^2})\boldsymbol{b} \cdot (\widehat{\boldsymbol{k}} \times \boldsymbol{\xi}_1) = 0.$$

The solutions of these equations are magnetoacoustic wave. One solution is

$$V^2 = v_{\mathrm{A}}^2 \cos^2\theta, \qquad (\boldsymbol{\xi}_1 \cdot \boldsymbol{k}) = 0, \qquad (\boldsymbol{\xi}_1 \cdot \boldsymbol{B}_0) = 0. \tag{5.57}$$

Since $\boldsymbol{\xi}_1$ of this solution is orthogonal to $\boldsymbol{k}$ and $\boldsymbol{B}_0$, this is called torsional Alfvén wave (see sec.10.4). The other solutions are given by

$$\left(\frac{V}{v_{\mathrm{A}}}\right)^4 - (1 + \frac{\gamma\beta}{2})\left(\frac{V}{v_{\mathrm{A}}}\right)^2 + \frac{\gamma\beta}{2}\cos^2\theta = 0, \tag{5.58}$$

$$\boldsymbol{B}_0 \cdot (\boldsymbol{k} \times \boldsymbol{\xi}_1) = 0.$$

Since $\boldsymbol{\xi}_1$ of these solutions are coplaner with $\boldsymbol{k}$ and $\boldsymbol{B}_0$, these solutions are compressional mode. If the velocity of sound is denoted by $c_{\rm s}^2 = \gamma p_0/\rho_{\rm m0}$, (5.58) becomes

$$V^4 - (v_{\rm A}^2 + c_{\rm s}^2)V^2 + v_{\rm A}^2 c_{\rm s}^2 \cos^2\theta = 0$$

and

$$V_{\rm f}^2 = \frac{1}{2}\left(v_{\rm A}^2 + c_{\rm s}^2) + ((v_{\rm A}^2 + c_{\rm s}^2)^2 - 4v_{\rm A}^2 c_{\rm s}^2 \cos^2\theta)^{1/2}\right), \tag{5.59}$$

$$V_{\rm s}^2 = \frac{1}{2}\left(v_{\rm A}^2 + c_{\rm s}^2) - ((v_{\rm A}^2 + c_{\rm s}^2)^2 - 4v_{\rm A}^2 c_{\rm s}^2 \cos^2\theta)^{1/2}\right). \tag{5.60}$$

The solution of (5.59) is called compressional Alfvén wave (see sec.10.4) and the solution of (5.60) is called *magnetoacoustic slow wave.* Characteristic velocity

$$v_{\rm A}^2 = \frac{B^2}{\mu_0 \rho_{\rm m0}}$$

is called *Alfvén velocity.* The plasma with zero resistivity is frozen to the magnetic field. There is tension $B^2/2\mu_0$ along the magnetic field line. As the plasma, of mass density $\rho_{\rm m}$, sticks to the field lines, the magnetoacoustic waves can be considered as waves propagating along the strings of magnetic field lines (see sec.10.4).

Ch.6 Equilibrium

In order to maintain a hot plasma, we must confine and keep it away from the vacuum-container wall. The most promising method for such confinement of a hot plasma is the use of appropriate strong magnetic fields. An equilibrium condition must be satisfied for such magnetic confinement systems.

6.1 Pressure Equilibrium

When a plasma is in the steady state, magnetohydrodynamic equation (5.30) yields the equilibrium equation

$$\nabla p = \boldsymbol{j} \times \boldsymbol{B}, \tag{6.1}$$

and

$$\nabla \times \boldsymbol{B} = \mu_0 \boldsymbol{j}, \tag{6.2}$$

$$\nabla \cdot \boldsymbol{B} = 0, \tag{6.3}$$

$$\nabla \cdot \boldsymbol{j} = 0. \tag{6.4}$$

From the equilibrium equation (6.1), it follows that

$$\boldsymbol{B} \cdot \nabla p = 0, \tag{6.5}$$

$$\boldsymbol{j} \cdot \nabla p = 0. \tag{6.6}$$

Equation (6.5) indicates that $\boldsymbol{B}$ and ∇p are orthogonal, and the surfaces of constant pressure coincide with the magnetic surfaces. Equation (6.6) shows that the current-density vector $\boldsymbol{j}$ is everywhere parallel to the constant-pressure surfaces. Substitution of (6.2) into (6.1) yields

$$\nabla \left(p + \frac{B^2}{2\mu_0} \right) = (\boldsymbol{B} \cdot \nabla) \frac{\boldsymbol{B}}{\mu_0} = B^2 \left(-\frac{1}{R} \boldsymbol{n} + \frac{\partial B / \partial l}{B} \boldsymbol{b} \right). \tag{6.7}$$

The following vector relations were used here;

$$\boldsymbol{B} \times (\nabla \times \boldsymbol{B}) + (\boldsymbol{B} \cdot \nabla) \boldsymbol{B} = \nabla (B^2/2), \qquad (\boldsymbol{B} \cdot \nabla) \boldsymbol{B} = B^2 [(\boldsymbol{b} \cdot \nabla) \boldsymbol{b} + \boldsymbol{b}((\boldsymbol{b} \cdot \nabla) B)/B].$$

R is the radius of curvature of the line of magnetic force and $\boldsymbol{n}$ is the unit vector directed toward a point on the line of magnetic force from the center of curvature. l is the length along the field line. We find the right-hand side of (6.7) can be neglected when the radius of curvature is much larger than the length over which the magnitude p changes appreciably, i.e., the size of the plasma, and the variation of $\boldsymbol{B}$ along the line of magnetic force is much smaller than the variation of $\boldsymbol{B}$ in the perpendicular direction. Then (6.7) becomes

$$p + \frac{B^2}{2\mu_0} \sim \frac{B_0^2}{2\mu_0},$$

where B_0 is the the value of the magnetic field at the plasma boundary (p=0).
When the system is axially symmetric and $\partial / \partial z = 0$, (6.7) exactly reduces to

$$\frac{\partial}{\partial r} \left(p + \frac{B_z^2 + B_\theta^2}{2\mu_0} \right) = -\frac{B_\theta^2}{r\mu_0}. \tag{6.8}$$

By the multiplification of (6.8) by r^2 and the integration by parts we obtain

$$\left(p+\frac{B_z^2+B_\theta^2}{2\mu_0}\right)_{r=a}=\frac{1}{\pi a^2}\int_0^a\left(p+\frac{B_z^2}{2\mu_0}\right)2\pi r\mathrm{d}r$$

i.e.,

$$\langle p\rangle+\frac{\langle B_z^2\rangle}{2\mu_0}=p_a+\frac{B_z^2(a)+B_\theta^2(a)}{2\mu_0}. \tag{6.9}$$

$\langle\ \rangle$ is the volume average. As $B^2/2\mu_0$ is the pressure of the magnetic field, (6.9) is the equation of pressure equilibrium. The ratio of plasma pressure to the pressure of the external magnetic field B_0

$$\beta\equiv\frac{p}{B_0^2/2\mu_0}=\frac{n(T_\mathrm{e}+T_\mathrm{i})}{B_0^2/2\mu_0} \tag{6.10}$$

is called the *beta ratio*. For a confined plasma, β is always smaller than 1, and is used as a figure of merit of the confining magnetic field. The fact that the internal magnetic field is smaller than the external field indicates the *diamagnetism* of the plasma.

6.2 Equilibrium Equation for Axially or Translationally Symmetric Systems

Let us use cylindrical coordinates (r,φ,z) and denote the magnetic surface by ψ. The magnetic surface ψ in an axisymmetric system is given by (see (3.24))

$$\psi=rA_\varphi(r,z) \tag{6.11}$$

where (r,φ,z) are cylindrical coordinates and the r and z components of the magnetic field are given by

$$rB_r=-\frac{\partial\psi}{\partial z},\qquad rB_z=\frac{\partial\psi}{\partial r}. \tag{6.12}$$

The relation $\boldsymbol{B}\cdot\nabla p=0$ follows from the equilibrium equation and is expressed by

$$-\frac{\partial\psi}{\partial z}\frac{\partial p}{\partial r}+\frac{\partial\psi}{\partial r}\frac{\partial p}{\partial z}=0.$$

Accordingly p is a functon of ψ only, i.e.,

$$p=p(\psi).$$

Similarly, from $\boldsymbol{j}\cdot\nabla p=0$ and $\nabla\times\boldsymbol{B}=\mu_0\boldsymbol{j}$, we may write

$$-\frac{\partial p}{\partial r}\frac{\partial(rB_\varphi)}{\partial z}+\frac{\partial p}{\partial z}\frac{\partial(rB_\varphi)}{\partial r}=0.$$

This means that rB_φ is a function of ψ only and

$$rB_\varphi=\frac{\mu_0 I(\psi)}{2\pi}. \tag{6.13}$$

Equation (6.13) indicates that $I(\psi)$ means the current flowing in the poloidal direction through the circular cross section within $\psi=rA_\varphi$ (fig.6.1). The r component of $\boldsymbol{j}\times\boldsymbol{B}=\nabla p$ leads to the equation on ψ :

$$L(\psi)+\mu_0 r^2\frac{\partial p(\psi)}{\partial\psi}+\frac{\mu_0^2}{8\pi^2}\frac{\partial I^2(\psi)}{\partial\psi}=0 \tag{6.14}$$

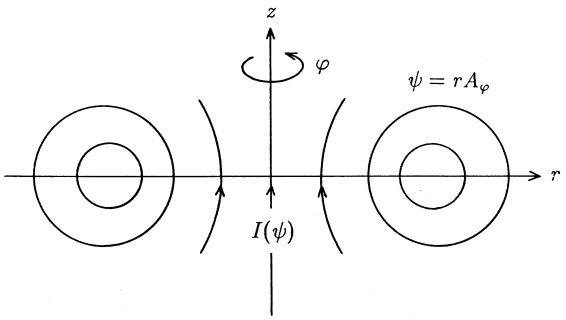

Fig.6.1 Magnetic surfaces $\psi = rA_\varphi$ and $I(\psi)$

where

$$L(\psi) \equiv \left(r\frac{\partial}{\partial r}\frac{1}{r}\frac{\partial}{\partial r} + \frac{\partial^2}{\partial z^2} \right) \psi.$$

This equation is called *Grad-Shafranov equation*. The current density is expressed in term of the function of the magnetic surface as

$$j_r = \frac{-1}{2\pi r}\frac{\partial I(\psi)}{\partial z}, \qquad j_z = \frac{1}{2\pi r}\frac{\partial I(\psi)}{\partial r},$$

$$j_\varphi = \frac{-1}{\mu_0}\left(\frac{\partial}{\partial r}\frac{1}{r}\frac{\partial \psi}{\partial r} + \frac{1}{r}\frac{\partial^2 \psi}{\partial z^2} \right) = -\frac{L(\psi)}{\mu_0 r}$$

$$= \frac{1}{\mu_0 r}\left(\mu_0 r^2 p' + \frac{\mu_0^2}{8\pi^2}(I^2)' \right)$$

or

$$\boldsymbol{j} = \frac{I'}{2\pi}\boldsymbol{B} + p' r \boldsymbol{e}_\varphi,$$

$$L(\psi) + \mu_0 r j_\varphi = 0.$$

The functions $p(\psi)$ and $I^2(\psi)$ are arbitrary functions of ψ. Let us assume that p and I^2 are linear functions of ψ. The ψ_b is the value of ψ at the plasma boundary. When the values at the boundary are $p = p_\mathrm{b},\ I^2 = I_\mathrm{b}^2$, then p and I^2 are expressed by

$$p(\psi) = p_\mathrm{b} - \frac{a}{\mu_0 R^2}(\psi - \psi_\mathrm{b}),$$

$$I^2(\psi) = I_\mathrm{b}^2 + \frac{8\pi^2}{\mu_0^2} b(\psi - \mathrm{b}).$$

Then we have

$$\mu_0 r j_\varphi = \left(\mu_0 r^2 p' + \frac{\mu_0^2}{8\pi^2}(I^2)' \right)(\psi - \psi_\mathrm{b}) = -\frac{a r^2}{R^2}(\psi - \psi_\mathrm{b}) - b(\psi - \psi_\mathrm{b})$$

$$= r^2 \left(\mu_0 (p - p_\mathrm{b}) - \frac{\mu_0^2}{8\pi^2}\left(\frac{I^2}{r^2} - \frac{I_\mathrm{b}^2}{r^2}\right) \right) = r^2 \mu_0 \left((p - p_\mathrm{b}) + \frac{1}{2\mu_0}(B_\varphi^2 - B_{\varphi\mathrm{B}}^2) \right),$$

$$\int_V \frac{1}{r^2}(\psi - \psi_\mathrm{b}) L(\psi) \mathrm{d}V = 2\pi \oint \frac{1}{r}(\psi - \psi_\mathrm{b}) \left((\nabla\psi)_r \mathrm{d}z + (\nabla\psi)_z \mathrm{d}r \right) - \int_V \frac{1}{r^2}(\nabla\psi)^2 \mathrm{d}V$$

$$= -\int_V (B_r^2 + B_z^2).$$

Equation (6.14) of equilibrium equation is reduced to

$$\int (p - p_{\rm s}) {\rm d}V = \int \frac{1}{2\mu_0} \left(B_{\varphi {\rm b}}^2 - B_\varphi^2 + 2(B_r^2 + B_z^2) \right) {\rm d}V.$$

This is the equation of pressure balance under the assumption made on $p(\psi)$ and $I(\psi)$.

Exact Solution of Grad -Shafranov equation

When the unit vectors with the directions of r, φ, z are denoted by $\boldsymbol{e}_r, \boldsymbol{e}_\varphi, \boldsymbol{e}_z$, respectively, then we have $\nabla\varphi = \boldsymbol{e}_\varphi / R$, $\boldsymbol{e}_r \times \boldsymbol{e}_\varphi = \boldsymbol{e}_z$, $\boldsymbol{e}_z \times \boldsymbol{e}_\varphi = -\boldsymbol{e}_r$. Therefore, $\boldsymbol{B}$ can be expressed from (6.12) and (6.13) as follows:

$$\boldsymbol{B} = \frac{\mu_0 I(\psi)}{2\pi} \nabla\varphi + \nabla\psi \times \nabla\varphi.$$

$p(\psi)$, $I^2(\psi)$ are arbitrary functions of ψ. When they are linear or quadratic functions of ψ, (6.14) becomes a linear differential equation. Let us consider a simple linear case of ψ. At the plasma boundary $\psi = \psi_{\rm b}$, we denote $p_{\rm b} = p(\psi_{\rm b})$ and $I_{\rm b}^2 = I^2(\psi_{\rm b})$; that is,

$$p(\psi) = p_{\rm b} - \frac{a}{\mu_0 R^2}(\psi - \psi_{\rm b}),$$

$$I^2(\psi) = I_{\rm b}^2 - \frac{8\pi^2}{\mu_0^2} b(\psi - \psi_{\rm b}).$$

Then (6.14) is reduced to

$$L(\psi) = a\frac{r^2}{R^2} + b = -\mu_0 r j_\varphi.$$

We set the position of the magnetic axis to $(R, 0)$. The following function

$$\psi - \psi_0 = \frac{b+a}{1+\epsilon} \left[\frac{1}{2} \left(1 + c\frac{r^2 - R^2}{R^2} \right) z^2 + \frac{\epsilon}{8R^2}(r^2 - R^2)^2 + \right.$$

$$\left. \frac{(1+\epsilon)b - (1-c)(b+a)}{24(b+a)R^4}(r^2 - R^2)^3 \right] \tag{6.15}$$

is the solution, which is correct up to the cubic of $(r - R), z$. The notations ϵ, c are constant and $\psi_0 = \psi(R, 0)$. When the coefficient of the third term of the right-hand side of (6.15) is 0, that is,

$$(1+\epsilon)b - (1-c)(b+a) = 0 \quad \rightarrow \quad \epsilon = -(c-1)(a/b) - c$$

(6.15) becomes the exact Solovev solution of the Grad-Shafranov equation (6.14). When we set $c = R^2/(R^2 - R_{\rm x}^2)$, ϵ becomes $\epsilon = -(a/b + R^2/R_{\rm x}^2)R_{\rm x}^2/(R^2 - R_{\rm x}^2)$ and then (6.15) is reduced to (ref.[1])

$$\psi = \frac{b}{2} \left(1 - \frac{r^2}{R_{\rm x}^2} \right) z^2 + \frac{a + (R^2/R_{\rm x}^2)b}{8R^2} \left((r^2 - R^2)^2 - (R^2 - R_{\rm x}^2)^2 \right). \tag{6.16}$$

(6.16) is an exact equilibrium solution in the interior region of plasma surrounded by the conductive wall specified by $\psi(r, z) = \psi_{\rm b}$. The surface $\psi(r, z) = 0$ is the separatrix surface (refer to fig.6.2). The separatrix points X are located at $(R_{\rm x}, \pm Z_{\rm x})$, where $Z_{\rm x}$ is $Z_{\rm x} = [-(a/b + R^2/R_{\rm x}^2)(1 - R_{\rm x}^2/R^2)/2]^{1/2} R_{\rm x}$. The maximum value $R_{\max}$ of r within the separatrix surface is $R_{\max} = (2 - R_{\rm x}^2/R^2)^{1/2} R$.

When we set the separatrix surface as the plasma boundary ($\psi_{\rm b} = 0$), the aspect ratio A, elongation ratio $\kappa_{\rm s}$, and central poloidal beta β_{p0} are

$$\frac{1}{A} = \frac{R_{\max} - R_{\rm x}}{2R} = \frac{(2 - R_{\rm x}^2/R^2)^{1/2} - R_{\rm x}/R}{2}$$

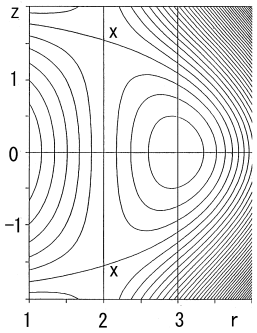

Fig.6.2 The contour (magnetic surface) of the flux function ψ of (6.16) in the case of $a/b = 4.4$, $R = 3$, $R_{\rm x} = 2$. Xs are the separatrix points and the magnetic surface passing X points is the separatix surface.

$$\kappa_{\rm s} = \frac{2Z_{\rm x}}{R_{\rm max} - R_{\rm x}} = \frac{AZ_{\rm x}}{R}$$

$$\beta_{p0} \equiv \frac{p(R,0) - p_{\rm b}}{B_z^2(R_{\rm x},0)/2\mu_0} = \frac{a}{a + (R^2/R_{\rm x}^2)b}.$$

When A and $\kappa_{\rm s}$ are specified, β_{p0} is fixed. To avoid this inadequateness, Weening (ref.[2]) added an additional particular solution $r^2\ln(r^2/R_\alpha^2) - r^2$ to Solovev solution; that is,

$$\psi = \frac{b+d}{2}\left(1 - \frac{r^2}{R_{\rm x}^2}\right)z^2 + \frac{a + (R^2/R_{\rm x}^2)(b+d)}{8R^2}\left((r^2 - R^2)^2 - (R^2 - R_{\rm x}^2)^2\right) \qquad (6.17)$$

$$-\frac{d}{4}\left(r^2\ln\frac{r^2}{R_{\rm x}^2} - (r^2 - R_{\rm x}^2)\right).$$

When the plasma boundary is chosen to be the separatrix $\psi(r,z) = 0$, the aspect ratio A, elongation ratio $\kappa_{\rm s}$, and central poloidal beta β_{p0} are

$$\frac{Z_{\rm x}^2}{R_{\rm x}^2} = -\frac{1}{2}\left(\frac{a}{b+d} + \frac{R^2}{R_{\rm x}^2}\right)\left(1 - \frac{R_{\rm x}^2}{R^2}\right)$$

$$\frac{R_{\rm max}^2}{R^2} = \left(2 - \frac{R_{\rm x}^2}{R^2}\right) + \frac{2d[x\ln x/(x-1) - 1]}{a + (R^2/R_{\rm x}^2)(b+d)}, \qquad x \equiv \frac{R_{\rm max}^2}{R_{\rm x}^2}$$

$$\frac{1}{A} = \frac{R_{\rm max}/R - R_{\rm x}/R}{2}, \quad \kappa_{\rm s} = \frac{AZ_{\rm x}}{R}$$

$$\beta_{p0} = \frac{a}{a + (R^2/R_{\rm x}^2)(b+d)}\left[1 + \frac{2d(\ln(R^2/R_{\rm x}^2) - (1 - R^2/R_{\rm x}^2))}{(a + (R^2/R_{\rm x}^2)(b+d))(1 - R_{\rm x}^2/R^2)}\right].$$

The magnetic surface ψ, the magnetic field $\boldsymbol{B}$ and the pressure p in translationally symmetric system ($\partial/\partial z = 0$) are given by

$$\psi = A_z(r,\theta),$$

$$B_r = \frac{1}{r}\frac{\partial\psi}{\partial\theta}, \quad B_\theta = -\frac{\partial\psi}{\partial r}, \quad B_z = \frac{\mu_0}{2\pi}I(\psi),$$

$$p = p(\psi).$$

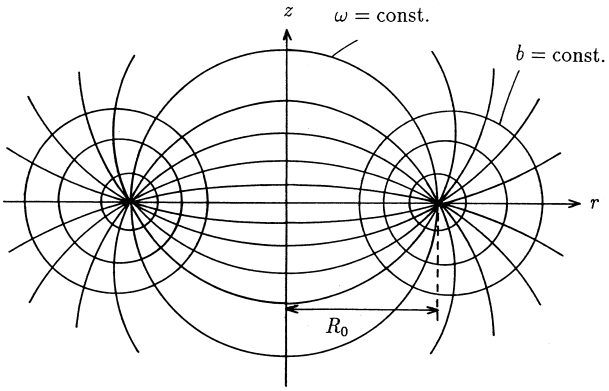

Fig.6.3 Toroidal coordinates.

The equilibrium equation is reduced to

$$\frac{1}{r}\frac{\partial}{\partial r}\left(r\frac{\partial \psi}{\partial r}\right)+\frac{1}{r^2}\frac{\partial^2 \psi}{\partial \theta^2}+\mu_0\frac{\partial p(\psi)}{\partial \psi}+\frac{\mu_0^2}{8\pi^2}\frac{\partial I^2(\psi)}{\partial \psi}=0,$$

$$\boldsymbol{j}=\frac{1}{2\pi}I'\boldsymbol{B}+p'\boldsymbol{e}_z,$$

$$\Delta\psi+\mu_0 j_z=0.$$

It is possible to drive the similar equilibrium equation in the case of helically symmetric system.

6.3 Tokamak Equilibrium (ref.[3])

The equilibrium equation for an axially symmetric system is given by (6.14). The 2nd and 3rd terms of the left-hand side of the equation are zero outside the plasma region. Let us use toroidal coordinates (b,ω,φ) (fig.6.3). The relations between these to cylindrical coordinates (r,φ,z) are

$$r=\frac{R_0\sinh b}{\cosh b-\cos\omega},\qquad z=\frac{R_0\sin\omega}{\cosh b-\cos\omega}.$$

The curves $b=b_0$ are circles of radius $a=R_0\sinh b_0$, centered at $r=R_0\coth b_0,\ z=0$. The curves $\omega=$const. are also circles with the center at $r=0, a=R_0\cos\omega/\sin\omega$. When the magnetic-surface function ψ is replaced by F, according to

$$\psi=\frac{F(b,\omega)}{2^{1/2}(\cosh b-\cos\omega)^{1/2}}$$

the function F satisfies

$$\frac{\partial^2 F}{\partial b^2}-\coth b\frac{\partial F}{\partial b}+\frac{\partial^2 F}{\partial \omega^2}+\frac{1}{4}F=0$$

outside the plasma region. When F is expanded as

$$F=\Sigma g_n(b)\cos n\omega,$$

the coefficient g_n satisfies

$$\frac{\mathrm{d}^2 g_n}{\mathrm{d}b^2}-\coth b\frac{\mathrm{d}g_n}{\mathrm{d}b}-\left(n^2-\frac{1}{4}\right)g_n=0.$$

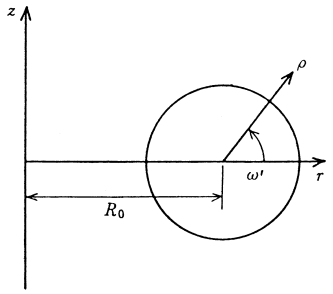

Fig.6.4 The coordinates r, z and ρ, ω'

There are two independent solutions:

$$\left(n^2 - \frac{1}{4}\right) g_n = \sinh b \frac{\mathrm{d}}{\mathrm{d}b} Q_{n-1/2}(\cosh b), \qquad \left(n^2 - \frac{1}{4}\right) f_n = \sinh b \frac{\mathrm{d}}{\mathrm{d}b} P_{n-1/2}(\cosh b).$$

$P_\nu(x)$ and $Q_\nu(x)$ are Legendre functions. If the ratio of the plasma radius to the major radius a/R_0 is small, i.e., when $e^{b_0} \gg 1$, then g_n and f_n are given by

$$g_0 = e^{b/2}, \quad g_1 = -\frac{1}{2} e^{-b/2}, \qquad f_0 = \frac{2}{\pi} e^{b/2}(b + \ln 4 - 2), \quad f_1 = \frac{2}{3\pi} e^{3b/2}.$$

If we take terms up to $\cos\omega$, F and ψ are

$$F = c_0 g_0 + d_0 f_0 + 2(c_1 g_1 + d_1 f_1)\cos\omega,$$

$$\psi = \frac{F}{2^{1/2}(\cosh b - \cos\omega)^{1/2}} \approx e^{-b/2}(1 + e^{-b}\cos\omega)F.$$

Use the coordinates ρ, ω' shown in fig.6.4. These are related to the cylindrical and toroidal coordinates as follows:

$$r = R_0 + \rho\cos\omega' = \frac{R_0 \sinh b}{\cosh b - \cos\omega} \qquad z = \rho\sin\omega' = \frac{R_0 \sin\omega}{\cosh b - \cos\omega}.$$

When b is large, the relations are

$$\omega' = \omega, \qquad \frac{\rho}{2R_0} \approx e^{-b}.$$

Accordingly the magnetic surface ψ is expressed by

$$\begin{aligned}\psi =& c_0 + \frac{2}{\pi} d_0 (b + \ln 4 - 2) \\ &+ \left[\left(c_0 + \frac{2}{\pi} d_0 (b + \ln 4 - 2)\right) e^{-b} + \left(\frac{4}{3\pi} d_1 e^b - c_1 e^{-b}\right)\right] \cos\omega \\ =& d_0' \left(\ln \frac{8R}{\rho} - 2\right) + \left(\frac{d_0'}{2R}\left(\ln \frac{8R}{\rho} - 1\right)\rho + \frac{h_1}{\rho} + h_2 \rho\right)\cos\omega.\end{aligned}$$

In terms of ψ, the magnetic-field components are given by

$$rB_r = -\frac{\partial\psi}{\partial z}, \qquad rB_z = \frac{\partial\psi}{\partial r},$$
$$rB_\rho = -\frac{\partial\psi}{\rho\partial\omega'}, \qquad rB_{\omega'} = \frac{\partial\psi}{\partial\rho}.$$

From the relation

$$-\frac{d_0'}{\rho} = r\overline{B}_{\omega'} \approx R\frac{-\mu_0 I_\mathrm{p}}{2\pi\rho},$$

the parameter d_0' can be taken as $d_0' = \mu_0 I_\mathrm{p} R/2\pi$. Here I_p is the total plasma current in the φ direction. The expression of the magnetic surface is reduced to

$$\psi = \frac{\mu_0 I_\mathrm{p} R}{2\pi}\left(\ln\frac{8R}{\rho} - 2\right) + \left(\frac{\mu_0 I_\mathrm{p}}{4\pi}\left(\ln\frac{8R}{\rho} - 1\right)\rho + \frac{h_1}{\rho} + h_2\rho\right)\cos\omega' \tag{6.18}$$

where R_0 has been replaced by R. In the case of $a/R \ll 1$, the equation of pressure equilibrium (6.9) is

$$\langle p\rangle - p_a = \frac{1}{2\mu_0}((B_{\varphi\mathrm{v}}^2)_a + (B_r^2 + B_z^2)_a - \langle B_\varphi^2\rangle).$$

Here $\langle\ \rangle$ indicates the volume average and p_a is the plasma pressure at the plasma boundary. The value of $B_r^2 + B_z^2$ is equal to $B_{\omega'}^2$. The ratio of $\langle p\rangle$ to $\langle B_{\omega'}^2\rangle/2\mu_0$ is called the *poloidal beta ratio* β_p. When $p_a = 0$, β_p is

$$\beta_\mathrm{p} = 1 + \frac{B_{\varphi\mathrm{v}}^2 - \langle B_\varphi^2\rangle}{B_{\omega'}^2} \approx 1 + \frac{2B_{\varphi\mathrm{v}}}{B_{\omega'}^2}\langle B_{\varphi\mathrm{v}} - B_\varphi\rangle.$$

B_φ and $B_{\varphi\mathrm{v}}$ are the toroidal magnetic fields in the plasma and the vacuum toroidal fields respectively. When B_φ is smaller than $B_{\varphi\mathrm{v}}$, the plasma is diamagnetic, $\beta_\mathrm{p} > 1$. When B_φ is larger than $B_{\varphi\mathrm{v}}$, the plasma is *paramagnetic*, $\beta_\mathrm{p} < 1$. When the plasma current flows along a line of magnetic force, the current produces the poloidal magnetic field $B_{\omega'}$ and a poloidal component of the plasma current appears and induces an additional toroidal magnetic field. This is the origin of the paramagnetism.

When the function (6.18) is used, the magnetic field is given by

$$\left.\begin{aligned} B_{\omega'} &= \frac{1}{r}\frac{\partial\psi}{\partial\rho} = \frac{-\mu_0 I_\mathrm{p}}{2\pi\rho} + \left(\frac{\mu_0 I_\mathrm{p}}{4\pi R}\ln\frac{8R}{\rho} + \frac{1}{R}\left(h_2 - \frac{h_1}{\rho^2}\right)\right)\cos\omega', \\ B_\rho &= -\frac{1}{r\rho}\frac{\partial\psi}{\partial\omega'} = \left(\frac{\mu_0 I_\mathrm{p}}{4\pi R}\left(\ln\frac{8R}{\rho} - 1\right) + \frac{1}{R}\left(h_2 + \frac{h_1}{\rho^2}\right)\right)\sin\omega'. \end{aligned}\right\} \tag{6.19}$$

The cross section of the magnetic surface is the form of

$$\psi(\rho,\omega') = \psi_0(\rho) + \psi_1\cos\omega'.$$

When $\Delta = -\psi_1/\psi_0'$ is much smaller than ρ, the cross section is a circle whose center is displaced by an amount (see fig.6.5)

$$\Delta(\rho) = \frac{\rho^2}{2R}\left(\ln\frac{8R}{\rho} - 1\right) + \frac{2\pi}{\mu_0 I_\mathrm{p} R}(h_1 + h_2\rho^2).$$

Let us consider the parameters h_1 and h_2. As will be shown in sec.6.4, the poloidal component $B_{\omega'}$ of the magnetic field at the plasma surface ($r = a$) must be

$$B_{\omega'}(a,\omega') = B_a\left(1 + \frac{a}{R}\Lambda\cos\omega'\right) \tag{6.20}$$

at equilibrium. a is the plasma radius and

$$\Lambda = \beta_\mathrm{p} + \frac{l_\mathrm{i}}{2} - 1 \tag{6.21}$$

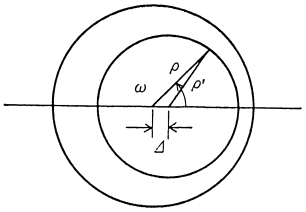

Fig.6.5 Displacement of the plasma column.
$\psi_0(\rho') = \psi_0(\rho) - \psi_0'(\rho)\Delta\cos\omega$, $\rho' = \rho - \Delta\cos\omega$.

and $\beta_{\rm p}$ is the poloidal beta ratio

$$\beta_{\rm p} = \frac{p}{(B_a^2/2\mu_0)} \tag{6.22}$$

and $l_{\rm i}$ is

$$l_{\rm i} = \frac{\int B_{\omega'}^2 \rho {\rm d}\rho {\rm d}\omega'}{\pi a^2 B_a^2}. \tag{6.23}$$

The parameters h_1 and h_2 must be chosen to satisfy $B_\rho = 0$ and $B_{\omega'} = B_a(1 + (a/R)\Lambda\cos\omega')$ at the plasma boundary, i.e.,

$$h_1 = \frac{\mu_0 I_{\rm p}}{4\pi} a^2 \left(\Lambda + \frac{1}{2}\right), \qquad h_2 = -\frac{\mu_0 I_{\rm p}}{4\pi}\left(\ln\frac{8R}{a} + \Lambda - \frac{1}{2}\right). \tag{6.24}$$

Accordingly ψ is given by

$$\psi = \frac{\mu_0 I_{\rm p} R}{2\pi}\left(\ln\frac{8R}{\rho} - 2\right) - \frac{\mu_0 I_{\rm p}}{4\pi}\left(\ln\frac{\rho}{a} + \left(\Lambda + \frac{1}{2}\right)\left(1 - \frac{a^2}{\rho^2}\right)\right)\rho\cos\omega'. \tag{6.25}$$

The term $h_2\rho\cos\omega'$ in ψ brings in the homogeneous vertical field

$$B_z = \frac{h_2}{R},$$

which is to say that we must impose a vertical external field. When we write $\psi_{\rm e} = h_2\rho\cos\omega'$ so that ψ is the sum of two terms, $\psi = \psi_{\rm p} + \psi_{\rm e}$, $\psi_{\rm e}$ and $\psi_{\rm p}$ are expressed by

$$\psi_{\rm e} = -\frac{\mu_0 I_{\rm p}}{4\pi}\left(\ln\frac{8R}{a} + \Lambda - \frac{1}{2}\right)\rho\cos\omega' \tag{6.26}$$

$$\psi_{\rm p} = \frac{\mu_0 I_{\rm p} R}{2\pi}\left(\ln\frac{8R}{\rho} - 2\right) + \frac{\mu_0 I_{\rm p}}{4\pi}\left(\left(\ln\frac{8R}{\rho} - 1\right)\rho + \frac{a^2}{\rho}\left(\Lambda + \frac{1}{2}\right)\right)\cos\omega'. \tag{6.27}$$

These formulas show that a uniform magnetic field in the z direction,

$$B_\perp = -\frac{\mu_0 I_{\rm p}}{4\pi R}\left(\ln\frac{8R}{a} + \Lambda - \frac{1}{2}\right), \tag{6.28}$$

must be applied in order to maintain a toroidal plasma in equilibrium (fig.6.6). This vertical field weakens the inside poloidal field and strengthens the outside poloidal field.

The amount of $B_\perp$ (6.28) for the equilibrium can be derived more intuitively. The *hoop force* by which the current ring of a plasma tends to expand is given by

$$F_{\rm h} = -\frac{\partial}{\partial R}\frac{L_{\rm p} I_{\rm p}^2}{2}\bigg|_{L_{\rm p}I_{\rm p}={\rm const.}} = \frac{1}{2} I_{\rm p}^2 \frac{\partial L_{\rm p}}{\partial R},$$

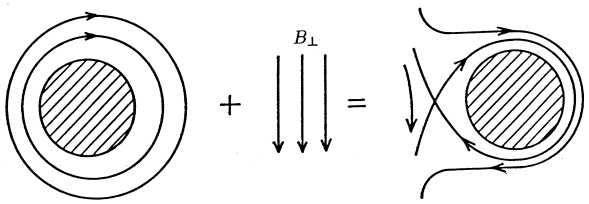

Fig.6.6 Poloidal magnetic field due to the combined plasma current and vertical magnetic field.

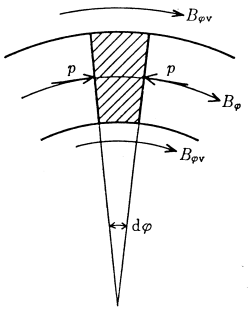

Fig.6.7 Equilibrium of forces acting on a toroidal plasma.

where L_p is the self-inductance of the current ring:

$$L_\mathrm{p} = \mu_0 R \left(\ln \frac{8R}{a} + \frac{l_\mathrm{i}}{2} - 2 \right).$$

Accordingly, the hoop force is

$$F_\mathrm{h} = \frac{\mu_0 I_\mathrm{p}^2}{2} \left(\ln \frac{8R}{a} + \frac{l_\mathrm{i}}{2} - 1 \right).$$

The outward force F_p exerted by the plasma pressure is (fig.6.7)

$$F_\mathrm{p} = \langle p \rangle \pi a^2 2\pi.$$

The inward (contractive) force F_{B1} due to the tension of the toroidal field inside the plasma is

$$F_{B1} = -\frac{\langle B_\varphi^2 \rangle}{2\mu_0} 2\pi^2 a^2$$

and the outward force F_B2 by the pressure due to the external magnetic field is

$$F_{B2} = \frac{B_{\varphi \mathrm{v}}^2}{2\mu_0} 2\pi^2 a^2.$$

The force F_I acting on the plasma due to the vertical field $B_\perp$ is

$$F_\mathrm{I} = I_\mathrm{p} B_\perp 2\pi R.$$

Balancing these forces gives

$$\frac{\mu_0 I_\mathrm{p}^2}{2} \left(\ln \frac{8R}{a} + \frac{l_\mathrm{i}}{2} - 1 \right) + 2\pi^2 a^2 \left(\langle p \rangle + \frac{B_{\varphi \mathrm{v}}^2}{2\mu_0} - \frac{\langle B_\varphi^2 \rangle}{2\mu_0} \right) + 2\pi R I_\mathrm{p} B_\perp = 0,$$

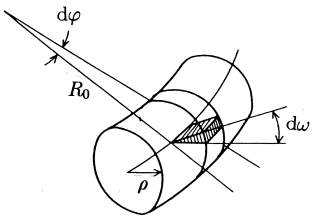

Fig.6.8 Volume element of a toroidal plasma.

and the amount of $B_\perp$ necessary is

$$B_\perp = \frac{-\mu_0 I_\mathrm{p}}{4\pi R}\left(\ln\frac{8R}{a} + \frac{l_\mathrm{i}}{2} - 1 + \beta_\mathrm{p} - \frac{1}{2}\right),$$

where $\Lambda = \beta_\mathrm{p} + l_\mathrm{i}/2 - 1$. Eq.(6.9) is used for the derivation.

6.4 Poloidal Field for Tokamak Equilibrium

The plasma pressure and the magnetic stress tensor are given by (ref.[4])

$$T_{\alpha\beta} = \left(p + \frac{B^2}{2\mu_0}\right)\delta_{\alpha\beta} - \frac{B_\alpha B_\beta}{\mu_0}.$$

Let us consider a volume element bounded by $(\omega, \omega+\mathrm{d}\omega)$, $(\varphi, \varphi+\mathrm{d}\varphi)$, and $(0, a)$ as is shown in fig.6.8. Denote the unit vectors in the directions r, z, φ and ρ, ω by $\boldsymbol{e}_r, \boldsymbol{e}_z, \boldsymbol{e}_\varphi$ and $\boldsymbol{e}_\rho, \boldsymbol{e}_\omega$, respectively. The relations between these are

$$\boldsymbol{e}_\rho = \boldsymbol{e}_r\cos\omega + \boldsymbol{e}_z\sin\omega, \qquad \boldsymbol{e}_\omega = \boldsymbol{e}_z\cos\omega - \boldsymbol{e}_r\sin\omega, \qquad \frac{\partial \boldsymbol{e}_\omega}{\partial\omega} = -\boldsymbol{e}_\rho, \qquad \frac{\partial \boldsymbol{e}_\rho}{\partial\omega} = \boldsymbol{e}_\omega.$$

(Here ω is the same as ω' of sec.6.3). Let $\mathrm{d}S_\rho,\ \mathrm{d}S_\omega,\ \mathrm{d}S_\varphi$ be surface-area elements with the normal vectors $\boldsymbol{e}_\rho, \boldsymbol{e}_\omega, \boldsymbol{e}_\varphi$. Then estimate the forces acting on the surfaces $\mathrm{d}S_\varphi(\varphi)$, $\mathrm{d}S_\varphi(\varphi+\mathrm{d}\varphi)$; $\mathrm{d}S_\omega(\varphi)$, $\mathrm{d}S_\omega(\omega+\mathrm{d}\omega)$; and $\mathrm{d}S_\rho(a)$. The sum $\boldsymbol{F}_\varphi$ of forces acting on $\mathrm{d}S_\varphi(\varphi)$ and $\mathrm{d}S_\varphi(\varphi+\mathrm{d}\varphi)$ is given by

$$\begin{aligned}\boldsymbol{F}_\varphi &= -\mathrm{d}\omega\mathrm{d}\varphi\int_0^a \left(T_{\varphi\varphi}\frac{\partial \boldsymbol{e}_\varphi}{\partial\varphi} + T_{\varphi\omega}\frac{\partial \boldsymbol{e}_\omega}{\partial\varphi} + T_{\varphi\rho}\frac{\partial \boldsymbol{e}_\rho}{\partial\varphi}\right)\rho\mathrm{d}\rho \\ &= -\mathrm{d}\omega\mathrm{d}\varphi\int_0^a \left(T^0_{\varphi\varphi}\left(\boldsymbol{e}_\omega\sin\omega - \boldsymbol{e}_\rho\cos\omega\right) - T^0_{\varphi\omega}\boldsymbol{e}_\varphi\sin\omega\right)\rho\mathrm{d}\rho.\end{aligned}$$

When the forces acting on $\mathrm{d}S_\omega(\omega)$ and $\mathrm{d}S_\omega(\omega+\mathrm{d}\omega)$ are estimated, we must take into account the differences in $\boldsymbol{e}_\omega,\ T_{\omega\alpha},\ \mathrm{d}S_\omega = (R+\rho\cos\omega)\,\mathrm{d}\rho\,\mathrm{d}\varphi$ at ω and $\omega+\mathrm{d}\omega$. The sum $\boldsymbol{F}_\omega$ of forces is

$$\begin{aligned}\boldsymbol{F}_\omega = -\mathrm{d}\omega\mathrm{d}\varphi\int_0^a \Bigg(&T_{\omega\omega}\frac{\partial}{\partial\omega}\left(\boldsymbol{e}_\omega\left(R+\rho\cos\omega\right)\right) \\ &+T_{\omega\varphi}\frac{\partial}{\partial\omega}\left(\boldsymbol{e}_\varphi\left(R+\rho\cos\omega\right)\right) + T_{\omega\rho}\frac{\partial}{\partial\omega}\left(\boldsymbol{e}_\rho\left(R+\rho\cos\omega\right)\right) \\ &+\frac{\partial T_{\omega\omega}}{\partial\omega}R\boldsymbol{e}_\omega + \frac{\partial T_{\omega\varphi}}{\partial\omega}R\boldsymbol{e}_\varphi + \frac{\partial T_{\omega\rho}}{\partial\omega}R\boldsymbol{e}_\rho\Bigg)\mathrm{d}\rho \\ = \mathrm{d}\omega\mathrm{d}\varphi\left(R\boldsymbol{e}_\rho\int_0^a T^0_{\omega\omega}\mathrm{d}\rho\right) &+ \mathrm{d}\omega\mathrm{d}\varphi\Bigg[\boldsymbol{e}_\rho\left(\cos\omega\int T^0_{\omega\omega}\rho\mathrm{d}\rho + R\int T^{(1)}_{\omega\omega}\mathrm{d}\rho\right) \\ &+\boldsymbol{e}_\omega\left(\sin\omega\int T^0_{\omega\omega}\rho\mathrm{d}\rho - R\int\frac{\partial T^{(1)}_{\omega\omega}}{\partial\omega}\mathrm{d}\rho\right)\Bigg]\end{aligned}$$

$$
\begin{aligned}
&+\mathrm{d}\omega\mathrm{d}\varphi\boldsymbol{e}_\varphi\left(\sin\omega\int T^0_{\omega\varphi}\rho\mathrm{d}\rho - R\int\frac{\partial T^{(1)}_{\omega\varphi}}{\partial\omega}\mathrm{d}\rho\right)\\
&+\mathrm{d}\omega\mathrm{d}\varphi\left(-\boldsymbol{e}_\omega R\int T^{(1)}_{\omega\rho}\mathrm{d}\rho - \boldsymbol{e}_\rho R\int\frac{\partial T^{(1)}_{\omega\rho}}{\partial\omega}\mathrm{d}\rho\right)\\
=\ &\mathrm{d}\omega\mathrm{d}\varphi\left(R\boldsymbol{e}_\rho\int_0^a T^0_{\omega\omega}\mathrm{d}\rho\right)\\
&+\mathrm{d}\omega\mathrm{d}\varphi\boldsymbol{e}_\rho\left(\cos\omega\int T^0_{\omega\omega}\rho\mathrm{d}\rho + R\int\left(T^{(1)}_{\omega\omega} - \frac{\partial T^{(1)}_{\omega\rho}}{\partial\omega}\right)\mathrm{d}\rho\right)\\
&+\mathrm{d}\omega\mathrm{d}\varphi\boldsymbol{e}_\omega\left(\sin\omega\int T^0_{\omega\omega}\rho\mathrm{d}\rho - R\int\left(T^{(1)}_{\omega\rho} + \frac{\partial T^{(1)}_{\omega\omega}}{\partial\omega}\right)\mathrm{d}\rho\right)\\
&+\mathrm{d}\omega\mathrm{d}\varphi\boldsymbol{e}_\varphi\left(\sin\omega\int T^0_{\omega\omega}\rho\mathrm{d}\rho - R\int\frac{\partial T^{(1)}_{\omega\varphi}}{\partial\omega}\mathrm{d}\rho\right).
\end{aligned}
$$

As $B_\rho(a)=0$, the force $\boldsymbol{F}_\rho$ acting on $\mathrm{d}S_\rho(a)$ is

$$\boldsymbol{F}_\rho = -\boldsymbol{e}_\rho T_{\rho\rho}(R+a\cos\omega)a\mathrm{d}\varphi\mathrm{d}\omega = \boldsymbol{e}_\rho(-T^0_{\rho\rho}Ra - (T^{(1)}_{\rho\rho}Ra + T^0_{\rho\rho}a^2\cos\omega)).$$

The equilibrium condition $\boldsymbol{F}_\varphi+\boldsymbol{F}_\omega+\boldsymbol{F}_\rho=0$ is reduced to

$$\int T^0_{\omega\omega}\mathrm{d}\rho = T^0_{\rho\rho}(a)a,$$

$$\frac{\partial}{\partial\omega}\int T^{(1)}_{\omega\varphi}\mathrm{d}\rho = \frac{2\sin\omega}{R}\int T^0_{\omega\varphi}\rho\mathrm{d}\rho, \tag{6.29}$$

$$\int\left(T^{(1)}_{\omega\rho} + \frac{\partial T^{(1)}_{\omega\omega}}{\partial\omega}\right)\mathrm{d}\rho = \frac{\sin\omega}{R}\int\left(T^0_{\omega\omega} - T^0_{\varphi\varphi}\right)\rho\mathrm{d}\rho, \tag{6.30}$$

$$\cos\omega\int(T^0_{\varphi\varphi}+T^0_{\omega\omega})\rho\mathrm{d}\rho + R\int\left(T^{(1)}_{\omega\omega} - \frac{\partial T^{(1)}_{\omega\rho}}{\partial\omega}\right)\mathrm{d}\rho - T^0_{\rho\rho}a^2\cos\omega - T^{(1)}_{\rho\rho}Ra = 0. \tag{6.31}$$

From $T^{(1)}\propto\sin\omega,\ \cos\omega$, it follows that $\partial^2T^{(1)}/\partial\omega^2 = -T^{(1)}$. So (6.30) is

$$\int\left(\frac{\partial T^{(1)}_{\omega\rho}}{\partial\omega} - T^{(1)}_{\omega\omega}\right)\mathrm{d}\rho = \frac{\cos\omega}{R}\int(T^0_{\omega\omega}-T^0_{\varphi\varphi})\rho\mathrm{d}\rho.$$

Using this relation, we can rewrite (6.31) as

$$T^{(1)}_{\rho\rho}(a) = \frac{a}{R}\cos\omega\left(-T^0_{\rho\rho}(a) + \frac{2}{a^2}\int_0^a T^0_{\varphi\varphi}.\rho\mathrm{d}\rho\right). \tag{6.32}$$

$T_{\rho\rho}$ and $T_{\varphi\varphi}$ are given by

$$T_{\rho\rho} = p + \frac{B_\omega^2}{2\mu_0} + \frac{B_\varphi^2}{2\mu_0},\quad T_{\varphi\varphi} = p + \frac{B_\omega^2}{2\mu_0} - \frac{B_\varphi^2}{2\mu_0}. \tag{6.33}$$

From (6.14), B_φ is

$$B_\varphi = \frac{\mu_0 I(\psi)}{2\pi r} = \frac{\mu_0 I(\psi)}{2\pi R}\left(1-\frac{\rho}{R}\cos\omega+\cdots\right) = B_\varphi(\rho)\left(1-\frac{\rho}{R}\cos\omega+\cdots\right). \tag{6.34}$$

When $B_\omega(a)$ is written as $B_\omega(a) = B_a + B^{(1)}_\omega$, (6.33) and (6.34) yield the expression

$$T^{(1)}_{\rho\rho}(a) = \frac{B_a B^{(1)}_\omega}{\mu_0} - \frac{B^2_{\varphi \mathrm{v}}(a)}{2\mu_0} 2\frac{a}{R}\cos\omega.$$

On the other hand, (6.9) and (6.32) give $T^{(1)}_{\rho\rho}(a)$ as

$$T^{(1)}_{\rho\rho}(a) = \frac{a}{R}\cos\omega\left(-p_a - \frac{B_a^2}{2\mu_0} - \frac{B^2_{\varphi \mathrm{v}}(a)}{2\mu_0} + \langle p\rangle + \frac{\langle B^2_\omega\rangle}{2\mu_0} - \frac{\langle B^2_\varphi\rangle}{2\mu_0}\right)$$

$$= \frac{a}{R}\cos\omega\left(\frac{B_a^2}{2\mu_0} l_{\mathrm{i}} + 2(\langle p\rangle - p_a) - \frac{B_a^2}{\mu_0} - \frac{B^2_{\varphi \mathrm{v}}(a)}{\mu_0}\right)$$

where l_{i} is the normalized internal inductance of the plasma per unit length (the internal inductance L_{i} of the plasma per unit length is given by $\mu_0 l_{\mathrm{i}}/4\pi$). Accordingly, $B^{(1)}_\omega$ must be

$$B^{(1)}_\omega = \frac{a}{R} B_a \cos\omega\left(\frac{l_{\mathrm{i}}}{2} + \frac{2\mu_0(\langle p\rangle - p_a)}{B_a^2} - 1\right).$$

B_a is ω component of the magnetic field due to the plasma current I_{p}, i.e.,

$$B_a = -\frac{\mu_0 I_{\mathrm{p}}}{2\pi a}.$$

When the poloidal ratio β_{p} (recall that this is the ratio of the plasma pressure p to the magnetic pressure due to B_a) is used, $B^{(1)}_\omega$ is given by

$$B^{(1)}_\omega = \frac{a}{R} B_a \cos\omega\left(\frac{l_{\mathrm{i}}}{2} + \beta_{\mathrm{p}} - 1\right). \tag{6.35}$$

6.5 Upper Limit of Beta Ratio

In the previous subsection, the value of B_ω necessary for equilibrium was derived. In this derivation, $(a/R)\Lambda < 1$ was assumed, i.e.,

$$\left(\beta_{\mathrm{p}} + \frac{l_{\mathrm{i}}}{2}\right) < \frac{R}{a}.$$

The vertical field $B_\perp$ for plasma equilibrium is given by

$$B_\perp = B_a \frac{a}{2R}\left(\ln\frac{8R}{a} + \Lambda - \frac{1}{2}\right).$$

The direction of $B_\perp$ is opposite to that of B_ω produced by the plasma current inside the torus, so that the resultant poloidal field becomes zero at some points in inside region of the torus and a separatrix is formed. When the plasma pressure is increased and β_{p} becomes large, the necessary amount of $B_\perp$ is increased and the separatrix shifts toward the plasma. For simplicity, let us consider a sharp-boundary model in which the plasma pressure is constant inside the plasma boundary, and in which the boundary encloses a plasma current I_{p}. Then the pressure-balance equation is

$$\frac{B_\omega^2}{2\mu_0} + \frac{B^2_{\varphi \mathrm{v}}}{2\mu_0} \approx p + \frac{B^2_{\varphi \mathrm{i}}}{2\mu_0}. \tag{6.36}$$

The φ components $B_{\varphi \mathrm{v}},\ B_{\varphi \mathrm{i}}$ of the field outside and inside the plasma boundary are proportional to $1/r$, according to (6.14). If the values of $B_{\varphi \mathrm{v}},\ B_{\varphi \mathrm{i}}$ at $r = R$ are denoted by $B^0_{\varphi \mathrm{v}},\ B^0_{\varphi \mathrm{i}}$ respectively, (6.36) may be written as

$$B_\omega^2 = 2\mu_0 p - ((B^0_{\varphi \mathrm{v}})^2 - (B^0_{\varphi \mathrm{i}})^2)\left(\frac{R}{r}\right)^2.$$

The upper limit of the plasma pressure is determined by the condition that the resultant poloidal field at $r = r_{\min}$ inside the torus is zero,

$$2\mu_0 p_{\max}\frac{r_{\min}^2}{R^2} = (B_{\varphi \mathrm{v}}^0)^2 - (B_{\varphi \mathrm{i}}^0)^2. \tag{6.37}$$

As r is expressed by $r = R + a\cos\omega$, (6.37) is reduced (with $(r_{\min} = R - a)$) to

$$B_\omega^2 = 2\mu_0 p_{\max}\left(1 - \frac{r_{\min}^2}{r^2}\right) = 8\mu_0 p_{\max}\frac{a}{R}\cos^2\frac{\omega}{2}.$$

Here $a/R \ll 1$ is assumed. From the relation $\oint B_\omega a \mathrm{d}\omega = \mu_0 I_{\mathrm{p}}$, the upper limit $\beta_{\mathrm{p}}^{\mathrm{c}}$ of the poloidal beta ratio is

$$\beta_{\mathrm{p}}^{\mathrm{c}} = \frac{\pi^2}{16}\frac{R}{a} \approx 0.5\frac{R}{a}. \tag{6.38}$$

Thus the upper limit of $\beta_{\mathrm{p}}^{\mathrm{c}}$ is half of the aspect ratio R/a in this simple model. When the rotational transform angle ι and the safety factor $q_{\mathrm{s}} = 2\pi/\iota$ are introduced, we find that

$$\frac{B_\omega}{B_\varphi} = \frac{a}{R}\left(\frac{\iota}{2\pi}\right) = \frac{a}{Rq_{\mathrm{s}}},$$

so that

$$\beta = \frac{p}{B^2/2\mu_0} \approx \frac{p}{B_\omega^2/2\mu_0}\left(\frac{B_\omega}{B_\varphi}\right)^2 = \left(\frac{a}{Rq_{\mathrm{s}}}\right)^2\beta_{\mathrm{p}}. \tag{6.39}$$

Accordingly, the upper limit of the beta ratio is

$$\beta^{\mathrm{c}} = \frac{0.5}{q_{\mathrm{s}}^2}\frac{a}{R}. \tag{6.40}$$

6.6 Pfirsch-Schlüter Current

When the plasma pressure is isotropic, the current $\boldsymbol{j}$ in the plasma is given by (6.1) and (6.4) as

$$\boldsymbol{j}_\perp = \frac{\boldsymbol{b}}{B} \times \nabla p$$

$$\nabla \cdot \boldsymbol{j}_\parallel = -\nabla \cdot \boldsymbol{j}_\perp = -\nabla \cdot \left(\frac{\boldsymbol{B}}{B^2} \times \nabla p\right) = -\nabla p \cdot \nabla \times \left(\frac{\boldsymbol{B}}{B^2}\right).$$

Then $j_\parallel$ is

$$\nabla \cdot \boldsymbol{j}_\parallel = -\nabla p \cdot \left(\left(\nabla \frac{1}{B^2} \times \boldsymbol{B}\right) + \frac{\mu_0 \boldsymbol{j}}{B^2}\right) = 2\nabla p \cdot \frac{\nabla B \times \boldsymbol{B}}{B^3} \tag{6.41}$$

$$\frac{\partial j_\parallel}{\partial s} = 2\nabla p \cdot \frac{(\nabla B \times \boldsymbol{b})}{B^2}, \tag{6.42}$$

where s is length along a line of magnetic force. In the zeroth-order approximation, we can put $B \propto 1/R$, $p = p(r)$, and $\partial/\partial s = (\partial\theta/\partial s)\partial/\partial\theta = (\iota/(2\pi R))\partial/\partial\theta$, where ι is the rotational transform angle. When s increases by $2\pi R$, θ increases by ι. Then (6.42) is reduced to

$$\frac{\iota}{2\pi R}\frac{\partial j_\parallel}{\partial\theta} = -\frac{\partial p}{\partial r}\frac{2}{RB}\sin\theta$$

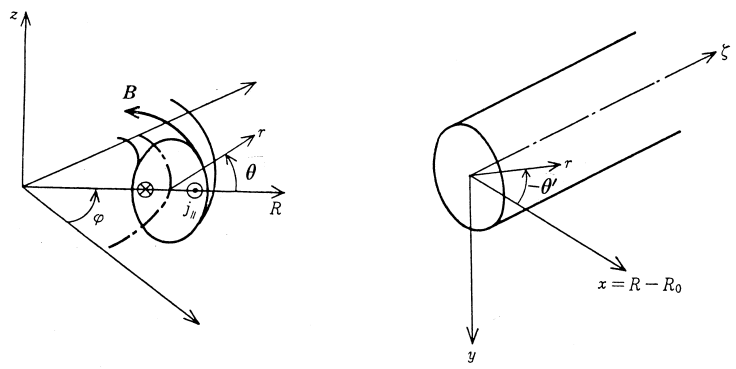

Fig.6.9 Pfirsch-Schlüter current $j_{\parallel}$ in a toroidal plasma.

i.e.,

$$\frac{\partial j_{\parallel}}{\partial \theta} = -\frac{4\pi}{\iota B}\frac{\partial p}{\partial r}\sin\theta, \qquad j_{\parallel} = \frac{4\pi}{\iota B}\frac{\partial p}{\partial r}\cos\theta. \tag{6.43}$$

This current is called the *Pfirsch-Schlüter current* (ref.[5]) (fig.6.9). These formulas are very important, and will be used to estimate the diffusion coefficient of a toroidal plasma. The Pfirsch-Schlüter current is due to the short circuiting, along magnetic-field lines, of toroidal drift polarization charges. The resultant current is inversely proportional to ι.

Let us take the radial variation in plasma pressure $p(r)$ and ι to be

$$p(r) = p_0\left(1 - \left(\frac{r}{a}\right)^m\right),$$

$$\iota(r) = \iota$$

respectively; then $j_{\parallel}$ is

$$j_{\parallel} = -\frac{4\pi m p_0}{B\iota a}\left(\frac{r}{a}\right)^{m-1}\cos\theta.$$

Let us estimate the magnetic field $\boldsymbol{B}^{\beta}$ produced by $j_{\parallel}$. As a/R is small, $\boldsymbol{B}^{\beta}$ is estimated from the corresponding linear configuration of fig.6.9. We utilize the coordinates (r, θ', ζ) and put $\theta = -\theta'$ and $j_{\parallel} \approx j_{\zeta}$ (ι is assumed not to be large). Then the vector potential $\boldsymbol{A}^{\beta} = (0, 0, A^{\beta}_{\zeta})$ for $\boldsymbol{B}^{\beta}$ is given by

$$\frac{1}{r}\frac{\partial}{\partial r}\left(r\frac{\partial A^{\beta}_{\zeta}}{\partial r}\right) + \frac{1}{r^2}\frac{\partial^2 A^{\beta}_{\zeta}}{\partial \theta'^2} = -\mu_0 j_{\zeta}.$$

When $A^{\beta}_{\zeta}(r, \theta') = A^{\beta}(r)\cos\theta'$, and parameters $s = m - 1,\ \alpha = 4\pi m p_0 \mu_0/(B\iota) = m\beta_0 B/(\iota/2\pi)$ (β_0 is beta ratio at the center) are used, we find

$$\frac{1}{r}\frac{\partial}{\partial r}\left(r\frac{\partial A^{\beta}}{\partial r}\right) - \frac{A^{\beta}}{r^2} = \frac{\alpha}{a}\left(\frac{r}{a}\right)^s.$$

In the plasma region ($r < a$), the vector potential is

$$A^{\beta}_{\rm in} = \left(\frac{\alpha r^{s+2}}{((s+2)^2 - 1)a^{s+1}} + \delta r\right)\cos\theta'$$

and $A^{\beta}_{\rm out}$ outside the plasma region ($r > a$) is

$$A^{\beta}_{\rm out} = \frac{\gamma}{r}\cos\theta',$$

where δ and γ are constants. Since B^{β}_{r}, $B^{\beta}_{\theta'}$ must be continuous at the boundary $r = a$, the solution for $\boldsymbol{B}^{\beta}$ inside the plasma is

$$\left.\begin{aligned} B^{\beta}_{r} &= -\frac{\alpha}{(s+2)^2-1}\left(\left(\frac{r}{a}\right)^{s+1} - \frac{s+3}{2}\right)\sin\theta', \\ B^{\beta}_{\theta'} &= -\frac{\alpha}{(s+2)^2-1}\left((s+2)\left(\frac{r}{a}\right)^{s+1} - \frac{s+3}{2}\right)\cos\theta' \end{aligned}\right\} \tag{6.44}$$

and the solution outside is

$$\begin{aligned} B^{\beta}_{r} &= \frac{\alpha}{(s+2)^2-1}\frac{s+1}{2}\left(\frac{a}{r}\right)^2\sin\theta', \\ B^{\beta}_{\theta} &= \frac{-\alpha}{(s+2)^2-1}\frac{s+1}{2}\left(\frac{a}{R}\right)^2\cos\theta' \end{aligned}$$

($B_r = r^{-1}\partial A_\zeta/\partial\theta'$, $B_{\theta'} = -\partial A_\zeta/\partial r$). As is clear from (6.44), there is a homogeneous vertical-field component

$$B_z = \frac{-(s+3)\alpha}{2((s+2)^2-1)} = \frac{-(m+2)m}{2((m+1)^2-1)}\frac{\beta}{(\iota/2\pi)}B \equiv -f_m\frac{\beta_0}{(\iota/2\pi)}B = -\frac{m+2}{m}f_m\frac{\langle\beta\rangle}{\iota/2\pi},$$

where $\langle\beta\rangle$ is the average beta value. This field causes the magnetic surface to be displaced by the amount Δ. From (3.42), Δ is given by

$$\frac{\Delta}{R} = \frac{-2\pi B_z}{\iota B} = \frac{m}{m+2}f_m\left(\frac{2\pi}{\iota}\right)^2\langle\beta\rangle.$$

The condition $\Delta < a/2$ gives the upper limit of the beta ratio:

$$\langle\beta\rangle_{\rm c} < \frac{1}{2}\frac{a}{R}\left(\frac{\iota}{2\pi}\right)^2,$$

in the case of $m = 2$. This critical value is the same as (6.40).

6.7 Virial Theorem

The equation of equilibrium $\boldsymbol{j}\times\boldsymbol{B} = (\nabla\times\boldsymbol{B})\times\boldsymbol{B} = \nabla p$ can be reduced to

$$\sum_i \frac{\partial}{\partial x_i}T_{ik} - \frac{\partial p}{\partial x_k} = 0 \tag{6.45}$$

where

$$T_{ik} = \frac{1}{\mu_0}(B_iB_k - \frac{1}{2}B^2\delta_{ik}). \tag{6.46}$$

This is called the magnetic stress tensor. From the relation (6.45), we have

$$\int_{\rm S}\left(\left(p + \frac{B^2}{2\mu_0}\right)\boldsymbol{n} - \frac{\boldsymbol{B}(\boldsymbol{B}\cdot\boldsymbol{n})}{\mu_0}\right)\,{\rm d}S = 0 \tag{6.47}$$

where $\boldsymbol{n}$ is the outward unit normal to the closed surface surrounding a volume V.

Since the other relation

$$\sum_i \frac{\partial}{\partial x_i}\left(x_k\left(T_{ik}-p\delta_{ik}\right)\right)=\left(T_{kk}-p\right)+x_k\sum_i\frac{\partial}{\partial x_i}\left(T_{ik}-p\delta_{ik}\right)=\left(T_{kk}-p\right)$$

holds,it follows that

$$\int_{\mathrm{V}}\left(3p+\frac{B^2}{2\mu_0}\right)\mathrm{d}V=\int_{\mathrm{S}}\left(\left(p+\frac{B^2}{2\mu_0}\right)(\boldsymbol{r}\cdot\boldsymbol{n})-\frac{(\boldsymbol{B}\cdot\boldsymbol{r})(\boldsymbol{B}\cdot\boldsymbol{n})}{\mu_0}\right)\mathrm{d}S. \tag{6.48}$$

This is called the virial theorem. When a plasma fills a finite region with $p=0$ outside the region, and no solid conductor carries the current anywhere inside or outside the plasma, the magnitude of the magnetic field is the order of $1/r^3$, so the surface integral approaches zero as the plasma surface approaches infinity ($r\to 0$). This contradicts that the volume integral of (6.48) is positive definite. In other words, a plasma of the finite extent cannot be in equilibrium unless there exist solid conductors to carry the current.

Let us apply the virial theorem (6.48) and (6.47) to a volume element of an axisymmetric plasma bounded by a closed toroidal surface S_{t} formed by the rotation of an arbitrary shaped contour $\mathrm{l_t}$. We denote the unit normal and tangent of the contour $\mathrm{l_t}$ by $\boldsymbol{n}$ and $\boldsymbol{l}$ respectively and a surface element of the transverse cross section by $\mathrm{d}S_\varphi$. The volume and the surface element are related by

$$\mathrm{d}V=2\pi r\mathrm{d}S_\varphi.$$

The magnetic field $\boldsymbol{B}$ is expressed by

$$\boldsymbol{B}=B_\varphi\boldsymbol{e}_\varphi+\boldsymbol{B}_{\mathrm{p}}$$

where $\boldsymbol{B}_{\mathrm{p}}$ is the poloidal field and B_φ is the magnitude of the toroidal field and $\boldsymbol{e}_\varphi$ is the unit vector in the φ direction.

Let us notice two relations

$$\int r^\alpha(\boldsymbol{r}\cdot\boldsymbol{n})\mathrm{d}S_{\mathrm{t}}=(\alpha+3)\int r^\alpha\mathrm{d}V \tag{6.49}$$

$$\begin{aligned}\int r^\alpha(\boldsymbol{e}_r\cdot\boldsymbol{n})\mathrm{d}S_{\mathrm{t}}&=\int\nabla\cdot(r^\alpha\boldsymbol{e}_r)\mathrm{d}V=\int\frac{1}{r}\frac{\partial}{\partial r}r^{\alpha+1}\mathrm{d}V\\&=(\alpha+1)\int r^{(\alpha-1)}\mathrm{d}V=2\pi(\alpha+1)\int r^\alpha\mathrm{d}S_\varphi\end{aligned} \tag{6.50}$$

where $\boldsymbol{e}_r$ is the unit vector in the r direction. Applying (6.48) to the full torus surrounded by S_{t}, we get

$$\begin{aligned}&\int\left(3p+\frac{B_\varphi^2+B_{\mathrm{p}}^2}{2\mu_0}\right)\mathrm{d}V=\int\left(\left(p+\frac{B_\varphi^2+B_{\mathrm{p}}^2}{2\mu_0}\right)(\boldsymbol{n}\cdot\boldsymbol{r})-\frac{B_n(\boldsymbol{B}\cdot\boldsymbol{r})}{\mu_0}\right)\mathrm{d}S_{\mathrm{t}}\\&=\int\left(\left(p+\frac{B_l^2-B_n^2}{2\mu_0}\right)(\boldsymbol{n}\cdot\boldsymbol{r})-\frac{B_nB_l}{\mu_0}(\boldsymbol{l}\cdot\boldsymbol{r})\right)\mathrm{d}S_{\mathrm{t}}+\int\frac{{B_\varphi}^2}{2\mu_0}(\boldsymbol{n}\cdot\boldsymbol{r})\,\mathrm{d}S_{\mathrm{t}},\end{aligned} \tag{6.51}$$

because of $\boldsymbol{B}_{\mathrm{p}}=B_l\boldsymbol{l}+B_n\boldsymbol{n}$ (see fig.6.10a). When the vacuum toroidal field (without plasma) is denoted by $B_{\varphi0}$, this is given by $B_{\varphi0}=\mu_0 I/(2\pi r)$, where I is the total coil current generating the toroidal field. By use of (6.50), (6.51) reduces to (ref.[6])

$$\begin{aligned}&\int\left(3p+\frac{B_{\mathrm{p}}^2+B_\varphi^2-B_{\varphi0}^2}{2\mu_0}\right)2\pi r\mathrm{d}S_\varphi\\&=\int\left(\left(p+\frac{B_l^2-B_n^2}{2\mu_0}\right)(\boldsymbol{n}\cdot\boldsymbol{r})-\frac{B_nB_l}{\mu_0}(\boldsymbol{l}\cdot\boldsymbol{r})\right)\mathrm{d}S_{\mathrm{t}}.\end{aligned} \tag{6.52}$$

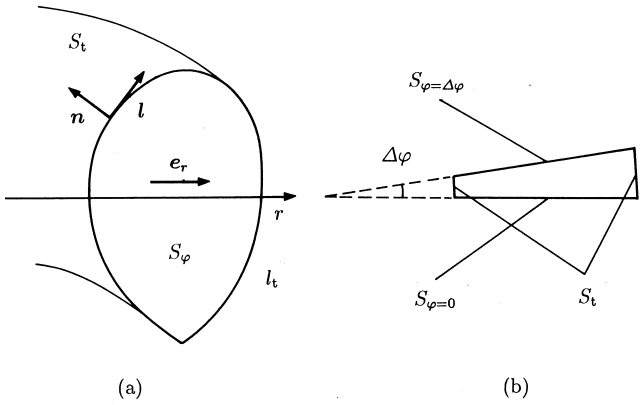

Fig.6.10 Integral region of Virial theorem (a) (6.48) and (b) (6.47).

Applying (6.47) to the sector region surrounded by $\varphi = 0, \varphi = \Delta\varphi$ and S_t (see fig.6.10b) and taking its r component gives (ref.[6])

$$-\Delta\varphi \int \left(p + \frac{B^2}{2\mu_0} - \frac{B_\varphi^2}{\mu_0} \right) \mathrm{d}S_\varphi + \frac{\Delta\varphi}{2\pi} \int \left(\left(p + \frac{B^2}{2\mu_0} \right) (\boldsymbol{n} \cdot \boldsymbol{e}_r) - \frac{(\boldsymbol{B} \cdot \boldsymbol{e}_r)(\boldsymbol{B} \cdot \boldsymbol{n})}{\mu_0} \right) \mathrm{d}S_t = 0$$

$$2\pi \int \left(p + \frac{B_p^2 - B_\varphi^2 + B_{\varphi 0}^2}{2\mu_0} \right) \mathrm{d}S_\varphi = \int \left(\left(p + \frac{B_l^2 - B_n^2}{2\mu_0} \right) (\boldsymbol{n} \cdot \boldsymbol{e}_r) - \frac{B_l B_n}{\mu_0} (\boldsymbol{l} \cdot \boldsymbol{e}_r) \right) \mathrm{d}S_t = 0. \tag{6.53}$$

Eqs. (6.52) and (6.53) are used to measure the poloidal beta ratio (6.18) and the internal plasma inductance per unit length (6.23) of arbitrary shaped axisymmetric toroidal plasma by use of magnetic probes surrounding the plasma.

References

[1] L. S. Solovev: Sov. Phys, JETP **26**, 400 (1968).
N. M. Zueva and L. S. Solovev: AtomnayaEnrggia **24**, 453 (1968).
[2] R. H. Weening: Phys. Plasmas **7**, 3654 (2000).
[3] V. S. Mukhovatov and V. D. Shafranov: Nucl. Fusion **11**, 605 (1971).
[4] V. D. Shafranov: Plasma Physics, J. of Nucl. Energy pt.**C5**, 251 (1963).
[5] D. Pfirsch and A. Schlüter: MPI/PA/7/62 Max-Planck Institut für Physik und Astrophysik, München (1962).
[6] V. D. Shafranov: Plasma Physics **13** 757 (1971).

Ch.7 Diffusion of Plasma, Confinement Time

Diffusion and confinement of plasmas are among the most important subjects in fusion research, with theoretical and experimental investigations being carried out concurrently. Although a general discussion of diffusion and confinement requires the consideration of the various instabilities (which will be studied in subsequent chapters), it is also important to consider simple but fundamental diffusion for the ideal stable cases. A typical example (sec.7.1) is classical diffusion, in which collisions between electrons and ions are dominant effect. The section 7.2 describe the neoclassical diffusion of toroidal plasmas confined in tokamak, for both the rare-collisional and collisional regions. Sometimes the diffusion of an unstable plasma may be studied in a phenomenological way, without recourse to a detailed knowledge of instabilities. In this manner, diffusions caused by fluctuations in a plasma are explained in secs.7.3 and 7.4.

The transport equation of particles is

$$\frac{\partial}{\partial t} n(\boldsymbol{r},t) + \nabla \cdot (n(\boldsymbol{r},t)\boldsymbol{V}(\boldsymbol{r},t)) = 0 \tag{7.1}$$

provided processes of the ionization of neutrals and the recombination of ions are negligible (see ch.5.1). The particle flux $\boldsymbol{\Gamma} = n\boldsymbol{V}$ is given by

$$n(\boldsymbol{r},t)\boldsymbol{V}(\boldsymbol{r},t) = -D(\boldsymbol{r},t)\nabla n(\boldsymbol{r},t)$$

in many cases, where D is diffusion coefficient. (Additional terms may be necessary in more general cases.)

Diffusion coefficient D and *particle confinement time* $\tau_{\rm p}$ are related by the diffusion equation of the plasma density n as follows:

$$\nabla \cdot (D\nabla n(\boldsymbol{r},t)) = \frac{\partial}{\partial t} n(\boldsymbol{r},t).$$

Substitution of $n(\boldsymbol{r},t) = n(\boldsymbol{r})\exp(-t/\tau_{\rm p})$ in diffusion equation yields

$$\nabla \cdot (D\nabla n(\boldsymbol{r})) = -\frac{1}{\tau_{\rm p}} n(\boldsymbol{r}).$$

When D is constant and the plasma column is a cylinder of radius a, the diffusion equation is reduced to

$$\frac{1}{r}\frac{\partial}{\partial r}\left(r\frac{\partial n}{\partial r}\right) + \frac{1}{D\tau_{\rm p}} n = 0.$$

The solution satisfying the boundary condition $n(a) = 0$ is

$$n = n_0 J_0\left(\frac{2.4r}{a}\right)\exp\left(-\frac{t}{\tau_{\rm p}}\right)$$

and the particle confinement time is

$$\tau_{\rm p} = \frac{a^2}{2.4^2 D} = \frac{a^2}{5.8D}, \tag{7.2}$$

where J_0 is the zeroth-order Bessel function. The relationship (7.2) between the particle confinement time $\tau_{\rm p}$ and D holds generally, with only a slight modification of the numerical factor. This formula is frequently used to obtain the diffusion coefficient from the observed values of the plasma radius and particle confinement time.

The equation of energy balance is given by (A.19), which will be derived in appendix A, as follows:

$$\frac{\partial}{\partial t}\left(\frac{3}{2}n\kappa T\right)+\nabla\cdot\left(\frac{3}{2}\kappa Tn\boldsymbol{v}\right)+\nabla\cdot\boldsymbol{q}=Q-p\nabla\cdot\boldsymbol{v}-\sum_{ij}\Pi_{ij}\frac{\partial \boldsymbol{v}_i}{\partial x_j}. \tag{7·3}$$

The first term in the right-hand side is the heat generation due to particle collisions per unit volume per unit time, the second term is the work done by pressure and the third term is viscous heating. The first term in the left-hand side is the time derivative of the thermal energy per unit volume, the second term is convective energy loss and the third term is conductive energy loss. Denoting the *thermal conductivity* by κ_{T}, the *thermal flux* due to heat conduction may be expressed by

$$\boldsymbol{q}=-\kappa_{\mathrm{T}}\nabla(\kappa T).$$

If the *convective loss* is neglected and the heat sources in the right-hand side of (7.3) is zero, we find that

$$\frac{\partial}{\partial t}\left(\frac{3}{2}n\kappa T\right)-\nabla\cdot\kappa_{\mathrm{T}}\nabla(\kappa T)=0.$$

In the case of $n=$ const., this equation reduces to

$$\frac{\partial}{\partial t}\left(\frac{3}{2}\kappa T\right)=\nabla\cdot\left(\frac{\kappa_{\mathrm{T}}}{n}\nabla(\kappa T)\right).$$

When the thermal diffusion coefficient χ_{T} is defined by

$$\chi_{\mathrm{T}}=\frac{\kappa_{\mathrm{T}}}{n},$$

the same equation on κT is obtained as (7.1). In the case of $\chi_{\mathrm{T}}=$ const., the solution is

$$\kappa T=\kappa T_0 J_0\left(\frac{2.4}{a}r\right)\exp\left(-\frac{t}{\tau_{\mathrm{E}}}\right),\qquad \tau_{\mathrm{E}}=\frac{a^2}{5.8(2/3)\chi_{\mathrm{T}}}. \tag{7.4}$$

The term τ_{E} is called *energy confinement time*.

7.1 Collisional Diffusion (Classical Diffusion)

7.1a Magnetohydrodynamic Treatment

A magnetohydrodynamic treatment is applicable to diffusion phenomena when the electron-to-ion collision frequency is large and the mean free path is shorter than the *connection length* of the inside regions of good curvature and the outside region of bad curvature of the torus; i.e.,

$$\frac{v_{\mathrm{Te}}}{\nu_{\mathrm{ei}}}\lesssim\frac{2\pi R}{\iota},$$

$$\nu_{\mathrm{ei}}\gtrsim\nu_{\mathrm{p}}\equiv\frac{1}{R}\frac{\iota}{2\pi}v_{\mathrm{Te}}=\frac{1}{R}\frac{\iota}{2\pi}\left(\frac{\kappa T_{\mathrm{e}}}{m_{\mathrm{e}}}\right)^{1/2}$$

where v_{Te} is electron thermal velocity and ν_{ei} is electron to ion collision frequency. From Ohm's law (5.28)

$$\boldsymbol{E}+\boldsymbol{v}\times\boldsymbol{B}-\frac{1}{en}\nabla p_{\mathrm{i}}=\eta\boldsymbol{j},$$

the motion of plasma across the lines of magnetic force is expressed by

$$n\boldsymbol{v}_{\perp}=\frac{1}{B}\left(\left(n\boldsymbol{E}-\frac{\kappa T_{\mathrm{i}}}{e}\nabla n\right)\times\boldsymbol{b}\right)-\frac{m_{\mathrm{e}}\nu_{\mathrm{ei}}}{e^2}\frac{\nabla p}{B^2}$$

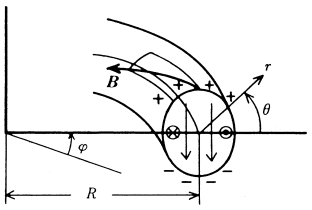

Fig.7.1 Electric field in a plasma confined in a toroidal field. The symbols ⊗ and ⊙ here show the direction of the Pfirsch-Schlüter current.

$$= \frac{1}{B}\left(\left(n\boldsymbol{E} - \frac{\kappa T_\mathrm{i}}{e}\nabla n\right) \times \boldsymbol{b}\right) - (\rho_{\Omega\mathrm{e}})^2 \nu_\mathrm{ei}\left(1 + \frac{T_\mathrm{i}}{T_\mathrm{e}}\right)\nabla n \tag{7.5}$$

where $\rho_{\Omega\mathrm{e}} = v_\mathrm{Te}/\Omega_\mathrm{e},\ v_\mathrm{Te} = (\kappa T_\mathrm{e}/m_\mathrm{e})^{1/2}$ and $\eta = m_\mathrm{e}\nu_\mathrm{ei}/e^2 n_\mathrm{e}$ (see sec.2.8).

If the first term in the right-hand side can be neglected, the particle diffusion coefficient D is given by

$$D = (\rho_{\Omega\mathrm{e}})^2 \nu_\mathrm{ei}\left(1 + \frac{T_\mathrm{i}}{T_\mathrm{e}}\right). \tag{7.6}$$

The *classical diffusion coefficient* D_ei is defined by

$$D_\mathrm{ei} \equiv (\rho_{\Omega\mathrm{e}})^2 \nu_\mathrm{ei} = \frac{n\kappa T_\mathrm{e}}{\sigma_\perp B^2} = \frac{\beta_\mathrm{e}\eta_\parallel}{\mu_0}, \tag{7.7}$$

where $\sigma_\perp = n_\mathrm{e}e^2/(m_\mathrm{e}\nu_\mathrm{ei}),\ \eta_\parallel = 1/2\sigma_\perp$.

However the first term of the right-hand side of (7.5) is not always negligible. In toroidal configuration, the charge separation due to the toroidal drift is not completely cancelled along the magnetic field lines due to the finite resistivity and an electric field $\boldsymbol{E}$ arises (see fig.7.1). Therefore the $\boldsymbol{E}\times\boldsymbol{b}$ term in (7.5) contributes to the diffusion. Let us consider this term. From the equilibrium equation, the diamagnetic current

$$\boldsymbol{j}_\perp = \frac{\boldsymbol{b}}{B} \times \nabla p, \qquad j_\perp = \left|\frac{1}{B}\frac{\partial p}{\partial r}\right|$$

flows in the plasma. From $\nabla \cdot \boldsymbol{j} = 0$, we find $\nabla \cdot \boldsymbol{j}_\parallel = -\nabla \cdot \boldsymbol{j}_\perp$. By means of the equation $B = B_0(1 - (r/R)\cos\theta)$, the Pfirsch-Schlüter current $j_\parallel$ is given by (refer to (6.43))

$$j_\parallel = 2\frac{2\pi}{\iota}\frac{1}{B_0}\frac{\partial p}{\partial r}\cos\theta. \tag{7.8}$$

If the electric conductivity along the magnetic lines of force is $\sigma_\parallel$, the parallel electric field is $E_\parallel = j_\parallel/\sigma_\parallel$. As is clear from fig.7.1, the relation

$$\frac{E_\theta}{E_\parallel} \approx \frac{B_0}{B_\theta}$$

holds. From $B_\theta/B_0 \approx (r/R)(\iota/2\pi)$, the θ component of the electric field is given by

$$E_\theta = \frac{B_0}{B_\theta}E_\parallel = \frac{R}{r}\frac{2\pi}{\iota}\frac{1}{\sigma_\parallel}j_\parallel = \frac{2}{\sigma_\parallel}\frac{R}{r}\left(\frac{2\pi}{\iota}\right)^2\frac{1}{B_0}\frac{\partial p}{\partial r}\cos\theta. \tag{7.9}$$

Accordingly (7.5) is reduced to

$$nV_\mathrm{r} = -n\frac{E_\theta}{B} - (\rho_{\Omega\mathrm{e}})^2\nu_\mathrm{ei}\left(1 + \frac{T_\mathrm{i}}{T_\mathrm{e}}\right)\frac{\partial n}{\partial r}$$

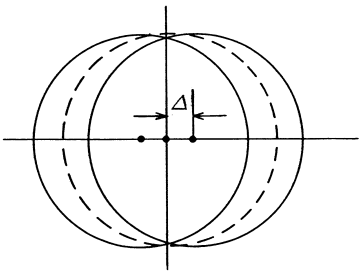

Fig.7.2 Magnetic surface (dotted line) and drift surfaces (solid lines).

$$= -\left(\frac{R}{r}\cdot 2\left(\frac{2\pi}{\iota}\right)^2 \frac{n\kappa T_\mathrm{e}}{\sigma_\parallel B_0^2}\cos\theta\left(1+\frac{r}{R}\cos\theta\right)\right.$$

$$\left.+\frac{n\kappa T_\mathrm{e}}{\sigma_\perp B_0^2}\left(1+\frac{r}{R}\cos\theta\right)^2\right)\times\left(1+\frac{T_\mathrm{i}}{T_\mathrm{e}}\right)\frac{\partial n}{\partial r}.$$

Noting that the area of a surface element is dependent of θ, and taking the average of nV_r over θ, we find that

$$\langle nV_\mathrm{r}\rangle = \frac{1}{2\pi}\int_0^{2\pi} nV_\mathrm{r}\left(1+\frac{r}{R}\cos\theta\right)\mathrm{d}\theta$$

$$= -\frac{n\kappa T_\mathrm{e}}{\sigma_\perp B_0^2}\left(1+\frac{T_\mathrm{i}}{T_\mathrm{e}}\right)\left(1+\frac{2\sigma_\perp}{\sigma_\parallel}\left(\frac{2\pi}{\iota}\right)^2\right)\frac{\partial n}{\partial r}. \tag{7.10}$$

Using the relation $\sigma_\perp = \sigma_\parallel/2$, we obtain the diffusion coefficient of a toroidal plasma:

$$D_\mathrm{P.S.} = \frac{nT_\mathrm{e}}{\sigma_\perp B_0^2}\left(1+\frac{T_\mathrm{i}}{T_\mathrm{e}}\right)\left(1+\left(\frac{2\pi}{\iota}\right)^2\right). \tag{7.11}$$

This diffusion coefficient is $(1+(2\pi/\iota)^2)$ times as large as the diffusion coefficient of (7.2). This value is called Pfirsch-Schlüter factor (ref.[1]). When the rotational tranform angle $\iota/2\pi$ is about 0.3, *Pfirsch-Schlüter factor* is about 10.

7.1b A Particle Model

The classical diffusion coefficient of electrons

$$D_\mathrm{ei} = (\rho_{\Omega\mathrm{e}})^2\nu_\mathrm{ei}$$

is that for electrons which move in a random walk with a step length equal to the Larmor radius. Let us consider a toroidal plasma. For rotational transform angle ι, the displacement Δ of the electron drift surface from the magnetic surface is (see fig.7.2)

$$\Delta \approx \pm\rho_{\Omega\mathrm{e}}\frac{2\pi}{\iota}. \tag{7.12}$$

The $\pm$ signs depend on that the direction of electron motion is parallel or antiparallel to the magnetic field (see sec.3.5). As an electron can be transferred from one drift surface to the other by collision, the step length across the magnetic field is

$$\Delta = \left(\frac{2\pi}{\iota}\right)\rho_{\Omega\mathrm{e}}. \tag{7.13}$$

Consequently, the diffusion coefficient is given by

$$D_{\mathrm{P.S.}} = \Delta^2 \nu_{\mathrm{ei}} = \left(\frac{2\pi}{\iota}\right)^2 (\rho_{\Omega \mathrm{e}})^2 \nu_{\mathrm{ei}}, \tag{7.14}$$

thus the Pfirsch-Schlüter factor has been reduced ($|2\pi/\iota| \gg 1$ is assumed).

7.2 Neoclassical Diffusion of Electrons in Tokamak

The magnitude B of the magnetic field of a tokamak is given by

$$B = \frac{RB_0}{R(1+\epsilon_{\mathrm{t}} \cos\theta)} = B_0(1 - \epsilon_{\mathrm{t}} \cos\theta), \tag{7.15}$$

where

$$\epsilon_{\mathrm{t}} = \frac{r}{R}. \tag{7.16}$$

Consequently, when the perpendicular component $v_\perp$ of a electron velocity is much larger than the parallel component $v_\parallel$, i.e., when

$$\left(\frac{v_\perp}{v}\right)^2 > \frac{R}{R+r},$$

that is,

$$\frac{v_\perp}{v_\parallel} > \frac{1}{\epsilon_{\mathrm{t}}^{1/2}}, \tag{7.17}$$

the electron is trapped outside of the torus, where the magnetic field is weak. Such an electron drifts in a banana orbit (see fig.3.9). In order to complete a circuit of the banana orbit, the effective collision time $\tau_{\mathrm{eff}} = 1/\nu_{\mathrm{eff}}$ of the trapped electron must be longer than one period τ_{b} of banana orbit

$$\tau_{\mathrm{b}} \approx \frac{R}{v_\parallel}\left(\frac{2\pi}{\iota}\right) = \frac{R}{v_\perp \epsilon_{\mathrm{t}}^{1/2}}\left(\frac{2\pi}{\iota}\right). \tag{7.18}$$

The effective collision frequency ν_{eff} of the trapped electron is the frequency in which the condition (7.17) of trapped electron is violated by collision. As the collision frequency ν_{ei} is the inverse of diffusion time required to change the directon of velocity by 1 radian, the effective collision frequency ν_{eff} is given by

$$\nu_{\mathrm{eff}} = \frac{1}{\epsilon_{\mathrm{t}}}\nu_{\mathrm{ei}}. \tag{7.19}$$

Accordingly, if $\nu_{\mathrm{eff}} < 1/\tau_{\mathrm{b}}$, i.e.,

$$\nu_{\mathrm{ei}} < \nu_{\mathrm{b}} \equiv \frac{v_\perp \epsilon_{\mathrm{t}}^{3/2}}{R}\left(\frac{\iota}{2\pi}\right) = \epsilon_{\mathrm{t}}^{3/2}\frac{1}{R}\left(\frac{\iota}{2\pi}\right)\left(\frac{\kappa T_{\mathrm{e}}}{m_{\mathrm{e}}}\right)^{1/2} \tag{7.20}$$

the trapped electron can travel the entire banana orbit. When the trapped electron collides, it can shift its position by an amount of the banana width (see sec.3.5(b))

$$\Delta_{\mathrm{b}} = \frac{mv_\parallel}{eB_{\mathrm{p}}} \approx \frac{mv_\perp}{eB}\frac{v_\parallel}{v_\perp}\frac{B}{B_{\mathrm{p}}} \approx \rho_{\Omega \mathrm{e}}\epsilon_{\mathrm{t}}^{1/2}\frac{R}{r}\frac{2\pi}{\iota} = \left(\frac{2\pi}{\iota}\right)\epsilon_{\mathrm{t}}^{-1/2}\rho_{\Omega \mathrm{e}}. \tag{7.21}$$

As the number of trapped electrons is $\epsilon_{\mathrm{t}}^{1/2}$ times the total number of electrons, the trapped-electron contribution to diffusion is

$$\begin{aligned} D_{\mathrm{G.S.}} &= \epsilon_{\mathrm{t}}^{1/2}\Delta_{\mathrm{b}}^2\nu_{\mathrm{eff}} = \epsilon_{\mathrm{t}}^{1/2}\left(\frac{2\pi}{\iota}\right)^2 \epsilon_{\mathrm{t}}^{-1}(\rho_{\Omega \mathrm{e}})^2\frac{1}{\epsilon_{\mathrm{t}}}\nu_{\mathrm{ei}} \\ &= \epsilon_{\mathrm{t}}^{-3/2}\left(\frac{2\pi}{\iota}\right)^2 (\rho_{\Omega \mathrm{e}})^2\nu_{\mathrm{ei}}. \end{aligned} \tag{7.22}$$

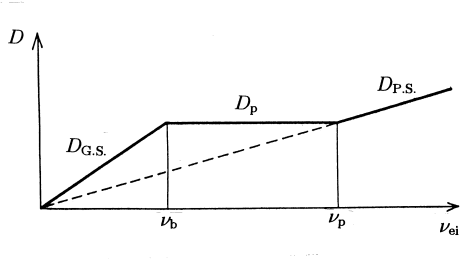

Fig.7.3 Dependence of the diffusion coefficient on collision frequency in a tokamak. $\nu_{\rm p} = (\iota/2\pi)v_{\rm Te}/R$, $\nu_{\rm b} = \epsilon_{\rm t}^{3/2}\nu_{\rm p}$.

This diffusion coefficient, introduced by Galeev-Sagdeev, is $\epsilon_{\rm t}^{-3/2} = (R/r)^{3/2}$ times as large as the diffusion coefficient for collisional case. This derivation is semi-quantitative discussion. The more rigorous discussion is given in (ref.[2]).

As was discussed in sec.7.1, MHD treatment is applicable if the electron to ion collision frequency is larger than the frequency $\nu_{\rm p}$ given by

$$\nu_{\rm p} = \frac{1}{R}\frac{\iota}{2\pi}v_{\rm Te} = \frac{1}{R}\left(\frac{\iota}{2\pi}\right)\left(\frac{\kappa T_{\rm e}}{m_{\rm e}}\right)^{1/2}. \tag{7.23}$$

When the electron to ion collision frequency is smaller than the frequency

$$\nu_{\rm b} = \epsilon_{\rm t}^{3/2}\nu_{\rm p}, \tag{7.24}$$

the electron can complete a banana orbit. The diffusion coefficients are witten by

$$D_{\rm P.S.} = \left(\frac{2\pi}{\iota}\right)^2(\rho_{\Omega{\rm e}})^2\nu_{\rm ei}, \quad \nu_{\rm ei} > \nu_{\rm p}, \tag{7.25}$$

$$D_{\rm G.S.} = \epsilon_{\rm t}^{-3/2}\left(\frac{2\pi}{\iota}\right)^2(\rho_{\Omega{\rm e}})^2\nu_{\rm ei}, \quad \nu_{\rm ei} < \nu_{\rm b} = \epsilon_{\rm t}^{3/2}\nu_{\rm p}. \tag{7.26}$$

If $\nu_{\rm ei}$ is in the region $\nu_{\rm b} < \nu_{\rm ei} < \nu_{\rm p}$, it is not possible to treat the diffusion phenomena of electrons in this region by means of a simple model. In this region we must resort to the drift approximation of Vlasov's equation. The result is that the diffusion coefficient is not sensitive to the collision frequency in this region and is given by (ref.[2],[3])

$$D_{\rm p} = \left(\frac{2\pi}{\iota}\right)^2(\rho_{\Omega{\rm e}})^2\nu_{\rm p}, \quad \nu_{\rm p} > \nu_{\rm ei} > \nu_{\rm b} = \epsilon_{\rm t}^{3/2}\nu_{\rm p}. \tag{7.27}$$

The dependence of the diffusion coefficient on the collision frequency is shown in fig.7.3. The region $\nu_{\rm ei} > \nu_{\rm p}$ is called the *MHD region* or *collisional region*. The region $\nu_{\rm p} > \nu_{\rm ei} > \nu_{\rm b}$ is the *platau region* or *intermediate region*; and the region $\nu_{\rm ei} < \nu_{\rm b}$ is called the *banana region* or *rare collisional region*. These diffusion processes are called neoclassical diffusion. There is an excellent review[3] on neoclassical diffusion.
The reason that the electron-electron collison frequency does not affect the electron's particle diffusion coefficient is that the center-of-mass velocity does not change by the Coulomb collision.

The neoclassical thermal diffusion coefficient $\chi_{\rm Te}$ is the same order as the particle diffusion coefficient ($\chi_{\rm Te} \sim D_{\rm e}$). Although ion collision with the same ion species does not affect the ion's particle diffusion coefficient, it does contribute thermal diffusion processes, if temperature gradient exists. Even if the ions are the same species with each other, it is possible to distinguish hot ion (with high velocity) and cold ion. Accordingly the ion's thermal diffusion coefficient in banana region is given by $\chi_{\rm Ti} \sim \epsilon_{\rm t}^{-3/2}(2\pi/\iota)^2\rho_{\Omega{\rm i}}^2\nu_{\rm ii}$, and $\chi_{\rm Ti} \sim (m_{\rm i}/m_{\rm e})^{1/2}D_{\rm ie}$ ($D_{\rm ie} \sim D_{\rm ei}$). Therefore ion's thermal diffusion coefficient is about $(m_{\rm i}/m_{\rm e})^{1/2}$ times as large as the ion's particle diffusion

coefficient.

7.3 Fluctuation Loss, Bohm, Gyro-Bohm Diffusion, and Stationary Convective Loss

In the foregoing sections we have discussed diffusion due to binary collision and have derived the confinement times for such diffusion as an ideal case. However, a plasma will be, in many cases, more or less unstable, and fluctuations in the density and electric field will induce collective motions of particles and bring about anomalous losses. We will study such losses here.

Assume the plasma density $n(\boldsymbol{r},t)$ consists of the zeroth-order term $n_0(\boldsymbol{r},t)$ and 1st-order perturbation terms $\tilde{n}_k(\boldsymbol{r},t) = n_k \exp i(\boldsymbol{kr} - \omega_k t)$ and

$$n = n_0 + \sum_k \tilde{n}_k. \tag{7.28}$$

Since n and n_0 are real, there are following relations:

$$\tilde{n}_{-k} = (\tilde{n}_k)^*, \quad n_{-k} = n_k^*, \quad \omega_{-k} = -\omega_k^*.$$

where $*$ denotes the complex conjugate. ω_k is generally complex and $\omega_k = \omega_{k\mathrm{r}} + i\gamma_k$ and

$$\omega_{-k\mathrm{r}} = -\omega_{k\mathrm{r}}, \quad \gamma_{-k} = \gamma_k.$$

The plasma is forced to move by perturbation. When the velocity is expressed by

$$\boldsymbol{V}(\boldsymbol{r},t) = \sum_k \tilde{\boldsymbol{V}}_k = \sum_k \boldsymbol{V}_k \exp i(\boldsymbol{k}\cdot\boldsymbol{r} - \omega_k t) \tag{7.29}$$

then $\boldsymbol{V}_{-k} = \boldsymbol{V}_k^*$ and the equation of continuity

$$\frac{\partial n}{\partial t} + \nabla\cdot(n\boldsymbol{V}) = 0$$

may be written as

$$\frac{\partial n_0}{\partial t} + \sum_k \frac{\partial \tilde{n}_k}{\partial t} + \nabla\cdot\left(\sum_k n_0\tilde{\boldsymbol{V}}_k + \sum_{k,k'} \tilde{n}_k\tilde{\boldsymbol{V}}_{k'}\right) = 0.$$

When the first- and the second-order terms are separated, then

$$\sum \frac{\partial \tilde{n}_k}{\partial t} + \nabla\cdot\sum n_0\tilde{\boldsymbol{V}}_k = 0, \tag{7.30}$$

$$\frac{\partial n_0}{\partial t} + \nabla\cdot\left(\sum_{k,k'} \tilde{n}_k\tilde{\boldsymbol{V}}_{k'}\right) = 0. \tag{7.31}$$

Here we have assumed that the time derivative of n_0 is second order. The time average of the product of (7.30) and $\tilde{n}_{-k}$ becomes

$$\left.\begin{aligned} &\gamma_k|n_k|^2 + \nabla n_0\cdot\mathrm{Re}(n_k\boldsymbol{V}_{-k}) + n_0\boldsymbol{k}\cdot\mathrm{Im}(n_k\boldsymbol{V}_{-k}) = 0, \\ &\omega_{k\mathrm{r}}|n_k|^2 + \nabla n_0\cdot\mathrm{Im}(n_k\boldsymbol{V}_{-k}) - n_0\boldsymbol{k}\cdot\mathrm{Re}(n_k\boldsymbol{V}_{-k}) = 0. \end{aligned}\right\} \tag{7.32}$$

If the time average of (7.31) is taken, we find that

$$\frac{\partial n_0}{\partial t} + \nabla\cdot\left(\sum \mathrm{Re}(n_k\boldsymbol{V}_{-k})\exp(2\gamma_k t)\right) = 0. \tag{7.33}$$

The diffusion equation is

$$\frac{\partial n_0}{\partial t} = \nabla\cdot(D\nabla n_0)$$

and the outer particle flux Γ is

$$\boldsymbol{\Gamma} = -D\nabla n_0 = \sum_k \mathrm{Re}(n_k \boldsymbol{V}_{-k}) \exp 2\gamma_k t. \tag{7.34}$$

Equation (7.32) alone is not enough to determine the quantity $\nabla n_0 \cdot \mathrm{Re}(n_k \boldsymbol{V}_{-k}) \exp 2\gamma_k t$. Denote $\beta_k = n_0 \boldsymbol{k} \cdot \mathrm{Im}(n_k \boldsymbol{V}_{-k}) / \nabla n_0 \cdot (\mathrm{Re}(n_k \boldsymbol{V}_{-k}))$; then (7.34) is reduced to

$$D|\nabla n_0|^2 = \frac{\sum \gamma_k |n_k|^2 \exp 2\gamma_k t}{1+\beta_k}$$

and

$$D = \sum_k \gamma_k \frac{|\tilde{n}_k|^2}{|\nabla n_0|^2} \frac{1}{1+\beta_k}. \tag{7.35}$$

This is the anomalous diffusion coefficient due to fluctuation loss.

Let us consider the case in which the fluctuation $\tilde{\boldsymbol{E}}_k$ of the electric field is electrostatic and can be expressed by a potential $\tilde{\phi}_k$. Then the perturbed electric field is expressed by

$$\tilde{\boldsymbol{E}}_k = -\nabla \tilde{\phi}_k = -i\boldsymbol{k} \cdot \phi_k \exp i(\boldsymbol{kr} - \omega_k t).$$

The electric field results in an $\tilde{\boldsymbol{E}}_k \times \boldsymbol{B}$ drift, i.e.,

$$\tilde{\boldsymbol{V}}_k = (\tilde{\boldsymbol{E}}_k \times \boldsymbol{B})/B^2 = -i(\boldsymbol{k} \times \boldsymbol{b})\tilde{\phi}_k / B \tag{7.36}$$

where $\boldsymbol{b} = \boldsymbol{B}/B$. Equation (7.36) gives the perpendicular component of fluctuating motion. The substitution of (7.36) into (7.30) yields

$$\tilde{n}_k = \nabla n_0 \cdot \left(\frac{\boldsymbol{b} \times \boldsymbol{k}}{B}\right) \frac{\tilde{\phi}_k}{\omega_k}. \tag{7.37}$$

In general ∇n_0 and $\boldsymbol{b}$ are orthogonal. Take the z axis in the direction of $\boldsymbol{b}$ and the x axis in the direction of $-\nabla n$, i.e., let $\nabla n = -\kappa_n n_0 \hat{\boldsymbol{x}}$, where κ_n is the inverse of the scale of the density gradient and $\hat{\boldsymbol{x}}$ is the unit vector in the x direction. Then (7.37) gives

$$\frac{\tilde{n}_k}{n_0} = \frac{\kappa_n}{B}\frac{k_y}{\omega_k}\tilde{\phi}_k = k_y \kappa_n \frac{\kappa T_\mathrm{e}}{eB\omega_k}\frac{e\tilde{\phi}_k}{\kappa T_\mathrm{e}} = \frac{\omega_k^*}{\omega_k}\frac{e\tilde{\phi}_k}{\kappa T_\mathrm{e}}$$

where k_y the y (poloidal) component of the propagation vector $\boldsymbol{k}$. The quantity

$$\omega_k^* \equiv k_y \kappa_n \frac{(\kappa T_\mathrm{e})}{eB}.$$

is called the *drift frequency*. If the frequency ω_k is real (i.e., if $\gamma_k = 0$), $\tilde{n}_k$ and $\tilde{\phi}_k$ have the same phase, and the fluctuation does not contribute to anomalous diffusion as is clear from (7.35). When $\gamma_k > 0$, so that ω is complex, there is a phase difference between $\tilde{n}_k$ and $\tilde{\phi}_k$ and the fluctuation in the electric field contributes to anomalous diffusion. (When $\gamma_k < 0$, the amplitude of the fluctuation is damped and does not contribute to diffusion.) Using the real parameters A_k, α_k of $\omega_k = \omega_{k\mathrm{r}} + i\gamma_k = \omega_k^* A_k \exp i\alpha_k$ ($A_k > 0$, α_k are both real), $\boldsymbol{V}_k$ is expressed by

$$\tilde{\boldsymbol{V}}_k = -i(\boldsymbol{k} \times \boldsymbol{b})\frac{\kappa T_\mathrm{e}}{eB}\frac{\tilde{\phi}_k}{\kappa T_\mathrm{e}} = -i(\boldsymbol{k} \times \boldsymbol{b})\frac{\kappa T_\mathrm{e}}{eB}\frac{\tilde{n}_k}{n_0}\frac{\omega_{k\mathrm{r}} + \gamma_k i}{\omega_k^*} = -i(\boldsymbol{k} \times \boldsymbol{b})\frac{\kappa T_\mathrm{e}}{eB}\frac{\tilde{n}_k}{n_0} A_k \exp i\alpha_k,$$

$$\tilde{V}_{kx} = k_y \frac{\tilde{n}_k}{n_0}\frac{\kappa T_\mathrm{e}}{eB}\frac{\gamma_k - \omega_{k\mathrm{r}} i}{\omega_k^*} = k_y \frac{\tilde{n}_k}{n_0}\frac{\kappa T_\mathrm{e}}{eB}(-iA_k \exp i\alpha_k).$$

Then the diffusion coefficient may be obtained from (7.34) as follows:

$$D = \frac{1}{\kappa_n n_0}\mathrm{Re}(\tilde{n}_k \tilde{V}_{-kx} = \left(\sum_k \frac{k_y \gamma_k}{\kappa_n \omega_k^*}\left|\frac{\tilde{n}_k}{n_0}\right|^2\right)\frac{\kappa T_\mathrm{e}}{eB} = \left(\sum_k \frac{k_y}{\kappa_n} A_k \sin\alpha_k \left|\frac{\tilde{n}_k}{n_0}\right|^2\right)\frac{\kappa T_\mathrm{e}}{eB}. \tag{7.38}$$

The anomalous diffusion coefficient due to fluctuation loss increases with time (from (7.35) and (7.38)) and eventually the term with the maximum growth rate $\gamma_k > 0$ becomes dominant.

However, the amplitude $|\tilde{n}_k|$ will saturate due to nonlinear effects; the saturated amplitude will be of the order of

$$|\tilde{n}_k| \approx |\nabla n_0| \Delta x \approx \frac{\kappa_n}{k_x} n_0,$$

where Δx is the correlation length of the fluctuation in the direction of x and the inverse of the propagation constant k_x in the x direction. Then (7.35) becomes

$$D = \frac{\gamma_k}{\kappa_n^2}\left|\frac{\tilde{n}_k}{n_0}\right|^2 \approx \frac{\gamma_k}{k_x^2} \approx (\Delta x)^2 \gamma_k \approx \frac{(\Delta x)^2}{\tau_\mathrm{c}}, \tag{7.39}$$

where τ_c is the autocorrelation time of the fluctuation and is nearly equal to the inverse of γ_k in the saturation stage of the fluctuation.

When the nondimensional coefficient inside the parentheses in (7.38) is at its maximum of 1/16, we have the *Bohm diffusion coefficient*

$$D_\mathrm{B} = \frac{1}{16}\frac{\kappa T_\mathrm{e}}{eB}. \tag{7.40}$$

It appears that (7.40) give the largest possible diffusion coefficient.

When the density and potential fluctuations $\tilde{n}_k$, $\tilde{\phi}_k$ are measured, $\tilde{\boldsymbol{V}}_k$ can be calculated, and the estimated outward particle flux Γ and diffusion coefficient D can be compared to the values obtained by experiment. As the relation of $\tilde{n}_k$ and $\tilde{\phi}_k$ is given by (7.37), the phase difference will indicate whether ω_k is real (oscillatory mode) or $\gamma_k > 0$ (growing mode), so that this equation is very useful in interpreting experimental results.

Let us take an example of the fluctuation driven by ion temperature gradient drift instability (refer to sec.8.6). The mode is described by

$$\phi(r,\theta,z) = \sum \phi_{mn}(r)\exp(-im\theta + inz/R).$$

The growth rate of the fluctuation has the maximum at around $k_\theta = (-i/r)\partial/\partial\theta = -m/r$ of (ref.[4],[5])

$$|k_\theta| = \frac{m}{r} \sim \frac{\alpha_\theta}{\rho_\mathrm{i}}, \qquad \alpha_\theta = 0.7 \sim 0.8.$$

Then the correlation length Δ_θ in θ direction is $\Delta_\theta \sim \rho_\mathrm{i}/\alpha_\theta$ (ρ_i is ion Larmor radius).

The propagation constant $k_\parallel$ along the line of magnetic force near the rational surface $q(r_m) = m/n$ is

$$k_\parallel = -i\boldsymbol{b}\cdot\nabla = \frac{B_\theta}{B}\left(\frac{-m}{r}\right) + \frac{B_\mathrm{t}}{B}\left(\frac{n}{R}\right) \approx \frac{1}{R}\left(n - \frac{m}{q(r)}\right)$$

$$= \frac{m}{rR}\frac{rq'}{q^2}(r - r_m) = \frac{s}{Rq}k_\theta(r - r_m)$$

where $q(r) \equiv (r/R)(B_\mathrm{t}/B_\theta)$ is the safety factor (B_θ and B_t are poloidal and toroidal fields, respectively) and s is the shear parameter (refer to Section 8.3c) $s \equiv rq'/q$. $|k_\parallel|$ is larger than

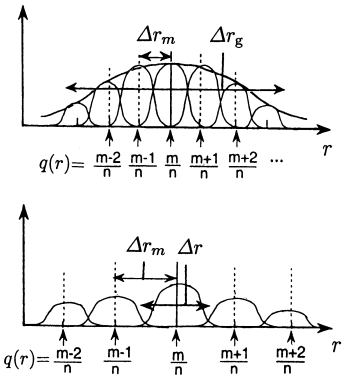

Fig.7.4 In the upper figure, the radial width of eigenmode Δr is larger than the radial separation of the rational surfaces Δr_m. A semi-global eigenmode structure $\Delta r_{\rm g}$ takes place due to the mode couplings. In the lower figure, the radial width of eigenmode Δr is smaller than the radial separation of the rational surfaces Δr_m. The modes with the radial width Δr are independent of each other.

the inverse of the connection length qR of torus and is less than the inverse of, say, the pressure gradient scale $L_{\rm p}$, that is

$$\frac{1}{qR} < |k_{\|}| < \frac{1}{L_{\rm p}}.$$

The radial width $\Delta r = |r - r_m|$ of the mode near the rational surface $r = r_m$ is roughly expected to be $\Delta r = |r - r_m| = (Rq/s)(k_{\|}/k_\theta) = (\rho_{\rm i}/s\alpha_\theta) \sim O(\rho_{\rm i}/s)$. The more accurate radial width of the eigenmode of ion temperature gradient driven drift turbulence is given by (ref.[5][6])

$$\Delta r = \rho_{\rm i} \left(\frac{qR}{sL_{\rm p}}\right)^{1/2} \left(\frac{\gamma_k}{\omega_{kr}}\right)^{1/2}.$$

The radial separation length Δr_m of the adjacent rational surface r_m and r_{m+1} is

$$q'\Delta r_m = q(r_{m+1}) - q(r_m) = \frac{m+1}{n} - \frac{m}{n} = \frac{1}{n}, \qquad \Delta r_m = \frac{1}{nq'} = \frac{m/n}{rq'}\frac{r}{m} \sim \frac{1}{sk_\theta}.$$

When the mode width Δr is larger than the radial separation of the rational surface Δr_m, the different modes are overlapped and the toroidal mode coupling takes place (see fig.7.4). The half width $\Delta r_{\rm g}$ of the envelope of coupled modes is estimated to be (ref.[6]-[8])

$$\Delta r_{\rm g} = \left(\frac{\rho_{\rm i} L_{\rm p}}{s}\right)^{1/2}.$$

The radial correlation length becomes the large value of $\Delta r_{\rm g}$ ($\Delta r_{\rm g}/\Delta r \sim (L_{\rm p}/\rho_{\rm i})^{1/2}$) and the radial propagation constant becomes $k_r \sim 1/\Delta r_{\rm g}$. In this case, the diffusion coefficient D is

$$D = (\Delta r_{\rm g})^2 \gamma_k \sim \frac{\rho_{\rm i} L_{\rm p}}{s} \omega_k^* \sim \frac{T}{eB}\frac{\alpha_\theta}{s}.$$

where ω_k^* is the drift frequency (sec.8.6, sec.9.2). This coefficient is of the Bohm type.

When the mode width Δr is less than Δr_m (weak shear case), there is no coupling between different modes and the radial correlation length is

$$\Delta r = \rho_{\rm i} \left(\frac{qR}{sL_{\rm p}}\right)^{1/2}.$$

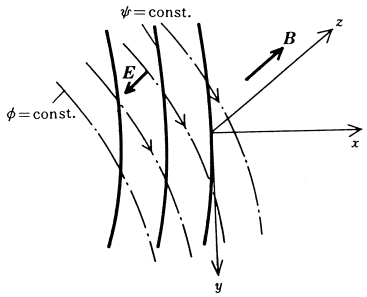

Fig.7.5 Magnetic surface $\psi = \text{const.}$ and electric-field equipotential $\phi = \text{const.}$ The plasma moves along the equipotential surfaces by virtue of $\boldsymbol{E} \times \boldsymbol{B}$.

The diffusion coefficient D in this case is

$$D \sim (\Delta r)^2 \omega_k^* \sim \rho_{\rm i}^2 \left(\frac{qR}{sL_{\rm p}}\right)\left(\frac{k_\theta T}{eBL_{\rm p}}\right) \sim \frac{T}{eB}\frac{\rho_{\rm i}}{L_{\rm p}}\left(\frac{\alpha_\theta qR}{sL_{\rm p}}\right) \propto \frac{T}{eB}\frac{\rho_{\rm i}}{L_{\rm p}}. \tag{7.41}$$

This is called *gyro-Bohm type diffusion coefficient*. It may be expected that the transport in toroidal systems becomes small in the weak shear region of negative shear configuration near the minimum q position (refer to sec.16.7).

Stationary Convective Loss

Next, let us consider *stationary convective losses* across the magnetic flux. Even if fluctuations in the density and electric field are not observed at a fixed position, it is possible that the plasma can move across the magnetic field and continuously escape. When a stationary electric field exists and the equipotential surfaces do not coincide with the magnetic surfaces $\phi = \text{const.}$, the $\boldsymbol{E} \times \boldsymbol{B}$ drift is normal to the electric field $\boldsymbol{E}$, which itself is normal to the equipotential surface. Consequently the plasma drifts along the equipotential surfaces (see fig.7.5) which cross the magnetic surfaces. The resultant loss is called stationary convective loss. The particle flux is given by

$$\Gamma_k = n_0 \frac{E_y}{B}. \tag{7.42}$$

The losses due to diffusion by binary collision are proportional to B^{-2}; but fluctuation or convective losses are proportional to B^{-1}. Even if the magnetic field is increased, the loss due to fluctuations does not decrease rapidly.

7.4 Loss by Magnetic Fluctuation

When the magnetic field in a plasma fluctuates, the lines of magnetic force will wander radially. Denote the radial shift of the field line by Δr and the radial component of magnetic fluctuation $\delta \boldsymbol{B}$ by δB_r respectively. Then we find

$$\Delta r = \int_0^L b_r \mathrm{d}l,$$

where $b_r = \delta B_r / B$ and l is the length along the line of magnetic force. The ensemble average of $(\Delta r)^2$ is given by

$$\begin{aligned}\langle (\Delta r)^2 \rangle &= \left\langle \int_0^L b_r \,\mathrm{d}l \int_0^L b_r \,\mathrm{d}l' \right\rangle = \left\langle \int_0^L \mathrm{d}l \int_0^L \mathrm{d}l'\, b_r(l)\, b_r(l') \right\rangle \\ &= \left\langle \int_0^L \mathrm{d}l \int_{-l}^{L-l} \mathrm{d}s\, b_r(l)\, b_r(l+s) \right\rangle \approx L \left\langle b_r^2 \right\rangle l_{\rm corr},\end{aligned}$$

where $l_{\rm corr}$ is

$$l_{\rm corr} = \frac{\left\langle \int_{-\infty}^{\infty} b_r(l)\, b_r(l+s)\, \mathrm{d}s \right\rangle}{\langle b_r^2 \rangle}.$$

If electrons run along the lines of magnetic force with the velocity $v_{\rm Te}$, the diffusion coefficient $D_{\rm e}$ of electrons becomes (ref.[9])

$$D_{\rm e} = \frac{\langle(\Delta r)^2\rangle}{\Delta t} = \frac{L}{\Delta t}\langle b_r^2\rangle l_{\rm corr} = v_{\rm Te} l_{\rm corr} \left\langle \left(\frac{\delta B_r}{B}\right)^2 \right\rangle . \tag{7.43}$$

We may take $l_{\rm corr} \sim R$ in the case of tokamak and $l_{\rm corr} \sim a$ in the case of reverse field pinch (RFP, refer sec.17.1).

References

[1] D. Pfirsh and A. Schlüter: MPI/PA/7/62, Max-Planck Institute für Physik und Astrophysik München (1962).

[2] A. A. Galeev and R. Z. Sagdeev: Sov. Phys. JETP **26**, 233 (1968).

[3] B. B. Kadomtsev and O. P. Pogutse: Nucl. Fusion **11**, 67 (1971).
F. L. Hinton and R. D. Hazeltine: Rev. Modern Phys. **48** 239 (1976).

[4] W. Horton: Phys. Rev. Lett. **37**, 1269 (1976).

[5] S. Hamaguchi and W. Horton: Phys. Fluids **B4**, 319 (1992).

[6] W. Horton, Jr., R. Esres, H. Kwak, and D.-I. Choi: Phys. Fluids **21**, 1366 (1978).

[7] F. Romanelli and F. Zonca: Phys. Fluids **B5**, 4081 (1993).
J. Y. Kim and M. Wakatani: Phys. Rev. Lett. **73**, 2200 (1994).

[8] Y. Kishimoto, J. Y. Kim, T. Fukuda, S. Ishida, T. Fujita, T. Tajima, W. Horton, G. Furnish, and M. J. LeBrun: 16th IAEA Fusion Energy Conf. (Conf. Proceedings, Motreal 1996) vol.**2**, 581 (1997) IAEA, Vienna.

[9] A. B. Rechester and M. N. Rosenbluth: Phys. Rev. Lett. **40**, 38 (1978).

Ch.8 Magnetohydrodynamic Instabilities

The stability of plasmas in magnetic fields is one of the primary research subjects in the area of controlled thermonuclear fusion and both theoretical and experimental investigations have been actively pursued. If a plasma is free from all possible instabilities and if the confinement is dominated by neoclassical diffusion in the banana region, then the energy confinement time $\tau_{\rm E}$ is given by

$$\tau_{\rm E} \approx \frac{(3/2)a^2}{5.8\chi_{\rm G.S.}} \approx \frac{(3/2)}{5.8}\left(\frac{\iota}{2\pi}\right)^2 \epsilon^{3/2}\left(\frac{a}{\rho_{\Omega \rm i}}\right)^2 \frac{1}{\nu_{\rm ii}}$$

where a is the plasma radius, $\rho_{\Omega \rm i}$ is the ion Larmor radius, and $\nu_{\rm ii}$ is the ion-ion collision frequency. For such an ideal case, a device of a reasonable size satisfies ignition condition. (For example, with $B = 5\,\mathrm{T}, a = 1\,\mathrm{m}$, $T_{\rm i} = 20\,\mathrm{keV}$, $\iota/2\pi \approx 1/3$, and inverse aspect ratio $\epsilon = 0.2$, the value of $n\tau_{\rm E} \sim 3.5 \times 10^{20}\,\mathrm{cm}^{-3} \cdot \mathrm{sec}$.)

A plasma consists of many moving charged particles and has many magnetohydrodynamic degrees of freedom as well as degrees of freedom in velocity space. When a certain mode of perturbation grows, it enhances diffusion. Heating a plasma increases the kinetic energy of the charged particles but at the same time can induce fluctuations in the electric and magnetic fields, which in turn augment anomalous diffusion.

Therefore, it is very important to study whether any particular perturbed mode is stable (damping mode) or unstable (growing mode). In the stability analysis, it is assumed that the deviation from the equilibrium state is small so that a linearized approximation can be used. In this chapter we will consider instabilities that can be described by linearized magnetohydrodynamic equations. These instabilities are called the *magnetohydrodynamic* (MHD) *instabilities* or *macroscopic instabilities*.

A small perturbation $\boldsymbol{F}(\boldsymbol{r}, t)$ of the first order is expanded in terms of its Fourier components

$$\boldsymbol{F}(\boldsymbol{r}, t) = \boldsymbol{F}(\boldsymbol{r}) \exp(-i\omega t) \qquad \omega = \omega_{\rm r} + i\omega_{\rm i}$$

and each term can be treated independently in the linearized approximation. The dispersion equation is solved for ω and the stability of the perturbation depends on the sign of the imaginary part $\omega_{\rm i}$ (unstable for $\omega_{\rm i} > 0$ and stable for $\omega_{\rm i} < 0$). When $\omega_{\rm r} \neq 0$, the perturbation is oscillatory and when $\omega_{\rm r} = 0$, it grows or damps monotonously.

In the following sections, typical MHD instabilities are introduced. In sec.8.1, interchange instability and kink instability are explained in an intuitive manner. In sec.8.2 the magnetohydrodynamic equations are linearized and the boundary conditions are implemented. The stability criterion is deduced from the energy principle (8.45) $\sim$ (8.48). In sec.8.3, a cylindrical plasma is studied as an important example; and the associated energy integrals are derived. Furthermore, important stability conditions, the Kruskal-Shafranov limit, (8.66), and the Suydam criterion, (8.97) are described. Tokamak and reversed field pinch configurations are taken approximately as cylindrical plasmas, and their stabilities are examined. In this chapter, only the most common and tractable magnetohydrodynamic instabilities are introduced; it should be understood that there are many other instabilities. General reviews of plasma instabilities may be found in (ref.[1]).

8.1 Interchange, Sausage and Kink Instabilities

Let us study simple examples of instabilities intuitively before discussing the general linear theory of instabilities.

8.1a Interchange Instability

Let $x = 0$ be the boundary between plasma and vacuum and let the z axis be taken in the direction of the magnetic field $\boldsymbol{B}$. The plasma region is $x < 0$ and the vacuum region is $x > 0$. It is assumed that the acceleration $\boldsymbol{g}$ is applied in the x direction (see fig.8.1). Ions and electrons drift in opposite directions to each other, due to the acceleration, with drift velocities

$$\boldsymbol{v}_{\rm G,i} = \frac{M}{e}\frac{\boldsymbol{g} \times \boldsymbol{B}}{B^2},$$

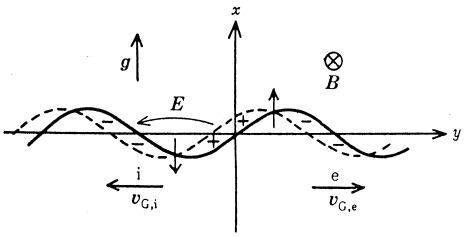

Fig.8.1 Ion and electron drifts and the resultant electric field for interchange instability.

$$\boldsymbol{v}_{\mathrm{G,e}} = -\frac{m}{e}\frac{\boldsymbol{g}\times\boldsymbol{B}}{B^2}.$$

Let us assume that, due to a perturbation, the boundary of the plasma is displaced from the surface $x = 0$ by the amount

$$\delta x = a(t)\sin(k_y y).$$

The charge separation due to the opposite ion and electron drifts yields an electric field. The resultant $\boldsymbol{E}\times\boldsymbol{B}$ drift enhances the original perturbation if the direction of the acceleration $\boldsymbol{g}$ is outward from the plasma. From fig.8.4b we see that this is the same as saying that the magnetic flux originally inside but near the plasma boundary is displaced so that it is outside the boundary, while the flux outside moves in to fill the depression thus left in the boundary; because of this geometrical picture of the process, this type of instability has come to be called *interchange instability* or *Rayleigh-Taylor instability*. As the perturbed plasma boundary is in the form of flutes along the magnetic lines of force (fig.8.4b), this instability is also called *flute instability*.

The drift due to the acceleration yields a surface charge on the plasma, of charge density

$$\sigma_s = \sigma(t)\cos(k_y y)\delta(x) \tag{8.1}$$

(see fig.8.1). The electrostatic potential ϕ of the induced electric field $\boldsymbol{E} = -\nabla\phi$ is given by

$$\epsilon_\perp\frac{\partial^2\phi}{\partial y^2} + \frac{\partial}{\partial x}\left(\epsilon_\perp\frac{\partial\phi}{\partial x}\right) = -\sigma_s. \tag{8.2}$$

The boundary condition is

$$\epsilon_0\left(\frac{\partial\phi}{\partial x}\right)_{+0} - \left(\epsilon_\perp\frac{\partial\phi}{\partial x}\right)_{-0} = -\sigma_s,$$

$$\phi_{+0} = \phi_{-0}.$$

Under the assumption $k_y > 0$, the solution ϕ is

$$\phi = \frac{\sigma(t)}{k_y(\epsilon_0+\epsilon_\perp)}\cos(k_y y)\exp(-k_y|x|). \tag{8.3}$$

The velocity of the boundary $\mathrm{d}(\delta x)/\mathrm{d}t$ is equal to $\boldsymbol{E}\times\boldsymbol{B}/B^2$ at $x = 0$, with $\boldsymbol{E}$ found from the potential (8.3). The velocity is

$$\frac{\mathrm{d}a(t)}{\mathrm{d}t}\sin(k_y y) = \frac{\sigma(t)}{(\epsilon_0+\epsilon_\perp)B}\sin(k_y y). \tag{8.4}$$

The charge flux in the y direction is

$$ne|\boldsymbol{v}_{\mathrm{G,i}}| = \frac{\rho_{\mathrm{m}}g}{B}$$

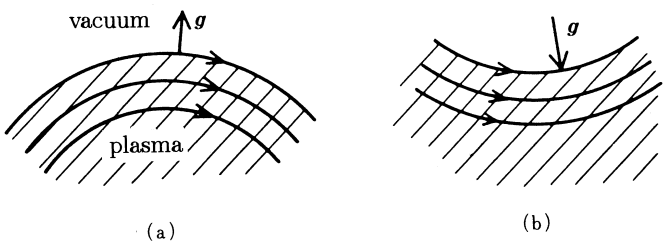

Fig.8.2 Centrifugal force due to the curvature of magnetic-force lines.

where $\rho_{\rm m} = nM$. Accordingly the changing rate of charge density is

$$\frac{{\rm d}\sigma(t)}{{\rm d}t}\cos(k_y y) = \frac{\rho_{\rm m} g}{B} a(t) \frac{\rm d}{{\rm d}y}\sin(k_y y) \tag{8.5}$$

and

$$\frac{{\rm d}^2 a}{{\rm d}t^2} = \frac{\rho_{\rm m} g k_y}{(\epsilon_0 + \epsilon_\perp) B^2} a. \tag{8.6}$$

The solution is in the form $a \propto \exp \gamma t$; the growth rate γ is given by

$$\gamma = \left(\frac{\rho_{\rm m}}{(\epsilon_0 + \epsilon_\perp) B^2}\right)^{1/2} (g k_y)^{1/2}. \tag{8.7}$$

In the low-frequency case (compared with the ion cyclotron frequency), the dielectric constant is given by

$$\epsilon_\perp = \epsilon_0 (1 + \frac{\rho_{\rm m}}{B^2 \epsilon_0}) \gg \epsilon_0 \tag{8.8}$$

as will be explained in ch.10. Accordingly the growth rate γ is (ref.[2])

$$\gamma = (g k_y)^{1/2}. \tag{8.9}$$

When the acceleration is outward, a perturbation with the propagation vector $\boldsymbol{k}$ normal to the magnetic field $\boldsymbol{B}$ is unstable; i.e.,

$$(\boldsymbol{k} \cdot \boldsymbol{B}) = 0. \tag{8.10}$$

However, if the acceleration is inward ($g < 0$), γ of (8.9) is imaginary and the perturbation is oscillatory and stable.

The origin of interchange instability is charge separation due to the acceleration. When the magnetic lines of force are curved, as is shown in fig.8.2, the charged particles are subjected to a centrifugal force. If the magnetic lines of force are convex outward (fig.8.2a), this centrifugal acceleration induces interchange instability. If the lines are concave outward, the plasma is stable. Accordingly, the plasma is stable when the magnitude B of the magnetic field increases outward. In other words, if B is a minimum at the plasma region the plasma is stable. This is the *minimum-B condition* for stability.

The drift motion of charged particles is expressed by

$$\boldsymbol{v}_{\rm g} = \frac{\boldsymbol{E} \times \boldsymbol{b}}{B} + \frac{\boldsymbol{b}}{\Omega} \times \left(\boldsymbol{g} + \frac{(v_\perp^2/2) + v_\parallel^2}{R}\boldsymbol{n}\right) + v_\parallel \boldsymbol{b}$$

where $\boldsymbol{n}$ is the normal unit vector from the center of curvature to a point on a line of magnetic force. R is the radius of curvature of line of magnetic force. The equivalent acceleration is

$$\boldsymbol{g} = \frac{(v_\perp^2/2) + v_\parallel^2}{R}\boldsymbol{n}. \tag{8.11}$$

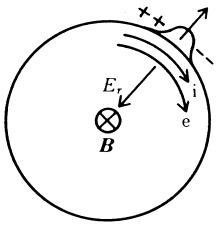

Fig.8.3 Charge separation due to the difference in velocities of ions and electrons.

The growth rate becomes $\gamma \approx (a/R)^{1/2}(v_{\rm T}/a)$ in this case. Analysis of interchange instability based on the linearlized equation of motion (8.32) with the acceralation term is described in (ref.[1]).

For a perturbation with propagation vector $\boldsymbol{k}$ normal to the magnetic field $\boldsymbol{B}$, i.e., $(\boldsymbol{k}\cdot\boldsymbol{B})=0$, another mechanism of charge separation may cause the same type of instability. When a plasma rotates with the velocity $v_\theta = E_r/B$ due to an inward radial electric field (fig.8.3), and if the rotation velocity of ions falls below that of electrons, the perturbation is unstable. Several possible mechanisms can retard ion rotation. The collision of ions and neutral particles delays the ion velocity and causes *neutral drag instability*.

When the growth rate $\gamma \sim (gk_y)^{1/2}$ is not very large and the ion Larmor radius $\rho_\Omega^{\rm i}$ is large enough to satisfy

$$(k_y\rho_\Omega^{\rm i})^2 > \frac{\gamma}{|\Omega_{\rm i}|}$$

the perturbation is stabilized (ref.[3]). When the ion Larmor radius becomes large, the average perturbation electric field felt by the ions is different that felt by the electrons, and the $\boldsymbol{E}\times\boldsymbol{B}/B^2$ drift velocities of the ion and the electrons are different. The charge separation thus induced has opposite phase from the charge separation due to acceleration and stabilizes the instabiltity.

8.1b Stability Criterion for Interchange Instability, Magnetic Well

Let us assume that a magnetic line of force has "good" curvature at one place B and 'bad" curvature at another place A (fig.8.4). Then the directions of the centrifugal force at A and B are opposite, as is the charge separation. The charge can easily be short circuited along the magnetic lines of the force, so that the problem of stability has a different aspect. Let us here consider perturbations in which the magnetic flux of region 1 is interchanged with that of region 2 and the plasma in the region 2 is interchanged with the plasma in the region 1 (interchange perturbations, fig.8.4b). It is assumed that the plasma is low-beta so that the magnetic field is nearly identical to the vacuum field. Any deviation from the vacuum field is accompanied by an increase in the energy of the disturbed field. This is the consequence of Maxwell equation. It can be shown that the most dangerous perturbations are those which exchange equal magnetic fluxes, as follows.
The energy of the magnetic field inside a magnetic tube is

$$Q_{\rm M} = \int {\rm d}\boldsymbol{r}\frac{B^2}{2\mu_0} = \int {\rm d}lS\frac{B^2}{2\mu_0} \tag{8.12}$$

where l is length taken along a line of magnetic force and S is the cross section of the magnetic tube. As the magnetic flux $\Phi = B\cdot S$ is constant, the energy is

$$Q_{\rm M} = \frac{\Phi^2}{2\mu_0}\int\frac{{\rm d}l}{S}.$$

The change $\delta Q_{\rm M}$ in the magnetic energy due to the interchange of the fluxes of regions 1 and 2 is

$$\delta Q_{\rm M} = \frac{1}{2\mu_0}\left(\left(\Phi_1^2\int_2\frac{{\rm d}l}{S}+\Phi_2^2\int_1\frac{{\rm d}l}{S}\right)-\left(\Phi_1^2\int_1\frac{{\rm d}l}{S}+\Phi_2^2\int_2\frac{{\rm d}l}{S}\right)\right). \tag{8.13}$$

If the exchanged fluxes Φ_1 and Φ_2 are the same, the energy change $\delta Q_{\rm M}$ is zero, so that perturbations resulting in $\Phi_1=\Phi_2$ are the most dangerous.

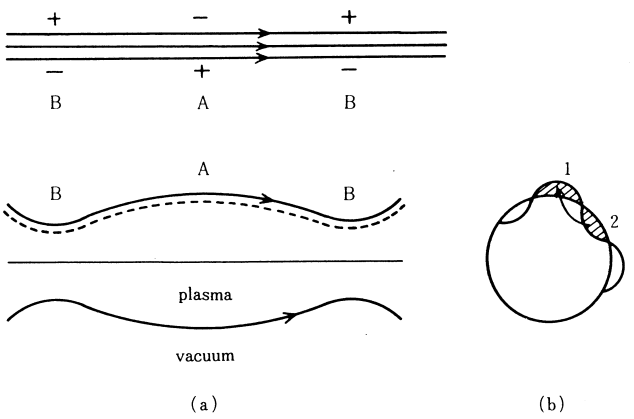

Fig.8.4 Charge separation in interchange instability. (a) The lower figure shows the unstable part A and the stable part B along a magnetic line of force. The upper figure shows the charge separation due to the acceleration along a flute. (b) Cross section of the perturbed plasma.

The kinetic energy $Q_{\rm p}$ of a plasma of volume $\mathcal{V}$ is

$$Q_{\rm p} = \frac{nT\mathcal{V}}{\gamma - 1} = \frac{p\mathcal{V}}{\gamma - 1} \tag{8.14}$$

where γ is the specific-heat ratio. As the perturbation is adiabatic,

$$p\mathcal{V}^{\gamma} = \text{const.}$$

is conserved during the interchange process. The change in the plasma energy is

$$\delta Q_{\rm p} = \frac{1}{\gamma - 1}\Big(p_2'\mathcal{V}_2 - p_1\mathcal{V}_1 + p_1'\mathcal{V}_1 - p_2\mathcal{V}_2\Big).$$

where p_2' is the pressure after interchange from the region $\mathcal{V}_1$ to $\mathcal{V}_2$ and p_1' is the pressure after interchange from the region $\mathcal{V}_2$ to $\mathcal{V}_1$. Because of adiabaticity, we have $p_2' = p_1\Big(\frac{\mathcal{V}_1}{\mathcal{V}_2}\Big)^{\gamma}$, $p_1' = p_2\Big(\frac{\mathcal{V}_2}{\mathcal{V}_1}\Big)^{\gamma}$ and $\delta Q_{\rm p}$ becomes

$$\delta Q_{\rm p} = \frac{1}{\gamma - 1}\left(p_1\left(\frac{\mathcal{V}_1}{\mathcal{V}_2}\right)^{\gamma}\mathcal{V}_2 - p_1\mathcal{V}_1 + p_2\left(\frac{\mathcal{V}_2}{\mathcal{V}_1}\right)^{\gamma}\mathcal{V}_1 - p_2\mathcal{V}_2\right). \tag{8.15}$$

Setting

$$p_2 = p_1 + \delta p,$$

$$\mathcal{V}_2 = \mathcal{V}_1 + \delta\mathcal{V}$$

we can write $\delta Q_{\rm p}$ as

$$\delta Q_{\rm p} = \delta p\delta\mathcal{V} + \gamma p\frac{(\delta\mathcal{V})^2}{\mathcal{V}}. \tag{8.16}$$

Since the stability condition is $\delta Q_{\rm p} > 0$, the sufficient condition is

$$\delta p\delta\mathcal{V} > 0.$$

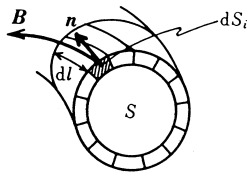

Fig.8.5 Specific volume of a toroidal field.

Since the volume is

$$\mathcal{V} = \int \mathrm{d}lS = \Phi \int \frac{\mathrm{d}l}{B}$$

the stability condition for interchange instability is written as

$$\delta p \delta \int \frac{\mathrm{d}l}{B} > 0.$$

Usually the pressure decreases outward ($\delta p < 0$), so that the stability condition is

$$\delta \int \frac{\mathrm{d}l}{B} < 0 \tag{8.17}$$

in the outward direction (ref.[4]). The integral is to be taken only over the plasma region.

Let the volume inside a magnetic surface ψ be V and the magnetic flux in the toroidal direction φ inside the magnetic surface ψ be Φ. We define the *specific volume* U by

$$U = \frac{\mathrm{d}V}{\mathrm{d}\Phi}. \tag{8.18}$$

If the unit vector of the magnetic field $\boldsymbol{B}$ is denoted by $\boldsymbol{b}$ and the normal unit vector of the infinitesimal cross-sectional area $\mathrm{d}S$ is denoted by $\boldsymbol{n}$, then we have

$$\mathrm{d}V = \int \sum_i (\boldsymbol{b}\cdot\boldsymbol{n})_i \mathrm{S}_i \mathrm{d}l, \qquad \mathrm{d}\Phi = \sum_i (\boldsymbol{b}\cdot\boldsymbol{n})_i B_i \mathrm{d}S_i.$$

When the magnetic lines of force close upon a single circuit of the torus, the specific volume U is

$$U = \frac{\oint \left(\sum_i (\boldsymbol{b}\cdot\boldsymbol{n})_i \mathrm{d}S_i \right) \mathrm{d}l}{\sum_i (\boldsymbol{b}\cdot\boldsymbol{n})_i B_i \mathrm{d}S_i} = \frac{\sum_i (\boldsymbol{b}\cdot\boldsymbol{n})_i B_i \mathrm{d}S_i \oint \frac{\mathrm{d}l}{B_i}}{\sum_i (\boldsymbol{b}\cdot\boldsymbol{n})_i B_i \mathrm{d}S_i}.$$

As the integral over l is carried out along a small tube of the magnetic field, $\sum_i (\boldsymbol{b}\cdot\boldsymbol{n})_i \mathrm{d}S_i B_i$ is independent of l (conservation of magnetic flux). As $\oint \mathrm{d}l/B_i$ on the same magnetic surface is constant, U is reduced to

$$U = \oint \frac{\mathrm{d}l}{B}.$$

When the lines of magnetic force close at N circuits, U is

$$U = \frac{1}{N} \int_N \frac{\mathrm{d}l}{B}. \tag{8.19}$$

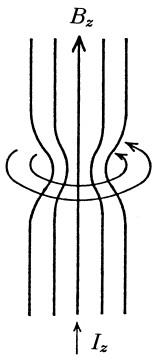

Fig.8.6 Sausage instability.

When the lines of magnetic force are *not* closed, U is given by

$$U = \lim_{N\to\infty} \frac{1}{N} \int_N \frac{\mathrm{d}l}{B}.$$

Therefore, U may be considered to be an average of $1/B$. When U decreases outward, it means that the magnitude B of the magnetic field increases outward in an average sense, so that the plasma region is the so-called *average minimum-B* region. In other word, the stability condition for interchange instability is reduced to average minimum-B condition;

$$\frac{\mathrm{d}U}{\mathrm{d}\Phi} = \frac{\mathrm{d}^2V}{\mathrm{d}\Phi^2} < 0. \tag{8.20}$$

When the value of U on the magnetic axis and on the outermost magnetic surface are U_0 and U_a respectively, we define a *magnetic well depth* $-\Delta U/U$ as

$$-\frac{\Delta U}{U} = \frac{U_0 - U_a}{U_0}. \tag{8.21}$$

8.1c Sausage Instability

Let us consider a cylindrical plasma with a sharp boundary. Only a longitudinal magnetic field B_z, exists inside the plasma region and only an azimuthal field $H_\theta = I_z/2\pi r$ due to the plasma current I_z exists outside the plasma region. We examine an azimuthally symmetric perturbation which constricts the plasma like a sausage (fig.8.6). When the plasma radius a is changed by δa, conservation of magnetic flux and the current in the plasma yields

$$\delta B_z = -B_z \frac{2\delta a}{a},$$

$$\delta B_\theta = -B_\theta \frac{\delta a}{a}.$$

The longitudinal magnetic field inside the plasma acts against the perturbation, while the external azimuthal field destabilizes the perturbation. The difference δp_m in the magnetic pressures is

$$\delta p_\mathrm{m} = -\frac{B_z^2}{\mu_0}\frac{2\delta a}{a} + \frac{B_\theta^2}{\mu_0}\frac{\delta a}{a}.$$

The plasma is stable if $\delta p_\mathrm{m} > 0$ for $\delta a < 0$, so that the stability condition is

$$B_z^2 > \frac{B_\theta^2}{2}. \tag{8.22}$$

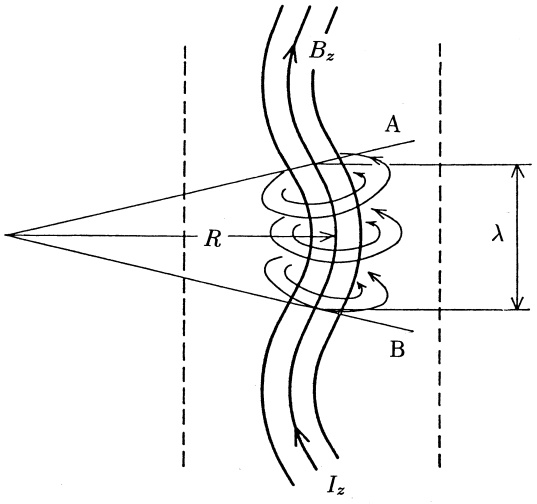

Fig.8.7 Kink instability.

This type of instability is called *sausage instability.*

8.1d Kink Instability

Let us consider a perturbation that kinks the plasma column as shown in fig.8.7. The configuration of the plasma is the same as that in the previous subsection (sharp boundary, an internal longitudinal field, an external azimuthal field). Denote the characteristic length of the kink by λ and its radius of curvature by R. The longitudinal magnetic field acts as a restoring force on the plasma due to the longitudinal tension; the restoring force on the plasma region of length λ is

$$\frac{B_z^2}{2\mu_0}\pi a^2\frac{\lambda}{R}.$$

The azimuthal magnetic field becomes strong, at the inner (concave) side of the kink and destabilizes the plasma column. In order to estimate the destabilizing force, we consider a cylindrical lateral surface of radius λ around the plasma and two planes A and B which pass through the center of curvature (see fig.8.7). Let us compare the contributions of the magnetic pressure on the surfaces enclosing the kink. The contribution of the magnetic pressure on the cylindrical surface is negligible compared with those on the planes A and B. The contribution of the magnetic pressure on the planes A and B is

$$\int_a^\lambda \frac{B_\theta^2}{2\mu_0}2\pi r\mathrm{d}r\times\frac{\lambda}{2R}=\frac{B_\theta^2(a)}{2\mu_0}\pi a^2\ln\frac{\lambda}{a}\times\frac{\lambda}{R}.$$

Accordingly

$$\frac{B_z^2}{B_\theta^2(a)}>\ln\frac{\lambda}{a} \tag{8.23}$$

is the stability condition (ref.[3]). However, the pressure balance

$$p+\frac{B_z^2}{2\mu_0}=\frac{B_\theta^2}{2\mu_0}$$

holds, so that perturbations of large λ are unstable. This type of instability is called *kink instability.*

In this section, a cylindrical sharp-boundary plasma has been analyzed in an intuitive way. The stability of a cylindrical plasma column will be treated in sec.8.2 in more general and systematic ways.

8.2 Formulation of Magnetohydrodynamic Instabilities

8.2a Linearization of Magnetohydrodynamic Equations

The stability problems of plasmas can be studied by analyzing infinitesimal perturbations of the equilibrium state. If the mass density, pressure, flow velocity, and magnetic field are denoted by $\rho_{\rm m}, p, \boldsymbol{V}$, and $\boldsymbol{B}$, respectively, the equation of motion, conservation of mass, Ohm's law, and the adiabatic relation are

$$\rho_{\rm m}\frac{\partial \boldsymbol{V}}{\partial t} = -\nabla p + \boldsymbol{j}\times\boldsymbol{B}, \qquad \frac{\partial \rho_{\rm m}}{\partial t} + \nabla\cdot(\rho_{\rm m}\boldsymbol{V}) = 0,$$

$$\boldsymbol{E} + \boldsymbol{V}\times\boldsymbol{B} = 0, \qquad \left(\frac{\partial}{\partial t} + \boldsymbol{V}\cdot\nabla\right)(p\rho_{\rm m}^{-\gamma}) = 0$$

respectively (γ is the ratio of specific heat). Maxwell's equations are then

$$\nabla\times\boldsymbol{E} = -\frac{\partial \boldsymbol{B}}{\partial t}, \qquad \nabla\times\boldsymbol{B} = \mu_0\boldsymbol{j}, \qquad \nabla\cdot\boldsymbol{B} = 0.$$

These are the magnetohydrodynamic equations of a plasma with zero specific resistivity (see sec.5.2). The values of $\rho_{\rm m}$, p, $\boldsymbol{V}$, and $\boldsymbol{B}$ in the equilibrium state are $\rho_{\rm m0}$, p_0, $\boldsymbol{V}_0 = 0$, and $\boldsymbol{B}_0$ respectively. The first-order small quantities are $\rho_{\rm m1}$, p_1, $\boldsymbol{V}_1 = \boldsymbol{V}$, and $\boldsymbol{B}_1$. The zeroth-order equations are

$$\nabla p_0 = \boldsymbol{j}_0\times\boldsymbol{B}_0, \qquad \nabla\times\boldsymbol{B}_0 = \mu_0\boldsymbol{j}_0, \qquad \nabla\cdot\boldsymbol{B}_0 = 0.$$

The first-order linearized equations are

$$\frac{\partial \rho_{\rm m1}}{\partial t} + \nabla\cdot(\rho_{\rm m0}\boldsymbol{V}) = 0, \tag{8.24}$$

$$\rho_{\rm m0}\frac{\partial \boldsymbol{V}}{\partial t} + \nabla p_1 = \boldsymbol{j}_0\times\boldsymbol{B}_1 + \boldsymbol{j}_1\times\boldsymbol{B}_0, \tag{8.25}$$

$$\frac{\partial p_1}{\partial t} + (\boldsymbol{V}\cdot\nabla)p_0 + \gamma p_0\nabla\cdot\boldsymbol{V} = 0, \tag{8.26}$$

$$\frac{\partial B_1}{\partial t} = \nabla\times(\boldsymbol{V}\times\boldsymbol{B}_0). \tag{8.27}$$

If displacement of the plasma from the equilibrium position $\boldsymbol{r}_0$ is denoted by $\boldsymbol{\xi}(\boldsymbol{r}_0, t)$, it follows that

$$\boldsymbol{\xi}(\boldsymbol{r}_0, t) = \boldsymbol{r} - \boldsymbol{r}_0, \qquad \boldsymbol{V} = \frac{{\rm d}\boldsymbol{\xi}}{{\rm d}t} \approx \frac{\partial \boldsymbol{\xi}}{\partial t}.$$

Equation (8.27) is reduced to

$$\frac{\partial \boldsymbol{B}_1}{\partial t} = \nabla\times\left(\frac{\partial \boldsymbol{\xi}}{\partial t}\times\boldsymbol{B}_0\right)$$

and

$$\boldsymbol{B}_1 = \nabla\times(\boldsymbol{\xi}\times\boldsymbol{B}_0). \tag{8.28}$$

From $\mu_0\boldsymbol{j} = \nabla\times\boldsymbol{B}$, it follows that

$$\mu_0\boldsymbol{j}_1 = \nabla\times\boldsymbol{B}_1. \tag{8.29}$$

Equations (8.24) and (8.26) yield

$$\rho_{\rm m1} = -\nabla\cdot(\rho_{\rm m0}\boldsymbol{\xi}) \tag{8.30}$$

$$p_1 = -\boldsymbol{\xi} \cdot \nabla p_0 - \gamma p_0 \nabla \cdot \boldsymbol{\xi}. \tag{8.31}$$

The substitution of these equations into (8.25) gives

$$\begin{aligned}\rho_{\mathrm{m}0} \frac{\partial^2 \boldsymbol{\xi}}{\partial t^2} &= \nabla(\boldsymbol{\xi} \cdot \nabla p_0 + \gamma p_0 \nabla \cdot \boldsymbol{\xi}) + \frac{1}{\mu_0}(\nabla \times \boldsymbol{B}_0) \times \boldsymbol{B}_1 + \frac{1}{\mu_0}(\nabla \times \boldsymbol{B}_1) \times \boldsymbol{B}_0 \\ &= -\nabla \left(p_1 + \frac{\boldsymbol{B}_0 \cdot \boldsymbol{B}_1}{\mu_0} \right) + \frac{1}{\mu_0}((\boldsymbol{B}_0 \cdot \nabla)\boldsymbol{B}_1 + (\boldsymbol{B}_1 \cdot \nabla)\boldsymbol{B}_0).\end{aligned} \tag{8.32}$$

This is the linearized equation of motion in terms of $\boldsymbol{\xi}$.

Next let us consider the boundary conditions. Where the plasma contacts an ideal conductor, the tangential component of the electric field is zero, i.e., $\boldsymbol{n} \times \boldsymbol{E} = 0$. This is equivalent to $\boldsymbol{n} \times (\boldsymbol{\xi} \times \boldsymbol{B}_0) = 0$, $\boldsymbol{n}$ being taken in the outward direction. The conditions $(\boldsymbol{\xi} \cdot \boldsymbol{n}) = 0$ and $(\boldsymbol{B}_1 \cdot \boldsymbol{n}) = 0$ must also be satisfied. At the boundary surface between plasma and vacuum, the total pressure must be continuous and

$$p - p_0 + \frac{B_{\mathrm{in}}^2 - B_{0,\mathrm{in}}^2}{2\mu_0} = \frac{B_{\mathrm{ex}}^2 - B_{0,\mathrm{ex}}^2}{2\mu_0}$$

where $\boldsymbol{B}_{\mathrm{in}}, \boldsymbol{B}_{0,\mathrm{in}}$ give the internal magnetic field of the plasma and $\boldsymbol{B}_{\mathrm{ex}}, \boldsymbol{B}_{0,\mathrm{ex}}$ give the external field. The boundary condition is reduced to

$$\begin{aligned}&-\gamma p_0 \nabla \cdot \boldsymbol{\xi} + \frac{\boldsymbol{B}_{0,\mathrm{in}} \cdot (\boldsymbol{B}_{1,\mathrm{in}} + (\boldsymbol{\xi} \cdot \nabla)\boldsymbol{B}_{0,\mathrm{in}})}{\mu_0} \\ &\quad = \frac{\boldsymbol{B}_{0,\mathrm{ex}} \cdot (\boldsymbol{B}_{1,\mathrm{ex}} + (\boldsymbol{\xi} \cdot \nabla)\boldsymbol{B}_{0,\mathrm{ex}})}{\mu_0}\end{aligned} \tag{8.33}$$

when $\boldsymbol{B}_{\mathrm{in}}(\boldsymbol{r}), \boldsymbol{B}_{\mathrm{ex}}(\boldsymbol{r})$ and $p(\boldsymbol{r})$ are expanded in $\boldsymbol{\xi} = \boldsymbol{r} - \boldsymbol{r}_0$ ($f(\boldsymbol{r}) = f_0(\boldsymbol{r}_0) + (\boldsymbol{\xi} \cdot \nabla) f_0(\boldsymbol{r}) + f_1$).

From Maxwell's equations, the boundary conditions are

$$\boldsymbol{n}_0 \cdot (\boldsymbol{B}_{0,\mathrm{in}} - \boldsymbol{B}_{0,\mathrm{ex}}) = 0, \tag{8.34}$$

$$\boldsymbol{n}_0 \times (\boldsymbol{B}_{0,\mathrm{in}} - \boldsymbol{B}_{0,\mathrm{ex}}) = \mu_0 \boldsymbol{K} \tag{8.35}$$

where $\boldsymbol{K}$ is the surface current.

Ohm's law yields

$$\boldsymbol{E}_{\mathrm{in}} + \boldsymbol{V} \times \boldsymbol{B}_{0,\mathrm{in}} = 0 \tag{8.36}$$

in the plasma. As the electric field $\boldsymbol{E}^*$ in coordinates moving with the plasma is $\boldsymbol{E}^* = \boldsymbol{E} + \boldsymbol{V} \times \boldsymbol{B}_0$ and the tangential component of the electric field $\boldsymbol{E}^*$ is continuous across the plasma boundary. The boundary condition can be written as

$$\boldsymbol{E}_t + (\boldsymbol{V} \times \boldsymbol{B}_{0,\mathrm{ex}})_{\mathrm{t}} = 0 \tag{8.37}$$

where the subscript t indicates the tangential component. Since the normal component of $\boldsymbol{B}$ is given by the tangential component of $\boldsymbol{E}$ by the relation $\nabla \times \boldsymbol{E} = -\partial \boldsymbol{B}/\partial t$, (8.37) is reduced to

$$(\boldsymbol{n}_0 \cdot \boldsymbol{B}_{1,\mathrm{ex}}) = \boldsymbol{n}_0 \cdot \nabla \times (\boldsymbol{\xi} \times \boldsymbol{B}_{0,\mathrm{ex}}). \tag{8.38}$$

The electric field $\boldsymbol{E}_{\mathrm{ex}}$ and the magnetic field $\boldsymbol{B}_{\mathrm{ex}}$ in the external (vacuum) region can be expressed in terms of a vector potential:

$$\boldsymbol{E}_{\mathrm{ex}} = -\frac{\partial \boldsymbol{A}}{\partial t}, \qquad \boldsymbol{B}_{1,\mathrm{ex}} = \nabla \times \boldsymbol{A}, \qquad \nabla \cdot \boldsymbol{A} = 0.$$

If no current flows in the vacuum region, $\boldsymbol{A}$ satisfies

$$\nabla \times \nabla \times \boldsymbol{A} = 0. \tag{8.39}$$

Using the vector potential, we may express (8.37) as

$$\boldsymbol{n}_0 \times \left(-\frac{\partial \boldsymbol{A}}{\partial t} + \boldsymbol{V} \times \boldsymbol{B}_{0,\mathrm{ex}} \right) = 0.$$

For $\boldsymbol{n}_0 \cdot \boldsymbol{B}_{0,\mathrm{in}} = \boldsymbol{n} \cdot \boldsymbol{B}_{0,\mathrm{ex}} = 0$, the boundary condition is

$$\boldsymbol{n}_0 \times \boldsymbol{A} = -\xi_n \boldsymbol{B}_{0,\mathrm{ex}}. \tag{8.40}$$

The boundary condition at the wall of an ideal conductor is

$$\boldsymbol{n} \times \boldsymbol{A} = 0. \tag{8.41}$$

The stability problem now becomes one of solving (8.32) and (8.39) under the boundary conditions (8.33),(8.38),(8.40) and (8.41). When a normal mode $\boldsymbol{\xi}(\boldsymbol{r}, t) = \boldsymbol{\xi}(\boldsymbol{r}) \exp(-i\omega t)$ is considered, the problem is reduced to the eigenvalue problem $\rho_0 \omega^2 \boldsymbol{\xi} = \boldsymbol{F}(\boldsymbol{\xi})$. If any eigenvalue is negative, the plasma is unstable; if all the eigenvalues are positive, the plasma is stable.

8.2b Energy Principle (ref.[5])

The eigenvalue problem is complicated and difficult to solve in general. When we introduce a potential energy associated with the displacement $\boldsymbol{\xi}$, the stability problem can be simplified. The equation of motion has the form

$$\rho_{\mathrm{m}0} \frac{\partial^2 \boldsymbol{\xi}}{\partial t^2} = \boldsymbol{F}(\boldsymbol{\xi}) = -\widehat{\boldsymbol{K}} \cdot \boldsymbol{\xi}. \tag{8.42}$$

This equation can be integrated:

$$\frac{1}{2} \int \rho_{\mathrm{m}0} \left(\frac{\partial \boldsymbol{\xi}}{\partial t} \right)^2 \mathrm{d}\boldsymbol{r} + \frac{1}{2} \int \boldsymbol{\xi} \cdot \widehat{\boldsymbol{K}} \boldsymbol{\xi} \mathrm{d}\boldsymbol{r} = \mathrm{const.}$$

The kinetic energy T and the potential energy W are

$$T \equiv \frac{1}{2} \int \rho_{\mathrm{m}0} \left(\frac{\partial \boldsymbol{\xi}}{\partial t} \right)^2 \mathrm{d}\boldsymbol{r}, \qquad W \equiv \frac{1}{2} \int \boldsymbol{\xi} \cdot \widehat{\boldsymbol{K}} \boldsymbol{\xi} \mathrm{d}\boldsymbol{r} = -\frac{1}{2} \int \boldsymbol{\xi} \cdot F(\boldsymbol{\xi}) \mathrm{d}\boldsymbol{r}$$

respectively. Accordingly if

$$W > 0$$

for all possible displacements, the system is stable. This is the stability criterion of the *energy principle*. W is called the *energy integral*.

It is possible to prove that the operator $\widehat{\boldsymbol{K}}$ is Hermite operator (self-adjoint operator) (ref.[6],[7]). A displacement $\boldsymbol{\eta}$ and a vector potential $\boldsymbol{Q}$ are introduced which satisfy the same boundary conditions as $\boldsymbol{\xi}$ and $\boldsymbol{A}$, i.e.,

$$\boldsymbol{n}_0 \times \boldsymbol{Q} = -\eta_n \boldsymbol{B}_{0,\mathrm{ex}}$$

at the plasma-vacuum boundary and

$$\boldsymbol{n}_0 \times \boldsymbol{Q} = 0$$

at the conducting wall. By substitution of (8.32), the integral in the plasma region V_{in} is seen to be

$$\int_{V_{\mathrm{in}}} \boldsymbol{\eta} \cdot \widehat{\boldsymbol{K}} \boldsymbol{\xi} \mathrm{d}\boldsymbol{r} = \int_{V_{\mathrm{in}}} \Big(\gamma p_0 (\nabla \cdot \boldsymbol{\eta})(\nabla \cdot \boldsymbol{\xi}) + (\nabla \cdot \boldsymbol{\eta})(\boldsymbol{\xi} \cdot \nabla p_0) + \frac{1}{\mu_0} (\nabla \times (\boldsymbol{\eta} \times \boldsymbol{B}_0)) \cdot \nabla \times (\boldsymbol{\xi} \times \boldsymbol{B}_0)$$

$$-\frac{1}{\mu_0}(\boldsymbol{\eta}\times(\nabla\times\boldsymbol{B}_0))\cdot\nabla\times(\boldsymbol{\xi}\times\boldsymbol{B}_0)\Big)\,\mathrm{d}\boldsymbol{r}$$

$$+\int_S \boldsymbol{n}_0\cdot\boldsymbol{\eta}\left(\frac{\boldsymbol{B}_{0,\mathrm{in}}\cdot\nabla\times(\boldsymbol{\xi}\times\boldsymbol{B}_{0,\mathrm{in}})}{\mu_0}-\gamma p_0(\nabla\cdot\boldsymbol{\xi})-(\boldsymbol{\xi}\cdot\nabla p_0)\right)\mathrm{d}S. \tag{8.43}$$

Next let us consider the surface integral in (8.43). Due to the boundary condition $\boldsymbol{n}_0\times\boldsymbol{Q}=-\eta_n\boldsymbol{B}_{0,\mathrm{ex}}$, we find that

$$\begin{aligned}\int_S \eta_n\boldsymbol{B}_{0,\mathrm{ex}}\cdot\boldsymbol{B}_{1,\mathrm{ex}}\mathrm{d}S&=\int_S\eta_n\boldsymbol{B}_{0,\mathrm{ex}}(\nabla\times\boldsymbol{A})\mathrm{d}S=-\int_S(\boldsymbol{n}_0\times\boldsymbol{Q})\cdot(\nabla\times\boldsymbol{A})\mathrm{d}S\\&=-\int_S\boldsymbol{n}_0\cdot(\boldsymbol{Q}\times(\nabla\times\boldsymbol{A}))\mathrm{d}S=\int_{V_{\mathrm{ex}}}\nabla\cdot(\boldsymbol{Q}\times(\nabla\times\boldsymbol{A}))\mathrm{d}\boldsymbol{r}\\&=\int_{V_{\mathrm{ex}}}((\nabla\times\boldsymbol{Q})\cdot(\nabla\times\boldsymbol{A})-\boldsymbol{Q}\cdot\nabla\times(\nabla\times\boldsymbol{A}))\,\mathrm{d}\boldsymbol{r}\\&=\int_{V_{\mathrm{ex}}}(\nabla\times\boldsymbol{Q})\cdot(\nabla\times\boldsymbol{A})\mathrm{d}\boldsymbol{r}.\end{aligned}$$

From the boundary condition (8.33), the difference between the foregoing surface integral and the surface integral in (8.43) is reduced to

$$\begin{aligned}&\int\eta_n\Big(\frac{\boldsymbol{B}_{0,\mathrm{in}}\cdot\boldsymbol{B}_{1,\mathrm{in}}-\boldsymbol{B}_{0,\mathrm{ex}}\cdot\boldsymbol{B}_{1,\mathrm{ex}}}{\mu_0}-\gamma p_0(\nabla\cdot\boldsymbol{\xi})-(\boldsymbol{\xi}\cdot\nabla)p_0\Big)\mathrm{d}S\\&\quad=\int_S\eta_n(\boldsymbol{\xi}\cdot\nabla)\Big(\frac{B_{0,\mathrm{ex}}^2}{2\mu_0}-\frac{B_{0,\mathrm{in}}^2}{2\mu_0}-p_0\Big)\mathrm{d}S\\&\quad=\int_S\eta_n\xi_n\frac{\partial}{\partial n}\Big(\frac{B_{0,\mathrm{ex}}^2}{2\mu_0}-\frac{B_{0,\mathrm{in}}^2}{2\mu_0}-p_0\Big)\mathrm{d}S\end{aligned}$$

where the relation $\boldsymbol{n}_0\times\nabla(p_0+B_{0,\mathrm{in}}^2/2\mu_0-B_{0,\mathrm{ex}}^2/2\mu_0)=0$ is used. The integral region V_{ex} is the region outside the plasma. Finally, the energy integral is reduced to

$$\begin{aligned}\int_{V_{\mathrm{in}}}\boldsymbol{\eta}\cdot\widehat{\boldsymbol{K}}\boldsymbol{\xi}\mathrm{d}\boldsymbol{r}=\int_{V_{\mathrm{in}}}\Big(&\gamma p_0(\nabla\cdot\boldsymbol{\eta})(\nabla\cdot\boldsymbol{\xi})+\frac{1}{\mu_0}(\nabla\times(\boldsymbol{\eta}\times\boldsymbol{B}_0))\cdot\nabla\times(\boldsymbol{\xi}\times\boldsymbol{B}_0)\\&+(\nabla\cdot\boldsymbol{\eta})(\boldsymbol{\xi}\cdot\nabla p_0)-\frac{1}{\mu_0}(\boldsymbol{\eta}\times(\nabla\times\boldsymbol{B}_0))\cdot\nabla\times(\boldsymbol{\xi}\times\boldsymbol{B}_0)\Big)\mathrm{d}\boldsymbol{r}+\frac{1}{\mu_0}\int_{V_{\mathrm{ex}}}(\nabla\times\boldsymbol{Q})\cdot(\nabla\times\boldsymbol{A})\mathrm{d}\boldsymbol{r}\\&+\int_S\eta_n\xi_n\frac{\partial}{\partial n}\Big(\frac{B_{0,\mathrm{ex}}^2}{2\mu_0}-\frac{B_{0,\mathrm{in}}^2}{2\mu_0}-p_0\Big)\mathrm{d}S.\end{aligned}\tag{8.44}$$

The energy integral W is divided into three parts W_{P}, W_{S}, and W_{V}, the contributions of the plasma internal region V_{in}, the boundary region S, and the external vacuum region V_{ex}, i.e.,

$$W=\frac{1}{2}\int_{V_{\mathrm{in}}}\boldsymbol{\xi}\cdot\widehat{\boldsymbol{K}}\boldsymbol{\xi}\mathrm{d}\boldsymbol{r}=W_{\mathrm{p}}+W_{\mathrm{S}}+W_{\mathrm{V}}, \tag{8.45}$$

$$\begin{aligned}W_{\mathrm{p}}=\frac{1}{2}\int_{V_{\mathrm{in}}}\Big(&\gamma p_0(\nabla\cdot\boldsymbol{\xi})^2+\frac{1}{\mu_0}(\nabla\times(\boldsymbol{\xi}\times\boldsymbol{B}_0))^2+(\nabla\cdot\boldsymbol{\xi})(\boldsymbol{\xi}\cdot\nabla p_0)\\&-\frac{1}{\mu_0}(\boldsymbol{\xi}\times(\nabla\times\boldsymbol{B}_0))\cdot\nabla\times(\boldsymbol{\xi}\times\boldsymbol{B}_0)\Big)\mathrm{d}\boldsymbol{r}\end{aligned}$$

$$= \frac{1}{2}\int_{V_{\rm in}} \left(\frac{\boldsymbol{B}_1^2}{\mu_0} - p_1(\nabla\cdot\boldsymbol{\xi}) - \boldsymbol{\xi}\cdot(\boldsymbol{j}_0\times\boldsymbol{B}_1)\right) \mathrm{d}\boldsymbol{r}, \tag{8.46}$$

$$W_{\rm S} = \frac{1}{2}\int_S \xi_n^2 \frac{\partial}{\partial n}\left(\frac{B_{0,\rm ex}^2}{2\mu_0} - \frac{B_{0,\rm in}^2}{2\mu_0} - p_0 \right) \mathrm{d}S, \tag{8.47}$$

$$W_{\rm V} = \frac{1}{2\mu_0}\int_{V_{\rm ex}} (\nabla\times\boldsymbol{A})^2 \mathrm{d}\boldsymbol{r} = \int_{V_{\rm ex}} \frac{\boldsymbol{B}_1^2}{2\mu_0}\mathrm{d}\boldsymbol{r}. \tag{8.48}$$

The stability condition is $W > 0$ for all possible $\boldsymbol{\xi}$. The frequency or growth rate of a perturbation can be obtained from the energy integral. When the perturbation varies as $\exp(-i\omega t)$, the equation of motion is

$$\omega^2 \rho_{\rm m0}\boldsymbol{\xi} = \widehat{\boldsymbol{K}}\boldsymbol{\xi}. \tag{8.49}$$

The solution of the eigenvalue problem is the same as the solution based on the calculus of variations $\delta W = 0$, where

$$\omega^2 = \frac{\int \boldsymbol{\xi}\cdot\widehat{\boldsymbol{K}}\boldsymbol{\xi}\mathrm{d}\boldsymbol{r}}{\int \rho_{\rm m0}\boldsymbol{\xi}^2\mathrm{d}\boldsymbol{r}}. \tag{8.50}$$

As $\widehat{\boldsymbol{K}}$ is a Hermitian operator, ω^2 is real. In the MHD analysis of an ideal plasma with zero resistivity, the perturbation either increases or decreases monotonically, or else the perturbed plasma oscillates with constant amplitude.

The energy integral (8.46) can be further rearranged to the more illuminating form. The reduction of the form is described in appendix B. The energy integral of axisymmetiric toroidal system is also described in appendix B.

8.3 Instabilities of a Cylindrical Plasma

8.3a Instabilities of Sharp-Boundary Configuration: Kruskal-Shafranov Condition

Let us consider a sharp-boundary plasma of radius a, with a longitudinal magnetic field B_{0z} inside the boundary and a longitudinal magnetic field $B_{\rm e}z$ and an azimuthal magnetic field $B_\theta = \mu_0 I/(2\pi r)$ outside. B_{0z} and B_{ez} are assumed to be constant. We can consider the displacement

$$\boldsymbol{\xi}(r)\exp(im\theta + ikz) \tag{8.51}$$

since any displacement may be expressed by a superposition of such modes. Since the term in $\nabla\cdot\boldsymbol{\xi}$ in the energy integral is positive, incompressible perturbation is the most dangerous. We examine only the worst mode,

$$\nabla\cdot\boldsymbol{\xi} = 0. \tag{8.52}$$

The perturbation of the magnetic field $\boldsymbol{B}_1 = \nabla\times(\boldsymbol{\xi}\times\boldsymbol{B}_0)$ is

$$\boldsymbol{B}_1 = ikB_{0z}\boldsymbol{\xi}. \tag{8.53}$$

The equation of motion (8.32) becomes

$$\left(-\omega^2\rho_{\rm m0} + \frac{k^2 B_{0z}^2}{\mu_0}\right)\boldsymbol{\xi} = -\nabla\left(p_1 + \frac{\boldsymbol{B}_0\cdot\boldsymbol{B}_1}{\mu_0}\right) \equiv -\nabla p^*. \tag{8.54}$$

As $\nabla\cdot\boldsymbol{\xi} = 0$, it follows that $\Delta p^* = 0$, i.e.,

$$\left(\frac{\mathrm{d}^2}{\mathrm{d}r^2} + \frac{1}{r}\frac{\mathrm{d}}{\mathrm{d}r} - \left(k^2 + \frac{m^2}{r^2}\right)\right) p^*(r) = 0. \tag{8.55}$$

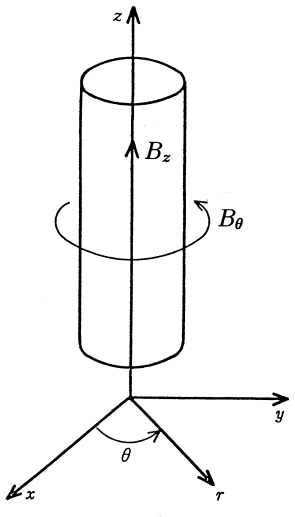

Fig.8.8 Sharp-boundary plasma.

The solution without singularity at $r = 0$ is given by the modified Bessel function $I_m(kr)$, so that $p^*(r)$ is

$$p^*(r) = p^*(a)\frac{I_m(kr)}{I_m(ka)}.$$

Accodingly, we find

$$\xi_r(a) = \frac{\dfrac{kp^*(a)}{I_m(ka)}}{\omega^2\rho_{\mathrm{m0}} - \dfrac{k^2B_0^2}{\mu_0}} I'_m(ka). \tag{8.56}$$

As the perturbation of the vacuum magnetic field $\boldsymbol{B}_{1\mathrm{e}}$ satisfies $\nabla \times \boldsymbol{B} = 0$ and $\nabla \cdot \boldsymbol{B} = 0$, $\boldsymbol{B}_{1\mathrm{e}}$ is expressed by $\boldsymbol{B}_{1\mathrm{e}} = \nabla\psi$. The scalar magnetic potential ψ satisfies $\Delta\psi = 0$ and $\psi \to 0$ as $r \to \infty$. Then

$$\psi = C\frac{K_m(kr)}{K_m(ka)}\exp(im\theta + ikz). \tag{8.57}$$

The boundary condition (8.33) is

$$\begin{aligned} p_1 + \frac{1}{\mu_0}\boldsymbol{B}_0 \cdot \boldsymbol{B}_1 &= \frac{1}{\mu_0}\boldsymbol{B}_{\mathrm{e}} \cdot \boldsymbol{B}_{1\mathrm{e}} + (\boldsymbol{\xi} \cdot \nabla)\left(\frac{B_{\mathrm{e}}^2}{2\mu_0} - \frac{B_0^2}{2\mu_0} - p_0\right) \\ &= \frac{1}{\mu_0}\boldsymbol{B}_{\mathrm{e}} \cdot \boldsymbol{B}_{1\mathrm{e}} + (\boldsymbol{\xi} \cdot \nabla)\left(\frac{B_\theta^2}{2\mu_0}\right). \end{aligned}$$

As $B_\theta \propto 1/r$, $p^*(a)$ is given by

$$p^*(a) = \frac{i}{\mu_0}(kB_{\mathrm{e}z} + \frac{m}{a}B_\theta)C - \frac{B_\theta^2}{\mu_0 a}\xi_r(a). \tag{8.58}$$

The boundary condition (8.38) is reduced to

$$Ck\frac{K'_m(ka)}{K_m(ka)} = i(kB_{\mathrm{e}z} + \frac{m}{a}B_\theta)\xi_r(a). \tag{8.59}$$

From (8.56), (8.58) and (8.59), the dispersion equation is

$$\frac{\omega^2}{k^2} = \frac{B_{0z}^2}{\mu_0\rho_{\mathrm{m0}}} - \frac{(kB_{\mathrm{e}z} + (m/a)B_\theta)^2}{\mu_0\rho_{\mathrm{m0}}k^2}\frac{I'_m(ka)}{I_m(ka)}\frac{K_m(ka)}{K'_m(ka)} - \frac{B_\theta^2}{\mu_0\rho_{\mathrm{m0}}}\frac{1}{(ka)}\frac{I'_m(ka)}{I_m(ka)}. \tag{8.60}$$

The 1st and 2nd terms represent the stabilizing effect of B_{0z} and B_{ez} ($K_m/K'_m < 0$). If the propagation vector $\boldsymbol{k}$ is normal to the magnetic field, i.e., if

$$(\boldsymbol{k} \cdot \boldsymbol{B}_{\rm e}) = kB_{ez} + \frac{m}{a}B_\theta = 0$$

the 2nd term (stabilizing term) of (8.60) becomes zero, so that a flutelike perturbation is indicated. The 3rd term is the destabilizing term.

(i) The $m = 0$ Mode with $B_{ez} = 0$ Let us consider the $m = 0$ mode with $B_{ez} = 0$. This configuration corresponds to that of the sausage instability described in sec.8.1c. Equation (8.60) reduces to

$$\omega^2 = \frac{B_{0z}^2 k^2}{\mu_0 \rho_{\rm m0}} \left(1 - \frac{B_\theta^2}{B_{0z}^2} \frac{I_0'(ka)}{(ka) I_0(ka)}\right). \tag{8.61}$$

Since $I_0'(x)/xI_0(x) < 1/2$, the stability condition is

$$B_{0z}^2 > B_\theta^2/2.$$

(ii) The $m = 1$ Mode with $B_{ez} = 0$ For the $m = 1$ mode with $B_{ez} = 0$, (8.60) is

$$\omega^2 = \frac{B_{0z}^2 k^2}{\mu_0 \rho_{\rm m0}} \left(1 + \frac{B_\theta^2}{B_{0z}^2} \frac{1}{(ka)} \frac{I_1'(ka)}{I_1(ka)} \frac{K_0(ka)}{K_1'(ka)}\right), \tag{8.62}$$

since $-K_1'(z) = K_0(z) + K_1(z)/z$.
For perturbations with long characteristic length, (8.62) becomes

$$\omega^2 = \frac{B_{0z}^2 k^2}{\mu_0 \rho_{\rm m0}} \left(1 - \left(\frac{B_\theta}{B_{0z}}\right)^2 \ln \frac{1}{ka}\right). \tag{8.63}$$

This dispersion equation corresponds to kink instability, which is unstable for the perturbation with long wavelength (refer (8.23)).

(iii) Instability in the Case of $|B_{ez}| > |B_\theta|$ When $|B_{ez}| \gg |B_\theta|$, the case $|ka| \ll 1$ predominates. Expanding the modified Bessel function ($m > 0$ is assumed), we find

$$\mu_0 \rho_{\rm m0} \omega^2 = k^2 B_{0z}^2 + \left(kB_{ez} + \frac{m}{a} B_\theta\right)^2 - \frac{m}{a^2} B_\theta^2. \tag{8.64}$$

ω^2 becomes minimum at $\partial\omega/\partial k = 0$, i.e., $k(B_{0z}^2 + B_{ez}^2) + (m/a)B_\theta B_{ez}$
$= 0$. In this case, ω^2 is

$$\omega_{\rm min}^2 = \frac{B_\theta^2}{\mu_0 \rho_{\rm m0} a^2} \left(\frac{m^2 B_{0z}^2}{B_{ez}^2 + B_{0z}^2} - m\right) = \frac{B_\theta^2}{\mu_0 \rho_{\rm m0} a^2} m \left(m \frac{1-\beta}{2-\beta} - 1\right), \tag{8.65}$$

where β is the beta ratio. Accordingly, the plasma is unstable when $0 < m < (2-\beta)/(1-\beta)$. For a low-beta plasma only the modes $m = 1$ and $m = 2$ become unstable. However, if

$$\left(\frac{B_\theta}{B_z}\right)^2 < (ka)^2 \tag{8.66}$$

is satisfied the plasma is stable even for $m = 1$. Usually the length of the plasma is finite so that k cannot be smaller than $2\pi/L$. Accordingly, when

$$\left|\frac{B_\theta}{B_z}\right| < \frac{2\pi a}{L}$$

the plasma is stable. This stability condition is called the *Kruskal- Shafranov condition* (ref.[8],[9])

When a cylindrical conducting wall of radius b surrounds the plasma, the scalar magnetic potential of the external magnetic field is

$$\psi = \left(c_1 \frac{K_m(kr)}{K_m(ka)} + c_2 \frac{I_m(kr)}{I_m(ka)} \right) \exp(im\theta + ikz)$$

instead of (8.57). The boundary condition $B_{1er} = 0$ at $r = b$ yields

$$\frac{c_1}{c_2} = -\frac{I'_m(kb)K_m(ka)}{K'_m(kb)I_m(ka)}.$$

The dispersion equation becomes

$$\begin{aligned}\frac{\omega^2}{k^2} =& \frac{B_{0z}^2}{\mu_0 \rho_{\mathrm{m0}}} - \frac{(kB_{\mathrm{e}z} + (m/a)B_\theta)^2}{\mu_0 \rho_{\mathrm{m0}} k^2} \frac{I'_m(ka)}{I_m(ka)} \\ & \times \left(\frac{K_m(ka)I'_m(kb) - I_m(ka)K'_m(kb)}{K'_m(ka)I'_m(kb) - I'_m(ka)K'_m(kb)} \right) \\ & - \frac{B_\theta^2}{\mu_0 \rho_{\mathrm{m0}}} \frac{1}{(ka)} \frac{I'_m(ka)}{I_m(ka)}.\end{aligned}$$

Expanding the modified Bessel functions under the conditions $ka \ll 1, kb \ll 1$, we find

$$\mu_0 \rho_{\mathrm{m0}} \omega^2 = k^2 B_{0z}^2 + \frac{1 + (a/b)^{2m}}{1 - (a/b)^{2m}} (kB_{\mathrm{e}z} + \frac{m}{a} B_\theta)^2 - \frac{m}{a^2} B_\theta^2.$$

The closer the wall to the plasma boundary, the more effective is the wall stabilization.

In toroidal systems, the propagation constant is $k = n/R$ where n is an integer and R is the major radius of the torus. If the *safety factor* q_a at the plasma boundary $r = a$

$$q_a = \frac{aB_{\mathrm{e}z}}{RB_\theta} \tag{8.67}$$

is introduced, $(\boldsymbol{k} \cdot \boldsymbol{B})$ may be written as

$$(\boldsymbol{k} \cdot \boldsymbol{B}) = (kB_{\mathrm{e}z} + \frac{m}{a} B_\theta) = \frac{nB_\theta}{a} \left(q_a + \frac{m}{n} \right).$$

The Kruskal-Shafranov condition (8.66) of $m = 1,\ n = -1$ mode can then be expressed in terms of the safety factor as

$$q_a > 1. \tag{8.68}$$

This is the reason why q_a is called the safety factor.

8.3b Instabilities of Diffuse-Boundary Configurations

The sharp-boundary configuration treated in sec.8.3a is a special case; in most cases the plasma current decreases gradually at the boundary. Let us consider the case of a diffuse-boundary plasma whose parameters in the equilibrium state are

$$p_0(r), \qquad \boldsymbol{B}_0(r) = (0, B_\theta(r), B_z(r)).$$

The perturbation $\boldsymbol{\xi}$ is assumed to be

$$\boldsymbol{\xi} = \boldsymbol{\xi}(r) \exp(im\theta + ikz).$$

The perturbation of the magnetic field $\boldsymbol{B}_1 = \nabla \times (\boldsymbol{\xi} \times \boldsymbol{B}_0)$ is

$$B_{1r} = i(\boldsymbol{k} \cdot \boldsymbol{B}_0)\xi_r, \tag{8.69}$$

$$B_{1\theta} = ikA - \frac{\mathrm{d}}{\mathrm{d}r}(\xi_r B_\theta), \tag{8.70}$$

$$B_{1z} = -\left(\frac{imA}{r} + \frac{1}{r} \frac{\mathrm{d}}{\mathrm{d}r}(r\xi_r B_z) \right) \tag{8.71}$$

where

$$(\boldsymbol{k}\cdot\boldsymbol{B}_0) = kB_z + \frac{m}{r}B_\theta, \tag{8.72}$$

$$A = \xi_\theta B_z - \xi_z B_\theta = (\boldsymbol{\xi}\times\boldsymbol{B}_0)_r. \tag{8.73}$$

Since the pressure terms $\gamma p_0(\nabla\cdot\boldsymbol{\xi})^2 + (\nabla\cdot\boldsymbol{\xi})(\boldsymbol{\xi}\cdot\nabla p_0) = (\gamma-1)p_0(\nabla\cdot\boldsymbol{\xi})^2 + (\nabla\cdot\boldsymbol{\xi})(\nabla\cdot p_0\boldsymbol{\xi})$ in the energy integral are nonnegative, we examine the incompressible displacement $\nabla\cdot\boldsymbol{\xi}=0$ again, i.e.,

$$\frac{1}{r}\frac{\mathrm{d}}{\mathrm{d}r}(r\xi_r) + \frac{im}{r}\xi_\theta + ik\xi_z = 0. \tag{8.74}$$

From this and (8.73) for A, ξ_θ and ξ_z are expressed in terms of ξ_r and A as

$$i(\boldsymbol{k}\cdot\boldsymbol{B})\xi_\theta = ikA - \frac{B_\theta}{r}\frac{\mathrm{d}}{\mathrm{d}r}(r\xi_r), \tag{8.75}$$

$$-i(\boldsymbol{k}\cdot\boldsymbol{B})\xi_z = \frac{imA}{r} + \frac{B_z}{r}\frac{\mathrm{d}}{\mathrm{d}r}(r\xi_r). \tag{8.76}$$

From $\mu_0\boldsymbol{j}_0 = \nabla\times\boldsymbol{B}_0$, it follows that

$$\mu_0 j_{0\theta} = -\frac{\mathrm{d}B_z}{\mathrm{d}r}, \tag{8.77}$$

$$\mu_0 j_{0z} = \frac{\mathrm{d}B_\theta}{\mathrm{d}r} + \frac{B_\theta}{r} = \frac{1}{r}\frac{\mathrm{d}}{\mathrm{d}r}(rB_\theta). \tag{8.78}$$

The terms of the energy integral are given by

$$\begin{aligned} W_\mathrm{p} =& \frac{1}{4}\int_{V_\mathrm{in}}\left(\gamma p_0|\nabla\cdot\boldsymbol{\xi}|^2 + (\nabla\cdot\boldsymbol{\xi}^*)(\boldsymbol{\xi}\cdot\nabla p_0) + \frac{1}{\mu_0}|\boldsymbol{B}_1|^2 - \boldsymbol{\xi}^*\cdot(\boldsymbol{j}_0\times\boldsymbol{B}_1)\right)\mathrm{d}\boldsymbol{r} \\ =& \frac{1}{4}\int\left(-p_1(\nabla\cdot\boldsymbol{\xi}) + \frac{1}{\mu_0}|\boldsymbol{B}_1|^2 - \boldsymbol{j}_0(\boldsymbol{B}_1\times\boldsymbol{\xi}^*)\right)\mathrm{d}\boldsymbol{r}, \end{aligned} \tag{8.79}$$

$$W_\mathrm{S} = \frac{1}{4}\int_S |\xi_n|^2\frac{\partial}{\partial n}\left(\frac{B_{0,\mathrm{ex}}^2}{2\mu_0} - \frac{B_{0,\mathrm{in}}^2}{2\mu_0} - p_0\right)\mathrm{d}S, \tag{8.80}$$

$$W_\mathrm{V} = \frac{1}{4\mu_0}\int_{V_\mathrm{ex}}|\boldsymbol{B}_1|^2\mathrm{d}\boldsymbol{r}. \tag{8.81}$$

ξ_θ and ξ_z can be eliminated by means of (8.75) and (8.76) and $\mathrm{d}B_z/\mathrm{d}r$ and $\mathrm{d}B_\theta/\mathrm{d}r$ can be eliminated by means of (8.77) and (8.78) in (8.79). Then W_p becomes

$$\begin{aligned} W_\mathrm{p} =& \frac{1}{4}\int_{V_\mathrm{in}}\frac{(\boldsymbol{k}\cdot\boldsymbol{B})^2}{\mu_0}|\xi_r|^2 + \left(k^2+\frac{m^2}{r^2}\right)\frac{|A|^2}{\mu_0} \\ &+ \frac{1}{\mu_0}\left|B_\theta\frac{\mathrm{d}\xi_r}{\mathrm{d}r} + \xi_r\left(\mu_0 j_z - \frac{B_\theta}{r}\right)\right|^2 + \frac{1}{\mu_0}\left|\frac{\xi_r B_z}{r} + B_z\frac{\mathrm{d}\xi_r}{\mathrm{d}r}\right|^2 \\ &+ \frac{2}{\mu_0}\mathrm{Re}\left(ikA^*\left(B_\theta\frac{\mathrm{d}\xi_r}{\mathrm{d}r} + \left(\mu_0 j_z - \frac{B_\theta}{r}\right)\xi_r\right) - \frac{imA^*}{r^2}\left(\xi_r B_z + rB_z\frac{\mathrm{d}\xi_r}{\mathrm{d}r}\right)\right) \\ &+ 2\mathrm{Re}\left(\xi_r^* j_{0z}\left(-B_\theta\frac{\mathrm{d}\xi_r}{\mathrm{d}r} - \frac{\xi_r\mu_0 j_z}{2} + ikA\right)\right)\mathrm{d}\boldsymbol{r}. \end{aligned}$$

The integrand of W_p is reduced to

$$\frac{1}{\mu_0}\left(k^2+\frac{m^2}{r^2}\right)\times\left|A + \frac{ikB_\theta((\mathrm{d}\xi_r/\mathrm{d}r) - \xi_r/r) - im(B_z/r)((\mathrm{d}\xi_r/\mathrm{d}r) + (\xi_r/r))}{k^2 + (m^2/r^2)}\right|^2$$

$$+\left(\frac{(\boldsymbol{k}\cdot\boldsymbol{B})^2}{\mu_0}-\frac{2j_zB_\theta}{r}\right)|\xi_r|^2+\frac{B_z^2}{\mu_0}\left|\frac{\mathrm{d}\xi_r}{\mathrm{d}r}+\frac{\xi_r}{r}\right|^2+\frac{B_\theta^2}{\mu_0}\left|\frac{\mathrm{d}\xi_r}{\mathrm{d}r}-\frac{\xi_r}{r}\right|^2$$

$$-\frac{|ikB_\theta((\mathrm{d}\xi_r/\mathrm{d}r)-(\xi_r/r))-im(B_z/r)((\mathrm{d}\xi_r/\mathrm{d}r)+(\xi_r/r))|^2}{\mu_0(k^2+(m^2/r^2))}.$$

Accordingly, the integrand is a minimum when

$$\begin{aligned}A&\equiv\xi_\theta B_z-\xi_zB_\theta\\&=-\frac{i}{k^2+(m^2/r^2)}\left(\left(kB_\theta-\frac{m}{r}B_z\right)\frac{\mathrm{d}\xi_r}{\mathrm{d}r}-\left(kB_\theta+\frac{m}{r}B_z\right)\frac{\xi_r}{r}\right).\end{aligned}$$

Then W_p is reduced to

$$W_\mathrm{p}=\frac{\pi}{2\mu_0}\int_0^a\left(\frac{|(\boldsymbol{k}\cdot\boldsymbol{B}_0)(\mathrm{d}\xi_r/\mathrm{d}r)+h(\xi_r/r)|^2}{k^2+(m/r)^2}+\left((\boldsymbol{k}\cdot\boldsymbol{B}_0)^2-\frac{2\mu_0j_zB_\theta}{r}\right)|\xi_r|^2\right)r\mathrm{d}r \tag{8.82}$$

where

$$h\equiv kB_z-\frac{m}{r}B_\theta.$$

Let us next determine W_S. From (6.8), it follows that $(\mathrm{d}/\mathrm{d}r)(p_0+(B_z^2+B_\theta^2)/2\mu_0)=-B_\theta^2/(r\mu_0)$. B_θ^2 is continuous across the boundary $r=a$, so that

$$\frac{\mathrm{d}}{\mathrm{d}r}\left(p_0+\frac{B_z^2+B_\theta^2}{2\mu_0}\right)=\frac{\mathrm{d}}{\mathrm{d}r}\left(\frac{B_{\mathrm{e}z}^2+B_{\mathrm{e}\theta}^2}{2\mu_0}\right).$$

Accordingly we find

$$W_\mathrm{S}=0 \tag{8.83}$$

as is clear from (8.80).

The expression for W_V can be obtained when the quantities in (8.82) for W_p are replaced as follows: $\boldsymbol{j}\to0$, $B_z\to B_{\mathrm{e}z}=B_\mathrm{s}(=\text{const.})$, $B_\theta\to B_{\mathrm{e}\theta}=B_aa/r$, $B_{1r}=i(\boldsymbol{k}\cdot\boldsymbol{B}_0)\xi_r\to B_{\mathrm{e}1r}=i(\boldsymbol{k}\cdot\boldsymbol{B}_{\mathrm{e}0})\eta_r$. This replacement yields

$$W_\mathrm{V}=\frac{\pi}{2\mu_0}\int_a^b\left(\left(kB_\mathrm{s}+\frac{m}{r}\frac{B_aa}{r}\right)^2|\eta_r|^2\right.$$

$$\left.+\frac{|[kB_\mathrm{s}+(m/r)(B_aa/r)](\mathrm{d}\eta_r/\mathrm{d}r)+[kB_\mathrm{s}-(m/r)(B_aa/r)]\eta_r/r|^2}{k^2+(m/r)^2}\right)r\mathrm{d}r. \tag{8.84}$$

By partial integration, W_p is seen to be

$$W_\mathrm{p}=\frac{\pi}{2\mu_0}\int_0^a\left(\frac{r(\boldsymbol{k}\cdot\boldsymbol{B}_0)^2}{k^2+(m/r)^2}\left|\frac{\mathrm{d}\xi_r}{\mathrm{d}r}\right|^2+g|\xi_r|^2\right)\mathrm{d}\boldsymbol{r}+\frac{\pi}{2\mu_0}\frac{k^2B_\mathrm{s}^2-(m/a)^2B_a^2}{k^2+(m/a)^2}|\xi_r(a)|^2 \tag{8.85}$$

$$g=\frac{1}{r}\frac{(kB_z-(m/r)B_\theta)^2}{k^2+(m/r)^2}+r(\boldsymbol{k}\cdot\boldsymbol{B}_0)^2-\frac{2B_\theta}{r}\frac{\mathrm{d}(rB_\theta)}{\mathrm{d}r}-\frac{\mathrm{d}}{\mathrm{d}r}\left(\frac{k^2B_z^2-(m/r)^2B_\theta^2}{k^2+(m/r)^2}\right). \tag{8.86}$$

Using the notation $\zeta\equiv rB_{\mathrm{e}1r}=ir(\boldsymbol{k}\cdot\boldsymbol{B}_{\mathrm{e}0})\eta_r$, we find that

$$W_\mathrm{V}=\frac{\pi}{2\mu_0}\int_a^b\left(\frac{1}{r(k^2+(m/r)^2)}\left|\frac{\mathrm{d}\zeta}{\mathrm{d}r}\right|^2+\frac{1}{r}|\zeta|^2\right)\mathrm{d}r. \tag{8.87}$$

The functions ξ_r or ζ that will minimize W_p or W_V are the solutions of Euler's equation:

$$\frac{\mathrm{d}}{\mathrm{d}r}\left(\frac{r(\boldsymbol{k}\cdot\boldsymbol{B}_0)^2}{k^2+(m/r)^2}\frac{\mathrm{d}\xi_r}{\mathrm{d}r}\right)-g\xi_r=0,\quad r\le a, \tag{8.88}$$

$$\frac{\mathrm{d}}{\mathrm{d}r}\left(\frac{1}{r(k^2+(m/r)^2)}\frac{\mathrm{d}\zeta}{\mathrm{d}r}\right)-\frac{1}{r}\zeta=0,\quad r>a\ . \tag{8.89}$$

There are two independent solutions, which tend to $\xi_r\propto r^{m-1}$, r^{-m-1} as $r\to 0$. As ξ_r is finite at $r=0$, the solution must satisfy the conditions

$$\begin{aligned} &r\to 0, && \xi_r\propto r^{m-1},\\ &r=a, && \zeta(a)=ia\left(kB_\mathrm{s}+\frac{m}{a}B_a\right)\xi_r(a),\\ &r=b, && \zeta(b)=0. \end{aligned}$$

Using the solution of (8.89), we obtain

$$W_\mathrm{V}=\frac{\pi}{2\mu_0}\frac{1}{r(k^2+(m/r)^2)}\left|\frac{\mathrm{d}\zeta}{\mathrm{d}r}\zeta^*\right|_a^b. \tag{8.90}$$

The solution of (8.89) is

$$\zeta=i\frac{I_m'(kr)K_m'(kb)-K_m'(kr)I_m'(kb)}{I_m'(ka)K_m'(kb)-K_m'(ka)I_m'(kb)}r\left(kB_\mathrm{s}+\frac{m}{a}B_a\right)\xi_r(a). \tag{8.91}$$

The stability problem is now reduced to one of examining the sign of $W_\mathrm{p}+W_\mathrm{V}$. For this we use

$$\left.\begin{aligned} W_\mathrm{p}&=\frac{\pi}{2\mu_0}\int_0^a\left(f\left|\frac{\mathrm{d}\xi_r}{\mathrm{d}r}\right|^2+g|\xi_r|^2\right)\mathrm{d}r+W_a,\\ W_a&=\frac{\pi}{2\mu_0}\frac{k^2B_\mathrm{s}^2-(m/a)^2B_a^2}{k^2+(m/a)^2}|\xi_r(a)|^2,\\ W_\mathrm{V}&=\frac{\pi}{2\mu_0}\frac{-1}{r(k^2+(m/a)^2)}\left|\frac{\mathrm{d}\zeta}{\mathrm{d}r}\zeta^*\right|_{r=a} \end{aligned}\right\} \tag{8.92}$$

where

$$f=\frac{r(kB_z+(m/r)B_\theta)^2}{k^2+(m/r)^2}, \tag{8.93}$$

$$\begin{aligned} g=&\frac{1}{r}\frac{(kB_z-(m/r)B_\theta)^2}{k^2+(m/r)^2}+r\left(kB_z+\frac{m}{r}B_\theta\right)^2\\ &-\frac{2B_\theta}{r}\frac{\mathrm{d}(rB_\theta)}{\mathrm{d}r}-\frac{\mathrm{d}}{\mathrm{d}r}\left(\frac{k^2B_z^2-(m/r)^2B_\theta^2}{k^2+(m/r)^2}\right). \end{aligned} \tag{8.94}$$

When the equation of equilibrium $\frac{\mathrm{d}}{\mathrm{d}r}(\mu_0p+B^2/2)=-B_\theta^2/r$ is used, (8.94) of g is reduced to

$$\begin{aligned} g=&\frac{2k^2}{k^2+(m/r)^2}\mu_0\frac{\mathrm{d}p_0}{\mathrm{d}r}+r(kB_z+\frac{m}{r}B_\theta)^2\frac{k^2+(m/r)^2-(1/r)^2}{k^2+(m/r)^2}\\ &+\frac{(2k^2/r)(k^2B_z^2-(m/r)^2B_\theta^2)}{(k^2+(m/r)^2)^2}. \end{aligned} \tag{8.95}$$

8.3c Suydam's Criterion

The function f in the integrand of $W_{\rm p}$ in the previous section is always $f \geq 0$, so that the term in f is a stabilizing term. The 1st and 2nd terms in (8.94) for g are stabilizing terms, but the 3rd and 4th terms may contribute to the instabilities. When a singular point

$$f \propto (\boldsymbol{k} \cdot \boldsymbol{B}_0)^2 = 0$$

of Euler's equation (8.88) is located at some point $r = r_0$ within the plasma region, the contribution of the stabilizing term becomes small near $r = r_0$, so that a local mode near the singular point is dangerous. In terms of the notation

$$r - r_0 = x, \qquad f = \alpha x^2, \qquad g = \beta, \qquad \beta = \frac{2B_\theta^2}{B_0^2}\mu_0 \frac{\mathrm{d}p_0}{\mathrm{d}r}\bigg|_{r=r_0},$$

$$\alpha = \frac{r_0}{k^2 r_0^2 + m^2}\left(kr\frac{\mathrm{d}B_z}{\mathrm{d}r} + kB_z + m\frac{\mathrm{d}B_\theta}{\mathrm{d}r}\right)^2_{r=r_0} = \frac{rB_\theta^2 B_z^2}{B^2}\left(\frac{\tilde{\mu}'}{\tilde{\mu}}\right)^2_{r=r_0}, \qquad \tilde{\mu} \equiv \frac{B_\theta}{rB_z}.$$

Euler's equation (8.88) with (8.95) of g is reduced to

$$\alpha \frac{\mathrm{d}}{\mathrm{d}r}(x^2 \frac{\mathrm{d}\xi_r}{\mathrm{d}x}) - \beta \xi_r = 0.$$

The solution is

$$\xi_r = c_1 x^{-n_1} + c_2 x^{-n_2} \tag{8.96}$$

where n_1 and n_2 are given by

$$n^2 - n - \frac{\beta}{\alpha} = 0, \qquad n_i = \frac{1 \pm (1 + 4\beta/\alpha)^{1/2}}{2}.$$

When $\alpha + 4\beta > 0$, n_1 and n_2 are real. The relation $n_1 + n_2 = 1$ holds always. For $n_1 < n_2$, we have the solution x^{-n_1}, called a *small solution*. When n is complex ($n = \gamma \pm i\delta$), ξ_r is in the form $\exp((-\gamma \mp i\delta)\ln x)$ and ξ_r is oscillatory.

Let us consider a local mode ξ_r, which is nonzero only in the neighborhood ε around $r = r_0$ and set

$$r - r_0 = \varepsilon t, \quad \xi_r(r) = \xi(t), \quad \xi(1) = \xi(-1) = 0.$$

Then $W_{\rm p}$ becomes

$$W_{\rm p} = \frac{\pi}{2\mu_0}\varepsilon \int_{-1}^{1}\left(\alpha t^2 \left|\frac{\mathrm{d}\xi}{\mathrm{d}t}\right|^2 + \beta|\xi|^2\right)\mathrm{d}t + O(\varepsilon^2).$$

Since Schwartz's inequality yields ($\int (uf(t) + g(t))^2 \mathrm{d}t = Au^2 + 2Bu + C > 0, AC > B^2$)

$$\int_{-1}^{1} t^2|\xi'|^2\mathrm{d}t \int_{-1}^{1}|\xi|^2\mathrm{d}t \geq \left|\int_{-1}^{1} t\xi'\xi^*\mathrm{d}t\right|^2 = \left(\frac{1}{2}\int_{-1}^{1}|\xi|^2\mathrm{d}t\right)^2$$

$W_{\rm p}$ is

$$W_{\rm p} > \frac{\pi}{2\mu_0}\frac{1}{4}(\alpha + 4\beta)\int_{-1}^{1}|\xi|^2\mathrm{d}t.$$

The stability condition is $\alpha + 4\beta > 0$, i.e.,

$$\frac{r}{4}\left(\frac{\tilde{\mu}'}{\tilde{\mu}}\right)^2 + \frac{2\mu_0}{B_z^2}\frac{\mathrm{d}p_0}{\mathrm{d}r} > 0. \tag{8.97}$$

$r(\tilde{\mu}'/\tilde{\mu})$ is called *shear parameter*. Usually the 2nd term is negative, since, most often, $dp_0/dr < 0$. The 1st term $(\tilde{\mu}'/\tilde{\mu})^2$ represents the stabilizing effect of shear. This condition is called *Suydam's*

criterion (ref.[10]). This is a necessary condition for stability; but it is not always a sufficient condition, as Suydam's criterion is derived from consideration of local-mode behavior only. Newcomb derived the necessary and sufficient conditions for the stability of a cylindrical plasma. His twelve theorems are described in (ref.[11]).

8.3d Tokamak Configuration

In this case the longitudinal magnetic field $B_{\rm s}$ is much larger than the poloidal magnetic field B_θ. The plasma region is $r \le a$ and the vacuum region is $a \le r \le b$ and an ideal conducting wall is at $r = b$. It is assumed that $ka \ll 1$, $kb \ll 1$. The function ζ in (8.90) for $W_{\rm V}$ is

$$\zeta = i\frac{(mB_a + kaB_{\rm s})}{1-(a/b)^{2m}}\xi_r(a)\frac{a^m}{b^m}\left(\frac{b^m}{r^m} - \frac{r^m}{b^m}\right)$$

(from (8.91)), and $W_{\rm V}$ becomes

$$W_{\rm V} = \frac{\pi}{2\mu_0}\frac{(mB_a + kaB_{\rm s})^2}{m}\xi_r^2(a)\lambda, \qquad \lambda \equiv \frac{1+(a/b)^{2m}}{1-(a/b)^{2m}}.$$

From the periodic condition for a torus, it follows that

$$\frac{2\pi n}{k} = -2\pi R \quad (n \text{ is an integer})$$

so that $(\boldsymbol{k}\cdot\boldsymbol{B})$ is given by

$$a(\boldsymbol{k}\cdot\boldsymbol{B}) = mB_a + kaB_{\rm s} = mB_a\left(1 - \frac{nq_a}{m}\right)$$

in terms of the safety factor. The W_a term in (8.92) is reduced to

$$\begin{aligned} k^2B_{\rm s}^2 - \left(\frac{m}{a}\right)^2 B_a^2 &= \left(kB_{\rm s} + \frac{m}{a}B_a\right)^2 - 2\frac{m}{a}B_a\left(kB_{\rm s} + \frac{m}{a}B_a\right) \\ &= \left(\frac{nB_a}{a}\right)^2\left(\left(1-\frac{nq_a}{m}\right)^2 - 2\left(1-\frac{nq_a}{m}\right)\right). \end{aligned}$$

Accordingly, the energy integral becomes

$$\begin{aligned} W_{\rm p} + W_{\rm V} = &\frac{\pi}{2\mu_0}B_a^2\xi_r^2(a)\left(\left(1-\frac{nq_a}{m}\right)^2(1+m\lambda) - 2\left(1-\frac{nq_a}{m}\right)\right) \\ &+ \frac{\pi}{2\mu_0}\int\left(f\left(\frac{{\rm d}\xi_r}{{\rm d}r}\right)^2 + g\xi_r^2\right){\rm d}r. \end{aligned} \tag{8.98}$$

The 1st term of (8.98) is negative when

$$1 - \frac{2}{1+m\lambda} < \frac{nq_a}{m} < 1. \tag{8.99}$$

The assumption $nq_a/m \sim 1$ corresponds to $ka \sim mB_a/B_{\rm s}$. As $B_a/B_{\rm s} \ll 1$, this is consistent with the assumption $ka \ll 1$. When $m = 1$, $(m^2-1)/m^2$ in the 2nd term of (8.95) for g is zero. The magnitude of g is of the order of k^2r^2, which is very small since $kr \ll 1$. The term in $f({\rm d}\xi_r/{\rm d}r)^2$ can be very small if ξ_r is nearly constant. Accordingly the contribution of the integral term in (8.98) is negligible. When $m = 1$ and $a^2/b^2 < nq_a < 1$, the energy integral becomes negative ($W < 0$). The mode $m = 1$ is unstable in the region specified by (8.99) irrespective of the current distribution. The Kruskal-Shafranov condition for the mode $m = 1$ derived from the sharp-boundary configuration is also applicable to the diffuse-boundary plasma. The growth rate $\gamma^2 = -\omega^2$ is

$$\gamma^2 \simeq \frac{-W}{\int(\rho_{\rm m0}|\boldsymbol{\xi}|^2/2){\rm d}\boldsymbol{r}} = \frac{1}{\langle\rho_{\rm m0}\rangle}\frac{B_a^2}{\mu_0 a^2}\left(2(1-nq_a) - \frac{2(1-nq_a)^2}{1-a^2/b^2}\right), \tag{8.100}$$

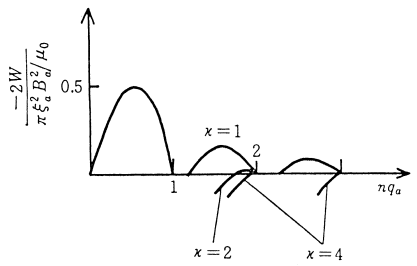

Fig.8.9 The relation of the growth rate γ and nq_a for kink instability ($-2W/(\pi\xi_a^2 B_a^2/\mu_0) = \gamma^2 a^2(\langle\rho_{\rm m0}\rangle\mu_0/B_a^2)$). After (ref.[12]).

$$\langle\rho_{\rm m0}\rangle = \frac{\int \rho_{\rm m0}|\boldsymbol{\xi}|^2 2\pi r\mathrm{d}r}{\pi a^2\xi_r^2(a)}.$$

The maximum growth rate is $\gamma_{\max}^2 \sim (1-a^2/b^2)B_a^2/(\mu_0\langle\rho\rangle a^2)$. When $m \neq 1$, $(m^2-1)/m^2$ in the 2nd term of (8.95) for g is large, and $g \sim 1$. Accordingly, the contribution of the integral term to $W_{\rm p}$ must be checked. The region $g<0$ is given by $\chi_1 < \chi < \chi_2$, when $\chi \equiv -krB_z/B_\theta = nq(r)$ and

$$\chi_{1,2} = m - \frac{2}{m(m^2-1)}k^2r^2 \pm \frac{2k^2r^2}{m(m^2-1)}\left(1 - \frac{m^2(m^2-1)}{2k^2r^2}\frac{\mu_0 r p_0'}{B_\theta^2}\right)^{1/2}. \tag{8.101}$$

Since $kr \ll 1$, the region $g<0$ is narrow and close to the singular point $nq(r)=m$ and the contribution of the integral term to $W_{\rm p}$ can be neglected. Therefore if nq_a/m is in the range given by (8.99), the plasma is unstable due to the displacement $\xi_r(a)$ of the plasma boundary. When the current distribution is $j(r) = j_0\exp(-\kappa^2r^2/a^2)$ and the conducting wall is at infinity ($b=\infty$), γ^2 can be calculated from (8.100), using the solution of Euler's equation; and the dependence of γ^2 on q_a can be estimated. The result is shown in fig.8.9.

When the value of nq_a/m is outside the region given by (8.99), the effect of the displacement of the plasma boundary is not great and the contribution of the integral term in $W_{\rm p}$ is dominant. However, the growth rate γ^2 is k^2r^2 times as small as that given by (8.100), as is clear from consideration of (8.101).

8.3e Reversed Field Pinch (ref.[13])

The characteristics of the Reversed field pinch is that B_a and $B_{\rm s}$ are of the same order of magnitude, so that the approximation based upon $ka \ll 1$ or $B_a \ll B_{\rm s}$ can no longer be used. As is clear from the expression (8.82) for $W_{\rm p}$, the plasma is stable if

$$2\mu_0 j_z\frac{B_\theta}{r} = 2\frac{B_\theta}{r^2}\frac{\mathrm{d}}{\mathrm{d}r}(rB_\theta) = \frac{1}{r^3}\frac{\mathrm{d}}{\mathrm{d}r}(rB_\theta)^2 < 0 \tag{8.102}$$

is satisfied everywhere. This is a sufficient condition; however, it can never be satisfied in real cases. When the expression (8.95) for g is rewritten in terms of $P \equiv rB_z/B_\theta$ ($2\pi P$ is the pitch of the magnetic-field lines), we find

$$g = \frac{2(kr)^2\mu_0}{m^2+(kr)^2}\frac{\mathrm{d}p_0}{\mathrm{d}r} + \frac{B_\theta^2/r}{(m^2+(kr)^2)^2}(kP+m)$$
$$\times\left(kP((m^2+k^2r^2)^2-(m^2-k^2r^2)) + m((m^2+k^2r^2)^2-(m^2+3k^2r^2))\right). \tag{8.103}$$

When $m=1$, g becomes

$$g = \frac{2(kr)^2\mu_0}{1+(kr)^2}\frac{\mathrm{d}p_0}{\mathrm{d}r} + \frac{(kr)^2B_\theta^2/r}{(1+(kr)^2)^2}(kP+1)(kP(3+k^2r^2)+(k^2r^2-1)). \tag{8.104}$$

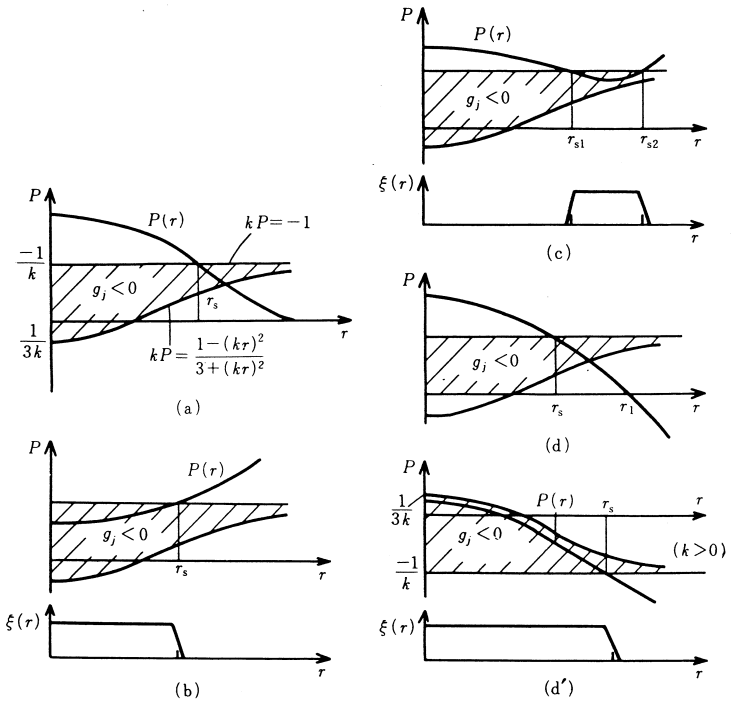

Fig.8.10 Dependence of pitch $P(r)$ on r, and the region $g_j(P,r) < 0$. The displacements $\xi_r(r)$ of the unstable modes are also shown. Parts a-d are for $k < 0$.

The 2nd term in (8.104) is quadratic with respect to P and has the minimum value

$$g(r) > 2\mu_0 \frac{\mathrm{d}p_0}{\mathrm{d}r} \frac{k^2r^2}{1+k^2r^2} - \frac{4B_\theta^2}{r} \frac{k^2r^2}{(1+k^2r^2)^2(3+k^2r^2)}.$$

The condition $g(r) > 0$ is reduced to

$$\frac{r\mu_0}{B_\theta^2} \frac{\mathrm{d}p_0}{\mathrm{d}r} > \frac{2}{(1+k^2r^2)(3+k^2r^2)} \tag{8.105}$$

($\mathrm{d}p_0/\mathrm{d}r$ must be positive). Accordingly if the equilibrium solution is found to satisfy the condition (8.105) near the plasma center and also to satisfy the condition (8.102) at the plasma boundary, the positive contribution of the integral term may dominate the negative contribution from the plasma boundary and this equilibrium configuration may be stable. Let us consider the 2nd term of (8.104):

$$g_j = \frac{k^2 r B_\theta^2}{(1+k^2r^2)^2}(kP+1)(kP(3+k^2r^2) + (k^2r^2-1)). \tag{8.106}$$

This term is positive when

$$kP < -1 \quad or \quad kP > (1-k^2r^2)/(3+k^2r^2). \tag{8.107}$$

The point $kP = -1$ is a singular point. The region $g_j < 0$ is shown in the P,r diagrams of fig.8.10a-d for given k (< 0). r_s is a singular point. Several typical examples of $P(r)$ are shown in the figure. It is clear that $\xi_r(r)$ shown in (b) and (c) makes W negative. The example (d) is the case where the longitudinal magnetic field B_z is reversed at $r = r_1$. If k (> 0) is chosen so that $kP(0) < 1/3$ and if the singular point r_s satisfying $kP(r_s) = -1$ is smaller than $r = b$ (i.e., r_s does not lie on the conducting wall $r = b$), the plasma is unstable for the displacement $\xi_r(r)$ shown in fig.8.10d′. The necessary condition for the stability of the reverse-field configuration is

$$-P(b) < 3P(0). \tag{8.108}$$

This means that B_θ cannot be very small compared with B_z and that the value of the reversed B_z at the wall cannot be too large.

When $m = 1$, (8.82) for W_p yields the sufficient condition of stability:

$$2\mu_0 j_z \frac{B_\theta}{r} < \frac{B_\theta^2}{r^2}(1 + kP)^2. \tag{8.109}$$

The most dangerous mode is $k = -1/P(a)$. With the assumption $B_\theta > 0$, the stability condition becomes

$$\mu_0 j_z < \frac{1}{2}\frac{B_\theta}{r}\left(-\frac{P(r)}{P(a)} + 1\right)^2. \tag{8.110}$$

Accordingly if the condition

$$\left|\frac{P(r)}{P(a)}\right| > 1 \tag{8.111}$$

is satisfied at small r and j_z is negative at r near the boundary, this configuration may be stable.

Let us consider limitations on the beta ratio from the standpoint of stability. For this purpose the dangerous mode $kP(a) = -1$ is examined, using (8.82) for W_p. The substitution

$$\xi_r(r) = \xi \qquad 0 \le r \le a - \varepsilon, \qquad \xi_r(r) = 0 \qquad r \ge a + \varepsilon$$

into (8.82) yields

$$W_\mathrm{p} = \frac{\pi}{2\mu_0}\xi^2 \int_0^a \frac{\mathrm{d}r}{r}\left(-2B_\theta \frac{\mathrm{d}}{\mathrm{d}r}(rB_\theta) + (krB_z + mB_\theta)^2 + \frac{(krB_z - mB_\theta)^2}{m^2 + k^2 r^2}\right).$$

When $m = 1$, then W_p is

$$W_\mathrm{p} = \frac{\pi}{2\mu_0}\xi^2 \int_0^a \frac{\mathrm{d}r}{r}\left(-2B_\theta \frac{\mathrm{d}}{\mathrm{d}r}(rB_\theta) + 2k^2 r^2 B_z^2 + 2B_\theta^2 - \frac{k^2 r^2 (krB_z - B_\theta)^2}{1 + k^2 r^2}\right).$$

Since the last term in the integrand is always negative, the integration of the other three terms must be positive, i.e.,

$$\frac{\pi}{2\mu_0}\xi^2\left(-B_\theta^2(a) + 2k^2 \int_0^a r B_z^2 \mathrm{d}r\right) > 0.$$

Using $kP(a) = -1$ and the equilibrium equation (6.9),

$$\frac{2}{a^2}\int_0^a \left(\mu_0 p_0 + \frac{B_z^2}{2}\right) r\mathrm{d}r = \left(\mu_0 p_0 + \frac{B_z^2 + B_\theta^2}{2}\right)_{r=a}$$

we can convert the necessary condition for stability to

$$a^2 B_\theta^2(a) > 4\mu_0 \int_0^a r p_0 \mathrm{d}r$$

i.e.,

$$\beta_\theta \equiv \left(\frac{2\mu_0}{B_\theta^2}\right)\frac{2\pi}{\pi a^2}\int p_0 r\mathrm{d}r < 1. \tag{8.112}$$

Next let us study the stability of the mode $m = 0$ in the reversed field pinch. It is assumed that B_z reverses at $r = r_1$. The substitution

$$\xi_r(r) = \lambda r \quad 0 \le r \le r_1 - \varepsilon, \qquad \xi_r(r) = 0 \qquad r > r_1 + \varepsilon$$

into (8.82) yields

$$W_{\rm p} = \frac{\pi}{2\mu_0}\lambda^2 \int_0^{r_1} r{\rm d}r \left(4B_z^2 - 2B_\theta \frac{\rm d}{{\rm d}r}(rB_\theta) + k^2 r^2 B_z^2\right).$$

Using the equilibrium equation (6.8), we obtain the necessary condition for stability:

$$\mu_0^{-1} r_1^2 B_\theta^2(r_1) > 8\int_0^{r_1} r p_0 {\rm d}r - 4r_1^2 p_0(r_1).$$

If $p_0(r_1) \sim 0$, we have the condition

$$\beta_\theta < \frac{1}{2}. \tag{8.113}$$

8.4 Hain-Lüst Magnetohydrodynamic Equation

When the displacement $\boldsymbol{\xi}$ is denoted by

$$\boldsymbol{\xi}(r,\theta,z,t) = \boldsymbol{\xi}(r)\exp i(m\theta + kz - \omega t)$$

and the equilibrium magnetic field $\boldsymbol{B}_0$ is expressed by

$$\boldsymbol{B}(r) = (0,\, B_\theta(r),\, B_z(r))$$

the (r,θ,z) components of magnetohydrodynamic equation of motion are given by

$$-\mu_0\rho_{\rm m}\omega^2\xi_r = \frac{\rm d}{{\rm d}r}\left(\mu_0\gamma p(\nabla\cdot\xi) + B^2\frac{1}{r}\frac{\rm d}{{\rm d}r}(r\xi_r) + iD(\xi_\theta B_z - \xi_z B_\theta)\right)$$
$$-\left(F^2 + r\frac{\rm d}{{\rm d}r}\left(\frac{B_\theta}{r}\right)^2\right)\xi_r - 2ik\frac{B_\theta}{r}(\xi_\theta B_z - \xi_z B_\theta), \tag{8.114}$$

$$-\mu_0\rho_{\rm m}\omega^2\xi_\theta = i\frac{m}{r}\gamma\mu_0 p(\nabla\cdot\boldsymbol{\xi}) + iDB_z\frac{1}{r}\frac{\rm d}{{\rm d}r}(r\xi_r) + 2ik\frac{B_\theta B_z}{r}\xi_r - H^2 B_z(\xi_\theta B_z - \xi_z B_\theta), \tag{8.115}$$

$$-\mu_0\rho_{\rm m}\omega^2\xi_z = ik\gamma\mu_0 p(\nabla\cdot\boldsymbol{\xi}) - iDB_\theta\frac{1}{r}\frac{\rm d}{{\rm d}r}(r\xi_r) - 2ik\frac{B_\theta^2}{r}\xi_r + H^2 B_\theta(\xi_\theta B_z - \xi_z B_\theta) \tag{8.116}$$

where

$$F = \frac{m}{r}B_\theta + kB_z = (\boldsymbol{k}\cdot\boldsymbol{B}), \quad D = \frac{m}{r}B_z - kB_\theta, \quad H^2 = \left(\frac{m}{r}\right)^2 + k^2,$$

$$\nabla\cdot\boldsymbol{\xi} = \frac{1}{r}\frac{\rm d}{{\rm d}r}(r\xi_r) + \frac{im}{r}\xi_\theta + ik\xi_z.$$

When ξ_θ, ξ_z are eliminated by (8.115),(8.116), we find

$$\frac{\rm d}{{\rm d}r}\left(\frac{(\mu_0\rho_{\rm m}\omega^2 - F^2)}{\Delta}(\mu_0\rho_{\rm m}\omega^2(\gamma\mu_0 p + B^2) - \gamma\mu_0 pF^2)\frac{1}{r}\frac{\rm d}{{\rm d}r}(r\xi_r)\right)$$
$$+\left[\mu_0\rho_{\rm m}\omega^2 - F^2 - 2B_\theta\frac{\rm d}{{\rm d}r}\left(\frac{B_\theta}{r}\right) - \frac{4k^2}{\Delta}\frac{B_\theta^2}{r^2}(\mu_0\rho_{\rm m}\omega^2 B^2 - \gamma\mu_0 pF^2)\right.$$
$$\left.+r\frac{\rm d}{{\rm d}r}\left(\frac{2kB_\theta}{\Delta r^2}\left(\frac{m}{r}B_z - kB_\theta\right)(\mu_0\rho_{\rm m}\omega^2(\gamma\mu_0 p + B^2) - \gamma\mu_0 pF^2)\right)\right]\xi_r$$
$$= 0 \tag{8.117}$$

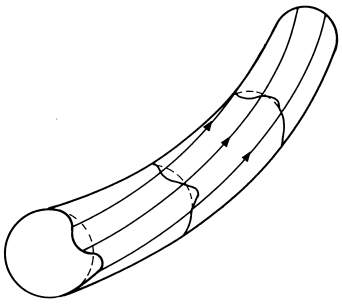

Fig.8.11 Ballooning mode

where Δ is

$$\Delta = \mu_0^2\rho_{\rm m}^2\omega^4 - \mu_0\rho_{\rm m}\omega^2 H^2(\gamma\mu_0 p + B^2) + \gamma\mu_0 p H^2 F^2.$$

This equation was derived by Hain-Lüst (ref.[14]). The solution of (8.117) gives $\xi_r(r)$ in the region of $0 < r < a$. The equations for the vacuum region $a < r < a_w$ (a_w is the radius of wall) are

$$\nabla \times \boldsymbol{B}_1 = 0, \qquad \nabla \cdot \boldsymbol{B}_1 = 0$$

so that we find

$$\boldsymbol{B}_1 = \nabla\psi, \qquad \triangle\psi = 0$$

and

$$\psi = (bI_m(kr) + cK_m(kr))\exp(im\theta + ikz),$$

$$B_{1r} = \frac{\partial\psi}{\partial r} = \left(bI_m'(kr) + cK_m'(kr)\right)\exp(im\theta + ikz). \tag{8.118}$$

B_{1r} in the plasma region is given by

$$B_{1r} = i(\boldsymbol{k}\cdot\boldsymbol{B})\xi_r = iF\xi_r$$

and the boundary conditions at $r = a$ are

$$B_{1r}(a) = iF\xi_r(a), \tag{8.119}$$

$$B_{1r}'(a) = i(F'\xi_r(a) + F\xi_r'(a)), \tag{8.120}$$

and the coefficients b,c can be fixed.

To deal with this equation as an eigenvalue problem, boundary conditions must be imposed on ξ_r; one is that $\xi_r \propto r^{m-1}$ at $r = 0$, and the other is that the radial component of the perturbed magnetic field at the perfect conducting wall $B_{1r}(a_w) = 0$. After finding suitable ω^2 to satisfy these conditions, the growth rate $\gamma^2 \equiv -\omega^2$ is obtained (ref.[15]).

8.5 Ballooning Instability

In interchange instability, the parallel component $k_\parallel = (\boldsymbol{k}\cdot\boldsymbol{B})/B$ of the propagation vector is zero and an average minimum-B condition may stabilize such an instability. Suydam's condition and the local-mode stability condition of toroidal-system are involved in perturbations with $k_\parallel = 0$. In this section we will study perturbations where $k_\parallel \neq 0$ but $|k_\parallel/k_\perp| \ll 1$. Although the interchange instability is stabilized by an average minimum-B configuration, it is possible that the perturbation

with $k_\parallel \neq 0$ can grow locally in the bad region of the average minimum-B field. This type of instability is called the *ballooning mode* (see fig.8.11). The energy integral δW is given by

$$\delta W = \frac{1}{2\mu_0}\int((\nabla\times(\boldsymbol{\xi}\times\boldsymbol{B}_0))^2 - (\boldsymbol{\xi}\times(\nabla\times\boldsymbol{B}_0))\cdot\nabla\times(\boldsymbol{\xi}\times\boldsymbol{B}_0) \\ +\gamma\mu_0 p_0(\nabla\cdot\boldsymbol{\xi})^2 + \mu_0(\nabla\cdot\boldsymbol{\xi})(\boldsymbol{\xi}\cdot\nabla p_0))\mathrm{d}\boldsymbol{r}.$$

Let us consider the case that $\boldsymbol{\xi}$ can be expressed by

$$\boldsymbol{\xi} = \frac{\boldsymbol{B}_0\times\nabla\phi}{B_0^2}, \tag{8.121}$$

where ϕ is considered to be the time integral of the scalar electrostatic potential of the perturbed electric field. Because of

$$\boldsymbol{\xi}\times\boldsymbol{B}_0 = \nabla_\perp\phi$$

the energy integral is reduced to

$$\delta W = \frac{1}{2\mu_0}\int\Bigg((\nabla\times\nabla_\perp\phi)^2 - \left(\frac{(\boldsymbol{B}_0\times\nabla_\perp\phi)\times\mu_0\boldsymbol{j}_0}{B_0^2}\right)\nabla\times\nabla_\perp\phi \\ +\gamma\mu_0 p_0(\nabla\cdot\boldsymbol{\xi})^2 + \mu_0(\nabla\cdot\boldsymbol{\xi})(\boldsymbol{\xi}\cdot\nabla p_0)\Bigg)\mathrm{d}\boldsymbol{r}.$$

$\nabla\cdot\boldsymbol{\xi}$ is given by

$$\nabla\cdot\boldsymbol{\xi} = \nabla\cdot\left(\frac{\boldsymbol{B}_0\times\nabla\phi}{B_0^2}\right) = \nabla\phi\cdot\nabla\times\left(\frac{\boldsymbol{B}_0}{B_0^2}\right) = \nabla\phi\cdot\left(\left(\nabla\frac{1}{B^2}\right)\times\boldsymbol{B} + \frac{1}{B^2}\nabla\times\boldsymbol{B}\right).$$

The 2nd term in ( ) is negligible compared with the 1st term in the low beta case. By means of $\nabla p_0 = \boldsymbol{j}_0\times\boldsymbol{B}_0$, δW is expressed by

$$\delta W = \frac{1}{2\mu_0}\int(\nabla\times\nabla_\perp\phi)^2 + \frac{\mu_0\nabla p_0\cdot(\nabla_\perp\phi\times\boldsymbol{B}_0)}{B_0^2}\left(\frac{\boldsymbol{B}_0\cdot\nabla\times\nabla_\perp\phi}{B_0^2}\right) \\ -\frac{\mu_0(\boldsymbol{j}_0\cdot\boldsymbol{B}_0)}{B_0^2}\nabla_\perp\phi\cdot\nabla\times\nabla_\perp\phi + \gamma\mu_0 p_0\left(\nabla\left(\frac{1}{B_0^2}\right)\cdot(\boldsymbol{B}_0\times\nabla_\perp\phi)\right)^2 \\ +\frac{\mu_0\nabla p_0\cdot(\boldsymbol{B}_0\times\nabla_\perp\phi)}{B_0^2}\left(\nabla\left(\frac{1}{B_0^2}\right)\cdot(\boldsymbol{B}_0\times\nabla_\perp\phi)\right)\mathrm{d}\boldsymbol{r}.$$

Let us use z coordinate as a length along a field line, r as radial coordinate of magnetic surfaces and θ as poloidal angle in the perpendicular direction to field lines. The r,θ,z components of ∇p_0, $\boldsymbol{B}$, and $\nabla\phi$ are approximately given by

$$\nabla p_0 = (p_0', 0, 0), \qquad \boldsymbol{B} = (0,\ B_\theta(r),\ B_0(1 - rR_\mathrm{c}^{-1}(z))),$$

$$\nabla\phi = (\partial\phi/\partial r, \partial\phi/r\partial\theta, \partial\phi/\partial z), \qquad \phi(r,\theta,z) = \phi(r,z)\mathrm{Re}(\exp im\theta).$$

$R_\mathrm{c}(z)$ is the radius of curvature of the line of magnetic force:

$$\frac{1}{R_\mathrm{c}(z)} = \frac{1}{R_0}\left(-w + \cos 2\pi\frac{z}{L}\right).$$

When $R_c(z) < 0$, the curvature is said to be good. If the configuration is average minimum-B, w and R_0 must be $1 > w > 0$ and $R_0 > 0$. Since $B_\theta/B_0, r/R_0, r/L$ are all small quantities, we find

$$\nabla_\perp \phi = \nabla\phi - \nabla_\parallel \phi \approx \mathrm{Re}\left(\frac{\partial\phi}{\partial r}, \frac{im}{r}\phi, 0\right),$$

$$\nabla \times (\nabla_\perp \phi) \approx \mathrm{Re}\left(\frac{-im}{r}\frac{\partial\phi}{\partial z}, \frac{\partial^2\phi}{\partial z \partial r}, 0\right),$$

$$\boldsymbol{B}_0 \times \nabla_\perp \phi \approx \mathrm{Re}\left(\frac{-im}{r}B_0\phi, B_0\frac{\partial\phi}{\partial r}, 0\right)$$

and δW is reduced to

$$\delta W = \frac{1}{2\mu_0}\int \frac{m^2}{r^2}\left(\left(\frac{\partial\phi(r,z)}{\partial z}\right)^2 - \frac{\beta}{r_p R_c(z)}(\phi(r,z))^2\right) 2\pi r \mathrm{d}r\mathrm{d}z$$

where $-p_0/p_0' = r_\mathrm{p}$ and $\beta = p_0/(B_0^2/2\mu_0)$. The 2nd term contributes to stability in the region $R_c(z) < 0$ and contributes to instability in the region of $R_c(z) > 0$. Euler's equation is given by

$$\frac{\mathrm{d}^2\phi}{\mathrm{d}z^2} + \frac{\beta}{r_\mathrm{p} R_c(z)}\phi = 0. \tag{8.122}$$

R_c is nearly equal to $B/|\nabla B|$. Equation (8.122) is a Mathieu differential equation, whose eigenvalue is

$$w = F(\beta L^2/2\pi^2 r_\mathrm{p} R_0).$$

Since

$$F(x) = x/4, \qquad x \ll 1, \qquad\qquad F(x) = 1 - x^{-1/2}, \quad x \gg 1,$$

we find the approximate relation

$$\beta_c \sim \frac{4w}{(1+3w)(1-w)^2}\frac{2\pi^2 r_\mathrm{p} R_0}{L^2}.$$

Since w is of the order of $r_\mathrm{p}/2R_0$ and the connection length is

$$L \approx 2\pi R_0(2\pi/\iota)$$

(ι being the rotational transform angle), the critical beta ratio β_c is

$$\beta_c \sim \left(\frac{\iota}{2\pi}\right)^2\left(\frac{r_\mathrm{p}}{R}\right). \tag{8.123}$$

If β is smaller than the critical beta ratio β_c, then $\delta W > 0$, and the plasma is stable. The stability condition for the ballooning mode in the shearless case is given by (ref.[16]).

$$\beta < \beta_c.$$

In the configuration with magnetic shear, more rigorous treatment is necessary. According to the analysis (ref.[17]-[19]) for ballooning modes with large toroidal mode number $n \gg 1$ and $m - nq \sim 0$ (see appendix B), the stable region in the shear parameter S and the measure of pressure gradient α of ballooning mode is shown in fig.8.12. The shear parameter S is defined by

$$S = \frac{r}{q}\frac{\mathrm{d}q}{\mathrm{d}r}$$

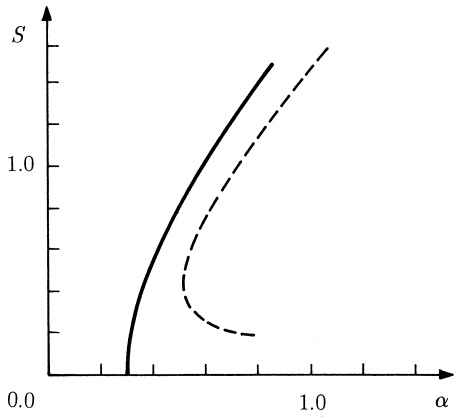

Fig.8.12 The maximum stable pressure gradient α as a function of the shear parameter S of ballooning mode. The dotted line is the stability boundary obtained by imposing a more restricted boundary condition on the perturbation (ref.[17]).

where q is the safety factor ($q \equiv 2\pi/\iota$: ι rotational transform angle) and the measure of pressure gradient α is defined by

$$\alpha = -\frac{q^2 R}{B^2/2\mu_0}\frac{\mathrm{d}p}{\mathrm{d}r}.$$

The straight-line approximation of the maximum pressure gradient in the range of large positive shear ($S > 0.8$) is $\alpha \sim 0.6S$ as is shown in fig.8.12. Since

$$\beta = \frac{1}{B_0^2/2\mu_0}\frac{1}{\pi a^2}\int_0^a p 2\pi r \mathrm{d}r = -\frac{1}{B_0^2/2\mu_0}\frac{1}{a^2}\int_0^a \frac{\mathrm{d}p}{\mathrm{d}r} r^2 \mathrm{d}r$$

the maximum ballooning stable beta is

$$\beta = 0.6\frac{a}{R}\left(\frac{1}{a^3}\int_0^a \frac{1}{q^3}\frac{\mathrm{d}q}{\mathrm{d}r} r^3 \mathrm{d}r\right).$$

Under an optimum q profile, the maximum beta is given by (ref.[19])

$$\beta_{\max} \sim 0.28\frac{a}{Rq_a} \qquad (q_a > 2) \tag{8.124}$$

where q_a is the safety factor at the plasma boundary. In the derivation of (8.124) $q_a > 2,\ q_0 = 1$ are assumed.

It must be notified that the ballooning mode is stable in the negative shear region of S, as is shown in fig.8.12. When the shear parameter S is negative ($q(r)$ decreases outwardly), the outer lines of magnetic force rotate around the magnetic axis more quickly than inner ones. When the pressure increases, the tokamak plasma tends to expand in a direction of major radius (Shafranov shift). This must be counter balanced by strengthening the poloidal field on the outside of tokamak plasma. In the region of strong pressure gradient, the necessary poloidal field increases outwardly, so on outer magnetic surfaces the magnetic field lines rotate around the magnetic axis faster than on inner ones and the shear parameter becomes more negative (ref.[20]).

In reality the shear parameter in a tokamak is positive in usual operations. However the fact that the ballooning mode is stable in negative shear parameter region is very important to develope tokamak configuration stable against ballooning modes. Since

$$\frac{r}{Rq} = \frac{B_\theta}{B_0} = \frac{1}{B_0}\frac{\mu_0}{2\pi r}\int_0^r j(r) 2\pi r \mathrm{d}r$$

the profile of safety factor $q(r)$ is

$$\frac{1}{q(r)} = \frac{R}{2B_0}\left(\frac{\mu_0}{\pi r^2}\int_0^r j 2\pi r \mathrm{d}r\right) \equiv \frac{\mu_0 R}{2B_0}\langle j(r)\rangle_r.$$

Therefore a negative shear configuration can be realized by a hollow current profile. The MHD stability of tokamak with hollow current profiles is analyzed in details in (ref.[21]).

8.6 $\eta_{\rm i}$ Mode due to Density and Temperature Gradient

Let us consider a plasma with the density gradient $\mathrm{d}n_0/\mathrm{d}r$, and the temperature gradient $\mathrm{d}T_{\rm e0}/\mathrm{d}r$, $\mathrm{d}T_{\rm i0}/\mathrm{d}r$ in the magnetic field with the z direction. Assume that the ion's density becomes $n_{\rm i} = n_{\rm i0} + \tilde{n}_{\rm i}$ by disturbance. The equation of continuity

$$\frac{\partial n_{\rm i}}{\partial t} + \boldsymbol{v}_{\rm i}\cdot\nabla n_{\rm i} + n_{\rm i}\nabla\cdot\boldsymbol{v}_{\rm i} = 0$$

is reduced, by the linearization, to

$$-i\omega\tilde{n}_{\rm i} + \tilde{v}_{\rm r}\frac{\partial n_0}{\partial r} + n_0 i k_\parallel \tilde{v}_\parallel = 0. \tag{8.125}$$

It is assumed that the perturbation terms changes as $\exp i(k_\theta r\theta + k_\parallel z - \omega t)$ and $k_\theta, k_\parallel$ are the θ and z components of the propagation vector. When the perturbed electrostatic potential is denoted by $\tilde{\phi}$, the $\boldsymbol{E}\times\boldsymbol{B}$ drift velocity is $\tilde{v}_{\rm r} = E_\theta/B = ik_\theta\tilde{\phi}/B$. Since the electron density follows Boltzmann distribution, we find

$$\frac{\tilde{n}_{\rm e}}{n_0} = \frac{e\tilde{\phi}}{kT_{\rm e}}. \tag{8.126}$$

The parallel component of the equation of motion to the magnetic field

$$n_{\rm i}m_{\rm i}\frac{\mathrm{d}v_\parallel}{\mathrm{d}t} = -\nabla_\parallel p_{\rm i} - en\nabla_\parallel\phi$$

is reduced, by the linearization, to

$$-i\omega n_{\rm i}m_{\rm i}\tilde{v}_\parallel = -ik_\parallel(\tilde{p}_{\rm i} + en_0\tilde{\phi}). \tag{8.127}$$

Similarly the adiabatic equation

$$\frac{\partial}{\partial t}(p_{\rm i}n_{\rm i}^{-5/3}) + \boldsymbol{v}\cdot\nabla(p_{\rm i}n_{\rm i}^{-5/3}) = 0$$

is reduced to

$$-i\omega\left(\frac{\tilde{p}_{\rm i}}{p_{\rm i}} - \frac{5}{3}\frac{\tilde{n}_{\rm i}}{n_{\rm i}}\right) - \frac{ik_\theta\tilde{\phi}}{B}\left(\frac{\mathrm{d}T_{\rm i0}}{\mathrm{d}r}\frac{1}{T_{\rm i0}} - \frac{2}{3}\frac{\mathrm{d}n_0}{\mathrm{d}r}\frac{1}{n_0}\right) = 0. \tag{8.128}$$

Let us define the *electron drift frequencies* $\omega^*_{\rm ne}, \omega^*_{Tee}$ and the *ion drift frequency* $\omega^*_{n\rm i}, \omega^*_{T\rm i}$ by

$$\omega^*_{ne} \equiv -\frac{k_\theta(\kappa T_{\rm e})}{eBn_{\rm e}}\frac{\mathrm{d}n_{\rm e}}{\mathrm{d}r}, \qquad \omega^*_{n\rm i} \equiv \frac{k_\theta(\kappa T_{\rm i})}{eBn_{\rm i}}\frac{\mathrm{d}n_{\rm i}}{\mathrm{d}r},$$

$$\omega^*_{T\rm e} \equiv -\frac{k_\theta}{eB}\frac{\mathrm{d}(\kappa T_{\rm e})}{\mathrm{d}r}, \qquad \omega^*_{T\rm i} \equiv \frac{k_\theta}{eB}\frac{\mathrm{d}(\kappa T_{\rm i})}{\mathrm{d}r}.$$

The ratio of the temperature gradient to the density gradient of electrons and ions is given by

$$\eta_{\rm e} \equiv \frac{{\rm d}T_{\rm e}/{\rm d}r}{T_{\rm e}} \frac{n_{\rm e}}{{\rm d}n_{\rm e}/{\rm d}r} = \frac{{\rm d}\ln T_{\rm e}}{{\rm d}\ln n_{\rm e}}, \qquad \eta_{\rm i} \equiv \frac{{\rm d}T_{\rm i}/{\rm d}r}{T_{\rm i}} \frac{n_{\rm i}}{{\rm d}n_{\rm i}/{\rm d}r} = \frac{{\rm d}\ln T_{\rm i}}{{\rm d}\ln n_{\rm i}}$$

respectively. There are following relations among these values;

$$\omega^*_{n{\rm i}} = -\frac{T_{\rm i}}{T_{\rm e}}\omega^*_{n{\rm e}}, \qquad \omega^*_{T{\rm e}} = \eta_{\rm e}\omega^*_{n{\rm e}}, \qquad \omega^*_{T{\rm i}} = \eta_{\rm i}\omega^*_{n{\rm i}}.$$

Then equations (8.125),(8.126),(8.127),(8.128) are reduced to

$$\frac{\tilde{n}_{\rm i}}{n_0} = \frac{\tilde{v}_\parallel}{\omega/k_\parallel} + \frac{\omega^*_{n{\rm e}}}{\omega}\frac{e\tilde{\phi}}{\kappa T_{\rm e}},$$

$$\frac{\tilde{n}_{\rm e}}{n_0} = \frac{e\tilde{\phi}}{\kappa T_{\rm e}},$$

$$\frac{\tilde{v}_\parallel}{\omega/k_\parallel} = \frac{1}{m_{\rm i}(\omega/k_\parallel)^2}\left(e\tilde{\phi} + \frac{\tilde{p}_{\rm i}}{n_0}\right),$$

$$\left(\frac{\tilde{p}_{\rm i}}{p_{\rm i0}} - \frac{5}{3}\frac{\tilde{n}}{n_0}\right) = \frac{\omega^*_{n{\rm e}}}{\omega}\left(\eta_{\rm i} - \frac{2}{3}\right)\frac{e\tilde{\phi}}{\kappa T_{\rm e}}.$$

Charge neutrality condition $\tilde{n}_{\rm i}/n_0 = \tilde{n}_{\rm e}/n_0$ yields the dispersion equation (ref.[22]).

$$1 - \frac{\omega^*_{n{\rm e}}}{\omega} - \left(\frac{v_{\rm Ti}}{\omega/k_\parallel}\right)^2\left(\frac{T_{\rm e}}{T_{\rm i}} + \frac{5}{3} + \frac{\omega^*_{n{\rm e}}}{\omega}\left(\eta_{\rm i} - \frac{2}{3}\right)\right) = 0.$$

($v^2_{\rm Ti} = \kappa T_{\rm i}/m_{\rm i}$). The solution in the case of $\omega \ll \omega^*_{n_{\rm e}}$ is

$$\omega^2 = -k^2_\parallel v^2_{\rm Ti}\left(\eta_{\rm i} - \frac{2}{3}\right).$$

The dispersion equation shows that this type of perturbation is unstable when $\eta_{\rm i} > 2/3$. This mode is called $\eta_{\rm i}$ *mode.*

When the propagation velocity $|\omega/k_\parallel|$ becomes the order of the ion thermal velocity $v_{T_{\rm i}}$, the interaction (Landau damping) between ions and wave (perturbation) becomes important as will be described in ch.11 and MHD treatment must be modified. When the value of $\eta_{\rm i}$ is not large, the kinetic treatment is necessary and the threshold of $\eta_{\rm i}$ becomes $\eta_{\rm i,cr} \sim 1.5$.

References

[1] G. Bateman: *MHD instabilities,* The MIT Press, Cambridge Mass. 1978.

[2] M. Kruskal and M. Schwarzschield: Proc. Roy. Soc. **A223**, 348 (1954).

[3] M. N. Rosenbluth, N. A. Krall and N. Rostoker: Nucl. Fusion Suppl. Pt.1 p.143 (1962).

[4] M. N. Rosenbluth and C. L. Longmire: Annal. Physics **1**, 120 (1957).

[5] I. B. Berstein, E. A. Frieman, M. D. Kruskal and R. M. Kulsrud: Proc. Roy. Soc. **A244**, 17 (1958).

[6] B. B. Kadmotsev: *Reviews of Plasma Physics* **2**, 153(ed. by M. A. Loentovich) Consultant Bureau, New York 1966.

[7] K. Miyamoto: *Plasma Physics for Nuclear Fusion* (revised edition) Chap.9, The MIT Press, Cambridge, Mass. 1988.

[8] M. D. Kruskal, J. L. Johnson, M. B. Gottlieb and L. M. Goldman: Phys. Fluids **1**, 421 (1958).

[9] V. D. Shafranov: Sov. Phys. JETP **6**, 545 (1958).

[10] B. R. Suydam: Proc. 2nd U. N. International Conf. on Peaceful Uses of Atomic Energy, Geneva, **31**, 157 (1958).
[11] W. A. Newcomb: Annal. Physics **10**, 232 (1960).
[12] V. D. Shafranov: Sov. Phys. Tech. Phys. **15**, 175 (1970).
[13] D. C. Robinson: Plasma Phys. **13**, 439 (1971).
[14] K. Hain and R. Lüst: Z. Naturforsh. **13a**, 936 (1958).
[15] K. Matsuoka and K. Miyamoto: Jpn. J. Appl. Phys. **18**, 817 (1979).
[16] R. M. Kulsrud: Plasma Phys. and Controlled Nucl. Fusion Research,**1**, 127, 1966 (Conf. Proceedings, Culham in 1965 IAEA Vienna).
[17] J. W. Connor, R. J. Hastie and J. B. Taylor: Phys. Rev. Lett. **40**, 393 (1978).
[18] J. W. Connor, R. J. Hastie and J. B. Taylor: Pro. Roy. Soc. **A365**, 1 (1979).
[19] J. A. Wesson, A. Sykes: Nucl. Fusion **25** 85 (1985).
[20] J. M. Greene, M. S. Chance: Nucl. Fusion **21**, 453 (1981).
[21] T. Ozeki, M. Azumi, S. Tokuda, S. Ishida: Nucl. Fusion **33**, 1025 (1993).
[22] B. B. Kadomtsev and O. P. Pogutse: *Reviews of Plasma Physics* **5**,304 (ed. by M. A. Leontovich) Consultant Bureau, New York 1970.

Ch.9 Resistive Instability

In the preceding chapter we have discussed instabilities of plasmas with zero resistivity. In such a case the conducting plasma is frozen to the line of magnetic force. However, the resistivity of a plasma is not generally zero and the plasma may hence deviate from the magnetic line of force. Modes which are stable in the ideal case may in some instances become unstable if a finite resistivity is introduced.

Ohm's law is

$$\eta \boldsymbol{j} = \boldsymbol{E} + \boldsymbol{V} \times \boldsymbol{B}. \tag{9.1}$$

For simplicity we here assume that $\boldsymbol{E}$ is zero. The current density is $\boldsymbol{j} = \boldsymbol{V} \times \boldsymbol{B}/\eta$ and the $\boldsymbol{j} \times \boldsymbol{B}$ force is

$$\boldsymbol{F}_{\mathrm{s}} = \boldsymbol{j} \times \boldsymbol{B} = \frac{\boldsymbol{B}(\boldsymbol{V} \cdot \boldsymbol{B}) - \boldsymbol{V}B^2}{\eta}. \tag{9.2}$$

When η tends to zero, this force becomes infinite and prevents the deviation of the plasma from the line of magnetic force. When the magnitude B of magnetic field is small, this force does not become large, even if η is small, and the plasma can deviate from the line of magnetic force. When we consider a perturbation with the propagation vector $\boldsymbol{k}$, only the parallel (to $\boldsymbol{k}$) component of the zeroth-order magnetic field $\boldsymbol{B}$ affects the perturbation, as will be shown later. Even if shear exists, we can choose a propagation vector $\boldsymbol{k}$ perpendicular to the magnetic field $\boldsymbol{B}$:

$$(\boldsymbol{k} \cdot \boldsymbol{B}) = 0. \tag{9.3}$$

Accordingly, if there is any force $\boldsymbol{F}_{\mathrm{dr}}$ driving the perturbation, this driving force may easily exceed the force $\boldsymbol{F}_{\mathrm{s}}$, which is very small for a perturbation where $(\boldsymbol{k} \cdot \boldsymbol{B}) = 0$, and the plasma becomes unstable. This type of instability is called *resistive instability.*

9.1 Tearing Instability

Let us consider a slab model in which the zeroth-order magnetic field $\boldsymbol{B}_0$ depends on only x and $\boldsymbol{B}$ is given as follows;

$$\boldsymbol{B}_0 = B_{0y}(x)\boldsymbol{e}_y + B_{0z}(x)\boldsymbol{e}_z. \tag{9.4}$$

From Ohm's law (9.1) we find

$$\frac{\partial \boldsymbol{B}}{\partial t} = -\nabla \times \boldsymbol{E} = \nabla \times ((\boldsymbol{V} \times \boldsymbol{B}) - \eta \boldsymbol{j}) = \nabla \times (\boldsymbol{V} \times \boldsymbol{B}) + \frac{\eta}{\mu_0}\Delta \boldsymbol{B} \tag{9.5}$$

where η is assumed to be constant. It is assumed that the plasma is incompressible. Since the growth rate of the resistive instability is small compared with the MHD characteristic rate (inverse of Alfven transit time) and the movement is slower than the sound velocity, the assumption of incompressibility is justified and it follows that

$$\nabla \cdot \boldsymbol{V} = 0. \tag{9.6}$$

The magnetic field $\boldsymbol{B}$ always satisfies

$$\nabla \cdot \boldsymbol{B} = 0. \tag{9.7}$$

The equation of motion is

$$\rho_{\mathrm{m}} \frac{\mathrm{d}\boldsymbol{V}}{\mathrm{d}t} = \frac{1}{\mu_0}(\nabla \times \boldsymbol{B}) \times \boldsymbol{B} - \nabla p$$

$$= \frac{1}{\mu_0}\left((\boldsymbol{B}_0\cdot\nabla)\boldsymbol{B}_1 + (\boldsymbol{B}_1\cdot\nabla)\boldsymbol{B}_0 - \frac{\nabla B^2}{2}\right) - \nabla p. \tag{9.8}$$

Let us consider the perturbation expressed by $f_1(\boldsymbol{r},t) = f_1(x)\exp(i(k_y y + k_z z) + \gamma t)$. Then (9.5) reduces to

$$\gamma B_{1x} = i(\boldsymbol{k}\cdot\boldsymbol{B})V_x + \frac{\eta}{\mu_0}\left(\frac{\partial^2}{\partial x^2} - k^2\right)B_{1x} \tag{9.9}$$

where $k^2 = k_y^2 + k_z^2$. The first term in the right-hand side of (9.8) becomes $(\boldsymbol{B}_0\cdot\nabla)\boldsymbol{B}_1 = i(\boldsymbol{k}\cdot\boldsymbol{B}_0)\boldsymbol{B}_1$. The rotation of (9.8) is

$$\mu_0\rho_{\mathrm{m}}\gamma\nabla\times\boldsymbol{V} = \nabla\times\left(i(\boldsymbol{k}\cdot\boldsymbol{B}_0)\boldsymbol{B}_1 + \left(B_{1x}\frac{\partial}{\partial x}\right)\boldsymbol{B}_0\right). \tag{9.10}$$

Equations (9.6),(9.7) reduce to

$$\frac{\partial B_{1x}}{\partial x} + ik_y B_{1y} + ik_z B_{1z} = 0, \tag{9.11}$$

$$\frac{\partial V_x}{\partial x} + ik_y V_y + ik_z V_z = 0. \tag{9.12}$$

Multiply k_y and z component of (9.10) and multiply k_z and the y component and take the difference. Use the relations of (9.11) and (9.12); then we find

$$\mu_0\rho_{\mathrm{m}}\gamma\left(\frac{\partial^2}{\partial x^2} - k^2\right)V_x = i(\boldsymbol{k}\cdot\boldsymbol{B}_0)\left(\frac{\partial^2}{\partial x^2} - k^2\right)B_{1x} - i(\boldsymbol{k}\cdot\boldsymbol{B}_0)''B_{1x} \tag{9.13}$$

where $'$ is differentiation in x. Ohm's law and the equation of motion are reduced to (9.9) and (9.13) (ref.[1]). It must be notified that the zeroth-order magnetic field $\boldsymbol{B}_0$ appears only in the form of $(\boldsymbol{k}\cdot\boldsymbol{B}_0)$. When we introduce a function

$$F(x) \equiv (\boldsymbol{k}\cdot\boldsymbol{B}_0) \tag{9.14}$$

the location of $F(x) = 0$ is the position where resistive instabilities are likely occurred. We choose this position to be $x = 0$ (see fig.9.1). $F(x)$ is equal to $(\boldsymbol{k}\cdot\boldsymbol{B}_0) \simeq (\boldsymbol{k}\cdot\boldsymbol{B}_0)'x$ near $x = 0$. As is clear from eqs.(9.9) and (9.13), B_{1x} is an even function and V_x is an odd function near $x = 0$. The term $|\Delta B_{1x}| \sim |\mu_0 k_y j_{1z}|$ can be large only in the region $|x| < \varepsilon$. Since the growth rate of resistive instability is much smaller than MHD growth rate, the left-hand side of the equation of motion (9.13) can be neglected in the region $|x| > \varepsilon$ and we have

$$\frac{\mathrm{d}^2 B_{1x}}{\mathrm{d}x^2} - k^2 B_{1x} = \frac{F''}{F}B_{1x}, \qquad |x| > \varepsilon. \tag{9.15}$$

The solution in the region $x > 0$ is

$$B_{1x} = e^{-kx}\left(\int_{-\infty}^{x} e^{2k\xi}\,\mathrm{d}\xi \int_{\infty}^{\xi}(F''/F)B_{1x}e^{-k\eta}\,\mathrm{d}\eta + A\right)$$

and the solution in the region $x < 0$ is

$$B_{1x} = e^{kx}\left(\int_{\infty}^{x} e^{-2k\xi}\,\mathrm{d}\xi \int_{\infty}^{\xi}(F''/F)B_{1x}e^{k\eta}\,\mathrm{d}\eta + B\right).$$

Let us define Δ' as the difference between $B'_{1x}(+\varepsilon)$ at $x = +\varepsilon$ and $B'_{1x}(-\varepsilon)$ at $x = -\varepsilon$ as follows;

$$\Delta' = \frac{B'_{1x}(+\varepsilon) - B'_{1x}(-\varepsilon)}{B_{1x}(0)}. \tag{9.16}$$

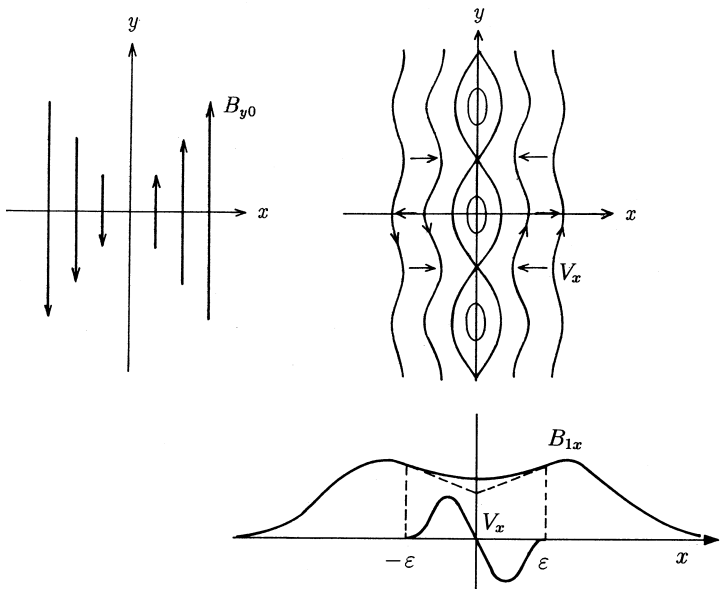

Fig.9.1 Zeroth-order magnetic configuration and magnetic islands due to tearing instability. Profiles of B_{1x} and V_x are also shown.

Then the value of Δ' obtained from the solutions in the region $|x| > \varepsilon$ is given by

$$\Delta' = -2k - \frac{1}{B_{1x}(0)} \left(\int_{-\infty}^{-\varepsilon} + \int_{\varepsilon}^{\infty} \right) \exp(-k|x|)(F''/F) B_{1x} \, \mathrm{d}x. \tag{9.17}$$

For a trial function of

$$F(x) = F_{\mathrm{s}} x / L_{\mathrm{s}} \quad (|x| < L_{\mathrm{s}}), \qquad F(x) = F_{\mathrm{s}} x / |x| \quad (x > |L_{\mathrm{s}}|)$$

we can solve (9.15) and Δ' is reduced to

$$\Delta' = \left(\frac{2\alpha}{L_{\mathrm{s}}} \right) \frac{\mathrm{e}^{-2\alpha} + (1 - 2\alpha)}{\mathrm{e}^{-2\alpha} - (1 - 2\alpha)} \approx \frac{2}{L_{\mathrm{s}}} \left(\frac{1}{\alpha} - \alpha \right)$$

Here $\alpha \equiv k L_{\mathrm{s}}$ was used and L_{s} is *shear length* defined by $L_{\mathrm{s}} = (F/F')_{x=0}$. For more general cases of $F(x)$, $B_{1x}(x)$ has logarithmic singularity at $x = 0$, since $F''/F \propto 1/x$ generally. Referene [2] describes the method to avoid difficulties arising from the corresponding logarithmic singularity.

Equations (9.9) and (9.13) in the region $|x| < \varepsilon$ reduce to

$$\frac{\partial^2 B_{1x}}{\partial x^2} - \left(k^2 + \frac{\gamma \mu_0}{\eta} \right) B_{1x} = -i \frac{\mu_0}{\eta} F' x V_x, \tag{9.18}$$

$$\frac{\partial^2 V_x}{\partial x^2} - \left(k^2 + \frac{(F')^2}{\rho_{\mathrm{m}} \eta \gamma} x^2 \right) V_x = i \left(F' x \frac{1}{\rho_{\mathrm{m}} \eta} - \frac{F''}{\mu_0 \rho_{\mathrm{m}} \gamma} \right) B_{1x}. \tag{9.19}$$

The value of Δ' obtained from the solution in the region $|x| < \varepsilon$ is given from (9.18) as follows;

$$\begin{aligned} \Delta' \times B_{1x}(0) &= \frac{\partial B_{1x}(+\varepsilon)}{\partial x} - \frac{\partial B_{1x}(-\varepsilon)}{\partial x} \\ &= \frac{\mu_0}{\eta} \int_{-\varepsilon}^{\varepsilon} \left(\left(\gamma + \frac{\eta}{\mu_0} k^2 \right) B_{1x} - i F' x V_x \right) \mathrm{d}x. \end{aligned} \tag{9.20}$$

The value Δ' of (9.20) must be equal to the value of Δ' of (9.17). This requirement gives the eigenvalue γ and the growth rate of this resistive instability can be obtained (ref.[1]). However we try to reduce the growth rate in qualitative manner in this section. In the region $|x| < \varepsilon$, it is possible to write

$$\frac{\partial^2 B_{1x}}{\partial x^2} \sim \frac{\Delta' B_{1x}}{\varepsilon}.$$

It is assumed that the three terms of (9.9), namely the term of induced electric field (the left-hand side), the $\boldsymbol{V} \times \boldsymbol{B}$ term (the first term in the right-hand side) and Ohm's term (the second term) are the same order:

$$\gamma B_{1x} \sim \frac{\eta}{\mu_0} \frac{\Delta' B_{1x}}{\varepsilon}, \tag{9.21}$$

$$\gamma B_{1x} \sim iF'\varepsilon V_x. \tag{9.22}$$

Then (9.21) yields

$$\gamma \sim \frac{\eta}{\mu_0} \frac{\Delta'}{\varepsilon}. \tag{9.23}$$

Accordingly

$$\Delta' > 0 \tag{9.24}$$

is the condition of instability. In order to get the value of γ, the evaluation of ε is necessary. Equation (9.13) reduces to

$$\mu_0 \rho_{\mathrm{m}} \gamma \left(\frac{-V_x}{\varepsilon^2} \right) \sim iF'\varepsilon \frac{\Delta' B_{1x}}{\varepsilon}. \tag{9.25}$$

If the terms V_x, B_{1x}, γ are eliminated by (9.21), (9.22) and (9.25), we find

$$\varepsilon^5 \sim \left(\frac{\eta}{\mu_0 a^2} \right)^2 (\Delta' a) \frac{\rho_{\mathrm{m}} \mu_0}{(F'a)^2} a^5,$$

$$\frac{\varepsilon}{a} \sim \left(\left(\frac{\tau_{\mathrm{A}}}{\tau_{\mathrm{R}}} \right)^2 (\Delta' a) \left(\frac{B_0}{F' a^2} \right)^2 \right)^{1/5} \sim S^{-2/5} (\Delta' a)^{1/5} \left(\frac{B_0}{(\boldsymbol{k} \cdot \boldsymbol{B}_0)' a^2} \right)^{2/5} \tag{9.26}$$

where the physical quantities

$$\tau_{\mathrm{R}} = \frac{\mu_0 a^2}{\eta},$$

$$\tau_{\mathrm{A}} = \frac{a}{B_0/(\mu_0 \rho_{\mathrm{m}})^{1/2}}$$

are the resistive diffusion time and Alfvén transit time respectively. A non-dimensional factor

$$S = \tau_{\mathrm{R}}/\tau_{\mathrm{A}}$$

is *magnetic Reynolds number* and a is a typical plasma size. Accordingly the growth rate γ is given by

$$\gamma = \frac{\eta}{\mu_0 a^2} \frac{a}{\varepsilon} (\Delta' a) = \frac{(\Delta' a)^{4/5}}{\tau_{\mathrm{R}}^{3/5} \tau_{\mathrm{A}}^{2/5}} \left(\frac{(\boldsymbol{k} \cdot \boldsymbol{B}_0)' a^2}{B_0} \right)^{2/5} = \frac{(\Delta' a)^{4/5}}{S^{3/5}} \left(\frac{(\boldsymbol{k} \cdot \boldsymbol{B}_0)' a^2}{B_0} \right)^{2/5} \frac{1}{\tau_{\mathrm{A}}}. \tag{9.27}$$

Since this mode is likely break up the plasma into a set of magnetic islands as is shown in fig.9.1, this mode is called *tearing instability* (ref.[1]).

The foregoing discussion has been based on the slab model. Let us consider this mode in a toroidal plasma. The poloidal and the toroidal components of the propagation vector $\boldsymbol{k}$ are m/r and $-n/R$ respectively. Accordingly there are correspondences of $k_y \leftrightarrow m/r$, and $k_z \leftrightarrow -n/R$, and

$$(\boldsymbol{k}\cdot\boldsymbol{B}_0) = \frac{m}{r}B_\theta - \frac{n}{R}B_{\rm z} = \frac{n}{r}B_\theta\left(\frac{m}{n}-q\right), \qquad q \equiv \frac{r}{R}\frac{B_z}{B_\theta}.$$

Therefore weak positions for tearing instability are given by $(\boldsymbol{k}\cdot\boldsymbol{B}_0)=0$ and these are rational surfaces satisfying $q(r_{\rm s}) = m/n$. The shear is given by

$$(\boldsymbol{k}\cdot\boldsymbol{B}_0)' = \frac{-n}{r}B_\theta\frac{{\rm d}q}{{\rm d}r}, \qquad \frac{(\boldsymbol{k}\cdot\boldsymbol{B}_0)' r_{\rm s}^2}{B_0} = -n\left(\frac{r_{\rm s}}{R}\right)\frac{q' r_{\rm s}}{q}.$$

The tearing mode is closely related to the internal disruption in tokamak and plays important role as is described in sec.16.3.

It has been assumed that the specific resistivity η and the mass density $\rho_{\rm m}$ are uniform and there is no gravitation (acceleration) $\boldsymbol{g}=0$. If η depends on x, the resistive term in (9.5) becomes $\nabla\times(\eta\nabla\times\boldsymbol{B})/\mu_0$. When there is temperature gradient ($\eta'\neq 0$), rippling mode with short wavelength ($kL_{\rm s}\gg 1$) may appear in the smaller-resistivity-side (high-temperature-side) of $x=0$ position. When there is gravitation, the term $\rho\boldsymbol{g}$ is added to the equation of motion (9.8). If the direction of $\boldsymbol{g}$ is opposit to $\nabla\rho_{\rm m}$ ($\boldsymbol{g}$ is toward low-density-side), gravitational interchange mode may appear (ref.[1]).

9.2 Resistive Drift Instability

A finite density and temperature gradient always exists at a plasma boundary. Configurations including a gradient may be unstable under certain conditions. Let us consider a slab model. The directon of the uniform magnetic field is taken in the z direction and $\boldsymbol{B}_0=(0,0,B_0)$. The x axis is taken in the direction of the density gradient with the positive direction outward from the plasma. The pressure is $p_0=p_0(x)$, (see fig.9.2). The zeroth-order plasma current is $\boldsymbol{j}_0=(0,p_0'/B_0,0)$ and we assume that the flow velocity and the electric field are zero $\boldsymbol{V}_0=0,\ \boldsymbol{E}_0=0$ in the zeroth order. The flow velocity due to classical diffusion is neglected here. Electron inertia and ion motion along magneitc lines of force are also neglected. The usual relations in this configuration are

$$Mn\frac{\partial\boldsymbol{V}}{\partial t} = \boldsymbol{j}\times\boldsymbol{B} - \nabla p, \tag{9.28}$$

$$\boldsymbol{E}+\boldsymbol{V}\times\boldsymbol{B} = \eta\boldsymbol{j} + \frac{1}{en}\left(\boldsymbol{j}\times\boldsymbol{B}-\nabla p_0\right), \tag{9.29}$$

$$\frac{\partial n}{\partial t} + \nabla\cdot(n\boldsymbol{V}) = 0, \tag{9.30}$$

$$\nabla\cdot\boldsymbol{j} = 0, \tag{9.31}$$

where M is the ion mass. In this configuration, electrostatic perturbations are considered here. The 1st-order electric field $\boldsymbol{E}_1$ is expressed by the electrostatic potential $\boldsymbol{E}_1=-\nabla\phi_1$ and the 1st-order magnetic field perturbation is zero $\boldsymbol{B}_1=0$ ($\partial B/\partial t=\nabla\times\boldsymbol{E}$). The characteristics of electrostatic perturbation will be explained in ch.10 in detail. For simplicity the ion temperature is assumed to be zero $T_{\rm i}=0$. Let us consider the mode

$$n_1(x,y,z,t) = n_1\exp i(ky+k_\parallel z-\omega t),$$
$$\phi_1(x,y,z,t) = \phi_1\exp i(ky+k_\parallel z-\omega t).$$

Equations (9.28),(9.29) reduce to

$$-i\omega Mn_0\boldsymbol{V}_1 = \boldsymbol{j}_1\times\boldsymbol{B}_0 - \kappa T_{\rm e}\nabla n_1, \tag{9.32}$$

$$\boldsymbol{j}_1\times\boldsymbol{B}_0 - \kappa T_{\rm e}\nabla n_1 = en_0(-\nabla\phi_1+\boldsymbol{V}_1\times\boldsymbol{B}_0-\eta\boldsymbol{j}_1). \tag{9.33}$$

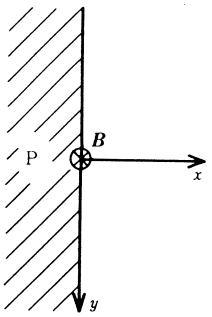

Fig.9.2 Slab model of resistive drift wave.

Equations (7.32),(7.33) yields

$$i\omega\left(\frac{M}{e}\right)\boldsymbol{V}_1 = \nabla\phi_1 - \boldsymbol{V}_1\times\boldsymbol{B}_0 + \eta\boldsymbol{j}_1. \tag{9.34}$$

When η is small ($\nu_{\rm ei} \ll \Omega_{\rm e}$), the contribution of $\eta\boldsymbol{j}$ can be neglected in (9.34), i.e., we may write

$$V_x = -ik\frac{\phi_1}{B_0}, \qquad V_y = \left(\frac{\omega}{\Omega_{\rm i}}\right)\frac{k\phi_1}{B_0}, \qquad V_z = \left(-\frac{\Omega_{\rm i}}{\omega}\right)\frac{k_\parallel\phi_1}{B_0}$$

$\Omega_{\rm i}$ is as usual, the ion cyclotron frequency ($\Omega_{\rm i} = -ZeB/M$). The wave frequency ω was assumed to be low $(\omega/\Omega_{\rm i})^2 \ll 1$. The x, y component of (9.32) and the z component of (9.33) are

$$j_x = -ik\frac{\kappa T_{\rm e} n_1}{B_0}, \qquad j_y = kn_0\left(\frac{\omega}{\Omega_{\rm i}}\right)\frac{e\phi_1}{B_0}, \qquad j_z = \frac{ik_\parallel}{e\eta}\left(\kappa T_{\rm e}\frac{n_1}{n_0} - e\phi_1\right).$$

Since (9.31) is $j_x' + ikj_y + ik_\parallel j_z = 0$, and (9.30) is $-i\omega n_1 + n_0' V_x + n_0 ikV_y + n_0 ik_\parallel V_z = 0$, we find

$$\frac{n_1}{n_0} - \left(1 + i\left(\frac{k}{k_\parallel}\right)^2\frac{\omega}{\Omega_{\rm i}}\frac{en_0\eta}{B_0}\right)\frac{e\phi_1}{\kappa T_{\rm e}} = 0, \tag{9.35}$$

$$\frac{n_1}{n_0} - \left(\left(\frac{k_\parallel}{\omega}\right)^2\frac{\kappa T_{\rm e}}{M} + k^2\frac{\kappa T_{\rm e}}{eB_0\Omega_{\rm i}} + \frac{k(-n_0'/n_0)\kappa T_{\rm e}}{eB_0}\frac{1}{\omega}\right)\frac{e\phi_1}{\kappa T_{\rm e}} = 0. \tag{9.36}$$

The dispersion equation is given by the determinant of the coefficients of (9.35),(9.36):

$$1 + i\left(\frac{k}{k_\parallel}\right)^2\frac{\omega}{\Omega_{\rm i}}\frac{\nu_{\rm ei}}{\Omega_{\rm e}} - \left(\frac{k_\parallel}{\omega}\right)^2 c_{\rm s}^2 + (k\rho_\Omega)^2 - \frac{\omega_{\rm e}^*}{\omega} = 0, \tag{9.37}$$

where $\eta = m_{\rm e}\nu_{\rm ei}/ne^2$, $B_0/(n_0 e\eta) = \Omega_{\rm e}/\nu_{\rm ei}$, $c_{\rm s}^2 \equiv \kappa T_{\rm e}/M$, $\rho_\Omega \equiv c_{\rm s}/|\Omega_{\rm i}|$ and $\omega_{\rm e}^* = k(-n_0'/n_0)(\kappa T_{\rm e}/m\Omega_{\rm e})$. The *drift velocities* $\boldsymbol{v}_{\rm di}, \boldsymbol{v}_{\rm de}$ of ions and electrons due to the density gradient ∇n_0 are given by

$$\boldsymbol{v}_{\rm di} = \frac{-(\kappa T_{\rm i}\nabla n_0/n_0)\times\boldsymbol{b}}{eB_0} = \frac{-\kappa T_{\rm i}}{eB_0}\left(\frac{-n_0'}{n_0}\right)\boldsymbol{e}_y,$$

$$\boldsymbol{v}_{\rm de} = \frac{(\kappa T_{\rm e}\nabla n_0/n_0)\times\boldsymbol{b}}{eB_0} = \frac{\kappa T_{\rm e}}{eB_0}\left(\frac{-n_0'}{n_0}\right)\boldsymbol{e}_y.$$

The *drift frequencies* of ions and electrons are defined by $\omega_{\rm i}^* \equiv kv_{\rm di}$ and $\omega_{\rm e}^* \equiv kv_{\rm de}$ respectively. As $n_0'/n_0 < 0$, $\omega_{\rm e}^* > 0$ and $\omega_{\rm i}^* = -(T_{\rm i}/T_{\rm e})\omega_{\rm e}^* < 0$. Since $\omega_{\rm e}^* = k(-n_0'/n_0)(\kappa T_{\rm e}/m\Omega_{\rm e})$, the dispersion equation is reduced to

$$\left(\frac{\omega}{\omega_{\rm e}^*}\right)^2 - i\left(1 + (k\rho_\Omega)^2 - \frac{\kappa T_{\rm e}}{M}\frac{k_\parallel^2}{\omega^2}\right)\frac{\Omega_{\rm e}\Omega_{\rm i}}{\nu_{\rm ei}\omega_{\rm e}^*}\left(\frac{k_\parallel}{k}\right)^2\left(\frac{\omega}{\omega_{\rm e}^*}\right) + i\frac{\Omega_{\rm e}\Omega_{\rm i}}{\nu_{\rm ei}\omega_{\rm e}^*}\left(\frac{k_\parallel}{k}\right)^2 = 0. \tag{9.38}$$

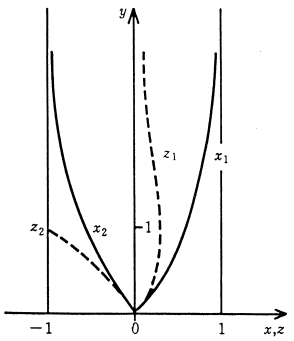

Fig.9.3 Dependence of $\omega/\omega_e^* = x + iz$ on $y \propto k_\parallel/k$ for resistive drift instability.

ρ_Ω is the ion Larmor radius when the ions are assumed to have the electron temperature T_e. Denote $\omega/\omega_e^* = x + iz$, and $-(\Omega_e\Omega_i\ /\nu_{ei}\omega_e^*)(k_\parallel/k)^2 = y^2$ and assume $(k\rho_\Omega)^2 - (\kappa T_e/M)(k_\parallel^2/\omega^2) \ll 1$. The dispersion equation is then

$$(x + iz)^2 + iy^2(x + iz) - iy^2 = 0. \tag{9.39}$$

The dependence of the two solutions $x_1(y), z_1(y)$ and $x_2(y), z_2(y)$ on $y \propto (k_\parallel/k)$, is shown in fig.9.3. As $z_2(y) < 0$, the mode corresponding to $x_2(y), z_2(y)$ is stable. This wave propagates in the direction of the ion drift. The solution $x_1, z_1 > 0$ propagates in the direction of the electron drift and it is unstable. If the value of $(k_\parallel/k)$ is adjusted to be $y \simeq 1.3$, the z_1 value becomes maximum to be $z_1 \approx 0.25$ and the growth rate is $\mathrm{Im}\,\omega \approx 0.25\,\omega_e^*$. If η is small, the wavelengh of the most unstable wave becomes long and the necessary number of collision to interrupt the electron motion along the magneitc line of force is maintained. If the lower limit of $k_\parallel$ is fixed by an appropriate method, the growth rate is

$$\mathrm{Im}(\omega/\omega_e^*) \approx y^{-2} = \frac{\nu_{ei}\omega_e^*}{\Omega_e|\Omega_i|}\left(\frac{k}{k_\parallel}\right)^2$$

and the growth rate is proportional to $\eta \propto \nu_{ei}$. This instability is called *resistive drift instability* or *dissipative drift instability.*

If the ion's inertia term can be neglected ($M \to 0, |\Omega_i| \to \infty$ in (9.37)), (9.37) reduces to $\omega^2 - \omega\omega^* - (k_\parallel c_s)^2 = 0$. The instability does not appear. This instability originates in the charge separation between electrons and ions due to ion inertia. The charge separation thus induced is neutralized by electrons motion along the lines of magnetic force. However, if the parallel motion of electrons is interrupted by collision,i.e.,resistivity, the charge separation grows and the wave becomes unstable (ref.[3],[4]). This instability is therefore also called *collisional drift instability.*

In collisionless case, (9.38) becomes

$$(1 + (k\rho_\Omega)^2)\omega^2 - \omega_e^*\omega - c_s^2k_\parallel^2 = 0. \tag{9.49}$$

The instability does not appear in the collisionless case as is seen from (9.37) in the framework of MHD theory. However the instability may occur even in the collisionless case when it is analyzed by the kinetic theory (see app.B). This instability is called *collisionless drift instability.*

References

[1] H. P. Furth, J. Killeen and M. N. Rosenbluth: Phys. Fluids **6**, 459 (1963)

[2] H. P. Furth, P. H. Rutherford and H. Selberg: Phys. Fluids **16**, 1054 (1973)
A. Pletzer and R. L. Dewar: J. Plasma Phys. **45**, 427 (1991)

[3] S. S. Moiseev and R. Z. Sagdeev: Sov. Phys. JETP **17**, 515 (1963),
Sov. Phys. Tech. Phys. **9**, 196 (1964)

[4] F. F. Chen: Phys. Fluids **8**, 912 and 1323 (1965)

Ch.10 Plasma as Medium of Electromagnetic Wave Propagation

A plasma is an ensemble of an enormous number of moving ions and electrons interacting with each other. In order to describe the behavior of such an ensemble, the distribution function was introduced in ch.4; and Boltzmann's and Vlasov's equations were derived with respect to the distribution function. A plasma viewed as an ensemble of a large number of particles has a large number of degrees of freedom; thus the mathematical description of plasma behavior is feasible only for simplified analytical models.

In ch.5, statistical averages in velocity space, such as mass density, flow velocity, pressure, etc., were introduced and the magnetohydrodynamic equations for these averages were derived. We have thus obtained a mathematical description of the magnetohydrodynamic fluid model; and we have studied the equilibrium conditions, stability problems, etc., for this model in chs. 6-9. Since the fluid model considers only average quantities in velocity space, it is not capable of describing instabilities or damping phenomena, in which the profile of the distribution function plays a significant role. The phenomena which can be handled by means of the fluid model are of low frequency (less than the ion or electron cyclotron frequency); high-frequency phenomena are not describable in terms of it.

In this chapter, we will focus on a model which allows us to study wave phenomena while retaining the essential features of plasma dynamics, at the same time maintaining relative simplicity in its mathematical form. Such a model is given by a homogeneous plasma of ions and electrons at 0K in a uniform magnetic field. In the unperturbed state, both the ions and electrons of this plasma are motionless. Any small deviation from the unperturbed state induces an electric field and a time-dependent component of the magnetic field, and consequently movements of ions and electrons are excited. The movements of the charged particles induce electric and magnetic fields which are themselves consistent with the previously induced small perturbations. This is called the kinetic model of a *cold plasma*. We will use it in this chapter to derive the dispersion relation which characterizes wave phenomena in the cold plasma.

Although this model assumes uniformity of the magnetic field, and the density and also the zero temperature, this cold plasma model is applicable for an nonuniform, warm plasma, if the typical length of variation of the magnetic field and the density is much larger than the wavelength and the phase velocity of wave is much larger than the thermal velocity of the particles.

It is possible to consider that the plasma as a medium of electromagnetic wave propagation with a dielectric tensor $\boldsymbol{K}$. This dielectric tensor $\boldsymbol{K}$ is a function of the magnetic field and the density which may change with the position. Accordingly plasmas are in general an nonuniform, anisotropic and dispersive medium.

When the temperature of plasma is finite and the thermal velocity of the particles is comparable to the phase velocity of propagating wave, the interaction of the particles and the wave becomes important. A typical interaction is Landau damping, which is explained in ch.11. The general mathematical analysis of the hot-plasma wave will be discussed in ch.12 and appendix C. The references [1]∼[4] describe the plasma wave in more detail.

10.1 Dispersion Equation of Waves in a Cold Plasma

In an unperturbed cold plasma, the particle density n and the magnetic field $\boldsymbol{B}_0$ are both homogeneous in space and constant in time. The ions and electrons are motionless.

Now assume that the first-order perturbation term $\exp i(\boldsymbol{k}\cdot\boldsymbol{r}-\omega t)$ is applied. The ions and electrons are forced to move by the perturbed electric field $\boldsymbol{E}$ and the induced magnetic field $\boldsymbol{B}_1$. Let us denote velocity by $\boldsymbol{v}_k$, where the sufix k indicates the species of particle (electrons, or ions of various kinds). The current $\boldsymbol{j}$ due to the particle motion is given by

$$\boldsymbol{j}=\sum_k n_k q_k \boldsymbol{v}_k. \tag{10.1}$$

n_k and q_k are the density and charge of the kth species, respectively. The electric displacement $\boldsymbol{D}$

is

$$\boldsymbol{D} = \epsilon_0 \boldsymbol{E} + \boldsymbol{P}, \tag{10.2}$$

$$\boldsymbol{j} = \frac{\partial \boldsymbol{P}}{\partial t} = -i\omega \boldsymbol{P} \tag{10.3}$$

where $\boldsymbol{E}$ is the electric intensity, $\boldsymbol{P}$ is the electric polarization, and ϵ_0 is the dielectric constant of vacuum. Consequently $\boldsymbol{D}$ is expressed by

$$\boldsymbol{D} = \epsilon_0 \boldsymbol{E} + \frac{i}{\omega}\boldsymbol{j} \equiv \epsilon_0 \boldsymbol{K} \cdot \boldsymbol{E}. \tag{10.4}$$

$\boldsymbol{K}$ is called *dielectric tensor*. The equation of motion of a single particle of the kth kind is

$$m_k \frac{\mathrm{d}\boldsymbol{v}_k}{\mathrm{d}t} = q_k(\boldsymbol{E} + \boldsymbol{v}_k \times \boldsymbol{B}). \tag{10.5}$$

Here $\boldsymbol{B}$ consists of $\boldsymbol{B} = \boldsymbol{B}_0 + \boldsymbol{B}_1$, where $\boldsymbol{v}_k$, $\boldsymbol{E}$, $\boldsymbol{B}_1$ are the first-order quantities. The linearized equation in these quantities is

$$-i\omega m_k \boldsymbol{v}_k = q_k(\boldsymbol{E} + \boldsymbol{v}_k \times \boldsymbol{B}_0). \tag{10.6}$$

When the z axis is taken along the direction of $\boldsymbol{B}_0$, the solution is given by

$$\left.\begin{aligned} v_{k,x} &= \frac{-iE_x}{B_0}\frac{\Omega_k \omega}{\omega^2 - \Omega_k^2} - \frac{E_y}{B_0}\frac{\Omega_k^2}{\omega^2 - \Omega_k^2}, \\ v_{k,y} &= \frac{E_x}{B_0}\frac{\Omega_k^2}{\omega^2 - \Omega_k^2} - \frac{iE_y}{B_0}\frac{\Omega_k \omega}{\omega^2 - \Omega_k^2}, \\ v_{k,z} &= \frac{-iE_z}{B_0}\frac{\Omega_k}{\omega} \end{aligned}\right\} \tag{10.7}$$

where Ω_k is the cyclotron frequency of the charged particle of the kth kind:

$$\Omega_k = \frac{-q_k B_0}{m_k} \tag{10.8}$$

($\Omega_\mathrm{e} > 0$ for electrons and $\Omega_\mathrm{i} < 0$ for ions). The components of $\boldsymbol{v}_k$ are the linear functions of $\boldsymbol{E}$ given by (10.7); and $\boldsymbol{j}$ of (10.1) and the electric displacement $\boldsymbol{D}$ of (10.4) are also the linear function of $\boldsymbol{E}$, so that the *dielectric tensor* is given by

$$\boldsymbol{K} \cdot \boldsymbol{E} = \begin{bmatrix} K_\perp & -iK_\times & 0 \\ iK_\times & K_\perp & 0 \\ 0 & 0 & K_\parallel \end{bmatrix} \begin{bmatrix} E_x \\ E_y \\ E_z \end{bmatrix} \tag{10.9}$$

where

$$K_\perp \equiv 1 - \sum_k \frac{\Pi_k^2}{\omega^2 - \Omega_k^2}, \tag{10.10}$$

$$K_\times \equiv -\sum_k \frac{\Pi_k^2}{\omega^2 - \Omega_k^2}\frac{\Omega_k}{\omega}, \tag{10.11}$$

$$K_\parallel \equiv 1 - \sum_k \frac{\Pi_k^2}{\omega^2}, \tag{10.12}$$

$$\Pi_k^2 \equiv \frac{n_k q_k^2}{\epsilon_0 m_k}. \tag{10.13}$$

According to the Stix notation, the following quantities are introduced:

$$\left.\begin{aligned} R &\equiv 1-\sum_k \frac{\Pi_k^2}{\omega^2}\frac{\omega}{\omega-\Omega_k} = K_\perp + K_\times, \\ L &\equiv 1-\sum_k \frac{\Pi_k^2}{\omega^2}\frac{\omega}{\omega+\Omega_k} = K_\perp - K_\times. \end{aligned}\right\} \tag{10.14}$$

From Maxwell's equation

$$\nabla \times \boldsymbol{E} = -\frac{\partial \boldsymbol{B}}{\partial t}, \tag{10.15}$$

$$\nabla \times \boldsymbol{H} = \boldsymbol{j} + \epsilon_0 \frac{\partial \boldsymbol{E}}{\partial t} = \frac{\partial \boldsymbol{D}}{\partial t} \tag{10.16}$$

it follows that

$$\boldsymbol{k} \times \boldsymbol{E} = \omega \boldsymbol{B}_1,$$

$$\boldsymbol{k} \times \boldsymbol{H}_1 = -\omega\epsilon_0 \boldsymbol{K} \cdot \boldsymbol{E}$$

and

$$\boldsymbol{k} \times (\boldsymbol{k} \times \boldsymbol{E}) + \frac{\omega^2}{c^2}\boldsymbol{K} \cdot \boldsymbol{E} = 0. \tag{10.17}$$

Let us define a dimensionless vector

$$\boldsymbol{N} \equiv \frac{\boldsymbol{k}c}{\omega}$$

(c is light velocity in vacuum). The absolute value $N = |\boldsymbol{N}|$ is the ratio of the light velocity to the phase velocity of the wave, i.e., N is the refractive index. Using $\boldsymbol{N}$, we may write (10.17) as

$$\boldsymbol{N} \times (\boldsymbol{N} \times \boldsymbol{E}) + \boldsymbol{K} \cdot \boldsymbol{E} = 0. \tag{10.18}$$

If the angle between $\boldsymbol{N}$ and $\boldsymbol{B}_0$ is denoted by θ (fig.10.1) and x axis is taken so that $\boldsymbol{N}$ lies in the z, x plane, then (10.18) may be expressed by

$$\begin{bmatrix} K_\perp - N^2\cos^2\theta & -iK_\times & N^2\sin\theta\cos\theta \\ iK_\times & K_\perp - N^2 & 0 \\ N^2\sin\theta\cos\theta & 0 & K_\parallel - N^2\sin^2\theta \end{bmatrix} \begin{bmatrix} E_x \\ E_y \\ E_z \end{bmatrix} = 0. \tag{10.19}$$

For a nontrivial solution to exist, the determinant of the matrix must be zero, or

$$AN^4 - BN^2 + C = 0 \tag{10.20},$$

$$A = K_\perp \sin^2\theta + K_\parallel \cos^2\theta, \tag{10.21}$$

$$B = (K_\perp^2 - K_\times^2)\sin^2\theta + K_\parallel K_\perp (1+\cos^2\theta), \tag{10.22}$$

$$C = K_\parallel (K_\perp^2 - K_\times^2) = K_\parallel RL. \tag{10.23}$$

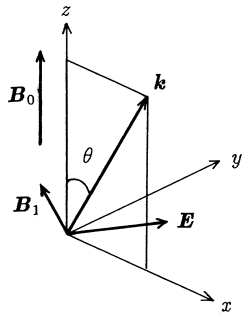

Fig.10.1 Propagation vector $\boldsymbol{k}$ and x, y, z coordinates

Equation (10.20) determines the relationship between the propagation vector $\boldsymbol{k}$ and the frequency ω, and it is called *dispersion equation*. The solution of (10.20) is

$$\begin{aligned} N^2 &= \frac{B \pm (B^2 - 4AC)^{1/2}}{2A} \\ &= ((K_\perp^2 - K_\times^2)\sin^2\theta + K_\parallel K_\perp(1+\cos^2\theta) \\ &\quad \pm[(K_\perp^2 - K_\times^2 - K_\parallel K_\perp)^2 \sin^4\theta + 4K_\parallel^2 K_\times^2 \cos^2\theta]^{1/2}) \\ &\quad \times \Big(2(K_\perp \sin^2\theta + K_\parallel \cos^2\theta)\Big)^{-1}. \end{aligned} \tag{10.24}$$

When the wave propagates along the line of magnetic force ($\theta = 0$), the dispersion equation (10.20) is

$$K_\parallel(N^4 - 2K_\perp N^2 + (K_\perp^2 - K_\times^2)) = 0, \tag{10.25}$$

and the solutions are

$$K_\parallel = 0, \quad N^2 = K_\perp + K_\times = R, \quad N^2 = K_\perp - K_\times = L. \tag{10.26}$$

For the wave propagating in the direction perpendicular to the magnetic field ($\theta = \pi/2$), the dispersion equation and the solutions are given by

$$K_\perp N^4 - (K_\perp^2 - K_\times^2 + K_\parallel K_\perp)N^2 + K_\parallel(K_\perp^2 - K_\times^2) = 0, \tag{10.27}$$

$$N^2 = \frac{K_\perp^2 - K_\times^2}{K_\perp} = \frac{RL}{K_\perp}, \qquad N^2 = K_\parallel. \tag{10.28}$$

10.2 Properties of Waves

10.2a Polarization and Particle Motion

The dispersion relation for waves in a cold plasma was derived in the previous section. We consider here the electric field of the waves and the resultant particle motion. The y component of (10.19) is

$$\begin{aligned} &iK_\times E_x + (K_\perp - N^2)E_y = 0, \\ &\frac{iE_x}{E_y} = \frac{N^2 - K_\perp}{K_\times}. \end{aligned} \tag{10.29}$$

The relation between the components of the particle velocity is

$$\frac{iv_{k,x}}{v_{k,y}} = \frac{i\left(\dfrac{-iE_x}{E_y}\dfrac{\omega}{\omega^2 - \Omega_k^2} - \dfrac{\Omega_k}{\omega^2 - \Omega_k^2}\right)}{\dfrac{E_x}{E_y}\dfrac{\Omega_k}{\omega^2 - \Omega_k^2} - i\dfrac{\omega}{\omega^2 - \Omega_k^2}}$$

$$= \frac{(\omega+\Omega_k)(N^2-L)+(\omega-\Omega_k)(N^2-R)}{(\omega+\Omega_k)(N^2-L)-(\omega-\Omega_k)(N^2-R)}. \tag{10.30}$$

The wave satisfying $N^2 = R$ at $\theta = 0$ has $iE_x/E_y = 1$ and the electric field is right-circularly polarized. In other word, the electric field rotates in the direction of the electron Larmor motion. The motion of ions and electrons is also right-circular motion. In the wave satisfying $N^2 = L$ at $\theta \to 0$, the relation $iE_x/E_y = -1$ holds and the electric field is left-circularly polarized. The motion of ions and electrons is also left-circular motion. The waves with $N^2 = R$ and $N^2 = L$ as $\theta \to 0$, are called the R *wave* and the L *wave*, respectively. The solution of the dispersion equation (10.25) at $\theta = 0$ is

$$N^2 = \frac{1}{2}\left(R + L \pm \frac{|K_\parallel|}{K_\parallel}|R-L|\right) \tag{10.31}$$

so that R and L waves are exchanged when $K_\parallel$ changes sign. When $K_\times = R - L$ changes sign, R and L waves are also exchanged.

When $\theta = \pi/2$, the electric field of the wave satisfying $N^2 = K_\parallel$ is $E_x = E_y = 0$, $E_z \neq 0$. For the wave safisfying $N^2 = RL/K_\perp$, the electric field satisfies the relations $iE_x/E_y = -(R-L)/(R+L) = -K_\times/K_\perp$, $E_z = 0$. The waves with $N^2 = K_\parallel$ and $N^2 = RL/K_\perp$ as $\theta \to \pi/2$ are called the ordinary wave (O) and the extraordinary wave (X), respectively. It should be pointed out that the electric field of the extraordinary wave at $\theta = \pi/2$ is perpendicular to the magnetic field ($E_z = 0$) and the electric field of the ordinary wave at $\theta = \pi/2$ is parallel to the magnetic field ($E_x = E_y = 0$). The dispersion relation (10.24) at $\theta = \pi/2$ is

$$\begin{aligned} N^2 &= \frac{1}{2K_\perp}(K_\perp^2 - K_\times^2 + K_\parallel K_\perp + |K_\perp^2 - K_\times^2 - K_\parallel K_\perp|) \\ &= \frac{1}{2K_\perp}(RL + K_\parallel K_\perp \pm |RL - K_\parallel K_\perp|) \end{aligned} \tag{10.32}$$

so that the ordinary wave and the extraordinary wave are exchanged at $RL - K_\parallel K_\perp = 0$.

Besides the classification into R and L waves, and O and X waves, there is another classification, namely, that of *fast* wave and *slow* wave, following the difference in the phase velocity. Since the term inside the square root of the equation $N^2 = (B \pm (B^2 - 4AC)^{1/2})/2A$ is always positive, as is clear from (10.24), the fast wave and slow wave do not exchange between $\theta = 0$ and $\theta = \pi/2$.

10.2b Cutoff and Resonance

The refractive index (10.24) may become infinity or zero. When $N^2 = 0$, the wave is said to be *cutoff* ; at cutoff the phase velocity

$$v_{\rm ph} = \frac{\omega}{k} = \frac{c}{N} \tag{10.33}$$

becomes infinity. As is clear from (10.20),(10.23), cutoff occurs when

$$K_\parallel = 0 \qquad R = 0 \qquad L = 0. \tag{10.34}$$

When $N^2 = \infty$, the wave is said to be at *resonance*; here the phase velocity becomes zero. The wave will be absorbed by the plasma at resonance (see ch.11). The resonance condition is

$$\tan^2\theta = -\frac{K_\parallel}{K_\perp}. \tag{10.35}$$

When $\theta = 0$, the resonance condition is $K_\perp = (R+L)/2 \to \pm\infty$. The condition $R \to \pm\infty$ is satisfied at $\omega = \Omega_{\rm e}$, $\Omega_{\rm e}$ being the electron cyclotron frequency. This is called *electron cyclotron resonance*. The condition $L \to \pm\infty$ holds when $\omega = |\Omega_{\rm i}|$, and this is called *ion cyclotron resonance*.

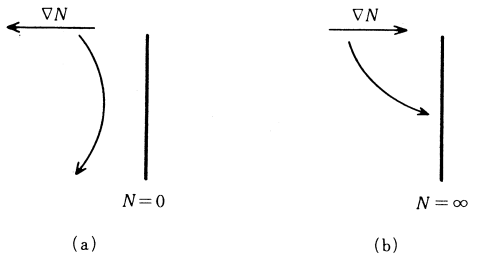

Fig.10.2 Wave propagation (a) near cutoff region and (b) near a resonance region

When $\theta = \pi/2$, $K_\perp = 0$ is the resonance condition. This is called *hybrid resonance*. When waves approach a cutoff region, the wave path is curved according to Snell's refraction law and the waves are reflected (fig.10.2a). When waves approach a resonance region, the waves propagate perpendicularly toward the resonance region. The phase velocities tend to zero and the wave energy will be absorbed.

10.3 Waves in a Two-Components Plasma

Let us consider a plasma which consists of electrons and of one kind of ion. Charge neutrality is

$$n_\mathrm{i} Z_\mathrm{i} = n_\mathrm{e}. \tag{10.36}$$

A dimensionless parameter is introduced for convenience:

$$\gamma = \frac{\mu_0 (n_\mathrm{i} m_\mathrm{i} + n_\mathrm{e} m_\mathrm{e}) c^2}{B_0^2}. \tag{10.37}$$

The quantity defined by (10.13), which was also introduced in sec.2.2,

$$\Pi_\mathrm{e}^2 = n_\mathrm{e} e^2/(\epsilon_0 m_\mathrm{e}) \tag{10.38}$$

is called electron plasma frequency. Then we have the relations

$$\left.\begin{aligned} &\Pi_\mathrm{e}^2/\Pi_\mathrm{i}^2 = m_\mathrm{i}/m_\mathrm{e} \gg 1, \\ &\frac{\Pi_\mathrm{i}^2 + \Pi_\mathrm{e}^2}{|\Omega_\mathrm{i}|\Omega_\mathrm{e}} = \gamma \approx \frac{\Pi_\mathrm{i}^2}{\Omega_\mathrm{i}^2}. \end{aligned}\right\} \tag{10.39}$$

$K_\perp$, $K_\times$, $K_\parallel$, and R, L are given by

$$\left.\begin{aligned} K_\perp &= 1 - \frac{\Pi_\mathrm{i}^2}{\omega^2 - \Omega_\mathrm{i}^2} - \frac{\Pi_\mathrm{e}^2}{\omega^2 - \Omega_\mathrm{e}^2}, \\ K_\times &= -\frac{\Pi_\mathrm{i}^2}{\omega^2 - \Omega_\mathrm{i}^2}\frac{\Omega_\mathrm{i}}{\omega} - \frac{\Pi_\mathrm{e}^2}{\omega^2 - \Omega_\mathrm{e}^2}\frac{\Omega_\mathrm{e}}{\omega}, \\ K_\parallel &= 1 - \frac{\Pi_\mathrm{e}^2 + \Pi_\mathrm{i}^2}{\omega^2} \simeq 1 - \frac{\Pi_\mathrm{e}^2}{\omega^2} \end{aligned}\right\} \tag{10.40}$$

$$R = 1 - \frac{\Pi_\mathrm{e}^2 + \Pi_\mathrm{i}^2}{(\omega - \Omega_\mathrm{i})(\omega - \Omega_\mathrm{e})} \simeq \frac{\omega^2 - (\Omega_\mathrm{i} + \Omega_\mathrm{e})\omega + \Omega_\mathrm{i}\Omega_\mathrm{e} - \Pi_\mathrm{e}^2}{(\omega - \Omega_\mathrm{i})(\omega - \Omega_\mathrm{e})}, \tag{10.41}$$

$$L = 1 - \frac{\Pi_\mathrm{e}^2 + \Pi_\mathrm{i}^2}{(\omega + \Omega_\mathrm{i})(\omega + \Omega_\mathrm{e})} \simeq \frac{\omega^2 + (\Omega_\mathrm{i} + \Omega_\mathrm{e})\omega + \Omega_\mathrm{i}\Omega_\mathrm{e} - \Pi_\mathrm{e}^2}{(\omega + \Omega_\mathrm{i})(\omega + \Omega_\mathrm{e})}. \tag{10.42}$$

The dispersion relations for the waves propagating parallel to $\boldsymbol{B}_0$ ($\theta = 0$) are found by setting

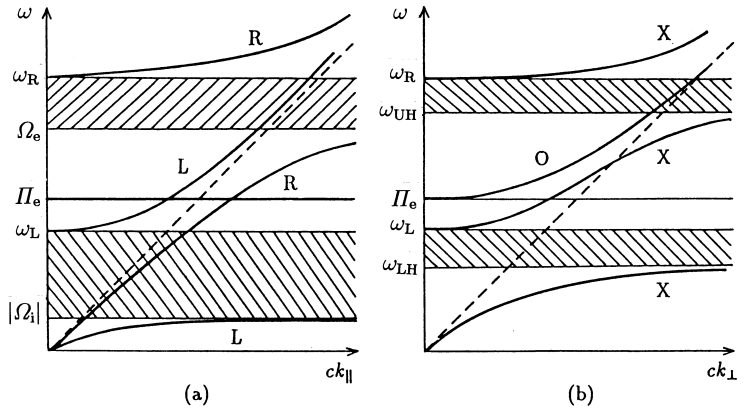

Fig.10.3 (a) Dispersion relations (ω - $ck_\parallel$) for R and L waves propagating parallel to the magnetic field ($\theta = 0$). (b) Dispersion relations (ω - $ck_\parallel$) for O and X waves propagating perpendicular to the magnetic field ($\theta = \pi/2$).

$K_\parallel = 0$, $N^2 = R$, and $N^2 = L$. Then

$$\omega^2 = \Pi_e^2, \tag{10.43}$$

$$\frac{\omega^2}{c^2k_\parallel^2} = \frac{1}{R} = \frac{(\omega-\Omega_i)(\omega-\Omega_e)}{\omega^2-\omega\Omega_e+\Omega_e\Omega_i-\Pi_e^2} = \frac{(\omega+|\Omega_i|)(\omega-\Omega_e)}{(\omega-\omega_R)(\omega+\omega_L)} \tag{10.44}$$

where ω_R, ω_L are given by

$$\omega_R = \frac{\Omega_e}{2} + \left(\left(\frac{\Omega_e}{2}\right)^2 + \Pi_e^2 + |\Omega_e\Omega_i|\right)^{1/2} > 0, \tag{10.45}$$

$$\omega_L = -\frac{\Omega_e}{2} + \left(\left(\frac{\Omega_e}{2}\right)^2 + \Pi_e^2 + |\Omega_e\Omega_i|\right)^{1/2} > 0, \tag{10.46}$$

$$\frac{\omega^2}{c^2k_\parallel^2} = \frac{1}{L} = \frac{(\omega+\Omega_i)(\omega+\Omega_e)}{\omega^2+\omega\Omega_e+\Omega_e\Omega_i-\Pi_e^2} = \frac{(\omega-|\Omega_i|)(\omega+\Omega_e)}{(\omega-\omega_L)(\omega+\omega_R)}. \tag{10.47}$$

Note that $\Omega_e > 0$, $\Omega_i < 0$ and $\omega_R > \Omega_e$. Plots of the dispersion relations $\omega - ck_\parallel$ are shown in fig.10.3a. The dispersion relations for the waves propagating perpendicular to $\boldsymbol{B}_0$ are found by setting $N^2 = K_\parallel$ (ordinary wave) and $N^2 = (K_\perp^2 - K_\times^2)/K_\perp$ (extraordinary wave). Then

$$\frac{\omega^2}{c^2k_\perp^2} = \frac{1}{K_\parallel} = \left(1 - \frac{\Pi_e^2}{\omega^2}\right)^{-1} = 1 + \frac{\Pi_e^2}{c^2k_\perp^2}, \tag{10.48}$$

$$\frac{\omega^2}{c^2k_\perp^2} = \frac{K_\perp}{K_\perp^2-K_\times^2} = \frac{K_\perp}{RL} = \frac{2(\omega^2-\Omega_i^2)(\omega^2-\Omega_e^2)-\Pi_e^2((\omega+\Omega_i)(\omega+\Omega_e)+(\omega-\Omega_i)(\omega-\Omega_e))}{2(\omega^2-\omega_L^2)(\omega^2-\omega_R^2)}$$

$$= \frac{\omega^4-(\Omega_i^2+\Omega_e^2+\Pi_e^2)\omega^2+\Omega_i^2\Omega_e^2-\Pi_e^2\Omega_i\Omega_e}{(\omega^2-\omega_L^2)(\omega^2-\omega_R^2)}. \tag{10.49}$$

Equation (10.48) is the dispersion equation of electron plasma wave (Langmuir wave). Let us define ω_{UH} and ω_{LH} by

$$\omega_{UH}^2 \equiv \Omega_e^2 + \Pi_e^2, \tag{10.50}$$

$$\frac{1}{\omega_{LH}^2} \equiv \frac{1}{\Omega_i^2+\Pi_i^2} + \frac{1}{|\Omega_i|\Omega_e}. \tag{10.51}$$

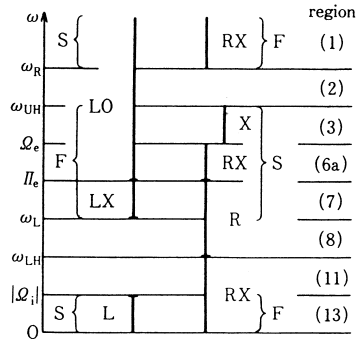

Fig.10.4 The ω regions of R and L waves at $\theta = 0$; O and X waves at $\theta = \pi/2$; F and S waves; in the case ($\omega_{\rm L} < \Pi_{\rm e} < \Omega_{\rm e}$). The numbers on the right identify regions shown in the CMA diagram, fig.10.5.

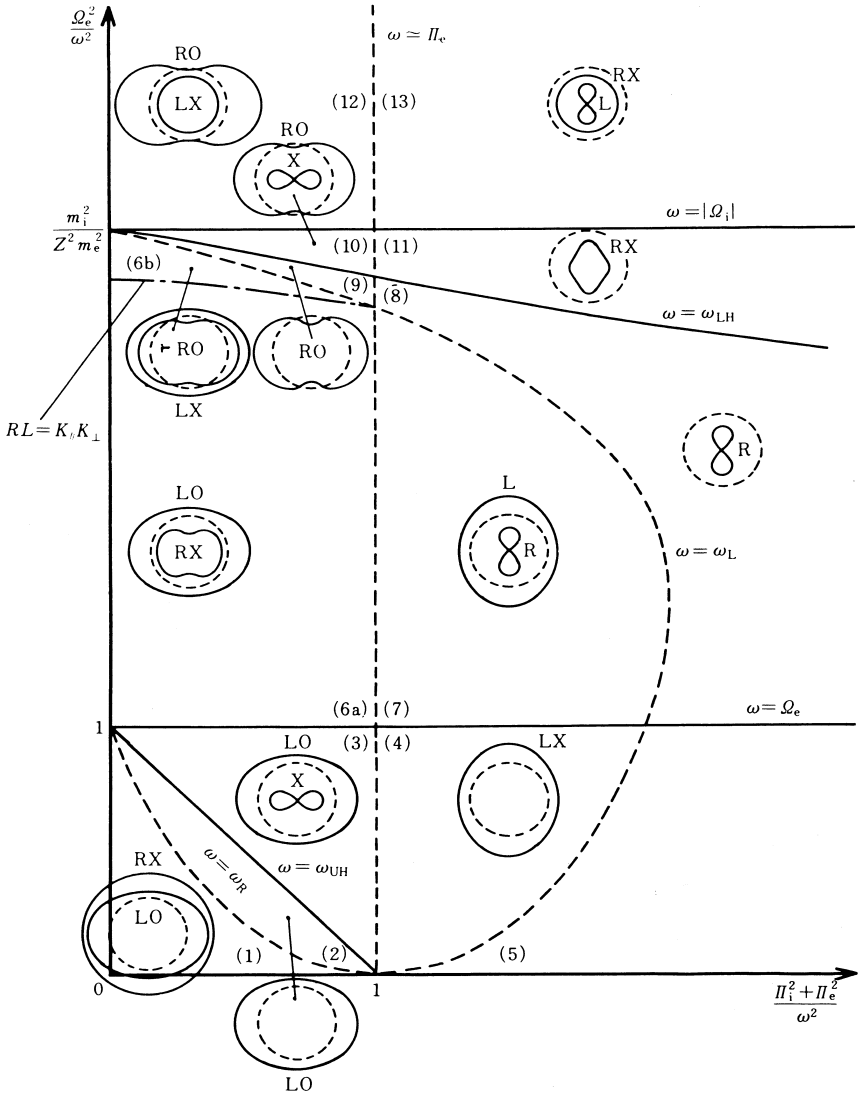

Fig.10.5 CMA diagram of a two-component plasma. The surfaces of constant phase are drawn in each region. The dotted circles give the wave front in vacuum. The magnetic field is directed toward the top of the diagram.

$\omega_{\rm UH}$ is called *upper hybrid resonant frequency* and $\omega_{\rm LH}$ is called *lower hybrid resonant frequency.* Using these, we may write (10.49) as

$$\frac{\omega^2}{c^2k_\perp^2}=\frac{(\omega^2-\omega_{\rm LH}^2)(\omega^2-\omega_{\rm UH}^2)}{(\omega^2-\omega_{\rm L}^2)(\omega^2-\omega_{\rm R}^2)}. \tag{10.52}$$

We have $\omega_{\rm R}>\omega_{\rm UH}>\mathit{\Pi}_{\rm e},\Omega_{\rm e}$ and $\omega_{\rm LH}^2<\Omega_{\rm e}|\Omega_{\rm i}|,\Omega_{\rm i}^2+\mathit{\Pi}^2$. Plots of the dispersion relation ω - $ck_\perp$ are shown in fig.10.3b. The gradient ω/ck in ω - $ck_\perp$ diagram is the ratio of the phase velocity $v_{\rm ph}$ to c. The steeper the gradient, the greater the phase velocity. The regions (in terms of ω) of R and L waves at $\theta=0$, and O and X waves at $\theta=\pi/2$, and F and S waves are shown in fig.10.4, for the case of $\omega_{\rm L}<\mathit{\Pi}_{\rm e}<\Omega_{\rm e}$.

We explain here the CMA diagram (fig.10.5), which was introduced by P. C. Clemmow and R. F. Mullaly and later modified by W. P. Allis (ref.[3]). The quantities $\Omega_{\rm e}^2/\omega^2$ and $(\mathit{\Pi}_{\rm i}^2+\mathit{\Pi}_{\rm e}^2)/\omega^2$ are plotted along the vertical and horizontal ordinates, respectively. The cutoff conditions $R=0\,(\omega=\omega_{\rm R})$, $L=0\,(\omega=\omega_{\rm L})$, $K_\parallel=0\,(\omega=\Omega_{\rm e})$ are shown by the dotted lines and the resonance conditions $R=\infty\,(\omega=\Omega_{\rm e})$, $L=\infty\,(\omega=\Omega_{\rm i})$, $K_\perp=0\,(\omega=\Omega_{\rm LH},\,\omega=\Omega_{\rm UH})$ are shown by solid lines. The cutoff and the resonance contours form the boundaries of the different regions. The boundary $RL=K_\parallel K_\perp$, at which O wave and X wave are exchanged, is also shown by broken and dotted line in fig.10.5. The surfaces of constant phase for R, L and O, X waves are shown for the different regions. As the vertical and horizontal ordinates correspond to the magnitude of B and the density $n_{\rm e}$, one can easily assign waves to the corresponding regions simply by giving their frequencies ω.

10.4 Various Waves

10.4a Alfvén Wave

When the frequency ω is smaller than the ion cyclotron frequency ($\omega\ll|\Omega_{\rm i}|$), the dielectric tensor $\boldsymbol{K}$ is expressed by

$$\left.\begin{aligned}K_\perp&=1+\gamma,\\K_\times&=0,\\K_\parallel&=1-\frac{\mathit{\Pi}_{\rm e}^2}{\omega^2}\end{aligned}\right\} \tag{10.53}$$

where $\gamma=\mu_0 n_{\rm i}m_{\rm i}c^2/B_0^2$. As $\mathit{\Pi}_{\rm e}^2/\omega^2=(m_{\rm i}/m_{\rm e})(\Omega_{\rm i}^2/\omega^2)\gamma$, we find $\mathit{\Pi}_{\rm e}^2/\omega^2\gg\gamma$. Assuming that $\mathit{\Pi}_{\rm e}^2/\omega^2\gg1$, we have $|K_\parallel|\gg|K_\perp|$; then A, B, C of (10.20) are given by

$$\left.\begin{aligned}A&\approx-\frac{\mathit{\Pi}_{\rm e}^2}{\omega^2}\cos^2\theta,\\B&\approx-\frac{\mathit{\Pi}_{\rm e}^2}{\omega^2}(1+\gamma)(1+\cos^2\theta),\\C&\approx-\frac{\mathit{\Pi}_{\rm e}^2}{\omega^2}(1+\gamma)^2\end{aligned}\right\} \tag{10.54}$$

and the dispersion relations are

$$\frac{c^2}{N^2}=\frac{\omega^2}{k^2}=\frac{c^2}{1+\gamma}=\frac{c^2}{1+\dfrac{\mu_0\rho_{\rm m}c^2}{B_0^2}}\simeq\frac{B_0^2}{\mu_0\rho_{\rm m}}, \tag{10.55}$$

$$\frac{c^2}{N^2}=\frac{\omega^2}{k^2}=\frac{c^2}{1+\gamma}\cos^2\theta \tag{10.56}$$

($\rho_{\rm m}$ is the mass density). The wave satisfying this dispersion relation is called the *Alfvén wave.* We define the *Alfvén velocity* by

$$v_{\rm A}^2=\frac{c^2}{1+\gamma}=\frac{c^2}{1+\dfrac{\mu_0\rho_{\rm m}c^2}{B_0^2}}\simeq\frac{B_0^2}{\mu_0\rho_{\rm m}}. \tag{10.57}$$

Equations (10.55) and (10.56) correspond to modes appearing in region (13) of the CMA diagram. Substitution of (10.55) and (10.56) into (10.19) shows that E_z for either mode is $E_z = 0$; $E_x = 0$ for the mode (10.55) (R wave, F wave, X wave) and $E_y = 0$ for mode (10.56) (L wave, S wave). From (10.6), we find for $\omega \ll |\Omega_\mathrm{i}|$ that

$$\boldsymbol{E} + \boldsymbol{v}_\mathrm{i} \times \boldsymbol{B}_0 = 0 \tag{10.58}$$

and $\boldsymbol{v}_\mathrm{i} = (\boldsymbol{E} \times \boldsymbol{B}_0)/\boldsymbol{B}_0^2$, so that $\boldsymbol{v}_\mathrm{i}$ of the mode (10.55) is

$$\boldsymbol{v}_\mathrm{i} \approx \hat{\boldsymbol{x}} \cos(k_x x + k_z z - \omega t) \tag{10.59}$$

and $\boldsymbol{v}_\mathrm{i}$ of the mode (10.56) is

$$\boldsymbol{v}_\mathrm{i} \approx \hat{\boldsymbol{y}} \cos(k_x x + k_z z - \omega t) \tag{10.60}$$

where $\hat{\boldsymbol{x}}$, $\hat{\boldsymbol{y}}$ are unit vectors along x and y axes, respectively. From these last equations, the fast mode (10.55) is called the *compressional mode* and the slow mode (10.56) is called the *torsional or shear mode*. The R wave (10.55) still exists, though it is deformed in the transition from region (13) to regions (11) and (8), but the L wave (10.56) disappears in these transitions.

As is clear from (10.58), the plasma is frozen to the magnetic field. There is tension $B^2/2\mu_0$ along the magnetic-field lines and the pressure $B^2/2\mu_0$ exerted perpendicularly to the magnetic field. As the plasma, of mass density ρ_m, sticks to the field lines, the wave propagation speed in the direction of the field is $B_0^2/(\mu_0\rho_\mathrm{m})$.

10.4b Ion Cyclotron Wave and Fast Wave

Let us consider the case where the frequency ω is shifted from low frequency toward the ion cyclotron frequency and $\Pi_\mathrm{e}^2/\omega^2 \gg 1$. The corresponding waves are located in regions (13) and (11) of the CMA diagram. When $|\omega| \ll \Omega_\mathrm{e}$, $\gamma \gg 1$, and $\Pi_\mathrm{e}^2/\omega^2 \gg 1$, the values of $K_\perp$, $K_\times$ and $K_\parallel$ are

$$K_\perp \approx \frac{-\gamma\Omega_\mathrm{i}^2}{\omega^2 - \Omega_\mathrm{i}^2}, \qquad K_\times \approx \frac{-\gamma\Omega_\mathrm{i}^2}{\omega^2 - \Omega_\mathrm{i}^2}\frac{\Omega}{\omega}, \qquad K_\parallel \approx -\frac{\Pi_\mathrm{e}^2}{\omega^2}. \tag{10.61}$$

$$R = K_\perp + K_\times = \frac{-\gamma\Omega_\mathrm{i}^2}{(\omega - \Omega_\mathrm{i})\omega}, \qquad L = K_\perp - K_\times = \frac{-\gamma\Omega_\mathrm{i}^2}{(\omega + \Omega_\mathrm{i})\omega},$$

Since $\Pi_\mathrm{e}^2/\omega^2 = (m_\mathrm{i}/m_\mathrm{e})(\Omega_\mathrm{i}^2/\omega^2)\gamma \gg \gamma$, the coefficients A, B, C are

$$\left.\begin{aligned} A &\approx -\frac{\Pi_\mathrm{e}^2}{\omega^2}\cos^2\theta, \\ B &\approx \frac{\Pi_\mathrm{e}^2}{\omega^2}\frac{\gamma\Omega_\mathrm{i}^2}{\omega^2 - \Omega_\mathrm{i}^2}(1 + \cos^2\theta) = -\frac{\Pi_\mathrm{e}^2}{\omega^2}K_\perp(1 + \cos^2\theta), \\ C &\approx -\frac{\Pi_\mathrm{e}^2}{\omega^2}\frac{\gamma^2\Omega_\mathrm{i}^2}{\omega^2 - \Omega_\mathrm{i}^2}\left(\frac{\Omega_\mathrm{i}}{\omega}\right)^2 = -\frac{\Pi^2}{\omega^2}RL. \end{aligned}\right\} \tag{10.62}$$

The dispersion equation becomes ($\Pi_\mathrm{i}^2 = \Omega_\mathrm{i}^2\gamma$, $v_\mathrm{A}^2 = c^2/\gamma$, $\Omega_\mathrm{i} < 0$)

$$N^4\cos^2\theta + N^2\frac{\gamma\Omega_\mathrm{i}^2}{\omega_\mathrm{i}^2 - \Omega^2}(1 + \cos^2\theta) + \frac{\gamma^2\Omega_\mathrm{i}^2}{\omega_\mathrm{i}^2 - \Omega^2}\left(\frac{\Omega_\mathrm{i}}{\omega}\right)^2 = 0. \tag{10.63}$$

Setting $N^2\cos^2\theta = N_\parallel^2$, and $N^2\sin^2\theta = N_\perp^2$, we may write (8.63) as

$$N_\parallel^2(N_\parallel^2 + N_\perp^2) - \frac{R+L}{2}(2N_\parallel^2 + N_\perp^2) + RL = 0,$$

$$N_\perp^2 = \frac{(N_\parallel^2 - R)(N_\parallel^2 - L)}{(K_\perp - N_\parallel^2)} \tag{10.64a}$$

$$\frac{k_\perp^2 v_{\rm A}^2}{\omega^2} \approx \frac{\Big((k_\parallel v_{\rm A}/\omega)^2 - \Omega_{\rm i}/(\omega-\Omega_{\rm i})\Big)\Big((k_\parallel v_{\rm A}/\omega)^2 - \Omega_{\rm i}/(\omega-\Omega_{\rm i})\Big)}{-\Omega_{\rm i}/(\omega^2-\Omega_{\rm i}^2) - (k_\parallel v_{\rm A}/\omega)^2} \tag{10.64b}$$

Therefore resonance occurs at $K_\perp - N_\parallel^2 = 0$, that is,

$$\omega^2 = \Omega_{\rm i}^2 \frac{k_\parallel^2 v_{\rm A}^2}{k_\parallel^2 v_{\rm A}^2 + \Omega_{\rm i}^2} \tag{10.65}$$

$$\left(\frac{\omega}{v_{\rm A} k_\parallel}\right)^2 = 1 - \left(\frac{\omega}{\Omega_{\rm i}}\right)^2.$$

The dispersion equation (10.63) approaches

$$N^2 \approx \frac{\gamma}{1+\cos^2\theta}, \tag{10.66}$$

$$N^2 \cos^2\theta \approx \gamma(1+\cos^2\theta)\frac{\Omega_{\rm i}^2}{\Omega_{\rm i}^2 - \omega^2} \tag{10.67}$$

as $|\omega|$ approaches $|\Omega_{\rm i}|$. The mode (10.66) corresponds to the Alfvén compressional mode (fast wave) and is not affected by the ion cyclotron resonance. The dispersion relation (10.67) is that of the *ion cyclotron wave*, and can be expressed by

$$\omega^2 = \Omega_{\rm i}^2 \left(1 + \frac{\Pi_{\rm i}^2}{k_\parallel^2 c^2} + \frac{\Pi_{\rm i}^2}{k_\parallel^2 c^2 + k_\perp^2 c^2}\right)^{-1}. \tag{10.68}$$

Note that here ω^2 is always less than $\Omega_{\rm i}^2$. The ions move in a left circular motion (i.e., in the direction of the ion Larmor motion) at $\omega \simeq |\Omega_{\rm i}|$ (refer to (10.30)).

The mode (10.66) satisfies $iE_x/E_y = 1$, i.e., it is circularly polarized, with the electric field rotating opposite to the ion Larmor motion.

The ion cyclotron wave satisfies

$$\frac{iE_x}{E_y} \approx -\frac{\omega}{|\Omega_{\rm i}|}\frac{1}{\left(1+\dfrac{k_\perp^2}{k_\parallel^2}\right)}, \tag{10.69}$$

i.e., the electric field is elliptically polarized, rotating in the same direction as the ion Larmor motion.

10.4c Lower Hybrid Resonance

The frequency at lower hybrid resonance at $\theta = \pi/2$ is given by

$$\omega^2 = \omega_{\rm LH}^2,$$

$$\frac{1}{\omega_{\rm LH}^2} = \frac{1}{\Omega_{\rm i}^2 + \Pi_{\rm i}^2} + \frac{1}{|\Omega_{\rm i}|\Omega_{\rm e}}, \qquad \frac{\omega_{\rm LH}^2}{|\Omega_{\rm i}|\Omega_{\rm e}} = \frac{\Pi_{\rm i}^2 + \Omega_{\rm i}^2}{\Pi_{\rm i}^2 + |\Omega_{\rm i}|\Omega_{\rm e} + \Omega_{\rm i}^2}. \tag{10.70}$$

When the density is high and $\Pi_{\rm i}^2 \gg |\Omega_{\rm i}|\Omega_{\rm e}$, it follows that $\omega_{\rm LH} = (|\Omega_{\rm i}|\Omega_{\rm e})^{1/2}$. When $\Pi_{\rm i}^2 \ll |\Omega_{\rm i}|\Omega_{\rm e}$, then $\omega_{\rm LH}^2 = \Pi_{\rm i}^2 + \Omega_{\rm i}^2$. At lower hybrid resonance, we have $E_y = E_z = 0$ and $E_x \neq 0$.

When the density is high (that is $\Pi_{\rm i}^2 > |\Omega_{\rm i}|\Omega_{\rm e}$), then $|\Omega_{\rm i}| \ll \omega_{\rm LH} \ll \Omega_{\rm e}$ and the analysis of the motions of ions and electrons becomes simple. From (10.7), the velocity is given by

$$v_{k,x} = \frac{i\epsilon_k E_x}{B_0}\frac{\omega|\Omega_k|}{\omega^2 - \Omega_k^2} \tag{10.71}$$

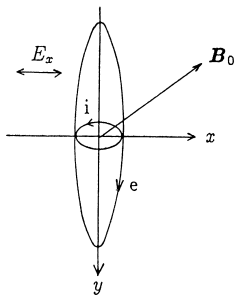

Fig.10.6 Orbits of ions and electrons at lower hybrid resonance.

and $v_{k,x} = \mathrm{d}x_k/\mathrm{d}t = -i\omega x_k$ yields

$$x_k = \frac{-\epsilon_k E_x}{B_0} \frac{|\Omega_k|}{\omega^2 - \Omega_k^2}. \tag{10.72}$$

At $\omega^2 = |\Omega_\mathrm{i}|\Omega_\mathrm{e}$, we find that $x_\mathrm{i} \approx -E_x/B_0\Omega_\mathrm{e}$ and $x_\mathrm{e} \simeq -E_x/B_0\Omega_\mathrm{e}$, or $x_\mathrm{i} \approx x_\mathrm{e}$ (see fig.10.6). Consequently, charge separation does not occur and the lower hybrid wave can exist.

We have been discussing lower hybrid resonance at $\theta = \pi/2$. Let us consider the case in which θ is slightly different from $\theta = \pi/2$. The resonance condition is obtained from (10.24) as follows:

$$K_\perp \sin^2\theta + K_\parallel \cos^2\theta = 0. \tag{10.73}$$

Using (10.46),(10.50) and (10.51), (10.73) is reduced to

$$\frac{(\omega^2 - \omega_\mathrm{LH}^2)(\omega^2 - \omega_\mathrm{UH}^2)}{(\omega^2 - \Omega_\mathrm{i}^2)(\omega^2 - \Omega_\mathrm{e}^2)} \sin^2\theta + \left(1 - \frac{\Pi_\mathrm{e}^2}{\omega^2}\right) \cos^2\theta = 0. \tag{10.74}$$

When θ is near $\pi/2$ and ω is not much different from ω_LH, we find that

$$\begin{aligned} \omega^2 - \omega_\mathrm{LH}^2 &= \frac{(\omega_\mathrm{LH}^2 - \Omega_\mathrm{e}^2)(\omega_\mathrm{LH}^2 - \Omega_\mathrm{i}^2)}{\omega_\mathrm{LH}^2 - \omega_\mathrm{UH}^2} \frac{\Pi_\mathrm{e}^2 - \omega_\mathrm{LH}^2}{\omega_\mathrm{LH}^2} \cos^2\theta \\ &\approx \frac{\Omega_\mathrm{e}^2 \Pi_\mathrm{e}^2}{\omega_\mathrm{UH}^2} \left(1 - \left(\frac{\Omega_\mathrm{i}}{\omega_\mathrm{LH}}\right)^2\right) \left(1 - \left(\frac{\omega_\mathrm{LH}}{\Pi_\mathrm{e}}\right)^2\right) \cos^2\theta. \end{aligned}$$

As $\omega_\mathrm{UH}^2\omega_\mathrm{LH}^2 = \Omega_\mathrm{i}^2\Omega_\mathrm{e}^2 + \Pi_\mathrm{e}^2|\Omega_\mathrm{i}|\Omega_\mathrm{e}$, ω^2 is expressed by

$$\omega^2 = \omega_\mathrm{LH}^2 \left[1 + \frac{m_\mathrm{i}}{Zm_\mathrm{e}} \cos^2\theta \frac{\left(1 - \left(\frac{\Omega_\mathrm{i}}{\omega_\mathrm{LH}}\right)^2\right) \left(1 - \left(\frac{\omega_\mathrm{LH}}{\Pi_\mathrm{e}}\right)^2\right)}{\left(1 + \frac{|\Omega_\mathrm{i}|\Omega_\mathrm{e}}{\Pi_\mathrm{e}^2}\right)}\right]. \tag{10.75}$$

When $\Pi_\mathrm{e}^2/|\Omega_\mathrm{i}|\Omega_\mathrm{e} \approx \gamma = c^2/v_\mathrm{A}^2 \gg 1$, (10.75) becomes

$$\omega^2 = \omega_\mathrm{LH}^2 \left(1 + \frac{m_\mathrm{i}}{Zm_\mathrm{e}} \cos^2\theta\right). \tag{10.76}$$

Even if θ is different from $\pi/2$ only slight amount $(Zm_\mathrm{e}/m_\mathrm{i})^{1/2}$, ω^2 becomes $\omega^2 \approx 2\omega_\mathrm{LH}^2$, so that (10.76) holds only in the region very near $\theta = \pi/2$.

10.4d Upper Hybrid Resonance

The upper hybrid resonant frequency ω_UH is given by

$$\omega_\mathrm{UH}^2 = \Pi_\mathrm{e}^2 + \Omega_\mathrm{e}^2. \tag{10.77}$$

Since this frequency is much larger than $|\Omega_\mathrm{i}|$, ion motion can be neglected.

10.4e Electron Cyclotron Wave (Whistler Wave)

Let us consider high-frequency waves, so that ion motion can be neglected. When $\omega \gg |\Omega_\mathrm{i}|$, we find

$$\left.\begin{aligned} K_\perp &\approx 1 - \frac{\Pi_\mathrm{e}^2}{\omega^2 - \Omega_\mathrm{e}^2}, \\ K_\times &\approx -\frac{\Pi_\mathrm{e}^2}{\omega^2 - \Omega_\mathrm{e}^2}\frac{\Omega_\mathrm{e}}{\omega}, \\ K_\parallel &= 1 - \frac{\Pi_\mathrm{e}^2}{\omega^2}. \end{aligned}\right\} \tag{10.78}$$

The solution of dispersion equation $AN^4 - BN^2 + C = 0$

$$N^2 = \frac{B \pm (B^2 - 4AC)^{1/2}}{2A}$$

may be modified to

$$\begin{aligned} N^2 - 1 &= \frac{-2(A - B + C)}{2A - B \pm (B^2 - 4AC)^{1/2}} \\ &= \frac{-2\Pi_\mathrm{e}^2(1 - \Pi_\mathrm{e}^2/\omega^2)}{2\omega^2(1 - \Pi_\mathrm{e}^2/\omega^2) - \Omega_\mathrm{e}^2 \sin^2\theta \pm \Omega_\mathrm{e}\Delta}, \end{aligned} \tag{10.79}$$

$$\Delta = \left(\Omega_\mathrm{e}^2 \sin^4\theta + 4\omega^2\left(1 - \frac{\Pi_\mathrm{e}^2}{\omega^2}\right)^2 \cos^2\theta\right)^{1/2}. \tag{10.80}$$

The ordinary wave and extraordinary wave will be obtained by taking the plus and minus sign, respectively, in (10.79). In the case of

$$\Omega_\mathrm{e}^2 \sin^4\theta \gg 4\omega^2\left(1 - \frac{\Pi_\mathrm{e}^2}{\omega^2}\right)^2 \cos^2\theta \tag{10.81}$$

we find

$$N^2 = \frac{1 - \Pi_\mathrm{e}^2/\omega^2}{1 - (\Pi_\mathrm{e}^2/\omega^2)\cos^2\theta}, \tag{10.82}$$

$$N^2 = \frac{(1 - \Pi_\mathrm{e}^2/\omega^2)^2\omega^2 - \Omega_\mathrm{e}^2 \sin^2\theta}{(1 - \Pi_\mathrm{e}^2/\omega^2)\omega^2 - \Omega_\mathrm{e}^2 \sin^2\theta}. \tag{10.83}$$

Equation (10.82) becomes $N^2 = K_\parallel = 1 - \Pi_\mathrm{e}^2/\omega^2$ at $\theta \sim \pi/2$ and does not depend on the magnitude of the magnetic field. This wave is used for density measurements by microwave interferometry. In the case of

$$\Omega_\mathrm{e}^2 \sin^4\theta \ll 4\omega^2\left(1 - \frac{\Pi_\mathrm{e}^2}{\omega^2}\right)^2 \cos^2\theta \tag{10.84}$$

with the additional condition

$$\Omega_\mathrm{e}^2 \sin^2\theta \ll \left| 2\omega^2\left(1 - \frac{\Pi_\mathrm{e}^2}{\omega^2}\right) \right| \tag{10.85}$$

the dispersion relations become

$$N^2 = 1 - \frac{\Pi_e^2}{(\omega + \Omega_e \cos\theta)\omega}, \tag{10.86}$$

$$N^2 = 1 - \frac{\Pi_e^2}{(\omega - \Omega_e \cos\theta)\omega}. \tag{10.87}$$

Equation (10.86) corresponds to the L wave, and (10.87) to the R wave. R-wave resonance occurs near the electron cyclotron frequency. This wave can propagate in regions (7) and (8) of the CMA diagram, where the frequency is less than the plasma frequency. This wave is called the *electron cyclotron wave*. It must be noticed that the assumptions (10.84) and (10.85) are not satisfied near $K_\parallel = 1 - \Pi_e^2/\omega^2 \simeq 0$.

The electron cyclotron wave is also called the *whistler wave*. Electromagnetic disturbances initiated by lighting flashes propagate through the ionosphere along magnetic-field lines. The frequency of a lightning-induced whistler wave falls in the audio region, and its group velocity increases with frequency; so that this wave is perceived as a whistle of descending tone. This is why it is called the whistler wave.

10.5 Conditions for Electrostatic Waves

When the electric field $\boldsymbol{E}$ can be expressed by an electrostatic potential

$$\boldsymbol{E} = -\nabla\phi = -i\boldsymbol{k}\phi \tag{10.88}$$

the resultant wave is called an *electrostatic wave*. The electric field $\boldsymbol{E}$ is always parallel to the propagation vector $\boldsymbol{k}$, so that the electrostatic wave is longitudinal. The magnetic field $\boldsymbol{B}_1$ of the electrostatic wave is always zero:

$$\boldsymbol{B}_1 = \boldsymbol{k} \times \boldsymbol{E}/\omega = 0. \tag{10.89}$$

Alfv́en waves are not electrostatic waves. We will here discuss the conditions for electrostatic waves. Since the dispersion relation is

$$\boldsymbol{N} \times (\boldsymbol{N} \times \boldsymbol{E}) + \boldsymbol{K} \cdot \boldsymbol{E} = 0$$

the scalar product with $\boldsymbol{N}$ becomes

$$\boldsymbol{N} \cdot \boldsymbol{K} \cdot (\boldsymbol{E}_\parallel + \boldsymbol{E}_\perp) = 0.$$

where $\boldsymbol{E}_\parallel$ and $\boldsymbol{E}_\perp$ are the components of the electric field parallel and perpendicular to $\boldsymbol{k}$. If $|\boldsymbol{E}_\parallel| \gg |\boldsymbol{E}_\perp|$, the wave is electrostatic and the dispersion relation becomes

$$\boldsymbol{N} \cdot \boldsymbol{K} \cdot \boldsymbol{N} = 0. \tag{10.90}$$

Rewriting the dispersion relation as

$$(N^2 - \boldsymbol{K}) \cdot \boldsymbol{E}_\perp = \boldsymbol{K} \cdot \boldsymbol{E}_\parallel$$

shows that $|\boldsymbol{E}_\parallel| \gg |\boldsymbol{E}_\perp|$ holds when

$$|N^2| \gg |K_{ij}| \tag{10.91}$$

is satisfied for all K_{ij}. The dispersion relation (10.90) for the electrostatic wave is then

$$k_x^2 K_{xx} + 2k_x k_z K_{xz} + k_z^2 K_{zz} = 0. \tag{10.92}$$

The condition (10.91) for the electrostatic wave indicates that the phase velocity $\omega/k = c/N$ of this wave is low. The K_{ij} have already been given by (10.9-10.12) for cold plasmas, and the general

formula for hot plasma will be discussed in chs.12-13. We have stated that magnetic field $\boldsymbol{B}_1$ of the electrostatic wave is zero. Disturbances of the magnetic field propagate with the Alfvén velocity $v_{\rm A} \simeq B_0^2/(\mu_0 n_{\rm i} m_{\rm i})$. If the phase velocity of the wave is much lower than $v_{\rm A}$, the disturbance of the magnetic field will be damped within a few cycles of the wave and the propagated magnetic-field disturbance becomes zero. When the electron thermal velocity $v_{\rm Te}$ is taken as a typical phase velocity for electrostatic waves, then the condition of $v_{\rm A} > v_{\rm Te}$ reduced to

$$\frac{B_0^2}{\mu_0 n_{\rm i} m_{\rm i} v_{\rm Te}^2} = \frac{2m_{\rm e}}{\beta_{\rm e} m_{\rm i}} > 1,$$

$$\beta_{\rm e} < \frac{2m_{\rm e}}{m_{\rm i}}.$$

This is a condition that a wave is electrostatic.

At resonance the refractive index N becomes infinite. As the K_{ij} are finite for lower hybrid and upper hybrid resonance, the condition (10.91) is satisfied so that these hybrid waves are electrostatic. Since some of the K_{ij} become infinite for the ion or electron cyclotron waves, these cyclotron waves are not always electrostatic.

References

[1] T. H. Stix: *The Theory of Plasma Waves*, McGraw-Hill, New York 1962.

[2] T. H. Stix: *Waves in Plasmas*, American Institute of Physics, New York, 1992.

[3] W. P. Allis, S. J. Buchsbanm and A. Bers: *Waves in AnisotropicPlasmas*, The MIT Press, Cambrige Mass. 1963.

[4] G. Bekefi: *Radiation Processes in Plasmas*, John Willey and Son Inc. Gordon and Breach Science Publishers Inc. New York, 1961.

Ch.11 Landau Damping and Cyclotron Damping

The existence of a damping mechanism by which plasma particles absorb wave energy even in a collisionless plasma was found by L.D.Landau, under the condition that the plasma is not cold and the velocity distribution is of finite extent. Energy-exchange processes between particles and wave are possible even in a collisionless plasma and play important roles in plasma heating by waves (wave absorption) and in the mechanism of instabilities (wave amplification). These important processes will be explained in terms of simplified physical models in this chapter. In succeeding chs.12, 13, and app.C, these processes will be described systematically. In hot plasma models, pressure term and particle-wave interaction term appear in the dielectric tensor that are absent in the dielectric tensor for a cold plasma.

11.1 Landau Damping (Amplification)

Let us assume that many particles drift with different velocities in the direction of the lines of magnetic force. When an electrostatic wave (a longitudinal wave with $\boldsymbol{k} \parallel \boldsymbol{E}$) propagates along the lines of magnetic force, there appears an interaction between the wave and a group of particles (see fig.11.1). Take the z axis in the direction of the magnetic field and denote the unit vector in this direction by $\hat{\boldsymbol{z}}$. Then the electric field and the velocity $\boldsymbol{v} = v\hat{\boldsymbol{z}}$ satisfy

$$\boldsymbol{E} = \hat{\boldsymbol{z}} E \cos(kz - \omega t), \tag{11.1}$$

$$m\frac{\mathrm{d}v}{\mathrm{d}t} = qE\cos(kz - \omega t). \tag{11.2}$$

The electric field $\boldsymbol{E}$ is a quantity of the 1st order. The zeroth-order solution of (11.2) is

$$z = v_0 t + z_0$$

and the 1st-order equation is

$$m\frac{\mathrm{d}v_1}{\mathrm{d}t} = qE\cos(kz_0 + kv_0 t - \omega t). \tag{11.3}$$

The solution of (11.3) for the initial condition $v_1 = 0$ at $t = 0$ is

$$v_1 = \frac{qE}{m}\frac{\sin(kz_0 + kv_0 t - \omega t) - \sin kz_0}{kv_0 - \omega}. \tag{11.4}$$

The kinetic energy of the particle becomes

$$\frac{\mathrm{d}}{\mathrm{d}t}\frac{mv^2}{2} = v\frac{\mathrm{d}}{\mathrm{d}t}mv = v_1\frac{\mathrm{d}}{\mathrm{d}t}mv_1 + v_0\frac{\mathrm{d}}{\mathrm{d}t}mv_2 + \cdots. \tag{11.5}$$

From (11.2),(11.4), we have the relation

$$\begin{aligned} m\frac{\mathrm{d}(v_1 + v_2)}{\mathrm{d}t} &= qE\cos(k(z_0 + v_0 t + z_1) - \omega t) \\ &= qE\cos(kz_0 + \alpha t) - qE\sin(kz_0 + \alpha t)kz_1, \end{aligned}$$

$$z_1 = \int_0^t v_1\,\mathrm{d}t = \frac{qE}{m}\left(\frac{-\cos(kz_0 + \alpha t) + \cos kz_0}{\alpha^2} - \frac{t\sin kz_0}{\alpha}\right)$$

where

$$\alpha \equiv kv_0 - \omega.$$

Using these, we may put (11.5) into the form

$$\frac{\mathrm{d}}{\mathrm{d}t}\frac{mv^2}{2} = \frac{q^2E^2}{m}\left(\frac{\sin(kz_0 + \alpha t) - \sin kz_0}{\alpha}\right)\cos(kz_0 + \alpha t)$$

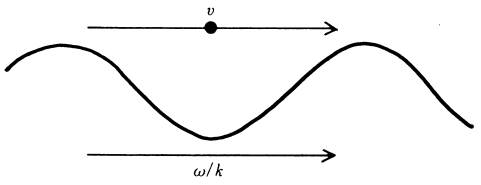

Fig.11.1 Propagation of wave and motion of particles in the process of Landau Damping.

$$-\frac{kv_0q^2E^2}{m}\left(\frac{-\cos(kz_0+\alpha t)+\cos kz_0}{\alpha^2}-\frac{t\sin kz_0}{\alpha}\right)\sin(kz_0+\alpha t).$$

The average of the foregoing quantitiy with respect to the initial position z_0 is

$$\left\langle \frac{\mathrm{d}}{\mathrm{d}t}\frac{mv^2}{2}\right\rangle_{z_0}=\frac{q^2E^2}{2m}\left(\frac{-\omega\sin\alpha t}{\alpha^2}+t\cos\alpha t+\frac{\omega t\cos\alpha t}{\alpha}\right). \tag{11.6}$$

When we take the velocity average of (11.6) over v_0 with the weighting factor i.e. distribution function $f(v_0)$ ($\alpha\equiv kv_0-\omega$)

$$f(v_0)=f\left(\frac{\alpha+\omega}{k}\right)=g(\alpha)$$

the rate of increase of the kinetic energy of the particles is obtained. The distribution function is normalized:

$$\int_{-\infty}^{\infty}f(v_0)\,\mathrm{d}v_0=\frac{1}{k}\int g(\alpha)\,\mathrm{d}\alpha=1.$$

The integral of the 2nd term of (11.6)

$$\frac{1}{k}\int g(\alpha)t\cos\alpha t\,\mathrm{d}\alpha=\frac{1}{k}\int g\left(\frac{x}{t}\right)\cos x\,\mathrm{d}x \tag{11.7}$$

approaches zero as $t\to\infty$. The integral of the 3rd term of (11.6) becomes

$$\frac{\omega}{k}\int\frac{g(\alpha)t\cos\alpha t}{\alpha}\,\mathrm{d}\alpha=\frac{\omega}{k}\int\frac{t}{x}g\left(\frac{x}{t}\right)\cos x\,\mathrm{d}x. \tag{11.8}$$

The function $g(\alpha)$ can be considered to be the sum of an even and an odd function. The even function does not contribute to the integral. The contribution of the odd function approaches zero when $t\to\infty$ if $g(\alpha)$ is continuous at $\alpha=0$. Therefore, only the contribution of the 1st term in (11.6) remains and we find

$$\left\langle \frac{\mathrm{d}}{\mathrm{d}t}\frac{mv^2}{2}\right\rangle_{z_0,v_0}=-\frac{\omega q^2E^2}{2mk}\mathrm{P}\int\frac{g(\alpha)\sin\alpha t}{\alpha^2}\,\mathrm{d}\alpha. \tag{11.9}$$

P denotes Cauchy's principal value of integral. The main contribution to the integral comes from near $\alpha=0$, so that $g(\alpha)$ may be expanded around $\alpha=0$:

$$g(\alpha)=g(0)+\alpha g'(0)+\frac{\alpha^2}{2}g''(0)+\cdots.$$

As $\sin\alpha t/\alpha^2$ is an odd function, only the 2nd term of the foregoing equation contributes to the integral and we find for large t that

$$\left\langle \frac{\mathrm{d}}{\mathrm{d}t}\frac{mv^2}{2}\right\rangle_{z_0,v_0}=-\frac{\omega q^2E^2}{2m|k|}\int_{-\infty}^{\infty}\frac{g'(0)\sin\alpha t}{\alpha}\,\mathrm{d}\alpha$$

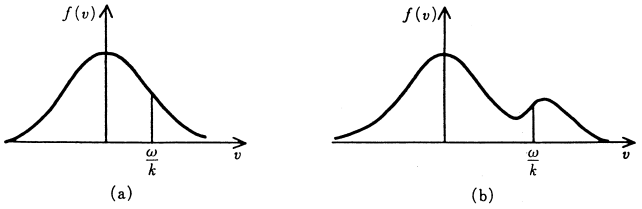

Fig.11.2 (a) Landau damping and (b) Landau amplification.

$$= \frac{-\pi q^2 E^2}{2m|k|}\left(\frac{\omega}{k}\right)\left(\frac{\partial f(v_0)}{\partial v_0}\right)_{v_0=\omega/k}. \tag{11.10}$$

If the number of particles slightly slower than the phase velocity of the wave is larger than the number slightly faster, i.e., if $v_0 \partial f_0/\partial v_0 < 0$, the group of particles as a whole gains energy from the wave and the wave is damped. On the contrary, when $v_0 \partial f_0/\partial v_0 > 0$ at $v_0 = \omega/k$, the particles gives their energy to the wave and the amplitude of the wave increases (fig.11.2). This mechanism is called *Landau damping* (ref.[1]) or *amplification*. Experimental verification of Landau damping of waves in a collisionless plasma was demonstrated by J.M.Malemberg and C.B.Wharton (ref.[2]) in 1965, twenty years after Landau's prediction.

The growth rate (11.10) of the kinetic energy of particles must be equal to the damping rate of wave energy. Therefore the growth rate γ of the amplitude of wave field is obtained by ($\gamma < 0$ in the case of damping)

$$n\left\langle \frac{\mathrm{d}}{\mathrm{d}t}\frac{mv^2}{2}\right\rangle_{z_0 v_0} = -2\gamma W$$

and the growth rate γ is given by

$$\frac{\gamma}{\omega} = \frac{\pi}{2}\left(\frac{\Pi}{\omega}\right)^2\left(\frac{\omega}{|k|}\right)\left(v_0\frac{\partial f(v_0)}{\partial v_0}\right)_{v_0=\omega/k} \tag{11.11}$$

where $\Pi^2 = nq^2/\epsilon_0 m,\ W \approx 2\epsilon_0 E^2/4,\ \int f(v)\mathrm{d}v = 1.$

There is a restriction on the applicability of linear Landau damping. When this phenomenon runs its course before the particle orbit deviates from the linear-approximation solution, the reductions leading to linear Landau damping are justified. The period of oscillation in the potential well of the electric field of the wave gives the time for the particle orbit to deviate from the linear approximation ($\omega^2 \sim eEk/m$ from $m\omega^2 x = eE$). The period of oscillation is

$$\tau_{\mathrm{osc}} = \frac{1}{\omega_{\mathrm{osc}}} \approx \left(\frac{m}{ekE}\right)^{1/2}.$$

Consequently the condition for the applicability of linear Landau damping is that the Landau damping time $1/\gamma$ is shorter than τ_{osc} or the collision time $1/\nu_{\mathrm{coll}}$ is shorter than τ_{osc}.

$$|\gamma\tau_{\mathrm{osc}}| > 1, \tag{11.12}$$

$$|\nu_{\mathrm{coll}}\tau_{\mathrm{osc}}| > 1. \tag{11.13}$$

On the other hand, it was assumed that particles are collisionless. The condition that the collision time $1/\nu_{\mathrm{coll}}$ is longer than λ/v_{rms} is necessary for the asymptotic approximation of the integral (11.9) as $t \to \infty$, where λ is the wavelength of the wave and v_{rms} is the spread in the velocity distribution;

$$\frac{1}{\nu_{\mathrm{coll}}} > \frac{2\pi}{kv_{\mathrm{rms}}}. \tag{11.14}$$

11.2 Transit-Time Damping

We have already described the properties of Alfvén waves in cold plasmas. There are compressional and torsional modes. The compressional mode becomes magnetosonic in hot plasmas, as is described in ch.5. In the low-frequency region, the magnetic moment $\mu_{\rm m}$ is conserved and the equation of motion along the field lines is

$$m\frac{{\rm d}v_z}{{\rm d}t} = -\mu_{\rm m}\frac{\partial B_{1z}}{\partial z}. \tag{11.15}$$

This equation is the same as that for Landau damping if $-\mu_{\rm m}$ and $\partial B_{1z}/\partial z$ are replaced by the electric charge and the electric field, respectively. The rate of change of the kinetic energy is derived similarly, and is

$$\left\langle \frac{\rm d}{{\rm d}t}\frac{mv^2}{2} \right\rangle_{z_0,v_0} = -\frac{\pi\mu_{\rm m}^2|k|}{2m}|B_{1z}|^2\left(\frac{\omega}{k}\right)\left(\frac{\partial f(v_0)}{\partial v_0}\right)_{v_0=\omega/k}. \tag{11.16}$$

This phenomena is called *transit-time damping*.

11.3 Cyclotron Damping

The mechanism of cyclotron damping is different from that of Landau damping. Here the electric field of the wave is perpendicular to the direction of the magnetic field and the particle drift and accelerates the particle perpendicularly to the drift direction. Let us consider a simple case in which the thermal energy of particles perpendicular to the magnetic field is zero and the velocity of particles parallel to the magnetic field $\boldsymbol{B}_0 = B_0\hat{\boldsymbol{z}}$ is V. The equation of motion is

$$m\frac{\partial \boldsymbol{v}}{\partial t} + mV\frac{\partial \boldsymbol{v}}{\partial z} = q(\boldsymbol{E}_1 + \boldsymbol{v}\times\hat{\boldsymbol{z}}B_0 + V\hat{\boldsymbol{z}}\times\boldsymbol{B}_1). \tag{11.17}$$

As our interest is in the perpendicular acceleration we assume $(\boldsymbol{E}_1\cdot\hat{\boldsymbol{z}}) = 0$. $\boldsymbol{B}_1$ is given by $\boldsymbol{B}_1 = (\boldsymbol{k}\times\boldsymbol{E})/\omega$. With the definitions $v^\pm = v_x \pm iv_y$, $E^\pm = E_x \pm iE_y$, the solution for the initial condition $\boldsymbol{v} = 0$ at $t = 0$ is

$$v^\pm = \frac{iqE^\pm(\omega - kV)\exp(ikz - i\omega t)}{m\omega}\frac{1-\exp(i\omega t - ikVt \pm i\Omega t)}{\omega - kV \pm \Omega}, \tag{11.18}$$

$$\Omega = \frac{-qB_0}{m}.$$

The macroscopic value of $\boldsymbol{v}_\perp$ is obtained by taking the average weighted by the distribution function $f_0(V)$ as follows:

$$\langle \boldsymbol{v}_\perp\rangle = \frac{iq\exp(ikz - i\omega t)}{2m}((c^+ + c^-)\boldsymbol{E}_\perp + i(c^+ - c^-)\boldsymbol{E}_\perp\times\hat{\boldsymbol{z}}), \tag{11.19}$$

$$c^\pm = \alpha^\pm - i\beta^\pm, \tag{11.20}$$

$$\alpha^\pm = \int_{-\infty}^{\infty}{\rm d}V\,\frac{f_0(V)(1-kV/\omega)(1-\cos(\omega - kV \pm \Omega)t)}{\omega - kV \pm \Omega}, \tag{11.21}$$

$$\beta^\pm = \int_{-\infty}^{\infty}{\rm d}V\,\frac{f_0(V)(1-kV/\omega)\sin(\omega - kV \pm \Omega)t}{\omega - kV \pm \Omega}. \tag{11.22}$$

As t becomes large we find that

$$\alpha^\pm \to P\int_{-\infty}^{\infty}{\rm d}V\,\frac{f_0(V)(1-kV/\omega)}{\omega - kV \pm \Omega}, \tag{11.23}$$

$$\beta^\pm \to \frac{\mp\pi\Omega}{\omega|k|}f_0\left(\frac{\omega\pm\Omega}{k}\right). \tag{11.24}$$

When

$$t \gg \frac{2\pi}{kV_{\rm rms}} \tag{11.25}$$

where $V_{\rm rms} = \langle V^2 \rangle^{1/2}$ is the spread of the velocity distribution, the approximations (11.19)∼(11.24) are justified. The absorption of the wave energy by the plasma particles is given by

$$\begin{aligned} &\langle {\rm Re}(q\boldsymbol{E}\exp(ikz - i\omega t))({\rm Re}\langle \boldsymbol{v}_\perp \rangle)\rangle_z \\ &\quad = \frac{q^2}{4m}(\beta^+ |E_x + iE_y|^2 + \beta^- |E_x - iE_y|^2). \end{aligned} \tag{11.26}$$

Let us consider the case of electrons ($\Omega_{\rm e} > 0$). As was described in sec.10.2, the wave $N^2 = R$ propagating in the direction of magnetic field ($\theta = 0$) satisfies $E_x + iE_y = 0$, so that the absorption power becomes

$$P_{\rm e} = \frac{q^2}{4m}\beta^- |E_x - iE_y|^2.$$

When $\omega > 0$, (11.24) indicates $\beta^- > 0$. In the case of $\omega < 0$, β^- is nearly zero since $f_0\left((\omega - \Omega_{\rm e})/k\right) \ll 1$.

Let us consider the case of ions ($-\Omega_{\rm i} > 0$). Similarly we find

$$P_{\rm i} = \frac{q^2}{4m}\beta^+ |E_x + iE_y|^2.$$

When $\omega > 0$, (11.24) indicates $\beta^+ > 0$. In the case of $\omega < 0$, β^+ is nearly zero, since $f_0\left(\omega + \Omega_{\rm i}/k\right) \ll 1$.

The *cyclotron velocity* $V_{\rm c}$ is defined so that the Doppler shifted frequency (the frequency of wave that a particle running with the velocity V feels) is equal to the cyclotron frequency, that is,

$$\begin{aligned} &\omega - kV_c \pm \Omega = 0, \\ &V_c = \frac{\omega}{k}\left(1 \pm \frac{\Omega}{\omega}\right). \end{aligned}$$

Accordingly particles absorb the wave energy when the absolute value of cyclotron velocity is smaller than the absolute value of phase velocity of the wave ($\pm\Omega/\omega < 0$)(see (11.24)). This phenomena is called *cyclotron damping*.

Let us consider the change in the kinetic energy of the particles in the case of cyclotron damping. Then the equation of motion is

$$m\frac{{\rm d}\boldsymbol{v}}{{\rm d}t} - q(\boldsymbol{v} \times \boldsymbol{B}_0) = q\boldsymbol{E}_\perp + q(\boldsymbol{v} \times \boldsymbol{B}_1).$$

Since $\boldsymbol{B}_1 = (\boldsymbol{k} \times \boldsymbol{E})/\omega$ and $E_z = 0$, we have

$$m\frac{{\rm d}v_z}{{\rm d}t} = \frac{qk_z}{\omega}(\boldsymbol{v}_\perp \cdot \boldsymbol{E}_\perp),$$

$$m\frac{{\rm d}\boldsymbol{v}_\perp}{{\rm d}t} - q(\boldsymbol{v}_\perp \times \boldsymbol{B}_0) = q\boldsymbol{E}_\perp\left(1 - \frac{k_z v_z}{\omega}\right)$$

so that

$$m\boldsymbol{v}_\perp \cdot \frac{{\rm d}\boldsymbol{v}_\perp}{{\rm d}t} = q(\boldsymbol{v}_\perp \cdot \boldsymbol{E}_\perp)\left(1 - \frac{k_z v_z}{\omega}\right).$$

Then

$$\frac{\rm d}{{\rm d}t}\left(\frac{mv_z^2}{2}\right) = \frac{k_z v_z}{\omega - k_z v_z}\frac{\rm d}{{\rm d}t}\left(\frac{mv_\perp^2}{2}\right),$$

$$v_\perp^2 + \left(v_z - \frac{\omega}{k_z}\right)^2 = \text{const.}$$

In the analysis of cyclotron damping we assumed that $v_z = V$ is constant; the condition of the validity of linearized theory is (ref.[3])

$$\frac{k_z^2 q^2 E_\perp^2 |\omega - k_z v_z| t^3}{24\omega^2 m^2} < 1.$$

We have discussed the case in which the perpendicular thermal energy is zero. When the perpendicular thermal energy is larger than the parallel thermal energy, so-called cyclotron instability may occur. The mutual interaction between particles and wave will be discussed again in chs.12 and 13 in relation to heating and instabilities.

11.4 Quasi-Linear Theory of Evolution in the Distribution Function

It has been assumed that the perturbation is small and the zeroth-order terms do not change. Under these assumption, the linearized equations on the perturbations are analyzed. However if the perturbations grow, then the zeroth-order quantities may change and the growth rate of the perturbations may change due to the evolution of the zeroth order quantities. Finally the perturbations saturate (growth rate becomes zero) and shift to steady state. Let us consider a simple case of $\boldsymbol{B} = 0$ and one dimensional electrostatic perturbation ($\boldsymbol{B}_1 = 0$). Ions are uniformly distributed. Then the distribution function $f(x, v, t)$ of electrons obeys the following Vlasov equation;

$$\frac{\partial f}{\partial t} + v\frac{\partial f}{\partial x} - \frac{e}{m}E\frac{\partial f}{\partial v} = 0. \tag{11.27}$$

Let the distribution function f be divided into two parts

$$f(x, v, t) = f_0(v, t) + f_1(x, v, t) \tag{11.28}$$

where f_0 is slowly changing zeroth order term and f_1 is the oscillatory 1st order term. It is assumed that the time derivatives of f_0 is the 2nd order term. When (11.28) is substituted into (11.27), the 1st and the 2nd terms satisfy following equations;

$$\frac{\partial f_1}{\partial t} + v\frac{\partial f_1}{\partial x} = \frac{e}{m}E\frac{\partial f_0}{\partial v}, \tag{11.29}$$

$$\frac{\partial f_0}{\partial t} = \frac{e}{m}E\frac{\partial f_1}{\partial v}. \tag{11.30}$$

f_1 and E may be expressed by Fourier integrals;

$$f_1(x, v, t) = \frac{1}{(2\pi)^{1/2}}\int f_k(v)\exp(i(kx - \omega(k)t))\mathrm{d}k, \tag{11.31}$$

$$E(x, t) = \frac{1}{(2\pi)^{1/2}}\int E_k\exp(i(kx - \omega(k)t))\mathrm{d}k. \tag{11.32}$$

Since f_1 and E are real, $f_{-k} = f_k^*$, $E_{-k} = E_k^*$, $\omega(-k) = -\omega^*(k)$ ($\omega(k) = \omega_\mathrm{r}(k) + i\gamma(k)$). The substitution of (11.31) (11.32) into (11.29) yields

$$f_k(v) = \frac{e}{m}\left(\frac{i}{\omega(k) - kv}\right)E_k\frac{\partial f_0}{\partial v}. \tag{11.33}$$

If (11.32) (11.33) are substituted into (11.30), we find

$$\frac{\partial f_0(v, t)}{\partial t} = \left(\frac{e}{m}\right)^2\frac{\partial}{\partial v}\left\langle\frac{1}{2\pi}\int E_{k'}\exp(i(k'x - \omega(k')t))\mathrm{d}k'\right.$$

$$\times \frac{i}{\omega(k)-kv} E_k \frac{\partial f_0(v,t)}{\partial v} \exp(i(kx-\omega(k)t))\mathrm{d}k \Big\rangle. \tag{11.34}$$

Statistical average of (11.34) (integration by x) is reduced to

$$\frac{\partial f_0(v,t)}{\partial t} = \frac{\partial}{\partial v}\left(D_\mathrm{v}(v)\frac{\partial f_0(v,t)}{\partial v}\right), \tag{11.35}$$

$$D_\mathrm{v}(v) = \left(\frac{e}{m}\right)^2 \frac{1}{L}\int_{-\infty}^{\infty} \frac{i|E_k|^2 \exp(2\gamma(k)t)}{\omega_\mathrm{r}(k)-kv+i\gamma(k)}\mathrm{d}k$$

$$= \left(\frac{e}{m}\right)^2 \frac{1}{L}\int_{-\infty}^{\infty} \frac{\gamma(k)|E_k|^2 \exp(2\gamma(k)t)}{(\omega_\mathrm{r}(k)-kv)^2+\gamma(k)^2}\mathrm{d}k,$$

where L is equal to the integral range of x for the statistical average. When $|\gamma(k)| \ll |\omega_\mathrm{r}(k)|$, the diffusion coefficient in velocity space is

$$D_\mathrm{v}(v) = \left(\frac{e}{m}\right)^2 \frac{\pi}{L}\int |E_k|^2 \exp(2\gamma(k)t)\,\delta(\omega_\mathrm{r}(k)-kv)\mathrm{d}k$$

$$= \left(\frac{e}{m}\right)^2 \frac{\pi}{L|v|}|E_k|^2 \exp(2\gamma(k)t)\Big|_{\omega/k=v}. \tag{11.36}$$

From Poisson's equation and (11.33), the dispersion equation can be derived:

$$\nabla \cdot \boldsymbol{E} = -\frac{e}{\epsilon_0}\int f_1 \mathrm{d}v,$$

$$ikE_k = -\frac{e}{\epsilon_0}\int f_k \mathrm{d}v,$$

$$1 + \frac{\Pi_\mathrm{e}^2}{k}\frac{1}{n}\int \left(\frac{1}{\omega(k)-kv}\right)\frac{\partial f_0}{\partial v}\mathrm{d}v = 0. \tag{11.37}$$

Under the assumption of $|\gamma| \ll |\omega_\mathrm{r}|(\omega = \omega_\mathrm{r} + i\gamma)$, the solution of (11.37) for γ is given by the same equation as (11.11).

Equation (11.35) is the diffusion equation in the velocity space. When the distribution function of electrons are given by the profile shown in fig.11.2(b), in which the positive gradient of $v\,\partial f/\partial v > 0$ exists near v_1. Then waves with the phase velocity of $\omega/k \approx v_1$ grow due to Landau amplification and the amplitude of $|E_k|$ increases. The diffusion coefficient D_v in velocity space becomes large and anomalous diffusion takes place in velocity space. The positive gradient of $\partial f/\partial v$ near $\sim v_1$ decreases and finally the profile of the distribution function becomes flat near $v \sim v_1$.

Let us consider the other case. When a wave is externally exited (by antenna) in a plasma with Maxwellian distribution function as is shown in fig.11.2(a), diffusion coefficient D_v at $v = \omega/k$ is increased. The gradient of the distribution function near $v = \omega/k$ becomes flat as will be seen in fig.16.21 of ch.16.

References

[1] L. D. Landau: J. Phys. (USSR) **10**, 45 (1946).

[2] J. H. Malmberg, C. B. Wharton and W. E. Drummond: Plasma Phys.and Controlled Nucl.Fusion Research **1**, 485 (1966) (Conf. Proceedings Culham in 1965, IAEA Vienna).

[3] T. H. Stix: *The Theory of Plasma Waves*, McGraw Hill, New York 1962.
T. H. Stix: *Waves in Plasmas*, American Institute of Physics, New York, 1992.

Ch.12 Wave Propagation and Wave Heating

Wave heating in ion cyclotron range of frequency (ICRF), lower hybrid wave heating (LHH), electron cyclotron heating (ECH), and other heating processes are being studied actively. The power sources of high-frequency waves are generally easier to construct than the beam source of neutral beam injection (NBI). Although the heating mechanism of NBI can be well explained by the classical process of Coulomb collision (refer sec(2.6)), the physical processes of wave heating are complicated and the interactions of waves and plasmas have a lot of variety, so that various applications are possible depending on the development of wave heating.

Waves are excited in the plasma by antennas or waveguides located outside the plasma (*excitation of wave, antenna-plasma coupling*). When the electric field of the excited wave is parallel to the confining magnetic field of the plasma, the electron, which can move along the magnetic field, may cancel the electric field. However, if the frequency of the wave is larger than the plasma frequency the electron can not follow the change in the electric field, and the wave then propagates through the plasma. When the electric field of the excited wave is perpendicular to the magnetic field, the electrons move in the direction of $\boldsymbol{E} \times \boldsymbol{B}$ (under the condition $\omega < \Omega_{\mathrm{e}}$) and thus they can not cancel the electric field. In this case the wave can propagate through the plasma even if the wave frequency is smaller than the plasma frequency. Excitation consists of pumping the high-frequency electromagnetic wave into plasma through the coupling system. If the strucure of the coupling system has the same periodicity as the eigenmode wave, the wave can be excited resonantly. The efficiency of wave excitation is not high except such *resonant excitation*.

Neutral beam injection and electron cyclotron heating can be launched in vacuum and propagate directly into the plasma without attenuation or interaction with the edge. Consequently the launching structures do not have to be in close proximity to the plasma and have advantage against thermal load and erosion by plasma.

Excited waves may propagate and pass through the plasma center without damping (heating) in some cases and may refract and turn back to the external region without passing the plasma center or may be reflected by the cutoff layer (see fig.12.1). The wave may be converted to the other type by the *mode conversion* (*wave propagation*).

The waves propagating in the plasma are absorbed and damped at the locations where Landau damping and cyclotron damping occur and heat the plasma. Therefore it is necessary for heating the plasma center that the waves be able to propagate into the plasma center without absorption and that they be absorbed when they reach the plasma center (*wave heating*).

12.1 Energy Flow

Energy transport and the propagation of waves in the plasma medium are very important in the wave heating of plasmas. The equation of energy flow is derived by taking the difference between the scalar product of $\boldsymbol{H}$ and (10.15) and the scalar product of $\boldsymbol{E}$ and (10.16):

$$\nabla \cdot (\boldsymbol{E} \times \boldsymbol{H}) + \boldsymbol{E} \cdot \frac{\partial \boldsymbol{D}}{\partial t} + \boldsymbol{H} \cdot \frac{\partial \boldsymbol{B}}{\partial t} = 0. \tag{12.1}$$

$\boldsymbol{P} \equiv \boldsymbol{E} \times \boldsymbol{H}$ is called *Poynting vector* and represents the energy flow of electromagnetic field. This Poynting equation does not include the effect of electric resistivity by electron-ion collision.

Plasmas are dispersive medium and the dielectric tensors are dependent on the propagation vector $\boldsymbol{k}$ and the frequency ω. Denote the Fourier components of $\boldsymbol{E}(\boldsymbol{r}, t)$ and $\boldsymbol{D}(\boldsymbol{r}, t)$ by $\boldsymbol{E}_\omega(\boldsymbol{k}, \omega)$ and $\boldsymbol{D}_\omega(\boldsymbol{k}, \omega)$, respectively. Then we find

$$\boldsymbol{D}_\omega = \frac{1}{(2\pi)^2} \int \boldsymbol{D}(\boldsymbol{r}, t) \exp(-i(\boldsymbol{k} \cdot \boldsymbol{r} - \omega t))\, \mathrm{d}\boldsymbol{r}\, \mathrm{d}t,$$

$$\boldsymbol{E}_\omega = \frac{1}{(2\pi)^2} \int \boldsymbol{E}(\boldsymbol{r}, t) \exp(-i(\boldsymbol{k} \cdot \boldsymbol{r} - \omega t))\, \mathrm{d}\boldsymbol{r}\, \mathrm{d}t.$$

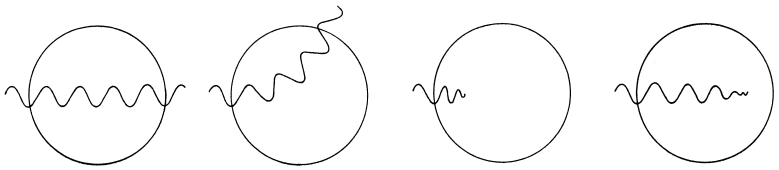

Fig.12.1 Passing through, refraction and reflection, absorption near boundary, and absorption at center of plasma.

There is following relation between them:

$$\boldsymbol{D}_\omega(\boldsymbol{k},\omega) = \epsilon_0 \boldsymbol{K}(\boldsymbol{k},\omega)\cdot\boldsymbol{E}_\omega(\boldsymbol{k},\omega),$$

and we have

$$\boldsymbol{D}(\boldsymbol{r},t) = \frac{1}{(2\pi)^2}\epsilon_0 \int \boldsymbol{K}(\boldsymbol{k},\omega)\cdot\boldsymbol{E}_\omega(\boldsymbol{k},\omega)\exp(i(\boldsymbol{k}\cdot\boldsymbol{r}-\omega t))\,\mathrm{d}\boldsymbol{k}\,\mathrm{d}\omega,$$

$$\boldsymbol{E}(\boldsymbol{r},t) = \frac{1}{(2\pi)^2}\int \boldsymbol{E}_\omega(\boldsymbol{k},\omega)\exp(i(\boldsymbol{k}\cdot\boldsymbol{r}-\omega t))\,\mathrm{d}\boldsymbol{k}\,\mathrm{d}\omega.$$

From the formula of Fourier integral, following equations are derived:

$$\boldsymbol{D}(\boldsymbol{r},t) = \epsilon_0 \int \widehat{\boldsymbol{K}}(\boldsymbol{r}-\boldsymbol{r}',t-t')\cdot\boldsymbol{E}(\boldsymbol{r}',t')\,\mathrm{d}\boldsymbol{r}'\,\mathrm{d}t'$$

where $\widehat{\boldsymbol{K}}(\boldsymbol{r},t)$ is

$$\widehat{\boldsymbol{K}}(\boldsymbol{r},t) = \frac{1}{(2\pi)^4}\int \boldsymbol{K}(\boldsymbol{k},\omega)\exp(-i(\boldsymbol{k}\cdot\boldsymbol{r}-\omega t))\,\mathrm{d}\boldsymbol{k}\,\mathrm{d}\omega.$$

Therefore analysis of general electromagnetic fields in dispersive medium is not simple. However if the electric field consists of Fourier component in narrow region of $\boldsymbol{k}$, ω and $\boldsymbol{K}$ changes slowly as $\boldsymbol{k}$, ω change, then we can use the following relation:

$$\boldsymbol{D}(\boldsymbol{r},t) = \epsilon_0 \boldsymbol{K}\cdot\boldsymbol{E}(\boldsymbol{r},t).$$

From now we will discuss this simple case. The relation between the magnetic induction $\boldsymbol{B}$ and the magnetic intensity $\boldsymbol{H}$ is

$$\boldsymbol{B} = \mu_0 \boldsymbol{H},$$

in plasmas.

The quasi-periodic functions $A,\ B$ may be expressed by

$$A = A_0 \exp\left(-i\int_{-\infty}^{t}(\omega_\mathrm{r}+i\omega_\mathrm{i})\mathrm{d}t'\right) = A_0\exp(-i\phi_\mathrm{r}+\phi_\mathrm{i}),$$
$$B = B_0 \exp\left(-i\int_{-\infty}^{t}(\omega_\mathrm{r}+i\omega_\mathrm{i})\mathrm{d}t'\right) = B_0\exp(-i\phi_\mathrm{r}+\phi_\mathrm{i})$$

where ϕ_r and ϕ_i are real. When the average of the multiplication of the real parts of A with the real part of B is denoted by $\overline{AB}$, then $\overline{AB}$ is given by

$$\overline{AB} = \frac{1}{2}\cdot\frac{1}{2}\langle(A_0\exp(-i\phi_\mathrm{r}+\phi_\mathrm{i}) + A_0^*\exp(i\phi_\mathrm{r}+\phi_\mathrm{i}))\times(B_0\exp(-i\phi_\mathrm{r}+\phi_\mathrm{i}) + B_0^*\exp(i\phi_\mathrm{r}+\phi_\mathrm{i}))\rangle$$

$$= \frac{1}{4}(A_0B_0^* + A_0^*B_0)\exp(2\phi_\mathrm{i}) = \frac{1}{2}\mathrm{Re}(AB^*)\,. \tag{12.2}$$

The averaging of the Poynting equation becomes

$$\nabla \cdot \boldsymbol{P} + \frac{\partial W}{\partial t} = 0, \tag{12.3}$$

$$\boldsymbol{P} = \frac{1}{2\mu_0}\mathrm{Re}(\boldsymbol{E}_0 \times \boldsymbol{B}_0^*) \exp 2\int_{-\infty}^{t} \omega_\mathrm{i} \mathrm{d}t', \tag{12.4}$$

$$\frac{\partial W}{\partial t} = \frac{1}{2}\mathrm{Re}\left(\left(\frac{\boldsymbol{B}^*}{\mu_0}\cdot\frac{\partial \boldsymbol{B}}{\partial t}\right) + \epsilon_0 \boldsymbol{E}^* \cdot \frac{\partial}{\partial t}(\boldsymbol{K}\cdot\boldsymbol{E})\right) = \frac{1}{2}\mathrm{Re}\left(-i\omega\frac{\boldsymbol{B}^*\cdot\boldsymbol{B}}{\mu_0} + \epsilon_0(-i\omega)\boldsymbol{E}^*\cdot\boldsymbol{K}\cdot\boldsymbol{E}\right)$$

$$= \frac{1}{2}\omega_\mathrm{i}\frac{\boldsymbol{B}\cdot\boldsymbol{B}^*}{\mu_0} + \frac{\epsilon_0}{2}\left(\omega_\mathrm{i}\mathrm{Re}(\boldsymbol{E}^*\cdot\boldsymbol{K}\cdot\boldsymbol{E}) + \omega_\mathrm{r}\mathrm{Im}(\boldsymbol{E}^*\cdot\boldsymbol{K}\cdot\boldsymbol{E})\right). \tag{12.5}$$

From the relations

$$\boldsymbol{E}^*\cdot\boldsymbol{K}\cdot\boldsymbol{E} = \sum_i E_i^* \sum_j K_{ij}E_j,$$

$$\boldsymbol{E}\cdot\boldsymbol{K}^*\cdot\boldsymbol{E}^* = \sum_i E_i \sum_j K_{ij}^* E_j^* = \sum_j E_j^* \sum_i (K_{ji}^\mathrm{T})^* E_i$$
$$= \sum_i E_i^* \sum_j (K_{ij}^\mathrm{T})^* E_j$$

we find

$$\mathrm{Re}(\boldsymbol{E}^*\cdot\boldsymbol{K}\cdot\boldsymbol{E}) = \boldsymbol{E}^*\cdot\frac{\boldsymbol{K}+(\boldsymbol{K}^\mathrm{T})^*}{2}\cdot\boldsymbol{E},$$

$$\mathrm{Im}(\boldsymbol{E}^*\cdot\boldsymbol{K}\cdot\boldsymbol{E}) = \boldsymbol{E}^*\cdot\frac{(-i)[\boldsymbol{K}-(\boldsymbol{K}^\mathrm{T})^*]}{2}\cdot\boldsymbol{E}.$$

$(\boldsymbol{K}^\mathrm{T})^*$ is the complex conjugate of transpose matrix $\boldsymbol{K}^\mathrm{T}$ (lines and rows of components are exchanged) of $\boldsymbol{K}$, i.e., $K_{ij}^\mathrm{T} \equiv K_{ji}$. When a matrix $\boldsymbol{M}$ and $(\boldsymbol{M}^\mathrm{T})^*$ are equal with each other, this kind of matrix is called *Hermite matrix*. For the Hermite matrix, $(\boldsymbol{E}^*\cdot\boldsymbol{M}\cdot\boldsymbol{E})$ is always real. The dielectric tensor may be decomposed to

$$\boldsymbol{K}(\boldsymbol{k},\omega) = \boldsymbol{K}_\mathrm{H}(\boldsymbol{k},\omega) + i\boldsymbol{K}_\mathrm{I}(\boldsymbol{k},\omega).$$

As is described in sec.12.3, $\boldsymbol{K}_\mathrm{H}$ and $\boldsymbol{K}_\mathrm{I}$ are Hermite, when $\boldsymbol{k}$, ω are real. It will be proved that the term $i\boldsymbol{K}_\mathrm{I}$ corresponds to Landau damping and cyclotron damping. When the imaginary part of ω is much smaller than the real part ($\omega = \omega_\mathrm{r} + i\omega_\mathrm{i}$, $|\omega_\mathrm{i}| \ll |\omega_\mathrm{r}|$) we may write

$$\boldsymbol{K}(\boldsymbol{k},\omega_\mathrm{r}+i\omega_\mathrm{i}) \approx \boldsymbol{K}_\mathrm{H}(\boldsymbol{k},\omega_\mathrm{r}) + i\omega_\mathrm{i}\frac{\partial}{\partial\omega_\mathrm{r}}\boldsymbol{K}_\mathrm{H}(\boldsymbol{k},\omega_\mathrm{r}) + i\boldsymbol{K}_\mathrm{I}(\boldsymbol{k},\omega_\mathrm{r}).$$

When the Hermite component of W (the term associated to $\boldsymbol{K}_\mathrm{H}$ in W) is denoted by W_0, W_0 is given by

$$W_0 = \frac{1}{2}\mathrm{Re}\left(\frac{\boldsymbol{B}_0^*\cdot\boldsymbol{B}_0}{2\mu_0} + \frac{\epsilon_0}{2}\boldsymbol{E}_0^*\cdot\boldsymbol{K}_\mathrm{H}\cdot\boldsymbol{E}_0 + \frac{\epsilon_0}{2}\boldsymbol{E}_0^*\cdot\left(\omega_\mathrm{r}\frac{\partial}{\partial\omega_\mathrm{r}}\boldsymbol{K}_\mathrm{H}\right)\cdot\boldsymbol{E}_0\right)$$

$$= \frac{1}{2}\mathrm{Re}\left(\frac{\boldsymbol{B}_0^*\cdot\boldsymbol{B}_0}{2\mu_0} + \frac{\epsilon_0}{2}\boldsymbol{E}_0^*\cdot\left(\frac{\partial}{\partial\omega}(\omega\boldsymbol{K}_\mathrm{H})\right)\cdot\boldsymbol{E}_0\right) \tag{12.6}$$

and (12.3),(12.5) yield

$$\frac{\partial W_0}{\partial t} = -\omega_\mathrm{r}\frac{1}{2}\epsilon_0\boldsymbol{E}_0^*\cdot\boldsymbol{K}_\mathrm{I}\cdot\boldsymbol{E}_0 - \nabla\cdot\boldsymbol{P}. \tag{12.7}$$

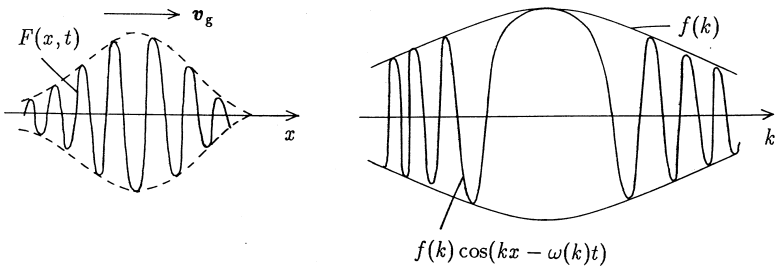

Fig.12.2 $F(x,t)$ and $f(k)\cos(kx - w(k)t)$

The 1st term in (12.6) is the energy density of the magnetic field and the 2nd term is the energy density of electric field which includes the kinetic energy of coherent motion associated with the wave. Equation (12.6) gives the energy density of the wave in a dispersive media. The 1st term in the right-hand side of (12.7) represents the Landau and cyclotron dampings and the 2nd term is the divergence of the flow of wave energy.

Let us consider the velocity of the wave packet

$$F(\boldsymbol{r},t) = \int_{-\infty}^{\infty} f(\boldsymbol{k}) \exp i(\boldsymbol{k}\cdot\boldsymbol{r} - \omega(\boldsymbol{k})t)\mathrm{d}\boldsymbol{k} \tag{12.8}$$

when the dispersion equation

$$\omega = \omega(\boldsymbol{k})$$

is given. If $f(\boldsymbol{k})$ varies slowly, the position of the maximum of $F(\boldsymbol{r},t)$ is the position of the stationary phase of

$$\frac{\partial}{\partial k_{\mathrm{i}}}(\boldsymbol{k}\cdot\boldsymbol{r} - \omega(\boldsymbol{k})t) = 0. \qquad (i = x,y,z)$$

(see fig.12.2). Consequently the velocity of the maximum position is

$$\left(\frac{x}{t} = \frac{\partial\omega(\boldsymbol{k})}{\partial k_x}, \qquad \frac{y}{t} = \frac{\partial\omega(\boldsymbol{k})}{\partial k_y}, \qquad \frac{z}{t} = \frac{\partial\omega(\boldsymbol{k})}{\partial k_z}\right)$$

that is,

$$\boldsymbol{v}_{\mathrm{g}} = \left(\frac{\partial\omega}{\partial k_x}, \frac{\partial\omega}{\partial k_y}, \frac{\partial\omega}{\partial k_z}\right). \tag{12.9}$$

This velocity is called *group velocity* and represents the velocity of energy flow.

12.2 Ray Tracing

When the wavelength of waves in the plasma is much less than the characteristic length (typically the minor radius a), the WKB approximation (geometrical optical approximation) can be applied. Let the dispersion relation be $D(\boldsymbol{k},\omega,\boldsymbol{r},t) = 0$. The direction of wave energy flow is given by the group velocity $\boldsymbol{v}_{\mathrm{g}} = \partial\omega/\partial\boldsymbol{k} \equiv (\partial\omega/\partial k_x,\ \partial\omega/\partial k_y,\ \partial\omega/\partial k_z)$, so that the optical ray can be given by $\mathrm{d}\boldsymbol{r}/\mathrm{d}t = \boldsymbol{v}_{\mathrm{g}}$. Although the quantities $(\boldsymbol{k},\omega)$ change according to the change of $\boldsymbol{r}$, they always satisfy $D = 0$. Then the optical ray can be obtained by

$$\frac{\mathrm{d}\boldsymbol{r}}{\mathrm{d}s} = \frac{\partial D}{\partial\boldsymbol{k}}, \qquad \frac{\mathrm{d}\boldsymbol{k}}{\mathrm{d}s} = -\frac{\partial D}{\partial\boldsymbol{r}}, \tag{12.10}$$

$$\frac{\mathrm{d}t}{\mathrm{d}s} = -\frac{\partial D}{\partial\omega}, \qquad \frac{\mathrm{d}\omega}{\mathrm{d}s} = \frac{\partial D}{\partial t}. \tag{12.11}$$

Here s is a measure of the length along the optical ray. Along the optical ray the variation δD becomes zero,

$$\delta D = \frac{\partial D}{\partial \boldsymbol{k}} \cdot \delta \boldsymbol{k} + \frac{\partial D}{\partial \omega} \cdot \delta \omega + \frac{\partial D}{\partial \boldsymbol{r}} \cdot \delta \boldsymbol{r} + \frac{\partial D}{\partial t} \cdot \delta t = 0 \tag{12.12}$$

and $D(\boldsymbol{k}, \omega, \boldsymbol{r}, t) = 0$ is satisfied. Equations (12.10),(12.11) reduce to

$$\frac{\mathrm{d}\boldsymbol{r}}{\mathrm{d}t} = \frac{\mathrm{d}\boldsymbol{r}}{\mathrm{d}s}\left(\frac{\mathrm{d}t}{\mathrm{d}s}\right)^{-1} = -\frac{\partial D}{\partial \boldsymbol{k}}\left(\frac{\partial D}{\partial \omega}\right)^{-1} = \left(\frac{\partial \omega}{\partial \boldsymbol{k}}\right)_{\boldsymbol{r}, t=\text{const.}} = \boldsymbol{v}_{\mathrm{g}}.$$

Equation (12.10) has the same formula as the equation of motion with Hamiltonian D. When D does not depend on t explicitly, $D = \text{const.} = 0$ corresponds to the energy conservation law. If the plasma medium does not depend on z, k_z =const. corresponds to the momentum conservation law and is the same as the Snell law, $N_{\parallel} = \text{const.}$.

When $\boldsymbol{k} = \boldsymbol{k}_{\mathrm{r}} + i\boldsymbol{k}_{\mathrm{i}}$ is a solution of $D = 0$ for a given real ω and $|\boldsymbol{k}_{\mathrm{i}}| \ll |\boldsymbol{k}_{\mathrm{r}}|$ is satisfied, we have

$$D(\boldsymbol{k}_{\mathrm{r}} + i\boldsymbol{k}_{\mathrm{i}}, \omega) = \mathrm{Re}D(\boldsymbol{k}_{\mathrm{r}}, \omega) + \frac{\partial \mathrm{Re}D(\boldsymbol{k}_{\mathrm{r}}, \omega)}{\partial \boldsymbol{k}_{\mathrm{r}}} \cdot i\boldsymbol{k}_{\mathrm{i}} + i\mathrm{Im}D(\boldsymbol{k}_{\mathrm{r}}, \omega) = 0.$$

Therefore this reduces to

$$\mathrm{Re}D(\boldsymbol{k}_{\mathrm{r}}, \omega) = 0,$$

$$\boldsymbol{k}_{\mathrm{i}} \cdot \frac{\partial \mathrm{Re}D(\boldsymbol{k}_{\mathrm{r}}, \omega)}{\partial \boldsymbol{k}_{\mathrm{r}}} = -\mathrm{Im}D(\boldsymbol{k}_{\mathrm{r}}, \omega). \tag{12.13}$$

Then the wave intensity $I(\boldsymbol{r})$ becomes

$$I(\boldsymbol{r}) = I(\boldsymbol{r}_0) \exp\left(-2\int_{\boldsymbol{r}_0}^{\boldsymbol{r}} \boldsymbol{k}_{\mathrm{i}} \mathrm{d}\boldsymbol{r}\right), \tag{12.14}$$

$$\int \boldsymbol{k}_{\mathrm{i}} \mathrm{d}\boldsymbol{r} = \int \boldsymbol{k}_{\mathrm{i}} \cdot \frac{\partial D}{\partial \boldsymbol{k}} \mathrm{d}s = -\int \mathrm{Im}D(\boldsymbol{k}_{\mathrm{r}}, \omega)\mathrm{d}s = -\int \frac{\mathrm{Im}D(\boldsymbol{k}_{\mathrm{r}}, \omega)}{|\partial D/\partial \boldsymbol{k}|}\mathrm{d}l. \tag{12.15}$$

where $\mathrm{d}l$ is the length along the optical ray. Therefore the wave absorption can be estimated from (12.14) and (12.15) by tracing many optical rays. The geometrical optical approximation can provide the average wave intensity with a space resolution of, say, two or three times the wavelength.

12.3 Dielectric Tensor of Hot Plasma, Wave Absorption and Heating

In the process of wave absorption by hot plasma, Landau damping or cyclotron damping are most important as was described in ch.11. These damping processes are due to the interaction between the wave and so called *resonant particles* satisfying

$$\omega - k_z v_z - \mathrm{n}\Omega = 0. \qquad \mathrm{n} = 0, \pm 1, \pm 2, \cdots$$

In the coordinates running with the same velocity, the electric field is static ($\omega = 0$) or of cyclotron harmonic frequency ($\omega = n\Omega$). The case of n = 0 corresponds to Landau damping and the case of n = 1 corresponds to electron cyclotron damping and the case of n = −1 corresponds to ion cyclotron damping ($\omega > 0$ is assumed).

Although nonlinear or stochastic processes accompany wave heating in many cases, the experimental results of wave heating or absorption can ususally well described by linear or quasi-linear theories. The basis of the linear theory is the dispersion relation with the dielectric tensor $\boldsymbol{K}$ of finite-temperature plasma. The absorbed power per unit volume of plasma P^{ab} is given by the 1st term in the right-hand side of (12.7):

$$P^{\mathrm{ab}} = \omega_{\mathrm{r}} \left(\frac{\epsilon_0}{2}\right) \boldsymbol{E}^* \cdot \boldsymbol{K}_{\mathrm{I}} \cdot \boldsymbol{E}.$$

Since $\boldsymbol{K}_{\rm H}$, $\boldsymbol{K}_{\rm I}$ is Hermit matrix for real $\boldsymbol{k}$, ω as will be shown later in this section, the absorbed power $P^{\rm ab}$ is given by

$$P^{\rm ab} = \omega_{\rm r}\left(\frac{\epsilon_0}{2}\right) {\rm Re}\left(\boldsymbol{E}^* \cdot (-i)\boldsymbol{K}\cdot\boldsymbol{E}\right)_{\omega=\omega_{\rm r}}. \tag{12.16}$$

As is clear from the expression (12.19) of $\boldsymbol{K}$, the absorbed power $P^{\rm ab}$ reduces to

$$P^{\rm ab} = \omega\frac{\epsilon_0}{2}\Big(|E_x|^2{\rm Im}K_{xx} + |E_y|^2{\rm Im}K_{yy} + |E_z|^2{\rm Im}K_{zz}$$

$$+2{\rm Im}(E_x^*E_y){\rm Re}K_{xy} + 2{\rm Im}(E_y^*E_z){\rm Re}K_{yz} + 2{\rm Im}(E_x^*E_z){\rm Re}K_{xz}\ \Big). \tag{12.17}$$

Since (10.3) gives $\boldsymbol{j} = -i\omega\boldsymbol{P} = -i\epsilon_0\omega(\boldsymbol{K}-\boldsymbol{I})\cdot\boldsymbol{E}$, (12.16) may be described by

$$P^{\rm ab} = \frac{1}{2}{\rm Re}(\boldsymbol{E}^*\cdot\boldsymbol{j})_{\omega=\omega_{\rm r}}. \tag{12.18}$$

The process to drive the dielectric tensor $\boldsymbol{K}$ of finite-temperature plasma is described in appendix C. When the plasma is bi-Maxwellian;

$$f_0(v_\perp, v_z) = n_0 F_\perp(v_\perp)F_z(v_z),$$

$$F_\perp(v_\perp) = \frac{m}{2\pi\kappa T_\perp}\exp\left(-\frac{mv_\perp^2}{2\kappa T_\perp}\right),$$

$$F_z(v_z) = \left(\frac{m}{2\pi\kappa T_z}\right)^{1/2}\exp\left(-\frac{m(v_z-V)^2}{2\kappa T_z}\right)$$

the dielectric tensor $\boldsymbol{K}$ is given by

$$\boldsymbol{K} = \boldsymbol{I} + \sum_{\rm i,e}\frac{\Pi^2}{\omega^2}\left[\sum_{\rm n}\left(\zeta_0 Z(\zeta_{\rm n}) - \left(1-\frac{1}{\lambda_{\rm T}}\right)(1+\zeta_{\rm n}Z(\zeta_{\rm n}))\right)e^{-b}\boldsymbol{X}_{\rm n} + 2\eta_0^2\lambda_{\rm T}\boldsymbol{L}\right], \tag{12.19}$$

$$\boldsymbol{X}_{\rm n} = \begin{bmatrix} {\rm n}^2 I_{\rm n}/b & i{\rm n}(I'_{\rm n}-I_{\rm n}) & -(2\lambda_{\rm T})^{1/2}\eta_{\rm n}\frac{\rm n}{\alpha}I_{\rm n} \\ -i{\rm n}(I'_{\rm n}-I_{\rm n}) & ({\rm n}^2/b+2b)I_{\rm n}-2bI'_{\rm n} & i(2\lambda_{\rm T})^{1/2}\eta_{\rm n}\alpha(I'_{\rm n}-I_{\rm n}) \\ -(2\lambda_{\rm T})^{1/2}\eta_{\rm n}\frac{\rm n}{\alpha}I_{\rm n} & -i(2\lambda_{\rm T})^{1/2}\eta_{\rm n}\alpha(I'_{\rm n}-I_{\rm n}) & 2\lambda_{\rm T}\eta_{\rm n}^2 I_{\rm n} \end{bmatrix} \tag{12.20}$$

$$Z(\zeta) \equiv \frac{1}{\pi^{1/2}}\int_{-\infty}^{\infty}\frac{\exp(-\beta^2)}{\beta-\zeta}\,{\rm d}\beta,$$

$I_{\rm n}(b)$ is the nth modified Bessel function

$$\eta_{\rm n} \equiv \frac{\omega+{\rm n}\Omega}{2^{1/2}k_z v_{{\rm T}z}}, \qquad \zeta_{\rm n} \equiv \frac{\omega-k_z V+{\rm n}\Omega}{2^{1/2}k_z v_{{\rm T}z}},$$

$$\lambda_{\rm T} \equiv \frac{T_z}{T_\perp}, \qquad b \equiv \left(\frac{k_x v_{{\rm T}\perp}}{\Omega}\right)^2, \qquad \alpha \equiv \frac{k_x v_{{\rm T}\perp}}{\Omega},$$

$$v_{{\rm T}z}^2 \equiv \frac{\kappa T_z}{m}, \qquad v_{{\rm T}\perp}^2 \equiv \frac{\kappa T_\perp}{m}.$$

The components of $\boldsymbol{L}$ matrix are zero except $L_{zz}=1$.

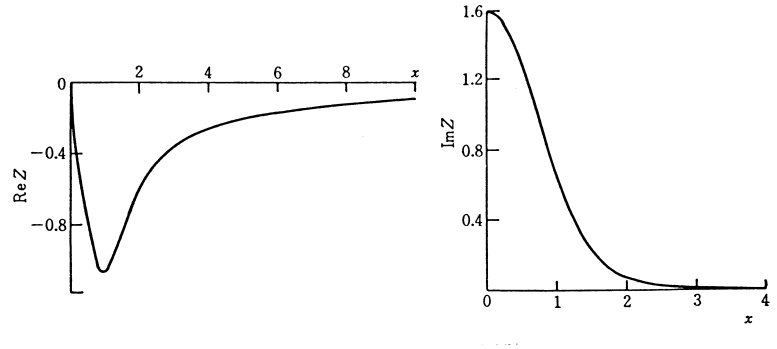

Fig.12.3 Real part $\mathrm{Re}\, Z$ and imaginary part $\mathrm{Im}\, Z$ of $Z(x)$ in the case of real x.

When the plasma is isotropic Maxwellian ($T_z = T_\perp$) and $V = 0$, then $\eta_\mathrm{n} = \zeta_\mathrm{n}$, and $\lambda_\mathrm{T} = 1$, and (12.19) reduces to

$$\boldsymbol{K} = \boldsymbol{I} + \sum_{\mathrm{i,e}} \frac{\Pi^2}{\omega^2} \left[\sum_{\mathrm{n}=-\infty}^{\infty} \zeta_0 Z(\zeta_\mathrm{n}) e^{-b} \boldsymbol{X}_\mathrm{n} + 2\zeta_0^2 \boldsymbol{L} \right]. \tag{12.21}$$

The real part $\mathrm{Re}\, Z(x)$ and the imaginary part $\mathrm{Im}\, Z(x)$ in the case of real x are shown in fig.12.3.

The series expansion of the plasma dispersion function $Z(\zeta)$ is

$$Z(\zeta) = i\pi^{1/2} \frac{k_z}{|k_z|} \exp(-\zeta^2) - 2\zeta \left(1 - \frac{2}{3}\zeta^2 + \frac{4}{15}\zeta^4 + \cdots \right)$$

in the case of $|\zeta| \ll 1$ (hot plasma). The asymptotic expansion of $Z(\zeta)$ is

$$Z(\zeta) = i\pi^{1/2} \sigma \frac{k_z}{|k_z|} \exp(-\zeta^2) - \frac{1}{\zeta} \left(1 + \frac{1}{2}\frac{1}{\zeta^2} + \frac{3}{4}\frac{1}{\zeta^4} + \cdots \right)$$

$$\sigma = 0 \ \text{ for } \ \mathrm{Im}\, \omega > 0, \qquad \sigma = 2 \ \text{ for } \ \mathrm{Im}\, \omega < 0,$$

but

$$\sigma = 1 \ \text{for} \ |\mathrm{Im}\, \zeta||\mathrm{Re}\, \zeta| \lesssim \pi/4, \ \text{and} \ |\zeta| \gg 1$$

in the case of $|\zeta| \ll 1$ (cold plasma) (ref.[1],[2]). Refer to appendix C for the derivation.
The part $i\pi^{1/2}(k_z/|k_z|)\exp(-\zeta^2)$ of $Z(\zeta)$ represents the terms of Landau damping and cyclotron damping as is described later in this section.

When $T \to 0$, that is, $\zeta_\mathrm{n} \to \pm\infty$, $b \to 0$, the dielectric tensor of hot plasma is reduced to the dielectric tensor (10.9)$\sim$(10.13) of cold plasma.

In the case of $b = (k_x \rho_\Omega)^2 \ll 1$ ($\rho_\Omega = v_{\mathrm{T}\perp}/\Omega$ is Larmor radius), it is possible to expand $e^{-b}\boldsymbol{X}_\mathrm{n}$ by b using

$$\begin{aligned} I_\mathrm{n}(b) &= \left(\frac{b}{2}\right)^\mathrm{n} \sum_{l=0}^{\infty} \frac{1}{l!(\mathrm{n}+l)!} \left(\frac{b}{2}\right)^{2l} \\ &= \left(\frac{b}{2}\right)^\mathrm{n} \left(\frac{1}{\mathrm{n}!} + \frac{1}{1!(\mathrm{n}+1)!}\left(\frac{b}{2}\right)^2 + \frac{1}{2!(\mathrm{n}+2)!}\left(\frac{b}{2}\right)^4 + \cdots \right). \end{aligned}$$

The expansion in b and the inclusion of terms up to the second harmonics in $\boldsymbol{K}$ give

$$K_{xx} = 1 + \sum_j \left(\frac{\Pi_j}{\omega}\right)^2 \zeta_0 \left((Z_1 + Z_{-1}) \left(\frac{1}{2} - \frac{b}{2} + \cdots \right) + (Z_2 + Z_{-2}) \left(\frac{b}{2} - \frac{b^2}{2} + \cdots \right) + \cdots \right)_j ,$$

$$K_{yy} = 1 + \sum_j \left(\frac{\Pi_j}{\omega}\right)^2 \zeta_0 \left(Z_0(2b + \cdots) + (Z_1 + Z_{-1}) \left(\frac{1}{2} - \frac{3b}{2} + \cdots\right) \right.$$
$$\left. + (Z_2 + Z_{-2}) \left(\frac{b}{2} - b^2 + \cdots\right) + \cdots \right)_j ,$$

$$K_{zz} = 1 - \sum_j \left(\frac{\Pi_j}{\omega}\right)^2 \zeta_0 \Big(2\zeta_0 W_0 (1 - b + \cdots) + (\zeta_1 W_1 + \zeta_{-1} W_{-1})(b + \cdots)$$
$$+ (\zeta_2 W_2 + \zeta_{-2} W_{-2}) \left(\frac{b^2}{4} + \cdots\right) + \cdots \Big)_j ,$$

$$K_{xy} = i \sum_j \left(\frac{\Pi_j}{\omega}\right)^2 \zeta_0 \left((Z_1 - Z_{-1}) \left(\frac{1}{2} - b + \cdots\right) + (Z_2 - Z_{-2}) \left(\frac{b}{2} + \cdots\right) + \cdots \right)_j ,$$

$$K_{xz} = 2^{1/2} \sum_j \left(\frac{\Pi_j}{\omega}\right)^2 b^{1/2} \zeta_0 \left((W_1 - W_{-1}) \left(\frac{1}{2} + \cdots\right) + (W_2 - W_{-2}) \left(\frac{b}{4} + \cdots\right) + \cdots \right)_j ,$$

$$K_{yz} = -2^{1/2} i \sum_j \left(\frac{\Pi_j}{\omega}\right)^2 b^{1/2} \zeta_0 \left(W_0 \left(-1 + \frac{3}{2} b + \cdots\right) \right.$$
$$\left. + (W_1 + W_{-1}) \left(\frac{1}{2} + \cdots\right) + (W_2 - W_{-2}) \left(\frac{b}{4} + \cdots\right) + \cdots \right)_j \tag{12.22}$$

$$K_{yx} = -K_{xy}, \quad K_{zx} = K_{xz}, \quad K_{zy} = -K_{zy}$$

where

$$Z_{\pm \mathrm{n}} \equiv Z(\zeta_{\pm \mathrm{n}}), \quad W_{\mathrm{n}} \equiv -\left(1 + \zeta_{\mathrm{n}} Z(\zeta_{\mathrm{n}})\right),$$
$$\zeta_{\mathrm{n}} = (\omega + \mathrm{n}\Omega)/(2^{1/2} k_z (\kappa T_z/m)^{1/2}).$$

When $x \gg 1$, $\mathrm{Re} W(x)$ is

$$\mathrm{Re}\, W(x) = (1/2) x^{-2} (1 + (3/2) x^{-2} + \cdots).$$

The absorbed power by Landau damping (including transit time damping) may be estimated by the terms associated with the imaginary part G_0 of $\zeta_0 Z(\zeta_0)$ in (12.22) of K_{ij}:

$$G_0 \equiv \mathrm{Im} \zeta_0 Z(\zeta_0) = \frac{k_z}{|k_z|} \pi^{1/2} \zeta_0 \exp(-\zeta_0^2).$$

Since

$$(\mathrm{Im} K_{yy})_0 = \left(\frac{\Pi_j}{\omega}\right)^2 2bG_0,$$

$$(\mathrm{Im} K_{zz})_0 = \left(\frac{\Pi_j}{\omega}\right)^2 2\zeta_0^2 G_0,$$

$$(\mathrm{Re}K_{yz})_0 = \left(\frac{\Pi_j}{\omega}\right)^2 2^{1/2} b^{1/2} \zeta_0 G_0$$

the contribution of these terms to the absorption power (12.17) is

$$P_0^{\mathrm{ab}} = 2\omega \left(\frac{\Pi_j}{\omega}\right)^2 G_0 \left(\frac{\epsilon_0}{2}\right) \left(|E_y|^2 b + |E_z|^2 \zeta_0^2 + \mathrm{Im}(E_y^* E_z)(2b)^{1/2}\zeta_0\right). \tag{12.23}$$

The 1st term is of transit time damping and is equal to (11.16). The 2nd term is of Landau damping and is equal to (11.10). The 3rd one is the term of the interference of both.

The absorption power due to cyclotron damping and the harmonic cyclotron damping is obtained by the contribution from the terms

$$G_{\pm \mathrm{n}} \equiv \mathrm{Im}\zeta_0 Z_{\pm \mathrm{n}} = \frac{k_z}{|k_z|}\pi^{1/2}\zeta_0 \exp(-\zeta_{\pm \mathrm{n}}^2)$$

and for the case $b \ll 1$,

$$(\mathrm{Im}K_{xx})_{\pm \mathrm{n}} = (\mathrm{Im}K_{yy})_{\pm \mathrm{n}} = \left(\frac{\Pi_j}{\omega}\right)^2 G_{\pm \mathrm{n}} \alpha_{\mathrm{n}},$$

$$(\mathrm{Im}K_{zz})_{\pm \mathrm{n}} = \left(\frac{\Pi_j}{\omega}\right)^2 2\zeta_{\pm \mathrm{n}}^2 G_{\pm \mathrm{n}} b \alpha_{\mathrm{n}} \mathrm{n}^{-2},$$

$$(\mathrm{Re}K_{xy})_{\pm \mathrm{n}} = -\left(\frac{\Pi_j}{\omega}\right)^2 G_{\pm \mathrm{n}} (\pm\alpha_{\mathrm{n}}),$$

$$(\mathrm{Re}K_{yz})_{\pm \mathrm{n}} = -\left(\frac{\Pi_j}{\omega}\right)^2 (2b)^{1/2} \zeta_{\pm \mathrm{n}} G_{\pm \mathrm{n}} \alpha_{\mathrm{n}} \mathrm{n}^{-1},$$

$$(\mathrm{Im}K_{xz})_{\pm \mathrm{n}} = -\left(\frac{\Pi_j}{\omega}\right)^2 (2b)^{1/2} \zeta_{\pm \mathrm{n}} G_{\pm \mathrm{n}} (\pm\alpha_{\mathrm{n}}) \mathrm{n}^{-1},$$

$$\alpha_{\mathrm{n}} = \mathrm{n}^2 (2 \cdot \mathrm{n}!)^{-1} \left(\frac{b}{2}\right)^{\mathrm{n}-1}.$$

The contribution of these terms to the absorbed power (12.17) is

$$P_{\pm \mathrm{n}}^{\mathrm{ab}} = \omega \left(\frac{\Pi_j}{\omega}\right)^2 G_{\mathrm{n}} \left(\frac{\epsilon_0}{2}\right) \alpha_{\mathrm{n}} |E_x \pm i E_y|^2. \tag{12.24}$$

Since

$$\zeta_{\mathrm{n}} = (\omega + \mathrm{n}\Omega_{\mathrm{i}})/(2^{1/2} k_z v_{\mathrm{Ti}}) = (\omega - \mathrm{n}|\Omega_{\mathrm{i}}|)/(2^{1/2} k_z v_{\mathrm{Ti}})$$

the term of $+\mathrm{n}$ is dominant for the *ion cyclotron damping* ($\omega > 0$), and the term of $-\mathrm{n}$ is dominant for *electron cyclotron damping* ($\omega > 0$), since

$$\zeta_{-\mathrm{n}} = (\omega - \mathrm{n}\Omega_{\mathrm{e}})/(2^{1/2} k_z v_{\mathrm{Te}}).$$

The relative ratio of $\boldsymbol{E}$ components can be estimated from the following equations:

$$\begin{aligned}
&(K_{xx} - N_\parallel^2)E_x + K_{xy}E_y + (K_{xz} + N_\perp N_\parallel)E_z = 0, \\
&-K_{xy}E_x + (K_{yy} - N_\parallel^2 - N_\perp^2)E_y + K_{yz}E_z = 0, \\
&(K_{xz} + N_\perp N_\parallel)E_x - K_{yz}E_y + (K_{zz} - N_\perp^2)E_z = 0.
\end{aligned} \tag{12.25}$$

For cold plasmas, $K_{xx} \to K_\perp$, $K_{yy} \to K_\perp$, $K_{zz} \to K_\parallel$, $K_{xy} \to -iK_\times$, $K_{xz} \to 0$, $K_{yz} \to 0$ can be substituted into (12.25), and the relative ratio is $E_x : E_y : E_z = (K_\perp - N^2) \times (K_\parallel - N_\perp^2) : -iK_x(K_\parallel - N_\perp^2) : -N_\parallel N_\perp (K_\perp - N^2)$.

In order to obtain the magnitude of the electric field, it is necessary to solve the Maxwell equation with the dielectric tensor of (12.19). In this case the density, the temperature, and the magnetic field are functions of the coordinates. Therefore the simplified model must be used for analytical solutions; otherwise numerical calculations are necessary to derive the wave field.

12.4 Wave Heating in Ion Cyclotron Range of Frequency

The dispersion relation of waves in the ion cyclotron range of frequency (ICRF) is given by (10.64);

$$N_\parallel^2 = \frac{N_\perp^2}{2[1-(\omega/\Omega_\mathrm{i})^2]}\left(-\left(1-\left(\frac{\omega}{\Omega_\mathrm{i}}\right)^2\right)+\frac{2\omega^2}{k_\perp^2 v_\mathrm{A}^2} \pm \left[\left(1-\left(\frac{\omega}{\Omega_\mathrm{i}}\right)^2\right)^2 + 4\left(\frac{\omega}{\Omega_\mathrm{i}}\right)^2\left(\frac{\omega}{k_\perp v_\mathrm{A}}\right)^4\right]^{1/2}\right).$$

The plus sign corresponds to the slow wave (L wave, ion cyclotron wave), and the minus sign corresponds to the fast wave (R wave, extraordinary wave). When $1 - \omega^2/\Omega_\mathrm{i}^2 \ll 2(\omega/k_\perp v_\mathrm{A})^2$, the dispersion relation becomes

$$k_z^2 = 2\left(\frac{\omega^2}{v_\mathrm{A}^2}\right)\left(1-\frac{\omega^2}{\Omega_\mathrm{i}^2}\right)^{-1}, \quad \text{(for slow wave)}$$

$$k_z^2 = -\frac{k_\perp^2}{2} + \frac{\omega^2}{2v_\mathrm{A}^2}. \quad \text{(for fast wave)}$$

Since the externally excited waves have propagation vectors with $0 < k_z^2 < (1/a)^2$, $k_\perp^2 > (\pi/a)^2$ usually, there are constraints

$$\frac{\omega^2}{v_\mathrm{A}^2}\frac{2}{(1-\omega^2/\Omega_\mathrm{i}^2)} < \left(\frac{\pi}{a}\right)^2,$$

$$n_{20}a^2 < 2.6\times 10^{-4}\frac{B^2(1-\omega^2/\Omega_\mathrm{i}^2)}{A}$$

for slow wave and

$$\frac{\omega^2}{2v_\mathrm{A}^2} > \left(\frac{\pi}{a}\right)^2,$$

$$n_{20}a^2 > 0.5\times 10^{-2}\frac{(\Omega_\mathrm{i}/\omega)^2}{A/Z^2}$$

for the fast wave (ref.[3]), where n_{20} is the ion density in $10^{20}\,\mathrm{m}^{-3}$, a is the plasma radius in meters, and A is the atomic number.

An ion cyclotron wave (slow wave) can be excited by a Stix coil (ref.[1]) and can propagate and heat ions in a low-density plasma. But it cannot propagate in a high-density plasma like that of a tokamak.

The fast wave is an extraordinary wave in this frequency range and can be excited by a loop antenna, which generates a high-frequency electric field perpendicular to the magnetic field (see sec.10.2). The fast wave can propagate in a high-density plasma. The fast wave in a plasma with a single ion species has $E_x + iE_y = 0$ at $\omega = |\Omega_\mathrm{i}|$ in cold plasma approximation, so that it is not absorbed by the ion cyclotron damping. However, the electric field of the fast wave in a plasma

with two ion species is $E_x + iE_y \neq 0$, so that the fast wave can be absorbed; that is, the fast wave can heat the ions in this case.

Let us consider the heating of a plasma with two ion species, M and m, by a fast wave. The masses, charge numbers, and densities of the M ion and m ion are denoted by $m_{\rm M}$, $Z_{\rm M}$, $n_{\rm M}$ and $m_{\rm m}$, $Z_{\rm m}$, $n_{\rm m}$, respectively. When we use

$$\eta_{\rm M} \equiv \frac{Z_{\rm M}^2 n_{\rm M}}{n_{\rm e}}, \qquad \eta_{\rm m} \equiv \frac{Z_{\rm m}^2 n_{\rm m}}{n_{\rm e}}$$

we have $\eta_{\rm M}/Z_{\rm M} + \eta_{\rm m}/Z_{\rm m} = 1$ since $n_{\rm e} = Z_{\rm M} n_{\rm M} + Z_{\rm m} n_{\rm m}$. Since $(\Pi_{\rm e}/\omega)^2 \gg 1$ in ICRF wave, the dispersion relation in the cold plasma approximation is given by (10.64) as follows:

$$N_\perp^2 = \frac{(R - N_\parallel^2)(L - N_\parallel^2)}{K_\perp - N_\parallel^2},$$

$$R = -\frac{\Pi_{\rm i}^2}{\omega^2}\left(\frac{(m_{\rm M}/m_{\rm m})\eta_{\rm m}\omega}{\omega + |\Omega_{\rm m}|} + \frac{\eta_{\rm M}\omega}{\omega + |\Omega_{\rm M}|} - \frac{\omega}{|\Omega_{\rm M}|/Z_{\rm M}}\right),$$

$$L = -\frac{\Pi_{\rm i}^2}{\omega^2}\left(\frac{(m_{\rm M}/m_{\rm m})\eta_{\rm m}\omega}{\omega - |\Omega_{\rm m}|} + \frac{\eta_{\rm M}\omega}{\omega - |\Omega_{\rm M}|} + \frac{\omega}{|\Omega_{\rm M}|/Z_{\rm M}}\right),$$

$$K_\perp = -\frac{\Pi_{\rm i}^2}{\omega^2}\left(\frac{(m_{\rm M}/m_{\rm m})\eta_{\rm m}\omega^2}{\omega^2 - \Omega_{\rm m}^2} + \frac{\eta_{\rm M}\omega^2}{\omega^2 - \Omega_{\rm M}^2}\right),$$

$$\Pi_{\rm i}^2 \equiv \frac{n_{\rm e} e^2}{\epsilon_0 m_{\rm M}}.$$

Therefore ion-ion hybrid resonance occurs at $K_\perp - N_\parallel^2 = 0$, that is,

$$\frac{\eta_{\rm m}(m_{\rm M}/m_{\rm m})\omega^2}{\omega^2 - \Omega_{\rm m}^2} + \frac{\eta_{\rm M}\omega^2}{\omega^2 - \Omega_{\rm M}^2} \approx -\frac{\omega^2}{\Pi_{\rm i}^2} N_\parallel^2 \approx 0,$$

$$\omega^2 \approx \omega_{\rm IH} \equiv \frac{\eta_{\rm M} + \eta_{\rm m}(\mu^2/\mu')}{\eta_{\rm M} + \eta_{\rm m}/\mu'}\Omega_{\rm m}^2,$$

$$\mu' \equiv \frac{m_{\rm m}}{\rm m_M}, \quad \mu \equiv \frac{\Omega_{\rm M}}{\Omega_{\rm m}} = \frac{m_{\rm m} Z_{\rm M}}{m_{\rm M} Z_{\rm m}}.$$

Figure 12.4 shows the ion-ion hybrid resonance layer; $K_\perp - N_\parallel^2 = 0$, the L cutoff layer; $L - N_\parallel^2 = 0$, and R cutoff layer; $R - N_\parallel^2 = 0$, of a tokamak plasma with the two ion species D^+ (M ion) and H^+ (m ion). Since the K_{zz} component of the dielectric tensor is much larger than the other component, even in a hot plasma, the dispersion relation of a hot plasma is (ref.[4])

$$\begin{vmatrix} K_{xx} - N_\parallel^2 & K_{xy} \\ -K_{xy} & K_{yy} - N_\parallel^2 - N_\perp^2 \end{vmatrix} = 0. \tag{12.26}$$

When we use the relation $K_{yy} \equiv K_{xx} + \Delta K_{yy}$, $|\Delta K_{yy}| \ll |K_{xx}|$,

$$N_\perp^2 = \frac{(K_{xx} - N_\parallel^2)(K_{xx} + \Delta K_{yy} - N_\parallel^2) + K_{xy}^2}{K_{xx} - N_\parallel^2}$$

$$\approx \frac{(K_{xx} + iK_{xy} - N_\parallel^2)(K_{xx} - iK_{xy} - N_\parallel^2)}{K_{xx} - N_\parallel^2}.$$

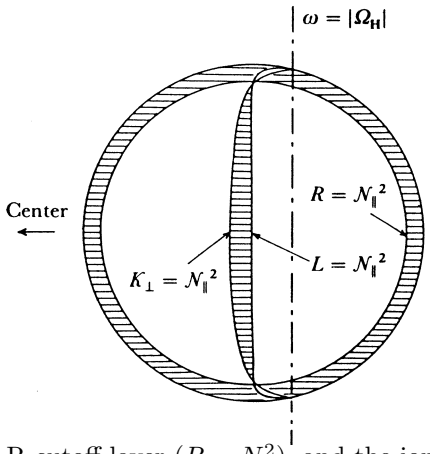

Fig.12.4 L cutoff layer($L = N_\parallel^2$), R cutoff layer ($R = N_\parallel^2$), and the ion-ion hybrid resonance layer ($K_\perp = N_\parallel^2$) of ICRF wave in a tokamak with two ion components D^+, H^+. The shaded area is the region of $N_\perp^2 < 0$.

When ω^2 is near ω_{IH}^2, K_{xx} is given by

$$K_{xx} = -\frac{\Pi_i^2}{\omega^2}\left(\frac{m_M}{2m_m}\eta_m\zeta_0 Z(\zeta_1) + \frac{\eta_M\omega^2}{\omega^2 - \Omega_M^2}\right).$$

The resonance condition is $K_{xx} = N_\parallel^2$. The value of $Z(\zeta_1)$ that appears in the dispersion equation is finite and $0 > Z(\zeta_1) > -1.08$. The condition

$$\eta_m \geq \eta_{cr} \equiv \frac{2}{1.08}\frac{m_m}{m_M}2^{1/2}N_\parallel\frac{v_{Ti}}{c}\left(\frac{\eta_M\omega^2}{\omega^2 - \Omega_M^2} + N_\parallel^2\frac{\omega^2}{\Pi_i^2}\right)$$

is necessary to obtain the resonance condition. This point is different from the cold plasma dispersion equation (note the difference between K_{xx} and $K_\perp$).

It is deduced from the dispersion equation (12.26) that the mode conversion (ref.[4]) from the fast wave to the ion Berstein wave occurs at the resonance layer when $\eta_m \geq \eta_{cr}$. When the L cutoff layer and the ion-ion hybrid resonance layer are close to each other, as shown in fig.12.4, the fast wave propagating from the outside torus penetrates the L cutoff layer partly by the tunneling effect and is converted to the ion Bernstein wave. The mode converted wave is absorbed by ion cyclotron damping or electron Landau damping. The theory of mode conversion is described in chapter 10 of (ref.[1]). ICRF experiments related to this topic were carried out in TFR.

When $\eta_m < \eta_{cr}$, $K_\perp = N_\parallel^2$ cannot be satisfied and the ion-ion hybrid resonance layer disappears. In this case a fast wave excited by the loop antenna outside the torus can pass through the R cutoff region (because the width is small) and is reflected by the L cutoff layer and bounced back and forth in the region surrounded by $R = N_\parallel^2$ and $L = N_\parallel^2$. In this region, there is a layer satisfying $\omega = |\Omega_m|$, and the minority m ions are heated by the fundamental ion cyclotron damping. The majority M ions are heated by the Coulomb collisions with m ions. If the mass of M ions is l times as large as the mass of m ions, the M ions are also heated by the lth harmonic ion cyclotron damping. This type of experiment was carried out in PLT with good heating efficiency. This is called *minority heating*. The absorption power P_{e0} due to electron Landau damping per unit volume is given by (12.23), and it is important only in the case $\zeta_0 \leq 1$. In this case we have $E_y/E_z \approx K_{zz}/K_{yz} \approx 2\zeta_0^2/(2^{1/2}b^{1/2}\zeta_0(-i))$ and P_{e0} is (ref.[5])

$$P_{e0} = \frac{\omega\epsilon_0}{4}|E_y|^2\left(\frac{\Pi_e}{\omega}\right)^2\left(\frac{k_\perp v_{Te}}{\Omega_e}\right)^2 2\zeta_{0e}\pi^{1/2}\exp(-\zeta_{0e}^2). \tag{12.27}$$

The absorption power P_{in} by the n-th harmonic ion cyclotron damping is given by (12.24) as follows;

$$P_{in} = \frac{\omega\epsilon_0}{2}|E_x + iE_y|^2\left(\frac{\Pi_i}{\omega}\right)^2\left(\frac{n^2}{2\times n!}\right)\left(\frac{b}{2}\right)^{n-1} \times \frac{\omega}{2^{1/2}k_z v_{Ti}}\pi^{1/2}\exp\left(-\frac{(\omega - n|\Omega_i|)^2}{2(k_z v_{Ti})^2}\right). \tag{12.28}$$

The absorption power due to the second harmonic cyclotron damping is proportional to the beta value of the plasma. In order to evaluate the absorption power by (12.27) and (12.28), we need the spatial distributions of E_x and E_y. They can be calculated in the simple case of a sheet model (ref.[6]).

In the range of the higher harmonic ion cyclotron frequencies ($\omega \sim 2\Omega_\mathrm{i}, 3\Omega_\mathrm{i}$), the direct excitation of the ion Bernstein wave has been studied by an external antenna or waveguide, which generates a high-frequency electric field parallel to the magnetic field (ref.[7]).

12.5 Lower Hybrid Wave Heating

Since $|\Omega_\mathrm{i}| \ll \Pi_\mathrm{i}$ in a tokamak plasma ($n_\mathrm{e} \geq 10^{13}, \mathrm{cm}^{-3}$), the lower hybrid resonance frequency becomes

$$\omega_\mathrm{LH}^2 = \frac{\Pi_\mathrm{i}^2 + \Omega_\mathrm{i}^2}{1 + \Pi_\mathrm{e}^2/\Omega_\mathrm{e}^2 + Zm_\mathrm{e}/m_\mathrm{i}} \approx \frac{\Pi_\mathrm{i}^2}{1 + \Pi_\mathrm{e}^2/\Omega_\mathrm{e}^2}.$$

There are relations $\Omega_\mathrm{e} \gg \omega_\mathrm{LH} \gg |\Omega_\mathrm{i}|$, $\Pi_\mathrm{i}^2/\Pi_\mathrm{e}^2 = |\Omega_\mathrm{i}|/\Omega_\mathrm{e}$. For a given frequency ω, lower hybrid resonance $\omega = \omega_\mathrm{LH}$ occurs at the position where the electron density satisfies the following condition:

$$\frac{\Pi_\mathrm{e}^2(x)}{\Omega_\mathrm{e}^2} = \frac{\Pi_\mathrm{res}^2}{\Omega_\mathrm{e}^2} \equiv p, \qquad p = \frac{\omega^2}{\Omega_\mathrm{e}|\Omega_\mathrm{i}| - \omega^2}.$$

When the dispersion equation (10.20) of cold plasma is solved about $N_\perp^2$ using $N^2 = N_\parallel^2 + N_\perp^2$, we have

$$N_\perp^2 = \frac{K_\perp \widetilde{K}_\perp - K_\times^2 + K_\parallel \widetilde{K}_\perp}{2K_\perp} \pm \left[\left(\frac{K_\perp \widetilde{K}_\perp - K_\times^2 + K_\parallel \widetilde{K}_\perp}{2K_\perp} \right)^2 + \frac{K_\parallel}{K_\perp}(K_\times^2 - \widetilde{K}_\perp^2) \right]^{1/2},$$

where $\widetilde{K}_\perp = K_\perp - N_\parallel^2$. The relations $h(x) \equiv \Pi_\mathrm{e}^2(x)/\Pi_\mathrm{res}^2$, $K_\perp = 1 - h(x)$, $K_\times = ph(x)\Omega_\mathrm{e}/\omega$, $K_\parallel = 1 - \beta_\Pi h(x)$, $\beta_\Pi \equiv \Pi_\mathrm{res}^2/\omega^2 \sim O(m_\mathrm{i}/m_\mathrm{e})$, $\alpha \equiv \Pi_\mathrm{res}^2/(\omega\Omega_\mathrm{e}) \sim O(m_\mathrm{i}/m_\mathrm{e})^{1/2}$ and $\beta_\Pi h \gg 1$ reduce this to

$$N_\perp^2(x) = \frac{\beta_\Pi h}{2(1-h)} \left(N_\parallel^2 - (1 - h + ph) \pm \left[(N_\parallel^2 - (1 - h + ph))^2 - 4(1-h)ph \right]^{1/2} \right). \tag{12.29}$$

The slow wave corresponds to the case of the plus sign in (12.29). In order for the slow wave to propagate from the plasma edge with low density ($h \ll 1$) to the plasma center with high density ($\Pi_\mathrm{e}^2 = \Pi_\mathrm{res}^2$, $h = 1$), $N_\perp(x)$ must real. Therefore following condition

$$N_\parallel > (1-h)^{1/2} + (ph)^{1/2}$$

is necessary. The right-hand side of the inequality has the maximum value $(1+p)^{1/2}$ in the range $0 < h < 1$, so that the accessibility condition of the resonant region to the lower hybrid wave becomes

$$N_\parallel^2 > N_{\parallel,\mathrm{cr}}^2 = 1 + p = 1 + \frac{\Pi_\mathrm{res}^2}{\Omega_\mathrm{e}^2}. \tag{12.30}$$

If this condition is not satisfied, the externally excited slow wave propagates into the position where the square root term in (12.29) becomes zero and transforms to the fast wave there. Then the fast wave returns to the low-density region (refer to fig.12.5). The slow wave that satisfies the accessibility condition can approach the resonance region and $N_\perp$ can become large, so that the dispersion relation of hot plasma must be used to examine the behavior of this wave. Near the lower hybrid resonance region, the approximation of the electrostatic wave, (13.1) or (C.36), is applicable. Since $|\Omega_\mathrm{i}| \ll \omega \ll \Omega_\mathrm{e}$, the terms of ion contribution and electron contribution are given by (13.3) and (13.4), respectively, that is,

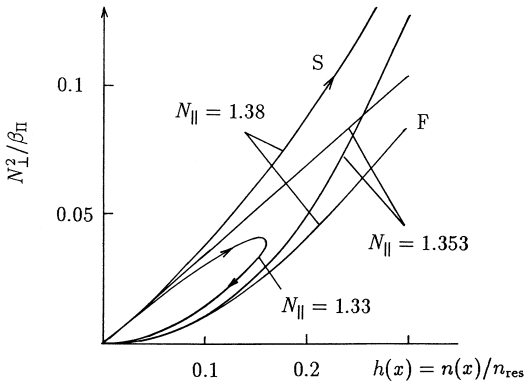

Fig.12.5 Trace of lower hybrid wave in $N_\perp^2 - h(x)\,(= \Pi_e^2(x)/\Pi_{res}^2)$ diagram for the case of $p = 0.353$, $N_{\parallel cr}^2 = 1 + p = 1.353$. This corresponds to the case of H^+ plasma in $B = 3\,\mathrm{T}$, and $f = \omega/2\pi = 10^9\,\mathrm{Hz}$. The electron density for the parameter $\beta_\Pi = 7.06 \times 10^3$ $(= \Pi_{res}^2/\omega^2)$ is $n_{res} = 0.31 \times 10^{20}\,\mathrm{m}^{-3}$.

$$1 + \frac{\Pi_e^2}{k^2}\frac{m_e}{T_e}(1 + I_0 e^{-b}\zeta_0 Z(\zeta_0)) + \frac{\Pi_i^2}{k^2}\frac{m_i}{T_i}(1 + \zeta Z(\zeta)) = 0,$$

where $\zeta_0 = \omega/(2^{1/2}k_z v_{Te})$, and $\zeta = \omega/(2^{1/2}k v_{Ti}) \approx \omega/(2^{1/2}k_\perp v_{Ti})$. Since $I_0 e^{-b} \approx 1 - b + (3/4)b^2$, $\zeta_0 \gg 1$, $\zeta \gg 1$, $1 + \zeta Z(\zeta) \approx -(1/2)\zeta^{-2} - (3/4)\zeta^{-4}$, we have

$$\left(\frac{3\Pi_i^2}{\omega^4}\frac{\kappa T_i}{m_i} + \frac{3}{4}\frac{\Pi_e^2}{\Omega_e^4}\frac{\kappa T_e}{m_e}\right)k_\perp^4 - \left(1 + \frac{\Pi_e^2}{\Omega_e^2} - \frac{\Pi_i^2}{\omega^2}\right)k_\perp^2 - \left(1 - \frac{\Pi_e^2}{\omega^2}\right)k_z^2 = 0. \tag{12.31}$$

Using the notations $\rho_i = v_{Ti}/|\Omega_i|$ and

$$s^2 \equiv 3\left(\frac{|\Omega_e\Omega_i|}{\omega^2} + \frac{1}{4}\frac{T_e}{T_i}\frac{\omega^2}{|\Omega_e\Omega_i|}\right) = 3\left(\frac{1+p}{p} + \frac{1}{4}\frac{T_e}{T_i}\frac{p}{1+p}\right),$$

we have

$$\left(\frac{3\Pi_i^2}{\omega^4}\frac{\kappa T_i}{m_i} + \frac{3}{4}\frac{\Pi_e^2}{\Omega_e^4}\frac{\kappa T_e}{m_e}\right) = \frac{\Pi_i^2}{\omega^2}\frac{m_e}{m_i}\frac{v_{Ti}^2 s^2}{\Omega_i}$$

$$\left(1 + \frac{\Pi_e^2}{\Omega_e^2} - \frac{\Pi_i^2}{\omega^2}\right) = \frac{1}{1+p}\frac{1-h}{h}\frac{\Pi_i^2}{\omega^2}$$

Then the dimensionless form of (12.31) is

$$(k_\perp\rho_i)^4 - \frac{1-h}{h}\frac{m_i}{m_e}\frac{1}{(1+p)s^2}(k_\perp\rho_i)^2 + \left(\frac{m_i}{m_e}\right)^2\frac{1}{s^2}(k_z\rho_i)^2 = 0. \tag{12.32}$$

This dispersion equation has two solutions. One corresponds to the slow wave in a cold plasma and the other to the plasma wave in a hot plasma. The slow wave transforms to the plasma wave at the location where (12.31) or (12.32) has equal roots (ref.[8]-[10]). The condition of zero discriminant is $1/h = 1 + 2k_z\rho_i(1+p)s$ and

$$\frac{\Pi_e^2(x)}{\Omega_e^2} = \frac{\Pi_{M.C.}^2}{\Omega_e^2} \equiv \frac{p}{1 + 2k_z\rho_i(1+p)s}.$$

Accordingly, the mode conversion occurs at the position satisfying

$$\frac{\omega^2}{\Pi_i^2} = \left(1 - \frac{\omega^2}{|\Omega_i|\Omega_e}\right) + \frac{N_\parallel v_{Te} 2\sqrt{3}}{c}\left(\frac{T_i}{T_e} + \frac{1}{4}\left(\frac{\omega^2}{\Omega_i\Omega_e}\right)^2\right)^{1/2}$$

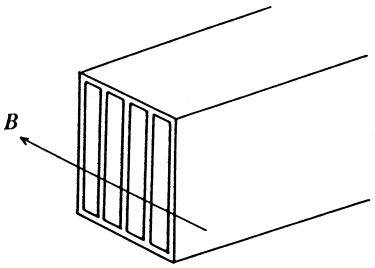

Fig.12.6 Array of waveguides to excite a lower hybrid wave (slow wave).

and the value of $k_\perp^2 \rho_\mathrm{i}^2$ at this position becomes

$$k_\perp^2 \rho_\mathrm{i}^2|_{\mathrm{M.C.}} = \frac{m_\mathrm{i}}{m_\mathrm{e}} \frac{k_z \rho_\mathrm{i}}{s}.$$

If the electron temperature is high enough at the plasma center to satisfy $v_\mathrm{Te} > (1/3)c/N_\parallel$, the wave is absorbed by electrons due to electron Landau damping.

After the mode conversion, the value $N_\perp$ becomes large so that $c/N_\perp$ becomes comparable to the ion thermal velocity ($c/N_\perp \sim v_\mathrm{Ti}$). Since $\omega \gg |\Omega_\mathrm{i}|$, the ion motion is not affected by the magnetic field within the time scale of ω^{-1}. Therefore the wave with phase velocity c/N is absorbed by ions due to ion Landau damping. When ions have velocity v_i larger than $c/N_\perp$ ($v_\mathrm{i} > c/N_\perp$), the ions are accelerated or decelerated at each time satisfying $v_\mathrm{i} \cos(\Omega_\mathrm{i} t) \approx c/N_\perp$ and are subjected to stochastic heating.

The wave is excited by the array of waveguides, as shown in fig.12.6, with an appropriate phase difference to provide the necessary parallel index $N_\parallel = k_z c/\omega = 2\pi c/(\lambda_z \omega)$. In the low-density region at the plasma boundary, the component of the electric field parallel to the magnetic field is larger for the slow wave than for the fast wave. Therefore the direction of wave-guides is arranged to excite the electric field parallel to the line of magnetic force. The coupling of waves to plasmas is discussed in detail in (ref.[11]) and the experiments of LHH are reviewed in (ref.[12]).

For the current drive by lower hybrid wave, the accessibility condition (12.30) and $c/N_\parallel \gg v_\mathrm{Te}$ are necessary. If the electron temperature is high and $\kappa T_\mathrm{e} \sim 10\,\mathrm{keV}$, then v_Te/c is already $\sim 1/7$. Even if $N_\parallel$ is chosen to be small under the accessibility condition, (12.30), the wave is subjected to absorbtion by electron damping in the outer part of the plasma, and it can not be expected that the wave can propagate into the central part of the plasma.

When the value of $N_\parallel$ is chosen to be $N_\parallel \sim (1/3)(c/v_\mathrm{Te})$, electron heating can be expected and has been observed experimentally. Under the condition that the mode conversion can occur, ion heating can be expected. However, the experimental results are less clear than those for electron heating.

12.6 Electron Cyclotron Heating

The dispersion relation of waves in the electron cyclotron range of frequency in a cold plasma is given by (10.79). The plus and minus signs in (10.79) correspond to ordinary and extraordinary waves, respectively. The ordinary wave can propagate only when $\omega^2 > \Pi_\mathrm{e}^2$ as is clear from (10.86) (in the case of $\theta = \pi/2$). This wave can be excited by an array of waveguides, like that used for lower hybrid waves (fig.12.6), which emits an electric field parallel to the magnetic field. The phase of each waveguide is selected to provide the appropriate value of the parallel index $N_\parallel = k_z c/\omega = 2\pi c/(\omega \lambda_z)$.

The dispersion relation of the extraordinary wave is given by (10.87). When $\theta = \pi/2$, it is given by (10.52). It is necessary to satisfy $\omega_\mathrm{UH}^2 > \omega^2 > \omega_\mathrm{L}^2, \omega_\mathrm{LH}^2$. As is seen from the CMA diagram of fig.10.5, the extraordinary wave can access the plasma center from the high magnetic field side (see fig.12.7) but can not access from the low field side because of $\omega = \omega_\mathrm{R}$ cutoff. The extraordinary wave can be excited by the waveguide, which emits an electric field perpendicular to the magnetic field (see sec.10.2a).

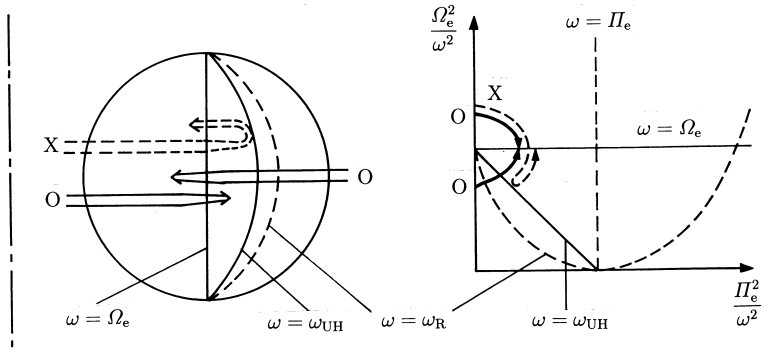

Fig.12.7 The locations of electron cyclotron resonance ($\omega = \Omega_e$), upperhybrid resonance ($\omega = \omega_{LH}$) and R cut off ($\omega = \omega_R$) in case of $\Omega_{e0} > \Pi_{e0}$, where Ω_{e0} and Π_{e0} are electron cyclotron resonance frequency and plasma frequency at the plasma center respectively (left-hand side figure). The right-hand side figure is the CMA diagram near electron cyclotron frequency region.

The ion's contribution to the dielectric tensor is negligible. When relations $b \ll 1$, $\zeta_0 \gg 1$ are satisfied for electron, the dielectric tensor of a hot plasma is

$$K_{xx} = K_{yy} = 1 + X\zeta_0 Z_{-1}/2, \qquad K_{zz} = 1 - X + N_\perp^2 \chi_{zz},$$

$$K_{xy} = -iX\zeta_0 Z_{-1}/2, \qquad K_{xz} = N_\perp \chi_{xz}, \qquad K_{yz} = iN_\perp \chi_{yz},$$

$$\chi_{xz} \approx \chi_{yz} \approx 2^{-1/2} XY^{-1} \frac{v_T}{c} \zeta_0 (1 + \zeta_{-1} Z_{-1}),$$

$$\chi_{zz} \approx XY^{-2} \left(\frac{v_T}{c}\right)^2 \zeta_0 \zeta_{-1} (1 + \zeta_{-1} Z_{-1}),$$

$$X \equiv \frac{\Pi_e^2}{\omega^2}, \qquad Y \equiv \frac{\Omega_e}{\omega}, \qquad \zeta_{-1} = \frac{\omega - \Omega_e}{2^{1/2} k_z v_T}, \qquad N_\perp = \frac{k_\perp c}{\omega}.$$

The Maxwell equation is

$$(K_{xx} - N_\parallel^2) E_x + K_{xy} E_y + N_\perp (N_\parallel + \chi_{xz}) E_z = 0,$$

$$-K_{xy} E_x + (K_{yy} - N_\parallel^2 - N_\perp^2) E_y + iN_\perp \chi_{yz} E_z = 0,$$

$$N_\perp (N_\parallel + \chi_{xz}) E_x - iN_\perp \chi_{yz} E_y + (1 - X - N_\perp^2 (1 - \chi_{zz})) E_z = 0.$$

The solution is

$$\frac{E_x}{E_z} = -\frac{iN_\perp^2 \chi_{xz} (N_\parallel + \chi_{xz}) + K_{xy} (1 - X - N_\perp^2 (1 - \chi_{zz}))}{N_\perp (i\chi_{xz} (K_{xx} - N_\parallel^2) + K_{xy} (N_\parallel + \chi_{xz}))},$$

$$\frac{E_y}{E_z} = -\frac{N_\perp^2 (N_\parallel + \chi_{xz})^2 - (K_{xx} - N_\parallel^2)(1 - X - N_\perp^2 (1 - \chi_{zz}))}{N_\perp (i\chi_{xz} (K_{xx} - N_\parallel^2) + K_{xy} (N_\parallel + \chi_{xz}))}.$$

The absorption power P_{-1} per unit volume is given by (12.24) as follows:

$$P_{-1} = \omega X \zeta_0 \frac{\pi^{1/2}}{2} \exp\left(-\frac{(\omega - \Omega_e)^2}{2k_z^2 v_{Te}^2}\right) \frac{\epsilon_0}{2} |E_x - iE_y|^2.$$

When $\omega = \Omega_e$, then $\zeta_{-1} = 0$, $Z_{-1} = i\pi^{1/2}$, $K_{xx} = 1 + ih$, $K_{xy} = h$, $\chi_{yz} = \chi_{xz} = 2^{1/2}X(v_{Te}/c)\zeta_0 = X/(2N_\parallel)$, $\chi_{zz} = 0$, $h \equiv \pi^{1/2}\zeta_0 X/2$. Therefore the dielectric tensor $\boldsymbol{K}$ becomes

$$\boldsymbol{K} = \begin{bmatrix} 1+ih & h & N_\perp\chi_{xz} \\ -h & 1+ih & iN_\perp\chi_{xz} \\ N_\perp\chi_{xz} & -iN_\perp\chi_{xz} & 1-X \end{bmatrix}.$$

For the ordinary wave (O wave), we have

$$\frac{E_x - iE_y}{E_z} = \frac{iN_\perp^2(\mathrm{O})N_\parallel(N_\parallel + \chi_{xz}) - i(1-N_\parallel^2)(1-X-N_\perp^2(\mathrm{O}))}{N_\perp(\mathrm{O})(N_\parallel h + i\chi_{xz}(1-N_\parallel^2))}.$$

When $N_\parallel \ll 1$ and the incident angle is nearly perpendicular, (10.82) gives $1 - X - N_\perp^2(\mathrm{O}) = (1-X)N_\parallel^2$. Since $\chi_{xz} = X/2N_\parallel$, $\chi_{xz} \gg N_\parallel$. Therefore the foregoing equation reduces to

$$\frac{E_x - iE_y}{E_z} = \frac{iN_\perp(\mathrm{O})N_\parallel\chi_{xz}}{N_\parallel h + i\chi_{xz}}.$$

For extraordinary wave (X wave), we have

$$\frac{E_x - iE_y}{E_y} = -\frac{iN_\perp^2(\mathrm{X})N_\parallel(N_\parallel + \chi_{xz}) - i(1-N_\parallel^2)(1-X-N_\perp^2(\mathrm{X}))}{N_\perp^2(\mathrm{X})(N_\parallel + \chi_{xz})^2 - (K_{xx} - N_\parallel^2)(1-X-N_\perp^2(\mathrm{X}))}.$$

When $N_\parallel \ll 1$ and $\omega = \Omega_e$, (10.83) gives $1 - X - N_\perp^2(\mathrm{X}) \approx -1 + N_\parallel^2$. Since $\chi_{xz}^2 = (2\pi)^{-1/2}(v_{Te}/cN_\parallel)Xh \ll h$, the foregoing equation reduces to

$$\frac{E_x - iE_y}{E_y} = \frac{-(1 + N_\perp^2(\mathrm{X})N_\parallel(N_\parallel + \chi_{xz}))}{h - i(1 + N_\perp^2(\mathrm{X})(N_\parallel + \chi_{xz})^2)} \sim \frac{-1}{h}.$$

The absorption power per unit volume at $\omega = \Omega_e$ is

$$P_{-1}(\mathrm{O}) \approx \frac{\omega\epsilon_0}{2}|E_z|^2 \frac{hN_\perp^2(\mathrm{O})N_\parallel^2\chi_{xz}^2}{(N_\parallel h)^2 + \chi_{xz}^2}\exp(-\zeta_{-1}^2)$$

$$\approx \frac{\omega\epsilon_0}{2}|E_z|^2 \frac{1}{(2\pi)^{1/2}}\left(\frac{\Pi_e}{\omega}\right)^2\left(\frac{v_{Te}}{cN_\parallel}\right)\frac{N_\perp^2(\mathrm{O})N_\parallel^2}{N_\parallel^2 + (v_{Te}/c)^2(2/\pi)}$$

for ordinary wave and

$$P_{-1}(\mathrm{X}) \sim \frac{\omega\epsilon_0}{2}|\mathrm{E_y}|^2\frac{1}{\mathrm{h}} = \frac{\omega\epsilon_0}{2}|\mathrm{E_y}|^2 2\left(\frac{2}{\pi}\right)^{1/2}\left(\frac{\Pi_e}{\omega}\right)^{-2}\left(\frac{\mathrm{N_\parallel v_{Te}}}{\mathrm{c}}\right).$$

for extraordinary wave (ref.[13]).

Since $P(\mathrm{O}) \propto n_e T_e^{1/2}/N_\parallel$, $P(\mathrm{X}) \propto N_\parallel T_e^{1/2}/n_e$, the ordinary wave is absorbed more in the case of higher density and perpendicular incidence, but the extraordinary wave has opposite tendency.

The experiments of electron cyclotron heating have been carried out by T-10, ISX-B, JFT-2, D-IIID, and so on, and the good heating efficiency of ECH has been demonstrated. Heating and current drive by electron cyclotron waves are reviewed in (ref.[14]).

References

[1] T. H. Stix: *The Theory of Plasma Waves*, McGraw-Hill, New York 1962.
T. H. Stix: *Waves in Plasmas*, American Institute of Physics, New York, 1992.
[2] B. D. Fried and S. D. Conte: *The Plasma Dispersion Function*, Academic Press, New York 1961.
[3] B.D.Fried and S. D. Conte: *The Plasma Dispersion Function* Academic Press, New York 1961
[4] M. Porkolab: *Fusion* (ed. by E. Teller) Vol.1, Part B, p.151, Academic Press, New York (1981).
[5] J. E. Scharer, B. D. McVey and T. K. Mau: Nucl. Fusion **17**, 297 (1977).
[6] T. H. Stix: Nucl. Fusion **15**, 737 (1975)
[7] A. Fukuyama, S.Nishiyama, K. Itoh and S.I. Itoh: Nucl. Fusion **23** 1005 (1983).
[8] M. Ono, T.Watari, R. Ando, J.Fujita *et al.*: Phys. Rev. Lett. **54**, 2339 (1985).
[9] T. H. Stix: Phys. Rev. Lett. **15**, 878 (1965).
[10] V. M. Glagolev: Plasma Phys. **14**, 301,315 (1972).
[11] M. Brambilla: Plasma Phys. **18**, 669 (1976).
[12] S. Bernabei, M. A. Heald, W. M. Hooke, R. W. Motley, F. J. Paoloni, M. Brambilla and W.D. Getty : Nucl. Fusion **17**, 929 (1977).
[13] S. Takamura: *Fundamentals of Plasma Heating*, Nagoya Univ. Press, 1986 (in Japanese).
[14] I. Fidone, G. Granata and G. Ramponi: Phys. Fluids **21**, 645 (1978).
[15] R. Pratter: Phys. Plasmas **11**, 2349 (2004).

Ch.13 Velocity Space Instabilities (Electrostatic Waves)

Besides the magnetohydrodynamic instabilities discussed in ch.8, there is another type of instabilities, caused by deviations of the velocity space distribution function from the stable Maxwell form. Instabilities which are dependent on the shape of the velocity distribution function are called *velocity space instabilities* or *microscopic instabilities*. However the distinction between microscopic and macroscopic or MHD instabilities is not always clear, and sometimes an instability belongs to both.

13.1 Dispersion Equation of Electrostatic Wave

In this chapter, the characteristics of the perturbation of electrostatic wave is described. In this case the electric field can be expressed by $\boldsymbol{E} = -\nabla\phi = -i\boldsymbol{k}\phi$. The dispersion equation of electrostatic wave is give by (sec.10.5)

$$k_x^2 K_{xx} + 2k_x k_z K_{xz} + k_z^2 K_{zz} = 0.$$

The process in derivation of dispersion equation of hot plasma will be described in details in appendix C. When the zeroth-order distribution function is expressed by

$$\begin{aligned} f_0(v_\perp, v_z) &= n_0 F_\perp(v_\perp) F_z(v_z), \\ F_\perp(v_\perp) &= \frac{m}{2\pi\kappa T_\perp} \exp\left(-\frac{m v_\perp^2}{2\kappa T_\perp}\right), \\ F_z(v_z) &= \left(\frac{m}{2n\kappa T_\perp}\right)^{1/2} \exp\left(-\frac{m v_z^2}{2\kappa T_z}\right) \end{aligned}$$

the dispersion equation is given by (C.36) as follows

$$k_x^2 + k_z^2 + \sum_{\mathrm{i,e}} \Pi^2 \frac{m}{\kappa T_z} \left(1 + \sum_{n=-\infty}^{\infty} \left(1 + \frac{T_z}{T_\perp}\frac{(-n\Omega)}{\omega_n}\right) \zeta_n Z(\zeta_n) I_n(b) e^{-b}\right) = 0 \tag{13.1}$$

where

$$\begin{aligned} &\zeta_n \equiv \frac{\omega_n}{2^{1/2} k_z v_{\mathrm{T}z}}, \qquad \omega_n \equiv \omega - k_z V + n\Omega, \\ &b = (k_x v_{\mathrm{T}\perp}/\Omega)^2, \qquad v_{\mathrm{T}z}^2 = \kappa T_z/m, \qquad v_{\mathrm{T}\perp}^2 = \kappa T_\perp/m, \\ &I_n(b) \text{ is } n\text{-th modified Bessel function} \\ &Z(\zeta) \text{ is plasma dispersion function.} \end{aligned}$$

When the frequency of the wave is much higher than cyclotron frequency ($|\omega| \gg |\Omega|$), then we find $\zeta_n \to \zeta_0,\ n\Omega \to 0,\ \sum I_n \exp(-b) = 1$, so that the dispersion equation is reduced to

$$k_x^2 + k_z^2 + \sum_{\mathrm{i,e}} \Pi^2 \frac{m}{\kappa T_z} (1 + \zeta_0 Z(\zeta_0)) = 0 \qquad (|\omega| \gg |\Omega|). \tag{13.2}$$

The dispersion equation in the case of $B = 0$ is given by

$$k^2 + \sum_{\mathrm{i,e}} \Pi^2 \frac{m}{\kappa T} (1 + \zeta Z(\zeta)) = 0. \qquad \left(\zeta = \frac{\omega - kV}{2^{1/2} k v_{\mathrm{T}}},\ \ B = 0\right) \tag{13.3}$$

When the frequency of wave is much lower than cyclotron frequency ($|\omega| \ll |\Omega|$), then we find $\zeta_n \to \infty\,(n \neq 0),\ \zeta_n Z_n \to -1$ and $\sum I_n(b) e^{-b} = 1$.

$$k_x^2 + k_z^2 + \sum_{\mathrm{i,e}} \Pi^2 \frac{m}{\kappa T_z} \left(I_0 e^{-b} (1 + \zeta_0 Z(\zeta_0)) + \frac{T_z}{T_\perp}\left(1 - I_0 e^{-b}\right)\right) = 0. \qquad (|\omega| \ll |\Omega|) \tag{13.4}$$

When the frequency of wave is much higher than cyclotron frequency or the magnetic field is very small, the dispersion equations (13.2),(13.3) are reduced to

$$k_x^2 + k_z^2 + \sum \Pi^2 \frac{m}{\kappa T_z} \left(k_z \frac{\kappa T_z}{m} \int \frac{\partial (f/n_0)}{\partial v_z} \frac{\mathrm{d}v_z}{\omega - k_z v_z} \right) = 0.$$

Partial integration gives

$$\frac{k_x^2 + k_z^2}{k_z^2} = \sum \Pi^2 \int \frac{(f/n_0)}{(\omega - k_z v_z)^2} \, \mathrm{d}v_z. \tag{13.5}$$

13.2 Two Streams Instability

The interaction between beam and plasma is important. Let us consider an excited wave in the case where the j particles drift with the velocity V_j and the spread of the velocity is zero. The distribution function is given by

$$f_i(v_z) = n_j \delta(v_z - V_j).$$

The dispersion equation of the wave propagating in the direction of the magnetic field ($k_x = 0$) is

$$1 = \sum_j \frac{\Pi_j^2}{(\omega - kV_j)^2}.$$

In the special case $\Pi_1^2 = \Pi_2^2$ ($n_1^2 q_1^2 / m_1 = n_2^2 q_2^2 / m_2$), the dispersion equation is quadratic:

$$(\omega - k\bar{V})^2 = \Pi_\mathrm{t}^2 \left(\frac{1 + 2x^2 \pm (1 + 8x^2)^{1/2}}{2} \right)$$

where

$$\Pi_\mathrm{t}^2 = \Pi_1^2 + \Pi_2^2, \qquad x = \frac{k(V_1 - V_2)}{2\Pi_\mathrm{t}}, \qquad \bar{V} = \frac{V_1 + V_2}{2}.$$

For the negative sign, the dispersion equation is

$$(\omega - k\bar{V})^2 = \Pi_\mathrm{t}^2 (-x^2 + x^3 + \cdots) \tag{13.6}$$

and the wave is unstable when $x < 1$, or

$$k^2 (V_1 - V_2)^2 < 4\Pi_\mathrm{t}^2.$$

The energy to excite this instability comes from the zeroth-order kinetic energy of beam motion. When some disturbance occurs in the beam motion, charged particles may be bunched and the electric field is induced. If this electric field acts to amplify the bunching, the disturbance grows. This instability is called *two-streams instability*.

13.3 Electron Beam Instability

Let us consider the interaction of a weak beam of velocity V_0 with a plasma which consists of cold ions and hot electrons. The dispersion equation (13.5) of a electrostatic wave with $k_x = 0$ ($E_x = E_y = 0,\ E_z \neq 0,\ \boldsymbol{B}_1 = 0$) is given by

$$K_{zz} = K_\parallel - \frac{\Pi_\mathrm{b}^2}{(\omega - kV_0)^2} = 1 - \frac{\Pi_\mathrm{i}^2}{\omega^2} - \Pi_\mathrm{e}^2 \int_{-\infty}^{\infty} \frac{f_\mathrm{e}(v_z)/n_0}{(\omega - kv_z)^2} \, \mathrm{d}v_z - \frac{\Pi_\mathrm{b}^2}{(\omega - kV_0)^2} = 0. \tag{13.7}$$

For the limit of weak beam ($\Pi_{\rm b}^2 \to 0$), the dispersion equation is reduced to $K_\parallel(\omega, k) \approx 0$, if $\omega \neq kV_0$. The dispersion equation including the effect of weak beam must be in the form of

$$\omega - kV_0 = \delta_\omega(k). \quad (\delta_\omega(k) \ll kV_0)$$

Using δ_ω^2 we reduce (13.7) to

$$\frac{\Pi_{\rm b}^2}{\delta_\omega^2} = K_\parallel(\omega = kV_0, k) + \left(\frac{\partial K_\parallel}{\partial \omega}\right)_{\omega = kV_0} \delta_\omega.$$

If $\omega = kV_0$ does not satisfy $K_\parallel = 0$, $K_\parallel \neq 0$ holds and the 2nd term in right-hand side of the foregoing equation can be neglected:

$$\frac{\Pi_{\rm b}^2}{\delta_\omega^2} = K_\parallel(\omega = kV_0, k).$$

The expression for $K_\parallel(\omega = kV_0, k)$ is

$$K_\parallel(\omega_{\rm r}) = K_{\rm R}(\omega_{\rm r}) + iK_{\rm I}(\omega_{\rm r}).$$

The $K_{\rm I}$ term is of the Laudau damping (see sec.12.3).

When the condition $\omega = kV_0$ is in a region where Landau damping is ineffective, then $|K_{\rm I}| \ll |K_{\rm R}|$ and the dispersion equation is reduced to

$$\frac{\Pi_{\rm b}^2}{(\omega - kV_0)^2} = K_{\rm R}. \tag{13.8}$$

Therefore if the condition

$$K_{\rm R} < 0 \tag{13.9}$$

is satisfied, δ_ω is imaginary and the wave is unstable. When the dielectric constant is negative, electric charges are likely to be bunched and we can predict the occurrence of this instability.

If $\omega = kV_0$ is in a region where Landau damping is effective, the condition of instability is that the wave energy density W_0 in a dispersive medium (12.6) is negative, because the absolute value of W_0 increases if $\partial W_0/\partial t$ is negative;

$$\frac{\partial W_0}{\partial t} = \frac{\partial}{\partial t}\left(\frac{\epsilon_0}{2} E_z^* \frac{\partial}{\partial \omega}(\omega K_{zz}) E_z\right) = -\frac{\omega_{\rm r}}{2}\epsilon_0 E_z^* K_{\rm I} E_z < 0.$$

When energy is lost from the wave by Landau damping, the amplitude of wave increases because the wave energy density is negative. Readers may refer to (ref.[1]) for more detailed analysis of beam-plasma interaction.

13.4 Harris Instability

When a plasma is confined in a mirror field, the particles in the loss cone ($(v_\perp/v)^2 < 1/R_{\rm m}$ $R_{\rm m}$ being mirror ratio) escape, so that anisotropy appears in the velocity-space distribution function. The temperature perpendicular to the magnetic field in the plasma heated by ion or electron cyclotron range of frequency is higher than the parallel one.

Let us consider the case where the distribution function is bi-Maxwellian. It is assumed that the density and temperature are uniform and there is no flow of particles ($V = 0$). In this case the dispersion equation (13.1) is

$$k_x^2 + k_z^2 + \sum_j \Pi_j^2 m_j \left(\frac{1}{\kappa T_z} + \sum_{l=-\infty}^{\infty} I_l(b) e^{-b}\left(\frac{1}{\kappa T_z} + \frac{1}{\kappa T_\perp}\frac{(-l\Omega)}{\omega + l\Omega}\right)\zeta_l Z(\zeta_l)\right)_j = 0, \tag{13.10}$$

$$\zeta_l = \frac{\omega + l\Omega}{(2\kappa T_z/m)^{1/2} k_z}.$$

We denote the real and imaginary parts of the right-hand side of (13.10) for real $\omega = \omega_\mathrm{r}$ by $K(\omega_\mathrm{r}) = K_\mathrm{r}(\omega_\mathrm{r}) + iK_\mathrm{i}(\omega_\mathrm{r})$. When the solution of (13.10) is $\omega_\mathrm{r} + i\gamma$, i.e., for $K(\omega_\mathrm{r} + i\gamma) = 0$, ω_r and γ are given by $K_\mathrm{r}(\omega_\mathrm{r}) = 0$, $\gamma = -K_\mathrm{i}(\omega_\mathrm{r})(\partial K_\mathrm{r}(\omega_\mathrm{r})/\partial\omega_\mathrm{r})^{-1}$ when $|\gamma| \ll |\omega_\mathrm{r}|$ and Taylor expansion is used. Accordingly we find

$$k_x^2 + k_z^2 + \sum_j \Pi_j^2 m_j \left(\frac{1}{\kappa T_z} + \frac{1}{(2\kappa T_z/m)^{1/2} k_z} \sum_{l=-\infty}^{\infty} I_l e^{-b} \left(\frac{\omega + l\Omega}{\kappa T_z} - \frac{l\Omega}{\kappa T_\perp} \right) Z_\mathrm{r}(\zeta_l) \right)_j = 0, \tag{13.11}$$

$$\gamma = -\frac{1}{A} \pi^{1/2} \sum_j \Pi_j^2 m_j \times \left(\sum_{l=-\infty}^{\infty} I_l e^{-b} \frac{1}{(2\kappa T_z/m)^{1/2} |k_z|} \left(\frac{\omega + l\Omega}{\kappa T_z} - \frac{l\Omega}{\kappa T_\perp} \right) \exp(-\zeta_l^2) \right)_j, \tag{13.12}$$

$$A = \sum_j \Pi_j^2 m_j \sum_{l=-\infty}^{\infty} \left[I_l e^{-b} \left(\frac{Z_\mathrm{r}(\zeta_l)/\kappa T_z}{(2\kappa T_z/m)^{1/2} k_z} + \frac{1}{(2\kappa T_z/m) k_z^2} \left(\frac{\omega + l\Omega}{\kappa T_z} - \frac{l\Omega}{\kappa T_\perp} \right) Z_\mathrm{r}'(\zeta_l) \right) \right]_j.$$

$Z_\mathrm{r}(\zeta_l)$ is real part of $Z(\zeta_l)$ and $Z_\mathrm{r}'(\zeta_l)$ is the derivatives by ζ_l.

Let us assume that the electron is cold ($b_\mathrm{e} \approx 0$, $|\zeta_{0\mathrm{e}}| \gg 1$) and the ion is hot. Then the contribution of the electron term is dominant in (13.11) and the ion term can be neglected. Equation (13.11) becomes

$$k^2 - \Pi_\mathrm{e}^2 \frac{k_z^2}{\omega_\mathrm{r}^2} = 0. \tag{13.13}$$

i.e.,

$$\omega_\mathrm{r} = \pm \Pi_\mathrm{e} \frac{k_z}{k}.$$

The substitution of ω_r into (13.12) yields

$$\gamma = \frac{\pi^{1/2}}{2k^2} \sum_j \Pi_j^2 \left(\frac{m}{\kappa T_z} \right)_j \frac{1}{(2\kappa T_z/m)_j^{1/2} |k_z|} \times \left(\sum_{l=-\infty}^{\infty} I_l e^{-b} \omega_\mathrm{r} \left(-(\omega_\mathrm{r} + l\Omega) + \frac{T_z}{T_\perp} l\Omega \right) \exp(-\zeta_l^2) \right)_j. \tag{13.14}$$

$\exp(-\zeta_l^2)$ has meaningful value only near $\omega_\mathrm{r} + l\Omega_\mathrm{i} = \omega_\mathrm{r} - l|\Omega_\mathrm{i}| \approx 0$. The first term in the braket of (13.14), $-(\omega_\mathrm{r} - l|\Omega_\mathrm{i}|)|$ can be destabilizing term and the 2nd term $-(T_z/T_\perp) l|\Omega_\mathrm{i}|$ is stabilizing term. Accordingly the necessary conditions for instability ($\gamma > 0$) are

$$\omega_\mathrm{r} \sim l|\Omega_\mathrm{i}|, \qquad \omega_\mathrm{r} < l|\Omega_\mathrm{i}|, \qquad \frac{T_z}{T_\perp} l < \frac{1}{2},$$

that is,

$$\omega_\mathrm{r} = \Pi_\mathrm{e} \frac{k_z}{k} < l|\Omega_\mathrm{i}|, \tag{13.15}$$

$$\frac{T_\perp}{T_z} > 2l. \tag{13.16}$$

When the density increases to the point that Π_e approaches $|\Omega_\mathrm{i}|$, then plasma oscillation couples to ion Larmor motion, causing the instability. When the density increases further, an oblique

Langmuir wave couples with an ion cyclotron harmonic wave $l|\Omega_\mathrm{i}|$ and an instability with $\omega_\mathrm{r} = \Pi_\mathrm{e} k_z/k \sim l|\Omega_\mathrm{i}|$ is induced. As is clear from (13.16), the degree of anisotropy must be larger for the instability in the region of higher frequency (l becomes large).

In summary, the instability with ion cyclotron harmonic frequencies appear one after another in a cold-electron plasma under the anisotropic condition (13.16) when the electron density satisfies

$$n_\mathrm{e} \sim l^2 Z^2 \frac{m_\mathrm{e}}{m_\mathrm{i}} \left(\frac{B^2}{\mu_0 m_\mathrm{i} c^2} \right) \frac{k^2}{k_z^2}. \qquad (l = 1,\ 2,\ 3,\ \cdots)$$

This instability is called *Harris instability* (ref.[2],[3]).

Velocity space instabilities in simple cases of homogeneous bi-Maxwellian plasma were described. The distribution function of a plasma confined in a mirror field is zero for loss cone region $(v_\perp/v)^2 < 1/R_\mathrm{M}$ (R_M is mirror ratio). The instability associated with this is called *loss-cone instability* (ref.[4]). In general plasmas are hot and dense in the center and are cold and low density. The instabilities driven by temperature gradient and density gradient are called *drift instability*. The electrostatic drift instability (ref.[5],[7]) of inhomogeneous plasma can be analyzed by the more general dispersion equation described in appendix C. In toroidal field, trapped particles always exist in the outside where the magnetic field is weak. The instabilities induced by the trapped particles is called *trapped particle instability* (ref.[6]).

References

[1] R. J. Briggs: *Electron-Stream Interaction with Plasma*, The MIT Press, Cambridge, Mass. 1964.

[2] E. G. Harris: Phys. Rev. Lett. **2**, 34 (1959)

[3] E. G. Harris: *Physics of Hot Plasma*, p.145 (ed. by B. J. Rye and J. B. Taylor) Oliver & Boyd, Edinburgh (1970).

[4] M. N. Rosenbluth and R. F. Post: Phys. Fluids **8**, 547 (1965).

[5] N. A. Krall and M. N. Rosenbluth: Phys. Fluids **8**, 1488 (1965).

[6] B. B. Kadomtsev and O. P. Pogutse: Nucl. Fusion **11**, 67 (1971).

[7] K. Miyamoto: *Plasma Physics for Nuclear Fusion* (revised edition) Chap.12, The MIT Press, Cambridge, Mass. 1989

Ch.14 Instabilities Driven by Energetic Particles

Sustained ignition of thermonuclear plasma depends on heating by highly energetic alpha particles produced from fusion reactions. Excess loss of the energetic particles may be caused by fishbone instability and toroidal Alfvén eigenmodes. Such losses can not only reduce the alpha particle heating efficiency, but also lead to excess heat loading and damage to plasma-facing components. These problems have been studied in experiments and analyzed theoretically. In this chapter basic aspects of theories on collective instabilities by energetic particles are described.

14.1 Fishbone Instability

Fishbone oscillations were first observed in PDX experiments with nearly perpendicular neutral beam injection. The poloidal magnetic field fluctuations associated with this instabilities have a characteristic skeletal signature on the Mirnov coils, that has suggested the name of fishbone oscillations. Particle bursts corresponding to loss of energetic beam ions are correlated with fishbone events, reducing the beam heating efficiency. The structure of the mode was identified as m=1, n=1 internal kink mode, with a precursor oscillation frequency close to the thermal ion diamagnetic frequency as well as the fast ion magnetic toroidal precessional frequency.

14.1a Formulation

Theoretical analysis of *fishbone instability* is described mainly according to L. Chen, White and Rosenbluth (ref.[1]). Core plasma is treated by the ideal MHD analysis and the hot component is treated by gyrokinetic description. The first order equation of displacement $\boldsymbol{\xi}$ is (refer to (8.25))

$$\rho_{\rm m}\gamma^2\boldsymbol{\xi} = \boldsymbol{j}\times\delta\boldsymbol{B} + \delta\boldsymbol{j}\times\boldsymbol{B} - \nabla\delta p_{\rm c} - \nabla\delta p_{\rm h}. \tag{14.1}$$

where $\delta p_{\rm c}$ is the first order pressure disturbance of core plasma $\nabla\delta p_{\rm c} = -\boldsymbol{\xi}\cdot\nabla p_{\rm c} - \gamma_{\rm s} p\nabla\cdot\boldsymbol{\xi}$. $\delta p_{\rm h}$ is the first order pressure disturbance of hot component. The following ideal MHD relations hold:

$$\delta\boldsymbol{E}_\perp = \gamma\boldsymbol{\xi}\times\boldsymbol{B}, \quad \delta\boldsymbol{E}_\parallel = 0, \quad \delta\boldsymbol{B} = \nabla\times(\boldsymbol{\xi}\times\boldsymbol{B}), \quad \delta\boldsymbol{j} = \nabla\cdot\delta\boldsymbol{B}.$$

By multiplying $\int {\rm d}\boldsymbol{r}\boldsymbol{\xi}^*$ on (14.1) and assuming a fixed conducting boundary, we have

$$\delta W_{\rm MHD} + \delta W_{\rm K} + \delta I = 0 \tag{14.2}$$

where

$$\delta I = \frac{\gamma^2}{2}\int \rho_{\rm m}|\boldsymbol{\xi}|^2 {\rm d}\boldsymbol{r} \tag{14.3}$$

$$\delta W_{\rm K} = \frac{1}{2}\int \boldsymbol{\xi}\cdot\nabla\delta p_{\rm h}{\rm d}\boldsymbol{r} \tag{14.4}$$

and $\delta W_{\rm MHD}$ is the potential energy of core plasma associated with the displacement $\boldsymbol{\xi}$, which was discussed in sec.8.2b and is given by (8.79). $\delta W_{\rm K}$ is the contribution from hot component.

14.1b MHD Potential Energy

Let us consider the MHD term of $\delta W_{\rm MHD}$, which consists of the contribution of $\delta W^{\rm s}_{\rm MHD}$ from singular region near rational surface and the contribution $\delta W^{\rm ext}_{\rm MHD}$ from the external region. External contribution $\delta W^{\rm ext}_{\rm MHD}$ of cylindrical circular plasma is already given by (8.92)

$$\frac{\delta W^{\rm ext}_{\rm MHDcycl}}{2\pi R} = \frac{\pi}{2\mu_0}\int_0^a \left(f\left|\frac{{\rm d}\xi_r}{{\rm d}r}\right|^2 + g|\xi_r|^2\right){\rm d}r \tag{14.5}$$

where f and g are given by (8.93) and (8.95). When $r/R \ll 1$ is assumed, f and g of (-m, n) mode are

$$f = \frac{r^3}{R^2}B_z^2\left(\frac{1}{q}-\frac{\mathrm{n}}{\mathrm{m}}\right)^2\left(1-\left(\frac{\mathrm{n}r}{\mathrm{m}R}\right)^2\right)$$

$$g = \frac{r}{R^2}B_z^2\left(\left(\frac{1}{q}-\frac{\mathrm{n}}{\mathrm{m}}\right)^2\left((\mathrm{m}^2-1)+\frac{\mathrm{n}^2r^2}{R^2}\right)\left(1-\left(\frac{\mathrm{n}r}{\mathrm{m}R}\right)^2-2\left(\frac{1}{q^2}-\left(\frac{\mathrm{n}}{\mathrm{m}}\right)^2\right)\left(\frac{\mathrm{n}r}{\mathrm{m}R}\right)^2\right)\right)$$
$$+2\left(\frac{\mathrm{n}r}{\mathrm{m}R}\right)^2\mu_0\frac{\mathrm{d}p_0}{\mathrm{d}r}$$

where $q(r) \equiv (rB_z/RB_\theta(r))$ is the safety factor. Let us consider the m=1 perturbation with the singular radius $r = r_\mathrm{s}$ $(q(r_\mathrm{s}) = \mathrm{m/n})$. In this case the displacement is ξ_r =const. for $0 < r < r_\mathrm{s}$ and $\xi_r = 0$ for $r_\mathrm{s} < r < a$ (refer sec.8.3b). Then $\delta W^{\mathrm{ext}}_{\mathrm{MHDcycl}}$ is reduced to (ref.[2])

$$\frac{\delta W^{\mathrm{ext}}_{\mathrm{MHDcycl}}}{2\pi R} = \frac{\pi B^2_{\theta\mathrm{s}}}{2\mu_0}|\xi_\mathrm{s}|^2\left(\frac{r_\mathrm{s}}{R}\right)^2\left(-\beta_\mathrm{p}-\int_0^1\rho^3\left(\frac{1}{q^2}+\frac{2}{q}-3\right)\mathrm{d}\rho\right) \tag{14.6}$$

where $\rho = r/r_\mathrm{s}$, $\beta_\mathrm{p} \equiv \langle p\rangle_\mathrm{s}/(B^2_{\theta\mathrm{s}}/2\mu_0)$ and $B_{\theta\mathrm{s}} \equiv (r_\mathrm{s}/Rq(r_\mathrm{s}))B_z$ is the poloidal field at $r = r_\mathrm{s}$. The pressure $\langle p\rangle_\mathrm{s}$ is defined by

$$\langle p\rangle_\mathrm{s} = -\int_0^{r_\mathrm{s}}\left(\frac{r}{r_\mathrm{s}}\right)^2\frac{\mathrm{d}p}{\mathrm{d}r}\mathrm{d}r = \frac{1}{r_\mathrm{s}^2}\int_0^{r_\mathrm{s}}(p-p_\mathrm{s})2r\mathrm{d}r. \tag{14.7}$$

MHD potential energy $\delta W^{\mathrm{ext}}_{\mathrm{MHDtor}}/2\pi R$ per unit length of toroidal plasma with circular cross section is given by (ref.[3])

$$\frac{\delta W^{\mathrm{ext}}_{\mathrm{MHDtor}}}{2\pi R} = \left(1-\frac{1}{\mathrm{n}^2}\right)\frac{\delta W^{\mathrm{ext}}_{\mathrm{MHDcycl}}}{2\pi R}+\frac{\pi B^2_{\theta\mathrm{s}}}{2\mu_0}|\xi_\mathrm{s}|^2\delta\hat{W}_\mathrm{T}, \qquad \delta\hat{W}_\mathrm{T} = \pi\left(\frac{r_\mathrm{s}}{R}\right)^2 3(1-q_0)\left(\frac{13}{144}-\beta^2_{\mathrm{ps}}\right). \tag{14.8}$$

In the case of m=1 and n=1, $\delta W^{\mathrm{ext}}_{\mathrm{MHDtor}}/2\pi R$ is reduced to only the term of $\delta\hat{W}_\mathrm{T}$.

Let us consider the contribution from singular region. In this case we must solve the displacement ξ_r in singular region near rational surface. The equation of motion in singular surface was treated in sec.9.1 of tearing instability. From (9.13) and (9.9), we have (in the limit of $x \ll 1$)

$$\mu_0\rho_\mathrm{m}\gamma^2\frac{\partial^2\xi_r}{\partial x^2} = iF\frac{\partial^2 B_{1r}}{\partial x^2} \tag{14.9}$$

$$\gamma B_{1r} = iF\gamma\xi_r+\frac{\eta}{\mu_0 r_\mathrm{s}^2}\frac{\partial^2}{\partial x^2}B_{1r} \tag{14.10}$$

where

$$F \equiv (\boldsymbol{k}\cdot\boldsymbol{B}) = \frac{-\mathrm{m}}{r}B_\theta+\frac{n}{R}B_z = \frac{B_\theta}{r}(-\mathrm{m}+\mathrm{n}q) = \frac{B_\theta \mathrm{n}}{r}\frac{\mathrm{d}q}{\mathrm{d}r}\Delta r = \frac{B_\theta \mathrm{n}s}{r_\mathrm{s}}x, \quad x \equiv \frac{r-r_\mathrm{s}}{r_\mathrm{s}}, \quad s \equiv r_\mathrm{s}\left.\frac{\mathrm{d}q}{\mathrm{d}r}\right|_{r_\mathrm{s}}.$$

By following normalizations

$$\psi \equiv \frac{iB_{1r}r_\mathrm{s}}{B_{\theta,s}s\mathrm{n}}, \qquad \tau_{\mathrm{A}\theta} \equiv \frac{r_\mathrm{s}}{(B^2_\theta/\mu_0\rho_\mathrm{m})^{1/2}}, \qquad \tau_\mathrm{R} \equiv \frac{\mu_0 r_\mathrm{s}^2}{\eta}, \qquad S_\mathrm{R} \equiv \frac{\tau_\mathrm{R}}{\tau_{\mathrm{A}\theta}},$$

we have

$$\gamma^2 \left(\frac{\tau_{\mathrm{A}\theta}}{\mathrm{n}s}\right)^2 \xi_r'' = x\psi'', \qquad \psi = -x\xi_r + \frac{1}{\gamma\tau_{\mathrm{A}\theta}S_{\mathrm{R}}}\psi''. \tag{14.11}$$

In the limit of $S_{\mathrm{R}} \to \infty$, (14.11) yields

$$\left(\left(\gamma\frac{\tau_{\mathrm{A}\theta}}{\mathrm{n}s}\right)^2 + x^2\right)\xi_r'' + 2x\xi_r' = 0$$

and the solution is (ref.[4])

$$\xi_r' = \frac{(\xi_0/\pi)(\gamma\tau_{\mathrm{A}\theta}/\mathrm{n}s)^{-1}}{x^2/(\gamma\tau_{\mathrm{A}\theta}/\mathrm{n}s)^2 + 1}, \qquad \xi_r(x) = \xi_\infty - \frac{\xi_0}{\pi}\tan^{-1}\left(\frac{x}{\gamma\tau_{\mathrm{A}\theta}/(\mathrm{n}s)}\right). \tag{14.12}$$

Since the external solution of m=1 is $\xi_r = \xi_{\mathrm{s}}$ as $x \to -\infty$ and $\xi_r = 0$ as $x \to \infty$, the matching conditions to external solution yield $\xi_\infty = \xi_{\mathrm{s}}/2$ and $\xi_0 = \xi_{\mathrm{s}}$.

The term $\delta W^{\mathrm{s}}_{\mathrm{MHD}}$ from singular region is

$$\frac{\delta W^{\mathrm{s}}_{\mathrm{MHD}}}{2\pi R} = \frac{\pi}{2\mu_0}\int_{r_{\mathrm{s}}-\Delta}^{r_{\mathrm{s}}+\Delta} r^3(\boldsymbol{k}\cdot\boldsymbol{B})^2\left(\frac{\partial\xi_r}{\partial r}\right)^2 \mathrm{d}r = \frac{\pi}{2\mu_0}\frac{B_{\theta\mathrm{s}}^2}{2\pi}s\mathrm{n}\gamma\tau_{\mathrm{A}\theta}|\xi_{\mathrm{s}}|^2. \tag{14.13}$$

Eq.(14.13) is the expression in the case of cylindrical plasma. For the toroidal plasma $\tau_{\mathrm{A}\theta}$ is replaced by $3^{1/2}r_{\mathrm{s}}/(B_\theta^2/\mu_0\rho)^{1/2}$, where $3^{1/2}$ is the standard toroidal factor $(1+2q^2)^{1/2}$ (ref.[6]).

Therefore the total sum of MHD contributions of m=1, n=1 is ($\gamma\tau_{\mathrm{A}\theta} \ll 1$ is assumed.)

$$\begin{aligned}\delta W_{\mathrm{MHD}} \ + \delta I &= 2\pi R\frac{B_{\theta\mathrm{s}}^2}{2\mu_0}|\xi_{\mathrm{s}}|^2\left(\delta\hat{W}^{\mathrm{T}} + \gamma\tau_{\mathrm{A}\theta}\frac{s}{2} + \pi\gamma^2\tau_{\mathrm{A}\theta}^2\right)\\ &\approx 2\pi R\frac{B_{\theta\mathrm{s}}^2}{2\mu_0}|\xi_{\mathrm{s}}|^2\left(\delta\hat{W}^{\mathrm{T}} + \gamma\tau_{\mathrm{A}\theta}\frac{s}{2}\right).\end{aligned} \tag{14.14}$$

14.1c Kinetic Integral of Hot Component

The perturbed distribution of hot ion component δF_{h} is given by gyrokinetic equation in the case of low beta and zero gyro-radius approximation as follow (ref.[5])

$$\delta F_{\mathrm{h}} \equiv \frac{e}{m}\delta\phi\frac{\partial}{\partial E}F_{0\mathrm{h}} + \delta H_{\mathrm{h}}, \qquad \left(v_\parallel\frac{\partial}{\partial l} - i(\omega - \hat{\omega}_{\mathrm{dh}})\right)\delta H_{\mathrm{h}} = i\frac{e}{m}Q(\delta\phi - v_\parallel\delta A_\parallel) \tag{14.15}$$

where $\delta A_\parallel = (-i/\omega)(\partial\delta\phi/\delta l)$ due to $E_\parallel = 0$ (see (14.43) and

$$E \equiv \frac{v^2}{2}, \quad \mu \equiv \frac{v_\perp^2}{2B}, \quad \omega_{\mathrm{c}} \equiv \frac{eB}{m}, \quad Q \equiv \left(\omega\frac{\partial}{\partial E} + \hat{\omega}_{*\mathrm{h}}\right)F_{0\mathrm{h}}, \quad \hat{\omega}_{\mathrm{dh}} \equiv -i\boldsymbol{v}_{\mathrm{dh}}\cdot\nabla,$$

$$\boldsymbol{v}_{\mathrm{dh}} \equiv \left(v_\parallel^2 + \frac{v_\perp^2}{2}\right)\frac{m}{eB}(\boldsymbol{b}\times\boldsymbol{\kappa}), \qquad \hat{\omega}_{*\mathrm{h}} \equiv -i\omega_{\mathrm{c}}^{-1}\frac{\boldsymbol{b}\times\nabla F_{0\mathrm{h}}}{F_{0\mathrm{h}}}\cdot\nabla \approx \frac{-m}{eBr}\frac{\partial}{\partial r}.$$

$\boldsymbol{v}_{\mathrm{dh}}$ is the magnetic drift velocity and $|\hat{\omega}_{\mathrm{dh}}|$ is diamagnetic drift frequency of hot ion. $\boldsymbol{\kappa} = (\boldsymbol{b}\cdot\nabla)\boldsymbol{b}$ is the vector toward the center of curvature of magnetic field line and the magnitude is R (refer sec.2.4). $\delta\phi$ is scaler potential and related by $\nabla\delta\phi = -i\omega\boldsymbol{\xi}\times\boldsymbol{B}$. When we set

$$\delta H_{\mathrm{h}} = -\frac{1}{\omega}\frac{e}{m}Q\delta\phi + \delta G_{\mathrm{h}} \tag{14.16}$$

we have

$$v_\parallel \frac{\partial \delta H_\mathrm{h}}{\partial l} = i(\omega - \hat{\omega}_\mathrm{dh})\delta G_\mathrm{h} + i\frac{\hat{\omega}_\mathrm{dh}}{\omega}\frac{e}{m}Q\delta\phi - \frac{1}{\omega}\frac{e}{m}v_\parallel \frac{\partial \delta\phi}{\partial l}Q.$$

Taking the average $\bar{A} \equiv \oint (A/v_\parallel)\mathrm{d}l / \oint \mathrm{d}l/v_\parallel$ of both side of the foregoing equation yields

$$\delta G_\mathrm{h} = -\frac{e}{m}Q\frac{1}{\omega - \overline{\hat{\omega}_\mathrm{dh}}}\overline{\frac{\hat{\omega}_\mathrm{dh}\delta\phi}{\omega}} \tag{14.17}$$

and

$$\frac{\hat{\omega}_\mathrm{dh}\delta\phi}{\omega} = -\frac{i}{\omega}\frac{m(v_\parallel^2 + v_\perp^2/2)}{eB}(\boldsymbol{b}\times\boldsymbol{\kappa})\cdot\nabla\delta\phi = -\frac{1}{\omega}\frac{m(v_\parallel^2 + v_\perp^2/2)}{eB}(\boldsymbol{b}\times\boldsymbol{\kappa})\cdot\omega(\boldsymbol{\xi}\times\boldsymbol{B})$$

$$= \frac{m(v_\parallel^2 + v_\perp^2/2)}{e}(\boldsymbol{\kappa}\cdot\boldsymbol{\xi}) = -\frac{m}{e}Jv^2 = -\frac{m}{e}J2E$$

where

$$J \equiv \frac{-1}{v^2}(v_\parallel^2 + v_\perp^2/2)(\boldsymbol{\kappa}\cdot\boldsymbol{\xi}) \approx \frac{v_\parallel^2 + v_\perp^2/2}{v^2}\frac{(\cos\theta\xi_r + \sin\theta\xi_\theta)}{R} \sim \frac{v_\parallel^2 + v_\perp^2/2}{v^2}\frac{e^{-i\theta}\xi_r}{R}. \tag{14.18}$$

One notes that frequencies $\omega,\ \omega_\mathrm{dh}$ are much smaller than the hot ion transit and bounce frequencies $v_\parallel/R,\ \epsilon^{1/2}v/qR$. For untrapped particles (δG_hu) and trapped particles (δG_ht), we have

$$\delta G_\mathrm{hu} \approx 0, \qquad \delta G_\mathrm{ht} \approx 2QE\frac{\bar{J}}{\omega - \overline{\hat{\omega}_\mathrm{dh}}}. \tag{14.19}$$

The perturbed pressure tensor due to hot ion component is

$$\delta P_\mathrm{h} = -\boldsymbol{\xi}_\perp\cdot\nabla(P_\perp I + (P_\parallel - P_\perp)\boldsymbol{bb}) + \delta P_\perp I + (\delta P_\parallel - \delta P_\perp)\boldsymbol{bb} \tag{14.20}$$

where

$$\delta P_\perp = \int \frac{mv_\perp^2}{2}\delta F_\mathrm{h} 2\pi v_\perp \mathrm{d}v_\perp \mathrm{d}v_\parallel$$

$$\delta P_\parallel = \int mv_\parallel^2 \delta F_\mathrm{h} 2\pi v_\perp \mathrm{d}v_\perp \mathrm{d}v_\parallel.$$

The first term of the right-hand side of (14.20) has similar form to the pressure term of core plasma. Since beta of hot ion component β_h is much smaller than β_c of core plasma, the first term in (14.20) can be neglected. Since $E = v^2/2$, $\mu = v_\perp^2/2B$ and $\alpha \equiv \mu/E$ are defined, we have

$$v_\parallel^2 = 2E(1-\alpha B), \quad v_\perp^2 = 2B\alpha E, \quad 2\pi v_\perp \mathrm{d}v_\perp \mathrm{d}v_\parallel = 2^2\pi\frac{BE}{v_\parallel}\mathrm{d}E\mathrm{d}\alpha = 2^{3/2}\pi B\frac{E^{1/2}}{(1-\alpha B)^{1/2}}\mathrm{d}\alpha\mathrm{d}E.$$

Then the perturbed pressure of hot ion component is reduced to

$$\delta P_\perp = 2^{3/2}\pi B\int \frac{E^{1/2}}{(1-\alpha B)^{1/2}}\mathrm{d}\alpha\mathrm{d}E\ m\alpha BE\delta F_\mathrm{h}$$

$$= 2^{5/2}mB\int_{B_\mathrm{max}^{-1}}^{B^{-1}} \mathrm{d}\alpha(1-\alpha B)^{1/2}\int_0^E \mathrm{d}E E^{3/2}\frac{\alpha B}{2(1-\alpha B)}\delta F_\mathrm{h} \tag{14.21a}$$

$$\delta P_\parallel = 2^{3/2}\pi B\int \frac{E^{1/2}}{(1-\alpha B)^{1/2}}\mathrm{d}\,\alpha\mathrm{d}E\; m2E(1-\alpha B)\delta F_\mathrm{h}$$

$$= 2^{5/2}mB\int_{B_\mathrm{max}^{-1}}^{B^{-1}}\mathrm{d}\alpha(1-\alpha B)^{1/2}\int_0^E \mathrm{d}E E^{3/2}\delta F_\mathrm{h}. \tag{14.22a}$$

The divergence of the second and the third pressure terms of (14.20) is

$$(\nabla\delta P_\mathrm{h})_\beta = \sum_\alpha \frac{\partial\delta P_\perp}{\partial x_\alpha}\delta_{\alpha\beta} + \sum_\alpha \frac{\partial(\delta P_\parallel - \delta P_\perp)}{\partial x_\alpha}b_\alpha b_\beta + (\delta P_\parallel - \delta P_\perp)\sum_\alpha (b_\alpha b_\beta)$$

$$= \frac{\partial\delta P_\perp}{\partial x_\beta} + b_\beta(\boldsymbol{b}\cdot\nabla)(\delta P_\parallel - \delta P_\perp) + (\delta P_\parallel - \delta P_\perp)((\boldsymbol{b}\cdot\nabla)b_\beta + b_\beta(\nabla\cdot\boldsymbol{b}))$$

$$(\nabla\delta P_\mathrm{h})_\perp = \nabla_\perp\delta P_\perp + (\delta P_\parallel - \delta P_\perp)(\boldsymbol{b}\cdot\nabla)\boldsymbol{b} = \nabla_\perp\delta P_\perp + (\delta P_\parallel - \delta P_\perp)\boldsymbol{\kappa} \tag{14.21b}$$

$$(\nabla\delta P_\mathrm{h})_\parallel = \nabla_\parallel\delta P_\perp + (\boldsymbol{b}\cdot\nabla)(\delta P_\parallel - \delta P_\perp) + (\delta P_\parallel - \delta P_\perp)\nabla\cdot\boldsymbol{b}. \tag{14.22b}$$

The kinetic integral δW_K is

$$\delta W_\mathrm{K} = \frac{1}{2}\int \boldsymbol{\xi}_\perp^*\cdot\nabla\delta P\mathrm{d}\boldsymbol{r} = \frac{1}{2}\int \boldsymbol{\xi}_\perp^*\cdot(\nabla_\perp\delta P_\perp + (\delta P_\parallel - \delta P_\perp)\boldsymbol{\kappa})\mathrm{d}\boldsymbol{r}$$

$$= -\frac{1}{2}\int \nabla\cdot\boldsymbol{\xi}_\perp^*\delta P_\perp - (\delta P_\parallel - \delta P_\perp)\boldsymbol{\xi}_\perp^*\cdot\boldsymbol{\kappa})\mathrm{d}\boldsymbol{r}$$

$$= -2^{3/2}\pi m\int \mathrm{d}\boldsymbol{r}B\int \mathrm{d}\alpha\mathrm{d}E\frac{E^{3/2}}{(1-\alpha B)^{1/2}}\left(\nabla\cdot\boldsymbol{\xi}_\perp^*\frac{v_\perp^2}{2v^2} - (\boldsymbol{\xi}_\perp^*\cdot\boldsymbol{\kappa})\frac{v_\parallel^2 - v_\perp^2/2}{v^2}\right)\delta F_\mathrm{h}.$$

Since $\nabla\cdot\boldsymbol{\xi}_\perp + 2(\boldsymbol{\xi}\cdot\boldsymbol{\kappa}) \approx 0$ (refer (B.7)), the term of ( ) in the integrand is

$$(\quad) = -\frac{v_\parallel^2 + v_\perp^2/2}{v^2}(\boldsymbol{\xi}_\perp^*\cdot\boldsymbol{\kappa}) \approx -\frac{1}{2}(\boldsymbol{\xi}_\perp^*\cdot\boldsymbol{\kappa}),$$

δW_K is reduced to

$$\frac{\delta W_\mathrm{K}}{2\pi R} = -\frac{2^{3/2}\pi}{2\pi R}m_\mathrm{h}\int \mathrm{d}\boldsymbol{r}B\int \mathrm{d}\alpha\mathrm{d}E\frac{E^{3/2}}{(1-\alpha B)^{1/2}}\frac{\bar{J}^*QE\bar{J}2}{\omega - \overline{\hat{\omega}_\mathrm{dh}}}$$

$$= -2^{5/2}\pi^2 m_\mathrm{h}\int \mathrm{d}r\, r\frac{1}{2\pi}\int \mathrm{d}\theta B\int \mathrm{d}\alpha\mathrm{d}E\frac{E^{3/2}}{(1-\alpha B)^{1/2}}\frac{\bar{J}^*QE\bar{J}2}{\omega - \overline{\hat{\omega}_\mathrm{dh}}}$$

$$= -2^{7/2}\pi^2 m_\mathrm{h}\int_0^{r_\mathrm{s}}\mathrm{d}r\, r\int_{(1-r/R)}^{(1+r/R)}\mathrm{d}(\alpha B)\int \mathrm{d}E K_\mathrm{b}E^{5/2}\frac{\bar{J}^*QE\bar{J}}{\omega - \overline{\overline{\hat{\omega}_\mathrm{dh}}}}$$

$$\approx 2^{3/2}\pi^2 m_\mathrm{h}\frac{|\boldsymbol{\xi}|^2}{R^2}\int_0^{r_\mathrm{s}}\mathrm{d}r\, r\int \mathrm{d}(\alpha B)\int \mathrm{d}E E^{5/2}\frac{K_2^2}{K_\mathrm{b}}\frac{Q}{\overline{\overline{\hat{\omega}_\mathrm{dh}}} - \omega} \equiv \frac{B_{\theta\mathrm{s}}^2}{2\mu_0}|\boldsymbol{\xi}_\mathrm{s}|^2\delta\hat{W}_\mathrm{K}, \tag{14.23}$$

where

$$K_\mathrm{b} = \oint\frac{\mathrm{d}\theta}{2\pi}\frac{1}{(1-\alpha B)^{1/2}} = \oint\frac{\mathrm{d}\theta}{2\pi}\frac{v}{v_\parallel}, \qquad K_2 = \oint\frac{\mathrm{d}\theta}{2\pi}\frac{\cos\theta}{(1-\alpha B)^{1/2}}.$$

Therefore dispersion relation (14.3) is reduced to

$$\frac{-i\omega}{\omega_{\rm A}} + \delta\hat{W}^{\rm T} + \delta\hat{W}_{\rm K} = 0, \tag{14.24}$$

where $\omega_{\rm A} \equiv (\tau_{\rm A} s/2)^{-1}$ and γ is relaced by $-i\omega$.

14.1d Growth Rate of Fishbone Instability

Let us assume a model distribution for slowing down hot ions with the initial velocity $v_{\rm mx}^2/2 = E_{\rm mx}$

$$F_{\rm h0} = c_0 \frac{\delta(\alpha - \alpha_0)}{E^{3/2}}, \quad (E < E_{\rm mx}). \tag{14.25}$$

Then the pressure $p_{\rm h}$ and the density $n_{\rm h}$ of hot ions are

$$p_{\rm h} = \int 2^{3/2}\pi B \frac{E^{1/2}}{(1-\alpha B)^{1/2}} {\rm d}\alpha {\rm d}E (mE) F_{\rm h0} = c_0 \int_0^{E_{\rm mx}} 2^{3/2}\pi B \frac{m}{(1-\alpha_0 B)^{1/2}} {\rm d}E \tag{14.26}$$

$$p_{\rm h} = c_0 2^{3/2}\pi B m K_{\rm b} E_{\rm mx}, \qquad c_0 = \frac{p_{\rm h}}{2^{3/2}\pi B m K_{\rm b} E_{\rm mx}}, \tag{14.27}$$

$$n_{\rm h} = \int_{T_{\rm c}}^{E_{\rm mx}} 2^{3/2}\pi B \frac{E^{1/2}}{(1-\alpha B)^{1/2}} {\rm d}\alpha {\rm d}E F_{\rm h0} = c_0 2^{3/2}\pi B m K_{\rm b} E_{\rm mx} = p_{\rm h} \frac{\ln(E_{\rm mx}/T_{\rm c})}{E_{\rm mx}}. \tag{14.28}$$

The kinetic integral is

$$\frac{\delta W_{\rm K}}{2\pi R} = \frac{r_{\rm s}^2}{R^2}|\boldsymbol{\xi}_{\rm s}|^2 \frac{1}{r_{\rm s}^2}\int_0^{r_{\rm s}} {\rm d}r\ r \int {\rm d}E 2^{3/2}\pi^2 m B E^{5/2} \left(\frac{K_2^2}{K_{\rm b}}\right) \frac{-(3/2)\omega c_0 E^{-5/2} - (\partial c_0/\partial r)(m/eBr)E^{-3/2}}{mE/(2eBRr) - \omega}$$

$$= \frac{r_{\rm s}^2}{R^2}\frac{B^2}{2\mu_0}|\boldsymbol{\xi}_{\rm s}|^2 \frac{1}{r_{\rm s}^2}\int_0^{r_{\rm s}} {\rm d}r\ r\pi \frac{K_2^2}{K_{\rm b}^2}\frac{1}{E_{\rm mx}}\int_0^{E_{\rm mx}} {\rm d}E \frac{-(3/2)\beta_{\rm h} - 2(\partial\beta_{\rm h}/\partial r)R(mE/2eBRr\omega)}{mE/(2eBRr\omega) - 1}$$

$$= \frac{r_{\rm s}^2}{R^2}\frac{B^2}{2\mu_0}|\boldsymbol{\xi}_{\rm s}|^2 \frac{1}{r_{\rm s}^2}\int_0^{r_{\rm s}} {\rm d}r\ r\pi \frac{K_2^2}{K_{\rm b}^2}\frac{\omega}{\omega_{\rm dh,mx}}\left(-(3/2)\beta_{\rm h}\int_0^{y_{\rm mx}} \frac{{\rm d}y}{y-1} - 2\frac{\partial\beta_{\rm h}}{\partial r}R\int \frac{y{\rm d}y}{y-1}\right)$$

$$= \frac{B_{\theta{\rm s}}^2}{2\mu_0}|\boldsymbol{\xi}_{\rm s}|^2 \frac{\pi}{2}\frac{K_2^2}{K_{\rm b}^2}\left((-3/2)\langle\beta_{\rm h}\rangle\frac{\omega}{\omega_{\rm dh,mx}}\ln\left(1-\frac{\omega_{\rm dh,mx}}{\omega}\right) - 2\langle\frac{\partial\beta_{\rm h}}{\partial r}\rangle R\left(1 + \frac{\omega}{\omega_{\rm dh,mx}}\ln\left(1-\frac{\omega_{\rm dh,mx}}{\omega}\right)\right)\right). \tag{14.29}$$

As the second term of $\langle(\partial\beta_{\rm h}/\partial r)\rangle R$ is dominant, the dispersion relation is reduced to

$$-i\Omega\frac{\omega_{\rm dh,mx}}{\omega_{\rm A}} + \delta\hat{W}^{\rm T} + \pi\frac{K_2^2}{K_{\rm b}^2}\langle -\frac{\partial\beta_{\rm h}}{\partial r}\rangle R\left(1 + \Omega\ln\left(1-\frac{1}{\Omega}\right)\right) = 0. \tag{14.30}$$

where

$$\Omega \equiv \frac{\omega}{\omega_{\rm dh,mx}}, \quad \omega_{\rm dh,mx} \equiv \frac{mv_{\rm mx}^2/2}{eBRr}, \quad \beta_{\rm h} \equiv \frac{p_{\rm h}}{B^2/2\mu_0}.$$

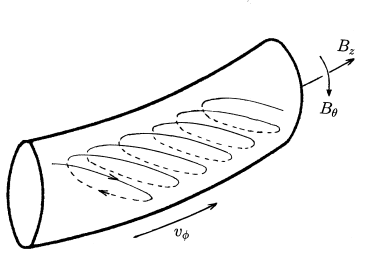

Fig.14.1 Toroidal precession of banana orbit of trapped ions

Let us consider the case of $\delta\hat{W}^{\mathrm{T}} = 0$. Then (14.30) is

$$-i\alpha_{\mathrm{h}}\Omega + \Omega \ln\left(1-\frac{1}{\Omega}\right) + 1 = 0, \tag{14.31}$$

where

$$\alpha_{\mathrm{h}} \equiv \frac{\omega_{\mathrm{dh,mx}}}{\omega_{\mathrm{A}}}\left(\pi\frac{K_2^2}{K_{\mathrm{b}}^2}\langle-\frac{\partial\beta_{\mathrm{h}}}{\partial r}\rangle R\right)^{-1}.$$

Under the assumption $(1-1/\Omega_{\mathrm{r}}) < 0$ and $|\Omega_{\mathrm{i}}| \ll |\Omega_{\mathrm{r}}|$, (14.31) is reduced to

$$-i\alpha_{\mathrm{h}}(\Omega_{\mathrm{r}} + i\Omega_{\mathrm{i}}) + (\Omega_{\mathrm{r}} + i\Omega_{\mathrm{i}})\left(\ln\left(\frac{1}{\Omega_{\mathrm{r}}} - 1\right) + \pi i - \frac{\Omega_{\mathrm{i}}}{(1/\Omega_{\mathrm{r}} - 1)\Omega_{\mathrm{r}}^2}i\right) + 1 = 0. \tag{14.32}$$

From the real and imaginary parts of (14.32), we have

$$\Omega_{\mathrm{i}} = \frac{\pi - \alpha_{\mathrm{h}}}{-\ln(1/\Omega_{\mathrm{r}} - 1) + (1 - (1/\Omega_{\mathrm{r}}))}\Omega_{\mathrm{r}} \tag{14.33}$$

$$\Omega_{\mathrm{r}} = \frac{1 - (\pi - \alpha_{\mathrm{h}})\Omega_{\mathrm{i}}}{-\ln(1/\Omega_{\mathrm{r}} - 1)}. \tag{14.34}$$

In the case of marginally unstable state $\pi = \alpha_{\mathrm{h}}$, that is, $\Omega_{\mathrm{i}} = 0$, Ω_{r} is given by

$$\Omega_{\mathrm{r}} = \frac{1}{-\ln(1/\Omega_{\mathrm{r}} - 1)}, \quad \rightarrow \quad \Omega_{\mathrm{r}} = \frac{1}{1 + \exp(-1/\Omega_{\mathrm{r}})} = \frac{1}{2}\left(1 + \tanh\frac{1}{2\Omega_{\mathrm{r}}}\right)$$

and $\Omega_{\mathrm{r}} \approx 0.75$. For the excitation of fishbone instability, the necessary condition is $\Omega_{\mathrm{i}} > 0$, that is, $\alpha_{\mathrm{h}} < \pi$ and

$$\langle-\frac{\partial\beta_{\mathrm{h}}}{\partial r}\rangle r_{\mathrm{s}} > \frac{r_{\mathrm{s}}}{R}\frac{\omega_{\mathrm{dh,mx}}}{\omega_{\mathrm{A}}}\frac{1}{\pi^2}\frac{K_{\mathrm{b}}^2}{K_2^2}.$$

There is a threshold for $\langle|\partial\beta_{\mathrm{h}}/\partial r|\rangle r_{\mathrm{s}}$ for the instability.

Banana orbits of trapped ions drift in toroidal direction as is shown in fig.14.1. The toroidal precession velocity and frequency are* (refer to (3.59))

$$v_\phi = \frac{mv_\perp^2/2}{eBr}, \qquad \omega_\phi = \frac{mv_\perp^2/2}{eBRr}. \tag{14.35}$$

Therefore $\omega_{\mathrm{dh,mx}}$ is equal to the toroidal precession frequency of trapped ions with the initial (maximum) velocity. It seems that the fishbone instability is due to an interaction between energetic particles and m=1, n=1 MHD perturbation. The interaction of resonant type is characterized by Landau damping. The resonance is between the toroidal wave velocity of instability and the toroidal precession of trapped energetic particles.

(* Note: The toroidal vertical drift velocity is $v_{\rm d} = (mv_\perp^2/2eBR)$, so that the poloidal displacement of particles between bounces is $r\delta\theta \sim v_{\rm d}\tau_{\rm d}$, $\tau_{\rm d}$ being the bounce period. Since $\mathrm{d}\phi/\mathrm{d}\theta = q$ along the magnetic line of field, the associated toroidal displacement between bounces is $R\mathrm{d}\phi = (Rqv_{\rm d}\tau_{\rm d}/r)$, $q = 1$. Thus toroidal precession velocity is given by (14.35).)

14.2 Toroidal Alfvén Eigenmode

Alfvén waves in homogeneous magnetic field in infinite plasma have been analyzed in sec.5.4. Shear Alfvén wave, fast and slow magnetosonic waves appear. In the case of incompressible plasma ($\nabla \cdot \boldsymbol{\xi} = 0$ or ratio of specific heat $\gamma \to \infty$), only the shear Alfvén wave can exists.

In the case of cylindrical plasma in the axisymmetric magnetic field, the displacement of MHD perturbation $\boldsymbol{\xi}(r,\theta,z) = \boldsymbol{\xi}(r)\exp i(-m\theta + kz - \omega t)$ is given by Hain-Lüst equations (8.114-117) as was discussed in sec.8.4. In the case of incompressible plasma, Hain-Lüst equation (8.117) is reduced to [In sec.8.4 perturbation is assumed to be $\boldsymbol{\xi}(r)\exp i(+m\theta + kz - \omega t)$]

$$\frac{\mathrm{d}}{\mathrm{d}r}\left(\frac{F^2 - \mu_0\rho_{\rm m}\omega^2}{\mathrm{m}^2/r^2 + k^2}\right)\frac{1}{r}\frac{\mathrm{d}}{\mathrm{d}r}(r\xi_r) + \left(-(F^2 - \mu_0\rho_{\rm m}\omega^2) + 2B_\theta\frac{\mathrm{d}}{\mathrm{d}r}\left(\frac{B_\theta}{r}\right)\right.$$

$$\left. + \frac{4k^2B_\theta^2F^2}{r^2(\mathrm{m}^2/r^2 + k^2)(F^2 - \mu_0\rho_{\rm m}\omega^2)} + 2r\frac{\mathrm{d}}{\mathrm{d}r}\left(\frac{(\mathrm{m}/r)FB_\theta}{r^2(\mathrm{m}^2/r^2 + k^2)}\right)\right)\xi_r = 0 \qquad (14.36)$$

where

$$F = (\boldsymbol{k}\cdot\boldsymbol{B}) = \left(\frac{-\mathrm{m}}{r}B_\theta(r) + \frac{\mathrm{n}}{R}B_z(r)\right) = \frac{B_z}{R}\left(\mathrm{n} - \frac{\mathrm{m}}{q(r)}\right), \qquad q(r) = \frac{R}{r}\frac{B_z}{B_\theta}.$$

The position at which $F^2 - \mu_0\rho_{\rm m}\omega^2 = 0 \to \omega^2 = \boldsymbol{k}_\parallel^2 v_{\rm A}^2$, $v_{\rm A}^2 \equiv B^2/\mu_0\rho_{\rm m}$ holds is singular radius. It was shown by Hasegawa and L.Chen (ref.[7]) that at this singular radius (resonant layer) shear Alfvén wave is mode converted to the kinetic Alfvén wave and absorbed by Landau damping. Therefore Alfvén wave is stable in the cylindrical plasma.

Alfvén waves were also treated in sec.10.4a, 10.4b by cold plasma model. The dispersion relation in homogenous infinite plasma is given by (10.64b) showing that Alfvén resonance occurs at $\omega^2 \approx k_\parallel^2 v_{\rm A}^2$ and cuts off of compressional Alfvén wave and shear Alfvén wave occur at $\omega^2 = k_\parallel^2 v_{\rm A}^2(1+\omega/\Omega_{\rm i})$ and $\omega^2 = k_\parallel^2 v_{\rm A}^2(1-\omega/\Omega_{\rm i})$ respectively.

14.2a Toroidicity Induced Alfvén Eigenmode

Let us consider shear Alfvén waves in toroidal plasma and the perturbation of (-m, n) mode given by

$$\phi(r,\theta,z,t) = \phi(r)\exp i(-m\theta + n\frac{z}{R} - \omega t) \qquad (14.37)$$

where R is major radius of torus and $k_\parallel$ is

$$k_\parallel = \frac{\boldsymbol{k}\cdot\boldsymbol{B}}{B} = \frac{1}{R}\left(\mathrm{n} - \frac{\mathrm{m}}{q(r)}\right).$$

The resonant conditions of m and m+1 modes in linear cylindrical plasma are

$$\frac{\omega^2}{v_{\rm A}^2} - k_{\parallel\mathrm{m}}^2 = 0$$

$$\frac{\omega^2}{v_{\rm A}^2} - k_{\parallel\mathrm{m+1}}^2 = 0.$$

However wave of m mode can couple with m±1 in toroidal plasma since the magnitude of toroidal

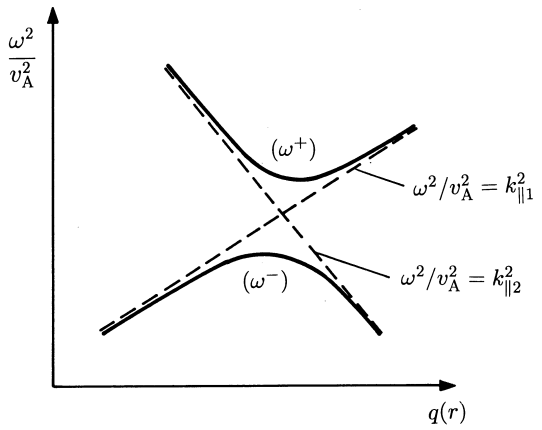

Fig.14.2 The Alfvén resonance frequency ω of toroidally coupled m and m+1 modes.

field changes as $B_z = B_{z0}(1-(r/R)\cos\theta)$, as will be shown in this section later. Then the resonant condition of m and m+1 modes in toroidal plasma becomes

$$\begin{vmatrix} \frac{\omega^2}{v_A^2} - k_{\parallel \mathrm{m}}^2 & \alpha\epsilon\frac{\omega^2}{v_A^2} \\ \alpha\epsilon\frac{\omega^2}{v_A^2} & \frac{\omega^2}{v_A^2} - k_{\parallel \mathrm{m}+1}^2 \end{vmatrix} = 0$$

where $\epsilon = r/R$ and α is a constant with order of 1. Then the solutions are

$$\frac{\omega_\pm^2}{v_A^2} = \frac{k_{\parallel \mathrm{m}}^2 + k_{\parallel \mathrm{m}+1}^2 \pm \left((k_{\parallel \mathrm{m}}^2 - k_{\parallel \mathrm{m}+1}^2)^2 + 4\alpha\epsilon^2 k_{\parallel \mathrm{m}}^2 k_{\parallel \mathrm{m}+1}^2\right)^{1/2}}{2(1-\alpha^2\epsilon^2)}. \tag{14.38}$$

The resonant condition (14.38) is plotted in fig.14.2. At the radius satisfying $k_{\parallel \mathrm{m}}^2 = k_{\parallel \mathrm{m}+1}^2$, the difference of $\omega_\pm$ becomes minimum and the radius is given by

$$\frac{1}{R}\left(\mathrm{n} - \frac{\mathrm{m}}{q(r)}\right) = -\frac{1}{R}\left(\mathrm{n} - \frac{\mathrm{m}+1}{q(r)}\right), \quad q(r_0) = \frac{\mathrm{m}+1/2}{\mathrm{n}}, \quad k_{\parallel \mathrm{m}} = -k_{\parallel \mathrm{m}+1} = \frac{1}{2q(r_0)R}. \tag{14.39}$$

$q(r_0) = 1.5$ for the case of m=1 and n=1. Therefore Alfvén resonance does not exist in the frequency gap $\omega_- < \omega < \omega_+$.

The continuum Alfvén waves correspond to the excitation of shear Alfvén waves on a given flux surface where the mode frequency is resonant $\omega^2 = k_{\parallel \mathrm{m}}^2 v_A^2(r)$ and such a resonance leads wave damping. However frequencies excited within the spectral gaps are not resonant with the continuum and hence will not damp in the gap region. This allows a discrete eigen-frequency of *toroidicty-induced Alfvén eigenmode* or *toroidal Alfvén eigenmode* (TAE) to be established. This TAE can easily be destabilized by the kinetic effect of energetic particles.

The equations of TAE will be described according to Berk, Van Dam, Guo, Lindberg (ref.[8]). The equations of the first order perturbations are

$$\nabla \cdot \boldsymbol{j}_1 = 0, \qquad \rho\frac{\mathrm{d}\boldsymbol{v}_1}{\mathrm{d}t} = (\boldsymbol{j} \times \boldsymbol{B})_1, \tag{14.40}$$

$$\boldsymbol{E}_1 = \nabla\phi_1 - \frac{\partial \boldsymbol{A}_1}{\partial t}, \qquad \boldsymbol{B}_1 = \nabla \times \boldsymbol{A}_1. \tag{14.41}$$

For ideal, low β MHD waves, we have following relations:

$$\boldsymbol{E}_\parallel = 0, \qquad \boldsymbol{B}_{\parallel 1} = 0, \qquad \boldsymbol{A}_1 = A_{\parallel 1}\boldsymbol{b} \tag{14.42}$$

so that

$$i\omega A_{\parallel 1} = \boldsymbol{b}\cdot\nabla\phi_1, \qquad \boldsymbol{v}_1 = \frac{\boldsymbol{E}_1\times\boldsymbol{b}}{B}. \tag{14.43}$$

From (14.40), we have

$$\nabla\cdot\boldsymbol{j}_{\perp 1} + \nabla\cdot(j_{\parallel 1}\boldsymbol{b}) = 0, \tag{14.44}$$

and

$$-i\omega\rho(\boldsymbol{v}_1\times\boldsymbol{b}) = (\boldsymbol{j}_{\perp 1}\times\boldsymbol{B})\times\boldsymbol{b} + (\boldsymbol{j}\times\boldsymbol{B}_1)\times\boldsymbol{b}, \qquad \boldsymbol{j}_{\perp 1} = -\frac{i\omega\rho}{B^2}\boldsymbol{E}_{\perp 1} + \frac{j_\parallel}{B}\boldsymbol{B}_{\perp 1}. \tag{14.45}$$

Equations (14.41-43) yield

$$\boldsymbol{B}_{\perp 1} = \nabla\times(A_{\parallel 1}\boldsymbol{b}) = \nabla\left(\frac{A_{\parallel 1}}{B}\right)\times\boldsymbol{B} + \frac{A_{\parallel 1}}{B}\nabla\times\boldsymbol{B} \approx \frac{-i}{\omega}\nabla\left(\frac{\boldsymbol{b}\cdot\nabla\phi_1}{B}\right)\times\boldsymbol{B} \tag{14.46}$$

$$j_{\parallel 1} = \boldsymbol{b}\cdot\boldsymbol{j}_1 = \frac{1}{\mu_0}\boldsymbol{b}\cdot\nabla\times\boldsymbol{B}_{\perp 1} = \frac{-i}{\omega\mu_0}\boldsymbol{b}\cdot\nabla\times\left(B^2\nabla_\perp\left(\frac{(\boldsymbol{B}\cdot\nabla)\phi_1}{B^2}\right)\times\frac{\boldsymbol{B}}{B^2}\right)$$
$$= \frac{i}{\omega\mu_0}\left(\boldsymbol{b}\cdot\frac{\boldsymbol{B}}{B^2}\right)\nabla\cdot\left(B^2\nabla_\perp\left(\frac{\boldsymbol{B}\cdot\nabla\phi_1}{B^2}\right)\right) = \frac{i}{\omega\mu_0 B}\nabla\cdot\left(B^2\nabla_\perp\left(\frac{\boldsymbol{B}\cdot\nabla\phi_1}{B^2}\right)\right). \tag{14.47}$$

Then (14.44-47) yield

$$\nabla\cdot\left(i\frac{\omega}{\mu_0}\frac{1}{v_{\rm A}^2}\nabla_\perp\phi_1\right) + \nabla\left(\frac{j_\parallel}{B}\boldsymbol{B}_{\perp 1}\right) + \nabla\left(\frac{j_{\parallel 1}}{B}\boldsymbol{B}\right) = 0$$

$$\nabla\cdot\left(\frac{\omega^2}{v_{\rm A}^2}\nabla_\perp\phi_1\right) + \mu_0\nabla\left(\frac{j_\parallel}{B}\right)\cdot\boldsymbol{B}\times\nabla\left(\frac{(\boldsymbol{B}\cdot\nabla)\phi_1}{B^2}\right) + (\boldsymbol{B}\cdot\nabla)\left(\frac{1}{B^2}\nabla\cdot\left(B^2\nabla_\perp\cdot\left(\frac{\boldsymbol{B}\cdot\nabla\phi_1}{B^2}\right)\right)\right) = 0. \tag{14.48}$$

When (R,φ,Z) and (r,θ,ζ) coordinates are introduced by,

$$R = R_0 + r\cos\theta, \qquad Z = r\sin\theta, \qquad \varphi = -\frac{\zeta}{R}$$

and following notations are used

$$\phi_1(r,\theta,\zeta,t) = \sum_{\rm m}\phi_{\rm m}(r)\exp i(-{\rm m}\theta + {\rm n}\varphi - \omega t), \qquad (\boldsymbol{b}\cdot\nabla)\phi_{\rm m} = \frac{i}{R_0}\left({\rm n} - \frac{\rm m}{q(r)}\right)\phi_{\rm m} = -ik_{\parallel{\rm m}}\phi_{\rm m},$$

$$k_{\parallel{\rm m}} = \frac{1}{R_0}\left({\rm n} - \frac{\rm m}{q(r)}\right), \qquad E_{\rm m} \equiv \frac{\phi_{\rm m}}{R},$$

(14.48) is reduced to (ref.[8])

$$\frac{\rm d}{{\rm d}r}\left(r^3\left(\frac{\omega^2}{v_{\rm A}^2} - k_{\parallel{\rm m}}^2\right)\frac{{\rm d}E_{\rm m}}{{\rm d}r}\right) + r^2E_{\rm m}\frac{\rm d}{{\rm d}r}\left(\frac{\omega}{v_{\rm A}}\right)^2 - ({\rm m}^2-1)\left(\frac{\omega^2}{v_{\rm A}^2} - k_{\parallel{\rm m}}^2\right)rE_{\rm m}$$
$$+\frac{\rm d}{{\rm d}r}\left(r^3\left(\frac{\omega}{v_{\rm A}}\right)^2\frac{2r}{R_0}\left(\frac{{\rm d}E_{{\rm m}+1}}{{\rm d}r} + \frac{{\rm d}E_{{\rm m}-1}}{{\rm d}r}\right)\right) = 0. \tag{14.49}$$

As is seen in fig.14.3, mode structure has a sharp transition of m=1 and m=2 components at the gap location. Therefore m and m+1 modes near gap location reduces

$$\left(\frac{\omega^2}{v_{\rm A}^2} - k_{\parallel{\rm m}}^2\right)\frac{{\rm d}E_{\rm m}}{{\rm d}r} + \frac{2r}{R_0}\left(\frac{\omega}{v_{\rm A}}\right)^2\frac{{\rm d}E_{{\rm m}+1}}{{\rm d}r} \approx 0$$

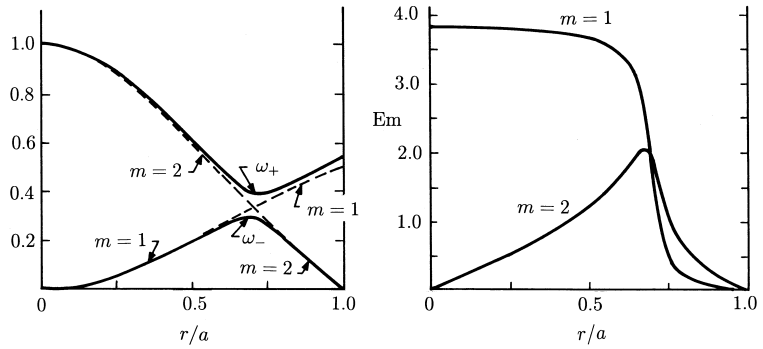

Fig.14.3 Left-hand side figure: The toroidal shear Alfvén resonance frequencies Ω that corresponds to (n=1, m=1) and (n=1. m=2), $q(r) = 1 + (r/a)^2$, $a/R = 0.25$, $\Omega \equiv \omega/(v_{\rm A}(0)/R_0)$. Right-hand side figure: The structure of the global mode amplitude as a function of radius.

$$\left(\frac{\omega^2}{v_{\rm A}^2} - k_{\parallel {\rm m}+1}^2\right)\frac{{\rm d}E_{{\rm m}+1}}{{\rm d}r} + \frac{2r}{R_0}\left(\frac{\omega}{v_{\rm A}}\right)^2\frac{{\rm d}E_{\rm m}}{{\rm d}r} \approx 0,$$

so that toroidal shear Alfvén resonance frequency is given by

$$\begin{vmatrix} \left(\frac{\omega^2}{v_{\rm A}^2} - k_{\parallel {\rm m}}^2\right) & 2\epsilon\left(\frac{\omega}{v_{\rm A}}\right)^2 \\ 2\epsilon\left(\frac{\omega}{v_{\rm A}}\right)^2 & \left(\frac{\omega^2}{v_{\rm A}^2} - k_{\parallel {\rm m}+1}^2\right) \end{vmatrix} = 0. \tag{14.50}$$

When Shafranov shift is included in the coordinates of (R, φ, Z) and (r, θ, ζ), coupling constant becomes 2.5ϵ instead of 2ϵ (ref.[8]). The energy integral from (14.49) without coupling term of m$\pm$1 modes is reduced to following equation by use of partial integral:

$$G(\omega, E_{\rm m}) \equiv {\rm P}\int_0^a {\rm d}r\, r\left(\left(r^2\left(\frac{{\rm d}E_{\rm m}}{{\rm d}r}\right)^2 + ({\rm m}^2-1)E_{\rm m}^2\right)\left(\frac{\omega^2}{v_{\rm A}^2} - k_{\parallel {\rm m}}^2\right) - \omega^2 r E_{\rm m}^2\frac{\rm d}{{\rm d}r}\frac{1}{v_{\rm A}^2}\right)$$

$$= E_{\rm m}(r_{\rm s}^-)C_{\rm m}(r_{\rm s}^-) - E_{\rm m}(r_{\rm s}^+)C_{\rm m}(r_{\rm s}^+) \tag{14.51}$$

where

$$C_{\rm m}(r) = \left(\frac{\omega^2}{v_{\rm A}^2} - k_{\parallel {\rm m}}^2\right) r^2\frac{{\rm d}E_{\rm m}}{{\rm d}r}, \qquad E_{\rm m}(a) = 0.$$

The radius $r = r_{\rm s}$ is singular at which $(\omega^2/v_{\rm A})^2 - k_{\parallel {\rm m}}^2 = 0$ and P is principal value of the integral. From this formulation, it is possible to estimate the damping rate of TAE and is given by (ref.[8])

$$\frac{\delta\omega}{\omega} = -i\pi\frac{{\rm sign}(\omega_0)C_{\rm m}(r_{\rm s})^2}{r_{\rm s}^3\left|\frac{\partial}{\partial r}\left(\frac{\omega^2}{v_{\rm A}^2} - k_{\parallel {\rm m}}^2\right)\right|\omega_0\frac{\partial G}{\partial\omega_0}}. \tag{14.52}$$

Since $\omega_0\partial G/\partial\omega_0 > 0$, ${\rm Im}(\delta\omega) < 0$. This is called continuum damping.

14.2b Instability of TAE Driven by Energetic Particles

Dynamics of energetic particles must be treated by kinetic theory. Basic equations will be described according to Betti and Freidberg (ref.[9]).

$$\frac{\partial f_{\rm j}}{\partial t} + \boldsymbol{v}\cdot f_{\rm j} + \frac{q_{\rm j}}{m_{\rm j}}(\boldsymbol{E} + \boldsymbol{v}\times\boldsymbol{B})\cdot\nabla_v f_{\rm j} = 0, \tag{14.53}$$

$$\frac{\partial n_{\rm j}}{\partial t} + \nabla \cdot (n_{\rm j}\boldsymbol{u}_{\rm j}) = 0, \tag{14.54}$$

$$m_{\rm j}\frac{\partial}{\partial t}(n_{\rm j}\boldsymbol{u}_{\rm j}) + \nabla \cdot P_{\rm j} = q_{\rm j}n_{\rm j}(\boldsymbol{E} + \boldsymbol{u}_{\rm j} \times \boldsymbol{B}), \tag{14.55}$$

$$P_{\rm j} = m_{\rm j}\int \boldsymbol{v}\boldsymbol{v}f_{\rm j}{\rm d}\boldsymbol{v}, \tag{14.56}$$

$$\boldsymbol{B}_1 = \nabla \times (\boldsymbol{\xi}_\perp \times \boldsymbol{B}), \tag{14.57}$$

$$\mu_0\boldsymbol{j}_1 = \nabla\boldsymbol{B}_1 = \nabla \times \nabla \times (\boldsymbol{\xi}_\perp \times \boldsymbol{B}), \tag{14.58}$$

$$\boldsymbol{j}_1 \times \boldsymbol{B} + \boldsymbol{j} \times \boldsymbol{B}_1 = \sum_{\rm j}(\nabla P_{1{\rm j}} - i\omega m_{\rm j}(n_{1{\rm j}}\boldsymbol{u}_{\rm j} + n_{\rm j}\boldsymbol{u}_{1{\rm j}})) \approx \sum_{\rm j}\left(\nabla P_{1{\rm j}} - \rho\omega^2\boldsymbol{\xi}_{\perp{\rm j}}\right). \tag{14.59}$$

$F_{\rm j}$ is equilibrium distribution function of axisymmetric torus. $F_{\rm j}(\varepsilon, p_\varphi)$ is assumed to be a function of constants of motion ε and p_φ, where

$$\varepsilon = \frac{m_{\rm j}}{2}v^2 + q_{\rm j}\phi, \quad p_\varphi = m_{\rm j}Rv_\varphi + q_{\rm j}\psi, \quad \psi = RA_\varphi \tag{14.60}$$

$$RB_Z = \frac{\partial\psi}{\partial R}, \qquad RB_R = -\frac{\partial\psi}{\partial Z},$$

$$\frac{\partial f_{1{\rm j}}}{\partial t} + \boldsymbol{v} \cdot f_{1{\rm j}} + \frac{q_{\rm j}}{m_{\rm j}}(\boldsymbol{v} \times \boldsymbol{B}) \cdot \nabla_v f_{1{\rm j}} = -\frac{q_{\rm j}}{m_{\rm j}}(\boldsymbol{E} + \boldsymbol{v} \times \boldsymbol{B}_1) \cdot \nabla_v F_{\rm j} \tag{14.61}$$

$$\nabla_v F_{\rm j} = \hat{\boldsymbol{\varphi}}\frac{\partial p_\varphi}{\partial v_\varphi}\frac{\partial F_{\rm j}}{\partial p_\varphi} + (\nabla_v\varepsilon)\frac{\partial F_{\rm j}}{\partial\varepsilon} = \hat{\boldsymbol{\varphi}}m_{\rm j}R\frac{\partial F_{\rm j}}{\partial p_\varphi} + m_{\rm j}\boldsymbol{v}\frac{\partial F_{\rm j}}{\partial\varepsilon}. \tag{14.62}$$

The solution is obtained by integral along the particle orbit (refer appendix sec.C.2)

$$f_{1{\rm j}} = -\frac{q_{\rm j}}{m_{\rm j}}\int_{-\infty}^{t}(\boldsymbol{E} + \boldsymbol{v} \times \boldsymbol{B}_1) \cdot \nabla_v F_{\rm j}{\rm d}t'. \tag{14.63}$$

It is assumed that the perturbations are in the form of

$$Q_1 = Q_1(R, Z)\exp i({\rm n}\varphi - \omega t).$$

The second term $m_{\rm j}\boldsymbol{v}(\partial F_{\rm j}/\partial\varepsilon)$ of the right-hand side of (14.62) contributes to the integral

$$-\frac{q_{\rm j}}{m_{\rm j}}\int_{-\infty}^{t}(\boldsymbol{E} + \boldsymbol{v} \times \boldsymbol{B}_1) \cdot m_{\rm j}\boldsymbol{v}\frac{\partial F_{\rm j}}{\partial\varepsilon}{\rm d}t' = -q_{\rm j}\frac{\partial F_{\rm j}}{\partial\varepsilon}\int_{-\infty}^{t}\boldsymbol{E} \cdot \boldsymbol{v}{\rm d}t'.$$

The contribution from the first term $m_{\rm j}R(\partial F_{\rm j}/\partial p_\varphi)$ is

$$-\frac{q_{\rm j}}{m_{\rm j}}\left(\int_{-\infty}^{t}(\boldsymbol{E}_\varphi m_{\rm j}R\frac{\partial F_{\rm j}}{\partial p_\varphi}{\rm d}t' + \int_{-\infty}^{t}m_{\rm j}R(\boldsymbol{v} \times \boldsymbol{B}_1)_\varphi\frac{\partial F_{\rm j}}{\partial p_\varphi}{\rm d}t'\right)$$

$$= -q_{\rm j}\frac{\partial F_{\rm j}}{\partial p_\varphi}\left(\int_{-\infty}^{t}\boldsymbol{E}_\varphi R{\rm d}t' + \int_{-\infty}^{t}R\boldsymbol{v} \times \left(\frac{(\nabla \times \boldsymbol{E})_\varphi}{-i\omega}\right){\rm d}t'\right)$$

$$= -q_{\rm j}\frac{\partial F_{\rm j}}{\partial p_\varphi}\left(\int_{-\infty}^{t}\frac{1}{-i\omega}\frac{\partial(E_\varphi R)}{\partial t}{\rm d}t' + \int_{-\infty}^{t}\left(\frac{\rm n}{\omega}(\boldsymbol{v} \cdot \boldsymbol{E}) - \frac{1}{i\omega}(\boldsymbol{v} \cdot \nabla)(E_\varphi R)\right){\rm d}t'\right)$$

$$= -q_{\rm j}\frac{\partial F_{\rm j}}{\partial p_\varphi}\left(\int_{-\infty}^{t}\frac{1}{-i\omega}\frac{{\rm d}(E_\varphi R)}{{\rm d}t}{\rm d}t' + \int_{-\infty}^{t}\frac{\rm n}{\omega}(\boldsymbol{v} \cdot \boldsymbol{E}){\rm d}t'\right).$$

The solution is

$$f_{1\mathrm{j}} = -\frac{q_\mathrm{j}}{\omega}\left(i\frac{\partial F_\mathrm{j}}{\partial p_\varphi}RE_\varphi + \left(\omega\frac{\partial F_\mathrm{j}}{\partial \varepsilon} + \mathrm{n}\frac{\partial F_\mathrm{j}}{\partial p_\varphi}\right)\int_{-\infty}^{t}(\boldsymbol{E}\cdot\boldsymbol{v})\mathrm{d}t'\right). \tag{14.64}$$

Since

$$E_{1\parallel} = 0, \qquad -i\omega\boldsymbol{\xi}_\perp = \frac{\boldsymbol{E}_\perp\times\boldsymbol{B}}{B^2}, \qquad \boldsymbol{E}_\perp = i\omega(\boldsymbol{\xi}_\perp\times\boldsymbol{B}),$$

$$RE_\varphi = i\omega(\boldsymbol{\xi}_\perp\times\boldsymbol{B})_\varphi R = i\omega(\xi_{\perp R}B_Z - \xi_{\perp Z}B_R)R = -i\omega(\boldsymbol{\xi}\cdot\nabla\psi),$$

$$\boldsymbol{E}\cdot\boldsymbol{v} = i\omega(\boldsymbol{\xi}_\perp\times\boldsymbol{B})\cdot\boldsymbol{v} = -i\omega\boldsymbol{\xi}_\perp\cdot(\boldsymbol{v}\times\boldsymbol{B}) = -i\omega\boldsymbol{\xi}_\perp\cdot\frac{m_\mathrm{j}}{q_\mathrm{j}}\frac{\mathrm{d}\boldsymbol{v}}{\mathrm{d}t}$$

$$= -i\omega\frac{m_\mathrm{j}}{q_\mathrm{j}}\boldsymbol{\xi}_\perp\cdot\frac{\mathrm{d}\boldsymbol{v}}{\mathrm{d}t} = -i\omega\frac{m_\mathrm{j}}{q_\mathrm{j}}\left(\frac{\mathrm{d}(\boldsymbol{\xi}_\perp\cdot\boldsymbol{v})}{\mathrm{d}t} - \boldsymbol{v}\cdot\frac{\mathrm{d}\boldsymbol{\xi}_\perp}{\mathrm{d}t}\right),$$

$f_{1\mathrm{j}}$ becomes

$$f_{1\mathrm{j}} = -q_\mathrm{j}\frac{\partial F_\mathrm{j}}{\partial p_\varphi}(\boldsymbol{\xi}\cdot\nabla\psi) + im_\mathrm{j}\left(\omega\frac{\partial F_\mathrm{j}}{\partial\varepsilon} + \mathrm{n}\frac{\partial F_\mathrm{j}}{\partial p_\varphi}\right)\left(\boldsymbol{\xi}_\perp\cdot\boldsymbol{v} - \int_{-\infty}^{t}\boldsymbol{v}\cdot\frac{\mathrm{d}\boldsymbol{\xi}_\perp}{\mathrm{d}t}\mathrm{d}t'\right)$$

$$= -q_\mathrm{j}\frac{\partial F_\mathrm{j}}{\partial\psi} + im_\mathrm{j}(\omega-\omega_{*\mathrm{j}})\frac{\partial F_\mathrm{j}}{\partial\varepsilon}(\boldsymbol{\xi}_\perp\cdot\boldsymbol{v} - s_\mathrm{j}) \tag{14.65}$$

where

$$s_\mathrm{j} \equiv \int_{-\infty}^{t}\boldsymbol{v}\cdot\frac{\mathrm{d}\boldsymbol{\xi}_\perp}{\mathrm{d}t}\mathrm{d}t', \qquad \omega_{*\mathrm{j}} \equiv -\frac{n\partial F_\mathrm{j}/\partial p_\varphi}{\partial F_\mathrm{j}/\partial\varepsilon}.$$

s_j is reduced to

$$s_\mathrm{j} = \int_{-\infty}^{t}\left(\frac{v_\perp^2}{2}\nabla\cdot\boldsymbol{\xi}_\perp + \left(\frac{v_\perp^2}{2} - v_\parallel^2\right)\boldsymbol{\xi}\cdot\boldsymbol{\kappa}\right)\mathrm{d}t' \tag{14.66}$$

as will be shown in the end of this subsection. The perturbed pressure tensor is

$$P_{1\mathrm{j}} = \int m_\mathrm{j}\boldsymbol{v}\boldsymbol{v}f_{1j}\mathrm{d}\boldsymbol{v} = P_{1\perp\mathrm{j}}I + (P_{1\parallel\mathrm{j}} - P_{1\perp\mathrm{j}})\boldsymbol{b}\boldsymbol{b} \tag{14.67}$$

and $\nabla P_{1\mathrm{j}}$ is given by (14.21b) and (14.22b). Then the equation of motion is

$$-\rho\omega^2\boldsymbol{\xi}_\perp = \boldsymbol{F}_\perp(\boldsymbol{\xi}_\perp) + i\boldsymbol{D}_\perp(\boldsymbol{\xi}_\perp), \tag{14.68}$$

$$\boldsymbol{F}_\perp(\boldsymbol{\xi}_\perp) = \boldsymbol{j}_1\times\boldsymbol{B} + \boldsymbol{j}\times\boldsymbol{B}_1 + \nabla(\boldsymbol{\xi}_\perp\cdot\nabla P_1), \tag{14.69}$$

$$\boldsymbol{D}_\perp(\boldsymbol{\xi}_\perp) = m_\mathrm{j}\int\left(\frac{v_\perp^2}{2}\nabla_\perp + \left(v_\parallel^2 - \frac{v_\perp^2}{2}\right)\boldsymbol{\kappa}\right)m_\mathrm{j}(\omega-\omega_{*\mathrm{j}})\frac{\partial F_\mathrm{j}}{\partial\varepsilon}s_\mathrm{j}\mathrm{d}\boldsymbol{v}. \tag{14.70}$$

$\boldsymbol{F}_\perp(\boldsymbol{\xi}_\perp)$ is the ideal MHD force operator for incompressible displacement. $\boldsymbol{D}_\perp(\boldsymbol{\xi}_\perp)$ contains the contribution of energetic particles. Eqs.(14.68-14.70) describe the low frequency, finite wave number stability of energetic particle-Alfvén waves in axisymmetric torus.

The energy integral of (14.68) consists of plasma kinetic energy normalization K_M, ideal MHD perpendicular potential energy δW_MHD and the kinetic contribution to the energy integral δW_K:

$$\omega^2 K_\mathrm{M} = \delta W_\mathrm{MHD} + \delta W_\mathrm{K}. \tag{14.71}$$

where

$$K_{\rm M} = \frac{1}{2}\int \rho|\boldsymbol{\xi}_\perp|^2 {\rm d}\boldsymbol{r},$$

$$\delta W_{\rm MHD} = -\frac{1}{2}\int \boldsymbol{\xi}_\perp^* \boldsymbol{F}_\perp(\boldsymbol{\xi}_\perp){\rm d}\boldsymbol{r},$$

$$\delta W_{\rm K} = -\frac{i}{2}\int \boldsymbol{\xi}_\perp^* \boldsymbol{D}_\perp(\boldsymbol{\xi}_\perp){\rm d}\boldsymbol{r}.$$

After a simple integration by parts, $\delta W_{\rm K}$ can be written as

$$\delta W_{\rm K} = \frac{i}{2}\sum_{\rm j}\int(\omega-\omega_{*\rm j})\frac{\partial F_{\rm j}}{\partial\varepsilon}s_{\rm j}\frac{{\rm d}s_{\rm j}^*}{{\rm d}t}{\rm d}\boldsymbol{v}{\rm d}\boldsymbol{r}, \tag{14.72}$$

since

$$\frac{{\rm d}s_{\rm j}^*}{{\rm d}t} = \left(\frac{v_\perp^2}{2}\nabla_\perp\cdot\boldsymbol{\xi}^* + \left(\frac{v_\perp^2}{2}-v_\parallel\right)\boldsymbol{\xi}_\perp\cdot\boldsymbol{\kappa}\right).$$

On the other hand ${\rm d}s_{\rm j}^*/{\rm d}t$ is given by

$$\frac{{\rm d}s_{\rm j}^*}{{\rm d}t} = i\omega^* s_{\rm j}^* + Ds_{\rm j}^*, \qquad D\equiv(\boldsymbol{v}\cdot\nabla)+\frac{q_{\rm j}}{m_{\rm j}}(\boldsymbol{v}\times\boldsymbol{B})\cdot\nabla_v.$$

With use of the notation $s_{\rm j}\equiv a_{\rm j}+ic_{\rm j}$ ($a_{\rm j}$ and $c_{\rm j}$ are real), we have

$$s_{\rm j}\frac{{\rm d}s_{\rm j}^*}{{\rm d}t} = i\omega^*|{\rm s_j}|^2 + i(c_{\rm j}Da_{\rm j}-a_{\rm j}Dc_{\rm j})+\frac{1}{2}D(a_{\rm j}^2+c_{\rm j}^2).$$

Contribution of the last term to the integral (14.72) by ${\rm d}\boldsymbol{r}{\rm d}\boldsymbol{v}$ is zero, since $F_{\rm j}$ and $\omega_{*\rm j}$ are functions of the constants of motion ε and p_φ and

$$\delta W_{\rm K} = \frac{1}{2}\sum_{\rm j}\int(\omega-\omega_{*\rm j})\frac{\partial F_{\rm j}}{\partial\varepsilon}(i\omega_{\rm i}|s_{\rm j}|^2+R_{\rm j}){\rm d}\boldsymbol{v}{\rm d}\boldsymbol{r},$$

$$R_{\rm j} = c_{\rm j}Da_{\rm j}-a_{\rm j}Dc_{\rm j}-\omega_{\rm r}|s_{\rm j}|^2.$$

The desired expression for the growth rate is obtained by setting the real and imaginary parts of (14.71) to to be equal individually:

$$\omega_{\rm r}^2 = \frac{\delta W_{\rm MHD}}{K_{\rm M}}+O(\beta). \tag{14.73}$$

$O(\beta)$ is the contribution of $R_{\rm j}$ term. In the limit of $\omega_{\rm i}\ll\omega_{\rm r}$, the imaginary part yields

$$\omega_{\rm i}\approx\frac{W_{\rm K}}{K_{\rm M}}, \qquad W_{\rm K}\equiv\lim_{\omega_{\rm i}\to0}\left(\frac{1}{4\omega_{\rm r}}\sum_{\rm j}\int(\omega-\omega_{*\rm j})\frac{\partial F_{\rm j}}{\partial\varepsilon}\omega_{\rm i}|s_{\rm j}|^2{\rm d}\boldsymbol{v}{\rm d}\boldsymbol{r}\right). \tag{14.74}$$

Let us estimate (14.74). Since $\nabla\cdot\boldsymbol{\xi}_\perp+2\boldsymbol{\xi}_\perp\cdot\boldsymbol{\kappa}\approx0$ (refer (B.7) of App. B), $s_{\rm j}$ is

$$s_{\rm j} = -m_{\rm j}\int_{-\infty}^{t}\left(v_\parallel^2+\frac{v_\perp^2}{2}\right)(\boldsymbol{\kappa}\cdot\boldsymbol{\xi}_\perp){\rm d}t' = m_{\rm j}\int_{-\infty}^{t}\left(v_\parallel^2+\frac{v_\perp^2}{2}\right)\frac{\xi_R}{R}{\rm d}t'$$

where

$$\xi_R = \xi_r\cos\theta-\xi_\theta\sin\theta = \xi_r\frac{e^{i\theta}+e^{-i\theta}}{2}-\xi_\theta\frac{e^{i\theta}-e^{-i\theta}}{2i}.$$

ξ_r and ξ_θ are ($\nabla\cdot\boldsymbol{\xi} = (1/r)(\partial(r\xi_r)/\partial r) - i(\mathrm{m}/r)\xi_\theta \approx 0$)

$$\xi_r = \sum_{\mathrm{m}} \xi_{\mathrm{m}}(r) e^{-i\mathrm{m}\theta}, \qquad \xi_\theta = -i\sum_{\mathrm{m}} \frac{(r\xi_{\mathrm{m}}(r))'}{\mathrm{m}} e^{-i\mathrm{m}\theta}.$$

Since the leading-order guiding center of orbits of energetic particles are given by

$$r(t') = r(t), \quad \theta(t') = \frac{v_\parallel B_\theta}{rB_\varphi}(t'-t) + \ \theta(t), \quad \varphi(t') = \frac{v_\parallel}{r}(t'-t) + \varphi(t)$$

perturbations along the orbit become

$$\exp i(-\mathrm{m}\theta(t') + \mathrm{n}\varphi(t') - \omega t') = \exp\left(i(-\frac{\mathrm{m}B_\theta}{rB_\varphi}v_\parallel + \frac{\mathrm{n}v_\parallel}{R} - \omega)(t'-t)\right)\exp i(-\mathrm{m}\theta(t) + \mathrm{n}\varphi(t) - \omega t)$$

$$= \exp\left(-i(\omega-\omega_{\mathrm{m}})(t'-t)\right)\exp i(-\mathrm{m}\theta(t) + \mathrm{n}\varphi(t) - \omega t)$$

where

$$\omega_{\mathrm{m}} = \frac{v_\parallel}{R}\left(\mathrm{n} - \frac{\mathrm{m}}{q}\right).$$

and

$$s_{\mathrm{j}} = \frac{m_{\mathrm{j}}(v_\parallel^2 + v_\perp^2/2)}{R}\frac{1}{2}\sum_{\mathrm{m}}(\xi_{\mathrm{m}-1} + \xi_{\mathrm{m}+1} - i\xi_{\theta(\mathrm{m}-1)} + i\xi_{\theta(\mathrm{m}+1)})\exp i(-m\theta + \mathrm{n}\varphi - \omega t)$$

$$\times \int_\infty^0 \exp(-i(\omega-\omega_{\mathrm{m}})t''\mathrm{d}t''$$

$$= i\frac{m_{\mathrm{j}}}{2R}\left(v_\parallel^2 + \frac{v_\perp^2}{2}\right)\sum_{\mathrm{m}}\left(\xi_{\mathrm{m}-1} + \xi_{\mathrm{m}+1} - i\frac{(r\xi_{\mathrm{m}-1})'}{(\mathrm{m}-1)} + i\frac{(r\xi_{\mathrm{m}+1})'}{(\mathrm{m}+1)}\right)\frac{\exp i(-i\mathrm{m}\theta + \mathrm{n}\varphi - \omega t)}{(\omega-\omega_{\mathrm{m}})}. \quad (14.75)$$

It is assumed that perturbation consists primarily of two toroidally coupled harmonics $\boldsymbol{\xi}_{\mathrm{m}}$ and $\boldsymbol{\xi}_{\mathrm{m}+1}$ and all other harmonics are essentially zero. Strong coupling occurs in a narrow region of thickness $\sim \epsilon a$ localized about the surface $r = r_0$ corresponding to $q(r_0) = (2\mathrm{m}+1)/2\mathrm{n} = q_0$. The mode localization implies that $\xi'_{\mathrm{m}\pm1}$ terms dominate in (14.75). Substituting these results into the expression for s_{j} and maintaining only these terms which do not average to zero in θ leads to the following expression for $|\mathrm{s_j}|^2$:

$$|\mathrm{s_j}|^2 = \frac{m_{\mathrm{j}}^2 r_0^2}{4R}\left(v_\parallel^2 + \frac{v_\perp^2}{2}\right)^2\left(\frac{|\xi'_{(\mathrm{m}+1)}|^2}{(\mathrm{m}+1)^2} + \frac{|\xi'_{\mathrm{m}}|^2}{\mathrm{m}^2}\right)\left(\frac{1}{|\omega-\omega_{\mathrm{m}}|^2} + \frac{1}{|\omega-\omega_{\mathrm{m}-1}|^2}\right)$$

since $\omega_{\mathrm{m}+1} = -\omega_{\mathrm{m}}$ and $\omega_{\mathrm{m}+2} = -\omega_{\mathrm{m}-1}$. K_{M} is given by

$$K_{\mathrm{M}} = \frac{r_0^2\rho_0}{2}\int\left(\frac{|\xi'_{\mathrm{m}}|^2}{\mathrm{m}^2} + \frac{|\xi'_{\mathrm{m}+1}|^2}{(\mathrm{m}+1)^2}\right)\mathrm{d}\boldsymbol{r}. \quad (14.76)$$

Using the relations $\omega_{\mathrm{r}} \approx k_\parallel v_{\mathrm{A}}$, $k_\parallel = 1/(2q_0R)$, $q_0 = (2\mathrm{m}+1/2\mathrm{n})$, we obtain the following expression for growth rate:

$$\frac{\omega_{\mathrm{i}}}{k_\parallel v_{\mathrm{A}}} = \lim_{\omega_{\mathrm{i}}\to 0}\sum_{\mathrm{j}}\frac{\mu_0 m_{\mathrm{j}}^2 q_0^2}{2B^2}\int\left(v_\parallel^2 + \frac{v_\perp^2}{2}\right)^2\left(\omega_{\mathrm{r}}\frac{\partial F_{\mathrm{j}}}{\partial\varepsilon} + \frac{\mathrm{n}}{q_{\mathrm{j}}}\frac{\partial F_{\mathrm{j}}}{\partial\psi}\right)\left(\frac{\omega_{\mathrm{i}}}{|\omega-\omega_{\mathrm{m}}|^2} + \frac{\omega_{\mathrm{i}}}{|\omega-\omega_{\mathrm{m}-1}|^2}\right)\mathrm{d}\boldsymbol{v}. \quad (14.77)$$

With use of the formula $\int_{-\infty}^{\infty}\epsilon/(x^2+\epsilon^2)\mathrm{d}x = \pi$, short calculation of integral by $v_\parallel$ yields

$$\frac{\omega_{\mathrm{i}}}{k_\parallel v_{\mathrm{A}}} = \sum_{\mathrm{j}}\frac{2\pi^2\mu_0 m_{\mathrm{j}}^2 R q_0^3}{2B^2}\int\left(v_\parallel^2 + \frac{v_\perp^2}{2}\right)^2\left(\omega_{\mathrm{r}}\frac{\partial F_{\mathrm{j}}}{\partial\varepsilon} + \frac{\mathrm{n}}{q_{\mathrm{j}}}\frac{\partial F_{\mathrm{j}}}{\partial\psi}\right)v_\perp\mathrm{d}v_\perp\Big|_{v_\parallel=v_{\mathrm{A}}} + \Big|_{v_\parallel=v_{\mathrm{A}}/3}.$$

(14.78)

(Note $\omega_{\rm m} = v_\parallel/(2q_0R)$, $\omega_{\rm m-1} = 3v_\parallel/(2q_0R)$, $\omega_{\rm r} = v_{\rm A}/2q_0R$.)
Equation (14.78) gives the TAE growth rate for arbitrary distribution function $F_{\rm j}(\varepsilon,\psi)$. The second term of (14.78) is due to sideband resonance.

The growth rate can be easily evaluated for a Maxwellian distribution

$$F_{\rm j} = n_{\rm j}\left(\frac{m_{\rm j}}{2\pi\kappa T_{\rm j}}\right)^{3/2}\exp\left(-\frac{m_{\rm j}v^2}{2\pi\kappa T_{\rm j}}\right).$$

Here $n_{\rm j} = n_{\rm j}(\psi)$ and $T_{\rm j} = T_{\rm j}(\psi)$. Some straightforward calculation leads to

$$\left(\frac{\omega_{\rm i}}{k_\parallel v_{\rm A}}\right)_{\rm j} = -q_0^2\beta_{\rm j}\left(G^{\rm T}_{\rm mj} - {\rm n}q_0\delta_{\rm j}\frac{H^{\rm T}_{\rm mj}+\eta_{\rm j}J^{\rm T}_{\rm mj}}{1+\eta_{\rm j}}\right) \tag{14.79}$$

where

$$\beta_{\rm j} = \frac{n_{\rm j}\kappa T_{\rm j}}{B^2/2\mu_0},\quad \delta_{\rm j} = -r_{\rm Lpj}\frac{{\rm d}p_{\rm j}/{\rm d}r}{p_{\rm j}},\quad r_{\rm Lpj}\equiv\frac{m_{\rm j}v_{\rm Tj}}{q_{\rm j}B_{\rm p}},\quad \eta_{\rm j}\equiv\frac{{\rm d}\ln T_{\rm j}}{{\rm d}\ln n_{\rm j}}.$$

Each of these quantities is evaluated at $r = r_0$. The functions $G^{\rm T}_{\rm mj}$, $H^{\rm T}_{\rm mj}$ and $J^{\rm T}_{\rm mj}$ are functions of single parameter $\lambda_{\rm j}\equiv v_{\rm A}/v_{\rm Tj}$ ($v^2_{\rm Tj}\equiv 2\kappa T_{\rm j}/m_{\rm j}$) and are given by

$$G^{\rm T}_{\rm mj} = g^{\rm T}_{\rm mj}(\lambda_{\rm j}) + g^{\rm T}_{\rm mj}(\lambda_{\rm j}/3),\quad g^{\rm T}_{\rm mj}(\lambda_{\rm j}) = (\pi^{1/2}/2)\lambda_{\rm j}(1+2\lambda_{\rm j}^2+2\lambda_{\rm j}^4)e^{-\lambda_{\rm j}^2}$$

$$H^{\rm T}_{\rm mj} = h^{\rm T}_{\rm mj}(\lambda_{\rm j}) + h^{\rm T}_{\rm mj}(\lambda_{\rm j}/3),\quad h^{\rm T}_{\rm mj}(\lambda_{\rm j}) = (\pi^{1/2}/2)(1+2\lambda_{\rm j}^2+2\lambda_{\rm j}^4)e^{-\lambda_{\rm j}^2} \tag{14.80}$$

$$J^{\rm T}_{\rm mj} = j^{\rm T}_{\rm mj}(\lambda_{\rm j}) + j^{\rm T}_{\rm mj}(\lambda_{\rm j}/3),\quad j^{\rm T}_{\rm mj}(\lambda_{\rm j}) = (\pi^{1/2}/2)(3/2+2\lambda_{\rm j}^2+\lambda_{\rm j}^4+2\lambda_{\rm j}^6)e^{-\lambda_{\rm j}^2}$$

For the alpha particles it is more reasonable to assume a slowing down distribution

$$F_\alpha = \frac{A}{(v^2+v_0^2)^{3/2}},\qquad (\,0<v<v_\alpha,\quad \frac{m_\alpha v_\alpha^2}{2} = 3.5{\rm MeV})$$

A and v_0 are related to the density and pressure as follows:

$$A\approx\frac{n_\alpha}{4\pi\ln(v_\alpha/v_0)},\qquad p_\alpha\approx\frac{n_\alpha m_\alpha v_\alpha^2/2}{3\ln(v_\alpha/v_0)},\qquad \frac{m_{\rm j}v_0^2}{2}\approx\kappa T_{\rm j}.$$

After another straightforward calculation we obtain an analogous expression for the alpha particle contribution to the growth rate:

$$\left(\frac{\omega_{\rm i}}{k_\parallel v_{\rm A}}\right)_\alpha = -q_0^2\beta_\alpha\left(G^{\rm T}_{{\rm s}\alpha} - nq_0\delta_\alpha H^{\rm T}_{{\rm s}\alpha}\right) \tag{14.82}$$

where

$$\beta_\alpha = \frac{p_\alpha}{B^2/2\mu_0},\quad \delta_\alpha = -\frac{2}{3}r_{{\rm L}\alpha}\frac{{\rm d}p_\alpha/{\rm d}r}{p_\alpha},\quad r_{{\rm Lp}\alpha} = \frac{m_\alpha v_\alpha}{q_\alpha B_{\rm p}}.$$

The functions $G^{\rm T}_{{\rm s}\alpha}$ and $H^{\rm T}_{{\rm s}\alpha}$ are functions of the parameter $\lambda_\alpha\equiv v_{\rm A}/v_\alpha$ and are given by

$$G^{\rm T}_{{\rm s}\alpha} = g^{\rm T}_{\rm s}(\lambda_\alpha) + g^{\rm T}_{\rm s}(\lambda_\alpha/3),\quad g^{\rm T}_{\rm s}(\lambda_\alpha) = (3\pi/16)\lambda_\alpha(3+4\lambda_\alpha-6\lambda_\alpha^2-\lambda_\alpha^4)H(1-\lambda_\alpha)$$

$$H_{\rm s}^{\rm T} = h_{\rm s}^{\rm T}(\lambda_\alpha) + h_{\rm s}^{\rm T}(\lambda_\alpha/3), \quad h_{\rm s\alpha}^{\rm T}(\lambda_\alpha) = (3\pi/16)(1 + 6\lambda_\alpha^2 - 4\lambda_\alpha^3 - 3\lambda_\alpha^4)H(1-\lambda_\alpha) \tag{14.83}$$

$H(1-\lambda_\alpha)$ is the Heaviside step function ($H(x) = 1$ for $x > 0$, $H(x) = 0$ for $x < 0$). The final form of the growth rate is obtained by combining the contributions of ions and electrons of core plasma and α particles:

$$\frac{\omega_{\rm i}}{k_\parallel v_{\rm A}} = -q_0^2 \left(\beta_{\rm i} G_{\rm mi}^{\rm T} + \beta_{\rm e} G_{\rm me}^{\rm T} + \beta_\alpha (G_{\rm s\alpha}^{\rm T} - {\rm n} q_0 \delta_\alpha H_{\rm s\alpha}^{\rm T})\right) \tag{14.84}$$

where $\beta_{\rm i}$, $\beta_{\rm e}$ and β_α are $\beta_{\rm j} \equiv n_{\rm j}\kappa T_{\rm j}/B^2/2\mu_0$ of ions and electrons of core plasma and α particles. The contributions of ions and electron of core plasma are Landau damping. The marginal condition for excitation of TAE is

$$\beta_\alpha > \frac{\beta_{\rm i} G_{\rm i}^{\rm T}(\lambda_{\rm i})}{{\rm n} q_0 \delta_\alpha H_{\rm s\alpha}^{\rm T} - G_{\rm s\alpha}^{\rm T}}, \qquad \delta_\alpha > \frac{G_{\rm s\alpha}}{{\rm n} q_0 H_{\rm s\alpha}^{\rm T}}. \tag{14.85}$$

Derivation of (14.66) is described as follow:

$$\boldsymbol{v}\cdot\frac{{\rm d}\boldsymbol{\xi}}{{\rm d}t} = \sum_{\rm i} v_{\rm i}\frac{{\rm d}\xi_{\rm i}}{{\rm d}t} = \sum_{\rm i} v_{\rm i}\frac{\partial\xi_{\rm i}}{\partial t} + \sum_{\rm i} v_{\rm i}(\boldsymbol{v}\cdot\nabla)\xi_{\rm i} = \sum_{\rm i} -i\omega v_{\rm i}\xi_{\rm i} + \sum_{\rm ij} v_{\rm i}v_{\rm j}\frac{\partial\xi_{\rm i}}{x_{\rm j}}$$

$$\boldsymbol{v} = v_\parallel \boldsymbol{b} + v_\perp \cos(\Omega t)\hat{\boldsymbol{e}}_\perp - v_\perp \sin(\Omega t)(\boldsymbol{b}\times\hat{\boldsymbol{e}}_\perp)$$

$$\overline{\boldsymbol{v}\boldsymbol{v}} = v_\parallel^2 \boldsymbol{b}\boldsymbol{b} + v_\perp^2 \overline{\cos(\Omega t)^2}\hat{\boldsymbol{e}}_\perp\hat{\boldsymbol{e}}_\perp + v_\perp^2\overline{\sin(\Omega t)^2}(\boldsymbol{b}\times\hat{\boldsymbol{e}}_\perp)(\boldsymbol{b}\times\hat{\boldsymbol{e}}_\perp)$$

$$= (v_\parallel^2 - v_\perp^2/2)\boldsymbol{b}\boldsymbol{b} + (v_\perp^2/2)(\boldsymbol{b}\boldsymbol{b} + \hat{\boldsymbol{e}}_\perp\hat{\boldsymbol{e}}_\perp + (\boldsymbol{b}\times\hat{\boldsymbol{e}}_\perp)(\boldsymbol{b}\times\hat{\boldsymbol{e}}_\perp)) = (v_\parallel^2 - v_\perp^2/2)\boldsymbol{b}\boldsymbol{b} + v_\perp^2/2)I,$$

$$\overline{\boldsymbol{v}\cdot\frac{{\rm d}\boldsymbol{\xi}}{{\rm d}t}} = -i\omega\overline{v_\parallel\xi_\parallel} + (v_\perp^2/2)\nabla\cdot\boldsymbol{\xi} + (v_\parallel^2 - v_\perp^2/2)\sum_{\rm ij} b_{\rm i}b_{\rm j}\frac{\partial\xi_{\rm i}}{\partial x_{\rm j}},$$

$$\sum_{\rm ij}\left(b_{\rm i}b_{\rm j}\frac{\partial\xi_{\rm i}}{\partial x_{\rm j}} + b_{\rm j}\xi_{\rm i}\frac{\partial b_{\rm i}}{\partial x_{\rm j}}\right) = \sum_{\rm ij} b_{\rm j}\frac{\partial}{\partial x_{\rm j}}(\xi_{\rm i}b_{\rm i})$$

$$\sum_{\rm ij} b_{\rm i}b_{\rm j}\frac{\partial\xi_{\rm i}}{\partial x_{\rm j}} = -\xi\cdot(\boldsymbol{b}\cdot\nabla)\boldsymbol{b} + (\boldsymbol{b}\cdot\nabla)(\boldsymbol{\xi}\cdot\boldsymbol{b}) = -\boldsymbol{\kappa}\cdot\boldsymbol{\xi} + (\boldsymbol{b}\cdot\nabla)\xi_\parallel,$$

$$\overline{\boldsymbol{v}\cdot\frac{{\rm d}\boldsymbol{\xi}}{{\rm d}t}} = (v_\perp^2/2)\nabla\cdot\boldsymbol{\xi} + (v_\perp^2/2 - v_\parallel^2)\boldsymbol{\kappa}\cdot\boldsymbol{\xi}_\perp - i\omega\overline{v_\parallel\xi_\parallel} + (v_\parallel^2 - v_\perp^2/2)\frac{\partial\xi_\parallel}{\partial l}.$$

Since $|\xi_\parallel| \ll |\boldsymbol{\xi}_\perp|$, we obtain

$$\boldsymbol{v}\cdot\frac{{\rm d}\boldsymbol{\xi}}{{\rm d}t} = (v_\perp^2/2)\nabla\cdot\boldsymbol{\xi} + (v_\perp^2/2 - v_\parallel^2)\boldsymbol{\kappa}\cdot\boldsymbol{\xi}_\perp + a_1 e^{-i\Omega t} + \cdots.$$

The third term is rapidly oscillating term and the contribution to (14.66) is small.

14.2c Various Alfvén Modes

In the previous subsection we discussed the excitation of weakly damped TAE by super-Alfvénic energetic particles. There are various Alfvén Modes.

In high-temperature plasmas, non-ideal effects such as finite Larmor radius of core plasma become important in gap region and cause the Alfvén continuum to split into a series of kinetic Alfvén eigenmodes (KTAE) at closely spaced frequencies above the ideal TAE frequency (ref.[10]).

In central region of the plasma, a low-shear version of TAE can arise, called the core-localized mode (CLM) (ref.[11]).

Noncicular shaping of the plasma poloidal cross section creates other gaps in the Alfvén continuum, at high frequency. Ellipticity creats a gap, at about twice of TAE frequency, within which

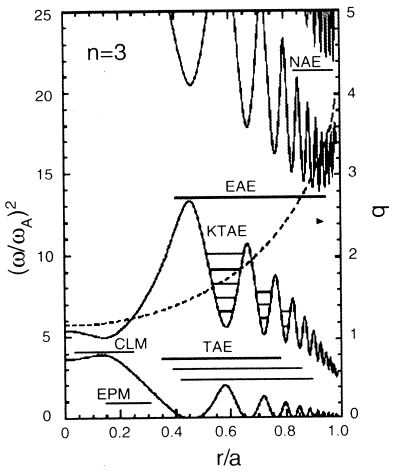

Fig.14.4 Representative shear Alfvén frequency continuum curves as function of minor radius r. Horizontal lines indicating the approximate radial location and mode width for toroidal Alfvén eigenmode (TAE), kinetic TAE mode (KTAE), core-localized TAE mode (CLM), ellipticity Alfvén eigenmode (EAE), noncicular triangularity Alfvén eigenmode (NAE), and energetic particle continuum mode (EPM).

exist ellipticity-induced Alfvén eigenmodes (EAE) (ref.[9]) and similarly for triangularity-induced Alfvén eigenmodes (NAE) (ref.[9]) at about three times the TAE frequency.

The ideal and kinetic TAE's are "cavity" mode, whose frequencies are determined by the bulk plasma. In addition, a "beam mode" can arise that is not a natural eigenmode of plasma but is supported by the presence of a population of energetic particles and also destabilized by them. This so-called energetic particle mode (EPM) (ref.[12]), which can also exit outside the TAE gaps, has a frequencies related to the toroidal precession frequency and poloidal transit/bounce frequency of the fast ions. The beta-induced Alfvén Eigenmode (BAE) (ref.[13]) exists in the beta-induced gap. The schematic in fig.14.4 illustrates these various modes.

Close interaction between theory and experiment has led many new discoveries on Alfvén eigenmodes in toroidal plasma. A great deal of theoretical work have been carried out on energetic particle drive and competing damping mechanism, such as continuum and radiative damping, ion Landau damping for both thermal and fast ions, electron damping and trapped electron collisional damping. For modes with low to moderate toroidal mode numbers n, typically continuum damping and ion Landau damping are dominant, where as high n modes, trapped collisional damping and radiative damping are strong stabilizing mechanism. There are excellent reviews on toroidal Alfvén eigenmode (ref.[14]).

References

[1] Liu Chen and R. B. White and M. N. Rosenbluth: Phys. Rev. Lett. **52**, 1122 (1984).
Y. Z. Zhang, H. L. Berk S. M. Mahajan: Nucl. Fusion **29**, 848 (1989).

[2] V. D. Shafranov: Sov. Phys. Tech. Phys. **15**, 175 (1970).

[3] M. N. Bussac, R. Pella, D. Edery and J. L. Soule: Phys. Rev. Lett. **35**, 1638 (1975).

[4] G. Ara, B.Basu, B.Coppi, G. Laval, M. N. Rosenbluth and B. V. Waddell: Annals of Phys. **112**, 443 (1978).

[5] P. J. Catto, W. M. Tang and D. E. Baldwin: Plasma Phys. **23**, 639 (1981).

[6] B. N. Kuvshinov, A. B. Mikhailovskii and E. G. Tatarinov: Sov. J. Plasma Phys. **14**, 239, (1988).

[7] A. Hasegawa and Liu Chen: Phys. Fluids: **19**, 1924 (1976).

[8] H. L. Berk, J. W. Van Dam, Z. Guo and D.M. Lindberg: Phys. Fluids **B4**, 1806 (1992).

[9] R. Betti and J. P. Freidberg: Phys. Fluids **B4**, 1465 (1992).

[10] J. Candy and N. M. Rosenbluth: Plasma Phys. Control. Fusion **35**, 957 (1993).
J. Candy and N. M. Rosenbluth: Phys. Plasmas **1**, 356 (1994).
R. R. Mett and S. M. Mahajan: Phys. Fluids **B4**, 2885 (1992).

[11] Y. Fu, C. Z. Cheng: Phys. Fluids **B2**, 985 (1990).
H. L. Berk, J.W. Van Dam, D. Borba, J. Candy, G. T. A. Huysmans, S. Sharapov: Phys. Plasmas **2**, 3401 (1995).

[12] F. Zonca and L.Chen: Phys. Fluids **B5**, 3668 (1993).
F. Zonca and L. Chen: Phys. Plasmas **3**, 323 (1996).

[13] M. S. Chu, J. M. Greene, L. L. Lao, A. D. Turnbull, M. S. Chance: Phys. Fluids **B4**, 3713 (1992)
A. D. Turnbull, E. J. Strait, W. W. Heidbrink, M. S. Chu, H. H. Duong, J. M. Greene,
L. L. Lao, T. S. Taylor, S. J. Thompson: Phys. Fluids **B5**, 2546 (1993)

[14] ITER Physics Basis: Nucl. Fusion **39**, No.12, p2495 (1999)
E. J. Strait, W. W. Heidbrik, A. D.Turnbull, M.S. Chu, H. H. Duong: Nucl. Fusion **33**, 1849 (1993)
King-Lap Wong: Plasma Phys. Control. Fusion **41** R1 (1999)A. Fukuyama and T. Ozeki: J. Plasma Fusion Res. **75**, 537 (1999) (in Japanese)

Ch.15 Development of Fusion Researches

The major research effort in the area of controlled nuclear fusion is focused on the confinement of hot plasmas by means of strong magnetic fields. The magnetic confinements are classified to toroidal and open end configurations. Confinement in a linear mirror field (sec.17.3) may have advantages over toroidal confinement with respect to stability and anomalous diffusion across the magnetic field. However, the end loss due to particles leaving along magnetic lines of force is determined solely by diffusion in the velocity space; that is, the confinement time cannot be improved by increasing the intensity of the magnetic field or the plasma size. It is necessary to find ways to suppress the end loss.

Toroidal magnetic confinements have no open end. In the simple toroidal field, ions and electrons drift in opposite directions due to the gradient of the magnetic field. This gradient B drift causes the charge separation that induces the electric field $\boldsymbol{E}$ directed parallel to the major axis of the torus. The subsequent $\boldsymbol{E} \times \boldsymbol{B}$ drift tends to carry the plasma ring outward. In order to reduce the $\boldsymbol{E} \times \boldsymbol{B}$ drift, it is necessary to connect the upper and lower parts of the plasma by magnetic lines of force and to short-circuit the separated charges along these field lines. Accordingly, a poloidal component of the magnetic field is essential to the equilibrium of toroidal plasmas, and toroidal devices may be classified according to the method used to generate the poloidal field. The tokamak (ch.16) and the reversed field (17.1) pinch devices use the plasma current along the toroid, whereas the toroidal stellarator (sec.17.2) has helical conductors or equivalent winding outside the plasma that produce appropriate rotational transform angles.

Besides the study of magnetic confinement systems, inertial confinement approaches are being actively investigated. If a very dense and hot plasma could be produced within a very short time, it might be possible to complete the nuclear fusion reaction before the plasma starts to expand. An extreme example is a hydrogen bomb. This type of confinement is called inertial confinement. In laboratory experiments, high-power laser beams or particle beams are focused onto small solid deuterium and tritium targets, thereby producing very dense, hot plasma within a short time. Because of the development of the technologies of high-power energy drivers, the approaches along this line have some foundation in reality. Inertial confinement will be discussed briefly in ch.18.

The various kinds of approaches that are actively investigated in controlled thermonuclear fusion are classified as follows:

- Magnetic confinement
  - Toroidal system
    - Axially symmetric
      - Tokamak
      - Reversed field pinch
      - Spheromak
    - Axially asymmetric
      - Stellarator system
      - Heliac
      - Bumpy torus
  - Open end system
    - Mirror, Tandem mirror
    - Field Reversal Configuration
    - Cusp
- Inertial confinement
  - Laser
  - Ion beam, Electron beam

From Secrecy to International Collaboration

Basic research into controlled thermonuclear fusion probably began right after World War II in the United States, the Soviet Union, and the United Kingdom in strict secrecy. There are on record many speculations about research into controlled thermonuclear fusion even in the 1940s. The United States program, called Project Sherwood, has been described in detail by Bishop (ref.[1]). Bishop states that Z pinch experiments for linear and toroidal configurations at the Los Alamos Scientific Laboratory were carried out in an attempt to overcome sausage and kink

instabilities. The astrophysicist L. Spitzer, Jr., started the figure-eight toroidal stellarator project at Princeton University in 1951. At the Lawrence Livermore National Laboratory, mirror confinement experiments were conducted. At the Atomic Energy Research Establishment in Harwell, United Kingdom, the Zeta experiment was started (ref.[2]) and at the I.V. Kurchatov Institute of Atomic Energy in the Soviet Union, experiments on a mirror called Ogra and on tokamaks were carried out (ref.[3]).

The first United Nations International Conference on the Peaceful Uses of Atomic Energy was held in Geneva in 1955. Although this conference was concerned with peaceful applications of nuclear fission, the chairman, H.J. Bhabha, hazarded the prediction that ways of controlling fusion energy that would render it industrially usable would be found in less than two decades. However, as we have seen, the research into controlled nuclear fusion encountered serious and unexpected difficulties. It was soon recognized that the realization of a practical fusion reactor was a long way off and that basic research on plasma physics and the international exchange of scientific information were absolutely necessary. From around that time articles on controlled nuclear fusion started appearing regularly in academic journals. Lawson's paper on the conditions for fusion was published in January 1957 (ref.[4]), and several important theories on MHD instabilities had by that time begun to appear (ref.[5],[6]). Experimental results of the Zeta (ref.[7]) (Zero Energy Thermonuclear Assembly) and Stellarator (ref.[8]) projects were made public in January 1958. In the fusion sessions of the second United Nations International Conference on the Peaceful Uses of Atomic Energy, held in Geneva, September 1-13, 1958 (ref.[9],[10]), many results of research that had proceeded in secrecy were revealed.
L.A.Artsimovich expressed his impression of this conference as "something that might be called a display of ideas." The second UN conference marks that start of open rather than secret international cooperation and competition in fusion research.

In Japan controlled fusion research started in Japan Atomic Energy Institute (JAERI) under the ministry of science and technology and in Institute of Plasma Physics, Nagoya University under the ministry of education and culture in early 1960's.

The First International Conference on Plasma Physics and Controlled Nuclear Fusion Research was held in Salzburg in 1961 under the auspices of the International Atomic Energy Agency (IAEA). At the Salzburg conference (ref.[11]) the big projects were fully discussed. Some of there were Zeta, Alpha, Stellarator C, Ogra, and DCX. Theta pinch experiments (Scylla, Thetatron, etc.) appeared to be more popular than linear pinches. The papers on the large scale experimental projects such as Zeta or Stellarator C all reported struggles with various instabilities. L.A. Artsimovich said in the summary on the experimental results: "Our original beliefs that the doors into the desired regions of ultra-high temperature would open smoothly...have proved as unfounded as the sinner's hope of entering Paradise without passing through Purgatory." The importance of the PR-2 experiments of M.S. Ioffe and others was soon widely recognized (vol.3, p.1045). These experiments demonstrated that the plasma confined in a minimum B configuration is MHD stable.

The Second International Conference on Plasma Physics and Controlled Nuclear Fusion Research was held at Culham in 1965 (ref.[12]) The stabilizing effect of minimum B configurations was confirmed by many experiments. An absolute minimum B field cannot be realized in a toroidal configuration. Instead of this, the average minimum B concept was introduced (vol.1, pp.103,145). Ohkawa and others succeeded in confining plasmas for much longer than the Bohm time with toroidal multipole configurations (vol.2, p.531) and demonstrated the effectiveness of the average minimum B configuration. Artsimovich and others reported on a series of tokamak experiments (T-5, vol.2, p.577; T-3, p.595; T-2, p.629; TM-2, p.647; TM-1, p.659). Further experiments with Zeta and Stellarator C were also reported. However, the confinement times for these big devices were only of the order of the Bohm time, and painful examinations of loss mechanisms had to be carried out. Theta pinch experiments were still the most actively pursued. The ion temperatures produced by means of theta pinches were several hundred eV to several keV, and confinement times were limited only by end losses. One of the important goals of the theta pinch experiments had thus been attained, and it was a turning point from linear theta pinch to toroidal pinch experiments.

In this conference, the effectiveness of minimum B, average minimum B, and shear configurations was thus confirmed. Many MHD instabilities were seen to be well understood experimentally as well as theoretically. Methods of stabilizing against MHD instabilities seemed to be becoming gradually clearer. The importance of velocity-space instabilities due to the non-Maxwellian distribution function of the confined plasma was recognized. There had been and were subsequently to be

reports on loss-cone instabilities (ref.[17]), Harris instability (ref.[18]) (1959), drift instabilities (ref.[19]) (1963, 1965),etc. The experiment by J.M.Malmberg and C.B.Wharton (vol.1,p.485) was the first experimental verification of Landau damping.
L.Spitzer,Jr., concluded in his summary talk at Culham that "most of the serious obstacles have been overcome, sometimes after years of effort by a great number of scientists. We can be sure that there will be many obstacles ahead but we have good reason to hope that these will be surmounted by the cooperative efforts of scientists in many nations."

Artsimovich Era

The Third International Conference (ref.[13]) was held in 1968 at Novosibirsk. The most remarkable topic in this conference was the report that Tokamak T-3 (vol.1, p.157) had confined a plasma up to 30 times the Bohm time (several milliseconds) at an electron temperature of 1 keV. In Zeta experiments a quiescent period was found during a discharge and MHD stability of the magnetic field configuration of the quiescent period was discussed. This was the last report of Zeta and HBTX succeeded this reversed field pinch experiment. Stellarator C (vol.1, pp.479, 495) was still confining plasmas only to several times the Bohm time at electron temperatures of only several tens to a hundred eV. This was the last report on Stellarator C; this machine was converted into the ST tokamak before the next conference (Madison 1971). However, various aspects of stellarator research were still pursued. The magnetic coil systems of Clasp (vol.1, p.465) were constructed accurately, and the confinement of high-energy electrons were examined using the β decay of tritium. It was demonstrated experimentally that the electrons ran around the torus more than 10^7 times and that the stellarator field had good charge-particle confinement properties. In WII the confinement of the barium plasma was tested, and resonant loss was observed when the magnetic surface was rational. Diffusion in a barium plasma in nonrational cases was classical. In 2X(vol.2, p.225) a deuterium plasma was confined up to an ion temperature of 6-8 keV at a density of $n < 5 \times 10^{13}\,\mathrm{cm}^{-3}$ for up to $\tau = 0.2\,\mathrm{ms}$. Laser plasmas appeared at this conference.

At the Novosibirsk conference toroidal confinement appeared to have the best overall prospects, and the mainstream of research shifted toward toroidal confinement. L.A.Artsimovich concluded this conference, saying; "We have rid ourselves of the gloomy spectre of the enormous losses embodied in Bohm's formula and have opened the way for further increases in plasma temperature leading to the physical thermonuclear level."

The Tokamak results were seen to be epoch making if the estimates of the electron temperature were accurate. R. S. Pease, the director of the Culham Laboratory, and L.A.Artsimovich agreed the visit of British team of researchers to Kurchatov Institute to measure the electron temperature of the T-3 plasma by laser scattering methods. The measurements supported the previous estimates by the tokamak group (ref.[20]). The experimental results of T-3 (refer to fig.15.1, (ref.[14])) had a strong impact on the next phase of nuclear fusion research in various nations. At the Princeton Plasma Physics Laboratory, Stellarator C was converted to the ST tokamak device; newly built were ORMAK at Oak Ridge National Laboratory, TFR at the Center for Nuclear Research, Fontaney aux Rose, Cleo at the Culham Laboratory, Pulsator at the Max Planck Institute for Plasma Physics, and JFT-2 at the Japan Atomic Energy Research Institute.

The Fourth International Conference was held in Madison, Wisconsin, in 1971 (ref.[15]). The main interest at Madison was naturally focused on the tokamak experiments. In T-4(vol.1, p.443), the electron temperature approached 3 keV at a confinement time around 10 ms. The ions were heated to around 600 eV by collision with the electrons. ST(vol.1, pp.451, 465) produced similar results.

Trek to Large Tokamaks (since around oil crisis)

Since then the IAEA conference has been held every two years; Tokyo in 1974 (ref.[16]), Berchtesgarden in 1976, Innsburg in 1978, Brussels in 1980, Baltimore in 1982, London in 1984, Kyoto in 1986, Nice in 1988, Washington D.C. in 1990, Würzburg in 1992, Seville in 1994, Montreal in 1996, Yokohama in 1998, Sorrento in 2000 $\cdots$. Tokamak research has made steady progress as the mainstream of magnetic confinement. Pease stated in his summary talk of the IAEA conference at Berchtesgarden in 1976 that "one can see the surprisingly steady progress that has been maintained.

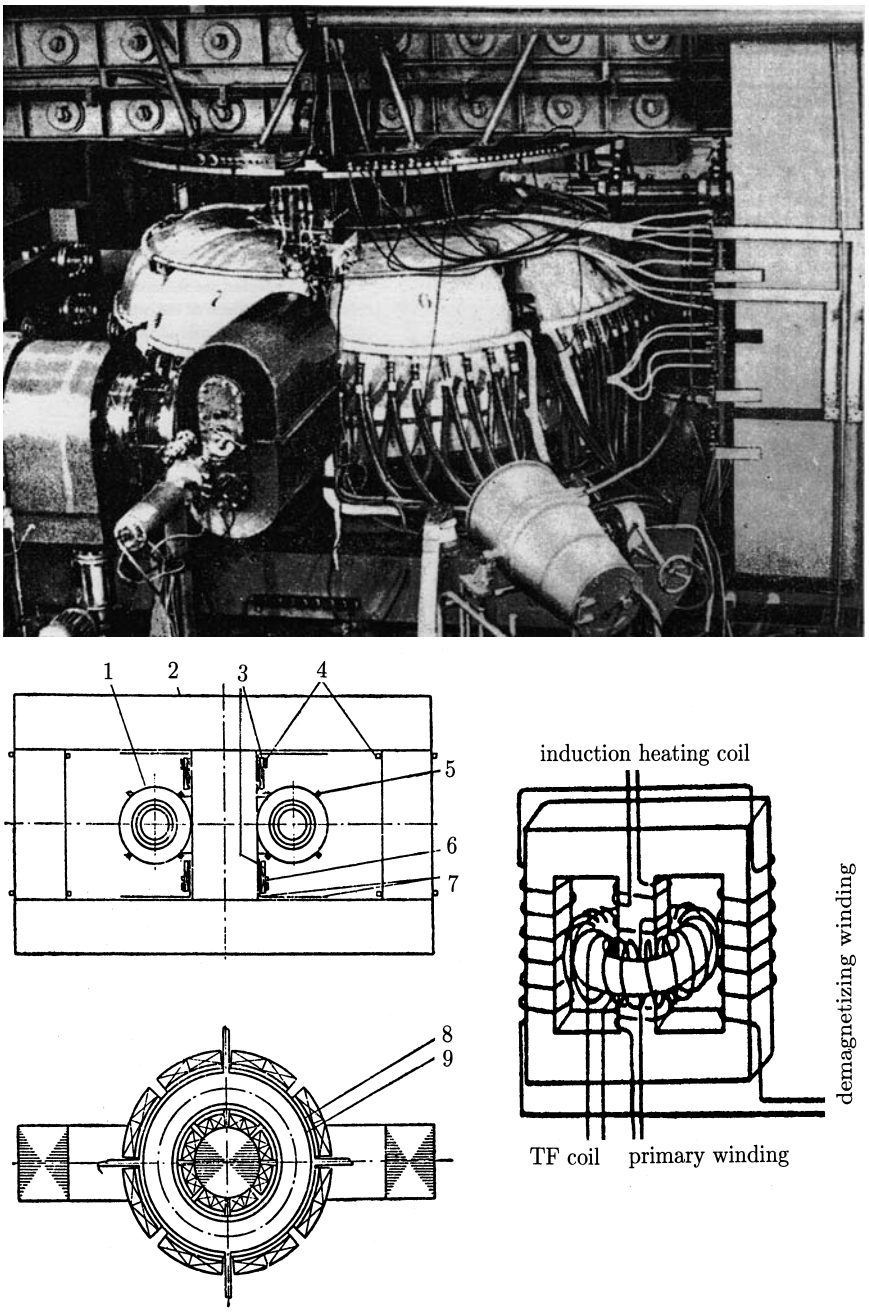

Fig.15.1 Photograph (top), schematic drawing (lower left) and circuits of toroidal field coil and primary winding of current tranaformer, demagnetization winding, induction heating coil (lower right) of Tokamak-T3 device. The numbers in shematic drawing indicate (1) toroidal field coil, (2) current transformer, (3) primary winding, (4) demagnetization winding, (5) compensating coil, (6) induction heating coil, (7) screening for primary winding, (8) external chamber, and (9) liner. After (ref.[14]).

Furthermore, looked at logarithmically, we have now covered the greater part of the total distance. What remains is difficult, but the difficulties are finite and can be summed up by saying that we do not yet have an adequate understanding or control of cross-field electron thermal conduction."

After the tokamaks of the first generation (T-4, T-6, ST, ORMAK, Alcator A, C. TFR, Pulsator, DITE, FT, JFT-2, JFT-2a, JIPP T-II, etc.), second generation tokamaks (T-10, PLT, PDX, ISX-B, Doublet III, ASDEX, etc.) began appearing around 1976. The energy confinement time of ohmically heated plasmas was approximately described by the Alcator scaling law ($\tau_{\rm E} \propto na^2$). The value of $n\tau_{\rm E}$ reached $2 \times 10^{13}\,{\rm cm}^{-3}$s in Alcator A in 1976. Heating experiments of neutral beam injection (NBI) in PLT achieved the ion temperature of 7keV in 1978, and the effective wave heating in an ion cyclotron range of frequency was demonstrated in TFR and PLT around 1980. The average β value of 4.6 % was realized in the Doublet III non-circular tokamak ($\kappa = 1.4$) in 1982 using 3.3 MW NBI. Noninductive drives for plasma current have been pursued. Current drive by the tangential injection of a neutral beam was proposed by Ohkawa in 1970 and was demonstrated in DITE experimentally in 1980. Current drive by a lower hybrid wave was proposed by Fisch in 1978 and demonstrated in JFT-2 in 1980 and in Versator 2, PLT, Alcator C, JIPP T-II, Wega, T-7 and so on. Ramp-up experiments of plasma current from 0 were succeeded by WT-2 and PLT in 1984. TRIAM-1M with superconducting toroidal coils sustained the plasma current of $I_{\rm p} = 22\,{\rm kA}, (n_{\rm e} \approx 2 \times 10^{18}\,{\rm m}^3)$ during 70 minutes by LHW in 1990.

The suppression of impurity ions by a divertor was demonstrated in JFT-2a (DIVA) in 1978 and was investigated by ASDEX and Doublet III in detail (1982). At that time the energy confinement time had deteriorated compared with the ohmic heating case as the heating power of NBI was increased (according to the Kaye-Goldston scaling law). However, the improved mode (named H mode) of the confinement time, increased by about 2 times compared with the ordinary mode (L mode), was found in the divertor configuration of ASDEX in 1982. The H mode was also observed in Doublet III, PDX, JFT-2M, and DIII-D. Thus much progress had been made to solve many critical issues of tokamaks.

Based on these achievements, experiments of third-generation large tokamaks started, with TFTR (United States) in the end of 1982, JET (European Community) in 1983 and JT-60 (Japan) in 1985. Originally these large tokamaks are planned in early 1970s. TFTR achieved $n_{\rm DT}(0)\tau_{\rm E} \sim 1.2 \times 10^{19}\,{\rm m}^{-3}{\cdot}{\rm s}$, $\kappa T_{\rm i}(0) = 44\,{\rm keV}$ by supershot (H mode-like). JET achieved $n_{\rm D}(0)\tau_{\rm E} \sim 3.2{\times}10^{19}\,{\rm m}^{-3}{\cdot}{\rm s}$, $\kappa T_{\rm i}(0) = 18.6\,{\rm keV}$ by H mode with divertor configuration. JT-60 drove a plasma current of 1.7 MA ($\bar{n}_{\rm e} = 0.3 \times 10^{13}\,{\rm cm}^{-3}$) by lower hybrid wave ($P_{\rm RF} = 1.2\,{\rm MW}$) in 1986 and upgraded to JT60U in 1991 (ref.[21]). JT60U achieved $n_{\rm D}(0)\tau_{\rm E} \sim 3.4 \times 10^{19}\,{\rm m}^{-3} \cdot {\rm s}$, $\kappa T_{\rm i}(0) = 45\,{\rm keV}$ by high $\beta_{\rm p}$ H mode. A high performance confinement mode with negative magnetic shear was demonstrated in TFTR, DIII-D, JT60U, JET, Tore Supra, T10 (ref.[22]).

JET performed a preliminary tritium injection experiment (ref.[23]) ($n_{\rm T}/(n_{\rm D} + n_{\rm T}) \simeq 0.11$) in 1991 and the production of 1.7 MW ($Q \sim 0.11$) of fusion power using 15MW of NBI. Extensive deuterium-tritium experiment was carried out on TFTR in 1994 (ref.[24]). Fusion power of 9.3 MW ($Q \sim 0.27$) was obtained using 34 MW of NBI in supershot ($I_{\rm p}$=2.5 MA). JET set records of DT fusion output of 16.1MW ($Q \sim 0.62$) using 25.7 MW of input power (22.3MW NBI + 3.1MW ICRF) (ref.[25]) in 1998. A pumped divertors were installed in JET, JT60U, DIIID, ASDEX-U and others in attempt to suppress impurity ions and the heat load on divertor plate. Now these large tokamaks are aiming at the scientific demonstration of required conditions of critical issues (plasma transport, steady operation, divertor and impurity control and so on) of fusion reactors.

Based on the development of tokamak researches, the design activities of tokamak reactors have been carried out. The International Tokamak Reactor (INTOR) (ref.[26]) (1979-1987) and The International Thermonuclear Experimental Reactor (ITER) (ref.[27]) (1988-2001) are collaborative efforts among Euratom, Japan, The United States of America and Russian Federation under the auspices of IAEA. The status of ITER (ref.[28]) is described in sec.16.12.

Alternative Aproaches

Potentail theoretical advantages of spherical tokamak was outlined by Peng and Strickler (ref.[29]), in which the aspect rato $A = R/a$ of standard tokamak is substantially reduces toward unity. Predicted advantages include a naturally high elongation ($\kappa_{\rm s} \sim 2$), high toroidal beta and tokamak like confinement. These predictions have been verified experimentally, in particular by START device (ref.[30]) at Culham ($R/a \approx 0.3/0.28 = 1.31, I_{\rm p} \approx 0.25{\rm MA}, B_{\rm t} \approx 0.15{\rm T}$). The toroidal beta reached

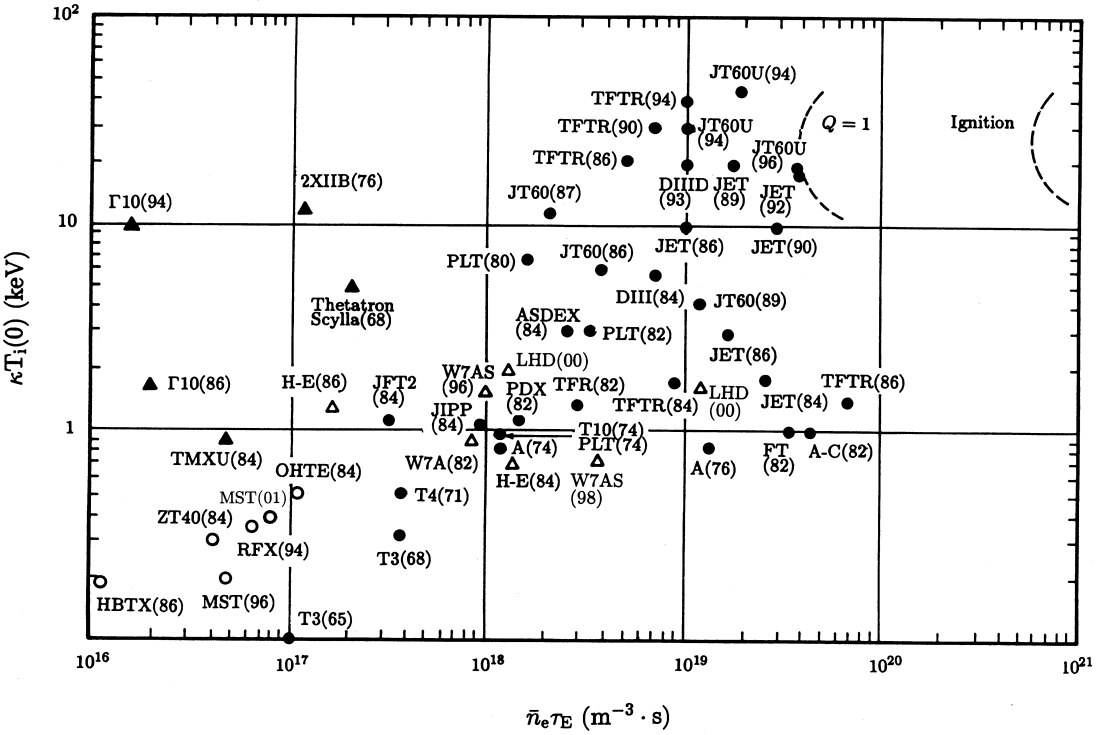

Fig.15.2 Development of confinement experiments in $\bar{n}_e\tau_E$ - $\kappa T_i(0)$ ($\bar{n}_e$ is the line average electron density, τ_E is the energy confinement time $\tau_E \equiv W/(P_{tot} - dW/dt - L_{thr})$, $T_i(0)$ is the ion temperature). tokamak(•), stellarator (△), RFP(○), tandem mirror, mirror, theta pinch(closed triangle). $Q = 1$ is the critical condition. W; total energy of plasma, P_{tot}; total heating power, L_{thr}; shine through of neutral beam heating.

40% and observed confinement times follow similar scaling of standard tokamaks. Spherical tokamak (ST) experiments were also conducted by Globus-M (Ioffe), Pegasus (Madison), TST (Tokyo), TS-3 (Tokyo). The next generation ST projects MAST (Culham) and NSTX (Princeton) started experiments in 1999 $\sim$ 2000.

Non-tokamak confinement systems have been investigated intensively to catch up with the achievements of tokamaks. The stellarator program proceeded from small-scale experiments (Wendelstein IIb, Clasp, Uragan-1, L-1, JIPP-I, Heliotron D) to middle-scale experiments (Wendelstein VIIA, Cleo, Uragan-2, L-2, JIPP T-II, Heliotron E). The plasmas with $T_e \sim T_i \approx$ several hundred eV to 1 keV, $n_e \sim$ several $10^{13}\,cm^{-3}$ were sustained by NBI heating without an ohmic heating current, and the possibility of steady-state operation of stellarators was demonstrated by WVIIA and Heliotron E. Scaling of confinement time of currentless plasma was studied in Heliotron E, CHS, ATF and WVII AS. Large helical device LHD started experiments in 1998 and advanced stellarator WVII-X is under construction.

The reversed field pinch (RFP) configuration was found in the stable quiescent period of Zeta discharge just before the shutdown in 1968. J.B. Taylor pointed out that RFP configuration is the minimum energy state under the constraint of the conservation of magnetic helicity in 1974 (see sec.17.1). RFP experiments have been conducted in HBTX-1B, ETA-BETA 2, TPE-1RM, TPE-1RM15, TPE-1RM20, ZT-40M, OHTE, REPUTE-1, STP-3M, MST. An average β of 10-15% was realized. ZT-40M demonstrated that RFP configuration can be sustained by relaxation phenomena (the so-called dynamo effect) as long as the plasma current is sustained (1982). The next step projects RFX is proceeding.

Spheromak configurations have been studied by S-1, CTX, and CTCC-1, and field reversed configurations have been studied by FRX, TRX, LSX, NUCTE and PIACE.

In mirror research, 2XIIB confined a plasma with an ion temperature of 13 keV and $n\tau_E \times 10^{11}\,cm^{-3}s$ in 1976. However, the suppression of the end loss is absolutely necessary. The concept of a tandem mirror, in which end losses are suppressed by electrostatic potential, was proposed in

1976-1977 (sec 17.3). TMX, TMX-U and GAMMA 10 are typical tandem mirror projects. The bumpy torus is the toroidal linkage of many mirrors to avoid end loss and this method was pursued in EBT and NBT.

Inertial confinement research has made great advances in the implosion experiment by using a Nd glass laser as the energy driver. Gekko XII (30 kJ, 1 ns, 12 beams), Nova (100 kJ, 1 ns, 10 beams), Omega X(4 kJ, 1 ns, 24 bemas), and Octal (2 kJ, 1 ns, 8 beams) investigated implosion using laser light of $\lambda = 1.06\,\mu$m and its higher harmonics $\lambda = 0.53\,\mu$m and $0.35\,\mu$m. It was shown that a short wavelength is favorable because of the better absorption and less preheating of the core. A high-density plasma, $200 \sim 600$ times as dense as the solid state, was produced by laser implosion (1990). Based on Nova results, Lawrence Livermore National Laboratory is in preparation on National Ignition Facility (NIF (ref.[31],[32]) (1.8MJ, 20ns, 0.35μm, 192 beams, Nd glass laser system).

Nuclear fusion research has been making steady progress through international collaboration and competition. A summary of the progress of magnetic confinement is given in fig.15.2 of the $\bar{n}_e\tau_E$ - $T_i(0)$ diagram. TFTR demonstrated $Q \sim 0.27$ DT experiments and JET demonstrated $Q \sim 0.62$ DT experiments. JET and JT60U achieved equivalent break-even condition by D-D plasma, that is, the extrapolated D-T fusion power output would be the same as the heating input power ($Q_{\rm equiv}$=1).

References

[1] A. S. Bishop: *Project Sherwood*, Addison Wesley, Reading Mass. (1958).

[2] R. S. Pease: Plasma Phys. and Controlled Fusion **28**, 397 (1986).

[3] L. A. Artsimovich: Sov. Phys. Uspekhi **91**, 117 (1967).

[4] J. D. Lawson: Proc. Phys. Soc. **70**B, 6 (1957).

[5] M. D. Kruskal and M. Schwarzschild: Proc. Roy. Soc. A**223**, 348 (1954).

[6] M. N. Rosenbluth and C. L. Longmire: Ann. Phys. **1**, 120 (1957).
I. B. Berstein, E. A. Frieman, M. D. Kruskal and R. M. Kulsrud: Proc. Roy. Soc. A**244**, 17 (1958).

[7] Nature **181**, No. 4604, p. 217, Jan. 25 (1958).

[8] L. Spitzer, Jr.: Phys. Fluids **1**, 253 (1958).

[9] Proceedings of the Second United Nations International Conference on the Peaceful Uses of Atomic Energy in Geneva Sep. 1–13 (1958),
Theoretical and Experimental Aspects of Controlled Nuclear Fusion, 32, Controlled Fusion Devices, United Nations Publication, Geneva (1958).

[10] The Second Geneva Series on the Peaceful Uses of Atomic Energy (editor of the series by J. G. Beckerley, Nuclear Fusion) D. Van Nostrand Co. Inc., New York (1960).

[11] Plasma Physics and Controlled Nuclear Fusion Research (Conference Proceeding, Salzburg, 1961) Nucl. Fusion Suppl. (1962) (Translation of Russian Papers: U.S. Atomic Energy Commission, Division of Technical Information Office of Tech. Service, Depart. of Commerce, Washington D.C.(1963)).

[12] ibid: (Conference Proceedings, Culham, 1965) International Atomic Energy Agency, (Vienna (1966) Translation of Russian Paper:U.S. Atomic Energy Commission, Division of Technical Information Oak Ridge, Tenn. (1966)).

[13] ibid: (Conference Proceedings, Novosibirsk, Aug.1–7 1968) International Atomic Energy Agency, Vienna (1969)(Translation of Russian Paper: Nucl. Fusion Suppl. (1969)).

[14] M. A.Gashev, G. K. Gustav, K. K. D'yachenco, E. G. Komar, I. F. Malyshev et al.: Sov. Atomic Energy **17**, 1017 (1964). (Atomnaya Energiya **17** 287 1964).

[15] ibid: (Conference Proceedings, Madison, 1971) International Atomic Energy Agency, Vienna(1971) (Translation of Russian Paper: Nucl. Fusion Suppl.(1972)).

[16] ibid: (Conference Proceedings, Tokyo. Nov. 11–15 1974) International Atomic Energy Agency, Vienna (1975).

[17] M. N. Rosenbluth and R. F. Post: Phys. Fluids **8**, 547 (1965).

[18] E. G. Harris: Phys. Rev. Lett. **2**, 34 (1959).

[19] A. B. Mikhailovskii and L. I. Rudakov: Sov. Phys. JETP **17**, 621 (1963)
N. A. Krall and M. N. Rosenbluth: Phys. Fluids **8**, 1488 (1965).

[20] M. J. Forrest, N. J. Peacock, D. C. Robinson, V. V. Sannikov and P. D. Wilcock: Culham Report CLM–R 107, July (1970).

[21] JT60U Team: Plasma Physics and Controlled Nucl. Fusion Research **1**, 31, (1995) (Conference Proceedings, Seville in 1994) IAEA, Vienna.

[22] O1-2, O1-6, O1-3, A5-5, O2-2 in 16th IAEA Fusion Energy Conference (Montreal in 1996) **1**, (1997) IAEA Vienna.

[23] JET Team: Nucl. Fusion **32**, 187 (1992)

[24] TFTR Team: Plasma Physics and Controlled Nucl. Fusion Research **1**, 11, (1995) (Conference Proceedings, Seville in 1994) IAEA, Vienna.

[25] JET Team: 17th IAEA Fusion Energy Conference (Yokohama in 1998) **1**, 29 (1999) IAEA Vienna.

[26] INTOR Team: Nucl. Fusion **23**, 1513, (1983)

[27] ITER PhysicsBasis: Nucl. Fusion **39** No.12 pp2137-2638 (1999).

[28] R. Aymar, Y. Shimonura, M. Huguet, V. Chuyanov an the ITER International and Participant Teams: 19th Fusion Energy Conf. (Lyon 2002) OV/1-1.
ITER-FEAT: Technical Basis for the ITER-FEAT Outline Design (Dec 1999) IAEA Vienna.

[29] Y-K M. Peng, D. J. Strickler: Nucl.Fusion **26**, 769 (1986).

[30] A. Sykes: 17th IEA Fusion Energy Conference (Yokohama in 1998) **1**, 129 (1999) IAEA Vienna.

[31] J. D. Lindl, M. M. Marinak: 16th IEA Fusion Energy Conference (Monreal in 1996) **3**, 43 (1997) IAEA Vienna.

[32] J. D. Lindl: *Inertial Confinement Fusion* AIP Press, Springer 1998.

Ch.16 Tokamak

The word "tokamak" is said to be a contraction of the Russian words for current (т о к), vessel (к а м е р), magnet (м а г н и т), and coil (к а т у щ к а). Tokamaks are axisymmetric, with the plasma current itself giving rise to the poloidal field essential to the equilibrium of toroidal plasmas. In a tokamak the toroidal field used to stabilize against MHD instabilities, is strong enough to satisfy the Kruskal-Shafranov condition. This characteristics is quite different from that of reversed field pinch, with its relatively weak toroidal field. There are excellent reviews and textbooks of tokamak experiments, (ref.[1],[2]) equilibrium, (ref.[3]) and diagnostics (ref.[4],[5]).

16.1 Tokamak Devices

The structure of the devices of large tokamaks JET, JT60U and TFTR are shown in figs.16.1, 16.2 and 16.3 as typical examples.

The toroidal field coils, equilibrium field coils (also called the poloidal field coils, which produce the vertical field and shaping field), ohmic heating coils (the primary windings of the current transformer), and vacuum vessel can be seen in the figures. Sometimes "poloidal field coils" means both the equilibrium field coils and the ohmic heating coils. By raising the current of the primary windings of the current transformer (ohmic heating coils), a current is induced in the plasma, which acts as the secondary winding. In the JET device, the current transformer is of the iron core type. The air-core type of current tranformer is utilized in JT60U and TFTR. The vacuum vessel is usually made of thin stainless steel or inconel so that it has enough electric resistance in the toroidal direction. Therefore the voltage induced by the primary windings can penetrate it. The thin vacuum vessel is called the linear. Before starting an experiment, the liner is outgassed by baking at a temperature of 150-400 ℃ for a long time under high vacuum.

Table 16.1 Parameters of tokamaks. R, a, b in m, B_t in T, and I_p in MA.

	R	$a(\times b)$	R/a	B_t	I_p	Remarks
T-4	1.0	0.17	5.9	5.0	0.3	
T-10	1.5	0.39	3.8	5.0	0.65	
PLT	1.32	0.4	3.3	3.2	0.5	
TFTR	2.48	0.85	2.9	5.2	2.5	compact
JET	2.96	1.25(×2.1)	2.4	3.45	7	noncircular
JT60U	3.4	1.1(×1.4)	3.1	4.2	6	JT60 upgraded

Furthermore, before running an experiment, a plasma is run with a weak toroidal field in order to discharge-clean the wall of the liner. Inside the liner there is a diaphragm made of tungsten, molybdenum, or graphite that limits the plasma size and minimizes the interaction of the plasma with the wall. This diaphragm is called a limiter. Furthermore a divertor configuration is introduced instead of the limiter, so that the magnetic surface, including the separatrix point, determines the plasma boundary (see sec.16.5). A conducting shell surrounds the plasma outside the liner and is used to maintain the positional equilibrium or to stabilize MHD instabilities during the skin time scale. The magnitude of the vertical field is feedback controlled to keep the plasma at the center of the liner always. Many improvements have been made in tokamak devices over the years. Accuracy of the magnetic field is also important to improve the plasma performance in tokamak and other toroidal devices. The parameters of typical tokamak devices are listed in table 16.1.

Measurements by magnetic probes are a simple and useful way to monitor plasma behavior. Loop voltage V_L and the plasma current I_p can be measured by the magnetic loop and Rogowsky coil, respectively (ref.[4]). Then the electron temperature can be estimated by the Spitzer formula from the resistivity of the plasma, which can be evaluated using V_L and I_p. From (6.18), the poloidal beta ratio β_p is given by

$$\beta_\mathrm{p} = 1 + \frac{2B_\varphi}{B_\omega^2}\langle B_{\varphi\mathrm{V}} - B_\varphi\rangle \tag{16.1}$$

where $|B_{\varphi\mathrm{V}} - B_\varphi| \ll |B_\varphi|$ and $B_\omega = \mu_0 I_\mathrm{p}/2\pi a$. Since the diamagnetic flux $\delta\Phi$ is

$$\delta\Phi = \pi a^2 \langle B_{\varphi\mathrm{V}} - B_\varphi\rangle$$

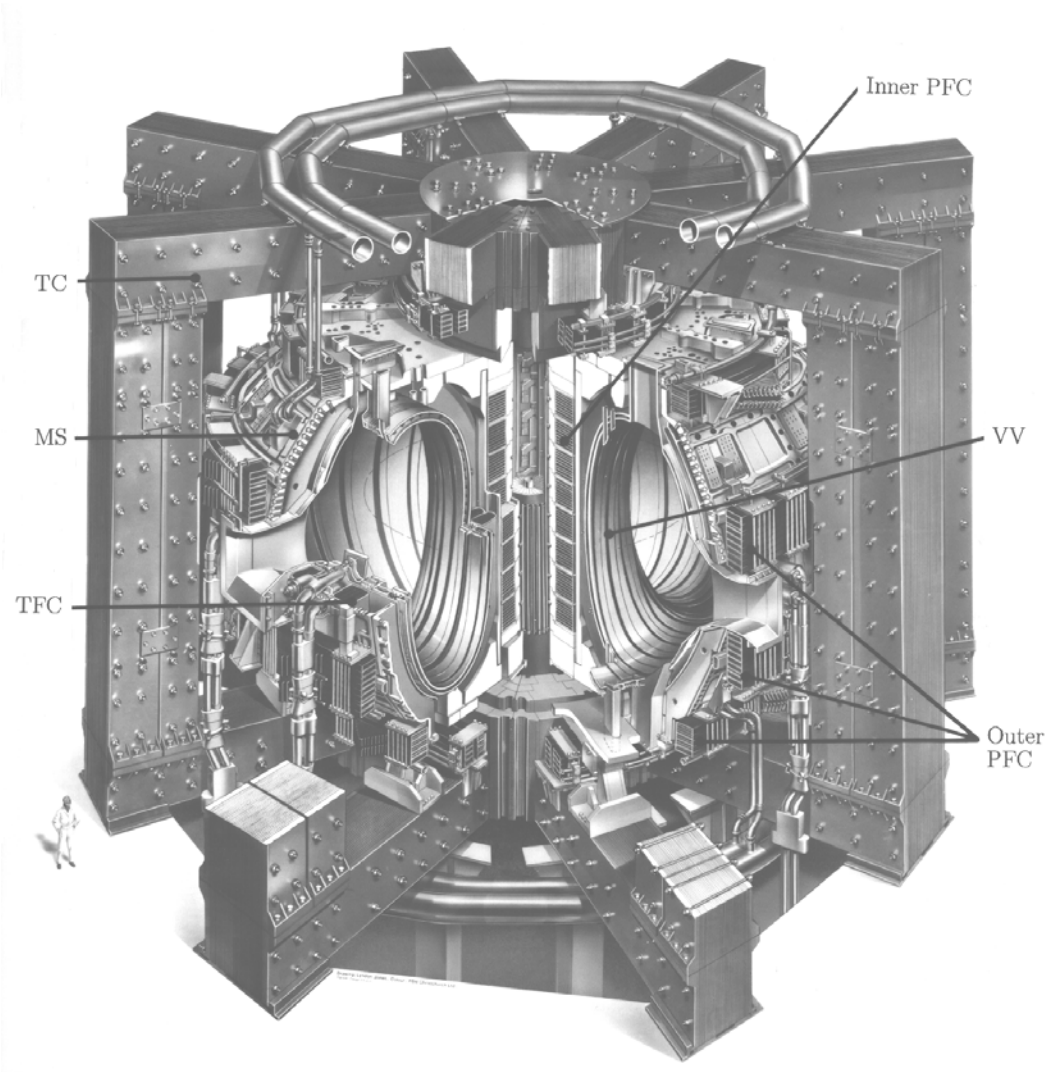

Fig.16.1 Artist's drawing of JET (Joint European torus), JET Joint Undertaking, Abingdon, Oxfordshire, England. The toroidal field coils (TFC) are arranged around the vacuum vessel(VV). The outer poloidal field coils (Outer PFC, equilibrium field coils) and inner poloidal field coils (Inner PFC, ohmic heating coils) are wound in the toroidal direction outside the toroidal field coils(TFC). JET uses an ion-core current transformer (TC). The mechanical structures (MS) support the toroidal field coils against the large amount of torque due to the equilibrium field. Reprinted with permission from JET Joint Undertaking.

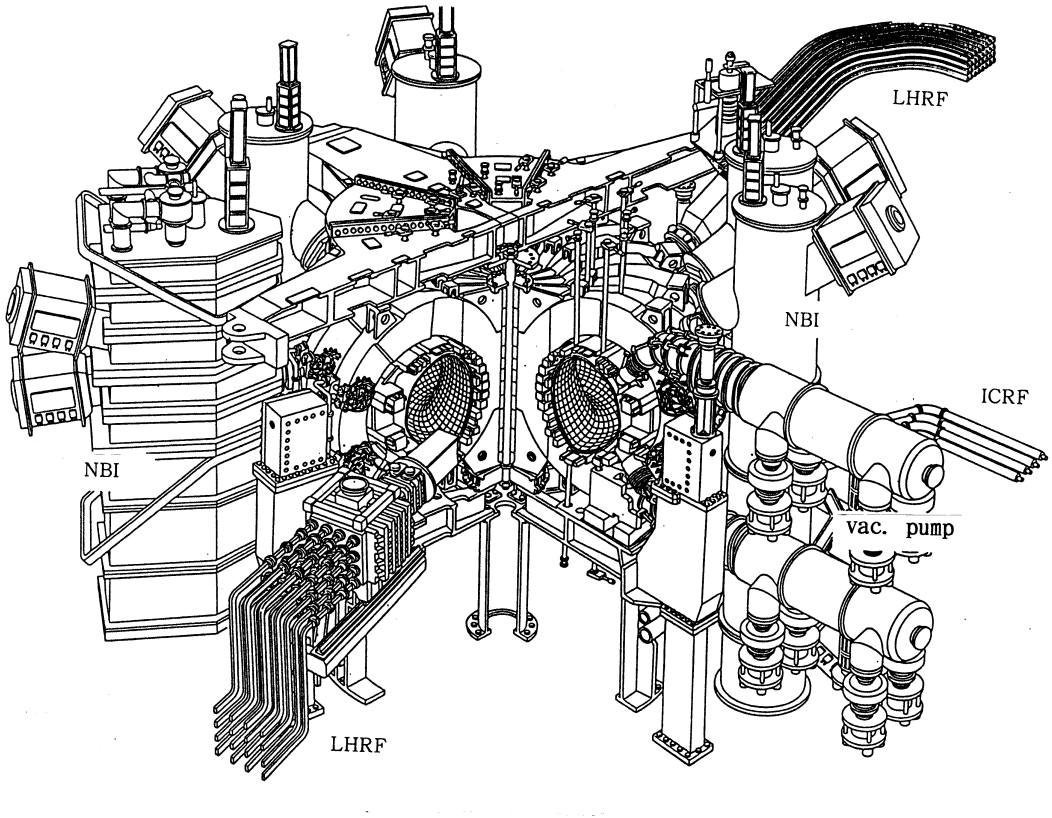

Fig.16.2 A birdview of JT60U, Japan Atomic Energy Research Institute.

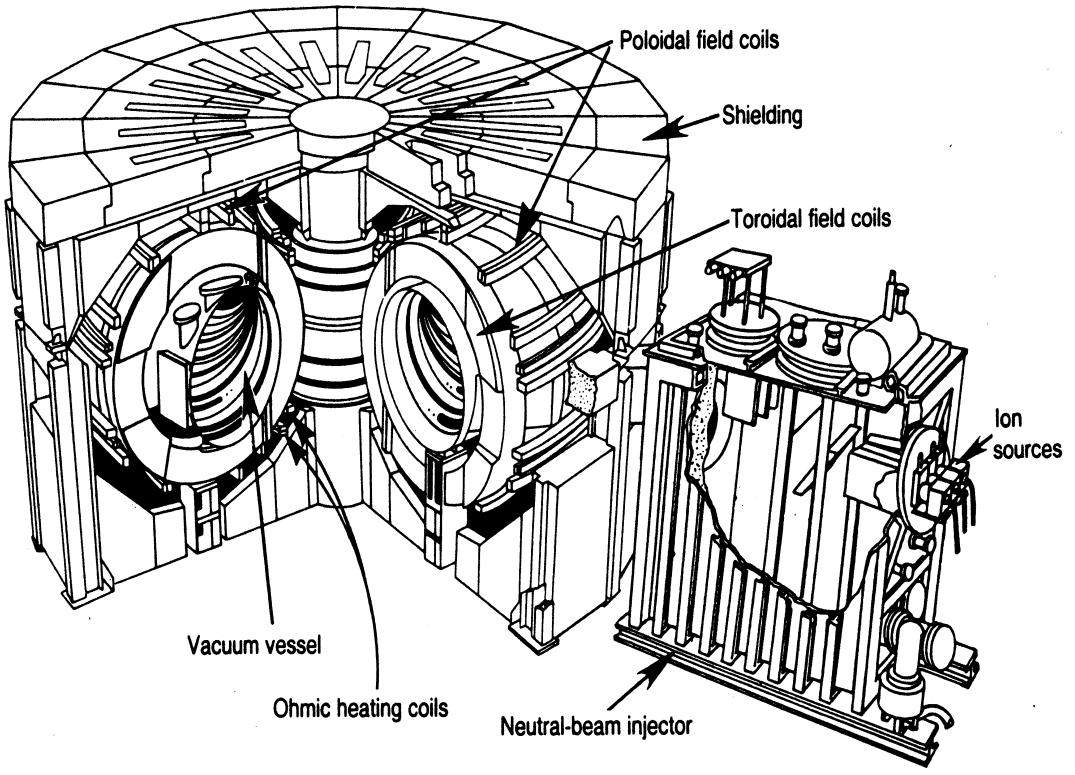

Fig.16.3 A birdview of TFTR(Tokamak Fusion Test Reactor), Plasma Physics Laboratory, Princeton University.

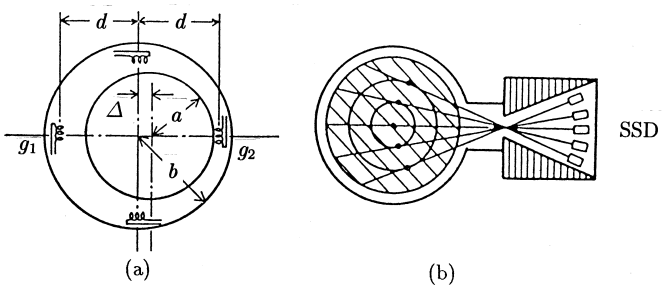

Fig.16.4 (a) Locations of magnetic probes around plasma (Δ) shown in the figure is minus) (b) an array of soft X ray solid-state detectors. Each detector's main contribution to a signal comes from the emission at the peak temperature along the line of sight of the detector. the fluctuation of the electron temperature at this point can be detected.

we have

$$\beta_{\rm p} = \frac{p}{B_\omega^2/2\mu_0} = 1 + \frac{8\pi B_\varphi}{\mu_0^2 I_{\rm p}^2}\delta\Phi. \tag{16.2}$$

Therefore measurement of the diamagnetic flux $\delta\Phi$ yields $\beta_{\rm p}$ and the plasma pressure. Magnetic probes $g_1,\ g_2$ located around the plasma, as shown in fig.16.4a, can be used to determine the plasma position. Since the necessary magnitude of the vertical field for the equilibrium $B_\perp$ is related to the quantity $\Lambda = \beta_{\rm p} + l_{\rm i}/2 - 1$, the value of Λ can be estimated from $B_\perp$ ($l_{\rm i}$ is the normalized internal inductance). The fluctuations in the soft X-ray (bremsstrahlung) signal follow the fluctuations in electron temperature. The fluctuations occur at the rational surfaces ($q_{\rm s}(r) = 1, 2, ...$). The mode number and the direction of the propagation can be estimated by arrays of solid-state detectors, as shown in fig.16.4b. When the positions of the rational surfaces can be measured, the radial current profile can be estimated for use in studies of MHD stability.

16.2 Equilibrium

The solution of the Grad-Shafranov equation (6.15) for the equilibrium gives the magnetic surface function $\Psi = rA_\varphi$ (A_φ is the φ component of the vector potential). Then the magnetic field $\boldsymbol{B}$ is described by

$$rB_r = -\frac{\partial\psi}{\partial z}, \qquad rB_z = \frac{\partial\psi}{\partial r}$$

and the current density $\boldsymbol{j}$ is

$$\boldsymbol{j} = \frac{I'}{2\pi}\boldsymbol{B} + rp'\boldsymbol{e}_\varphi$$

where $'$ means $\partial/\partial\psi$. When the plasma cross section is circular, the magnetic surface $\psi(\rho,\omega)$ outside the plasma is given by (6.25) as follows:

$$\psi(\rho,\omega) = \frac{\mu_0 I_{\rm p} R}{2\pi}\left(\ln\frac{8R}{\rho} - 2\right) - \frac{\mu_0 I_{\rm p}}{4\pi}\left(\ln\frac{\rho}{a} + \left(\Lambda + \frac{1}{2}\right)\left(1 - \frac{a^2}{\rho^2}\right)\right)\rho\cos\omega. \tag{16.3}$$

The plasma boundary is given by $\rho = a$, that is, by

$$\psi(\rho,\omega) = \frac{\mu_0 I_{\rm p} R}{2\pi}\left(\ln\frac{8R}{a} - 2\right). \tag{16.4}$$

16.2a Case with Conducting Shell

When a conducting shell of radius b surrounds the plasma, the magnetic surface ψ must be constant at the conducting shell. Therefore the location of the shell is given by

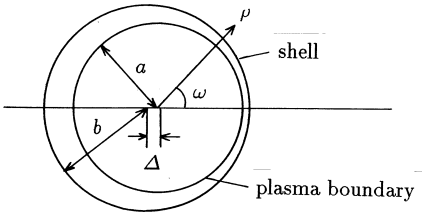

Fig.16.5 Positions of plasma boundary and shell

$$\psi(\rho,\omega)=\frac{\mu_0 I_\mathrm{p} R}{2\pi}\left(\ln\frac{8R}{b}-2\right).$$

(In practice, the position of the shell is fixed, and the plasma settles down to the appropriate equilibrium position; the important point is their relative position). When the magnetic surface is expressed by

$$\psi(\rho,\omega)=\psi_0(\rho)+\psi_1\cos\omega$$

the magnetic surface is a circle with the shifted center by the amount of $\Delta=-\psi_1/\psi_0'$. Therefore the plasma center is displaced from the center of the shell by an amount Δ_0 given by (see fig. 16.5. $\rho'=\rho-\Delta\cos\omega, \Phi_0(\rho')=\Phi_0(\rho)-(\partial\Phi_0/\partial\rho)\Delta\cos\omega$)

$$\Delta_0(b)=-\frac{b^2}{2R}\left(\ln\frac{b}{a}+\left(\Lambda+\frac{1}{2}\right)\left(1-\frac{a^2}{b^2}\right)\right).$$

($\Delta_0<0$ means that the plasma center is outside the center of the shell.)

16.2b Case without Conducting Shell

If the vertical field $B_\perp$ is uniform in space, the equilibrium is neutral with regard to changes to plasma position. When the lines of the vertical field are curved, as shown in fig.16.6, the plasma position is stable with regard to up and down motion. The z component F_z of the magnetic force applied to a plasma current ring with mass M is

$$F_z=-2\pi R I_\mathrm{p} B_R.$$

From the relation $(\partial B_R/\partial z)-(\partial B_z/\partial R)=0$,

$$M\ddot{z}=-2\pi R I_\mathrm{p}\frac{\partial B_R}{\partial z}z=2\pi I_\mathrm{p}B_z\left(-\frac{R}{B_z}\frac{\partial B_z}{\partial R}\right)z.$$

As $I_\mathrm{p}B_z<0$, the stability condition for decay index n is

$$n\equiv-\frac{R}{B_z}\frac{\partial B_z}{\partial R}>0. \tag{16.5}$$

The horizontal component $F_R=2\pi R I_\mathrm{p}(B_z-B_\perp)$ of the magnetic force is

$$M\frac{\mathrm{d}^2(\Delta R)}{\mathrm{d}t^2}=2\pi\frac{\partial R I_\mathrm{p}(B_z-B_\perp)}{\partial R}\Delta R\approx 2\pi R I_\mathrm{p}\left(\frac{\partial B_z}{\partial R}-\frac{\partial B_\perp}{\partial R}\right)=2\pi I_\mathrm{p}B_z\left(-n+1-\frac{R}{I_\mathrm{p}}\frac{\partial I_\mathrm{p}}{\partial z}\right).$$

The amount of $B_\perp$ necessary for plasma equilibrium (refer to (6.28)) is

$$B_\perp=\frac{-\mu_0 I_\mathrm{p}}{4\pi R}\left(\ln\frac{8R}{a}+\Lambda-\frac{1}{2}\right),\qquad \Lambda=\frac{l_\mathrm{i}}{2}+\beta_\mathrm{p}-1.$$

When the plasma is ideally conductive, the magnetic flux inside the plasma ring is conserved and

$$\frac{\partial}{\partial R}(L_\mathrm{p}I_\mathrm{p})+2\pi R B_\perp=0.$$

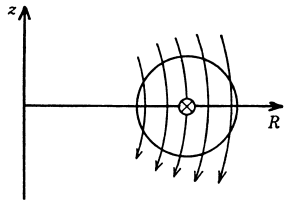

Fig.16.6 Vertical field for plasma equilibrium

Here the self-inductance is $L_\mathrm{p} = \mu_0 R(\ln(8R/a) + l_\mathrm{i}/2 - 2)$. Then we have $-R(\partial I_\mathrm{p}/\partial R)/I_\mathrm{p} = 1/2$. Therefore the equation of motion is

$$M\frac{\mathrm{d}^2(\Delta R)}{\mathrm{d}t^2} = 2\pi I_\mathrm{p} B_\perp \left(\frac{3}{2} - n\right)\Delta R$$

under the assumption $\ln(8R/a) \gg 1$. Then the stability condition for horizontal movement is

$$\frac{3}{2} > n. \tag{16.6}$$

16.2c Equilibrium Beta Limit of Tokamaks with Elongated Plasma Cross Sections

The poloidal beta limit of a circular tokamak is given by $\beta_\mathrm{p} = 0.5R/a$, as was given by (6.38). The same poloidal beta limit is derived by similar consideration for the elongated tokamak with horizontal radius a and vertical radius b. When the length of circumference along the poloidal direction is denoted by $2\pi aK$ for the elongated plasma and the average of poloidal field is $\bar{B}_\mathrm{p} = \mu_0 I_\mathrm{p}/(2\pi aK)$, the ratio of the poloidal and toroidal field is $\bar{B}_\mathrm{p}/B_\mathrm{t} = aK/(Rq_\mathrm{I})$, where K is approximately given by $K = [(1 + (b/a)^2)/2]^{1/2}$. Therefore the beta limit of an elongated tokamak is $\beta = \beta_\mathrm{p}(aK/Rq_\mathrm{I})^2 = 0.5K^2 a/(Rq_\mathrm{I}^2)$ and is K^2 times as large as that of circular one. In order to make the plasma cross section elongated, the decay index n of the vertical field must be negative, and the elongated plasma is positionally unstable in the up-down motion. Therefore feedback control of the variable horizontal field is necessary to keep the plasma position vertically stable (ref.[6]).

16.3 MHD Stability and Density Limit

A possible MHD instability in the low-beta tokamak is kink modes, which were treated in sec.8.3. Kink modes can be stabilized by tailoring the current profile and by appropriate choice of the safety factor q_a. When the plasma pressure is increased, the beta value is limited by the ballooning modes (sec.8.5). This instability is a mode localized in the bad curvature region driven by a pressure gradient. The beta limit of ballooning mode is given by $\beta_\mathrm{max} \sim 0.28(a/Rq_a)$ (ref.[7]) (refer to (8.124)).

Even if a plasma is ideally MHD stable, tearing modes can be unstable for a finite resistive plasma. When Δ' is positive at the rational surfaces (see sec.9.1) in which the safety factor $q(r)$ is rational $q(r) = 1, 3/2, 2$, tearing modes grow and magnetic islands are formed, as shown in fig.16.7. When the profile of the plasma current is peaked, then the safety factor at the center becomes $q(0) < 1$ and the tearing mode with $m = 1,\ n = 1$ grows at the rational surface $q(r) = 1$, and the hot core of the plasma is pushed out when the reconnection of magnetic surfaces occurs and the current profile is flattened (fig.16.8). The thermal energy in the central hot core is lost in this way (ref.[8]). Since the electron temperature in the central part is higher than in the outer region and the resistance in the central part is smaller, the current profile is peaked again and the same process is repeated. This type of phenomenon is called *internal disruption or minor disruption* .

The stable operational region of a tokamak with plasma current I_p and density n_e is limited. With Greenwald normalized density or Greenwald-Hugill-Murakami parameter, defined by

$$N_\mathrm{G} \equiv \frac{n_{20}}{I_\mathrm{p}(\mathrm{MA})/\pi a(\mathrm{m})^2} \tag{16.7}$$

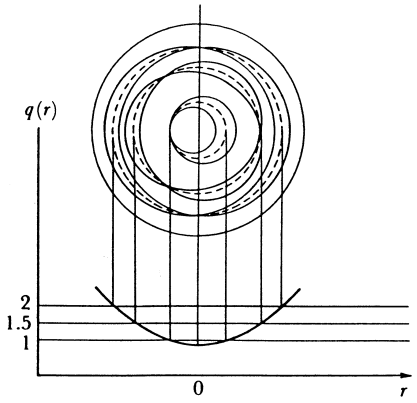

Fig.16.7 Magnetic islands of $m = 1, m = 3/2, m = 2$ appears at $q(r)$=1,3/2,2.

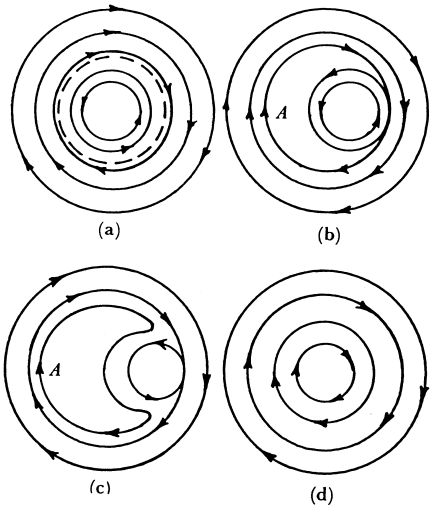

Fig.16.8 The hot core in the center is expelled by the reconnection of magnetic surfaces

an empirical scaling

$$N_{\rm G} < 1 \tag{16.8}$$

is hold for most of tokamak experiments (ref.[9]), where n_{20} is the electron density in the unit of $10^{20}{\rm m}^{-3}$. $N_{\rm G}$ is expressed by the other form (refer to sec.16.4)

$$N_{\rm G} = \frac{0.628}{K^2}\frac{n_{20}}{B_{\rm t}({\rm T})/R({\rm m})}q_{\rm I}.$$

The upper limit of the electron density depends critically on the plasma wall interaction and tends to increase as the heating power increases, although the scaling $N_{\rm GHM} < 1$ does not reflect the power dependence. When hydrogen ice pellets are injected into a plasma for fueling from high field side of ASDEX-U with advanced divertor (ref.[10]), $N_{\rm G}$ becomes up to ~ 1.5. Therefore there is possibility to increase $N_{\rm G}$ furthermore. The safety factor q_a at the plasma boundary is $q_a > 3$ in most cases. Beyond the stable region ($N_{\rm G} < 1,\ q_a < 2 \sim 3$), strong instability, called *disruptive instability*, occurs in usual operations. Negative spikes appear in the loop voltage due to the rapid expansion of the current channel (flattened current profile), that is, the rapid reduction of the internal inductance. The thermal energy of the plasma is lost suddenly. The electron temperature drops rapidly, and the plasma resistance increases. A positive pulse appears in the loop voltage. Then the plasma discharge is terminated rapidly. In some cases, the time scale of disruption is much faster than the time scale (9.27) predicted by the resistive tearing mode. For possible mechanisms of the disruptive instability, overlapping of the magnetic islands of $m = 2/n = 1\,(q(r) = 2)$ and $m = 3/n = 2\,(q(r) = 1.5)$ or the reconnection of $m = 2/n = 1, m = 1/n = 1$ magnetic islands are being discussed. Reviews of the MHD instabilities of tokamak plasmas and plasma transport are given in (ref.[11]-[14]).

16.4 Beta Limit of Elongated Plasma

The output power density of nuclear fusion is proportional to $n^2\langle\sigma v\rangle$. Since $\langle\sigma v\rangle$ is proportional to $T_{\rm i}^2$ in the region near $T_{\rm i} \sim 10\,{\rm keV}$, the fusion output power is proportional to the square of plasma pressure $p = n\kappa T$. Therefore the higher the beta ratio $\beta = p/(B^2/2\mu_0)$, the more economical the possible fusion reactor. The average beta of $\langle\beta\rangle \sim 3\%$ was realized by NBI experiments in ISX-B, JET-2, and PLT. All these tokamaks have a circular plasma cross section.

Troyon et al. (ref.[15]) evaluate the maximum growth rates of MHD instabilities in many cases of elongated tokamak plasma by ERATO code and derive the beta scaling on the upper limit of stable beta value under the optimized conditions as follows:

$$\beta_{\rm c}(\%) = \beta_{\rm N}\frac{I_{\rm p}({\rm MA})}{a({\rm m})B_t({\rm T})}. \tag{16.9}$$

$\beta_{\rm N}$ is called the Troyon factor or normalized beta ($\beta_{\rm N} = 2 \sim 4$). Figure 16.9 shows the poloidal plasma flow associated with an unstable mode which develops when β exceeds the limit.

In non-circular tokamak DIII-D, $\langle\beta\rangle = 11\%$ was realized in 1990 (ref.[17]), in which $a = 0.45\,{\rm m}$, $B_{\rm t} = 0.75\,{\rm T}$, $I_{\rm p} = 1.29\,{\rm MA}$, $I_{\rm p}/aB_{\rm t} = 3.1\,{\rm MA/Tm}$, $\beta_N \sim 3.6$, $\kappa_{\rm s} = 2.35$ and $R = 1.43{\rm m}$. Fig.16.10 shows the experimental data of DIII-D on the observed beta versus $I_{\rm p}/aB_{\rm t}$.

When the following definitions

$$\bar{B}_{\rm p} \equiv \frac{\mu_0 I_{\rm p}}{2\pi aK}, \qquad q_{\rm I} \equiv K\frac{a}{R}\frac{B_{\rm t}}{\bar{B}_{\rm p}} \tag{16.10}$$

are used, the critical beta is reduced to

$$\beta_{\rm c}(\%) = 5\beta_{\rm N}K^2\frac{a}{Rq_{\rm I}}$$

where $2\pi Ka$ is the the length of circumference of the plasma boundary and K is approximately given by

$$K^2 \simeq (1+\kappa_{\rm s}^2)/2$$

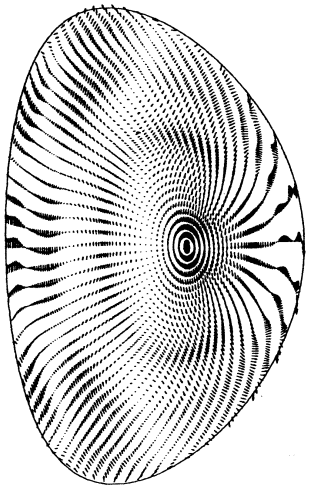

Fig.16.9 Unstable global $n = 1$ mode. After (ref.[15]). The singular surfaces $q = 2, 3$, and 4 are visible because of the peaked shear velocity on them. $q_0 = 1.35, \beta = 3\%$

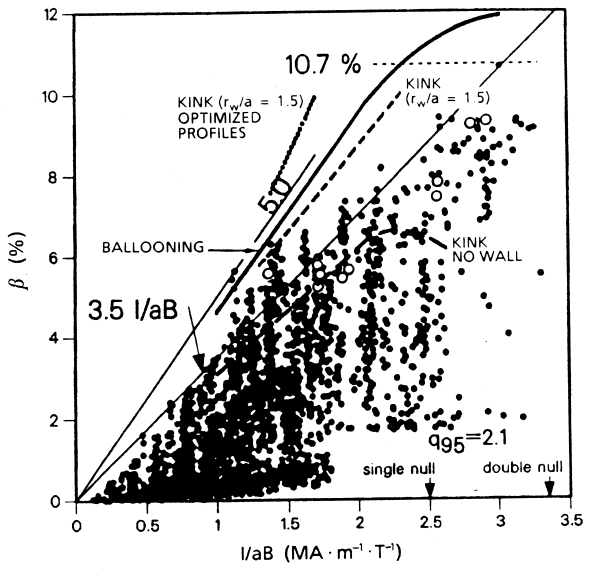

Fig.16.10 The observed beta versus I/aB for DIII-D. Various β limit calculations are summarized in the curves with different assumptions on the location of a conducting wall (r_w/a). After (ref.[17]).

and κ_s is the ratio of the vertical radius b to the horizontal radius a. q_I is called cylindrical safety factor, as q_I is the safety factor in the limiting case of large aspect ratio. In this case, there is the following relation between $\beta_c(\%)$ and β_p:

$$\beta_c(\%)\beta_p = 0.25\beta_N^2 K^2$$

The safety factor q_ψ at a magnetic surface ψ is given by

$$q_\psi = \frac{1}{2\pi}\oint \frac{B_t}{RB_p}\mathrm{d}l = \frac{1}{2\pi \mathrm{d}\psi}\oint B_t \frac{\mathrm{d}\psi}{RB_p}\mathrm{d}l$$

$$= \frac{1}{2\pi \mathrm{d}\psi}\oint B_t \mathrm{d}s\mathrm{d}l = \frac{1}{2\pi}\frac{\mathrm{d}\Phi}{\mathrm{d}\psi}$$

where Φ is the toroidal flux through the magnetic surface ψ. It must be notified that q_I is different from q_ψ in the finite aspect ratio. As an approximate fitting formula of the safety factor at the magnetic surface including 95% of the total toroidal magnetic flux through the total plasma cross-section, the following equation is used (refer to p.2160 of (ref.[16]):

$$q_{95} = q_I f_\delta f_A = \frac{a^2 B}{(\mu_0/2\pi)RI}\frac{1+\kappa_s^2}{2} f_\delta f_A, \tag{16.11}$$

where

$$f_\delta = \frac{1+\kappa_s^2(1+2\delta^2-1.2\delta^3)}{1+\kappa_s^2}, \qquad f_A = \frac{1.17-0.65/A}{(1-1/A^2)^2}.$$

δ is triangularity of the plasma shape defined in sec.16.12 or $\delta \approx \Delta/a$ (refer to fig.16.11). f_δ is the factor due to the triangularity of the plasma cross-section and f_A is the factor due to the finite aspect ratio.

16.5 Impurity Control, Scrape-Off Layer and Divertor

Radiation loss power P_{brems} by bremsstrahlung due to electron collision with ion per unit volume is

$$P_{\mathrm{brems}} = 1.5\times 10^{-38} Z_{\mathrm{eff}} n_e^2 (\kappa T_e/e)^{1/2}. \qquad (\mathrm{W/m^3})$$

The loss time due to bremsstrahlung defined by $\tau_{\mathrm{brems}} = (3/2)n_e\kappa T_e\ / P_{\mathrm{brems}}$ is

$$\tau_{\mathrm{brems}} = 0.16\frac{1}{Z_{\mathrm{eff}} n_{20}}\left(\frac{\kappa T_e}{e}\right)^{1/2} \qquad (\mathrm{sec})$$

where n_{20} is in units of $10^{20}\,\mathrm{m}^{-3}$ $\kappa T_e/e$ is in unit of eV . When $n_e \sim 10^{20}\,\mathrm{m}^{-3}$, and $\kappa T_e \sim 10\,\mathrm{keV}$, then we have $\tau_{\mathrm{brems}} \sim 8/Z_{\mathrm{eff}}(\mathrm{s})$. Therefore if the radiation losses such as bremsstrahlung, recombination radiation and line spectre emission are enhanced much by impurity ions, fusion core plasma can not be realized even by the radiation losses only. When the temperature of the plasma increases, the ions from the plasma hit the walls of the vacuum vessel and impurity ions are sputtered. When the sputtered impurities penetrate the plasma, the impurities are highly ionized and yield a large amount of radiation loss, which causes radiation cooling of the plasma. Therefore impurity control is one of the most important subjects in fusion research.

The light impurities, such as C and O, can be removed by baking and discharge-cleaning of the vacuum vessel. The sputtering of heavy atoms (Fe, etc.) of the wall material itself can be avoided by covering the metal wall by carbon tiles. Furthermore a divertor, as shown in fig.16.11, is very effective to reduce the plasma-wall interaction. Plasmas in *Scrap-off layer* flow at the velocity of sound along the lines of magnetic force just outside the *separatrix* S into the neutralized plates, where the plasmas are neutralized. Even if the material of the neutralized plates is sputtered, the atoms are ionized within the divertor regions near the neutralized plates. Since the thermal velocity of the heavy ions is much smaller than the flow velocity of the plasma (which is the same as the thermal velocity of hydrogen ions), they are unlikely to flow back into the main plasma.

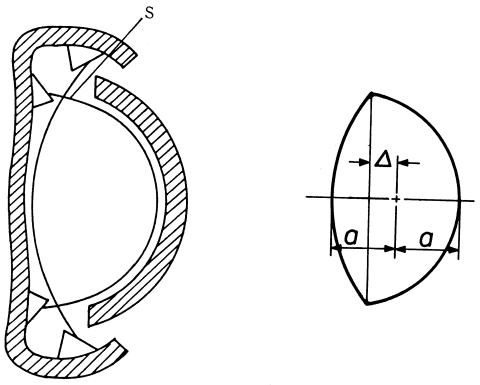

Fig.16.11 Divertor configuration using separatrix S of the magnetic surface (lefthand side). Definition of the triangularity $\delta = \Delta/a$ (righthand side)

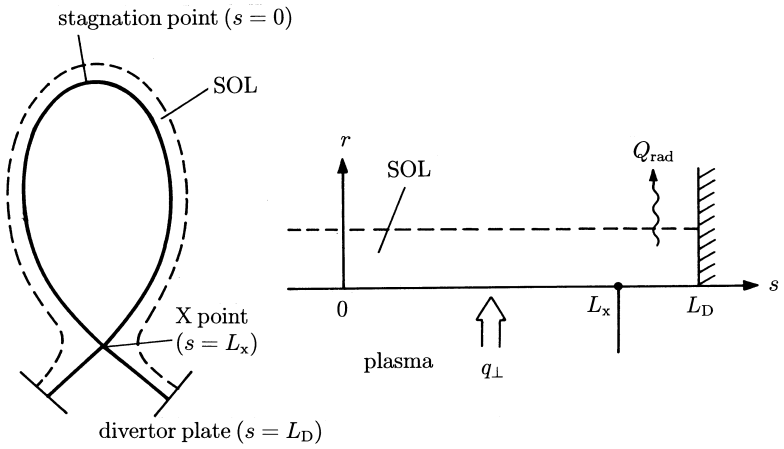

Fig.16.12 Configuration of scrape-off layer (SOL) and divertor. The coordinate of the slab model (right-hand side)

In the divertor region the electron temperature of the plasma becomes low because of impurity radiation cooling. Because of pressure equilibrium along the lines of magnetic force, the density in the divertor region near the neutralized plates becomes high. Therefore the velocity of ions from the plasma into the neutralized plates is collisionally damped and sputtering is suppressed. A decrease in the impurity radiation in the main plasma can be observed by using a divertor configuration.

However the scrape off layer of divertor is not broad and most of the total energy loss is concentrated to the narrow region of the target divertor plate. The severe heat load to the divertor plate is one of the most critical issues for a reactor design. Physical processes in scrape-off layer and divertor region are actively investigated experimentally and theoretically (ref.[18]).

Let us consider the thermal transport in scrape-off layer. It is assumed that the thermal transport parallel to the magnetic line of force is dominated by classical electron thermal conduction and the thermal transport perpendicular to the magnetic field is anomalous thermal diffusion. We use a slab model as is shown in fig.16.12 and omit Boltzmann constant in front of temperature in this section. Then we have

$$\nabla q_{\parallel} + \nabla q_{\perp} + Q_{\mathrm{rad}} = 0 \tag{16.12}$$

$$q_{\parallel} = -\kappa_{\mathrm{c}} \frac{\partial T_{\mathrm{e}}}{\partial s} = -\kappa_0 T_{\mathrm{e}}^{5/2} \frac{\partial T_{\mathrm{e}}}{\partial s} = -\frac{2}{7}\kappa_0 \frac{\partial T_{\mathrm{e}}^{7/2}}{\partial s} \tag{16.13}$$

$$q_{\perp} = -n\left(\chi_{\perp}^{\mathrm{e}} \frac{\partial T_{\mathrm{e}}}{\partial r} + \chi_{\perp}^{\mathrm{i}} \frac{\partial T_{\mathrm{i}}}{\partial r}\right) - \frac{3}{2} D(T_{\mathrm{e}} + T_{\mathrm{i}}) \frac{\partial n}{\partial r} \tag{16.14}$$

$$\kappa_{\rm c} \sim 3n\lambda_{\rm ei}^2\nu_{\rm ei} = \frac{3\times 51.6\pi^{1/2}\epsilon^2 T^{5/2}}{m_{\rm e}^{1/2}Ze^4\ln\Lambda} \sim \frac{2\times 10^{22}}{Z}\left(\frac{T_{\rm e}}{e}\right)^{5/2} \quad ({\rm m\cdot s})^{-1} \qquad \left(\frac{T_{\rm e}}{e} \text{ in unit of eV}\right).$$

Here $q_\parallel$ and $q_\perp$ are heat fluxes in the directions of parallel and perpendicular to the magnetic field and $Q_{\rm rad}$ is radiation loss. $\kappa_{\rm c}$ is heat conductivity and $\chi_\perp^{\rm e}, \chi_\perp^{\rm i}$ are thermal difusion coefficients and D is diffusion coefficient of particles. The stagnation point of heat flow is set as $s = 0$ and the X point of separatrix and divertor plate are set as $s = L_{\rm x}$ and $s = L_{\rm D}$ respectively. Then the boundary condition at $s = 0$ and $s = L_{\rm D}$ are

$$q_{\parallel 0} = 0 \tag{16.15}$$

$$\begin{aligned} q_{\parallel {\rm D}} &= \gamma T_{\rm D} n_{\rm D} d_{\rm D} + \frac{1}{2} m_{\rm i} u_{\rm D}^2 n_{\rm D} u_{\rm D} + \xi n_{\rm D} u_{\rm D} \\ &= n_{\rm D} M_{\rm D} c_{\rm s}((\gamma + M_{\rm D}^2)T_{\rm D} + \xi) \end{aligned} \tag{16.16}$$

where $u_{\rm D}$ is flow velocity of plasma at the divertor plate and $M_{\rm D}$ is Mach number $M_{\rm D} = u_{\rm D}/c_{\rm s}$. $\gamma \approx 7$ is sheath energy transfer coefficient and $\xi \approx 20 \sim 27$eV is ionization energy. The sound velocity is $c_{\rm s} = \tilde{c}_{\rm s} T_{\rm D}^{1/2}$, $\tilde{c}_{\rm s} = 0.98(2/A_{\rm i})^{1/2}10^4 {\rm ms}^{-1}({\rm eV})^{-1/2}$, $A_{\rm i}$ being ion atomic mass. The first and the second terms of (16.16) are the power flux into the sheath and the third term is power consumed within the recycling process. The equations of particles and momentum along the magnetic lines of force are

$$\frac{\partial(nu)}{\partial s} = S_{\rm i} - S_{\rm cx,r} - \nabla_\perp(nu_\perp) \approx S_{\rm i} - S_{\rm cx,r} \tag{16.17}$$

$$mnu\frac{\partial u}{\partial s} = -\frac{\partial p}{\partial s} - muS_{\rm m} \tag{16.18}$$

where $S_{\rm m} = nn_0\langle\sigma v\rangle_{\rm m}$ is the loss of momentum of plasma flow by collision with neutrals, $S_{\rm i} = nn_0\langle\sigma v\rangle_{\rm i}$ is the ionization term and $S_{\rm cx,r} = nn_0\langle\sigma v\rangle_{\rm cx,r}$ is ion loss by charge exchange and radiation recombination. Eqs.(16.17) and (16.18) reduce to

$$\frac{\partial(nmu^2 + p)}{\partial s} = -mu(S_{\rm m} + S_{\rm cx,r}) + muS_{\rm i} \tag{16.19}$$

The flow velocities at $s = 0$ and $s = L_{\rm D}$ are $u_0 = 0$ and $u_{\rm D} = M_{\rm D}c_{\rm s}, M_{\rm D} \approx 1$ respectively. Eqs.(16.12),(16.13) and the boundary conditions (16.15),(16.16) reduce to

$$\frac{2\kappa_0}{7}\frac{\partial^2}{\partial s^2}T_{\rm e}^{7/2} = \nabla_\perp q_\perp + Q_{\rm rad} \tag{16.20}$$

$$\frac{2\kappa_0}{7}(T_{\rm e}^{7/2}(s) - T_{\rm eD}^{7/2}) = \int_{L_{\rm D}}^{s} {\rm d}s' \int_0^{s'} (\nabla_\perp q_\perp + Q_{\rm rad}){\rm d}s''. \tag{16.21}$$

When $\nabla_\perp q_\perp$ =const. $Q_{\rm rad} = 0$ in $0 < s < L_{\rm x}$ and $\nabla_\perp q = 0$, $Q_{\rm rad}$ =const. in $L_{\rm x} < s < L_{\rm D}$, we have

$$\frac{2\kappa_0}{7}(T_{\rm e}^{7/2}(s) - T_{\rm eD}^{7/2}) = 0.5(-\nabla_\perp q_\perp)(2L_{\rm x}L_{\rm D} - L_{\rm x}^2 - s^2) + 0.5Q_{\rm rad}(L_{\rm D} - L_{\rm x})^2 \qquad (0 < s < L_{\rm x}).$$

When radiation term is negligible, $T_{\rm e0} \equiv T_{\rm e}(0)$ becomes

$$T_{\rm e0}^{7/2} = T_{\rm eD}^{7/2} + \frac{7}{4\kappa_0}\left(\frac{2L_{\rm D}}{L_{\rm x}} - 1\right)(-\nabla_\perp q_\perp)L_{\rm x}^2.$$

If $T_{\rm eD} < 0.5T_{\rm e0}$ and $L_{\rm D} - L_{\rm x} \ll L_{\rm x}$, we have

$$T_{\rm e0} \approx 1.17\left(\frac{(-\nabla_\perp q_\perp)L_{\rm x}^2}{\kappa_0}\right)^{2/7} = 1.17\left(\frac{q_\perp L_{\rm x}^2}{\kappa_0\lambda_q}\right)^{2/7} \tag{16.22}$$

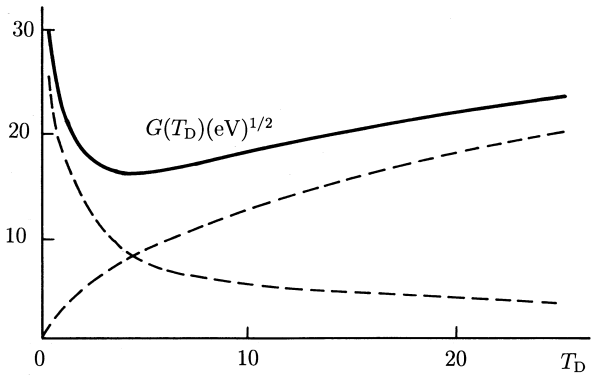

Fig.16.13 Dependence of $G(T_{\rm D})({\rm eV})^{1/2}$ on $T_{\rm D}({\rm eV})$

where $1/\lambda_q \equiv -\nabla_\perp q_\perp/q_\perp$. When the scale lengths of gradients of temperature and density are λ_T and λ_n respectively ($T(r) = T\exp(-r/\lambda_T)$, $n(r) = n\exp(-r/\lambda_n)$) and $\chi^{\rm i}_\perp \ll \chi^{\rm e}_\perp$ and$D \sim \chi^{\rm e}_\perp$ are assumed, (16.14) becomes

$$q_\perp = n\chi^{\rm e}_\perp \frac{T_{\rm e}}{\lambda_T}\left(1 + \frac{3}{2}(1 + \frac{T_{\rm i}}{T_{\rm e}})\frac{\lambda_T}{\lambda_n}\right). \tag{16.23}$$

Therefore if $\chi^{\rm e}$ is known as a function $\chi^{\rm e}(T_{\rm e}, n, B)$, λ_T is given as $\lambda_T(T_{\rm e}, n, B, q_\perp)$.

Let us consider the relations between $n_{\rm s}, T_{\rm es}, T_{\rm is}$ at stagnation point $s = 0$ and $n_{\rm D}, T_{\rm D}$ at divertor plate $s = L_{\rm D}$. The momentum flux at divertor region decreases due to collision with neutrals, charge exchange and ionization and becomes smaller than that at stagnation point.

$$f_p = \frac{2(1 + n_{\rm D}^2)n_{\rm D}T_{\rm D}}{n_{\rm s}(T_{\rm es} + T_{\rm is})} < 1. \tag{16.24}$$

The power flux to divertor plate is reduced by radiation loss from the power flux $q_\perp L_{\rm x}$ into scrape-off layer through the separatrix with length of $L_{\rm x}$

$$\int_0^\infty q_\parallel {\rm d}r = (1 - f_{\rm rad})q_\perp L_{\rm x} \tag{16.25}$$

where $f_{\rm rad}$ is the fraction of radiation loss. Eqs.(16.25) and(16.16) reduce

$$M_{\rm D}n_{\rm D}\tilde{c}_{\rm s}T_{\rm D}^{1/2}\left(\frac{(\gamma + M_{\rm D}^2)T_{\rm D}}{3/2\lambda_T + 1/\lambda_n} + \frac{\xi}{1/(2\lambda_T) + 1/\lambda_n}\right) = (1 - f_{\rm rad})q_\perp L_{\rm x}$$

that is

$$(1 - f_{\rm rad})q_\perp L_{\rm x} = \frac{\tilde{c}_{\rm s}f_p\lambda_T}{1.5 + \lambda_T/\lambda_n}n_{\rm s}\frac{T_{\rm es} + T_{\rm is}}{2}G(T_{\rm D}) \tag{16.26}$$

$$G(T_{\rm D}) \equiv \frac{M_{\rm D}}{1 + M_{\rm D}^2}(\gamma + M_{\rm D})T_{\rm D}^{1/2}\left(1 + \frac{1}{\gamma + M_{\rm D}}\frac{\bar{\xi}}{T_{\rm D}}\right). \tag{16.27}$$

The curve of $G(T_{\rm D})$ as the function of $T_{\rm D}$ is shown in fig.16.13 and $G(T_{\rm D})$ has a minimum at $T_{\rm D} = \bar{\xi}/(\gamma + M_{\rm D}^2)$. In the case of $M_{\rm D} \approx 1, \gamma \approx 7, \xi = 24{\rm eV}$, $G(T_{\rm D})$ is

$$G_{\rm D} = 4T_{\rm D}^{1/2}\left(1 + \frac{4.5}{T_{\rm D}}\right).$$

$G(T_{\rm D})$ is roughly proportional to $T_{\rm D}^{1/2}$ when $T_{\rm D} > 15{\rm eV}$ in this case. Since $T_{\rm es}$ depends on $n_{\rm s}$ through $\lambda_q^{-2/7}$ as is seen in (16.22), the dependence of $T_{\rm es}$ on $n_{\rm s}$ is very weak. From (16.26) and (16.24), we have roughly following relations

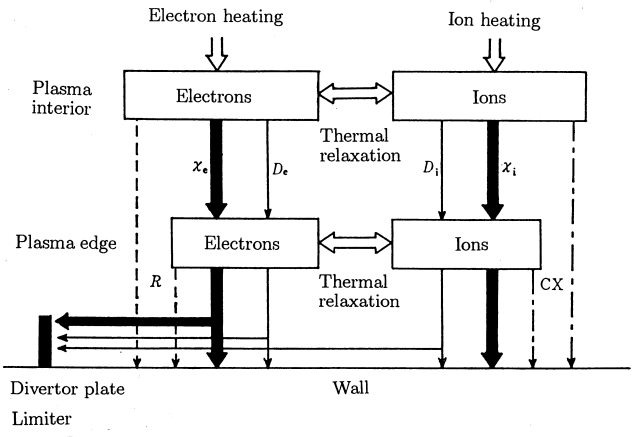

Fig.16.14 Energy flow of ions and electrons in a plasma. Bold arrows, thermal conduction (χ). Light arrows, convective loss (D). Dashed arrow, radiation loss (R). Dot-dashed arrows, charge exchange loss (CX).

$$T_{\rm D} \propto n_{\rm s}^{-2} \qquad n_{\rm D} \propto n_{\rm s}^{3} \tag{16.28}$$

and the density $n_{\rm D}$ at divertor increases nonlinearly with the density $n_{\rm s}$ of upstream scrape-off layer.

When the upstream density $n_{\rm s}$ increases while keeping the left-hand side of (16.26) constant, the solution $T_{\rm D}$ of (16.26) can not exists beyond a threshold density, since $G(T_{\rm D})$ has the minimum value (fig.16.13). This is related to the phenomenon of detached plasma above a threshold of upstream density (ref.[18]). The heat load $\phi_{\rm D}$ of divertor normal to the magnetic flux surface is given by

$$\phi_{\rm D} \approx \frac{(1-f_{\rm rad})P_{\rm sep}}{2\pi R 2\lambda_{\phi D}} = (1-f_{\rm rad})\pi K \frac{a}{\lambda_T} q_\perp \left(1.5 + \frac{\lambda_T}{\lambda_n}\right) \frac{B_{\theta \rm D}}{B_\theta} \tag{16.29}$$

where $P_{\rm sep}$ is the total power flux across the separatrix surface and $\lambda_{\phi D}$ is the radial width of heat flux at divertor plate

$$P_{\rm sep} = 2\pi a K 2\pi R q_\perp \qquad \lambda_{\phi D} = \lambda_T \frac{1}{1.5 + \lambda_T/\lambda_n} \frac{B_\theta}{B_{\theta \rm D}}.$$

The term $B_\theta / B_{\theta \rm D} = 2 \sim 3$ is the ratio of separations of magnetic flux surfaces at stagnation point and divertor plate. If the divertor plate is inclined with angle α against the magnetic flux surface, the heat load of the inclined divertor plate becomes $\sin\alpha$ times as small as that of the divertor normal to magnetic flux surface.

16.6 Confinement Scaling of L Mode

The energy flow of ions and electrons inside the plasma is schematically shown in fig.16.14. Denote the heating power into the electrons per unit volume by $P_{\rm he}$ and the radiation loss and the energy relaxation of electrons with ions by R and $P_{\rm ei}$, respectively; then the time derivative of the electron thermal energy per unit volume is given by

$$\frac{\rm d}{{\rm d}t}\left(\frac{3}{2} n_{\rm e} \kappa T_{\rm e}\right) = P_{\rm he} - R - P_{\rm ei} + \frac{1}{r}\frac{\partial}{\partial r} r \left(\chi_{\rm e} \frac{\partial \kappa T_{\rm e}}{\partial r} + D_{\rm e} \frac{3}{2} \kappa T_{\rm e} \frac{\partial n_{\rm e}}{\partial r}\right).$$

where $\chi_{\rm e}$ is the electron thermal conductivity and $D_{\rm e}$ is the electron diffusion coefficient. Concerning the ions, the same relation is derived, but instead of the radiation loss the charge exchange loss $L_{\rm ex}$ of ions with neutrals must be taken into account, and then

$$\frac{\rm d}{{\rm d}t}\left(\frac{3}{2} n_{\rm i} \kappa T_{\rm i}\right) = P_{\rm hi} - L_{\rm cx} + P_{\rm ei} + \frac{1}{r}\frac{\partial}{\partial r} r \left(\chi_{\rm i} \frac{\partial \kappa T_{\rm i}}{\partial r} + D_{\rm i} \frac{3}{2} \kappa T_{\rm i} \frac{\partial n_{\rm i}}{\partial r}\right).$$

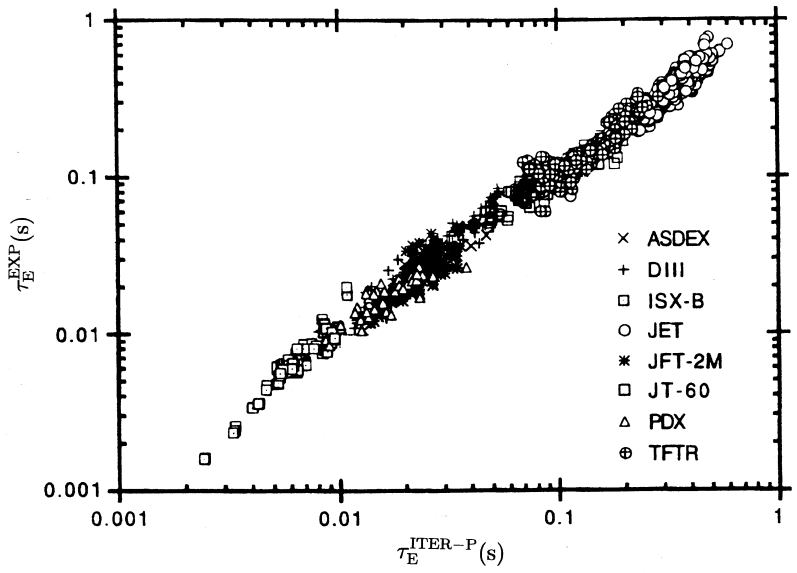

Fig.16.15 Comparison of confinement scaling $\tau_{\mathrm{E}}^{\mathrm{ITER-P}}$ with experimental data of energy confinement time $\tau_{\mathrm{E}}^{\mathrm{EXP}}$ of L mode. After (ref.[20]).

The experimental results of heating by ohmic one and neutral beam injection can be explained by classical processes. The efficiency of wave heating can be estimated fairly accurately by theoretical analysis. The radiation and the charge exchange loss are classical processes. In order to evaluate the energy balance of the plasma experimentally, it is necessary to measure the fundamental quantities $n_{\mathrm{e}}(r,t), T_{\mathrm{i}}(r,t), T_{\mathrm{e}}(r,t)$, and others. According to the many experimental results, the energy relaxation between ions and electrons is classical, and the observed ion thermal conductivities in some cases are around $2 \sim 3$ times the neoclassical thermal conductivity;

$$\chi_{\mathrm{i,nc}} = n_{\mathrm{i}} f(q,\varepsilon) q^2 (\rho_{\Omega \mathrm{i}})^2 \nu_{\mathrm{ii}}.$$

($f = 1$ in the Pfirsch-Schlüter region and $f = \epsilon_{\mathrm{t}}^{-3/2}$ in the banana region) and the observed ion thermal conductivities in some other cases are anomalous. The electron thermal conduction estimated by the experimental results is always anomalous and is much larger than the neoclassical one (more than one order of magnitude larger). In most cases the energy confinement time of the plasma is determined mostly by electron thermal conduction loss. The energy confinement times τ_{E} is defined by

$$\tau_{\mathrm{E}} \equiv \frac{\int (3/2)(n_{\mathrm{e}} \kappa T_{\mathrm{e}} + n_{\mathrm{i}} \kappa T_{\mathrm{i}}) \mathrm{d}V}{P_{\mathrm{in}}}.$$

in steady case. The energy confinement time τ_{OH} of an ohmically heated plasma is well described by Alcator (neo-Alcator) scaling as follows (units are $10^{20}\mathrm{m}^{-3}$, m):

$$\tau_{\mathrm{OH}}(\mathrm{s}) = 0.103 q^{0.5} \bar{n}_{\mathrm{e}20} a^{1.04} R^{2.04}.$$

However, the linearity of τ_{OH} on the average electron density $\bar{n}_{\mathrm{e}}$ deviates in the high-density region $n_{\mathrm{e}} > 2.5 \times 10^{20}\,\mathrm{m}^{-3}$ and τ_{OH} tends to saturate. When the plasma is heated by high-power NBI or wave heating, the energy confinement time degrades as the heating power increases. Kaye and Goldston examined many experimental results of NBI heated plasma and derived so-called Kaye-Goldston scaling on the energy confinement time (ref.[19]), that is,

$$\tau_{\mathrm{E}} = (1/\tau_{\mathrm{OH}}^2 + 1/\tau_{\mathrm{AUX}}^2)^{-1/2}$$

$$\tau_{\mathrm{AUX}}(\mathrm{s}) = 0.037 \kappa_{\mathrm{s}}^{0.5} I_{\mathrm{p}} P_{\mathrm{tot}}^{-0.5} a^{-0.37} R^{1.75}$$

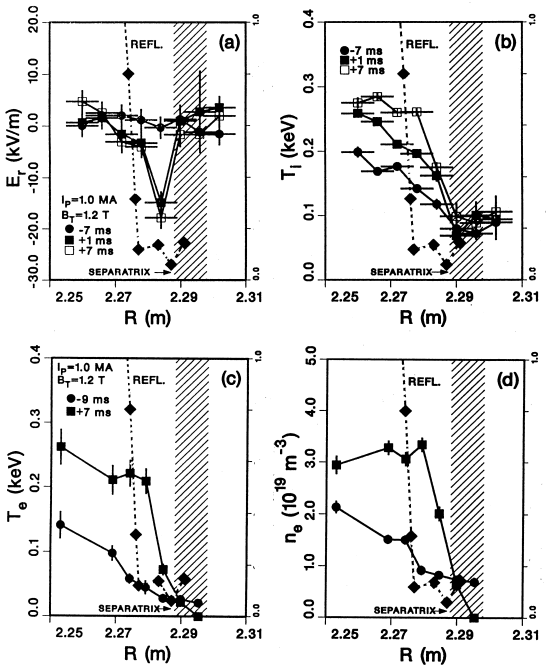

Fig.16.16 Plots of various edge plasma profiles at times spanning the L-H transition in DIIID. (a) E_r profile, (b) Profiles of the ion temperature measured by CVII charge exchange recombination spectroscopy, (c)(d) Profiles of electron temperature and electron density measured by Thomson scattering. After (ref.[24]).

where units are MA, MW, m and κ_s is the elongation ratio of noncircularity and P_{tot} is the total heating power in MW.

ITER team assembled data from larger and more recent experiments. Analysis of the data base of L mode experiments (see next section) led to the proposal of following ITER-P scaling (ref.[20]);

$$\tau_E^{ITER-P}(s) = 0.048 I_p^{0.85} R^{1.2} a^{0.3} \bar{n}_{20}^{0.1} B^{0.2} (A_i \kappa_s / P)^{1/2} \tag{16.31}$$

where unite are MA, m, T, MW and the unit of $\bar{n}_{20}$ is $10^{20}m^{-3}$. P is the heating power corrected for radiation P_R ($P = P_{tot} - P_R$). A comparison of confinement scaling τ_E^{ITER-P} with the experimental data of L mode is presented in fig.16.15.

16.7 H Mode and Improved Confinement Modes

An improved confinement state "*H mode* " was found in the ASDEX (ref.[21],[22]) experiments with divertor configuration. When the NBI heating power is larger than a threshold value in the divertor configuration, the D_α line of deuterium (atom flux) in the edge region of the deuterium plasma decreases suddenly (time scale of 100 μs) during discharge, and recycling of deuterium atoms near the boundary decreases. At the same time there is a marked change in the edge radial electric field E_r (toward negative). Furthermore the electron density and the thermal energy density increase and the energy confinement time of NBI heated plasma is improved by a factor of about 2. H mode was observed in PDX, JFT-2, DIII-D, JET, JT60U and so on. The confinement state following Kaye-Goldston scaling is called the "*L mode*". In the H mode, the gradients of electron temperature and the electron density become steep just at the inside of the plasma boundary determined by the separatrix. In the spontaneous H mode, and E_r becomes more negative (inward) (see fig.16.16) (ref.[23][24]). The ion orbit loss near the plasma edge was pointed out and analyzed as a possible cause of the change of radial electric field on L-H transition (ref.[25][26]). The radial electric field causes plasma rotation with the velocity of $v_\theta = -E_r/B$ in the poloidal direction

and with the velocity $v_\phi = -(E_r/B)(B_\theta/B)$ in the toroidal direction. If the gradient of E_r exists, sheared poloidal rotation and sheared toroidal rotation are generated. The importance of sheared flow for supression of edge turbulence and for improved confinement was pointed out in (ref.[27]).

Let us consider the following fluid model

$$\left(\frac{\partial}{\partial t} + (\boldsymbol{v}_0 + \tilde{\boldsymbol{v}}) \cdot \nabla + L_\mathrm{d}\right) \tilde{\xi} = \tilde{s} \tag{13.32}$$

where $\tilde{\xi}$ is the fluctuating field. $\boldsymbol{v}_0$ is taken to be the equilibrium $\boldsymbol{E} \times \boldsymbol{B}$ flow. $\tilde{s}$ represents a driving source of the turbulence and L_d is an operator responsible for dissipation of turbulence. The mutual correlation function $\langle\tilde{\xi}(1)\tilde{\xi}(2)\rangle$ of the fluctuating field $\tilde{\xi}(1)$ at a point 1 and $\tilde{\xi}(2)$ at a point 2 is given by (ref.[28])

$$\left(\frac{\partial}{\partial t} + (v'_\theta - v_\theta/r_+)r_+\frac{\partial}{\partial y_-} - \frac{\partial}{\partial r_+}D(r_+, y_-)\frac{\partial}{\partial r_+} + L_\mathrm{d}\right)\langle\tilde{\xi}(1)\tilde{\xi}(2)\rangle = T \tag{16.33}$$

where D is radial diffusion coefficient of turbulence and T is the driving term and $r_+ = (r_1 + r_2)/2$, $\theta_- = \theta_1 - \theta_2$, $y_- = r_+\theta_-$. The decorrelation time τ_d in the poloidal direction is the time in which the relative poloidal displacement between point 1 and point 2 due to sheared flow becomes the space correlation length of the turbulence k_{0k}^{-1}, that is,

$$k_{0k}\delta y \sim 1,$$

$$\delta y = v'_\theta(\Delta r)\tau_\mathrm{d},$$

$$\tau_\mathrm{d} = \frac{1}{v'_\theta \Delta r k_{0k}}.$$

The decorrelation rate ω_s in the poloidal direction is

$$\omega_\mathrm{s} = \frac{1}{\tau_\mathrm{d}} = (\Delta r k_{0k})v'_\theta.$$

When Δr is the radial correlation length of the turbulence, the radial decorrelation rate $\Delta\omega_\mathrm{t}$ is given by

$$\Delta\omega_\mathrm{t} = \frac{D}{(\Delta r)^2}.$$

Since there is strong mutual interaction between radial and poloidal decorrelation processes, the decorrelation rate $1/\tau_\mathrm{corr}$ becomes a hybrid of two decorrelation rates, that is,

$$\frac{1}{\tau_\mathrm{corr}} = (\omega_\mathrm{s}^2\Delta\omega_\mathrm{t})^{1/3} = \left(\frac{\omega_\mathrm{s}}{\Delta\omega_\mathrm{t}}\right)^{2/3}\Delta\omega_\mathrm{t}. \tag{16.34}$$

The decorrelation rate $1/\tau_\mathrm{corr}$ becomes $(\omega_\mathrm{s}/\Delta\omega_\mathrm{t})^{2/3}$ times as large as $\Delta\omega_\mathrm{t}$; $\Delta\omega_\mathrm{t}$ is the decorrelation rate of the turbulence in the case of shearless flow. Since the saturation level of fluctuating field $\tilde{\xi}$ is

$$|\tilde{\xi}|^2 \sim T \times \tau_\mathrm{corr}$$

the saturation level of fluctuating field is reduce to

$$\frac{|\tilde{\xi}|^2}{|\tilde{\xi}_0|^2} \sim \left(\frac{\Delta\omega_\mathrm{t}}{\omega_\mathrm{s}}\right)^{2/3} \sim \left(\frac{1}{(\mathrm{d}v_\theta/\mathrm{d}r)t_0}\right)^{2/3}\frac{1}{(k_{0y}\Delta r)^2},$$

$$t_0^{-1} \equiv \langle k_{0y}^2\rangle D$$

where $|\tilde{\xi}_0|$ is the level in the case of shearless flow. The effect of sheared flow on the saturated resistive pressure gradient driven turbulence is shown in fig.16.17. The coupling between poloidal

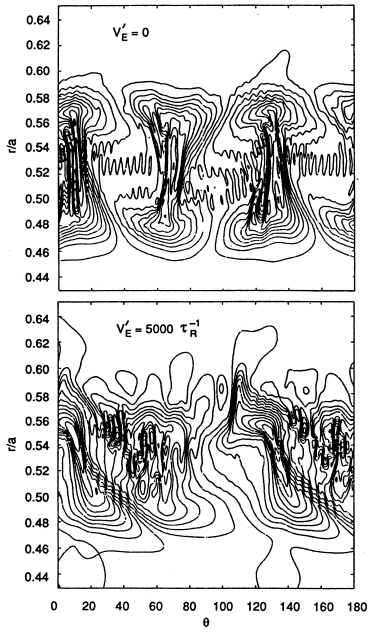

Fig.16.17 Snapshot of equidensity contour for shearless (top) and strongly-sheared (bottom) flows. After Bigrali et al: ref.[27]).

and radial decorrelation in shearing fluctuation is evident in this figure. Since the thermal diffusion coefficient is proportional to $|\tilde{\xi}|^2$, the thermal diffusion is reduced, that is, thermal barrier near the plasma edge is formed.

Active theoretical studies on H mode physics are being carried out.

In addition to the standard H mode as observed in ASDEX and others, the other types of improved confinement modes have been observed. In the TFTR experiment (ref.[29]) outgassing of deuterium from the wall and the carbon limiter located on the inner (high-field) side of the vacuum torus was extensively carried out before the experiments. Then balanced neutral beam injections of co-injection (beam direction parallel to the plasma current) and counterinjection (beam direction opposite to that of co-injection) were applied to the deuterium plasma, and an improved confinement "supershot" was obsered. In supershot, the electron density profile is strongly peaked ($n_{\rm e}(0)/\langle n_{\rm e}\rangle = 2.5 \sim 3$).

In DIII-D experiment, VH mode (ref.[30]) was observed, in which the region of strong radial electric field was expanded from the plasma edge to the plasma interior ($r/a \sim 0.6$) and $\tau_{\rm E}/\tau_{\rm E}^{\rm ITER-P}$ becomes 3.6.

In JT60U experiment, high beta-poloidal H mode (ref.[31]) was observed, in which $\beta_{\rm p}$ was high (1.2∼1.6) and the density profile was peaked ($n_{\rm e}(0)/\langle n_{\rm e}\rangle = 2.1 \sim 2.4$). Furthermore the edge thermal barrier of H mode was formed.

Hinton *et al* (ref.[32]) pointed out the peaked pressure and density profiles induce the gradient of the radial electric field. From the radial component of the equation of motion (5.7) of ion fluid or (5.28), we have

$$E_r \simeq B_{\rm p} u_{\rm t} - B_{\rm t} u_{\rm p} + \frac{1}{e n_{\rm i}} \frac{{\rm d}p_{\rm i}}{{\rm d}r}. \tag{16.35}$$

Differentiation of E_r by r is

$$\frac{{\rm d}E_r}{{\rm d}r} \sim -\frac{1}{e n_{\rm i}^2} \frac{{\rm d}n_{\rm i}}{{\rm d}r} \frac{{\rm d}p_{\rm i}}{{\rm d}r}$$

since the contribution from the other terms is small in usual experimental condition of H mode.

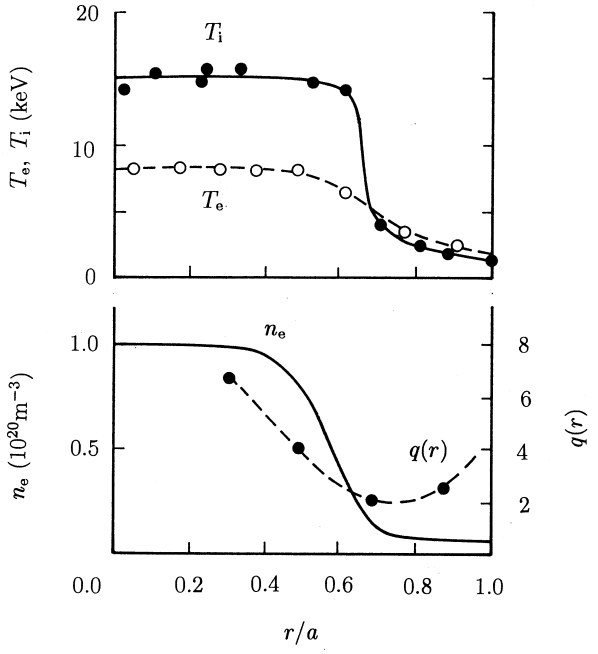

Fig.16.18 Radial profiles of ion and electron temperatures and density and q profiles in the negative magnetic shear configuration of JT60U.

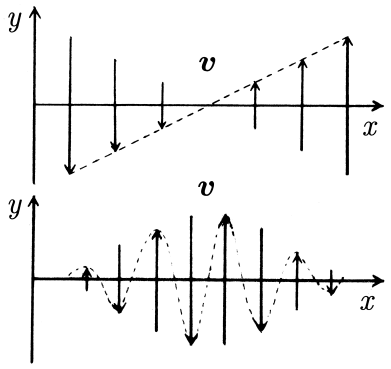

Fig.16.19 Upper figure: Sheared mean flow. Lower figure: Zonal flow.

High performance modes of negative magnetic shear configuration are demonstrated in DIII-D, TFTR, JT60U, JET and Tore Supra (ref.[33]). As described in sec.8.5, ballooning mode is stable in the negative shear region.

$$S = \frac{r}{q}\frac{\mathrm{d}q}{\mathrm{d}r} < 0. \tag{16.36}$$

Furthermore the scale of drift modes becomes smaller in weak shear region (gyro-Bohm diffusion) near the minimum q value as is discussed in sec.7.3. An example of radial profiles of temperature, density and q profile of JT60U is shown in fig.16.18. By combination of the central heating and the magnetic negative shear, the steep gradients in temperature and density appear at around the q minimum point.

The structure of sheard mean flow is macroscopic scale and the stabilizing effect of sheared flow on drift turbulence was discussed. Recently the theoretical researches on turbulence and zonal flow are greatly advanced and zonal flows have been observed experimentally (ref.[34]). The scale of zonal flow is mesoscopic as is described in appendix E in details. The difference of sheared mean flow and zonal flow is illustrated in fig.16.19.

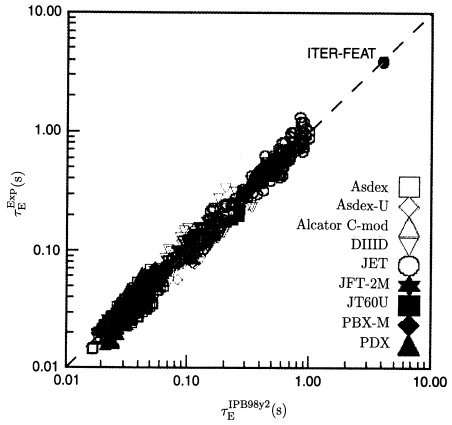

Fig.16.20 Comparison of IPB98y2 confinement scaling $\tau_{\mathrm{E\,th,\,scaling}}$ with experimental data of energy confinement time $\tau_{\mathrm{E\,th}}$ of H mode. After (ref.[36]).

Zonal flows in ITG (ion temperature gradient mode) are pumped by modulational instability of the drift waves. Magnetic field structures with $m = 0,\ n = 0$ (poloidal and toroidal modes) and finite k_r (radial mode), called zonal field, can be generated by drift wave turbulence. Zonal flows can modify the onset criterion for turbulence and turbulent transport.
Understanding of the zonal flow drive and damping has suggested several routes to improving confinement via externally driven flow shear amplification or by tuning the configuration design to lower the zonal flow damping (ref.[35]).

As a measure of high performance of improved confinement mode, the ratio, H_{L} factor, of observed energy confinement time $\tau_{\mathrm{E}}^{\mathrm{EXP}}$ to ITER-P scaling $\tau_{\mathrm{E}}^{\mathrm{ITER-P}}$ is widely used.

$$H_{\mathrm{L}} \equiv \frac{\tau_{\mathrm{E}}^{\mathrm{EXP}}}{\tau_{\mathrm{E}}^{\mathrm{ITER-P}}}. \tag{16.37}$$

Observed H_{L} factors are in the range of 2∼3.

ITER H mode database working group assembled standard experimental data of H mode from ASDEX, ASDEX-U, DIII-D, JET, JFT-2M, PDX, PBX, Alcator C-Mod, and so on. Results of regression analysis of H mode experiments led to the following thermal energy confinement time (chap. 2 in ref.[36]):

$$\tau_{\mathrm{E,th}}^{\mathrm{IPB98y2}} = 0.0562 I_{\mathrm{p}}^{0.93} B_{\mathrm{t}}^{0.15} P^{-0.69} M_{\mathrm{i}}^{0.19} R^{1.97} \bar{n}_{\mathrm{e19}}^{0.41} \epsilon^{0.58} \kappa^{0.78}, \tag{16.38}$$

where units of sec, MA, T, MW, amu, m, $10^{19}\mathrm{m}^{-3}$ are used and the total heating power corrected for shine-through of NBI heating, orbit loss, and charge exchange loss, less the time derivative of stored energy. This scaling is used when edge-localized-modes (ELM) exist. A comparison of thermal energy confinement scaling with experimental data of ELMy H mode is presented in fig.16.20.

In most experiments of hot plasmas, neutral beam injections are used to heat the plasma. With improved confinement mode operations, such as H mode, supershot and high β_{p} mode in large tokamaks, fusion grade plasmas are produced by neutral beam injection. The plasma parameters of typical shots of JET (ref.[37]), JT60U (ref.[31]), and TFTR (ref.[29]) are listed in Table 16.2.

Deuterium-tritium experiments were carried out on TFTR (ref.[29]). Fusion power of 9.3 MW ($Q \sim 0.27$) was obtained in supershot (refer to Table 16.2). JET set records of DT fusion output of 16.1 MW ($Q \sim 0.62$) with the heating power of 25.7 MW (ref.[37]).

In the present neutral beam source, the positive hydrogen ions are accelerated and then passed through the cell filled with neutral hydrogen gas, where ions are converted to a fast neutral beam by charge exchange (attachment of electron). However, the conversion ratio of positive hydrogen ions to neutral becomes small when the ion energy is larger than 100 keV (2.5% at 200 keV of H^+). On the other hand, the conversion ratio of negative hydrogen ions (H^-) to neutral (stripping of

Table 16.2 Plasma parameters of large tokamaks JET (ref.[37]), JT60U (ref.[31]) and TFTR (ref.[29]). $n_{\rm i}(0)\tau_{\rm E}^{\rm tot}T_{\rm i}(0)$ is fusion triple product. $\kappa_{\rm s}$ is the ratio of vertical radius to horizontal radius. q's are the effective safety factors near plasma boundary with different definitions. q_{95} is the safety factor at 95% flux surface. $q_{\rm eff}$ and q^* are defined in (ref.[31]) and (ref.[29]) respectively. $q_{\rm I}$ is the factor defined in sec.16.4. $E_{\rm NB}$ is a particle energy of neutral beam injection.

	JET	JT60U	TFTR
	ELM free No.26087	ELMy No.E21140	supershot
$I_{\rm p}$(MA)	3.1	2.2	2.5
$B_{\rm t}$(T)	2.8	4.4	5.1
R/a(m/m)	3.15/1.05	3.05/0.72	∼2.48/0.82
$\kappa_{\rm s}$	1.6	1.7	1
q's	q_{95}=3.8	$q_{\rm eff}$=4.6	q^*=3.2
$q_{\rm I}$	2.8	3.0	2.8
$n_{\rm e}(0)(10^{19}m^{-3})$	5.1	7.5	8.5
$n_{\rm e}(0)/\langle n_{\rm e}\rangle$	1.45	2.4	-
$n_{\rm i}(0)(10^{19}m^{-3})$	4.1	5.5	6.3
$T_{\rm e}(0)$(keV)	10.5	10	11.5
$T_{\rm e}(0)/\langle T_{\rm e}\rangle$	1.87	-	-
$T_{\rm i}$(keV)	18.6	30	44
$W_{\rm dia}$ (MJ)	11.6	7.5	6.5
${\rm d}W_{\rm dia}/{\rm d}t$(MJ/s)	6.0	-	7.5
$Z_{\rm eff}$	1.8	2.2	2.2
$\beta_{\rm p}$	0.83	1.2	∼1.1
$\beta_{\rm t}$(%)	2.2	∼1.3	∼1.2
g(Troyon factor)	2.1	∼1.9	2
$P_{\rm NB}$(MW)	14.9	24.8	33.7
$E_{\rm NB}$(keV)	135, 78	95	110
$\tau_{\rm E}^{\rm tot}=W/P_{\rm tot}$(s)	0.78	0.3	0.2
$H=\tau_{\rm E}^{\rm tot}/\tau_{\rm E}^{\rm ITER-P}$	∼ 3.0	∼ 2.1	∼ 2.0
$n_{\rm i}(0)\tau_{\rm E}^{\rm tot}T_{\rm i}(0)(10^{20}{\rm keVm^{-3}s})$	5.9	5	5.5
$n_{\rm T}(0)/(n_{\rm T}(0)+n_{\rm D}(0))$	0	0	0.5
$P_{\rm fusion}$(MW)	-	-	9.3

electron) does not decrease in the high energy range (∼60%); a neutral beam source with a *negative ion source* is being developed as a high-efficiency source.

Wave heating is another method of plasma heating and was described in ch.12. The similar heating efficiency of wave heating in ICRF (ion cyclotron range of frequency) to that of NBI was observed in PLT. In the ICRF experiments of JET, the parameters $T_{\rm i}(0) = 5.4\,{\rm keV}, T_{\rm e}(0) = 5.6\,{\rm keV}$, $n_{\rm e}(0) = 3.7 \times 10^{13}\,{\rm cm}^{-3}$, $\tau_{\rm E} \sim 0.3\,{\rm s}$ were obtained by $P_{\rm ICRF} = 7\,{\rm MW}$.

16.8 Noninductive Current Drive

As long as the plasma current is driven by electromagnetic induction of the current transformer in a tokamak device, the discharge is a necessarily pulsed operation with finite duration. If the plasma current can be driven in a noninductive way, a steady-state tokamak reactor is possible in principle. Current drive by neutral beam injection has been proposed by Ohkawa (ref.[38]) and current drive by traveling wave has been proposed by Wort (ref.39). The momenta of particles injected by NBI or of traveling waves are transferred to the charged particles of the plasma, and the resultant charged particle flow produces the plasma current. Current drive by NBI was demonstrated by DITE, TFTR, etc. Current drive by a lower hybrid wave (LHW), proposed by Fisch (ref.[40]) was demonstrated by JFT-2, JIPPT-II, WT-2, PLT, Alcator C, Versator 2, T-7, Wega, JT-60 and so on. Current drive by electron cyclotron wave was demonstrated by Cleo, T-10, WT-3, Compass-D, DIII-D, TCV and so on.

16.8a Lower Hybrid Current Drive

The theory of current drive by waves is described here according to Fisch and Karney (ref.[40]). When a wave is traveling along the line of magnetic force, the velocity distribution function near the phase velocity of the wave is flattened by the diffusion in velocity space. Denote the diffusion coefficient in velocity space by the wave by $D_{\rm rf}$; then the Fokker-Planck equation is given by (ref.[41]) (refer to sec.4.3)

$$\frac{\partial f}{\partial t} + \boldsymbol{v} \cdot \nabla_{\rm r} f + \left(\frac{\boldsymbol{F}}{m}\right) \cdot \nabla_{\rm v} f = \frac{\partial}{\partial v_z}\left(D_{\rm rf}\frac{\partial f}{\partial v_z}\right) + \left(\frac{\delta f}{\delta t}\right)_{\rm F.P.} \tag{16.39}$$

where $(\delta f/\delta t)_{\rm F.P.}$ is Fokker-Planck collision term

$$\left(\frac{\delta f}{\delta t}\right)_{\rm F.P.} = -\sum_{\rm i,e}\left(\frac{1}{v^2}\frac{\partial}{\partial v}(v^2 J_{\rm v}) + \frac{1}{v\sin\theta}\frac{\partial}{\partial\theta}(\sin\theta J_\theta)\right), \tag{16.40}$$

$$J_{\rm v} = -D_\parallel \frac{\partial f}{\partial v} + Af, \quad J_\theta = -D_\perp \frac{1}{v}\frac{\partial f}{\partial \theta}. \tag{16.41}$$

When the velocity v of a test particle is larger than the thermal velocity $v_{\rm T}^*$ of field particles ($v > v_{\rm T}^*$), the diffusion tensor in velocity space $D_\parallel, D_\perp$ and the coefficient of dynamic friction A are reduced to

$$D_\parallel = \frac{v_{\rm T}^{*2}\nu_0}{2}\left(\frac{v_{\rm T}^*}{v}\right)^3, \quad D_\perp = \frac{v_{\rm T}^{*2}\nu_0}{2}\frac{v_{\rm T}^*}{2v},$$

$$A = -D_\parallel \frac{m}{m^*}\frac{v}{v_{\rm T}^{*2}}$$

where $v_{\rm T}^*$ and ν_0 are

$$v_{\rm T}^{*2} = \frac{T^*}{m^*}, \qquad \nu_0 = \left(\frac{qq^*}{\epsilon_0}\right)^2 \frac{n^*\ln\Lambda}{2\pi v_{\rm T}^{*3} m^2}. = \Pi^{*4}\frac{\ln\Lambda}{2\pi v_{\rm T}^{*3} n^*}$$

where $\Pi^{*2} \equiv qq^*n^*/(\epsilon_0 m)$. (v, θ, ψ) are spherical coordinates in velocity space. $v_{\rm T}^*,\ q^*,\ n^*$ are the thermal velocity, charge, and density of field particles, respectively, and $v,\ q,\ n$ are quantities of test particles. Let us consider the electron distribution function in a homogeneous case in space without

external force ($\boldsymbol{F} = 0$). Collision terms of electron-electron and electron-ion (charge number = Z) are taken into account. When dimensionless quantities $\tau = \nu_{0e}t$, $u = v/v^*_{Te}$, $w = v_z/v^*_{Te}$, $D(w) = D_{rf}/v^{*2}_{Te}\nu_{0e}$ are introduced, the Fokker-Planck equation reduces to

$$\frac{\partial f}{\partial \tau} = \frac{\partial}{\partial w}\left(D(w)\frac{\partial f}{\partial w}\right) + \frac{1}{2u^2}\frac{\partial}{\partial u}\left(\frac{1}{u}\frac{\partial f}{\partial u} + f\right) + \frac{1+Z}{4u^3}\frac{1}{\sin\theta}\frac{\partial}{\partial \theta}\left(\sin\theta\frac{\partial f}{\partial \theta}\right).$$

When Cartesian coordinates in velocity space $(v_x,\ v_y,\ v_z) = (v_1,\ v_2,\ \ v_3)$ are used in stead of spherical coordinates in velocity space, the Fokker-Planck collision term in Cartesian coordinates is given as follows ($v > v^*_T$ is assumed):

$$A_i = -D_0 v^*_T \frac{m}{m^*}\frac{v_i}{v^3} \tag{16.42}$$

$$D_{ij} = \frac{D_0}{2}\frac{v^*_T}{v^3}\left((v^2\delta_{ij} - v_i v_j) + \frac{v^{*2}_T}{v^2}(3v_i v_j - v^2\delta_{ij})\right) \tag{16.43}$$

$$J_i = A_i f - \sum_j D_{ij}\frac{\partial f}{\partial v_j} \tag{16.44}$$

$$D_0 \equiv \frac{(qq^*)^2\, n^* \ln\Lambda}{4\pi\epsilon_0^2 m^2 v^*_T} \equiv \frac{v^{*2}_T \nu_0}{2} \tag{16.45}$$

$$\left(\frac{\delta f}{\delta t}\right)_{F.P.} = -\nabla_v \cdot \boldsymbol{J}.$$

A_i is the *coefficient of dynamic friction* and D_{ij} is the component of *diffusion tensor*. Let us assume that the distribution function of the perpendicular velocities $v_x,\ v_y$ to the line of magnetic force is Maxwellian. Then the one-dimensional Fokker-Planck equation on the distribution function $F(w) = \int f\, dv_x\, dv_y$ of parallel velocity $w = v_z/v^*_{Te}$ can be deduced by $(v_x,\ v_y)$ integration:

$$\iint \left(\frac{\delta f}{\delta t}\right)_{F.P.} dv_x dv_y = \iint (-\nabla_v \cdot \boldsymbol{J})\, dv_x dv_y$$

$$= \iint \frac{\partial}{\partial v_z}\left(-A_z f + \sum_j D_{zj}\frac{\partial f}{\partial v_j}\right) dv_x dv_y.$$

When $|v_z| \gg |v_x|,\ |v_y|$, the approximation $v \approx |v_z|$ can be used. The resultant one-dimensional Fokker-Planck equation on $F(w)$ is

$$\frac{\partial F}{\partial \tau} = \frac{\partial}{\partial w}\left(D(w)\frac{\partial F}{\partial w}\right) + \left(1 + \frac{Z}{2}\right)\frac{\partial}{\partial w}\left(\frac{1}{w^3}\frac{\partial}{\partial w} + \frac{1}{w^2}\right)F(w)$$

and the steady-state solution is

$$F(w) = C\ \exp\int^w \frac{-w dw}{1 + w^3 D(w)/(1 + Z/2)},$$

and $F(w)$ is shown in fig.16.21 schematically (when $D(w) = 0$, this solution is Maxwellian). $F(w)$ is asymmetric with respect to $w = 0$, so that the current is induced. The induced current density J is

$$J = env^*_{Te} j$$

where $j = \int wF(w)dw$, and

$$j \approx \frac{w_1 + w_2}{2} F(w_1)(w_2 - w_1). \tag{16.46}$$

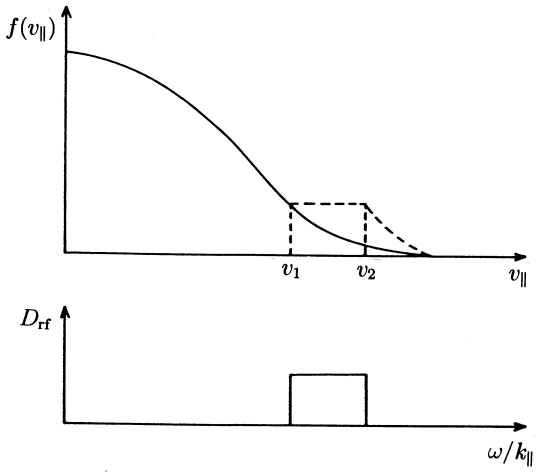

Fig.16.21 Distribution function $f(v_\parallel)$ of electrons is flatten in the region from $v_1 = c/N_1$ to $v_2 = c/N_2$ due to the interaction with the lower hybrid wave whose spectra of parallel index $N_\parallel$ ranges from N_1 to N_2.

On the other hand, this current tends to dissipate by Coulomb collision. Dissipated energy must be supplied by the input energy from the wave in order to sustain the current. Necessary input power $P_{\rm d}$ is

$$P_{\rm d} = -\int \frac{nmv^2}{2}\left(\frac{\delta f}{\delta t}\right)_{\rm F.P.} {\rm d}\boldsymbol{v} = \int \frac{nmv^2}{2}\frac{\partial}{\partial v_z}\left(D_{\rm rf}\frac{\partial f}{\partial v_z}\right){\rm d}\boldsymbol{v}$$

$$= nmv_{\rm Te}^{*2}\nu_0 \int \frac{w^2}{2}\frac{\partial}{\partial w}\left(D(w)\frac{\partial F}{\partial w}\right) {\rm d}w = nmv_{\rm Te}^{*2}\nu_0 p_{\rm d}$$

where $p_{\rm d}$ is given by use of the steady-state solution of $F(w)$, under the assumption of $w^3 D(w) \gg 1$, as follows:

$$p_{\rm d} = \left(1+\frac{Z}{2}\right)F(w_1)\,\ln\left(\frac{w_2}{w_1}\right) \approx \left(1+\frac{Z}{2}\right)F(w_1)\frac{w_2-w_1}{w_1}.$$

and

$$\frac{j}{p_{\rm d}} = \frac{1.5}{1+0.5Z_{\rm i}}\frac{2}{3}w^2. \tag{16.47}$$

More accurately, this ratio is (ref.[40])

$$\frac{j}{p_{\rm d}} = \frac{1.12}{1+0.12Z_{\rm i}}1.7w^2.$$

The ratio of the current density J and the necessary input power $P_{\rm d}$ per unit volume to sustain the current is given by

$$\frac{J}{P_{\rm d}} = \frac{env_{\rm Te}^* j}{nT_{\rm e}\nu_0 p_{\rm d}} = 0.16\frac{\kappa T_{\rm keV}}{n_{19}}\langle w^2\rangle\frac{1.12}{1+0.12Z_{\rm i}}\left(\frac{\rm A/m^2}{\rm W/m^3}\right) \tag{16.48}$$

where $\kappa T_{\rm keV}$ is the electron temperature in 1 keV units and n_{19} is the electron density in $10^{19}{\rm m}^{-3}$ units.
The ratio of total driven current $I_{\rm CD}$ to LHCD power $W_{\rm LH}$ is

$$\frac{I_{\rm CD}}{W_{\rm LH}} = \frac{1}{2\pi R}\frac{\int J 2\pi r{\rm d}r}{\int P_{\rm d}2\pi r{\rm d}r}$$

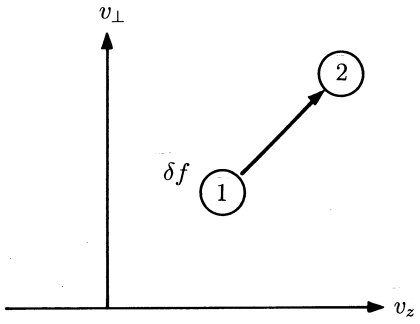

Fig.16.22 The displacement in velocity space of small number, δf , of electrons from coordinates to be subscripted 1 to those to be subscripted 2.

and the current drive efficiency of LHCD $\eta^{\mathrm{T}}_{\mathrm{LH}}$ is

$$\eta^{\mathrm{T}}_{\mathrm{LH}} \equiv \frac{Rn_{19}I_{\mathrm{CD}}}{W_{\mathrm{LH}}} = \frac{\int \eta_{\mathrm{LH}}(r)P_{\mathrm{d}}(r)2\pi r\mathrm{d}r}{\int P_{\mathrm{d}}(r)2\pi r\mathrm{d}r}\left(10^{19}\frac{\mathrm{A}}{Wm^2}\right)$$

where $\eta_{\mathrm{LH}}(r)$ is local current drive efficiency given by

$$\eta_{\mathrm{LH}}(r) = \frac{Rn_{19}J(r)}{2\pi RP_{\mathrm{d}}(r)} = 0.026(\kappa T_{\mathrm{e}})_{\mathrm{keV}}\langle w^2\rangle\frac{1.12}{1+0.12Z_{\mathrm{i}}}\left(10^{19}\frac{\mathrm{A}}{Wm^2}\right) \tag{16.49}$$

(R is the major radius in meter). The square average $\langle w^2\rangle$ of the ratio of the phase velocity (in the direction of magnetic field) of traveling waves to the electron thermal velocity is of the order of $20 \sim 50$. In the experiment (1994) of JT60U, a plasma current of $I_{\mathrm{p}} = 3\,\mathrm{MA}$ was driven by a lower hybrid wave with $W_{\mathrm{LH}} = 4.8\,\mathrm{MW}$ when $n = 1.2 \times 10^{19}\,\mathrm{m}^{-3}$, $\langle \kappa T_{\mathrm{e}}\rangle \sim 2\,\mathrm{keV}$, R=3.5 m and B_{t}=4 T ($\eta_{\mathrm{LH}}\sim$ 2.6). These results are consistent with the theoretical results.

The necessary power of current drive is proportional to the density, and the current cannot be driven beyond a threshold density in the case of lower hybrid current drive because of accessibility condition (refer sec.12.5). Other possible methods, such as drive in cyclotron range of frequencies (refer sec.16.8b), fast wave and by neutral beam injection (refer sec.16.8c) are also being studied.

A ramp-up experiment of the plasma current from zero was carried out first by WT-2 and PLT and others by the application of a lower hybrid wave to the target plasma produced by electron cyclotron heating and other types of heating. When the plasma current is ramped up in the low-density plasma and the density is increased after the plasma current reaches a specified value, all the available magnetic flux of the current transformer can be used only for sustaining the plasma current, so that the discharge duration can be increased several times.

16.8b Electron Cyclotron Current Drive

Electron Cyclotron Current Drive (ECCD) relies on the generation of an asymmetric resistivity due to the selective heating of electrons moving in a particular toroidal direction. N. J. Fisch and A. H. Boozer (ref.[41]) proposed that the collisionality of plasma is somehow altered so that, for example, electrons moving the left collide less frequently with ions than do electrons moving to the right. There would result a net electric current with electrons moving, on average, to the left and ions moving to the right.

Consider the displacement in velocity space of small number, δf, of electrons from coordinates to be subscripted 1 to those to be subscripted 2 as is shown in fig.16.22. The energy expended to produce this displacement is given by

$$\Delta E = (E_2 - E_1)\delta f$$

where E_i is the kinetic energy associated with velocity-space location i. Electrons at different coordinates will lose their momentum parallel to the magnetic field, which is in the z direction, at a rate ν_1, but now lose it at a rate ν_2. The z-directed current density is then given by

$$j(t) = -e\delta f(v_{z2}\exp(-\nu_2 t) - v_{z1}\exp(-\nu_1 t)). \tag{16.50a}$$

Consider the time-smoothed current J over a time interval δt which is large compared with both $1/\nu_1$ and $1/\nu_2$ so that

$$J = \frac{1}{\Delta t}\int_0^{\Delta t} j(t)\mathrm{d}t = -\frac{e\delta f}{\Delta t}\left(\frac{v_{z2}}{\nu_2} - \frac{v_{z1}}{\nu_1}\right).$$

Therefore the necessary input power density P_d to induce the current density is

$$P_\mathrm{d} = \frac{\Delta E}{\Delta t} = \frac{E_2 - E_1}{\Delta t}\delta f.$$

The ratio of J/P_d becomes

$$\frac{J}{P_\mathrm{d}} = -e\frac{v_{z2}/\nu_2 - v_{z1}/\nu_1}{E_2 - E_1} \Rightarrow -e\frac{\boldsymbol{s}\cdot\nabla(v_z/\nu)}{\boldsymbol{s}\cdot\nabla E} \tag{16.51}$$

where $\boldsymbol{s}$ is the unit vector in the direction of the displacement in velocity space. Let us estimate ν of (16.51). The deceleration rate of momentum of a test electron by collision with electrons and ions is expressed by (refer (2.14),(2.20))

$$\frac{\mathrm{d}p}{\mathrm{d}t} = -\frac{p}{\tau_{\mathrm{ee}\|}} - \frac{p}{\tau_{\mathrm{ei}\|}} = -\left(1 + \frac{Z_\mathrm{i}}{2}\right)\frac{\nu_0}{u^3}p$$

where

$$\nu_0 = \left(\frac{e^2 n_\mathrm{e}}{\epsilon_0 m_\mathrm{e}}\right)^2 \frac{\ln\Lambda}{2\pi n_\mathrm{e} v_\mathrm{Te}^3}, \qquad u \equiv \frac{v}{v_\mathrm{Te}}.$$

$v_\mathrm{Te} = (T_\mathrm{e}/m_\mathrm{e})^{1/2}$ is electron thermal velocity. Therefore we have

$$\frac{\mathrm{d}p}{\mathrm{d}t} = -\nu_\mathrm{M} p, \qquad \nu_\mathrm{M} \equiv (2 + Z_\mathrm{i})\frac{\nu_0}{2u^3}.$$

In order to estimate $\mathrm{d}u/\mathrm{d}t$, we must use the energy relaxation time $\tau_\mathrm{ee}^\epsilon$ (refer (2.27))

$$\frac{\mathrm{d}E}{\mathrm{d}t} = -\frac{E}{\tau_\mathrm{ee}^\epsilon}, \qquad E = \frac{m_\mathrm{e}}{2}u^2 v_\mathrm{Te}^2$$

that is

$$\frac{\mathrm{d}u}{\mathrm{d}t} = -\frac{u}{2\tau_\mathrm{ee}^\epsilon} = -\frac{\nu_0}{2u^3}u.$$

Each term in (16.50a) of $j(t)$ must be modified as follow:

$$j(t) = j_0\exp(-\int \nu_\mathrm{M}\mathrm{d}t) = j_0\left(\frac{u(t)}{u_0}\right)^{2+Z_\mathrm{i}} \tag{16.50b}$$

because of

$$-\int \nu_\mathrm{M}\mathrm{d}t = -\int \nu_\mathrm{M}\frac{\mathrm{d}t}{\mathrm{d}u}\mathrm{d}u = (2 + Z_\mathrm{i})\int\frac{\mathrm{d}u}{u} = (2 + Z_\mathrm{i})\ln\frac{u(t)}{u_0}.$$

Then the integral of $j(t)$ of (16.50b) reduces to

$$\int_0^\infty j(t)\mathrm{d}t = j_0 \int_{u_0}^0 \left(\frac{u(t)}{u_0}\right)^{2+Z_\mathrm{i}} \frac{\mathrm{d}t}{\mathrm{d}u}\mathrm{d}u = \frac{j_0}{\nu_0}\frac{2u_0^3}{5+Z_\mathrm{i}}.$$

Accordingly ν in (16.51) is

$$\nu = \nu_0 \frac{5+Z_\mathrm{i}}{2u^3} \tag{16.52}$$

and

$$\frac{J}{P_\mathrm{d}} = \frac{en_\mathrm{e}v_\mathrm{Te}}{n_\mathrm{e}T_\mathrm{e}\nu_0}\frac{j}{p_\mathrm{d}}, \qquad \frac{j}{p_\mathrm{d}} \equiv \frac{4}{5+Z_\mathrm{i}}\frac{\boldsymbol{s}\cdot\nabla(u^3w)}{\boldsymbol{s}\cdot\nabla u^2}$$

where $w \equiv v_z/v_\mathrm{Te}$. In the case of ECCD we have $j/p_\mathrm{d} \approx 6wu/(5+Z_\mathrm{i})$ and

$$\frac{J}{P_\mathrm{d}} = \frac{en_\mathrm{e}v_\mathrm{Te}}{n_\mathrm{e}T_\mathrm{e}\nu_0}\frac{\langle 6wu\rangle}{5+Z_\mathrm{i}} = 0.096\frac{(\kappa T_\mathrm{e})_\mathrm{keV}}{n_{19}}\frac{\langle 6wu\rangle}{5+Z_\mathrm{i}} \tag{16.53}$$

The ratio of driven current I_CD to ECCD power W_EC is

$$\frac{I_\mathrm{CD}}{W_\mathrm{EC}} = \frac{1}{2\pi R}\frac{\int J2\pi r\mathrm{d}r}{\int P_\mathrm{d}2\pi r\mathrm{d}r}$$

and the current drive efficiency $\eta_\mathrm{EC}^\mathrm{T}$ of ECCD is

$$\eta_\mathrm{EC}^\mathrm{T} \equiv \frac{Rn_{19}I_\mathrm{CD}}{W_\mathrm{CD}} = \frac{\int \eta_\mathrm{EC}(r)P_\mathrm{d}(r)2\pi r\mathrm{d}r}{\int P_\mathrm{d}2\pi r\mathrm{d}r}$$

where $\eta_\mathrm{EC}(r)$ is local current drive efficiency given by

$$\eta_\mathrm{EC}(r) = \frac{Rn_{19}J(r)}{2\pi RP_\mathrm{d}} = 0.015(\kappa T_\mathrm{e})_\mathrm{keV}\frac{\langle 6wu\rangle}{5+Z_\mathrm{i}}\left(10^{19}\frac{\mathrm{A}}{\mathrm{Wm}^2}\right). \tag{16.54}$$

16.8c Neutral Beam Current Drive

When a fast neutral beam is injected into a plasma, it changes to a fast ion beam by charge exchange or ionization processes. When the fast ions have higher energy than $E_\mathrm{cr} = m_\mathrm{b}v_\mathrm{cr}^2/2$ given by (2.33), they are decelerated mainly by electrons in the plasma and the fast ions with $E < E_\mathrm{cr}$ are decelerated mainly by ions in the plasma. The distribution function of the ion beam can be obtained by solving the Fokker-Planck equations. The Fokker-Planck collision term (16.40) of the fast ions with $E \gg E_\mathrm{cr}$ is dominated by the dynamic friction term in (16.41) due to electrons. The dynamic friction term of electrons on the fast ion in the case of $v < v_\mathrm{T}^*$ is given by

$$A = -\frac{v}{2\tau_\mathrm{be}^\epsilon}.$$

Then the Fokker-Planck equation is reduced to

$$\frac{\partial f_\mathrm{b}}{\partial t} + \frac{\partial}{\partial v}\left(\frac{-vf_\mathrm{b}}{2\tau_\mathrm{be}^\epsilon}\right) = \phi\delta(v-v_\mathrm{b}) \tag{16.55}$$

where v_b is the initial injection velocity and $\tau_\mathrm{be}^\epsilon$ is the energy relaxation time of beam ions and electrons as described by (2.34). The right-hand side is the source term of beam ions. The steady-state solution of the Fokker-Planck equation is

$$f_\mathrm{b} \propto 1/v.$$

However, the dynamic friction term due to ions or the diffusion term dominates the collision term in the region of $v < v_{\rm cr}$. Therefore the approximate distribution function of the ion beam is given by $f_{\rm b} \propto v^2/(v^3 + v_{\rm cr}^3)$, that is,

$$f_{\rm b}(v) = \frac{n_{\rm b}}{\ln(1 + (v_{\rm b}/v_{\rm cr})^3)^{1/3}} \frac{v^2}{v^3 + v_{\rm cr}^3} \qquad (v \le v_{\rm b}) \tag{16.56}$$

$$f_{\rm b}(v) = 0. \qquad (v > v_{\rm b})$$

The necessary ion injection rate ϕ per unit time per unit volume to keep the steady-state condition of the beam is derived by substitution of the solved $f_{\rm b}(v)$ into the Fokker-Planck equation

$$\phi = \frac{n_{\rm b}}{2\tau_{\rm be}^{\epsilon}} \frac{(1 + (v_{\rm cr}/v_{\rm b})^3)^{-1}}{(\ln(1 + (v_{\rm b}/v_{\rm cr})^3))^{1/3}}$$

and necessary power is

$$P_{\rm b} = \frac{m_{\rm b} v_{\rm b}^2}{2}\phi \approx \frac{m_{\rm b} v_{\rm b}^2 n_{\rm b}}{4\ln(v_{\rm b}/v_{\rm cr})\tau_{\rm be}^{\epsilon}}. \tag{16.57}$$

The average velocity of the decelerating ion beam is

$$\bar{v}_{\rm b} = v_{\rm b}(ln(v_{\rm b}/v_{\rm cr}))^{-1}. \tag{16.58}$$

Then the current density J driven by the fast ion's beam consists of terms due to fast ions and bulk ions and electrons of the plasma:

$$J = Z_{\rm i} e n_{\rm i} \bar{v}_{\rm i} + Z_{\rm b} e n_{\rm b} \bar{v}_{\rm b} - e n_{\rm e} \bar{v}_{\rm e}$$

$$n_{\rm e} = Z_{\rm i} n_{\rm i} + Z_{\rm b} n_{\rm b},$$

where $\bar{v}_{\rm i}$ and $\bar{v}_{\rm e}$ are the average velocities of ions with density $n_{\rm i}$ and electrons with density $n_{\rm e}$, respectively. The electrons of the plasma receive momentum by collision with fast ions and lose it by collision with plasma ions, that is

$$m_{\rm e} n_{\rm e} \frac{{\rm d}\bar{v}_{\rm e}}{{\rm d}t} = m_{\rm e} n_{\rm e}(\bar{v}_{\rm b} - \bar{v}_{\rm e})\nu_{\rm eb\|} + m_{\rm e} n_{\rm e}(\bar{v}_{\rm i} - \bar{v}_{\rm e})\nu_{\rm ei\|} = 0$$

so that

$$(Z_{\rm i}^2 n_{\rm i} + Z_{\rm b}^2 n_{\rm b})\bar{v}_{\rm e} = Z_{\rm b}^2 n_{\rm b}\bar{v}_{\rm b} + Z_{\rm i}^2 n_{\rm i}\bar{v}_{\rm i}.$$

Since $n_{\rm b} \ll n_{\rm i}$,

$$n_{\rm e}\bar{v}_{\rm e} = \frac{Z_{\rm b}^2}{Z_{\rm i}} n_{\rm b}\bar{v}_{\rm b} + Z_{\rm i} n_{\rm i}\bar{v}_{\rm i}$$

so that (ref.[38])

$$J = \left(1 - \frac{Z_{\rm b}}{Z_{\rm i}}\right) Z_{\rm b} e n_{\rm b}\bar{v}_{\rm b}. \tag{16.59}$$

The driven current density consists of the fast ion beam term $Z_{\rm b} e n_{\rm b}\bar{v}_{\rm b}$ and the term of dragged electrons by the fast ion beam, $-Z_{\rm b}^2 e n_{\rm b}\bar{v}_{\rm b}/Z_{\rm i}$. Then the ratio of $J/P_{\rm d}$ becomes

$$\frac{J}{P_{\rm d}} = (1 - Z_{\rm b}/Z_{\rm i})\frac{Z_{\rm b} e n_{\rm b}\bar{v}_{\rm b}}{m_{\rm b} n_{\rm b} v_{\rm b}\bar{v}_{\rm b}/4\tau_{\rm be}^{\epsilon}} = \frac{2eZ_{\rm b}(2\tau_{\rm be}^{\epsilon})}{m_{\rm b} v_{\rm b}}\left(1 - \frac{Z_{\rm b}}{Z_{\rm i}}\right). \tag{16.60}$$

When the charge number of beam ions is equal to that of the plasma ions, that is, when $Z_\mathrm{b} = Z_\mathrm{i}$, the current density becomes zero for linear (cylindrical) plasmas. For toroidal plasmas, the motion of circulating electrons is disturbed by collision with the trapped electrons (banana electrons), and the term of the dragged electrons is reduced. Thus J/P_d becomes (ref.[42])

$$\frac{J}{P_\mathrm{d}} = \frac{2eZ_\mathrm{b}(2\tau_\mathrm{be}^\epsilon)}{m_\mathrm{b}v_\mathrm{b}}\left(1 - \frac{Z_\mathrm{b}}{Z_\mathrm{i}}(1 - G(Z_\mathrm{eff}, \epsilon))\right) \tag{16.61}$$

$$G(Z_\mathrm{eff}, \epsilon) = \left(1.55 + \frac{0.85}{Z_\mathrm{eff}}\right)\epsilon^{1/2} - \left(0.2 + \frac{1.55}{Z_\mathrm{eff}}\right)\epsilon$$

where ϵ is inverse aspect ratio. When the effect of pitch angle of ionized beam is taken into account, the factor $\xi \equiv v_\parallel/v = R_\mathrm{tang}/R_\mathrm{ion}$ must be multiplied to (16.61), where R_tang is the minimum value of R along the neutral beam path and R_ion is R of ionization position.

The driving efficiency calculated by the bounce average Fokker Planck equation becomes

$$\frac{J}{P_\mathrm{d}} = \frac{2eZ_\mathrm{b}(2\tau_\mathrm{be}^\epsilon)}{m_\mathrm{b}v_\mathrm{b}}\left(1 - \frac{Z_\mathrm{b}}{Z_\mathrm{i}}(1 - G(Z_\mathrm{eff}, \epsilon))\right)\xi_0 F_\mathrm{nc} x_\mathrm{b} J_0(x_\mathrm{b}, y)$$

and

$$\frac{J}{P_\mathrm{d}} = \frac{2eZ_\mathrm{b}(2\tau_\mathrm{be}^\epsilon)}{m_\mathrm{b}v_\mathrm{cr}}\left(1 - \frac{Z_\mathrm{b}}{Z_\mathrm{i}}(1 - G(Z_\mathrm{eff}, \epsilon))\right)\xi_0 F_\mathrm{nc} J_0(x_\mathrm{b}, y) \tag{16.62}$$

where

$$x_\mathrm{b} \equiv \frac{v_\mathrm{b}}{v_\mathrm{cr}}, \qquad y = 0.8\frac{Z_\mathrm{eff}}{A_\mathrm{b}}$$

$$J_0(x, y) = \frac{x^2}{x^3 + (1.39 + 0.61y^{0.7})x^2 + (4 + 3y)}$$

and $F_\mathrm{nc} = 1 - b\epsilon^\sigma$ is the correction factor (ref.[43]). Finally we have

$$\frac{J}{P_\mathrm{d}}\left(\frac{\mathrm{Am}}{W}\right) = \frac{15.8(\kappa T_\mathrm{e})_\mathrm{keV}\xi_0}{Z_\mathrm{b}n_\mathrm{e19}}\left(1 - \frac{Z_\mathrm{b}}{Z_\mathrm{i}}(1 - G)\right)(1 - b\epsilon^\sigma)J_0(x_\mathrm{b}, y) \tag{16.63}$$

The local current drive efficiency η_NB of NBCD is

$$\eta_\mathrm{NB} \equiv \frac{Rn_\mathrm{e19}J}{2\pi RP_\mathrm{d}}\left(10^{19}\frac{\mathrm{A}}{\mathrm{Wm}^2}\right)$$

$$= 2.52(\kappa T_\mathrm{e})_\mathrm{keV}\xi_0\left(1 - \frac{Z_\mathrm{b}}{Z_\mathrm{i}}(1 - G)\right)(1 - b\epsilon^\sigma)J_0(x_\mathrm{b}, y). \tag{16.64}$$

When $Z_\mathrm{b} = 1, Z_\mathrm{eff} = 1.5, A_\mathrm{b} = 2, x_\mathrm{b}^2 = 4$, then $((1 - b\epsilon^\sigma)J_0) \sim 0.2$. When $\langle\epsilon\rangle \sim 0.15$, then $\eta_\mathrm{NB} \sim 0.29(\kappa T_\mathrm{e})_\mathrm{keV}(10^{19})\mathrm{A/Wm}^2)$. The current drive by NBI is demonstrated by the experiments of DITE, TFTR JT60U and JET.

When the application of a current drive to the fusion grade plasma with $n_\mathrm{e} \sim 10^{20}\mathrm{m}^{-3}$ is considered, the necessary input power for any current drive of full plasma current occupies a considerable amount of the fusion output. Therefore substantial part of plasma current must be driven by bootstrap current as is described in the next section.

16.8d Bootstrap Current

It was predicted theoretically that radial diffusion induces a current in the toroidal direction and the current can be large in banana region (ref.[44],[45]). Later this current called '*bootstrap current*'

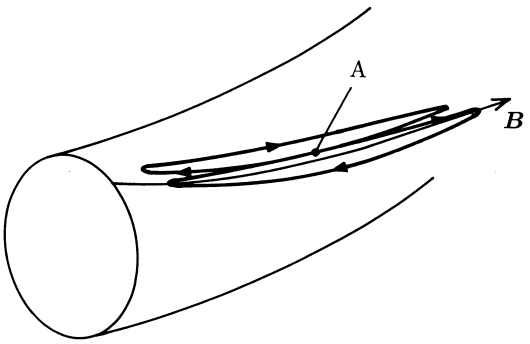

Fig.16.23 Banana orbits of trapped electrons those induce the bootstrap current

had been well confirmed experimentally. This is an important process which can provide the means to sustain the plasma current in tokamak in steady state.

As was described in sec.7.2, electrons in collisionless region $\nu_{\rm ei} < \nu_{\rm b}$ make complete circuit of the banana orbit. When density gradient exists, there is a difference in particles number on neighboring orbit passing through a point A, as is shown in fig.16.23. The difference is $({\rm d}n_{\rm t}/{\rm d}r)\Delta_{\rm b}$, $\Delta_{\rm b}$ being the width of the banana orbit. As the component of velocity parallel to magnetic field is $v_{\parallel} = \epsilon^{1/2} v_{\rm T}$, the current density due to the trapped electrons with the density $n_{\rm t}$ is

$$j_{\rm banana} = -(ev_{\parallel}) \left(\frac{{\rm d}n_{\rm t}}{{\rm d}r} \Delta_{\rm b} \right) = -\epsilon^{3/2} \frac{1}{B_{\rm p}} \frac{{\rm d}p}{{\rm d}r}.$$

The untrapped electrons start to drift in the same direction as the trapped electrons due to the collisions between them and the drift becomes steady state due to the collisions with ions. The drift velocity $V_{\rm untrap}$ of untrapped electrons in steady state is given by

$$m_{\rm e} V_{\rm untrap} \nu_{\rm ei} = \frac{\nu_{\rm ee}}{\epsilon} m_{\rm e} \left(\frac{j_{\rm banana}}{-en_{\rm e}} \right)$$

where $\nu_{\rm ee}/\epsilon$ is effective collision frequency between trapped and untrapped electrons. The current density due to the drift velocity $V_{\rm untrap}$ is

$$j_{\rm boot} \approx -\epsilon^{1/2} \frac{1}{B_{\rm p}} \frac{{\rm d}p}{{\rm d}r}. \tag{16.65}$$

This current is called '*bootstrap current*'. When the average poloidal beta is $\beta_{\rm p} = \langle p \rangle / (B_{\rm p}^2/2\mu_0)$ is used, the ratio of the total bootstrap current $I_{\rm b}$ to the plasma current $I_{\rm p}$ to form $B_{\rm p}$ is given by

$$\frac{I_{\rm b}}{I_{\rm p}} \sim c \left(\frac{a}{R} \right)^{1/2} \beta_{\rm p} \tag{16.66}$$

where $c \sim 0.3$ is constant. This value can be near 1 if $\beta_{\rm p}$ is high ($\beta_{\rm p} \sim R/a$) and the pressure profile is peaked. Experiments on bootstrap current were carried out in TFTR, JT60U and JET. 70 %$\sim$ 80 % of $I_{\rm p}$=1 MA was bootstrap driven in high $\beta_{\rm p}$ operation.

As the bootstrap current profile is hollow, it can produce negative magnetic shear q profile, which is stable against ballooning. MHD stability of hollow current profile is analyzed in details in (ref.[46]).

16.9 Neoclassical Tearing Mode

Much attention has been focused on tokamak operational pressure limit imposed by non-ideal

MHD instabilities, such as the effects of bootstrap current driven magnetic islands. At high $\beta_{\rm p}$ (poloidal beta) and low collisionality, the pressure gradient in the plasma gives rise to a bootstrap current (refer sec.16.8d). If an island develops, the pressure within the island tends to flatten out, thereby removing the drive for the bootstrap current. This gives rise to a helical 'hole' in the bootstrap current, which increases the size of the island (refer fig.16.24).

Tearing instability was treated in slab model in sec.9.1. The zero order magnetic field $\boldsymbol{B}_0$ depends on only x and is given by $\boldsymbol{B}_0 = B_{0y}(x)\boldsymbol{e}_y + B_{0z}\boldsymbol{e}_z$, $|B_{0y}(x)| \ll |B_{0z}|$, B_{0z}=const.. The basic equations are

$$\rho\left(\frac{\partial \boldsymbol{v}}{\partial t} + (\boldsymbol{v}\cdot\nabla)\boldsymbol{v}\right) = -\nabla p + \boldsymbol{j}\times\boldsymbol{B} \tag{16.67}$$

$$-\boldsymbol{E} = \boldsymbol{v}\times\boldsymbol{B} - \eta\boldsymbol{j} = \frac{\partial \boldsymbol{A}}{\partial t}, \qquad \boldsymbol{A} = (0,0,-\psi) \qquad B_x = -\frac{\partial\psi}{\partial y}, \quad B_y = \frac{\partial\psi}{\partial x}$$

$$-\frac{\partial\psi}{\partial t} = (v_x B_y - v_y B_x) - \eta j_z = (\boldsymbol{v}\cdot\nabla)\psi - \eta j_z \tag{16.68}$$

$$\nabla^2\psi = \mu_0 j_z \tag{16.69}$$

Since

$$\boldsymbol{v} = \frac{\boldsymbol{E}\times\boldsymbol{B}}{B^2} = \left(\frac{E_y}{B_{0z}}, -\frac{E_x}{B_{0z}}, 0\right) = \left(-\frac{1}{B_{0z}}\frac{\partial\phi}{\partial y}, \frac{1}{B_{0z}}\frac{\partial\phi}{\partial x}, 0\right),$$

it is possible to introduce a stream function φ such as

$$v_x = -\frac{\partial\varphi}{\partial y}, \qquad v_y = \frac{\partial\varphi}{\partial x}.$$

Furthermore z component of vorticity $w_z = (\nabla\times\boldsymbol{v})_z$ is introduced, then $w_z = \nabla^2\varphi$. Rotation of (16.67) yieds

$$\rho\frac{\partial w_z}{\partial t} + (\boldsymbol{v}\cdot\nabla)w_z = (\nabla\times(\boldsymbol{j}\times\boldsymbol{B}))_z = (\boldsymbol{B}\cdot\nabla)j_z - (\boldsymbol{j}\cdot\nabla)B_z = (\boldsymbol{B}\cdot\nabla)j_z \tag{16.70}$$

The relations $\nabla\cdot\boldsymbol{B} = 0$, $\nabla\cdot\boldsymbol{j} = 0$ were used here. The 0th order flux function ψ_0 and the first order perturbation $\tilde{\psi}$ are

$$\psi_0(x) = B'_{0y}\frac{x^2}{2}, \qquad \boldsymbol{B}_0 = (0, B'_{0y}x, B_{0z})$$

$$\tilde{\psi}(y,t) = \frac{B_{1x}(t)}{k}\cos ky, \qquad \boldsymbol{B}_1 = (B_{1x}(t))\sin ky, 0, 0), \qquad \tilde{\psi}_{\rm A}(t) \equiv \frac{B_{1x}(t)}{k}$$

$$\psi(x,y,t) = \psi_0(x) + \tilde{\psi}(y,t) = B'_{0y}\frac{x^2}{2} + \frac{B_{1x}(t)}{k}\cos ky = \frac{B'_{0y}}{2}x^2 + \tilde{\psi}_{\rm A}(t)\cos ky \tag{16.71}$$

$x = 0$ is the location of singular layer. The separatrix of islands is given by

$$B'_{0y}\frac{x^2}{2} + \frac{B_{1x}(t)}{k}\cos ky = \frac{B_{1x}(t)}{k}, \qquad x_{\rm s} = 2\left(\frac{B_{1x}}{kB'_{0y}}\right)^{1/2},$$

and the full width w of the island is

$$w = 4\left(\frac{B_{1x}}{kB'_{0y}}\right)^{1/2} = 4\left(\frac{\tilde{\psi}_{\rm A}(t)}{B'_{0y}}\right)^{1/2}. \tag{16.72}$$

The perturbation $B_{1x}(t)\sin ky$ growing with the growth rate γ induces a current $j_{1z} = E_{1z}/\eta = \gamma B_{1x}/\eta k$, which provides the x direction linear force $f_{1x} = -j_{1z}B'_{0y}x$ indicated on fig.16.24. These drive the flow pattern of narrow vortices. Moving away from the resistive singular layer, the induced electric field produces a flow $v_x = -E_z/B_y = -\gamma B_{1x}\cos ky/(kB'_{0y}x)$. For incompressible flow (in

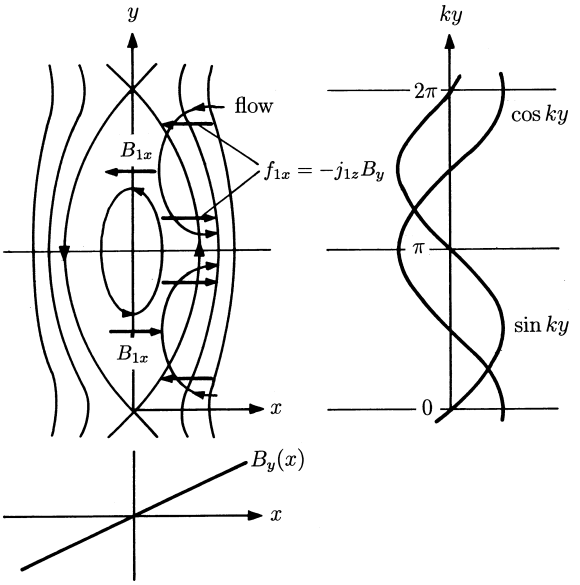

Fig.16.24 Tearing mode structure in the singular layer

strong equilibrium field B_{0z}), this requires a strongly sheared flow $v_y(x)$ over the layer $x \sim x_{\rm T}$, that is the narrow vortex pattern shown in fig.16.24 and we have

$$v_y x_{\rm T} \sim v_x/k, \qquad v_y \sim v_x/kx_{\rm T} \sim \gamma B_{1x}/(k^2 B'_{0y} x_{\rm T}^2).$$

That this shear flow be driven against inertia by the torque produced by the linear forces requires

$$x_{\rm T} j_{1z} B_{0y} = \gamma\rho v_y/k, \qquad B_{0y} = B'_{0y} x_{\rm T}, \quad \rightarrow \quad x_{\rm T}^4 = \frac{\gamma\rho}{j_{1z}kB'_{0y}} \frac{\gamma B_{1x}}{k^2 B'_{0y}} = \frac{\gamma\rho\eta}{(kB'_{0y})^2}.$$

since $j_{1z} = E_z/\eta = \gamma B_{1x}/\eta k$. Thus determined width of perturbation is

$$x_{\rm T} = \frac{(\gamma\rho\eta)^{1/4}}{(kB'_{0y})^{1/2}}. \tag{16.73}$$

Rutherford showed that the growth of the mode is drastically slowed and perturbation grows only linearly in time, when non-linear effects are taken into account (ref.[47]). The vortex flow will induce the second order y-independent eddy current $\delta j_{1z} = -v_y B_{1x}/\eta \sim \gamma B_{1x}^2/(\eta k^2 B'_{0y} x_{\rm T}^2)$. The y-direction third order nonlinear forces $\delta f_y \sim \delta j_z B_{1x}$ indicated on fig.16.25 provide a torque opposing vortex flow and decelerate v_y flow.

We restrict ourselves to the case where the inertia may be neglected in (16.70).

$$(\boldsymbol{B}\cdot\nabla) j_z = -\frac{\partial\psi}{\partial y}\frac{\partial j_z}{\partial x} + \frac{\partial\psi}{\partial x}\frac{\partial j_z}{\partial y} = 0, \qquad \rightarrow \qquad j_z = j_z(\psi).$$

Eq.(16.68) yields

$$\frac{\partial\psi_0}{\partial t} + \frac{\partial\tilde{\psi}}{\partial t} = -v_x B'_{0y} x + \eta j_{1z}, \quad \frac{\partial\psi_0}{\partial t} = \eta j_{0z}, \quad \rightarrow \quad \frac{\partial\tilde{\psi}}{\partial t} = -\frac{\partial\varphi}{\partial y} B'_{0y} x + \eta j_{1z} - \eta j_{0z} \tag{16.74}$$

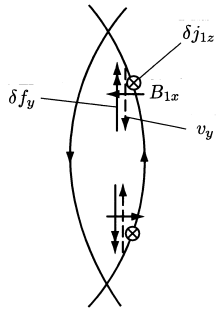

Fig.16.25 Nonlinear forces decelerating v_y flow in tearing mode.

We may eliminate φ from (16.74) by dividing by x and averaging over y at constant ψ. From (16.71), x is given by

$$x = \left(\frac{2}{B'_{0y}}(\psi - \tilde{\psi})\right)^{1/2} = \left(\frac{2}{B'_{0y}}\right)^{1/2} \tilde{\psi}_{\rm A}^{1/2}(W - \cos ky)^{1/2}, \qquad W \equiv \frac{\psi}{\tilde{\psi}_{\rm A}}$$

and

$$\left\langle \frac{1}{(\psi - \tilde{\psi})^{1/2}} \right\rangle (\eta j_{1z}(\psi) - \eta j_{0z}(\psi)) = \left\langle \frac{\partial \tilde{\psi}(y,t)/\partial t}{(\psi - \tilde{\psi}(y,t))^{1/2}} \right\rangle,$$

$$j_{1z}(\psi) = j_{0z}(\psi) + \frac{1}{\eta} \left\langle \frac{\partial \tilde{\psi}/\partial t}{(\psi - \tilde{\psi})^{1/2}} \right\rangle \left\langle (\psi - \tilde{\psi})^{-1/2} \right\rangle^{-1} \tag{16.75}$$

where

$$\langle f \rangle \equiv \frac{k}{2\pi} \int_0^{2\pi/k} f \mathrm{d}y.$$

For the outer solution we require the discontinuity in the logarithmic derivatives across singularity. We must match the logarithmic discontinuity from the solution within the singular layer to that of outer solution:

$$\Delta' \equiv \left(\frac{\partial \tilde{\psi}_{\rm A}}{\partial x}\bigg|_{+0} - \frac{\partial \tilde{\psi}_{\rm A}}{\partial x}\bigg|_{-0} \right) \frac{1}{\tilde{\psi}_{\rm A}} = \frac{\partial}{\partial x} \ln \tilde{\psi}_{\rm A} \bigg|_{-0}^{+0}.$$

We utilize $\nabla^2 \tilde{\psi} = \mu_0 j_{1z}$ and $\partial^2 \tilde{\psi}/\partial x^2 \approx \mu_0 j_{1z}$ and

$$\Delta' \tilde{\psi}_{\rm A} = 2\mu_0 \left\langle \cos ky \int_{-\infty}^{\infty} j_{1z} \mathrm{d}x \right\rangle, \qquad \mathrm{d}x = \left(\frac{1}{2B'_{0y}}\right)^{1/2} \frac{\mathrm{d}\psi}{(\psi - \tilde{\psi})^{1/2}}. \tag{16.76}$$

Insertion of (16.75) into (16.76) yields

$$\Delta' \tilde{\psi}_{\rm A} = 2\frac{\mu_0}{\eta} \int_{-\infty}^{\infty} \left\langle \frac{\partial \tilde{\psi}/\partial t}{(\psi - \tilde{\psi})^{1/2}} \right\rangle \left\langle (\psi - \tilde{\psi})^{-1/2} \right\rangle^{-1} \left\langle \left(\frac{1}{2B'_{0y}}\right)^{1/2} \frac{\cos ky}{(\psi - \tilde{\psi})^{1/2}} \right\rangle \mathrm{d}\psi$$

$$= \frac{4\mu_0}{\eta (2B'_{0y})^{1/2}} \int_{\psi_{\min}}^{\infty} \mathrm{d}\psi \frac{\partial \tilde{\psi}_{\rm A}}{\partial t} \left\langle \frac{\cos ky}{(\psi - \tilde{\psi})^{1/2}} \right\rangle \left\langle (\psi - \tilde{\psi})^{-1/2} \right\rangle^{-1} \left\langle \frac{\cos ky}{(\psi - \tilde{\psi})^{1/2}} \right\rangle.$$

Since

$$\int \mathrm{d}\psi \left\langle \frac{\cos ky}{(\psi - \tilde{\psi})^{1/2}} \right\rangle^2 \frac{1}{\left\langle (\psi - \tilde{\psi})^{-1/2} \right\rangle} = \int \left\langle \frac{\cos ky}{(W - \cos ky)^{1/2}} \right\rangle^2 \frac{\mathrm{d}W \tilde{\psi}_{\rm A}^{1/2}}{\langle (W - \cos ky)^{-1/2} \rangle} \equiv A \tilde{\psi}_{\rm A}^{1/2},$$

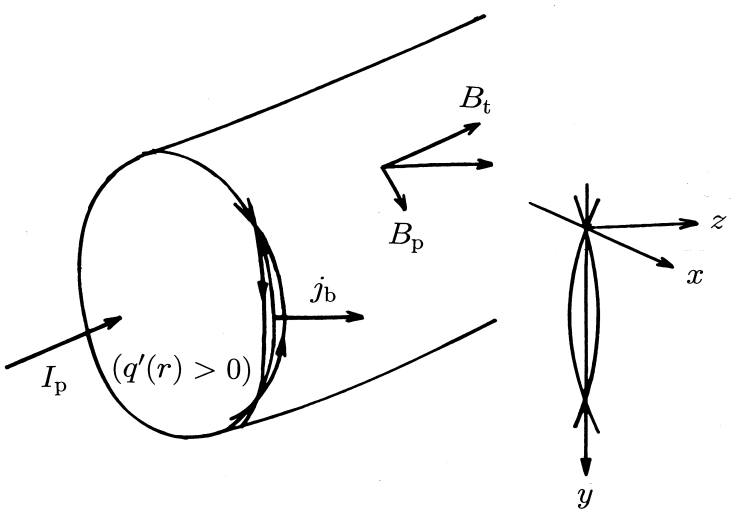

Fig.16.26 The coordinates in slab model and the coordinates in toroidal plasma. The coordinates (x, y, z) correspond radial coordinate $(r - r_s)$, poloidal coordinate $(\sim r\theta)$ and the direction of the magnetic field at the rational surface respectively. The arrows in the island indicate the direction of magnetic field $B_p - (nr/mR)B_t$ (refer to (16.79)).

we obtain

$$\Delta'\tilde{\psi}_A = \frac{4\mu_0 A}{\eta(2B'_{0y})^{1/2}}\frac{\partial\tilde{\psi}_A}{\partial t}\tilde{\psi}_A^{1/2}$$

and

$$\frac{\partial}{\partial t}\tilde{\psi}_A^{1/2} = \frac{\eta(2B'_{0y})^{1/2}}{8\mu_0 A}\Delta'.$$

Taking note (16.72), the time variation of the island width is reduced to (ref.[47])

$$\frac{dw}{dt} = \frac{1}{2^{1/2}A}\frac{\eta}{\mu_0}\Delta' \approx \frac{\eta}{\mu_0}\Delta', \qquad \tau_R\frac{d}{dt}\frac{w}{r_s} = \Delta' r_s \qquad \tau_R \equiv \frac{\mu_0 r_s^2}{\eta}. \tag{16.77}$$

Let us consider a toroidal plasma as is shown in fig.16.26. The magnetic field

$$B_p - \frac{nr}{nR}B_t = \left(\frac{1}{q(r)} - \frac{1}{q_s}\right)\frac{r}{R}B_t, \qquad (q_s = \frac{m}{n})$$

corresponds B_{0y} in slab model near singular radius. The coordinates (x, y, z) in slab model correspond radial coordinate $(r - r_s)$, poloidal coordinate $(\sim r\theta)$ and the direction of the magnetic field at the rational surface respectively. The flux function is

$$\psi(x, y) = \int_0^{r-r_s}\left(\frac{1}{q(r)} - \frac{1}{q_s}\right)\frac{r}{R}B_t dx + \frac{B_{1x}}{k}\cos ky \tag{16.78}$$

and the magnetic field is given by

$$B_{1x} = -\frac{\partial\psi}{\partial y} = B_{1x}\sin ky, \qquad B_{0y} = \frac{\partial\psi}{\partial x} = \left(\frac{1}{q(r)} - \frac{1}{q_s}\right)\frac{r}{R}B_t = -\frac{q'}{q}B_p x = B'_{0y}x \tag{16.79}$$

Eq.(16.78) is reduced to

$$\psi(x, y) = B'_{0y}\frac{x^2}{2} + \frac{B_{1x}}{k}\cos ky$$

The change of bootstrap current $\delta j_{1z}^{\rm b}$ induces the change in flux function $\delta\psi_{\rm b}$ and elecric field E_z.

$$E_z = \frac{\partial \psi_{\rm b}}{\partial t} = \eta \delta j_{1z}^{\rm b}.$$

Discontinuity of logarithmic derivative due to $\delta j_{1z}^{\rm b}$ is

$$\Delta'_{\rm b} = \frac{1}{\tilde{\psi}_{\rm A}} \left(\left. \frac{\partial \tilde{\psi}_{\rm A}^{\rm b}}{\partial r} \right|_{r_{\rm s}+} - \left. \frac{\partial \tilde{\psi}_{\rm A}^{\rm b}}{\partial r} \right|_{r_{\rm s}-} \right) = \frac{1}{\tilde{\psi}_{\rm A}} \int_{r_{\rm s}-}^{r_{\rm s}+} \mu_0 \delta j_{1z}^{\rm b} {\rm d}r$$

where

$$\tilde{\psi}_{\rm A} = \frac{B_{1x}}{k} = \frac{w^2 B'_{0y}}{16}$$

so that

$$\Delta'_{\rm b} = \frac{16}{w^2 B'_{0y}} \int_{r_{\rm s}-}^{r_{\rm s}+} \mu_0 \delta j_{1z}^{\rm b} {\rm d}r.$$

Because of flattening of pressure profile due to the formation of island, $\delta j_{1z}^{\rm b}$ is given by (refer (16.65))

$$\delta j_{1z}^{\rm b} = 0 - \left(-\frac{\epsilon_{\rm s}^{1/2}}{B_{\rm p}} \frac{{\rm d}p}{{\rm d}r} \right) = \frac{\epsilon_{\rm s}^{1/2}}{B_{\rm p}} \frac{{\rm d}p}{{\rm d}r} \tag{16.80}$$

This is called by helical hole of bootstrap current. Thus discontinuity of logarithmic derivative due to $\delta j_{1z}^{\rm b}$ is reduced to

$$\Delta'_{\rm b} r_{\rm s} = \frac{16\mu_0}{w^2 B'_{0y}} \left(\frac{\epsilon_{\rm s}^{1/2}}{B_{\rm p}} \frac{{\rm d}p}{{\rm d}r} \right)_{r_{\rm s}} w r_{\rm s} = \frac{8 r_{\rm s}}{w} \frac{p}{B_{\rm p}^2/2\mu_0} \epsilon_{\rm s}^{1/2} \frac{L_q}{L_p}, \qquad B'_{0y} = -\frac{q'}{q} B_{\rm p} \equiv -\frac{B_{\rm p}}{L_q}, \qquad \frac{{\rm d}p}{{\rm d}r} \equiv -\frac{p}{L_p}.$$

Then the time variation of island's width is given by

$$\tau_{\rm R} \frac{\rm d}{{\rm d}t} \frac{w}{r_{\rm s}} = \Delta' r_{\rm s} + a \epsilon_{\rm s}^{1/2} \beta_{\rm p} \frac{L_q}{L_p} \frac{r_{\rm s}}{w}, \qquad\qquad a \sim 8. \tag{16.81a}$$

The first term of right-hand side of (16.81) is Rutherford term and the second is the destabilizing term of bootstrap current. This is the equation of neoclassical tearing mode. When the transport across the island is taken into account, a reduction in the bootstrap current takes place. Then the term of bootstrap current is modified to

$$\tau_{\rm R} \frac{\rm d}{{\rm d}t} \frac{w}{r_{\rm s}} = \Delta' r_{\rm s} + a \epsilon_{\rm s}^{1/2} \beta_{\rm p} \frac{L_q}{L_p} \frac{r_{\rm s} w}{w^2 + w_{\rm c}^2}. \tag{16.81b}$$

where $w_{\rm c}$ is the effect of transport across the island parameterizing the magnitude of the contribution of the $\chi_\perp/\chi_\parallel$ model (ref.[48]) and being given by the relation

$$w_{\rm c} = 1.8 r_{\rm s} \left(\frac{8RL_q}{r_{\rm s}^2 {\rm n}} \right)^{1/2} \left(\frac{\chi_\perp}{\chi_\parallel} \right)^{1/4}.$$

Figure 16.27 shows the curve of (16.81b). When the effect of $w_{\rm c}$ is included, there is a threshold $w_{\rm th}$ for the onset of neoclassical tearing mode. When w becomes large, destabilizing term of bootstap current becomes weak and the island width is saturated. It is possible to control neoclassical tearing mode by local current drive in rational (singular) surface (ref.[49]).

16.10 Resistive Wall Mode

MHD kink instabilities in tokamak are of major importance because they have a beta limit. In

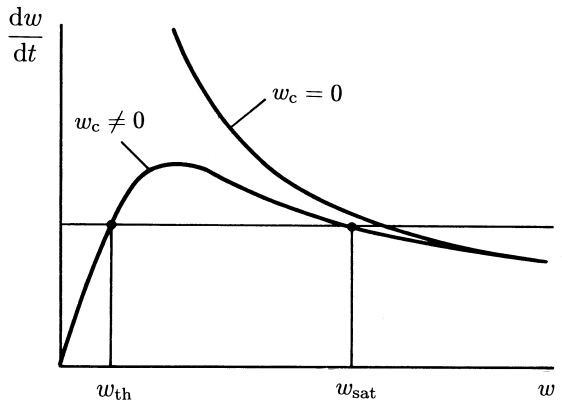

Fig.16.27 The curve of (16.81b). $w_{\rm th}$ is the threshold width of island for the onset of neoclassical tearing mode and $w_{\rm sat}$ is the saturated width.

the absence of a conducting wall, the results obtained in (ref.[15]) with a variety of current and pressure profile show that this beta limit is of form $\beta/(I_{\rm p}/aB) \equiv \beta_{\rm N} < 2.8$ (refer (16.9)).

However the external kink can be stabilized at higher value of $\beta_{\rm N}$ by including a closely fitting conducting wall. The situation is complicated by the existence of resistive wall in the case when an ideal MHD instability is stabilized by perfect conducting wall, but unstable if the wall is removed. In this situation, there is a resistive wall mode that grows on the resistive time of wall. Furthermore it is an interesting issue whether this resistive wall mode is stabilized by plasma rotation or not. In this section the analysis of resistive mode is described.

16.10a Growth Rate of Resistive Wall Mode

Basic equations of motion in slab model are already given by (9.9) and (9.13), that is,

$$B_{1x} = i(\boldsymbol{k}\cdot\boldsymbol{B})\xi_x$$

$$\mu_0\gamma^2\nabla\rho_{\rm m}\nabla\xi_x = i(\boldsymbol{k}\cdot\boldsymbol{B})\nabla B_{1x} - i(\boldsymbol{k}\cdot\boldsymbol{B})'' B_{1x}$$

For cylindrical coordinates, the same mathematical process as for the slab model leads to

$$(rB_{1r}) = iF(r\xi_r) \tag{16.82}$$

$$\frac{\mu_0\gamma^2}{F}\nabla\rho_{\rm m}\nabla(ir\xi_r) = -\nabla^2(rB_{1r}) + \frac{F''}{F}(rB_{1r}) \tag{16.83a}$$

where

$$F = (\boldsymbol{k}\cdot\boldsymbol{B}) = \left(\frac{-{\rm m}}{r}B_\theta + \frac{\rm n}{R}B_z\right) = \frac{B_z}{R}\left({\rm n} - \frac{\rm m}{q(r)}\right) = \frac{B_\theta}{r}({\rm n}q(r) - {\rm m}).$$

The flux function $\psi = A_z(r,\theta) = A_z(r)\exp(-{\rm m}\theta)$, z component of vector potential, is introduced and then

$$B_{1r} = \frac{1}{r}\frac{\partial A_z}{\partial\theta} = -i\frac{\rm m}{r}\psi, \qquad B_z = -\frac{\partial A_z}{\partial r} = -\frac{\partial\psi}{\partial r}.$$

(16.83) is reduced to

$$\frac{\mu_0\gamma^2}{F}\nabla\rho_{\rm m}\nabla_\perp\frac{\psi}{F} = -\nabla^2\psi - \frac{{\rm m}\mu_0}{F}\frac{j'}{r}\psi, \qquad F'' \approx -\frac{{\rm m}\mu_0 j'}{r} \tag{16.83b}$$

Firstly a step function model of cylindrical plasma presented by Finn (ref.[50]) is used for analysis. The mass density and plasma current profiles are flat within the plasma $r < a$ as is shown in fig.16.28, that is,

$$j(r) = j_0, \quad \rho(r) = \rho_0, \quad q(r) = q, \qquad \text{for } r < a,$$

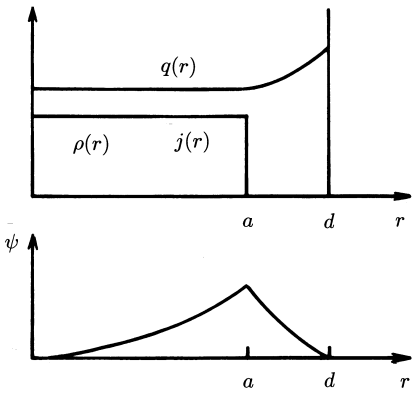

Fig.16.28 Upper figure: Profiles of mass density $\rho(r)$, current density $j(r)$ and q profile $q(r)$. The plasma radius is $r = a$ and the wall is located at $r = d$. Lower figure: Profile of flux function $\psi(r)$ in the case of conducting wall.

and $j(r) = 0, \quad \rho(r) = 0, \quad q(r) = q(r)$ for $r > a$. Then (16.83b) for $r < a$ yields

$$\left(1 + \frac{\mu_0 \rho_0 \gamma^2}{F^2}\right) \nabla^2 \psi = 0, \qquad \psi(r) = \psi_0 \left(\frac{r}{a}\right)^{\mathrm{m}}, \qquad \frac{\psi(a_-)'}{\psi(a)} = \frac{\mathrm{m}}{a} \tag{16.83c}$$

and (16.83b) for $r > a$ yields

$$\nabla^2 \psi = 0, \qquad \psi(r) = \frac{\psi(a)}{1-\alpha} \left(\left(\frac{r}{a}\right)^{-\mathrm{m}} - \alpha \left(\frac{r}{a}\right)^{\mathrm{m}} \right).$$

When a conducting wall is located at $r = d$, $\psi(d) = 0$ must be satisfied and $\alpha = (a/d)^{2\mathrm{m}}$. Then

$$\frac{\psi'(a_+)}{\psi(a)} = -\frac{\mathrm{m}}{a} \frac{1 + (a/d)^{2\mathrm{m}}}{1 - (a/d)^{2\mathrm{m}}}. \tag{16.83d}$$

At the plasma boundary, (16.83b) yields

$$\frac{\psi'(a_+)}{\psi(a)} - \left(1 + \frac{\mu_0 \rho_0 \gamma^2}{B_\theta^2 (\mathrm{n}q - \mathrm{m})^2 / a^2}\right) \frac{\psi'(a_-)}{\psi(a)} = \frac{\mathrm{m}\mu_0}{Fa} j_0 = \frac{\mathrm{m}}{a} \frac{2}{(\mathrm{n}q - \mathrm{m})}, \tag{16.84}$$

since $\mu_0 j_0 = 2B_\theta / a$ for flat current profile. The growth rate $\gamma_{\mathrm{c}}(d)$ of the MHD perturbation in the case of conducting wall at $r = d$ is reduced from (16.83c, 83d) and (16.84) as follow:

$$\gamma_{\mathrm{c}}(d)^2 \tau_{\mathrm{A}\theta}^2 = -2(\mathrm{n}q - \mathrm{m}) \left(1 + \frac{(\mathrm{n}q - \mathrm{m})}{1 - (a/d)^{2\mathrm{m}}}\right). \tag{16.85}$$

The stable region in d/a-q diagram is shown in fig.16.29.

When a thin resistive wall is located at $r = d$ instead of conducting wall, the external solution of ψ is modified and is given by (see fig.16.30)

$$\psi(r) = \psi(d)(r/d)^{-\mathrm{m}}, \quad (r > d), \qquad \psi(r) = \frac{\psi(d)}{1 - \alpha_{\mathrm{res}}} \left((r/d)^{-\mathrm{m}} - \alpha_{\mathrm{res}} (r/d)^{\mathrm{m}}\right), \quad (d > r > a). \tag{16.86a}$$

When the wall current and wall specific resistivity are denoted by j_{w} and η_{w}, there are following relations:

$$\nabla^2 \psi = -\mu_0 j_{\mathrm{w}}, \qquad j_{\mathrm{w}} = E_z / \eta_{\mathrm{w}} = -\frac{\gamma}{\eta_{\mathrm{w}}} \psi.$$

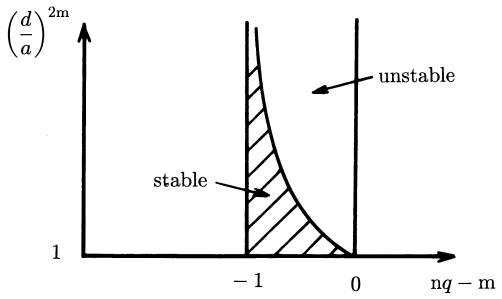

Fig.16.29 Stable region in $nq-m$-d/a-diagram.

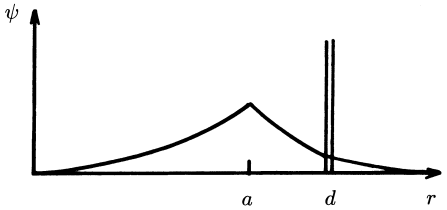

Fig.16.30 Profile of $\psi(r)$ in the case of resistive wall at $r=d$.

Then the discontinuity of logarithmic derivative at $r=d$ is

$$\frac{\psi(d_+)'-\psi(d_-)'}{\psi(d)}=-\frac{\mu_0\int j_w dr}{\psi}=\frac{\mu_0\gamma/\eta_w\int\psi dr}{\psi}=\frac{\mu_0\gamma\delta_w}{\eta_w}=\frac{\gamma\tau_w}{d},\qquad \tau_w\equiv\mu_0 d\delta_w\eta_w$$

where δ_w is the wall thickness and we obtain

$$\frac{\psi(d_-)'}{\psi(d)}=-\frac{m}{d}-\frac{\gamma_{res}\tau_w}{d}.$$

Thus α_{res} in (16.86a) is given by

$$\alpha_{res}=\frac{\gamma_{res}\tau_w/(2m)}{1+\gamma_{res}\tau_w/(2m)}.$$

We have already $\psi'(a_+)/\psi(a)$ from (16.84) as follow:

$$\frac{\psi'(a_+)}{\psi(a)}=\frac{m}{a}\left(1+\frac{\gamma_{res}^2\tau_{A\theta}^2}{(nq-m)^2}+\frac{2}{(nq-m)}\right).$$

On the other hand $\psi'(a_+)/\psi(a)$ is also given by (16.86a) as follow:

$$\frac{\psi'(a_+)}{\psi(a)}=-\frac{m}{a}\frac{1+\alpha_{res}(a/d)^{2m}}{1-\alpha_{res}(a/d)^{2m}}.\tag{16.86b}$$

Therefore the growth rate of the mode in the resistive wall is given by

$$\gamma_{res}(d)^2\tau_{A\theta}^2=-2(nq-m)\left(1+\frac{(nq-m)}{1-\alpha_{res}(a/d)^{2m}}\right).\tag{16.87}$$

Since

$$\frac{1}{1-\alpha_{res}(a/d)^{2m}}=\frac{1}{1+R}+\frac{R}{1+R}\frac{1}{1-(a/d)^{2m}},\qquad R=(1-(a/d)^{2m})\frac{\gamma_{res}(d)\tau_w}{2m}$$

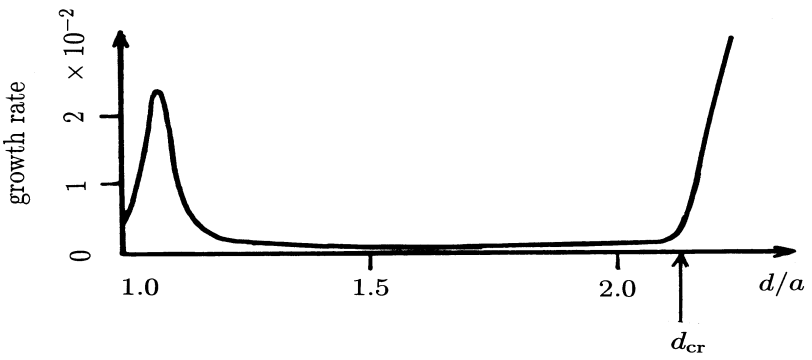

Fig.16.31 The growth rate $\gamma_{\mathrm{res}}(d)$ versus resistive wall position d/a in the case of $\omega_{\mathrm{rot}} = 0.5$. $\gamma_{\mathrm{res}}(d)$ and ω_{rot} are in unit of $\tau_{\mathrm{A}}^{-1} = B/(a(\mu_0\rho)^{1/2}) = (B/B_\theta)\tau_{\mathrm{A}\theta}^{-1}$, $d_{\mathrm{cr}} = 2.115$. $(R/a = 5, q_0 = 1.05$, m=2, n=1, $\tau_{\mathrm{A}}/\tau_{\mathrm{w}} = 5 \times 10^{-4})$. Afer (ref.[50]).

(16.87) is reduced to

$$\gamma_{\mathrm{res}}(d)^2 = \frac{\gamma_{\mathrm{c}}^2(\infty) + R\gamma_{\mathrm{c}}^2(d)}{1+R}. \tag{16.88}$$

Let us consider the case where the mode is stable with the conducting wall at $r = d$ and is unstable without the wall, that is, $\gamma_{\mathrm{c}}^2(d) < 0$ and $\gamma_{\mathrm{c}}^2(\infty) > 0$. Then the growth rate of the mode with thin resistive wall at $r = d$ is (under the assumption of $\gamma_{\mathrm{res}}(d)^2 \ll \gamma_{\mathrm{c}}^2(d), \gamma_{\mathrm{c}}^2(\infty)$)

$$R = -\frac{\gamma_{\mathrm{c}}^2(\infty)}{\gamma_{\mathrm{c}}^2(d)}, \qquad \gamma_{\mathrm{res}}(d)\tau_{\mathrm{w}} = \frac{2\mathrm{m}}{1-(a/d)^{2\mathrm{m}}}\left(-\frac{\gamma_{\mathrm{c}}^2(\infty)}{\gamma_{\mathrm{c}}^2(d)}\right). \tag{16.89}$$

Therefore the growth rate is order of inverse resistive wall time constant. For $d \to a$, $\gamma_{\mathrm{res}}(d)\tau_{\mathrm{w}} \to -2\mathrm{m}(1+\mathrm{n}q-\mathrm{m})/(\mathrm{n}q-\mathrm{m})$ is remains finite. This mode is called resistive wall mode (RWM). When wall position d approaches to critical one d_{cr}, where ideal MHD mode becomes unstable even with conducting wall $\gamma_{\mathrm{c}}(d_{\mathrm{cr}}) = 0$, the growth rate of RWM becomes infinity as is seen in (16.89) and connects to ideal MHD mode.

When plasmas rotate rigidly and perturbations also rotate without slip in the plasmas, the effect of rigid rotation is included by adding a Doppler shift

$$\gamma \to \gamma + i\boldsymbol{k}\cdot\boldsymbol{v} = \gamma + i\left(\frac{\mathrm{n}}{R}v_z - \mathrm{m}\omega_\theta\right) = \gamma + i\omega_{\mathrm{rot}} \text{ on the left−hand side of (16.88)},$$

but not on the right-hand side of (16.88). Fig.16.31 shows the dependence of the growth rate $\gamma_{\mathrm{res}}(d)$ on the resistive wall position d/a while Ω is fixed for the case of $\omega_{\mathrm{rot}}\tau_{\mathrm{A}} = 0.5$, $\tau_{\mathrm{A}}^{-1} \equiv B/(a(\mu_0\rho)^{1/2}) = (B/B_\theta)\tau_{\mathrm{A}\theta}^{-1}$, $R/a = 5, q_0 = 1.05$, m=2, n=1, $\tau_{\mathrm{A}}/\tau_{\mathrm{w}} = 5 \times 10^{-4}$. When d/a increases beyond d_{cr}/a, plasma becomes unstable in ideal MHD time scale. For d/a approaching near unity, there is an enhancement in the growth rate due to the inductance factor $(1-(a/d)^{2\mathrm{m}})$. Due to the fact the effective flux decay time becomes shorter, the resistive wall behaves as if the wall is more resistive. There is an initial increase in the growth rate with ω_{rot}, after which the growth rate decreases, but does not go to zero as $\omega_{\mathrm{rot}} \to \infty$.

Ward and Bondeson (ref.[51]) analyzed the full toroidal plasma with resistive wall by numerical code. Numerical analysis indicates that there are two modes. One is the mode that has zero frequency in the frame of plasma and perturbation hardly penetrates the resistive wall, the "plasma mode". In other word resistive wall behaves as if the wall is ideal when $\omega_{\mathrm{rot}} \gg \tau_{\mathrm{w}}^{-1}$. The other one is the mode that the perturbation rotates slowly with resistive wall, the "resistive wall mode". In other word perturbation rotates with respect to the plasma. The two modes are influenced in opposite way by the wall distance. The plasma mode is destabilized as the wall is moved farther from the plasma, while the resistive wall mode is stabilized. Therefore there can be a finite window

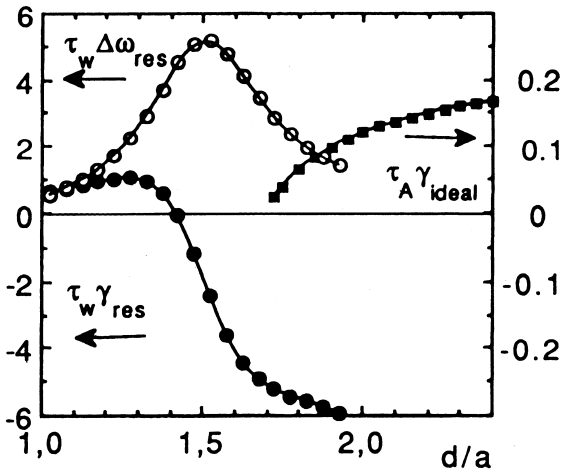

Fig.16.32 The growth rate $\gamma_{\rm res}$ and slip frequency $\Delta\omega_{\rm slip} = \omega_{\rm rot} - \omega_{\rm res}$ of resistive wall mode and the growth rate $\gamma_{\rm ideal}$ of plasma mode versus resistive wall radius d/a for n=1. $\omega_{\rm rot} = 0.06$ is unit of $\tau_{\rm A}^{-1} = B/(a(\mu_0\rho)^{1/2}) = (B/B_\theta)\tau_{{\rm A}\theta}^{-1}$. (Afer ref.[51]).

for the wall position such that both modes are stable (see fig.16.32). They suggest that important aspects of stabilization mechanism are that inertial effects become important near the resonant layers in the plasma where the rotation speed exceeds the local Alfvén frequency $k_\parallel v_{\rm A}$ and that coupling to sound waves contributes to the stabilization.

These numerical results can be interpreted by analytical consideration. In the case of resistive wall at $r = d$, $\psi'(a_+)/\psi(a)$ is already given by (16.86b). Formally $\psi'(a_-)/\psi(a)$ can be expressed by

$$\frac{\psi'(a_-)}{\psi(a)} = -\frac{\rm m}{a}(1+Z)$$

Z should be calculated by solving ψ for a given plasma model. Then the dispersion relation is given by

$$(1+Z) = \frac{1+\alpha_{\rm res}(a/d)^{2\rm m}}{1-\alpha_{\rm res}(a/d)^{2\rm m}} = \frac{(1+\gamma'_{\rm res})+\gamma'_{\rm res}(a/d)^{2\rm m}}{(1+\gamma'_{\rm res})-\gamma'_{\rm res}(a/d)^{2\rm m}}, \qquad \gamma'_{\rm res} = \frac{\gamma_{\rm res}\tau_{\rm w}}{2\rm m}$$

and the growth rate is given by

$$\frac{\gamma_{\rm res}\tau_{\rm w}}{2\rm m}\left(1-(a/d)^{2\rm m}\right) = \frac{Z}{w-Z}, \qquad w \equiv \frac{2(a/d)^{2\rm m}}{1-(a/d)^{2\rm m}} = \frac{2}{(d/a)^{2\rm m}-1}. \tag{16.90}$$

In the case when plasma does no rotate, Z is real $Z = x$ and positive and the resistive wall mode is unstable for $w > x$ or equivalently for

$$(1+2/x) > (d/a)^{2\rm m}, \qquad a < d < d_{\rm ideal} = a(1+2/x)^{1/2\rm m}.$$

As the wall radius approaches to $d_{\rm ideal}$ ($w \to x$), $\gamma_{\rm res}$ tends to increase to infinity and the resistive wall mode connects to ideal MHD instability, which is ideally unstable for $d > d_{\rm ideal}$.

When plasma rotates, the logarithmic derivative has non zero imaginary part $Z = x + yi$ and the growth rate is

$$\gamma_{\rm res}\tau_{\rm w}2\rm m\left(1-(a/d)^{2\rm m}\right) = \frac{wx - x^2 - y^2 + iwy}{(w-x)^2+y^2}.$$

This eliminates the zero in the demominator of above equation and $\gamma_{\rm res}$ remains finite and complex

for all wall distances. The resistive wall mode does not connect to the ideal instability. When $wx < (x^2 + y^2)$, the resistive wall mode becomes stable. This condition becomes

$$d > d_{\rm res}, \qquad d_{\rm res} \equiv (1 + 2x/(x^2 + y^2))^{1/2{\rm m}}.$$

These results are consistent with numerical results.

16.10b Feedback Stabilization of Resistive Wall Mode

Feedback stabilization of resistive wall mode is discussed according to (ref.[52]) by Okabayashi, Pomphrey and Hatcher. We begin with the eigenmode equation used to determine the stability of a large aspect ratio tokamak with low beta (ref.[53]).

$$\frac{\rm d}{{\rm d}r}\left((\gamma\tau_{\rm A}^2 + F^2)r\frac{\rm d}{{\rm d}r}(r\xi_r)\right) - \left({\rm m}^2(\gamma\tau_{\rm A}^2 + F^2) + r\frac{{\rm d}F^2}{{\rm d}r}\right)\xi_r = 0 \tag{16.91}$$

$$F = \left(-\frac{\rm m}{r}B_\theta + \frac{\rm n}{R}B_z\right) = \frac{B_\theta}{r}({\rm n}q - {\rm m}).$$

This formula can be derived from (14.36) under the assumption $\epsilon = r/R \ll 1$. In the vacuum, the perturbation of magnetic field $\boldsymbol{B}_1 = \nabla\phi$ is the the solution of

$$\nabla^2\phi = 0, \qquad \phi = A\left((r/b_{\rm w})^{-{\rm m}} + \alpha_{\rm w}(r/b_{\rm w})^{\rm m}\right)\exp(-i{\rm m}\theta + {\rm n}z/R). \tag{16.92}$$

A plasma-vacuum boundary condition at plasma edge $r = a$ is of the form of (ref.[53])

$$(\gamma^2\tau^2 + f^2)\frac{1}{\xi_r}\frac{{\rm d}(r\xi_r)}{{\rm d}r} = f^2\left(\frac{a\psi'(a_+)}{\psi(a)} - \frac{2{\rm m}}{f}\right) \tag{16.93}$$

where $f = {\rm n}q - {\rm m}$ and ψ is the flux function of external perturbation $\boldsymbol{B}_{1{\rm ex}}$. The flux function $\psi = \psi(r)\exp(-i{\rm m}\theta)$ (z component of vector potential A_z) in the vacuum is given by $\psi = rB_{1r}/{\rm m}$. This formula can be derived from the plasma-vacuum boundary condition (8.33) and (8.38). The boundary condition (8.38) $\boldsymbol{n}\cdot\boldsymbol{B}_{1{\rm ex}} = \boldsymbol{n}\cdot\nabla\times(\boldsymbol{\xi}\times\boldsymbol{B})$ becomes $\partial\phi/\partial r = r^{-1}\partial(\xi_r B_\theta/\partial\theta + \partial(\xi_r B_z)/\partial z$ and determines A in (16.92) as follow:

$$A = -i\frac{\xi_r F}{({\rm m}/a)\left((a/b_{\rm w})^{-{\rm m}} - \alpha_{\rm w}(a/b_{\rm w})^{\rm m}\right)}.$$

The constant $\alpha_{\rm w}$ is to be determined by the boundary condition on the wall at $r = b_{\rm w}$. The boundary condition (8.33) becomes

$$B_\theta B_{1\theta{\rm in}} + B_z B_{1z{\rm in}} = B_\theta B_{1\theta{\rm ex}} + B_z B_{1z{\rm ex}}$$

where $\boldsymbol{B}_{1{\rm in}} = \nabla\times(\boldsymbol{\xi}\times\boldsymbol{B})$ is given by (8.69-71) and $\boldsymbol{B}_{1{\rm ex}}$ is given by (16.92). $\boldsymbol{\xi}$ is given by Hain-Lüst equation (8.114-116), in which low β and incompressivility are assumed. Two boundary conditions yield (16.93).

The boundary condition (16.93) is used to provide a circuit equation for the plasma by defining $\beta_0 \equiv (1/\xi_r)({\rm d}(r\xi_r)/{\rm d}r)|_a$. In principle, β_0 would be determined by (16.91) and (16.93) selfconsistentely. The flux function $2\pi R\psi(a_+)$ is the perturbed poloidal flux of (m, n) mode in the vacuum region ($B_{1\theta} = -(\partial\psi/\partial r)$. $2\pi R\psi(a_+)$ consists of contributions from the perturbed current I_1, resistive wall current I_2 and circuit current I_3 corresponding to active feedback coil for (m, n) mode, that is,

$$2\pi R\psi(a_+) = L_1 I_1 + M_{12} I_2 + M_{13} I_3$$
$$2\pi R\psi'(a_+) = L_1' I_1 + M_{12}' I_2 + M_{13}' I_3.$$

Therefore (16.93) is reduced to

$$\left((\gamma^2\tau^2 + f^2)\beta_0 - f^2\frac{aL_1'}{L_1} + 2{\rm m}\right)L_1 I_1 + \left((\gamma^2\tau^2 + f^2)\beta_0 - f^2\frac{aM_{12}'}{M_{12}} + 2{\rm m}\right)M_{12} I_2$$

$$+\left((\gamma^2\tau^2+f^2)\beta_0 - f^2\frac{aM'_{13}}{M_{13}}+2\mathrm{m}\right)M_{13}I_3=0.$$

For circuit corresponding to resistive wall, the flux function at resistive wall ($r=r_\mathrm{w}$) is given by

$$2\pi R\frac{\partial\psi(r_\mathrm{w})}{\partial t}=L_2\frac{\partial I_2}{\partial t}+M_{21}\frac{\partial I_1}{\partial t}+M_{23}\frac{\partial I_3}{\partial t}$$

and

$$2\pi R\frac{\partial\psi(r_\mathrm{w})}{\partial t}=-2\pi R\eta_\mathrm{w}j_\mathrm{w}=-R_2I_2$$

where

$$I_2\equiv 2\pi r_\mathrm{w}\delta_\mathrm{w}j_\mathrm{w}/(2\mathrm{m}),\qquad R_2\equiv 2\mathrm{m}\frac{\eta_\mathrm{w}2\pi R}{2\pi r_\mathrm{w}\delta_\mathrm{w}}.$$

For the circuit corresponding the active feedback control, a voltage term to drive the feedback current must be included and

$$M_{31}\frac{\partial I_1}{\partial t}+M_{32}\frac{\partial I_2}{\partial t}+M_{31}\frac{\partial I_3}{\partial t}+R_3I_3=V_3.$$

The form of the feedback voltage V_3 should be applied to minimize $\psi(a_+)$ by use of appropriate sensors of the perturbations.

16.11 Steady-State Operation

Non-Inductive Current Drives and Bootstrap Current

As long as the plasma current is driven by electromagnetic induction of a current transformer in a tokamak device, the discharge is a pulsed operation with finite duration. In such cases, heat cycles of heavy thermal load to the first wall (plasma faced wall) may cause serious technological difficulty. Furthermore, pulsed reactors are not competitive as commercial power plants. If the plasma current is driven by the non-inductive way, a steady-state operation of tokamak is possible.

However, if the total plasma current is driven by non-inductive current drive, the substantial part of fusion output is necessary by the present experimental results and theoretical predictions.

On the other hand, bootstrap current driven by plasma itself is predicted by neoclassical theory (refer to sec.16.8d). It is demonstrated by experiments that the fraction of bootstrap current can reach 70∼80% of the total plasma current in the case of high poloidal beta β_p operation. The experimental results of full non-inductive current drive operation with large bootstrap current fraction in JT60U (ref.[54]) and DIIID (ref.[55]) are shown in fig.16.33. Radial profiles of measured total current density and the sum of calculated bootstrap current density and beam driven current density are compared and they are in good agreement within the experimental error. The parameters of experimental conditions and measured data are listed in Table 16.3.

Although the plasma currents in these experiments are relatively low in order to obtain high poloidal beta plasma, steady-state plasmas with high bootstrap current fraction and full non-inductive current drive are realized with good energy confinement HH_{98y2} in the cases of $\beta_\mathrm{p}\sim 3$ and these are very encouraging results.

Neoclassical Tearing Mode

When the duration of sustaining high toroidal beta plasma is longer than the resistive diffusion time scale $\tau_\mathrm{R}=\mu_0a_\mathrm{s}^2/\eta$ (η is specific resistivity of plasma at the radius a_s of rational surface), neoclassical tearing mode (NTM) appears in the magnetic island, when the poloidal beta exceeds critical values. Physics of neoclassical tearing mode was described in sec.16.9. It is possible to control neoclassical tearing mode by local current drive in rational surface (ref.[49]).

Resistive Wall Mode

When the discharge duration exceeds the resistive skin time $\tau_\mathrm{w}=\mu_0d\delta w/\eta_\mathrm{w}$ (η_w is specific resistivity of the wall with radius d and thickness δw), the resistive wall mode (RWM) appears as is described in sec.16.10. In such case, high beta plasma in the configuration of perfect conducting

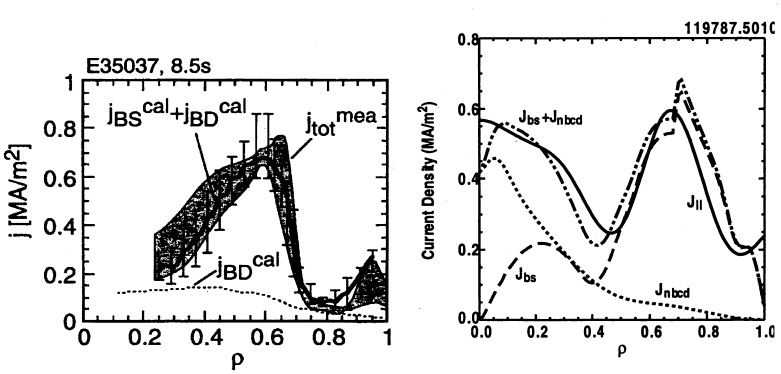

Fig.16.33 Left-hand side: Radial profiles of measured total current density $j_{\rm tot}^{\rm mea}$, calculated beam driven current density $j_{\rm BD}^{\rm cal}$, and sum of calculated bootstrap current density $j_{\rm BS}^{\rm cal}$ and $j_{\rm BD}^{\rm cal}$ of JT60U discharge E35037. After (ref.[54]).
Right-hand side: Current profiles for discharge 119787 of DIIID: total ($J_{\|}$), bootstrap ($J_{\rm bs}$), beam driven ($J_{\rm NBCD}$) current densities, and the sum of the bootstrap and beam-driven current densities. After (ref.[55]).

Table 16.3 Experimental data of full non-inductive current drive with large fraction of bootstrap current in JT60U and DIIID.

	JT60U (E35037) Reversed shear config.	DIIID (119787) ELMy H, standard q profile
R(m)	3.34	(1.66)
a(m)	0.8	(0.67)
$I_{\rm p}$(MA)	0.8	0.6
$B_{\rm t}$(T)	3.4	(< 2.1)
κ	1.5	1.85
δ	0.42	0.7
q_{95}	$\sim$9	$\sim$10
$q_{\rm min}$	3.6	2.94
$P_{\rm NB}$(MW)	5	–
$E_{\rm b}$(keV)	85	–
$\beta_{\rm N}$	1.9$\sim$2.2	3.08
$\beta_{\rm p}$	2.7$\sim$3.0	3.18
$\beta_{\rm t}$(%)	0.65	1.5
$\tau_{\rm E}$(s)	0.4$\sim$0.5	0.098
HH_{98y2}	2.1$\sim$2.3	2.03
$n_{\rm e19}(0)/\langle n_{\rm e19}\rangle$	3.5/–	6.7/4.37
$T_{\rm i}(0))/\langle T_{\rm i}\rangle$(keV)	7.5/–	3.8/2.08
$T_{\rm e}(0))/\langle T_{\rm e}\rangle$(keV)	5.0/–	2.5/1.49
$f_{\rm BS}$(%)	$(78 \sim 84) \pm 11$	80.8
$f_{\rm BD}$(%)	$\sim$25	19.2
$\tau_{\rm duration}$(s)	2.7	0.7

HH_{98y2} is energy confinement enhance factor over IPB98y2 scaling and $\tau_{\rm duration}$ is the duration time of steady-state, high bootstrap current fraction and full current drive. $f_{\rm BS}$ and $f_{\rm BD}$ are fractions of bootstrap current and beam driven current, respectively. δ is triangularity of plasma shape. The parameters of R, a, $B_{\rm t}$ in the DIIID column are not given in (ref.[55]), so the parameters are refered from (ref.[56]).

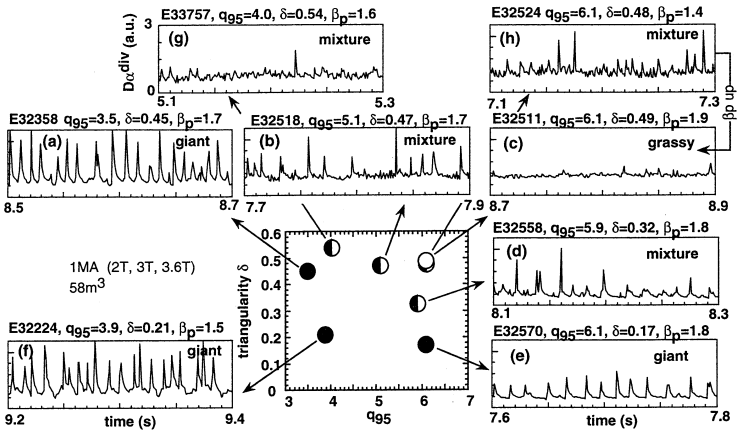

Fig.16.34 Change of ELM activity (divertor D_α signal) with δ, q_{95} and β_p at $I_p = 1$MA. Giant ELMs are replaced by grassy ELMs as q_{95} increases with fixed δ and β_p ((a) to (b) to (c)); as δ increases with fixed q_{95} and β_p ((e) to (d) to (c)); and as β_p increases with fixed δ and q_{95} ((h) to (c)). After (ref.[60]).

wall is no longer stable and the beta ratio of confined plasma decreases to the beta ratio in the configuration without conductive wall.

It is demonstrated in DIIID as well as the other devices that RWM with long wavelength external kink mode is stabilized by the feedback control of internal coil currents, which produces non-symmetric magnetic field (ref.[57]) (Ex/3-1Ra). Beta ratio well above the no-wall limit is sustained beyond the resistive time of resistive wall.

Furthermore, rapid toroidal plasma rotation past a resistive wall affects the stability of high beta plasma (ref.[57]) (Ex/3-1Rb). When the plasma rotation frequency is the order of a few percent of the inverse Alfv́en transit time, RWM is stabilized.

Edge Localized Mode

The improved confinement regime H mode is often perturbed by the onset of a quasi-periodic series of relaxation oscillations involving bursts of MHD activity and D_α emission, known as edge localized mode (ELM). These transit bursts of energy and particles into SOL produce high peak heat load and erosion on the divertor plates. On the other hand, the ELMs are effective in removing density and impurities accumlation. ELMy H mode is a standard operation of ITER. There are reviews on ELM (ref.[58],[59]).

ELM activities are classified as three types:

Type I ELMs: ELM repetition frequency $\nu_{\rm ELM}$ increases with heating power. In this case, the plasma edge is always close to the stability limit of normalized pressure gradient $\alpha \sim \alpha_{\rm cr}$. They appear as isolated sharp bursts on D_α

Type III ELMs: ELM repetition frequency decreases with heating power, contrary to the type I. The plasma edge pressure gradient is below the ideal ballooning limit $0.3 < \alpha/\alpha_{\rm cr} < 0.5$.

Type II ELMs: They become more frequent and the magnitude of D_α burst decreases (grassy ELM, small ELM).

H mode operation with grassy or small ELM is one of the candidates to satisfy good confinement with low impurities without high peak heat load to the divertor. There are trials to control ELMs. An example is the control of plasma shape by increase of triangularity. At a higher triangularity of $\delta = 0.54$, almost pure grassy phase appears even at a relatively low $q_{95} = 4.5$ in JT60U as is seen in fig.16.34 (ref.[60]). ASDEX-U experiment confirms that periodic injections of deuterium ice-pellet into plasma mitigate the type I ELM (ref.[61]).

Disruption Control

Loss of the plasma equilibrium control at the burning phase of tokamak fusion reactors such as ITER will cause serious damage to the first wall materials and divertor plate due to the high heat flux on the wall and due to the generation of high energy runaway electrons. Furthermore, toroidally asymmetric halo current generated at the vertical displacement during the plasma current quench causes intense electromagnetic force locally which may break in-vessel materials. Halo current, which flows helically along the wall-intersecting plasma flux surfaces, makes a complete circuit by

flowing from the strike points at one end of the open SOL field lines, through the conducting first wall structures and out onto the other end of the SOL field lines.

It is demonstrated in the experiments (ref.[62],[63]) that the injection of a solid impurity pellet (commonly termed *killer pellet*) into a tokamak plasma is capable of effecting a non-disruptive fast plasma energy and current shutdown, provided that the pellet size and velocity are chosen such that the pellet can penetrate deeply into the plasma core.

Massive-gas-injection is also effective to disruption mitigation (ref.[64]).

16.12 Parameters of Tokamak Reactors

Although there are many parameters to specify a tokamak device, there are also many relations and constrains between them (ref.[65]). If the plasma radius a, toroidal field B_t and the aspect rato A are specified, the other parameters of tokamak are determined by use of scaling laws of electron density, beta, energy confinement time and burning condition, when safety factor q_I (or q_{95}), the elongation ratio κ_s, triangularity δ of plasma cross section are given. By the definition of q_I, we have

$$q_\mathrm{I} \equiv \frac{Ka}{R}\frac{B_\mathrm{t}}{B_\mathrm{p}} = \frac{5K^2 a B_\mathrm{t}}{AI_\mathrm{p}}, \qquad B_\mathrm{p} = \frac{\mu_0 I_\mathrm{p}}{2\pi Ka} = \frac{I_\mathrm{p}}{5Ka}$$

the plasma current is

$$I_\mathrm{p} = \frac{5K^2 a B_\mathrm{t}}{Aq_\mathrm{I}}$$

where $K^2 = (1+\kappa_\mathrm{s}^2)/2$ (I_p in MA, B_t in T and a in m).
The safety factor q_{95} is approximately given by (refer to (16.11))

$$q_{95} \approx q_\mathrm{I} f_\delta f_\mathrm{A} \tag{16.94}$$

$$f_\delta = \frac{1+\kappa^2(1+2\delta^2-1.2\delta^3)}{1+\kappa^2} \qquad f_\mathrm{A} = \frac{1.17-0.65/A}{(1-1/A^2)^2}.$$

The volume average electron density n_{20} in unit of $10^{20}\mathrm{m}^{-3}$ is

$$n_{20} = N_\mathrm{G}\frac{I_\mathrm{p}}{\pi a^2} \tag{16.95}$$

where N_G is Greenwald normalized density. The beta ratio of thermal plasma

$$\beta_\mathrm{th} \equiv \frac{\langle p\rangle}{B_\mathrm{t}^2/2\mu_0} = 0.0403(1+f_\mathrm{DT}+f_\mathrm{He}+f_\mathrm{I})\frac{\langle n_{20}T\rangle}{B_\mathrm{t}^2}$$

is expressed by

$$\beta_\mathrm{th} = f_\mathrm{th}\beta_\mathrm{total}, \quad \beta_\mathrm{total} = 0.01\beta_\mathrm{N}\frac{I_\mathrm{p}}{aB_\mathrm{t}}, \tag{16.96}$$

where β_N is normalized beta. β_total is the sum of β_th (thermal plasma) and β_fast (fast (α) particle component) and $f_\mathrm{th} = \beta_\mathrm{th}/\beta_\mathrm{total}$. The notations f_DT, f_He, and f_I are the ratios of fuel DT, He, and impurity density to electron density respectively and the unit of T is keV. $\langle X\rangle$ means volume average of X. Thermal energy of plasma W is

$$W_\mathrm{th} = \frac{3}{2}\beta_\mathrm{th}\frac{B_\mathrm{t}^2}{2\mu_0}V = 0.5968\beta_\mathrm{th}B_\mathrm{t}^2 V \tag{16.97}$$

where W_th is in unit of MJ and plasma volume V is in unit of m^{-3}. Plasma shape with elongation ratio κ_s and triangularity δ is given by

$$R = R_0 + a\cos(\theta + \delta\sin\theta)$$

$$z = a\kappa_{\rm s}\sin\theta$$

Plasma volume V is given by

$$V \approx 2\pi^2 a^2 R\kappa_{\rm s} f_{\rm shape}$$

where $f_{\rm shape}$ is a correction factor due to triangularity

$$f_{\rm shape} = 1 - \frac{\delta}{8} + \frac{\delta^4}{192} - \frac{a}{4R}\left(\delta - \frac{\delta^3}{3}\right).$$

We utilize the thermal energy confinement scaling of IPB98y2 (ref.[34])

$$\tau_{\rm E} = 0.0562 \times 10^{0.41} H_{\rm y2} I^{0.93} B_{\rm t}^{0.15} M^{0.19} n_{20}^{0.41} a^{1.97} A^{1.39} \kappa_{\rm s}^{0.78} P^{-0.69} \tag{16.98}$$

where $M(=2.5)$ is average ion mass unit and P is loss power in MW by transport and is equal to necessary absorbed heating power subtracted by radiation loss power $P_{\rm rad}$. The total α particle fusion output power P_α is

$$P_\alpha = \frac{Q}{4}\langle n_{\rm DT}^2 \langle\sigma v\rangle_v\rangle V$$

where $Q_\alpha = 3.515$MeV. $\langle\sigma v\rangle_v$ is a function of T and a fitting equation for $\langle\sigma v\rangle_v$ is given in (1.5). Since the fusion rate σv near T =10keV is approximated by

$$\langle\sigma v\rangle_v \approx 1.1 \times 10^{-24} T_{\rm keV}^2 ({\rm m}^3/s)$$

the folowing Θ ratio is introduced:

$$\Theta(\langle T\rangle) \equiv \frac{\langle n_{\rm DT}^2 \langle\sigma v\rangle_v\rangle}{1.1 \times 10^{-24}\langle n_{\rm DT}^2 T^2\rangle}.$$

Θ is a function of average temperature $\langle T\rangle$ in keV and the profiles of density and temperature and has a peak of around 1 near $\langle T\rangle \approx 8 \sim 10$keV. The curves of Θ versus $\langle T\rangle$ in cases of $n(\rho) = \langle n\rangle (1-\rho^2)^{\alpha_n}(1+\alpha_n)$, $T(\rho) = \langle T\rangle(1-\rho^2)^{\alpha_T}(1+\alpha_T)$ is shown in fig.16.35 (ref.[66]).

Then P_α is reduced to

$$P_\alpha = 0.9551 \frac{f_{\rm prof} f_{\rm DT}^2}{(1 + f_{\rm DT} + f_{\rm He} + f_{\rm I})^2} \beta_{\rm th}^2 B_{\rm t}^4 \Theta V \tag{16.99}$$

where $f_{\rm prof} \equiv \langle n^2 T^2\rangle / \langle nT\rangle^2 \approx (\alpha_n + \alpha_T + 1)^2/(2\alpha_n + 2\alpha_T + 1)$ is the profile effect of temperature and density.

When absorbed auxiliary heating power is denoted by $P_{\rm aux}$ and heating efficiency of α heating is f_α, the total heating power is $f_\alpha P_\alpha + P_{\rm aux}$. When the fraction of radiation loss power to the total heating power is $f_{\rm R}$, the heating power to sustain buring plasma is given by

$$P = (1 - f_{\rm R})(f_\alpha P_\alpha + P_{\rm aux}).$$

. When Q ratio is defined by the ratio of total fusion output power $P_{\rm n} + P_\alpha = 5P_\alpha$ ($P_{\rm n}$ is neutron output power) to absorbed auxiliary heating power $P_{\rm aux}$, Q is

$$Q = \frac{5P_\alpha}{P_{\rm aux}}$$

Then P is reduced to

$$P = (1 - f_{\rm R})\left(f_\alpha + \frac{5}{Q}\right) P_\alpha.$$

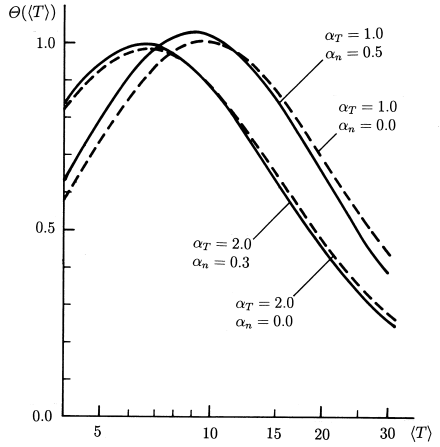

Fig.16.35 Θ is function of average temperature $\langle T\rangle$(keV) in cases with profile parameters $(\alpha_T = 1.0, \alpha_n = 0.0)$, $(\alpha_T = 2.0, \alpha_n = 0.0)$, $(\alpha_T = 1.0, \alpha_n = 0.5)$ and $(\alpha_T = 2.0, \alpha_n = 0.3)$

Therefore burning condition

$$\frac{W_{\rm th}}{\tau_{\rm E}} = (1 - f_{\rm R})\left(f_\alpha + \frac{5}{Q}\right) \tag{16.100}$$

From (16.97) and (6.100), we have

$$\beta_{\rm th} B_{\rm t}^2 \tau_{\rm E} = 0.625 \frac{(1 + f_{\rm DT} + f_{\rm He} + f_{\rm I})^2 / f_{\rm DT}^2}{(1 - f_{\rm rad})(f_\alpha + 5/Q) f_{\rm prof} \Theta(T)}.$$

The term in the left-hand side is proportional to the triple product $\langle n_{20} T_{\rm keV}\rangle \tau_{\rm E}$. Equations (16.98), (16.99) and (16.100) reduce to the following burning condition (ref.[66]):

$$\frac{B_{\rm t}^{0.73} a^{0.42}}{A^{0.26}} (f_\alpha + \frac{5}{Q})^{0.31} = 1.95 \Big[\frac{(1 + f_{\rm DT} + f_{\rm He} + f_{\rm I})^2}{(1 - f_{\rm rad}) f_{\rm prof} f_{\rm DT}^2 \Theta}\Big]^{0.31} \times \frac{q_{\rm I}^{0.96} (f_{\rm th}\beta_{\rm N})^{0.38} f_{\rm shape}^{0.69}}{H_{\rm y2} M^{0.19} N_{\rm G}^{0.41} K^{1.92} \kappa_{\rm s}^{0.09}}. \tag{16.101}$$

When Kaye-Goldston scaling (L mode) in sec.16.7 is used instead of IPB98y2 scaling, the burning condition becomes

$$\frac{I_{\rm p} A^{1.25}}{a^{0.12}} \left(f_\alpha + \frac{5}{Q}\right)^{0.5} = \frac{75.1 f_{\rm shape}(1 + f_{\rm DT} + f_{\rm He} + f_{\rm I})}{H_{\rm KG}[(1 - f_{\rm rad}) f_{\rm prof} \Theta]^{0.5} f_{\rm DT}}.$$

$H_{\rm KG}$ is the improved factor of energy confinement time over the Kaye-Goldston scaling. The value of $H_{\rm KG}$ necessary for the case of ITER parameters is 2.57. It is interesting to note that the burning condition mainly depends on $AI_{\rm p}$ in the case of Kaye-Goldston scaling.

When parameters a, $B_{\rm t}$, A are specified, then Q value and other parameters can be evaluated and are shown in Table 16.4. The result of this simple analysis are relatively consistent with ITER design parameters given by Table 16.5.

When the distance of plasma separatrix and the conductor of toroidal field coil is Δ and the maximum field of toroidal field coil is $B_{\rm mx}$ (see fig.16.36), there is a constraint of

$$\frac{B_{\rm t}}{B_{\rm mx}} = \frac{R - a - \Delta}{R} = 1 - \left(1 + \frac{\Delta}{a}\right)\frac{1}{A}$$

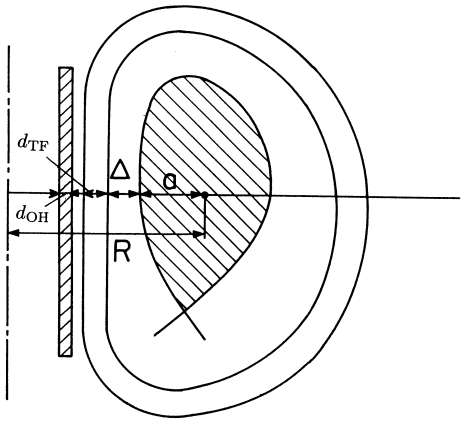

Fig.16.36 Geometry of plasma, toroidal field coil and central solenoid of current transformer in tokamak

and

$$1 - \frac{2}{A} < \frac{B_t}{B_{mx}} < \frac{1}{A}$$

under the assumption $a > \Delta > 0$. By specification of Δ and B_{mx}, B_t is a function of a.

The ratio ξ of the flux swing $\Delta\Phi$ of ohmic heating coil and the flux of plasma ring $L_p I_p$ is given by

$$\xi \equiv \frac{\Delta\Phi}{L_p I_p} = \frac{5B_{mx}((R_{OH} + d_{OH})^2 + 0.5d_{OH}^2)}{(\ln(8A/\kappa_s^{1/2}) + l_i - 2)RI_p}$$

where $R_{OH} = R - (a + \Delta + d_{TF} + d_s + d_{OH})$, d_{TF} and d_{OH} being the thickness of TF and OH coil conductors and d_s being the separation of TF and OH coil conductors (refer fig.16.35). The average current densities j_{TF}, j_{OH} of TF and OH coil conductors in MA/m^2=A/m^2 are

$$j_{TF} = \frac{2.5}{\pi}\frac{B_{mx}}{d_{TF}}\frac{1}{1 - 0.5d_{TF}/(R - a - \Delta)}$$

$$j_{OH} = \frac{2.5}{\pi}\frac{B_{mx}}{d_{OH}}.$$

The conceptual design of tokamak reactors has been actively pursued according to the development of tokamak experimental research. INTOR (International Tokamak Reactor) (ref.[68]) and ITER (International Thermonuclear Experimental Reactor) (ref.[67]) are representative of international activity in this field.

ITER aims achievement of extended burn in inductively driven plasmas with $Q \sim 10$ and aims at demonstrating steady state operation using non-inductive drive with $Q \sim 5$.

A cross section of ITER-FEAT outline design in 2000 is shown in fig.16.37.

Table 16.4 (a) Specified design parameters.

a	B_t	A	q_{95}	κ_s	δ	f_rad	f_α	$\beta_\mathrm{N}/f_\mathrm{th}$	N_G	f_DT	f_shape	H_{y2}
2.0	5.3	3.1	3.0	1.7	0.35	0.27	0.95	1.77/0.928	0.85	0.82	0.995	1.05

Specified value of β_N is the normalized beta of plasma which includes the contribution of energetic ion components. ($\alpha_T = 1.0, \alpha_n = 0.1$ and $f_\mathrm{He} = 0.04,\ f_\mathrm{I} = 0.02$ are assumed.)

(b) Reduced parameters.

Q	R	I_p	τ_E	n_{20}	$\langle T \rangle$	W_th	P_n	P_α	P_aux	P_rad	β_total	q_I	Θ
11	6.2	15.0	3.7	1.01	8.7	325	425	85	41	32.6	0.025	2.22	0.95

$P_\mathrm{n}, P_\alpha, P_\mathrm{aux}, P_\mathrm{rad}$ are in the unit of MW and W_th is in the unit of MJ.

Table 16.5 Parameters of ITER.

	inductive operation	non-inductive operation
I_p(MA)	15	9
B_t(T)	5.3	5.17
R/a(m)	6.2/2.0	6.35/1.84
A	3.1	3.45
$\kappa_{\mathrm{s}\,95}/\delta_{95}$	1.7/0.33	1.84/0.41
$\langle n_\mathrm{e} \rangle (10^{20}\mathrm{m}^{-3})$	1.01	0.67
N_G	0.85	0.83
$\langle 0.5 \times (T_\mathrm{e} + T_\mathrm{i}) \rangle$(keV)	8.5	∼11
$W_\mathrm{thermal}/W_\mathrm{fast}$(MJ)	325/25	273/60∼255/50
$\tau_\mathrm{E}^\mathrm{tr}$(s)	3.7	2.54∼2.32
$H_{y2} = \tau_\mathrm{E}^\mathrm{tr}/\tau_\mathrm{E}^\mathrm{IPB98y2}$	1.0	1.41∼1.3
P_fus(MW)	410	361∼338
P_aux(MW)	41	P_NB=34/P_LH=29∼33.7
P_rad(MW)	48	
Z_eff	1.65	2.2∼2.17
β_t(%)	2.5	2.64∼2.42
β_p	0.67	3.55∼3.26
β_N	1.77	2.8∼2.56
q_{95}	3.0	5.16∼5.13
q_I	2.22	3.44
l_i	0.86	2.2∼2.17
Q	10	5
f_R	0.39	
$f_\mathrm{DT}/f_\mathrm{He}$(%)	82/4.1	/
$f_\mathrm{Be}/f_\mathrm{Ar}$(%)	2/0.12	/

Inductive operation scenario in outline design in 2000 and non-inductive operation scenario in 2002 (ref.[67]). In non-inductive operation scenario, the bootstrap current and driven current are 5 MA and 4 MA, respectively.

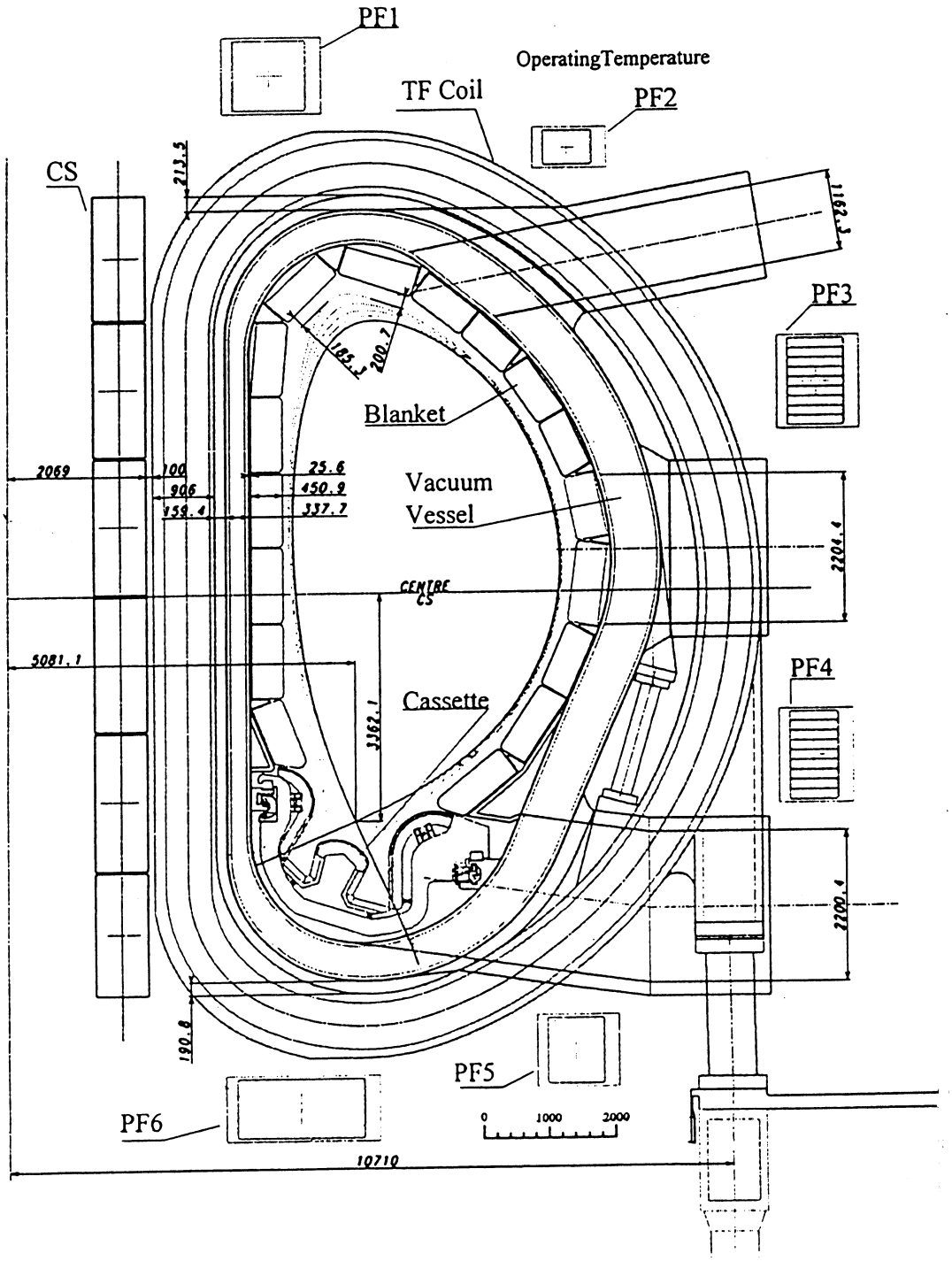

Fig.16.37 Toroidal cross section of ITER outline design in 2000.

16.13 Trials to Innovative Tokamaks

16.13a Spherical Tokamak

Potential theoretical advantages of spherical tokamak (ST) have been outlined by Peng and Strickler (ref.[69]), in which aspect ratio A/a of the standard tokamak is substantially reduced toward unity. Predicted advantages include a natural high elongation ($\kappa_s > 2$), high toroidal beta and tokamak-like confinement. These predictions have been confirmed experimentally, in particular by START (Small Tight Aspect Ratio Tokamak) (ref.[70]) at Culham ($R/a = 0.3/0.28 = 1.31$), $I_p \approx 0.25$MA, $B_t \approx 0.15$T. The toroidal beta reached 40% $\beta_N = 3.5 \sim 5.9$ (ref.[71]). Observed energy confinement times follow similar scaling to standard tokamak and it was demonstrated experimentally that the energy confinement times follow ITER98y2 scaling up to $\tau_E \sim 0.1$ s in the experment NSTX (National Spherical Torus Experiment) in Princeton (ref.[72]) ($R/a = 0.85/0.65 = 1.3$, $L_p = 1.5$MA, $B_t = 0.3 \sim 0.6$T) and MAST (Mega Ampere ST) in Culham (ref.[73]) ($R/a = 0.85/0.65 = 1.3$, $I_p = 1.35$MA, $B_t = 0.52$T (see fig.16.38). Density scaling is $N_G \sim 1$. Therefore, the fundamental scalings are almost the same as those of standard tokamaks (ITER) except a slight modification of q_{95} dependence on the aspect ratio in the region ($A < 3$); that is,

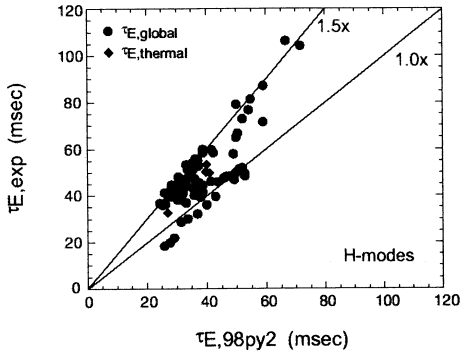

Fig.16.38 NSTX H-mode experimental confinement data points are shown compared to ITER98y2 H-mode scaling. After (ref.[72]).

$$q_I \equiv \frac{aB_t}{RB_p} = \frac{5K^2 aB_t}{AI_p} = \frac{5}{AI_N}\frac{1+\kappa_s^2}{2}, \qquad I_N \equiv \frac{I_p}{aB_t},$$

$$q_{95} = \left(\frac{5}{AI_N}\frac{1+\kappa_s^2}{2}\right)\frac{1.22-0.68/A}{(1-1/A^2)^2} \qquad (A<3), \tag{16.102}$$

$$\beta_c(\%) = \beta_N I_N, \quad \beta_c(\%)\beta_p = 0.25\beta_N^2 K^2,$$

$$S \equiv q_{95} I_N, \qquad \beta_c(\%) = \frac{\beta_N S}{q_{95}}, \qquad I_p = aB_t\frac{S}{q_{95}}, \tag{16.103}$$

$$n_{e\,20} = N_G \frac{I_p}{\pi a^2},$$

$$\tau_E = 0.0562 \times 10^{0.41} H_{y2} I^{0.93} B_t^{0.15} M^{0.19} n_{20}^{0.41} a^{1.97} A^{1.39} \kappa_s^{0.78} P^{-0.69},$$

where units of R, a, B_t, and I_p are m, T, and MA, respectively. I_N is normalized current and S is called by shape parameter. In addition, there are advantageous characteristics of ST. Refering to fig.16.39, in the center of plasma, the flux surfaces appear as in a standard tokamak but near the edge of plasma (if very low aspect ratio), the field lines dwell in the high field inboard side, so that q in edge is greatly increased. As A approaches toward 1, q_{95} becomes large as is seen in (16.102), even if the cylindrical safety factor $q_I \approx 2$. Therefore, it is possible to take I_N large value regardless of MHD stability limit (say $q_{95} > 3$). Accordingly Troyon limit of β_c can be large and the diamagnetic effect of high beta plasma counters the paramagnetic effect of the high normalized current I_N. This should improve MHD stability (ref.[71]).

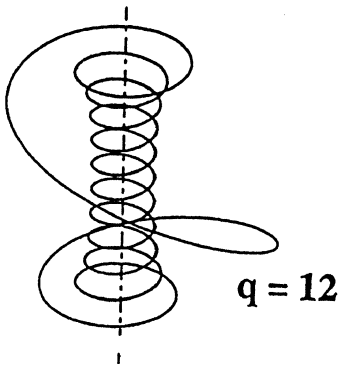

Fig.16.39 Magnetic field line in the plasma edge of ST. After (ref.[71]).

Table 16.6 Parameters of STPP, ARIES-ST and Vector, SlimCS.

	STPP	ARIES-ST	Vector('02)	SlimCS
R/a(m)	3.42 / 2.44	3.20 / 2.00	3.75 / 1.9	5.5 / 2.1
A	1.4	1.6	2	2.6
κ_s/δ	3.2 / 0.55	3.42 / 0.64	3.75 /$\sim$ 0.1	2.0 /$\sim$0.4
I_p(MA)	31	30.8	18.3	16.7
B_t/B_{max}(T)	1.77 / -	2.14 / 7.6	4.7 / 19.6	6.0 / 16.4
q_0/q_{edge}	3 / 15	- / -	- / 5.2	- / 5.4
$\beta_t(\%)/\beta_N$	59 / 8.2	54 / 8	7.7 / 3.75	5.7 / 4.3
$\langle n_{e\,20}\rangle/\bar{n}_{e\,20}$	1.08 /	- / 2.74	1.6 /	1.18 /
n_G	1.66	2.45	1.6	1.2
N_G	0.65	1.12	1	0.98
$\langle T_e\rangle$(keV)	22	-	-	17.0
$H_{98y2}/H_{ITER93H}$	1.6 /	- / 1.83	1.8 /	1.3 /
P_{fusion}(GW)	3.1	2.86	1.8	3
CD power (MW)	50	31	$\sim$40	59
BS current fraction (%)	92.6	95	$\sim$0.8	0.77
neutron wall load (MW/m^2)	3.5	4.1	3.5	3.2
TF coil ohmic loss (MW)	-	288	$\sim$0	$\sim$0
recirculating power fraction		0.32	$Q\sim 45$	$Q\sim 52$

Notations are the same as Table 16.5. TF coils of STPP and ARIES-ST are normal conductor and TF coils of Vector and SlimCS are super-conductor.

16.13b Trials to Innovative Tokamak Reactors

There are several trials of ST reactors with use of a solid copper center rod for TF (toroidal field) coils. The parameters of STPP (ST Power Plant) (ref.[74]), ARIES-ST (ref.[75]) are given in Table 16.6. TF coils of STPP and ARIES-ST use a solid copper center rod, so that B_t is small and requirements of $\beta_N \sim 8$ and $H_{98y2} \sim 1.6$ or 1.8 are demanding. Design of ST reactor NSST (Next Step ST) with the other name CTF (compact Component Test Facility) is being carried out as a volume neutron source (ref.[76]).

The other trials are tight aspect ratio tokamaks with super-conductinf TF coils. Vector (Very Compact Tokamak Reactor) (ref.[77]) and SlimCS (ref.[78]) are given in Table 16.6.

Vector is a tokamak reactor with super-conducting TF coils (Bi2212/Ag/AgMgSb (20 K)) and low aspect ratio $A \sim 2$ by removing the center solenoid (CS) coil system from standard tokamak ($A \sim 3$). This brings relatively high beta plasma due to low aspect ratio, low recirculating power fraction. However, research and development of superconducting TF coils with very high magnetic field (19.6T) are required. Issue of start-up feasibility and current ramp up are being studied experimentally (ref.[79]).

Motivated by the Vector concept, the more realistic demo reactor SlimCS is proposed. The parameters are $A = 2.6$, $B_{max} = 16.4$T (Nb_3Al), $\beta_N = 4.3$ and $H_{98y2} = 1.3$ (refer to Table 16.6). Slim CS is capable of raising the plasma current up to 3.8MA, while the full plasma current in steady-state is 16.7 MA.

Equilibrium and stability of ST including the effect of a large fraction of bootstrap current is analyzed in (ref.[80]).

Tight aspect ratio tokamak experimental device JT-60SA with all super-conducting coils is under the construction. The parameters are $I_{\rm p} = 5.5$MA, $B_{\rm t} = 2.25$T, $R = 2.96$m, $a = 1.18$m, $A = 2.5$, $\kappa_{\rm s} = 1.95$, triangularity $\delta = 0.53$, shape parameter (refer to (16.103)) $S = 6.7$, $q_{95} \sim 3$ (ref.[81]).

References

[1] L. A. Artsimovich: Nucl. Fusion **12**, 215 (1972)
H. P. Furth: Nucl. Fusion **15**, 487 (1975)
[2] J. Wesson: *Tokamaks*, Clarendon Press, Oxford 1997
ITER Physics Basis: Nucl. Fusion **39**, No.12, 2138-2638 (1999)
[3] V. S. Mukhovatov and V. D. Shafranov: Nucl. Fusion **11**, 605 (1971)
[4] Equip TFR: Nucl. Fusion **18**, 647 (1978)
[5] J. Sheffield: *Plasma Scattering of Electromagnetic Radiation*, Academic Press, New York(1975)
[6] Y. Nagayama, Y. Ohki and K. Miyamoto: Nucl. Fusion **23**, 1447 (1983)
[7] A. Sykes, M. F. Turner and S. Patel: Proc. 11th European Conference on Controlled Fusion and Plasma Physics, Aachen Part II, 363 (1983)
T. Tuda, M. Azumi, K. Itoh, G. Kurita, T. Takeda *et al.*: Plasma Physics and Controlled Nuclear Fusion Research **2**, 173 (1985) (Conference Proceedings, London in 1984, IAEA Vienna)
[8] B. B. Kadomtsev: Sov. J. Plasma Phys. **1**, 389 (1975)
[9] M. Greenwald, J. L. Terry, S, M. Wolfe, S. Ejima, M. G. Bell, S. M. Kaye, G. H. Nelson: Nucl. Fusion **28**, 2199, (1988)
[10] ASDEX-U Team: IAEA Fusion Energy Conference, O1-5 (Montreal in 1990) IAEA, Vienna
[11] J. A. Wesson: Nucl. Fusion **18**, 87 (1978)
[12] B. B. Kadomtsev and O. P. Pogutse: Nucl. Fusion **11**, 67 (1971)
[13] J. W. Connor and H. R. Wilson: Plasma Phys. Control. Fusion **36**, 719 (1994)
[14] F. Wagner and U. Stroth: Plasma Phys. Control. Fusion **35**, 1321 (1993)
[15] F. Troyon, R. Gruber, H. Saurenmann, S. Semenzato and S. Succi: Plasma Phys. and Controlled Fusion **26**, 209 (1984)
[16] ITER Physics Basis: Nucl. Fusion **39**, No. 12 (1999).
[17] DIII-D team: Plasma Physics and Controlled Nuclear Fusion Research **1**, 69, 1991 (Conference Proceedings, Washington D. C. in 1990) IAEA, Vienna
[18] K. Borrass: Nucl. Fusion: **31**, 1035, (1991)
K. Borrass, R. Farengo, G. C. Vlases: Nucl. Fusion **36**, 1389, (1996)
B. LaBombard, J. A. Goetz, I. Hutchinson, D. Jablonski, J. Kesner *et al*: Nucl. Materials **241-243**,149 (1997)
[19] R. J. Goldston: Plasma Physics and Controlled Fusion **26**, 87, (1984)
M. Kaye: Phys. Fluids **28**, 2327 (1985)
[20] P. N. Yushmanov, T. Takizuka, K. S. Riedel, D. J. W. F. Kardaun, J. G. Cordey, S. M. Kaye, D. E. Post: Nucl. Fusion **30**, 1999, (1990)
N. A. Uckan, P. N. Yushmanov, T. Takizuka, K. Borras, J. D. Callen, *et al*: Plasma Physics and Controlled Nuclear Fusion Research **3**, 307 (1991) (Conference Proceedings, Washington D. C. in 1990) IAEA, Vienna
[21] F. Wagner, G. Becker, K. Behringer *et al*: Phys. Rev.Lett.**49**, 1408 (1982)
F. Wagner, G. Becker, K. Behringer, D. Campbell, M. Keilhacker *et al.*: Plasma Physics and Controlled Nuclear Fusion Research **1**, 43, (1983) (Conference Proceedings, Baltimore in 1982) IAEA, Vienna
[22] ASDEX Team: Nucl. Fusion **29**, 1959 (1989)
[23] R. J. Groebner: Phys. Fluids **B5**, 2343 (1993)
[24] E. J. Doyle, C. L. Rettig, K. H. Burrell, P. Gohil, R. J. Groebner *et al*: Plasma Physics and Controlled Nucl. Fusion Research **1**, 235 (1992) (Conference Proceedings, Würzburg in 1992) IAEA, Vienna
[25] S. I. Itoh and K. Itoh: Phys. Rev. Lett. **60**, 2276 (1988)
[26] K. C. Shaing and E. C. Crume: Phy. Rev. Lett. **63**, 2369 (1989)
[27] H. Bigrali, D. H. Diamond, Y.-B. Kim, B. A. Carreras, V. E.Lynch, F. L. Hinton *et al*: Plasma Physics an Controlled Nucl. Fusion Research **2**, 191, (1991) (Conference Proceedings, Washington D.C. in 1990) IAEA Vienna
[28] T. H. Dupree: Phys. Fluids: **15**, 334 (1972)
T. Boutros-Ghali and T. H. Dupree: Phys. Fluids: **24**, 1839 (1981)
[29] TFTR Team: Plasma Physics and Controlled Nucl. Fusion Research **1**, 11, (1995) (Conference Proceedings, Seville in 1994) IAEA Vienna
ibid. **1**, 9, (1991) (Conference Proceedings, Washington D.C. in 1990)
[30] T. S. Taylor, T. H. Osborne, K. H. Burrel *et al*: Plasma Physics and Controlled Nuclear Fusion Research **1**, 167, (1992) (Conference Proceedings, Würzburg in 1992) IAEA, Vienna
[31] JT60U Team: ibid, **1**, 31, (1995) (Conference Proceedings, Seville in 1994) IAEA Vienna
[32] F. L. Hinton and G. M. Staebner: Phys. Fluids **B5**, 1281 (1993)
[33] O1-6, O1-2, O1-3, A5-5, O2-2 in IAEA Fusion Energy Conference (Montreal in 1996) IAEA, Vienna

[34] A. Fujisawa, K. Itoh, H. Iguchi, K. Matsuoka, S. Okamomura et al.: Plasma. Phys. Rev. Lett. **93**, 165002 (2004).
G. D. Conway, B. Scott, J. Schirmer, M. Reich, A. Kendl and ASDEX-U Team: Plasma Phys. Contr. Fusion **47**, 1165 (2005).
[35] P. H. Diamond, S.-L. Itoh, K. Itoh, and T. S. Hahm: Plasma Phys. Contr. Fusion **47**, R35 (2005).
P. H. Diamond, K. Itoh, S.-I. Itoh, and T. S. Hahm: 20th Fusion Energy Conf. (Vilamoura 2004) OV/2-1.
P. H. Diamond, K. Itoh, S.-I. Itoh: *Modern Plasma Physics* vol.1 Physical Kinetics of Turbulent Plasmas, Cambridge Univ. Press 2010.
[36] ITER Physics Basis, Chapter 2 in Nucl. Fusion **39**, No.12 (1999).
[37] JET Team: Nucl. Fusion **32**, 187 (1992).
[38] T. Ohkawa: Nucl. Fusion **10**, 185 (1970).
[39] D. J. H. Wort: Plasma Phys. **13**, 258 (1971).
[40] N. J. Fisch: Phys. Rev. Lett. **41**, 873 (1978).
C. F. F. Karney and N. J. Fisch: Phys. Fluids **22**, 1817 (1979).
[41] N. J. Fisch and A. H. Boozer: Phys. Rev. Lett **45**, 720 (1980).
[42] D. F. H. Start, J. G. Cordey and E. M. Jones: Plasma Phys. **22**, 303 (1980).
[43] K. Okano: Nucl. Fusion **30**, 423 (1990).
[44] R. J. Bickerton, J. W. Connor and J. B. Taylor: Nature Physical Science **229**, 110 (1971)
A. A. Galeev: Sov. Phys. JETP **32**, 752 (1971)
[45] M. N. Rosenbluth, R. D. Hazeltine and F. L. Hinton: Phys.Fluids **15**, 116 (1972)
D. J. Sigmar: Nucl. Fusion **13**, 17 (1973)
[46] T. Ozeki, M. Azumi, S. Tokuda, S. Ishida: Nucl. Fusion **33**, 1025, (1993)
[47] P. H. Rutherford: Phys. Fluids **16**, 1903, (1973)
[48] R. Fitzpatrick: Phys. Plasmas **2**, 825, (1995)
[49] D. A. Gates, B. Lloyd, A. W. Morris, G. McArdle, M. R. O'Brien *et.al.*: Nucl. Fusion **37**, 1593, (1997)
[50] J. M. Finn: Phys. Plasmas **2**, 198, (1995)
[51] D. J. Ward, A. Bondeson: Phys. Plasmas: **2**, 1570, (1995)
[52] M. Okabayashi, N. Pomphrey, R. E. Hatcher: Nucl. Fusion **38**, 1607, (1998)
[53] J. A. Wesson: Nucl. Fusion **18**, 87, (1978)
[54] T. Fujita, S. Ide, Y. Kamada, T. Suzuki, T. Oikawa et al.: Phys. Rev. Lett. **87**, 085001 (2001).
[55] P. A. Politzer, A. W. Hyatt, T. C. Luce, F. W. Perkins, R. Prater et al.: Nucl. Fusion **45**, 417 (2005).
[56] J. L. Luxon: Nucl. Fusion **42**, 614 (2002).
[57] M. Okabayashi, J. Bialek, A. Bodeson, M. S. Chance, M. S. Chu et al.: 20th IAEA Fusion Energy Conf. (Vilamoura 2004) EX/3-1Ra.
H. Reimerdes, J. Bialek, M. S. Chance, M. S. Chu, A. M. Garofalo et al.: 20th IAEA Fusion Energy Conf. (Vilamoura 2004) EX/3-1Rb.
[58] H. Zohn: Plasma Phys. Contr. Fusion **38**, 105 (1996).
[59] J. W. Connor: Plasma Phys. Contr. Fusion **40** 191 (1998).
M. Becoulet, G. Huysmans, Y. Sarazin, X. Garbet, Ph Ghendrih et al.: Plasma Phys. Control. Fusion **45**, A93 (2003).
[60] Y. Kamada, T. Oikawa, L. Lao, T. Takizuka, T. Hatae et al.: Plasma Phys. Contrl. Fusion **42**, A247 (2000).
[61] P. T. Lang, A. Kallenbach, J. Bucalossi, G. D. Conway, A. Degeling et al. (ASDEX-U Team): 20th IAEA Fusion Energy Conf. (Vilamoura 2004) EX/2-6.
[62] R. Yoshino, Y. Neyatani, N. Isei, A. Tanga, D. J.Cambell et al.: Plasma Phys. Contr. Nucl. Fusion Res. (Conf. Proceedings, Seville 1994) vol. **1**, 685, (1995) IAEA, Vienna.
R. Yoshino, T. Kondoh, Y. Neyatani, K. Itami, Y. Kawano, and N. Isei: Plasma Phys. Contr. Fusion **39**, 313 (1997).
[63] G. Pautasso, K. Büchl, J. C. Fuchs, O. Gruber, A. Herrmann et al.: Nucl. Fusion **36**, 1291 (1996).
[64] D. G. Whyte T. C. Jernigan, D. A. Humphreys, A. W. Hyatt, C. J. Lasnier et al: Phys. Rev. Lett. **89**, 055001 (2002).
[65] ITER Team: ITER: Plasma Phys. Contr. Nucl. Fusion Res. (Conf. Proceedings, Washington D.C. 1990) vol. **3**, 413, (1991) IAEA, Vienna.
[66] K. Miyamoto: J. Plasma Fusion Res. **76**, 166 (2000).
[67] R. Aymar, V. Chuyanov, M. Huguet, and Y. Shimonura: 18th IAEA Fusion Energy Conf. (Sorrento 2000) OV/1.
Technical Bases for the ITER-FEAT Outline Design Dec. 1999 (Draft for TAC Review).
M. Shimada, V. Mukhavatov, G. Federici, Y. Gribov, A. Kukushkin et al: 19th IAEA Fusion Energy Conf. (Lyon in 2002) CT-2.
[68] INTOR Team: International Tokamak Reactor - Phase Two A Part l. Nucl Fusion **23**, 1513 (1983).
[69] Y. K.M. Peng, and D. J. Strickler: Nucl. Fusion **26**, 769 (1986).
[70] D. A. Gates, R. Akers, L. Appel, P. G. Carolan, N. Conway et al.: Phys. Plasmas **5**, 1775 (1988).
[71] D. C. Robinson: Plasma Phys. Contrl. Fusion **41**, A143 (1999).
[72] B. P. LeBlanc, R. E. Bell, S. M. Kaye, D. Stutman, M. G. Bell et al.: Nucl. Fusion **44**, 513 (2004).
M. Ono, M. G. Bell, R. E. Bell, T. Bigelow, M. Bitter et al.: Plasma Phys. Control. Fusion **45**, A335 (2003).
[73] R. J. Akers, J. W. Ahn, G Y Antar, L. C. Appel, D. Applegate *et. al.*: Plasma Phys. Contr. Fusion **45**, A175 (2003).

[74] H. R. Wilson, G. Voss, J-W Ahn, R. J. Akers, L. Appel et al.: 19th IAEA Fusion Energy Conf. (Lyon 2002) FT/1-5.
R. J. Akers, A. Bond, R. J. Buttery, P. C. Carolan, G. F. Counsell et al.: Nucl. Fusion **40**, 1223 (2000).
[75] F. Najmabadi, S. Jardin, M. Tillack, R. Miller, T. K. Mau et. al.: 17th IAEA Fusion Energy Conf. (Yokohama 1998) FTP-08.
[76] M. Ono, M. Peng, C. Kessel, C. Neumeyer, J. Schmidt et al.: Nucl. Fusion **44**, 452 (2004).
[77] . Nishio, K. Tobita, S. Konishi, T. Ando, S. Hiroki et al.: 19th IAEA Fusion Energy Conf. (Lyon 2002) FT/P1-21.
S. Nishio, K. Tobita, K. Tokimatsu, K. Shinya, I. Senda et al.: 20th IAEA Fusion Energy Conf. (Vilamoura 2004) FT/P7-35.
[78] K. Tobita, S. Nishio, M. Enoeda, M. Sato, T. Isono et al.: Fusion Eng. Des. **81**, 1151 (2006).
[79] S. Shiraiwa, S. Ide et al.: Phys. Rev. Lett. **92**, 035001 (2004).
Y. Takase, T. Fukuda, G. Xiang, M. Gyaznevich, S. Ide et al. J. Plasma Fusion Res. **78**, 719 (2002).
[80] R. L. Miller, Y. R. Lin-Liu, A. D. Turnbull and V. S. Chan et. al.: Phys. Plasmas **4**, 1062 (1997).
C. P. C. Wong, and R. D. Stambaugh: Fusion Eng. Des. **51-52**, 387 (2000).
Y. R. Lin-Liu and R. D. Stambaugh: Nucl. Fusion **44**, 548 (2004).
[81] S. Ishida, P. Barabaschi, Y. Kamada and the JT-60SA Team: 23rd IAEA Fusion Energy Conf. (Daejeon, 2010) OV/P-4.

Ch.17 Non-Tokamak Confinement System

17.1 Reversed Field Pinch

17.1a Reversed Field Pinch Configuration

Reversed field pinch (RFP) is an axisymmetric toroidal field used as a tokamak. The magnetic field configuration is composed of the poloidal field $B_{\rm p}$ produced by the toroidal component of the plasma current and the toroidal field $B_{\rm t}$ produced by the external toroidal field coil and the poloidal component of the plasma current. The particle orbit loss is as small as that of tokamak. However, RFP and tokamaks have quite different characteristics. In RFP, the magnitudes of the poloidal field $B_{\rm p}$ and the toroidal field $B_{\rm t}$ are comparable and the safety factor

$$q_{\rm s}(r) = \frac{r}{R}\frac{B_z(r)}{B_\theta(r)}$$

is much less than 1 ($q_{\rm s}(0) \sim a/(R\Theta)$, $\Theta \sim 1.6$). The radial profile of the toroidal field is shown in fig.17.1. The direction of the boundary toroidal field is reversed with respect to the direction of the on-axis field, and the magnetic shear is strong. Therefore high-beta ($\langle\beta\rangle = 10 \sim 20\%$) plasmas can be confined in an MHD stable way. Since the plasma current can be larger than the Kruskal-Shafranov limit ($q < 1$), there is a possibility of reaching the ignition condition by ohmic heating only (although it depends on the confinement scaling).

RFP started in an early phase of nuclear fusion research. A stable quiescent phase of discharge was found in Zeta in Harwell in 1968 (ref.[1]). The configuration of the magnetic field in the quiescent phase was the reversed field pinch configuration, as shown in fig.17.1. The electron temperature, the energy confinement time, and the average beta of Zeta were $\kappa T_{\rm e} = 100 \sim 150$eV, $\tau_{\rm E} =$ 2ms, $\langle\beta\rangle \sim 10\%$ at the time of IAEA conference at Novosibirsk. However, the epoch-making result of tokamak T-3 ($\kappa T_{\rm e} = 1$keV, $\tau_{\rm E} =$ several ms, $\beta \sim 0.2\,\%$) was also presented in the same conference, and Zeta was shut down because of the better confinement characteristics in tokamaks. On the other hand, RFP can confine higher beta plasma and has been actively investigated to improve the confinement characteristics (ZT-40 M, OHTE, HBTX1-B, TPE-1RM 20, MST and RFX, TPE-RX) (ref.[2]-[5]). The important issues of RFP are confinement scaling and impurity control in the high-temperature region.

17.1b Taylor's Relaxation Theory

Even if the plasma is initially MHD unstable in the formation phase, it has been observed in RFP experiments that the plasma turns out to be a stable RFP configuration irrespective of the initial condition. J.B.Taylor pointed out in 1974 that RFP configuration is a minimum energy state by relaxation processes under certain constraints (ref.[6]).

Let us introduce a physical quantity "*magnetic helicity*" for the study of this subject. By use of scalar and vector potentials ϕ, $\boldsymbol{A}$ of electric and magnetic field $\boldsymbol{E}$, $\boldsymbol{B}$, the magnetic helicity K is defined by the integral of the scalar product $\boldsymbol{A}\cdot\boldsymbol{B}$ over the volume V surrounded by a magnetic surface

$$K = \int_V \boldsymbol{A}\cdot\boldsymbol{B}\mathrm{d}\boldsymbol{r} \tag{17.1}$$

where $\mathrm{d}\boldsymbol{r} \equiv \mathrm{d}x\,\mathrm{d}y\,\mathrm{d}z$. Since

$$\boldsymbol{E} = -\nabla\phi - \frac{\partial \boldsymbol{A}}{\partial t}, \qquad \boldsymbol{B} = \nabla\times\boldsymbol{A}$$

we find from Maxwell equations that (ref.[7])

$$\frac{\partial}{\partial t}(\boldsymbol{A}\cdot\boldsymbol{B}) = \frac{\partial \boldsymbol{A}}{\partial t}\cdot\boldsymbol{B} + \boldsymbol{A}\cdot\frac{\partial \boldsymbol{B}}{\partial t} = (-\boldsymbol{E}-\nabla\phi)\cdot\boldsymbol{B} - \boldsymbol{A}\cdot(\nabla\times\boldsymbol{E})$$

$$= -\boldsymbol{E}\cdot\boldsymbol{B} - \nabla\cdot(\phi\boldsymbol{B}) + \nabla\cdot(\boldsymbol{A}\times\boldsymbol{E}) - \boldsymbol{E}\cdot(\nabla\times\boldsymbol{A})$$

$$= -\nabla \cdot (\phi \boldsymbol{B} + \boldsymbol{E} \times \boldsymbol{A}) - 2(\boldsymbol{E} \cdot \boldsymbol{B}).$$

When the plasma is surrounded by a perfect conductive wall, then the conditions $(\boldsymbol{B} \cdot \boldsymbol{n}) = 0$, $\boldsymbol{E} \times \boldsymbol{n} = 0$ are hold ($\boldsymbol{n}$ is unit outward vector normal to the wall), so that we find

$$\frac{\partial K}{\partial t} = \frac{\partial}{\partial t} \int_V \boldsymbol{A} \cdot \boldsymbol{B} \mathrm{d}\boldsymbol{r} = -2 \int_V \boldsymbol{E} \cdot \boldsymbol{B} \mathrm{d}\boldsymbol{r}. \tag{17.2}$$

The right-hand side in (17.2) is the loss term of the magnetic helicity. When the Ohm's law

$$\boldsymbol{E} + \boldsymbol{v} \times \boldsymbol{B} = \eta \boldsymbol{j}$$

is applicable, the loss term is reduced to

$$\frac{\partial K}{\partial t} = -2 \int_V \eta \boldsymbol{j} \cdot \boldsymbol{B} \mathrm{d}\boldsymbol{r}. \tag{17.3}$$

When $\eta = 0$, the magnetic helicity is conserved; in other words, if a plasma is perfectly conductive, K integral over the volume surrounded by arbitrary closed magnetic surfaces is constant. However, if there is small resistivity in the plasma, the local reconnections of the lines of magnetic force are possible and the plasma can relax to a more stable state and the magnetic helicity may change locally. But J. B. Taylor postulates that the global magnetic helicity K_T integrated over the whole region of the plasma changes much more slowly. It is assumed that K_T is constant within the time scale of relaxation processes. Under the constraint of K_T invariant

$$\delta K_\mathrm{T} = \int \boldsymbol{B} \cdot \delta \boldsymbol{A} \mathrm{d}\boldsymbol{r} + \int \delta \boldsymbol{B} \cdot \boldsymbol{A} \mathrm{d}\boldsymbol{r} = 2 \int \boldsymbol{B} \cdot \delta \boldsymbol{A} \mathrm{d}\boldsymbol{r} = 0$$

the condition of minimum energy of magnetic field

$$(2\mu_0)^{-1} \delta \int (\boldsymbol{B} \cdot \boldsymbol{B}) \, \mathrm{d}\boldsymbol{r} = \mu_0^{-1} \int \boldsymbol{B} \cdot \nabla \times \delta \boldsymbol{A} \mathrm{d}\boldsymbol{r} = \mu_0^{-1} \int (\nabla \times \boldsymbol{B}) \cdot \delta \boldsymbol{A} \mathrm{d}\boldsymbol{r}$$

can be obtained by the method of undetermined multipliers, and we have

$$\nabla \times \boldsymbol{B} - \lambda \boldsymbol{B} = 0. \tag{17.4}$$

This solution is the minimum energy state in the force-free or pressureless plasma ($\boldsymbol{j} \times \boldsymbol{B} = \nabla p = 0$, $\boldsymbol{j} \| \boldsymbol{B}$). The axisymmetric solution in cylindrical coordinates is

$$B_r = 0, \qquad B_\theta = B_0 J_1(\lambda r), \qquad B_z = B_0 J_0(\lambda r) \tag{17.5}$$

and is called a *Besssel function model*. The profiles of $B_\theta(r)$ and $B_z(r)$ are shown in fig.17.1(a). In the region $\lambda r > 2.405$, the toroidal field B_z is reversed. The pinch parameter Θ and the field reversal ratio F are used commonly to characterize the RFP magnetic field as follows:

$$\Theta \equiv \frac{B_\theta(a)}{\langle B_z \rangle} = \frac{(\mu_0/2) I_\mathrm{p} a}{\int B_z 2\pi r \, \mathrm{d}r}, \qquad F \equiv \frac{B_z(a)}{\langle B_z \rangle}$$

where $\langle B_z \rangle$ is the volume average of the toroidal field. The values of F and Θ for the Bessel function model are

$$\Theta = \frac{\lambda a}{2}, \qquad F = \frac{\Theta J_0(2\Theta)}{J_1(2\Theta)} \tag{17.6}$$

and the F-Θ curve is plotted in fig.17.1(b). The quantity

$$\lambda = \frac{\mu_0 \boldsymbol{j} \cdot \boldsymbol{B}}{B^2} = \frac{(\nabla \times \boldsymbol{B}) \cdot \boldsymbol{B}}{B^2} = \text{const.}$$

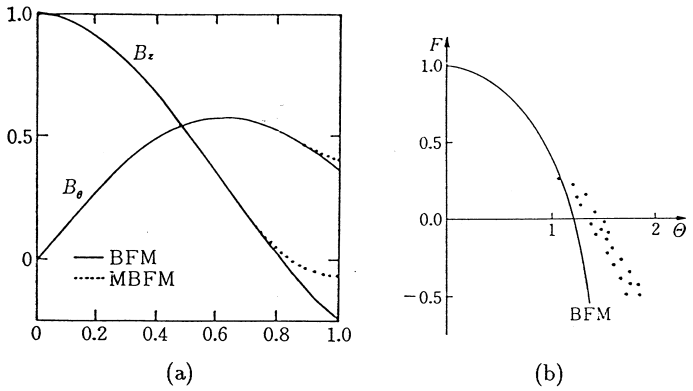

Fig.17.1 (a) Toroidal field $B_z(r)$ and poloidal field $B_\theta(r)$ of RFP. The radial profiles of the Bessel function model (BFM) and the modified Bessel function model (MBFM) are shown. (b) F-Θ curve

is constant in Taylor model. The observed RFP fields in experiments deviate from the Bessel function model due to the finite beta effect and the imperfect relaxation state. The λ value is no longer constant in the outer region of plasma and tends to 0 in the boundary. The solution of $\nabla \times \boldsymbol{B} - \lambda \boldsymbol{B} = 0$ with $\lambda(r)$ is called modified Bessel Function model (MBFM).

The stability condition of the local MHD mode (ref.[8]) is

$$\frac{1}{4}\left(\frac{q_s'}{q_s}\right)^2 + \frac{2\mu_0 p'}{rB_z^2}(1 - q_s^2) > 0.$$

This formula indicates that the strong shear can stabilize the RFP plasma in the $p'(r) < 0$ region but that the flat pressure profile, $p'(r) \sim 0$, is preferable in the central region of weak shear. When $q_s^2 < 1$, the local MHD mode is unstable near $q_s' = 0$ (*pitch minimum*).

When the effect of finite resistivity of a plasma is taken into account, it is expected by the classical process of magnetic dissipation that the RFP configuration can be sustained only during the period of $\tau_{\rm cl} = \mu_0 \sigma a^2$, where σ is the specific conductivity. However, ZT-40M experiments[9] demonstarated that RFP discharge was sustained more than three times ($\sim 20\,$ms) as long as $\tau_{\rm cl}$. This is clear evidence that the regeneration process of the toroidal flux exists during the relaxation process, which is consumed by classical magnetic dissipation, so that that the RFP configuration can be sustained as long as the plasma current is sustained.

17.1c Relaxation Process

As the electron temperature in the core of RFP plasma is higher than in the outer region and the parallel component of inductive toroidal electric field to the magnetic field line is large in the core region compared with the outer region (even reversed in the edge region due to RFP configuration), the current profile tends to be a peaked one. The $m = 1$ modes become unstable and relaxation phenomena occurs like the internal disruption of tokamak. But the physical process is quite different from the Kadomtsev type one.

When the current profile is peaked and $q(0)$ becomes below $1/n$, global non-linear deformation of the flux surface builds up the antiparallel radial components of the magnetic field near the separatrix on the rear side of the displacement. Then the non-linear driven reconnection starts to develop. According to the topology of magnetic flux, the rational surface appears and the $q(0)$ value increases larger than $1/n$ after reconnection (refer to fig.17.2). The current profile becomes more flat and the RFP plasma is relaxed to a more stable state. The time variation of $q(0)$, which was measured in REPUTE RFP plasma (ref.[9]), is consistent with this scenario. If Kadomtsev type reconnection happens in RFP $q(r)$ profile (reversed shear) configuration, the $q(0)$ value decreases after the reconnection and current profile is more peaked according to the topology of the magnetic flux. Then $m = 1$ global mode becomes unstable.

Studies of full MHD non-linear simulations have been done extensively (ref.[10],[11]). Contour

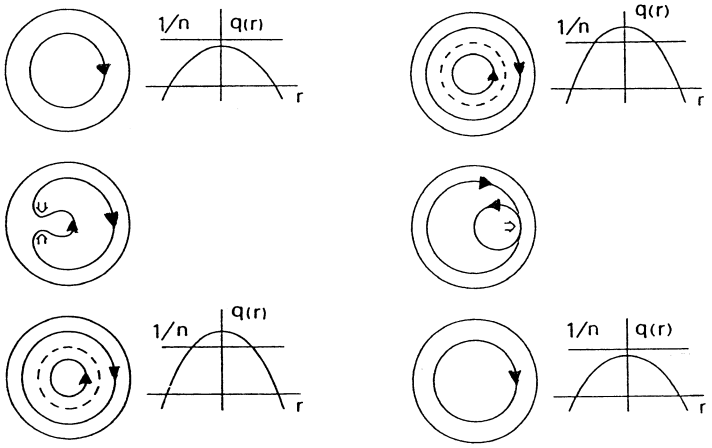

Fig.17.2 Driven reconnection by $m = 1$ global mode (left-hand side) and Kadomtsev type reconnction by tearing mode at the rational surface (right-hand side).

plots of the helical flux for $m/n = 1/5$ mode which are extracted from mutiple helicity simulation are shown in fig.17.3 (ref.[10]). As is evident in this figure, the occurrence of helical driven reconnection is observed in the period of $12\sim 20\tau_{\rm A}$ (Alfvén transit time). In the multiple helicity relaxation, unstable $m = 1$ modes with different n feed most of their energy to (0,1) mode by non-linear coupling and axisymmetric non-linear reconnection of the $m = 0$ islands play a more dominant role in the relaxation process than helical non-linear reconnection of $m = 1$ islands. In the helical non-linear reconnection, the reconnection line is the helical line and the converging flow leads reconnection. After the reconnection, the magnetic fields with toroidal and poloidal components is created. In the axisymmetric non-linear driven reconnection, the reconnection line is a poloidal ring and toroidal field only is created by axisymmetric reconnection. The latter process is more efficient for the generation of axisymmetric reversed field (positive field in the inner region and reversed field in the outer region of rational surface).

When there are fluctuations in plasmas, the magnetic field $\boldsymbol{B}$ in the plasma is expressed by the sum $\boldsymbol{B} = \langle \boldsymbol{B} \rangle_{\rm t} + \tilde{\boldsymbol{B}}$ of the time average $\langle \boldsymbol{B} \rangle_{\rm t}$ and the fluctuation term $\tilde{\boldsymbol{B}}$. The time average of Ohm's law (5.21)

$$\boldsymbol{E} + \left(\boldsymbol{v} - \frac{\boldsymbol{j}}{en_{\rm e}} \right) \times \boldsymbol{B} + \frac{1}{en_{\rm e}} \nabla p_{\rm e} = \eta \boldsymbol{j}$$

is reduced to

$$\langle \boldsymbol{E} \rangle_{\rm t} + \langle \boldsymbol{v} \rangle_{\rm t} \times \langle \boldsymbol{B} \rangle_{\rm t} + \langle \tilde{\boldsymbol{v}} \times \tilde{\boldsymbol{B}} \rangle_{\rm t} - \frac{1}{en_{\rm e}} \langle \tilde{\boldsymbol{j}} \times \tilde{\boldsymbol{B}} \rangle = \langle \eta \boldsymbol{j} \rangle_{\rm t} \tag{17.7}$$

where $\langle \ \ \rangle_{\rm t}$ denotes the time average. New terms appear due to fluctuations. The third term in the left-hand side of (17.7) is called MHD dynamo and the forth term is called Hall dynamo (ref.[12]). Since the time average of the toroidal flux $\Phi_z = \int B_z {\rm d}S$ within the plasma cross-section is constant during quasi-stationary state, the time average of the electric field in θ direction is ($\oint E_\theta {\rm d}l = -{\rm d}\Phi_z/{\rm d}t = 0$) and $\langle \boldsymbol{v}_r \rangle_{\rm t} = 0$. Steady-state RFP plasmas require the following condition:

$$\langle \eta j_\theta \rangle_{\rm t} = \langle (\tilde{\boldsymbol{v}} \times \tilde{\boldsymbol{B}})_\theta \rangle_{\rm t} - \frac{1}{en_{\rm e}} \langle (\tilde{\boldsymbol{j}} \times \tilde{\boldsymbol{B}})_\theta \rangle_{\rm t}. \tag{17.8}$$

In other words, resistive dissipation is compensated for by the effective electric field due to the fluctuations. This process is called *dynamo mechanism*.

When electron mean free path is very long, local relations such as Ohm's law may not be applicable. Instead of MHD dynamo theory, kinetic dynamo theory was proposed in (ref.[13]), in which anomalous transport of electron momentum across magnetic surfaces plays an essential role in sustaining RFP configuration.

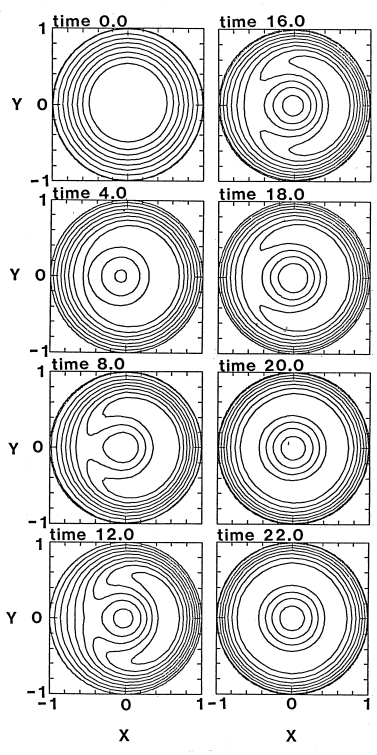

Fig.17.3 Contour plots of the helical flux of helicity $m = 1, n = 5$ mode which are extracted from mutiple helicity simulation. $\tau_{\rm A}$ is Alfvén transit time (ref.[10]).

Magnetic fluctuations of dynamo sustaining the poloidal plasma current, on the other hand, enhance the electron diffusion, since the electron diffusion coefficient is given by $D_{\rm e} \sim v_{\rm Te} a \langle (\delta B_r/B)^2 \rangle$ and the energy confinement of RFP is deteriorated.

17.1d Confinement of RFP

The energy confinement time $\tau_{\rm E}$ in an ohmically heated plasma can be obtained by energy balance equation

$$\frac{(3/2)\langle n\kappa(T_{\rm e}+T_{\rm i})\rangle_{\rm v} 2\pi R\pi a^2}{\tau_{\rm E}} = V_z I_{\rm p}$$

where V_z is the loop voltage and $I_{\rm p}$ is the plasma current. The notation $\langle\ \ \rangle_{\rm v}$ means the volume average. Using the definition of the poloidal beta

$$\beta_\theta \equiv \frac{\langle n\kappa(T_{\rm e}+T_{\rm i})\rangle_{\rm v}}{B_\theta^2/2\mu_0} = \frac{8\pi^2 a^2 \langle n\kappa(T_{\rm e}+T_{\rm i})\rangle_{\rm v}}{\mu_0 I_{\rm p}^2}$$

the energy confinement time is given by

$$\tau_{\rm E} = \frac{3\mu_0}{8} R\beta_\theta \frac{I_{\rm p}}{V_z}. \tag{17.9}$$

Therefore the scalings of β_θ and V_z are necessary for the scaling of $\tau_{\rm E}$. In order to apply a loop voltage on RFP plasma, a cut in the toroidal direction is necessary in the shell conductor surrounding the plasma. In this case, the contribution of surface integral must be added in (17.1) of magnetic helicity as follows:

$$\frac{\partial K}{\partial t} = -2\int \boldsymbol{E}\cdot\boldsymbol{B}\,{\rm d}\boldsymbol{r} - \int (\phi\boldsymbol{B} + \boldsymbol{E}\times\boldsymbol{A})\cdot\boldsymbol{n}\,{\rm d}S.$$

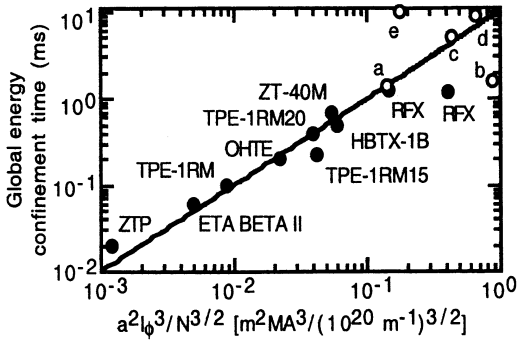

Fig.17.4 Scaling of energy confinement time of RFP in standard operation. I_ϕ in the figure is equivalent to I_p (ref.[15]).

The induced electric field in the (conductive) shell surface is zero and is concentrated between the both edge of shell cut. The surface integral consists of the contribution $2V_z\Phi_z$ from the shell cut and the contribution from the other part of surface S_-, that is,

$$\frac{\partial K}{\partial t} = -2\int \eta \boldsymbol{j}\cdot\boldsymbol{B}\,\mathrm{d}\boldsymbol{r} + 2V_z\Phi_z - \int_{\mathrm{S}_-}(\phi\boldsymbol{B}+\boldsymbol{E}\times\boldsymbol{A})\cdot\boldsymbol{n}\,\mathrm{d}S \tag{17.10}$$

where Φ_z is the volume average of toroidal magnetic flux $\Phi_z = \pi a^2\langle B_z\rangle_\mathrm{v}$. In quasi-steady state, the time average $\langle\partial K/\partial t\rangle_\mathrm{t}$ is zero. Then the time average of (17.2) yields

$$V_z = \frac{\int\langle\eta\boldsymbol{j}\cdot\boldsymbol{B}\rangle_\mathrm{t}\mathrm{d}\boldsymbol{r} + (1/2)\int_{\mathrm{S}_-}\langle\phi\boldsymbol{B}+\boldsymbol{E}\times\boldsymbol{A}\rangle_\mathrm{t}\cdot\boldsymbol{n}\,\mathrm{d}S}{\langle\Phi_z\rangle_\mathrm{t}}$$

$$= \frac{2\pi R}{\pi a^2}\eta_0 I_\mathrm{p}\zeta + V_\mathrm{B},$$

$$V_\mathrm{B} = \frac{2\pi R}{a}\frac{\langle\langle(\phi\boldsymbol{B}+\boldsymbol{E}\times\boldsymbol{A})\cdot\boldsymbol{n}\rangle_\mathrm{t}\rangle_{\mathrm{S}_-}}{\langle\langle B_z\rangle_\mathrm{t}\rangle_\mathrm{v}}$$

where $\langle\ \ \rangle_{\mathrm{S}_-}$ is the average in the surface region S_-. The notation ζ is a non-dimensional factor determined by the radial profiles of specific resistivity and magnetic field as follows:

$$\zeta \equiv \frac{\langle\langle\eta\boldsymbol{j}\cdot\boldsymbol{B}\rangle_\mathrm{t}\rangle_\mathrm{v}}{\eta_0\langle\langle j_z\rangle_\mathrm{t}\rangle_\mathrm{v}\langle\langle B_z\rangle_\mathrm{t}\rangle_\mathrm{v}} = \frac{\langle\langle\eta\boldsymbol{j}\rangle_\mathrm{t}\cdot\langle\boldsymbol{B}\rangle_\mathrm{t}\rangle_\mathrm{v} + \langle\langle\widetilde{(\eta\boldsymbol{j})}\cdot\widetilde{\boldsymbol{B}}\rangle_\mathrm{t}\rangle_\mathrm{v}}{\eta_0\langle\langle j_z\rangle_\mathrm{t}\rangle_\mathrm{v}\langle\langle B_z\rangle_\mathrm{t}\rangle_\mathrm{v}}.$$

Here η_0 is the specific resistivity at the plasma center. When the term of fluctuation is negligible, the value ζ of modified Bessel function model is $\zeta\sim 10$, but the value is generally $\zeta > 10$ due to fluctuation. The value of V_B is 0 when whole plasma boundary is conductive shell. In reality, plasma boundary is liner or protecting material for the liner. Lines of magnetic force can cross the wall by the magnetic fluctuation or shift of plasma position ($\boldsymbol{B}\cdot\boldsymbol{n}\neq 0$, $\boldsymbol{E}\neq 0$). Then the term V_B has a finite value. The substitution of V_z into the equation of energy confinement time τ_E gives

$$\tau_\mathrm{E} = \frac{3}{8}\beta_\theta\left(\frac{\mu_0 a^2}{\eta_0}\frac{1}{2\zeta}\right)\left(1+\frac{V_\mathrm{B}/2\pi R}{aB_\theta(a)}\frac{\mu_0 a^2}{\eta_0}\frac{1}{2\zeta}\right)^{-1}.$$

When plasmas become hot, the resistive term becomes small and the contribution of V_B is no longer negligible.

Energy confinement scaling of RFPs (ohmic heating only) was presented by ZT-40M group from

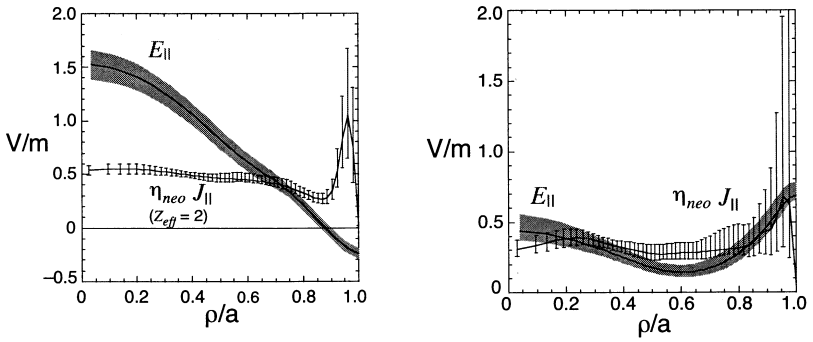

Fig.17.5 Radial profile of mean electric field and current density terms in Ohm's law for standard operation (left-hand side) and PPCD operation (right-hand side). The difference between the two curves indicates the dynamo effect (ref.[12]).

the data of ZT-40M, RFX, TPE-1RM and the others as follows (ref.[14]):

$$\tau_{\mathrm{E\,stand.}} = 10.2 a^2 I_{\mathrm{p}}^{1.5} \left(\frac{I_{\mathrm{p}}}{N}\right)^{1.5}, \tag{17.11}$$

where units are τ_{E}(ms), I_{p}(MA) and line density $N = \pi a^2 n_{\mathrm{e}}(10^{20}\mathrm{m}^{-1})$. I_{p}/N in (17.11) has been used as an important parameter to specify PFP plasmas, since the experiments of RFP started and is the same as the inverse of the normalized Greenwald density, that is, $I_{\mathrm{p}}/N = n_{\mathrm{G}}^{-1}$. I_{p}/N is usually larger than 2 and the lowest limit is 1 as tokamaks (ref.[16]). Experimental results of energy confinement time from various RFP devices are compared with the scaling (17.11) and are shown in fig.17.4 (ref.[14],[15]). Open circles in the figure are results of MST including improved confinement plasmas, which will described in the next paragraph.

Pulsed Parallel Current Drive (PPCD)

In recent years confinement has improved greatly in RFP through current density profile control. In standard operation of RFP, the parallel electric field to the magnetic field is strongly peaked in the center due to RFP configuration. The resulting peaked current density profile is unstable to tearing instability as well as global kink mode. The instabilities grow and force the current density profile to one that is less peaked through the robust reconnections. The magnetic fluctuations in the saturated state cause substantial anomalous transport. To improve confinement, the applied electric field is adjusted so that the plasma current induced by the electric field is less peaked, yielding a more stable plasma with smaller fluctuation. During a plasma discharge, an additional ohmic electric field is applied that has a strong parallel (mostly poloidal) component in the outer region of plasma, a technique that is often referred to as pulsed parallel current drive (PPCD). By PPCD, the energy confinement time of MST was doubled (2.2 ms) in 1994 (ref.[17]) and energy confinement time in PPCD improved up to 10 ms in 2001 (ref.[15]) and the dynamo strongly reduced.

The presence of the dynamo is most clearly seen through measurement of the terms in the parallel mean-field Ohm's law (ref.[12]). Figure 17.5 shows the measured radial profiles of the parallel electric field and current density terms in Ohm's law. In standard plasma (fig.17.5, left-hand side), the current density profile is much different than the electric field profile. In the core, current density is smaller than would be expected from the electric field, while in the edge the current density is directed opposite the electric field. A strong dynamo exists which drives current opposite to the electric field over much of the cross-section. In PCCD plasma (fig.17.5, right-hand side), the electric field profile changes substantially and, within experimental uncertainty, the current is fully accounted for by the applied electric field over most of the plasma cross-section.

Parameters of operating conditions and confinement properties in PCCD experiments of MST, RFX, and TPE-RX are listed in Table 17.1. Note for the plasma confined in MST with $\beta = 18\%$, $\tau_{\mathrm{E}} = 10$ ms listed in the second line of Table 17.1, the toroidal field at the plasma edge (field of TF coil) is only 0.024T.

Table 17.1 Parameters of operating conditions and confinement properties in PPCD experiments of MST, RFX, and TPE-RX.

	R/a	I_p	I_p/N	$\bar{n}_{\mathrm{e}\,20}$	$T_{\mathrm{e}\,0}/T_{\mathrm{i}\,0}$	F/Θ	β	τ_E	Ref.
MST	1.5/0.5	0.34	4.0	0.1	0.39/0.2	-0.65/2.2	9	5	[18]
MST	1.5/0.5	0.21	3.5	0.07	0.6/0.18	-2.1/3.5	18	10	[15]
MST	1.5/0.5	0.4	5.1	0.1	0.8/0.3			5	[19]
MST$^\mathrm{s}$	1.5/0.5	0.4	5.1	0.1	0.32/0.3			1	[19]
RFX	2/0.46	0.79	2.5	0.47	0.33/0.33	-0.20/1.5	6	1.9	[20]
TPE-RX	1.72/0.45	0.34	8.0	0.067	0.84/0.37	-0.69/2.0	9	3.5	[21]

Values are evaluated around the time when the energy confinement time has a peak value in PPCD period. Line density is evaluated by $N \equiv \bar{n}_\mathrm{e}\pi a^2$ where $\bar{n}_\mathrm{e}$ is line average electron density, as the profile of n_e is not available from the references. MST$^\mathrm{s}$ in the third line means standard operating conditions in MST. Units are R, a(m), I_p(MA), $I_\mathrm{p}/N(10^{-20}\mathrm{MA\,m})$, $\bar{n}_{\mathrm{e}\,20}(10^{20}\mathrm{m}^{-3})$, $T_{\mathrm{e}\,0}, T_{\mathrm{i}\,0}$(keV), $\beta(\%)$, τ_E(ms). Referred from ((ref.[19],[22]).

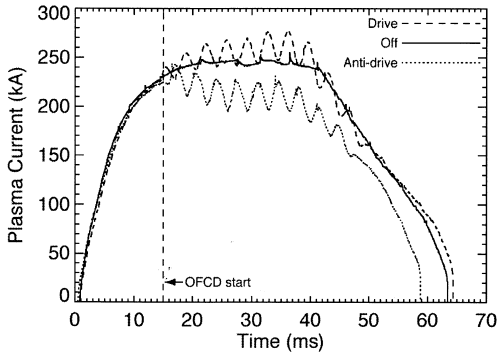

Fig.17.6 Plasma current vs. time for three cases. Oscillating field current drive (OFCD) with toloidal and poloidal loop voltages relative phases set for maximum helicity injection (dashed curve), OFCD with voltage phases set for maximum helicity removal, and OFCD off. After (ref.[12]).

It is desirable that pulsed parallel current drive is replaced by stationary current drive, and experiments of additional heating are accelerated in RFP researches.

Oscillating Field Current Drive

RFP plasmas tend to be MBFM due to non-linear phenomena of MHD relaxaton. Oscillating field current drive (OFCD) was proposed (ref.[23]) for sustaining the plasma current and preliminary experiments have been done (ref.[24]). More recently, experiment of OFCD is tested in MST (ref.[12]). The result is shown in fig.17.6. If terms V_z and Φ_z of the second term in the right-hand side of the magnetic helicity balance equation (17.11) are modulated as $V_z(t) = \tilde{V}_z \cos\omega t$, $\Phi_z(t) = \Phi_{z0} + \tilde{\Phi}_z \cos\omega t$, a time average of the product of $2V_z \cdot \Phi_z$ becomes $\tilde{V}_z\tilde{\Phi}_z$ and compensates the resistive loss of the magnetic helicity. The period of the oscillating field must be longer than the characteristic time of relaxation and must be shorter than magnetic diffusion time. The disturbing effect of the oscillating field to RFP plasma must be evaluated further.

17.2 Stellarator

A stellarator field can provide a steady-state magnetohydrodynamic equilibrium configuration of plasma only by the external field produced by the coils outside the plasma. The rotational transform, which is necessary to confine the toroidal plasma, is formed by the external coils so that the stellarator has the merit of steady-state confinement. Although Stellarator C (ref.[25]) was rebuilt as the ST tokamak in 1969, at the Princeton Plasma Physics Laboratory, confinement experiments by Wendelstein 7AS and large helical device LHD are being carried out, since there is a merit of steady-state confinement, without current-driven instabilities. Advanced stellarator WVII-X is under construction.

17.2a Helical Field

Let us consider a magnetic field of helical symmetry. By means of cylindrical coordinates $(r,\ \theta,\ z)$, we can express the field in terms of $(r,\ \varphi \equiv \theta - \delta\alpha z)$, where $\alpha > 0,\ \delta = \pm 1$. A magnetic field in a current-free region ($\boldsymbol{j} = 0$) can be expressed by a scalar potential ϕ_B, satisfying $\Delta\phi_B = 0$, and we can write

$$\phi_B = B_0 z + \frac{1}{\alpha}\sum_{l=1}^{\infty} b_l I_l(l\alpha r)\sin(l\varphi), \tag{17.12}$$

$$\varphi \equiv \theta - \delta\alpha z.$$

The field components $(B_r,\ B_\theta,\ B_z)$ of $\boldsymbol{B} = \nabla\phi_B$ are given by

$$B_r = \sum_{l=1}^{\infty} l b_l I_l'(l\alpha r)\sin(l\varphi), \tag{17.13}$$

$$B_\theta = \sum_{l=1}^{\infty}\left(\frac{1}{\alpha r}\right) l b_l I_l(l\alpha r)\cos(l\varphi), \tag{17.14}$$

$$B_z = B_0 - \delta\sum_{l=1}^{\infty} l b_l I_l(l\alpha r)\cos(l\varphi). \tag{17.15}$$

The vector potential corresponding to this field has components

$$A_r = -\frac{\delta}{\alpha^2 r}\sum_{l=1}^{\infty} b_l I_l(l\alpha r)\sin(l\varphi),$$

$$A_\theta = \frac{B_0}{2} r - \frac{\delta}{\alpha}\sum_{l=1}^{\infty} b_l I_l'(l\alpha r)\cos(l\varphi),$$

$$A_z = 0.$$

Using these, we can write

$$B_r = -\frac{\partial A_\theta}{\partial z}, \qquad B_\theta = \frac{\partial A_r}{\partial z}, \qquad B_z = \frac{1}{r}\frac{\partial (r A_\theta)}{\partial r} - \frac{1}{r}\frac{\partial A_r}{\partial \theta}.$$

The magnetic surface $\psi = A_z + \delta\alpha r A_\theta = \delta\alpha r A_\theta = \text{const.}$ is given by

$$\psi(r,\varphi) = B_0\frac{\delta\alpha r^2}{2} - r\sum_{l=1}^{\infty} b_l I_l'(l\alpha r)\cos(l\varphi) = \text{const.} \tag{17.16}$$

Such a helically symmetric field can be produced by a helical current distribution as is shown in fig.17.7.

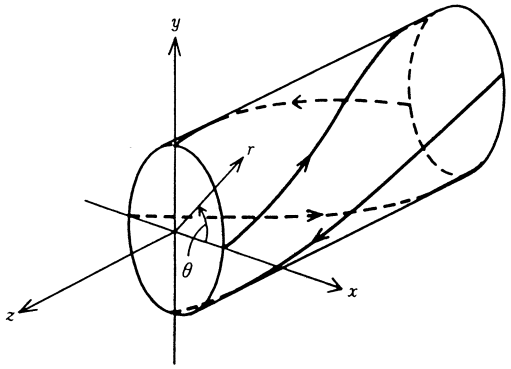

Fig.17.7 Current of helical coils

Let the magnetic fluxes in z and θ directions inside the magnetic surface be denoted by Φ and X (X is the integral over the pitch along z, i.e., over $2\pi/\alpha$); then these may be expressed by

$$\Phi = \int_0^{2\pi} \int_0^{r(\varphi)} B_z(r,\ \varphi) r \,\mathrm{d}r \,\mathrm{d}\theta,$$

$$X = \int_0^{2\pi/\alpha} \int_0^{r(\varphi)} B_\theta(r,\ \varphi) \,\mathrm{d}r \,\mathrm{d}z = \frac{1}{\alpha} \int_0^{2\pi} \int_0^{r(\varphi)} B_\theta(r,\ \varphi) \,\mathrm{d}r \,\mathrm{d}\theta.$$

Since $\alpha r B_z - \delta B_\theta = \alpha \partial (r A_\theta)/\partial r = \delta \partial \psi / \partial r$, we find that

$$\Phi - \delta X = 2\pi\psi/\delta\alpha.$$

Let us consider only one harmonic component of the field. The scalar potential and the magnetic surface are expressed by

$$\phi_B = B_0 z + \frac{b}{\alpha} I_l(l\alpha r) \sin(l\theta - \delta l \alpha z),$$

$$\psi = \frac{B_0}{2\delta\alpha} \left((\alpha r)^2 - \frac{2\delta(\alpha r) b}{B_0} I_l'(l\alpha r) \cos(l\theta - \delta l \alpha z) \right) = \frac{B_0}{2\delta\alpha} (\alpha r_0)^2.$$

The singular points $(r_\mathrm{s}, \theta_\mathrm{s})$ in the $z = 0$ plane are given by

$$\frac{\partial \psi}{\partial r} = 0, \qquad \frac{\partial \psi}{\partial \theta} = 0.$$

Since the modified Bessel function $I_l(x)$ satisfies

$$I_l''(x) + \frac{1}{x} I_l'(x) - \left(1 + \frac{l^2}{x^2} \right) I_l = 0,$$

the singular points are given by

$$\sin(l\theta_\mathrm{s}) = 0,$$

$$\alpha r \left(1 - \frac{\delta b l}{B_0} \left(1 + \frac{1}{(\alpha r_\mathrm{s})^2} \right) l_l(l\alpha r_\mathrm{s}) \cos(l\theta_\mathrm{s}) \right) = 0$$

or

$$\theta_\mathrm{s} = 2\pi(j-1)/l, \qquad \delta b / B_0 > 0,$$

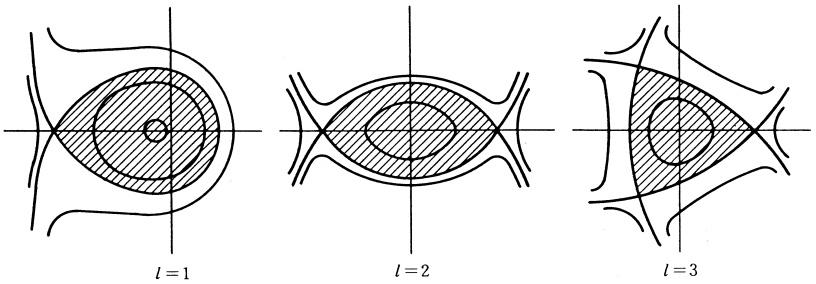

Fig.17.8 Magnetic surfaces, showing separatrix points and separatrices, of the helical field.

$$= 2\pi\left(j - \frac{1}{2}\right)/l, \qquad \delta b/B_0 < 0, \qquad j = 1, \cdots, l,$$

$$\left|\frac{\delta b l}{B_0}\right| = \frac{1}{(1 + (\alpha r_{\rm s})^{-2}) I_l(l\alpha r_{\rm s})}.$$

The magnetic surfaces for $l = 1,\ l = 2,\ l = 3$ are shown in fig.17.8. The magnetic surface which passes through the hyperbolic singular point is called *separatrices*. When $x \ll 1$, the modified Bessel function is

$$I_l(x) \approx \frac{1}{l!}\left(\frac{x}{2}\right)^l.$$

The magnetic surfaces in the region $\alpha r \ll 1$ is expressed by

$$(\alpha r)^2 - \frac{\delta b (l/2)^{l-1}}{B_0 (l-1)!}(\alpha r)^l \sin l(\theta - \delta\alpha z) = \text{const.}$$

The magnitude B is

$$\left(\frac{B}{B_0}\right)^2 = 1 - 2\frac{\delta l b}{B_0} I_l \cos(l\varphi) + \left(\frac{lb}{B_0}\right)^2 \left(I_l^2\left(1 + \frac{1}{(\alpha r)^2}\right)\cos^2(l\varphi) + (I_l')^2 \sin^2(l\varphi)\right).$$

The magnitude B at the separatrix $(r_{\rm s}, \theta_{\rm s})$ is

$$\left(\frac{B}{B_0}\right)^2 = 1 - \frac{(\alpha r)^2}{1 + (\alpha r)^2}$$

and B at the point $(r_{\rm s}, \theta_{\rm s} + \pi/l)$ is

$$\left(\frac{B}{B_0}\right)^2 = 1 + \frac{(\alpha r)^2}{1 + (\alpha r)^2}.$$

Therefore the magnitude B is small at the separatrix points. Let us estimate the rotational transform angle ι. As the line of magnetic force is expressed by

$$\frac{{\rm d}r}{B_r} = \frac{r{\rm d}\theta}{B_\theta} = \frac{{\rm d}z}{B_z}$$

the rotational transform angle is given by

$$\frac{r\iota}{2\pi R} = \left\langle \frac{r{\rm d}\theta}{{\rm d}z} \right\rangle = \left\langle \frac{B_\theta}{B_z} \right\rangle = \left\langle \frac{(1/\alpha r) l b I_l(l\alpha r)\cos l(\theta - \delta z)}{B_0 - l b I_l(l\alpha r)\cos l(\theta - \delta z)} \right\rangle.$$

Here r and θ are the values on the line of magnetic force and are functions of z and $\langle\ \ \rangle$ denotes the average over z. In a vaccum field, $\oint B_\theta {\rm d}l = \int (\nabla \times \boldsymbol{B}) \cdot {\rm d}\boldsymbol{S} = 0$ is holds, so that the rotational

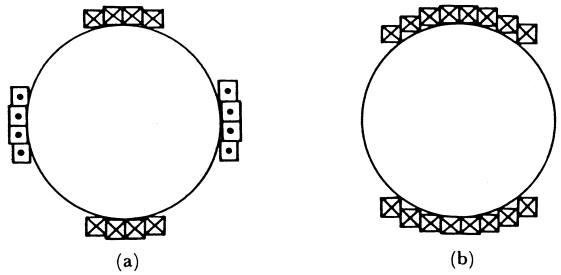

Fig.17.9 Cross-sectional views of helical coils in the $l = 2$ case. (a) standard stellarator. (b) heliotron/torsatron.

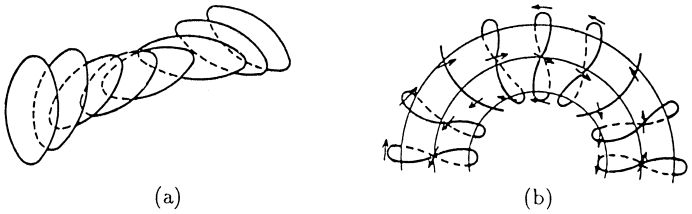

Fig.17.10 (a) Arrangement of elliptical coils used to produce an $l = 2$ linear helical field. (b) twisted toroidal coils that produce the $l = 2$ toroidal helical field.

transform angle is 0 in the first order of b/B_0. However the first order components of B_θ and B_z resonate to yield the resultant second order rotational transform angle. The average method gives the formula of the *rotational transform angle* (ref.[26],[27])

$$\frac{\iota}{2\pi} = \delta \left(\frac{b}{B}\right)^2 \frac{l^3}{2} \left(\frac{\mathrm{d}}{\mathrm{d}x}\left(\frac{I_l I_l'}{x}\right)\right)_{x=l\alpha r} \frac{R}{r}. \tag{17.17}$$

By use of the expansion

$$I_l(x) = \left(\frac{x}{2}\right)^l \left(\frac{1}{l!} + \frac{1}{(l+1)!}x^2 + \frac{1}{2!(l+2)!}x^4 + \cdots\right)$$

we find

$$\frac{\iota}{2\pi} = \delta \left(\frac{b}{B}\right)^2 \left(\frac{1}{2^l l!}\right)^2 l^5 (l-1)\alpha R \left((l\alpha r)^{2(l-2)} + \ldots\right). \qquad (l \geq 2) \tag{17.18}$$

An example of the analysis of toroidal helical field is given in the (ref.[28]).

17.2b Stellarator Devices

Familiar helical fields are of pole number $l = 2$ or $l = 3$. The three dimensional magnetic axis system of Heliac has l=1 component. When the ratio of the minor radius a_h of a helical coil to the helical pitch length R/m (R is the major radius and m is the number of field periods) is much less than 1, that is, $ma_h/R \ll 1$, the rotaional transform angle is $\iota_2(r) =$ const. for $l = 2$ and $\iota_3(r) = \iota(r/a)^2$ for $l = 3$. In this case the shear is small for the $l = 2$ configuration, and $\iota_3(r)$ is very small in the central region for the $l = 3$ configuration. However, if $ma_h/R \sim 1$, then $\iota_2(r) = \iota_0 + \iota_2(r/a)^2 + \cdots$, so that the shear can be large even when $l = 2$.

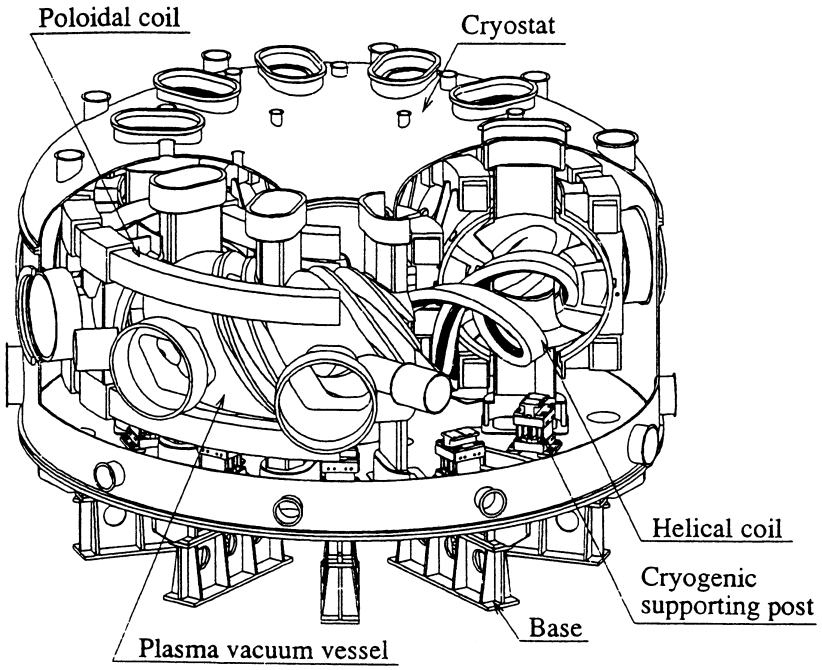

Fig.17.11 Schematic view of the LHD device in Toki (R=3.9m, $a \sim 0.6$m, B=3T).

The arrangement of coils in the $l = 2$ case is shown in fig.17.9. Figure 17.9 (a) is the standard type of stellarator (ref.[29],[30]), and fig.17.9(b) is a heliotron/torsatron type (ref.[31],[32]). Usually stellarator fields are produced by the toroidal field coils and the helical coils. In the heliotron/torsatron configuration the current directions of the helical coils are the same so that the toroidal field and the helical field can be produced by the helical coils alone by choosing an appropriate helical pitch (ref.[33],[34]) Therefore if the pitch is properly chosen, closed magnetic surfaces can be formed even without toroidal field coils (ref.[35],[36]). The typical devices of this type are Heliotron E, ATF and LHD. The device of LHD is shown in fig.17.11.

When elliptical coils are arranged as shown in fig.17.10(a), an l=2 helical field can be obtained (ref.[37]). The currents produced by the twisted toroidal coil system shown in fig.17.10(b) can simulate the currents of toroidal field coils and the helical coils taken together (ref.[38]). The typical devices of this modular coil type are Wendelstein 7AS and 7X. Modular coil system of Wendelstein 7X is shown in fig.17.12.

For linear helical fields the magnetic surface $\Psi = rA_\theta$ exists due to its helical symmetry. However, the existence of magnetic surfaces in toroidal helical fields has not yet been proven in the strict mathematical sense. According to numerical calculations, the magnetic surfaces exist in the central region near the magnetic axis, but in the outer region the lines of magnetic force behave ergodically and the magnetic surfaces are destroyed. Although the helical coils have a relatively complicated structure, the lines of magnetic force can be traced by computer, and the design of helical field devices becomes less elaborate. The effect of the geometrical error to the helical field can be estimated, and accurate coil windings are possible with numerically controlled devices ($\Delta l/R < 0.05 \sim 0.1\%$).

17.2c Neoclassical Diffusion in Helical Field

For the analysis of classical diffusion due to coulomb collision, the study of the orbit of charged particles is necessary. In a helical field or even in a tokamak toroidal field produced by finite number of coils, there is an asymmetric inhomogenous term in the magnitude B of magnetic field

$$\frac{B}{B_0} \approx 1 - \epsilon_{\rm h} \cos(l\theta - m\varphi) - \epsilon_t \cos\theta \tag{17.19}$$

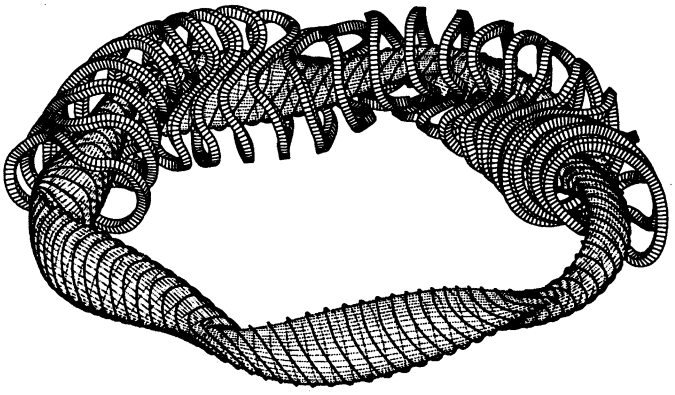

Fig.17.12 Modular coil system and a magnetic surface of the optimized stellerator Wendelstein 7-X in Greifswald (R=5.5m, a=0.55m, B=3T).

in addition to the toroidal term $-\epsilon_{\rm t}\cos\theta$. The variation of B along lines of magnetic force is shown in fig.17.13. Particles trapped by the inhomogeneous field of helical ripples drift across the magnetic surfaces and contribute to the particle diffusion in addition to the banana particles as was discussed in tokamak. The curvature of line of magnetic force near the helically trapped region is convex toward outward and is denoted by $R_{\rm h}, \epsilon_{\rm h} \approx r/R_{\rm h}$. Helically trapped particles drift in poloidal direction (θ direction) due to ∇B drift with the velocity of $v_{\rm h} \approx mv_{\perp}^2/(qBR_{\rm h})$ (see fig.17.14). The angular velocity of poloidal rotation is

$$w_{\rm h} = v_{\rm h}/r \approx (r/R_{\rm h})(kT/qBr^2). \tag{17.20}$$

Exact derivation is described in the paragraph 'precession of helical banana' in the end of this section 17.2. In the case of linear helical field ($\epsilon_{\rm t} = 0$), helically trapped particles rotate along the magnetic surface. However in the case of toroidal helical field, the toroidal drift is superposed and the toroidal drift velocity is $v_{\rm v} = kT/(qBR)$ in the vertical direction (see (3.40) in sec.3.5). When the effective collision time $(\nu_{\rm eff})^{-1} = (\nu/\epsilon_{\rm h})^{-1}$ is shorter than one period $(\omega_{\rm h})^{-1}$ of poloidal rotation, the deviation of orbit of helical banana from the magnetic surface is

$$\Delta_{\rm h1} = v_{\rm v}\frac{\epsilon_{\rm h}}{\nu} = \epsilon_{\rm h}\frac{kT}{qBR}\frac{1}{\nu}.$$

Then the coefficient of particle diffusion becomes (ref.[39])

$$D_{\rm h1} \sim \epsilon_{\rm h}^{1/2}\Delta_{\rm h1}^2\nu_{\rm eff} = \epsilon_{\rm h}^{3/2}\left(\frac{kT}{qBR}\right)^2\frac{1}{\nu} = \epsilon_t^2\epsilon_{\rm h}^{3/2}\left(\frac{kT}{qBr^2}\frac{1}{\nu}\right)\left(\frac{kT}{qB}\right).$$

Since $R_{\rm h} \sim r/\epsilon_{\rm h}$, the other expression is

$$D_{\rm h1} \sim \gamma_{\rm h}\epsilon_{\rm h}^{1/2}\epsilon_{\rm t}^2\left(\frac{\omega_{\rm h}}{\nu}\right)\left(\frac{kT}{qB}\right), \quad (\nu/\epsilon > \omega_{\rm h}) \tag{17.21}$$

where $\gamma_{\rm h}$ is a coefficient with the order of $O(1)$ (fig.17.15).

When the effective collision time $(\nu_{\rm eff})^{-1}$ is longer than $(\omega_{\rm h})^{-1}$, the deviation $\Delta_{\rm h2}$ of the orbit and the magnetic surface is

$$\Delta_{\rm h2} \approx v_{\rm v}/\omega_{\rm h} \approx \frac{R_{\rm h}}{R}r \sim \frac{\epsilon_{\rm t}}{\epsilon_{\rm h}}r,$$

and the $D_{\rm h2}$ becomes (fig.17.15)

$$D_{\rm h2} \approx \epsilon_{\rm h}^{1/2}\Delta_{\rm h2}^2\nu_{\rm eff} = \left(\frac{\epsilon_{\rm t}}{\epsilon_{\rm h}}\right)^2\frac{1}{\epsilon_{\rm h}^{1/2}}r^2\nu. \qquad (\nu/\epsilon_{\rm h} < \omega_{\rm h})$$

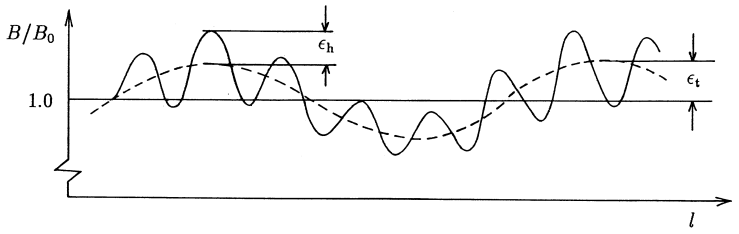

Fig.17.13 Variation of the magnitude B along the length l of line of magnetic force.

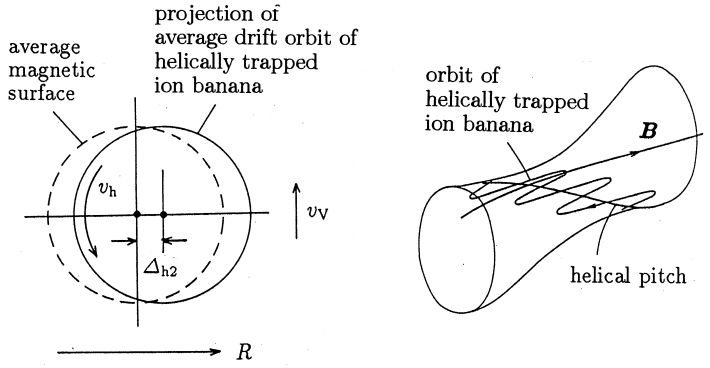

Fig.17.14 Orbit of helical banana ion trapped in helical ripple.

When a particle is barely trapped in a local helical mirror, the particle moves very slowly near the reflection point where the magnetic field is locally maximum and the field line is concave to outward. The effective curvature, which the particle feels in time average, becomes negative (concave). The orbit of the trapped particle in this case becomes so called *superbanana* (ref.[39]). However this theoretical treatment is based on the assumption of the longitudinal adiabatic invariant $J_{\|}$ =const. along the orbit of helically trapped particle. The adiabatic invariance is applicable when the poloidal rotation angle, during the one period of back and forth motion in the helical local mirror, is small. As the one period of back and forth motion of barely trapped particles becomes long, the adiabatic invariance may not be applicable in this case. The orbit trace by numerical calculations shows that the superbanana does not appear (ref.[40]) in the realistic case of $\epsilon_{\rm h} \sim \epsilon_{\rm t}$. If a particle orbit crosses the wall, the particle is lost. This is called orbit loss. A loss region in velocity space appears due to orbit loss in some case (ref.[41]) . When a radial electric field appears, the angular frequency of the poloidal drift rotation becomes $\omega_{\rm h} + \omega_{\rm E}$ ($\omega_{\rm E} = E_r/B_0$), the orbit is affected by the radial electric field.

The thermal diffusion coefficient $\chi_{\rm h1}$ due to helically trapped particles in the region of $\nu/\epsilon_{\rm h} > \omega_{\rm h}$ is given by

$$\chi_{\rm h1} \sim \gamma_{\rm T} \epsilon_{\rm t}^2 \epsilon_{\rm h}^{3/2} \left(\frac{kT}{qBr}\right)^2 \frac{1}{\nu}. \quad (\gamma_{\rm T} \sim 50) \tag{17.22}$$

Since $\nu \propto T^{-1.5}$, it means $\chi_{\rm h1} \propto T^{3.5}$. This may suggest that the thermal conduction loss becomes large in hot plasma and the suppression of helical ripple loss is very important (ref.[42]-[44]).

Since toroidal helical systems lose helical symmetry as well as axisymmetry, the generalized momentum correponding cyclic coordinate is not conserved (angular momentum $mr^2\dot{\theta} + qrA_\theta$ = const. for axisymmetric system $\boldsymbol{A}(r,z)$ and $m(\dot{z} + \alpha r^2\dot{\theta}) + q(A_z + \alpha r A_\theta)$ = const. for helically symmetric system $\boldsymbol{A}(r, \theta - \alpha z)$). Therefore, the orbit loss of energetic ions produced by heatings or fusion produced alpha particles with 3.5 MeV becomes large and the heating efficiencies may be deteriorated.

If quasi-symmetric stellarators are designed, particle orbits are quasi-closed due to the constant of motion. The neoclassical diffusion in classical stellarator field must be modified. There are active efforts to design quasi-axisymmetric, quasi-helically symmetric, and quasi-isodynamic or

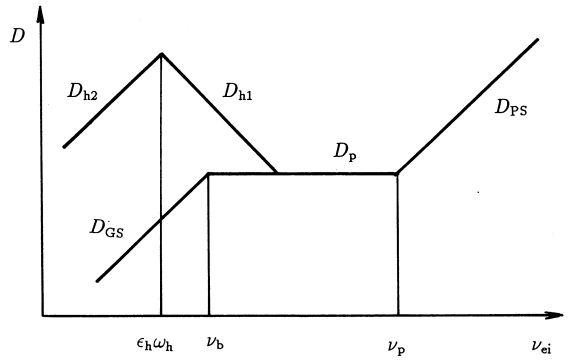

Fig.17.15 Dependence of the neoclassical diffusion coefficient of helical field on collision frequency. $\nu_{\rm p} = (\iota/2\pi)v_{\rm Te}/R,\ \ \nu_{\rm b} = \epsilon_{\rm t}^{3/2}\nu_{\rm p},\ \omega_{\rm h} = \epsilon_{\rm h}\kappa T_{\rm e}/(qBr^2)$.

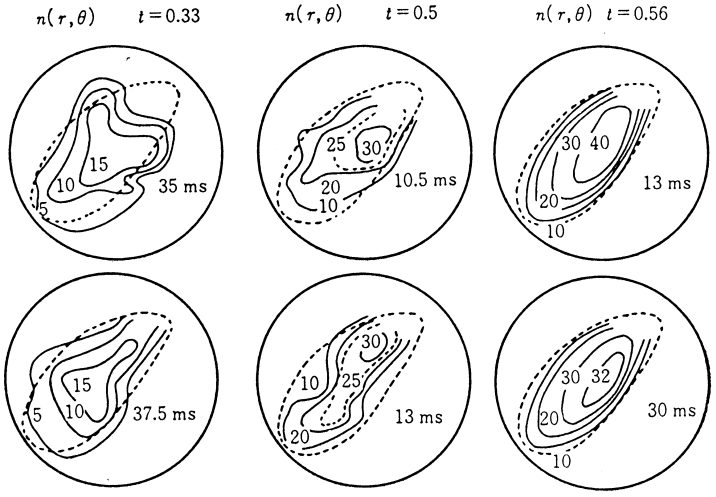

Fig.17.16 Equidensity contours of plasmas confined in JIPP I-b stellarator ($l = 2$) with the rotational transform angles of $\iota/2\pi = 1/2,\ 1/3$ and 0.56 (ref.[46]).

quasi-omnigenous stellerators, which will be introduced in section 17.2e.

17.2d Confinement of Stellarator (ref.[45]-[47])

After Stellarator C, the basic experiments were carried out in small but accurate stellarator devices (Clasp, Proto Cleo, Wendelstein IIb, JIPP I, Heliotron D, L1, Uragan 1). Alkali plasmas, or afterglow plasmas produced by wave heating or gun injection, were confined quiescently. The effect of shear on the stability and confinement scaling were investigated.

The l=2 stellarators with long helical pitch, such as Wendelstein IIa or JIPP I-b, have nearly constant rotational transform angles and the shears are small. When the transform angle is rational, $\iota/2\pi = n/m$, a line of magnetic force comes back to the initial position after m turns of the torus and is closed. If electric charges are localized in some place, they cannot be dispersed uniformly within the magnetic surface in the case of rational surfaces. A resistive drift wave or resistive MHD instabilities are likely to be excited, and convective loss is also possible. The enhanced loss is observed in the rational case (fig.17.16). This is called resonant loss. Resonant loss can be reduced by the introduction of shear.

Medium-scale stellarator devices (Wendelstein VIIA, Cleo, JIPP T-II, Heliotron-E, L2, Uragan 2, Uragan 3) have been constructed. The confinement time of the ohmically heated plasmas ($T_{\rm e} <$ 1 keV) is smilar to that of tokamaks with the same scale. When the rotational transform angle

Table 17.2 The maximal plasma parameters achieved in W7-AS.

	B_t	$\widehat{\iota}$	P_{NB}/P_{EC}	n_e	T_{e0}	T_{i0}	β	τ_E	$n_eT_{i0}\tau_E$	Remarks
T_{e0}	2.5	0.34	/2	0.2	6.8					e-ルート
T_{i0}	2.5	0.52	1.3/0.5	0.5		1.7				H-NBI
n_e	2.5	0.55	2.4/	4	0.35			10		HDH
β	0.9	0.5	2.8/	2	~ 0.37		3.4			HDH
τ_E	2.5	0.345	0.33/	1.1				60		H-NBI
$n_eT_{i0}\tau_E$	2.5	0.345	0.85/0.35	0.6					50	HDH

Units are T, MW, $10^{20}\mathrm{m}^{-3}$, keV, %, and ms. $\widehat{\iota} \equiv \iota/2\pi$. The triple product $n_eT_{i0}\tau_E$ in units of $10^{20}\mathrm{m}^{-3}\mathrm{eV}\cdot\mathrm{s}$.

is larger than $\iota_h/2\pi > 0.14$, the major disruption observed in tokamaks is suppressed (W VIIA, JIPP T-II). NBI heating or wave heatings, which were developed in tokamaks, have been applied to plasma production in helical devices. In Wendelstein VIIA, a target plasma was produced by ohmic heating; then the target plasma was sustained by NBI heating while the plasma current was gradually decreased, and finally a high-temperature plasma with $\kappa T_i \sim$ several hundred eV, $n_e \sim$ several $10^{13}\,\mathrm{cm}^{-3}$ was confined without plasma current (1982). In Heliotron-E, a target plasma was produced by electron cyclotron resonance heating with $\kappa T_e \sim 800\,\mathrm{eV}, n_e \sim 0.5\times10^{13}\,\mathrm{cm}^{-3}$, and the target plasma was heated by NBI heating with 1.8 MW to the plasma with $\kappa T_i \sim 1\mathrm{keV}, n_e = 2\times10^{13}\mathrm{cm}^{-3}$ (1984). The average beta, $\langle\beta\rangle \sim 2\%$, was obtained in the case of $B = 0.94\,\mathrm{T}$ and NBI power $P_{NB} \sim 1\,\mathrm{MW}$. These experimental results demonstrate the possibility of steady-state confinement by stellarator configurations. Experimental scaling laws of energy confinement time are presented from Heliotron-E group as follows; (ref.[48])

$$\tau_E^{\mathrm{LHD}} = 0.17a^{2.0}R^{0.75}n_{20}^{0.69}B^{0.84}P^{-0.58} \tag{17.23}$$

where the unit of n_{20} is $10^{20}\mathrm{m}^{-3}$. W7AS group presented W7AS confinement scaling (ref.[49]) of

$$\tau_E^{\mathrm{W7AS}} = 0.115A^{0.74}a^{2.95}n_{19}^{0.5}B^{0.73}P^{-0.54}\left(\frac{\iota}{2\pi}\right)^{0.43} \tag{17.24}$$

The scaling law of the international stellarator database (ref.[49]) is

$$\tau_E^{\mathrm{ISS95}} = 0.079a^{2.21}R^{0.65}n_{19}^{0.51}B^{0.83}P^{-0.59}\left(\frac{\iota}{2\pi}\right)^{0.4} \tag{17.25}$$

where the unit of n_{19} is $10^{19}\mathrm{m}^{-3}$ and $\iota/2\pi$ is the value at $r = (2/3)a$. Units are s, m, T, MW. The density scaling proposed by (ref.[48]) is

$$n_{20}^{s} = 0.25N_s\left(\frac{PB_t}{a^2R}\right)^{0.5}. \tag{17.26}$$

Electron thermal transport barrier was observed in ECH heated plasma of Compact Helical System (CHS) (R=1m, a=0.2m, B_t=1T) in 1999 (ref.[50]). When the ECH power is increased from 150 kW to 200 kW, L state to H state transition occurs. The electrostatic potential profile measured by HIBP (heavy ion beam probe) in H state exhibits a prominent peak around the core that is not seen in the L state. The electron temperature increases from 1.4 keV to 2.0 keV. The development of the electron root with positive (outward) electric field gives rise to low core transport in H state. Electron thermal transport barrier is also observed in W7AS (ref.[51]) and LHD (ref.[52, 53]). Furthermore zonal flow, which will be discussed in appendix E, is identified by use of two sets of HIBP in CHS (ref.[54]).

W7-AS is a stellarator with modular field coils ($l = 2, 3/n = 5$) which were designed to optimize the magnetic configuration with respect to low neoclassical transport and a reduction of Pfirsch-Schlüter current ($R = 2\,\mathrm{m}$, $a = 0.17\,\mathrm{m}$, $B_t = 2.5\,\mathrm{T}$). Confinement of W7-AS L mode discharge follows W7AS scaling (17.24) which is about 25% enhanced compared to ISS95 scaling (7.25).

Table 17.3 The maximal plasma parameters achieved in LHD.

	B_t/R	P_{NB}/P_{EC}	n_e	$T_{e\,0}$	$T_{i\,0}$	β	τ_E	$n_eT_{i0}\tau_E$	Ref.
T_{e0}	∼3/∼3.75	1.3/0.88	0.02	9.5					[53]
T_{i0}	2.75/3.6	1.8/	0.13	3.3	3.5		90		[58]
T_{i0}			0.07		5				[52]
n_e	∼2.8/3.6	11/	1.6						[59]
β	0.45/3.6	1.2/	0.3			4.1			[59]
τ_E	2.75/3.6	1.8/	0.65	1.1			300		[59]
$n_eT_{i0}\tau_E$		1.5(P_{abs})	0.48		1.3		360	220	[52]

Units are T, m, MW, $10^{20}\mathrm{m}^{-3}$, keV, %, and ms. The triple product $n_eT_{i0}\tau_E$ in units of $10^{20}\mathrm{m}^{-3}\mathrm{eV}\cdot\mathrm{s}$.

High confinement NBI discharge (H-NBI) (ref.[55]) of W7-AS was found in 1998. $\boldsymbol{E}\times\boldsymbol{B}$ shear flow and transport barrier are formed at $r/a\sim 0.7$ and confinement time is enhanced by a factor of 2 of W7AS scaling, that is, up to factor of 2.5 above ISS95 scaling.

High Density H mode (HDH) (ref.[56]) was observed in 2002. The density reaches $2\sim 4\times 10^{20}\mathrm{m}^{-3}$. Observed confinement time is around $2\tau_E^{W7AS}$ and the maximum density is about 1.6 times the density n_{20}^s (17.26).

The maximal plasma parameters achieved in W7-AS are listed in Table 17.2 (ref.[57]).

Large Helical Device (LHD) is a superconducting device with $R=3.5\sim 3.9\,\mathrm{m}$, $a\sim 0.6\,\mathrm{m}$, $B_t=0.45\sim 3\,\mathrm{T}$, $l=2,\ m=10$, $P_{NBI}=13\,\mathrm{MW}$ with the beam energy of 180 keV, $P_{ECH}=2\mathrm{MW}$ with 168 GHz and 84 GHz and $P_{ICRF}=2.7\,\mathrm{MW}$ with 38.5MHz (see fig.17.11). The energy confinement time in the LHD inward shifted discharge ($R_{axis}=3.6\,\mathrm{m}$) is consistent to ISS95 scaling with an enhancement factor of up to 1.5. The maximal parameters achieved in LHD are listed in Table 17.3.

17.2e Quasi-Symmetric Stellarator System

The particle orbits in Boozer coordinates depend on the magnetic field strength $|B|$ and do not depend on the components of $\boldsymbol{B}$ as is seen in (D.47) or (D55) in app.D. If $|B|$ can be made symmetric, the particle orbit is closed, subject to a constant of motion. There are three types of symmetry: (1) axisymmetry $B(\rho,\theta)$, (2) helical symmetry $B(\rho,\theta-\alpha\zeta)$, and (3) poloidal symmetry $B(\rho,\zeta)$ in Boozer coordinates.

Quasi-Axisymmetric Stellarator (QAS)
NCSX (National Compact Stellarator Experiment) is repesentative QAS in Princeton. Optimized modular coils of NCSX and radial profile of non-axisymmetric components of magnetic field strength are shown in fig.17.17. NCSX has $R=1.4\,\mathrm{m}$, $B_t=1.2\sim 2.0\,\mathrm{T}$, $A=4\sim 4.4$. It is expected theoretically that, even with bootstrap current consistent profiles, they are passively stable to the ballooning, kink, mercier, and neoclassical tearing mode for $\beta>4\%$ (ref.[60]).

Quasi-Helically Symmetric Stellarator (QHS)
HSX is QHS with $B/B_0\approx(1+\varepsilon_H\cos(\theta-4\zeta))$ ($R=1.2\,\mathrm{m},\ a=0.15\,\mathrm{m},\ B_t=1\,\mathrm{T}$). Experiments are carried out at University of Wisconsin (ref.[61]).

Quasi-Poloidally Symmetric Stellarator (QPS)
QPS device with $R=0.9\,\mathrm{m},\ A=2.7, B_t=1\,\mathrm{T}$ is in ORNL. QPS coil set has two field periods and will operate in an external vacuum tank (ref.[62]). Contours of magnetic field strength at $\psi/\psi_{edge}=0.25$ is shown in fig.17.18.

Quasi-Isodynamic or Quasi-Omnigenous Stellarator
Quasi-isodynamicity addresses the property that trapped particle gyrocenters precess poloidally with the confinement of thermal and energetic particles ensured by poloidally closed contours of the longitudinal invariant $J_\parallel$. Wendelstein-7X is fully optimized following the quasi-isodynamicity

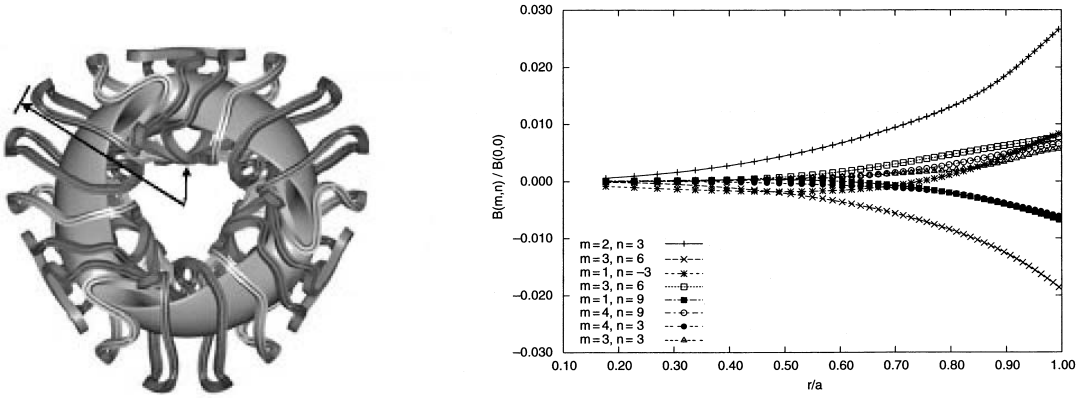

Fig.17.17 Left-hand side figure: NCSX plasma and modular coils (six each of three coil types). Right-hand side figure: radial profile of non-axisymmetric components of magnetic field strength (ref.[60]).

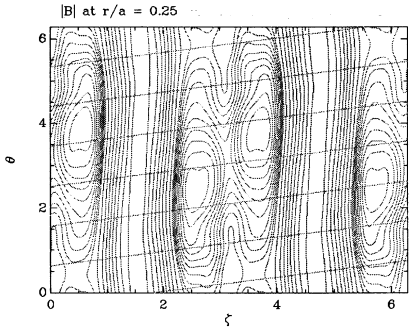

Figure 17.18 Contours of magnetic field strength and magnetic field lines of QPS (straight lines in Boozer coordinates on the flux surface $(\psi/\psi_{\rm edge})^{1/2} = 0.25$ (ref.[62]). $B > 1$T in the regions that contain closed contours plotted with thin lines and $B < 1$T in the regions without closed contours. θ is the poloidal angle variable and ζ is the toroidal angle variable.

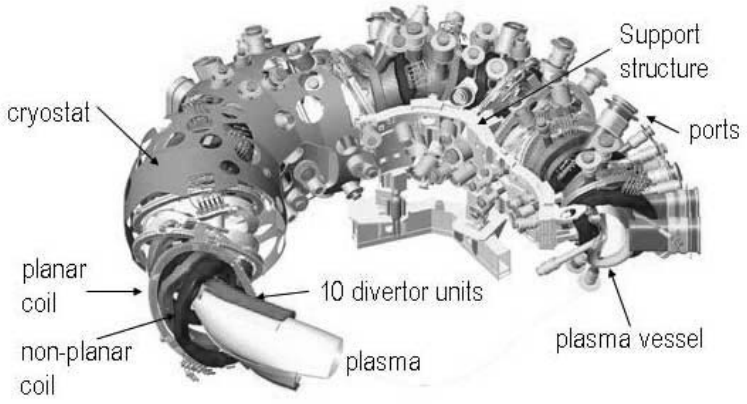

Fig.17.19 Components of W7-X device (ref.[63]).

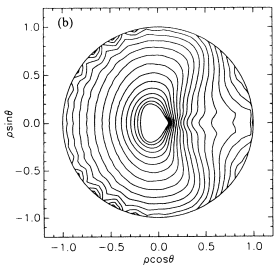

Fig.17.20 $J_\parallel$ contours for trapped particles. Concentric circles are the flux surfaces. After (ref.[64]).

principle. The optimization of W7-X leads to good and nested flux surfaces, low Shafranov shift due to $\langle j_\parallel^2/j_\perp^2\rangle \sim 0.5$, equilibrium and stability of $\langle\beta\rangle \sim 5\%$, and low neoclassical flux with a confinement determined by turbulent transport (ref.[63]). Device parameters are $R = 5.5\,\mathrm{m}$, $a = 0.55\,\mathrm{m}$, $B_\mathrm{t} = 2.5\,\mathrm{T}$ (superconductor coils), volume of plasma $V = 30\,\mathrm{m}^3$, pulse duration 30 min., $P_\mathrm{ECH} = 60\,\mathrm{MW}$, $P_\mathrm{NBI} = 5\,\mathrm{MW}(20^*)$ and $P_\mathrm{ICRF} = 3\,\mathrm{MW}(9^*)$ (*: stage II heating). Components of W7-X device are shown in Figure 17.19.

Quasi-omnigenous approach targets to align second (longitudinal) invariant $J_\parallel$ contours for the trapped particles with magnetic flux surfaces (ref.[64]). An example of $J_\parallel$ contours is shown in fig.17.20. Concentric circles are the flux surfaces.

These new concepts of stellarator configurations are reviewed in (ref.[65]).

17.2f Conceptual Design of Stellarator Reactor

Burning Condition of Stellarator Reactor can be reduced in the same way as that of tokamak (sec.16.12). We use (16.97), (16.99), and (16.100), ISS95 energy confinement scaling (17.25), and density scaling (17.26). Then burning condition with use of ISS95 scaling is given by

$$a^{1.09}B^{1.745} = \frac{13.26(1+f_\mathrm{DT}+f_\mathrm{He}+f_\mathrm{I})^{1.33}}{H^\mathrm{ISS95}N_\mathrm{s}^{0.51}\beta_\mathrm{th}[(1-f_\mathrm{rad\,c})(f_\alpha+5/Q)f_\mathrm{prof}f_\mathrm{DT}^2\Theta]^{0.665}(\iota/2\pi)^{0.4}A^{0.06}}, \tag{17.27}$$

Table 17.4 The parameters of HSR5/22 and FFHR2m2 reactors.

	HSR5/22 modular coils	FFHR2m2 LHD type coils
R / a(m)	22 / 1.8	16 / 2.8
$V(\mathrm{m}^3)$	1400	-
No. of field period	5	$l = 2$ $m = 10$
B_t(T)	4.75	4.43
B_max(T)	10	13
coil radius (m)	5.4	4.33
W_mag(GJ)	100	142
fusion power (GW)	3	3
$\bar{n}_\mathrm{e}$ $(10^{20}\mathrm{m}^{-3})$	2.12	
$n_\mathrm{e}(0)$ $(10^{20}\mathrm{m}^{-3})$	3.0	1.9
$\langle T_\mathrm{e}\rangle$(keV)	4.96	-
$T_\mathrm{e0}/T_\mathrm{i0}$(keV)	15 / -	/ 16.1
$\beta(\%)$	4.24	4.1
τ_E(s) (required)	1.62	-
$\tau_\mathrm{E}^\mathrm{ISS95}$(s)	0.96	-
H_ISS95	1.69	1.76

V: volume of plasma, W_mag: stored energy of magnetic field.
The number of the module coils in HSR5/22 is 50.

where $H^{\rm ISS95}$ is confinement enhancement factor over ISS95 scaling.

The Helias stellerator reactor is an upgraded version of the Wendelstein 7-X device taking into account the design criteria of a power reactor (ref.[66]). FFHR2 is LHD-type D-T demo-reactor (ref.[67]). The parameters of two reactors are listed in Table 17.4.

Precession of Helical Banana in Stellarator

Longitudinal adiabatic invariant $J_\parallel$ of stellarator is given by

$$J_\parallel(u^1,u^2,W,\mu_{\rm m}) = (2m)^{1/2}\oint\Big(W-q\phi-\mu_{\rm m}B(1-\epsilon_{\rm t}\cos\theta-\epsilon_{\rm h}\cos(l\theta-n\varphi))\Big)^{1/2}{\rm d}l$$

$$= (2m\mu_{\rm m}B\epsilon_{\rm h})^{1/2}\oint(2\kappa^2+\cos\zeta-1)^{1/2}{\rm d}\zeta = 16(m\mu_{\rm m}B\epsilon_{\rm h})^{1/2}Rn^{-1}(E(\kappa)-(1-\kappa^2)K(\kappa)),$$

where

$$\kappa^2(r,\theta,W,\mu_{\rm m}) = \frac{W-\mu_{\rm m}B(1-\epsilon_{\rm t}\cos\theta-\epsilon_{\rm h})-q\phi(r)}{2\mu_{\rm m}B\epsilon_{\rm h}},$$

and $\zeta = l\theta-n\varphi$, $\epsilon_{\rm h}\propto r^l$, $\epsilon_{\rm t}\propto r$, ${\rm d}l\approx{\rm d}R\varphi\approx Rn^{-1}{\rm d}\zeta$. Since

$$\frac{\partial\kappa^2}{\partial r} = -\frac{l}{r}(\kappa^2-1/2)+\frac{\epsilon_{\rm t}\cos\theta}{2\epsilon_{\rm h}r}-\frac{q\partial\phi/\partial r}{2\epsilon_{\rm h}\mu_m B}, \qquad \frac{\partial\kappa^2}{\partial\theta} = -\frac{\epsilon_{\rm t}\sin\theta}{2\epsilon_{\rm h}}$$

we have

$$\frac{\partial J_\parallel}{\partial r} = 16(m\mu_{\rm m}B\epsilon_{\rm h})^{1/2}Rn^{-1}\left((E(\kappa)-(1-\kappa^2)K(\kappa))\frac{l}{2r}+\frac{K}{2}\kappa K(\kappa)\frac{1}{2\kappa}\frac{\partial\kappa^2}{\partial r}\right)$$

$$= 16(m\mu_{\rm m}B\epsilon_{\rm h})^{1/2}Rn^{-1}\left((E-K/2)\frac{l}{2r}+\frac{K}{2}\left(\frac{\epsilon_{\rm t}\cos\theta}{2\epsilon_{\rm h}r}-\frac{q\partial\phi/\partial r}{2\epsilon_{\rm h}\mu_{\rm m}B}\right)\right),$$

$$\frac{\partial J_\parallel}{\partial\theta} = 16(m\mu_{\rm m}B\epsilon_{\rm h})^{1/2}Rn^{-1}\frac{K}{2}\left(-\frac{\epsilon_{\rm t}\sin\theta}{2\epsilon_{\rm h}}\right), \quad \frac{\partial J_\parallel}{\partial W} = 16(m\mu_{\rm m}B\epsilon_{\rm h})^{1/2}Rn^{-1}\frac{K}{2}\frac{1}{2\mu_{\rm m}B\epsilon_{\rm h}}.$$

Since the center of helical banana is in $l\theta-n\varphi=0$, where the magnitude of magnetic field of stellarator in minimum, we have

$$u^2 = \theta-(\iota/2\pi)\varphi = (1-(\iota/2\pi)(l/n))\theta, \qquad \frac{\partial J_\parallel}{\partial u^2} = \frac{1}{(1-(\iota/2\pi)(l/n))}\frac{\partial J_\parallel}{\partial\theta}.$$

The precession of helical banana is

$$\frac{{\rm d}\theta}{{\rm d}t} = \frac{1}{1-(\iota/2\pi)(l/n)}r\frac{{\rm d}u^2}{{\rm d}t} = \frac{1}{1-(\iota/2\pi)(l/n)}\frac{-1}{qBr}\frac{\partial J_\parallel/\partial r}{\partial J_\parallel/\partial W}$$

$$= \left(\frac{1}{1-(\iota/2\pi)(l/n)}\right)\left(-V_{\rm t\,drift}\cos\theta-\frac{E_r}{B}-\frac{2l}{r}(\frac{E}{K}-\frac{1}{2})\frac{\epsilon_{\rm h}\mu_m B}{qBr}\right), \tag{17.28}$$

$$\frac{{\rm d}r}{{\rm d}t} = \frac{1}{qBr}\frac{\partial J_\parallel/\partial u^2}{\partial J_\parallel/\partial W} = \frac{1}{(1-(\iota/2\pi)(l/n))}\frac{1}{qBr}\frac{\partial J_\parallel/\partial\theta}{\partial J_\parallel/\partial W}$$

$$= -\frac{1}{(1-(\iota/2\pi)(l/n))}\frac{\epsilon_{\rm t}\mu_m B}{qBr}\sin\theta = -\frac{1}{(1-(\iota/2\pi)(l/n))}V_{\rm t\,drift}\sin\theta.$$

17.3 Open End Systems

Open end magnetic field systems are of a simpler configuration than toroidal systems. The attainment of absolute minimum-B configurations is possible with mirror systems, whereas only average minimum-B configurations can be realized in toroidal systems. Although absolute minimum-B configurations are MHD stable, the velocity distribution of the plasma becomes non-Maxwellian due to end losses, and the plasma will be prone to velocity-space instabilities.

The most critical issue of open-end systems is the supression of end loss. The end plug of the mirror due to electrostatic potential has been studied by tandem mirrors. The bumpy torus, which is a toroidal linkage of many mirrors, was used in other trials to avoid end loss.

A cusp field is another type of open-end system. It is rotationally symmetric and absolute minimum-B. However, the magneitc field becomes zero at the center, so the magnetic momentum is no longer invariant and the end loss from the line and point cusps are severe.

17.3a Confinement Times in Mirrors and Cusps

Particles are trapped in a mirror field when the velocity components $v_\perp$ and $v_\parallel$, perpendicular and parallel to the magnetic field, satisfy the condition

$$\frac{v_\perp^2}{v^2} > \frac{b_0}{b_\mathrm{L}}, \qquad (v^2 = v_\perp^2 + v_\parallel^2)$$

where b_0 and b_L are the magnitudes of the magnetic field at the center and at the end, respectively. Denoting the mirror ratio b_L/b_0 by R_M, so that

$$\frac{b_0}{b_\mathrm{L}} = \frac{1}{R_\mathrm{M}} = \sin^2\alpha_\mathrm{L}$$

the trapping condition is reduced to

$$\frac{v_\perp}{v} > \sin\alpha_\mathrm{L}.$$

When the particles enter the loss cone, they escape immediately, so that the confinement time is determined by the velocity space diffusion to the loss cone. The *particle confinement time* τ_p of a mirror field is essentially determined by the ion-ion collision time τ_ii as follow: (ref.[68])

$$\tau_\mathrm{p} \approx \tau_\mathrm{ii} \ln R_\mathrm{M}. \tag{17.29}$$

Even if the mirror ratio R_M is increased, the confinement time is increased only as fast as $\ln R_\mathrm{M}$. The time is independent of the magnitude of the magnetic field and the plasma size. If the density is $n \approx 10^{20}\,\mathrm{m}^{-3}$, the ion temperature $\kappa T_\mathrm{i} \approx 100\mathrm{keV}$, the atomic mass number $A = 2$, and ion charge $Z = 1$, the ion-ion collision time is $\tau_\mathrm{ii} = 0.3\mathrm{s}$, so that $n\tau_\mathrm{p} = 0.3 \times 10^{20}\mathrm{m}^{-3}\mathrm{s}$. This value is not enough for a fusion reactor. It is necessary to increase the efficiency of recovery of the kinetic energy of charged particles escaping through the ends or to suppress the end loss.

Next let us consider cusp losses. Since the magnetic field is zero at the cusp center 0, the magnetic moment is not conserved. Therefore the end losses from the line cusp and the point cusp (fig.17.21) are determined by the hole size and average ion velocity $\bar{v}_\mathrm{i}$. The flux of particles from the line cusp of width δ_L and radius R is given by

$$F_\mathrm{L} = \frac{1}{4} n_\mathrm{L} \bar{v}_\mathrm{i} 2\pi R \cdot \delta_\mathrm{L}, \qquad \bar{v}_\mathrm{i} = \left(\frac{8}{\pi}\frac{\kappa T_\mathrm{i}}{M}\right)^{1/2}$$

where n_L is the particle density at the line cusp and T_i and M are the temperature and mass of the ions. The flux of particles from two point cusps of radius δ_p is (ref.[69])

$$F_\mathrm{p} = \frac{1}{4} n_\mathrm{p} \bar{v}_\mathrm{i} \pi \delta_\mathrm{p}^2 \times 2.$$

The observed value of δ_L is about that of the ion Larmor radius. As the lines of magnetic force are given by

$$r A_\theta = a r^2 z = \text{const.}$$

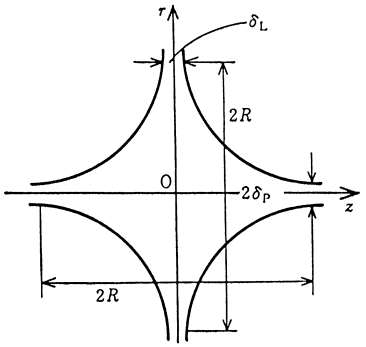

Fig.17.21 Line cusp width δ_L and point cusp radius δ_p.

we have

$$\delta_p^2 R \approx R^2 \frac{\delta_L}{2}, \qquad \delta_p^2 = \frac{R\delta_L}{2}$$

so that $F_p \approx F_L/2$. The total end-loss flux is

$$F \approx \frac{1}{4}\bar{v}_i 2\pi R\delta_L \left(n_L + \frac{n_p}{2}\right)$$

and the volume V of the cusp field is (fig.17.21)

$$V = \pi R^2 \delta_L \left(\ln \frac{2R}{\delta_L} + 1\right).$$

The *confinement time of cusp* is now given by

$$\tau = \frac{nV}{F} \approx \frac{R}{\bar{v}_i}\left(\ln \frac{2R}{\delta_L} + 1\right)\frac{4}{3}\frac{n}{n_L + n_p/2} \tag{17.30}$$

where n is the average density. When $R = 10\,\mathrm{m}$, $B = 10\mathrm{T}$, $\kappa T_i = 20\mathrm{keV}$, $A = 2$, and $\delta_L = \rho_B^i$, then $\tau \approx 0.1\,\mathrm{ms}$, which is 10-20 times the transit time $R/\bar{v}_i$. Even if the density is $n \approx 10^{22}\mathrm{m}^{-3}$, the product of $n\tau$ is of the order of $10^{18}\mathrm{m}^{-3}\mathrm{s}$, or 10^{-2} times smaller than fusion plasma condition.

17.3b Confinement Experiments with Mirrors

One of the most important mirror confinement experiments was done by Ioffe and his colleagues, who demonstrated that the minimum-B mirror configuration is quite stable (ref.[70]). Addition of stabilizing coils as shown in fig.17.22(a) results in a mirror field with the minimum-B property (fig.17.22(c)).

Define the *wall mirror ratio* as the ratio of the magnitude of the magnetic field at the radial boundary to its magnitude at the center. When the wall mirror ratio is increased, flute instability disappears and the confinement time becomes long. In the PR-5 device, a plasma of density $10^9 \sim 10^{10}\mathrm{cm}^{-3}$ and ion temperature $3 \sim 4$ keV has been confined for 0.1 s (ref.[71]). However, when the density is larger than $10^{10}\mathrm{cm}^{-3}$ ($\Pi_i > |\Omega_i|$), the plasma suffers from loss-cone instability.

One of the most promising mirror confinement results was brought about in the 2X experiments (ref.[72]). Here a plasmoid of mean energy of 2.5 keV produced by a plasma gun is injected into a quadrupole mirror and then compressed. The initial density of the trapped plasma is $n \approx 3 \times 10^{13}\mathrm{cm}^{-3}$, and $n\tau \approx 10^{10}\mathrm{cm}^{-3}\mathrm{s}$. The magnitude of the magnetic field is 1.3 T and $\beta \approx 5\%$. The average energy of the ions is 6-8 keV, and the electron temperature is about 200 eV. Since $n\tau$ for an ideal case (classical coulomb collision time) is $n\tau \approx 3 \times 10^{10}\mathrm{cm}^{-3}\mathrm{s}$, the results obtained are $1/3 \sim 1/15$ that of the ideal. In the 2XIIB experiment (ref.[73]), microscopic instability is suppressed by adding a small stream of warm plasma to smooth out the loss cone. A 15-19 keV, 260 A neutral beam is injected, and the resulting plasma, of 13 keV ion temperature, is confined to

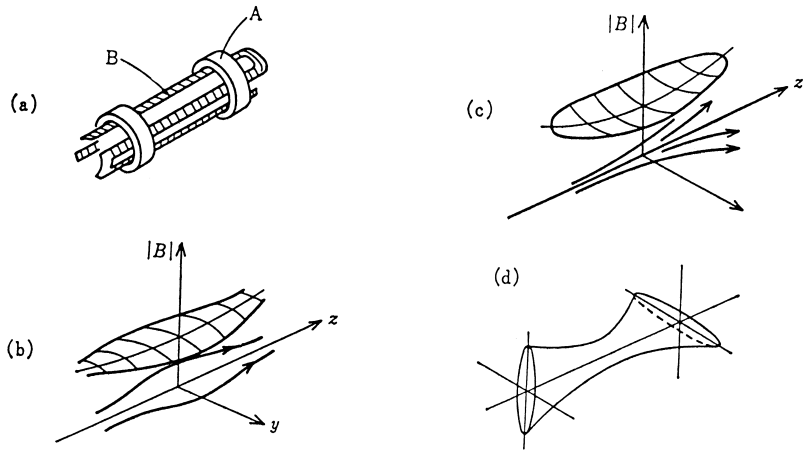

Fig.17.22 Minimum-B mirror field. (a) Coil system with mirror coil (A) and stabilizing coils (Ioffe bars) (B). (b) Magnitude of the magnetic field in a simple mirror. (c) Magnitude of the magnetic field in the minimum-B mirror field. (d) The shape of a quadrupole minimum-B (fishtail).

$n\tau \approx 10^{11}\,\mathrm{cm}^{-3}\mathrm{s}$ ($n \approx 4 \times 10^{13}\mathrm{cm}^{-3}$).

17.3c Instabilities in Mirror Systems

Instabilities of mirror systems are reviewed in (ref.[74]-[76]). MHD instability can be suppressed by the minimum-B configuration. However, the particles in the loss-cone region are not confined, and the non-Maxwellian distribution gives rise to electrostatic perturbations at the ion cyclotron frequency and its harmonics, which scatter the particles into the loss cone region and so enhance the end loss. It can be shown that instabilities are induced when the cyclotron wave couples with other modes, such as the electron plasma wave or the drift wave.

(i) Instability in the Low-Density Region ($\Pi_\mathrm{e} \approx l|\Omega_\mathrm{i}|$) Let us consider the low-density case. When the plasma electron frequency Π_e reaches the ion cyclotron frequency $|\Omega_\mathrm{i}|$, there is an interaction between the ion Larmor motion and the electron Langmuir oscillation, and *Harris instability* occurs (ref.[77]) (sec.13.4).

When the density increases further, the oblique Langmuir wave with $\omega = (k_\parallel/k_\perp)\Pi_\mathrm{e}$ couples with the harmonics $l|\Omega_\mathrm{i}|$ of the ion cyclotron wave. The condition $\omega \approx k_\perp v_{\perp\mathrm{i}}$ is necessary for the ions to excite the instability effectively; and, if $\omega > 3k_\parallel v_{\parallel\mathrm{e}}$, then the Landau damping due to electrons is ineffective. Thus excitation will occur when

$$\omega \approx l|\Omega_\mathrm{i}| \approx \Pi_\mathrm{e} k_\parallel/k \approx k_\perp v_{\perp\mathrm{i}} > 3k_\parallel v_{\parallel\mathrm{e}}$$

where $k_\parallel$, $k_\perp$ are the parallel and perpendicular components of the propagation vector and $v_\parallel$, $v_\perp$ are the parallel and perpendicular components of the velocity. Therefore the instability condition is

$$\frac{\Pi_\mathrm{e}}{l|\Omega_\mathrm{i}|} > \left(1 + \frac{9v_{\parallel\mathrm{e}}^2}{v_{\perp\mathrm{i}}^2}\right)^{1/2} \approx \left(1 + \frac{9MT_\mathrm{e}}{mT_\mathrm{i}}\right)^{1/2}. \tag{17.31}$$

Let L be the length of the device. As the relation $\kappa_\parallel > 2\pi/L$ holds, we have (ref.[78],[79])

$$\frac{L}{\rho_{\Omega\mathrm{i}}} > \frac{6\pi}{l}\frac{v_{\parallel\mathrm{e}}}{v_{\perp\mathrm{i}}}.$$

Harris instability has been studied in detail experimentally (ref.[80]).

(ii) Instability in the High Density ($\Pi_\mathrm{i} > |\Omega_\mathrm{i}|$) When the density increases further, so that Π_i is larger than $|\Omega_\mathrm{i}|$ (while $\Omega_\mathrm{e} > \Pi_\mathrm{i}$ still holds), *loss-cone instability* with $\omega_\mathrm{r} \approx \omega_\mathrm{i} \approx \Pi_\mathrm{i}$ will occur (ref.[81]). This is a convective mode and the length of the device must be less than a critical

length, given by

$$L_{\rm crit} = 20A\rho_{\Omega \rm i}\left(\frac{\Omega_{\rm e}^2}{\Pi_{\rm e}^2}+1\right)^{1/2} \tag{17.32}$$

for stability. Here A is of the order of 5 ($A \approx 1$ for complete reflection and $A \approx 10$ for no reflection at the open end). Therefore the instability condition is $L > 100\rho_{\rm B}^{\rm i}$. Loss-cone instability can occur for a homogeneous plasma. When there is a density gradient, this type of instability couples with the drift wave, and drift cyclotron loss-cone instability may occur (ref.[81]). When the characteristic length of the density gradient is comparable to the radial dimension $R_{\rm p}$ of the plasma, the instability condition of this mode is

$$R_{\rm p} < \rho_{\Omega \rm i}\left(\frac{\Pi_{\rm i}}{|\Omega_{\rm i}|}\left(1+\frac{\Pi_{\rm e}^2}{\Omega_{\rm e}^2}\right)^{-1/2}\right)^{4/3}. \tag{17.33}$$

(iii) Mirror Instability When the beta ratio becomes large, the anisotropy of plasma pressure induces electromagnetic-mode *mirror instabilities*. (Note that the Harris and loss-cone instabilities are electrostatic.) The instability condition is

$$\left(\frac{T_{\perp \rm i}}{T_{\parallel \rm i}}-1\right)2\beta > 1. \tag{17.34}$$

To avoid the instabilities described in (i)-(iii), the following stability conditions must be met:

$$L < 100 \sim 200\rho_{\Omega \rm i}, \tag{17.35}$$

$$R_{\rm p} > 200\rho_{\Omega \rm i}, \tag{17.36}$$

$$\beta < \frac{1}{2}\left(\frac{T_{\perp \rm i}}{T_{\parallel \rm i}}-1\right)^{-1} \approx 0.3 \sim 0.5. \tag{17.37}$$

(iv) Negative Mass Instability Let us assume that charged particles in Larmor motion are uniformly distributed at first and then a small perturbation occurs, so that positive charge (for example) accumulates at the region A shown in fig.17.23. The electric field decelerates ions in the region to the right of A, and their kinetic energy ϵ corresponding to the velocity component perpendicular to the magnetic field is decreased. Ions to the left of A are accelerated, and their ϵ is increased. When the rotational frequency ω depends on ϵ through the relation $\mathrm{d}\omega/\mathrm{d}\epsilon < 0$, the frequency ω of the ions in the region to the right of A is increased and the ions approach A despite the deceleration. These ions behave as if they had negative mass. This situation is exactly the same for the ions in the left-hand region. Therefore the charge accumulates at A, and the perturbation is unstable. This type of instability is called *negative mass* instability (ref.[82]). The condition $\mathrm{d}\omega/\mathrm{d}\epsilon < 0$ is satisfied when the magnitude of the magnetic field decreases radially. Thus, as expected, simple mirrors, where B decreases radially and the Larmor radius is large, have been reported to exhibit negative mass instability (ref.[83]). The PR-5 device is of minimum-B configuration, so that the magnitude of the magnetic field increases radially. However, here another type of negative mass instability is observed (ref.[84]). When the perpendicular energy ϵ decreases, ions can enter the mirror region more deeply, so that the ion cyclotron frequency is increased. Thus the condition $\mathrm{d}\omega/\mathrm{d}\epsilon < 0$ is satisfied even in PR-5.

(v) Instability in Hot Electron Plasmas A hot electron plasma can be produced by electron cyclotron resonant heating in mirror fields. The temperature of the hot component is raised up to the range of several keV to several hundred keV, and the density range is $10^{10} \sim 10^{11}\,\mathrm{cm}^{-3}$. The electromagnetic *whistler instability* (ref.[84],[85]) is excited by anistropy of the velocity distribution

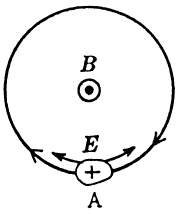

Fig.17.23 Negative mass instability.

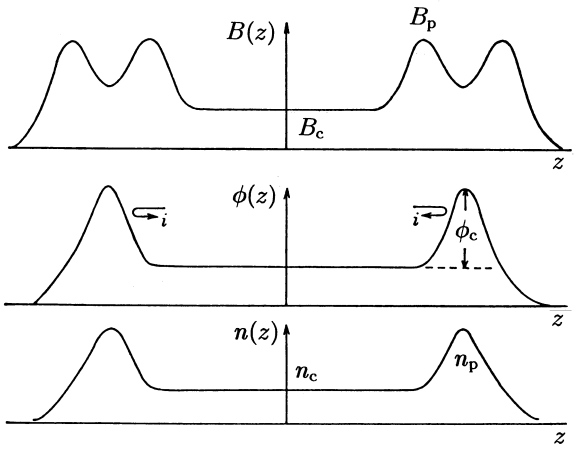

Fig.17.24 The magnitudes of magnetic field $B(z)$, electrostatic potential $\phi(z)$, and density $n(z)$ along the z axis (mirror axis) of a tandem mirror.

function ($T_\perp > T_\parallel$). This whistler instability of hot electron plasmas has been observed experimentally (ref.[86])

17.3d Tandem Mirrors

Theory

The input and output energy balance of a classical mirror reactor is quite marginal even in the ideal confinement condition. Therefore the suppression of the end loss is the critical issue for realistic mirror reactors. This section describes the research on the end plug by the use of electrostatic potential. In a simple mirror case, the ion confinement time is of the order of ion-ion collision time, and the electron confinement time is of the order of electron-electron or electron-ion collision times,($\tau_{ee} \sim \tau_{ei}$). Since $\tau_{ee} \ll \tau_{ii}$, the plasma is likely to be ion rich, and the plasma potential in the mirror tends to be positive. When the two mirrors are arranged in the ends of th central mirror in tandem, it is expected that the plasma potentials in the plug mirrors (plug cell) at both ends become positive with respect to the potential of the central mirror (central cell). This configuration is called a tandem mirror (ref.[87],[88]). The loss-cone region in velocity space of the tandem mirror, as shown in fig.17.24, is given by

$$\left(\frac{v_\perp}{v}\right)^2 < \frac{1}{R_m}\left(1 - \frac{q\phi_c}{mv^2/2}\right) \tag{17.38}$$

where q is the charge of the particle and R_m is the mirror ratio. The loss-cone regions of electrons and ions are shown in fig.17.25 in the positive case of the potential ϕ_c. Solving the Fokker-Planck equation, Pastukhov (ref.[89]) derived the *ion confinement time of a tandem mirror* with positive

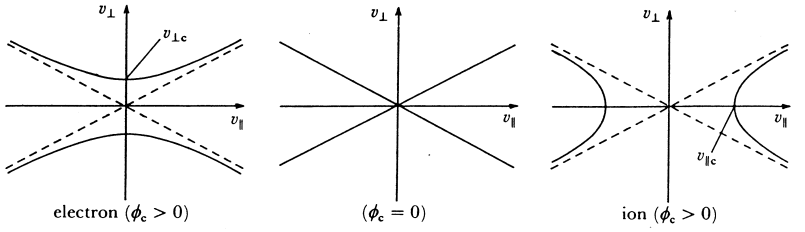

Fig.17.25 Loss-cone regions of an ion ($q = Ze$) and electron ($-e$) for positive electrostatic potential $\phi_c > 0$ and the mirror ratio R_m. $(v_{\perp c}/v)^2 = (e\phi_c/(R_m - 1))/(m_e v^2/2)$, in the electron case. $(v_{\parallel c}/v)^2 = Ze\phi_c/(m_i v^2/2)$ in the ion case.

potential as

$$\tau_{PAST} = \tau_{ii} g(R_m) \left(\frac{e\phi_c}{\kappa T_{ic}}\right) \exp\left(\frac{e\phi_c}{\kappa T_{ic}}\right) \tag{17.39}$$

$$g(R_m) = \pi^{1/2}(2R_m + 1)(4R_m)^{-1} \ln(4R_m + 2)$$

where T_{ic} is the ion temperature of the central cell and ϕ_c is the potential difference of the plug cells in both ends with respect to the central cell. Denote the electron densities of the central cell and the plug cell by n_c and n_p respectively; then the Boltzmann relation $n_p = n_c \exp(e\phi_c/\kappa T_e)$ gives

$$\phi_c = \frac{\kappa T_e}{e} \ln\left(\frac{n_p}{n_c}\right). \tag{17.40}$$

By application of neutral beam injection into the plug cell, it is possible to increase the density in the plug cell to be larger than that of the central cell. When $R_m \sim 10$ and $e\phi_c/\kappa T_{ic} \sim 2.5$, $\tau_{PAST} \sim 100\tau_{ii}$, so that the theoretical confinement time of the tandem mirror is longer than that of the simple mirror.

In this type of tandem mirror it is necessary to increase the density n_p in the plug cell in order to increase the plug potential ϕ_c, and the necessary power of the neutral beam injection becomes large. Since the plug potential ϕ_c is proportional to the electron temperature T_e, an increase in T_e also increases ϕ_c. If the electrons in the central cell and the electrons in the plug cells can be thermally isolated, the electrons in the plug cells only can be heated, so that efficient potential plugging may be expected. For this purpose a *thermal barrier* (ref.[90]) is introduced between the central cell and the plug cell, as shown in fig.17.26. When a potential dip is formed in the thermal barrier in an appropriate way, the electrons in the plug cell and the central cell are thermally isolated.

Since the electrons in the central cell are considered to be Maxwellian with temperature T_{ec}, we have the relation

$$n_c = n_b \exp\left(\frac{e\phi_b}{\kappa T_{ec}}\right). \tag{17.41}$$

The electrons in the plug cell are modified Maxwellian (ref.[91]) and the following relation holds:

$$n_p = n_b \exp\left(\frac{e(\phi_b + \phi_c)}{\kappa T_{ep}}\right) \times \left(\frac{T_{ep}}{T_{ec}}\right)^\nu \tag{17.42}$$

where $\nu \sim 0.5$. These relations reduce to

$$\phi_c = \frac{\kappa T_{ep}}{e} \ln\left(\frac{n_p}{n_b}\left(\frac{T_{ec}}{T_{ep}}\right)^\nu\right) - \frac{\kappa T_{ec}}{e} \ln\left(\frac{n_c}{n_b}\right)$$

$$= \frac{\kappa T_{ep}}{e} \ln\left(\frac{n_p}{n_c}\left(\frac{T_{ec}}{T_{ep}}\right)^\nu\right) + \left(\frac{T_{ep}}{T_{ec}} - 1\right) \frac{\kappa T_{ec}}{e} \ln\left(\frac{n_c}{n_b}\right), \tag{17.43}$$

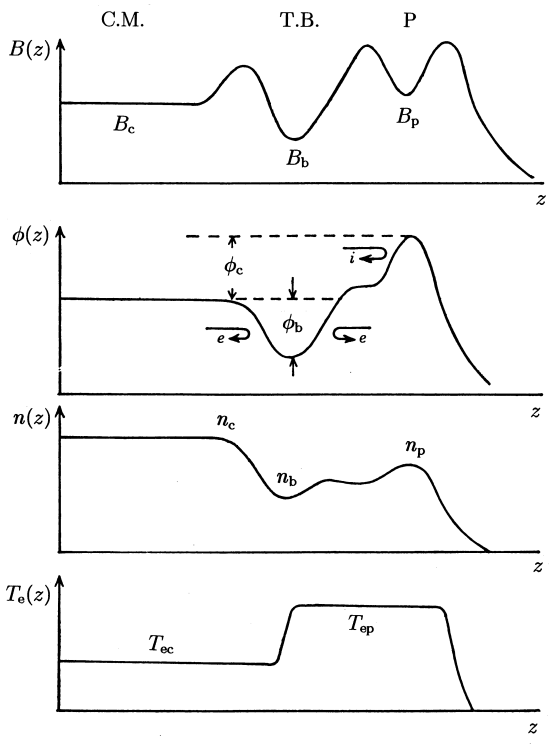

Fig.17.26 The magnitudes of magnetic field $B(z)$, electrostatic potential $\phi(z)$, density $n(z)$, and electron temperature $T_e(z)$ in tandem mirror with the thermal barrier. C.M., central mirror. T.B., thermal barrier. P, plug mirror.

$$\phi_b = \frac{\kappa T_{ec}}{e} \ln\left(\frac{n_c}{n_b}\right). \tag{17.44}$$

Therefore, if the electron temperature T_{ep} in the plug cell is increased, ϕ_c can be increased without the condition $n_p > n_c$; thus efficient potential plugging may be expected. Experiments with tandem mirrors have been carried out in TMX-U, GAMMA-10.

Experiments

Schematic diagram of **TMX** (tandem mirror experiment) at Lawrence Livermore Laboratory is shown in fig.17.27. At both sides of central solenoid coils confining the center-cell plasma, baseball coil type minimum B plugs provide an average minimum B configuration (refer to sec.17.3b) against interchange instability. Neutral beams with 13 keV×200 A (equivalent) per plug are injected and about 400 kW is trapped by the end plug plasmas provided by titanium-washer gun of the type used in 2XIIB. Axial profile data of magnetic field, electron density, and plasma potential are plotted in fig.17.27 (ref.[92]). In plug cells, the densities are higher than that of center-cell and ion confining potentials are formed. The mean temperature of center-cell plasma is $T_i \sim T_e \sim 70\,\text{eV}$ and center-cell β value as high as 5∼10% is observed. Ion confining potential is $\phi_c \sim 120\,\text{V}$ and center-cell confinement parameter is $n_e\tau_p \sim 3\times10^{10}\,\text{cm}^{-3}\cdot\text{s}$,($n_e \sim 0.5\times10^{13}\ \text{cm}^{-3}$). Electrostatic enhancement in confinement is ∼4.

TMX-U is the tandem mirror with thermal barrier and demonstrates the formation of microstable sloshing-ion distribution. By sloshing-ion produced by neutral beam injectors and electron cyclotron resonance heating of electrons, both ion confining potential ϕ_c and thermal barrier potential ϕ_b are formed in single plug cell (ref.[93]). When the neutral beam is injected with the appropriate angle to the magnetic field, fast neutrals are ionized and are trapped and bounce back and forth in the plug cell. The density profile of sloshing-ions is higher in the reflecting regions than in the middle region (double peaks). Furthermore, when the electrons at the (outside) peak region are heated by ECRH with fundamental cyclotron frequency (ω_{ce}), hot electrons are produced. Hot

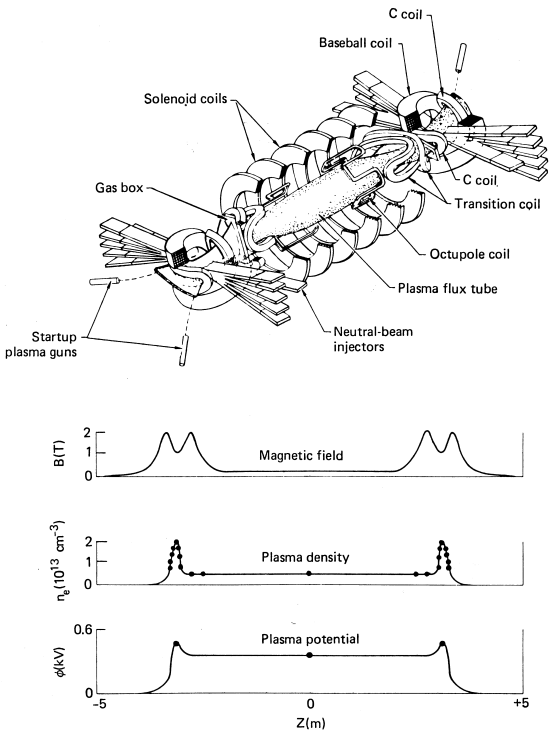

Fig.17.27 Schematic diagram of TMX magnet geometry and measured axial profiles of magnetic field, electron density, and plasma potential. After (ref.[92]).

electrons are pushed out by the force $-\mu\nabla B$ and ion confining potential ϕ_c is built up to keep the charge neutrality. Furthermore, when hot electrons are produced by 2nd harmonic ECRH ($2\omega_{ce}$) in the middle region of the plug cell, the thermal barrier potential ϕ_b (17.44) is modified to

$$e\phi_b = \kappa T_{ec} \ln\left(\frac{n_c}{n_b - n_{hot}}\right), \tag{17.45}$$

where n_{hot} is the density of hot electrons, which are trapped in the plug cell and cannot transit to the center-cell. The thermal barrier is then formed.

Axial profile of the magnetic field and axial measured potential profile are shown in fig.17.28. When both sloshing-ions and ECRH powers are present, fig.17.28 shows remarkable reduction of the end-loss currents out one end. The pulsed nature of the end-loss current seen in fig.17.28 results from sweeping the analyzer ion-repeller voltage to measure the energy distribution. Ion confining potential ϕ_c is larger than 1.5 kV and barrier potential ϕ_b is 0.45 kV. The center-cell beta resulting mainly from the neutral beam injected ions reaches 6% average over the radius to the limiter. During strong end plugging at low density ($7 \times 10^{11}\,cm^{-3}$), the axial ion confinement time $\tau_{\parallel}$ reaches 50∼100 ms, while the non-ambipolar radial ion confinement time $\tau_{\perp}$ is 14 ms. At high densitiy and lower ion confining potential, $\tau_{\parallel}$ is 6∼12 ms and $\tau_{\perp}$ exceeds 100 ms. Ions have been heated up to $T_{\perp i} \sim 2$ keV.

GAMMA 10 at University of Tukuba is the tandem mirror with axisymmetrized end plugging with thermal barrier with use of neutral beam injection and ECRH. Schematics of GAMMA 10 device and magnetic flux tube, together with heating systems, are shown in fig.17.29. The device length is 27 m. It consists of a center-cell ($B \sim 0.5$T), anchor cells and axisymmetric end mirror cells with thermal barrier and ion confining potential. The anchor cell is a minimum B mirror for suppressing interchange instability. Ramp coils set at both ends of the center cell throttle the fraction of passing particles flowing into the minimum B anchors and plug/barrier cells. When the axial potential hill is kept low in the anchor transition region, the center-cell ions are either reflected by the ramp coils or pass through the anchors and are reflected by the axisymmetric plugs with thermal barrier by use of NBI for sloshing-ions and ECRH. Axisymmetric plugs could reduce the resonant diffusion of ions trapped by non-axisymmetric plugs. Axial profile of magnetic field,

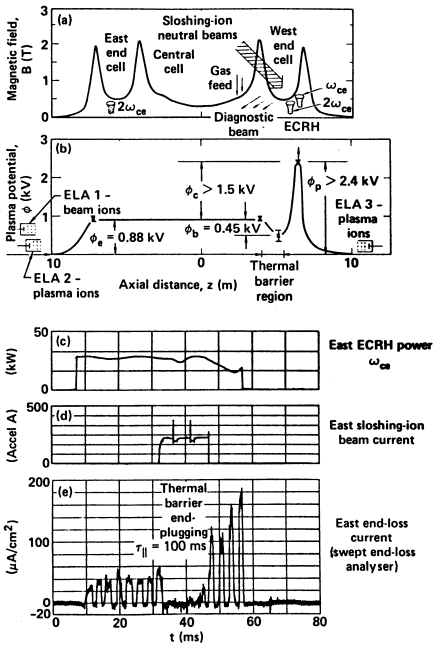

Fig.17.28 Thermal barrier measurements in TMX-U. (a) Axial profile of the magnetic field with illustration of heating systems used for single-end plugging operation, (b) axial measured potential profile, (c) time history of ECRH power, (d) time history of sloshing-beam current, and (e) time history of resulting end-loss current measured with a sweep end-loss analyzer showing that both ECRH and sloshing beam are required to reduce end losses. After (ref.[93]).

potential, and density are shown in fig.17.29 (ref.[94]).

The improvement of plasma confinement in the hot ion mode was obtained in 1998 (ref.[95]). RF heating in the ion cyclotron range of frequency (ICRF) is mainly used for plasma production and heating in center-cell. ECRHs are used for the formation of ion confining potential without sloshing-ions. The optimizations of the axisymmetrized heating patterns of ECRH and ICRH heating power are made. Furthermore, conducting plates in anchor cells are installed near the surface of plasma with the fanning magnetic flux tube in order to fix the potential at the boundary for reducing irregular electric field. Center-cell line density and end-loss currents to the end-loss ion energy analyzer (ELA) located in the east and west open ends are shown in fig.17.30. The effects of potential confinement are clearly seen in fig.17.30. The center-cell plasma with average ion temperature of 2.8 keV ($T_{i0} \sim 4.5$ keV) and the density on axis of 2.7×10^{12} cm^{-3} are obtained. An ion confining potential is ~ 0.6 kV. The particle confinement time is $\tau_{\parallel} \approx 40$ ms, which is one order of magnitude improvement due to potential confinement. The observed energy confinement time is $\tau_E \approx 10$ ms. The electron temperature is $\sim$80 eV.

A factor of 3 progresses up to 2.1 kV in the formation of ion confining potential was achieved in the hot ion mode with ion temperature of several keV and $n_e \sim 2 \times 10^{12}$ cm^{-3} in 2004 (ref.[96]). The advance in the potential formation gives the basis for finding the remarkable effects of sheared flow due to radial electric field on the suppression of turbulent fluctuations in GAMMA 10. From the viewpoint of both higher potential confinement in the axial direction and the suppressed turbulence due to a strong shear flow, a high potential formation plays a role in providing improved ion confinement both radially and axially simultaneously. In the case of $\phi_c = 0.84$ kV, particle confinement time is $\tau = 75$ ms ($\tau_{\parallel} = 95$ ms, $\tau_{\perp} > 4\tau_{\parallel}$) and Pastukhov's ion energy confinement time is $\tau_{E\,Pastu} = 50$ ms.

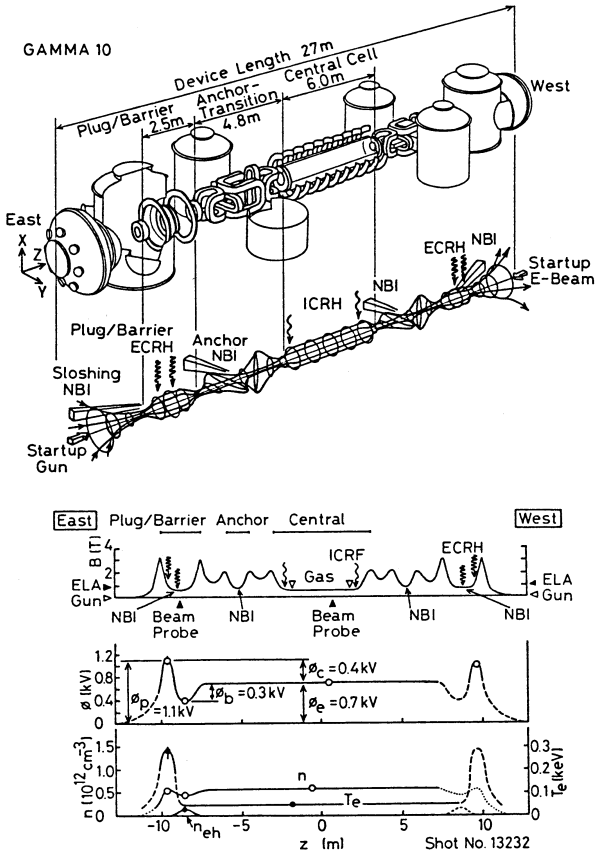

Fig.17.29 Schematics of GAMMA 10 device and magnetic flux tube with heating systems. Axial distribution of magnetic field strength and positions of heating, potential distribution measured by center-cell and barrier beam probes and end-loss analyzer, and axial distribution of density, electron temperature. After (ref.[94]).

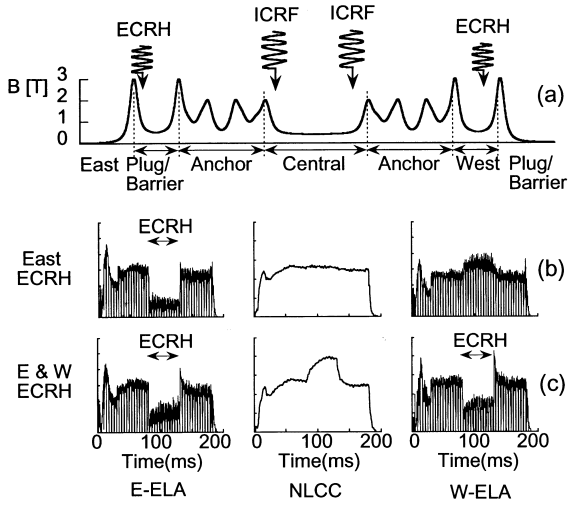

Fig.17.30 (a) Axial profile of magnetic field and location of heating systems in GAMMA 10. (b) and (c) Center-cell line density (NLCC) and end-loss currents to the east end-loss ion energy analyzer (E-ELA) and west (W-ELA), where one division of NLCC is $10^{13}\,\mathrm{cm}^{-2}$ and that of ELA is $10^{-4}\,\mathrm{A/cm}^2$. ECRH is applied from 80 ms to 130 ms. After (ref.[95]).

References

17.1 Revered Field Pinch

[1] D. C. Robinson and R. E. King: Plasma Physics and Controlled Nuclear Fusion Research **1**, (1969) (Conference Proceedings, Novosibirsk in 1968) IAEA Vienna
[2] H. A. B. Bodin and A. A. Newton: Nucl. Fusion **20**, 1255 (1980)
[3] H. A. B. Bodin: Plasma Phys. and Controlled Fusion **29**, 1297 (1987)
[4] MST Team: Plasma Physics and Controlled Nuclear Fusion Research **2**, 519 (1991) (Conference Proceedings, Washington D. C. in 1990) IAEA Vienna
TPE-1RM20 Team: 19th Fusion Energy Conference **2**, 95 (1997) (Conference Proceedings, Montreal in 1996) IAEA Vienna
[5] EX4/3(RFX), EX4/4(TPE-RX): 17th Fusion Energy Conference **1** 367, 375 (1999) (Conference Proceedings, Yokohama in 1998 IAEA Vienna
[6] J. B. Taylor: Phys. Rev. Lett. **33**, 1139 (1974)
[7] T. H. Jensen and M. S. Chu: Phys. Fluids **27**, 2881 (1984)
[8] V. D. Shafranov and E. I. Yurchenko: Sov. Phys. JETP **26**, 682 (1968)
[9] K. Miyamoto: Plasma Phys. and Controlled Fusion **30**, 1493 (1988)
[10] K. Kusano and T. Sato: Nucl. Fusion **26**, 1051 (1986)
[11] D. D. Schnack, E. J. Caramana and R. A. Nebel: Phys. Fluids **28**, 321 (1985)
[12] S. C. Prager, J. Adney, A. Almagri, J. Anderson, A. Blair et al.: 20th IAEA Fusion Energy Conf. (Vilamoura 2004) OV/4-2.
[13] A. R. Jacobson and R. W. Moses: Phys. Rev. A**29** 3335 (1984)
[14] K. A. Werley, J. N. Dimarco, R. A. Krakowski, and C. G. Bathke: Nucl. Fusion **36**, 629 (1996).
[15] B. E. Chapman, J. K. Anderson, T. M. Biewer, D. L. Brower, S. Castillo et al.: Phys. Rev. Lett. **87**, 205001 (2001).
B. E. Chapman, A. F. Almagri, J. K. Anderson, T. M. Biewer, P. K. Chattopadhyay et al.: Phys. Plasmas **9**, 2061 (2002).
[16] M. Valisa, F. Auriemma, A. Canton, L. Carraro, R. Lorenzini et al.: 20th IAEA Fusion Energy Conf. (Vilamoura 2004) EX/P4-13.
[17] J. S. Sarff, S. A. Hokin, H. Ji, S. C. Prager, and C. R. Sovinec: Phys. Rev. Lett. **72**, 3670 (1994).
[18] J. S. Sarff, N. E. Lanier, S. C. Prager, and M. R. Stoneking: Phys. Rev. Lett. **78**, 62 (1997).
[19] J. S. Sarff, A. F. Almagri, J. K. Anderson, T. M. Biewer, D. L. Brower et al.: 19th IAEA Fusion Energy Conf. (Lyon 2002) OV/4-3.
[20] R. Bartiromo, P. Martin, S. Martini, T. Bolzonella, A. Canton, and P. Innocente: Phys. Rev. Lett. **82**, 1462 (1999).
[21] Y. Yagi, H. Koguchi, Y. Hirano, T. Shimada, H. Sakakita, and S. Sekine: Phys. Plasmas **10**, 2925 (2003).
[22] Y. Yagi, H. Koguchi, Y. Hirano, H. Sakakita, and L. Frassinetti: Nucl. Fusion **45**, 138 (2005).
[23] M. K. Bevir and J. W. Gray: Proc of Reversed Field Pinch Theory Workshop (LANL Los Alamos, 1981) Report No–8944–C, p.176
M. K. Bevir and C. G. Gimblett: Phys. Fluids **28**, 1826 (1985)
[24] K. F. Schoenberg, J. C. Ingraham, C. P. Munson, P.G. Weber et al: Phys. Fluids **31**, 2285 (1988)

17.2 Stellarator

[25] L. Spitzer, Jr.: Phys. Fluids **1**, 253 (1958)
[26] A. I. Morozov and L. S. Solovév: *Reviews of Plasma Physics* **2**, 1 (ed. by M. A. Leontovich) Consultants Bureau, New York 1966
[27] K. Miyamoto: *Plasma Physics for Nuclear Fusion* (revised edition) Chap.2 The MIT Press 1989
[28] K. Nagasaki, K. Itoh, M. Wakatani and A. Iiyoshi: J.Phys. Soc. Japan **57**, 2000 (1988)
[29] W VIIA Team: Plasma Physics and Controlled Nuclear Fusion Research **2**, 241 (1983) (Conference Proceedings, Baltimore in 1982) IAEA Vienna
[30] E. D. Andryukhina, G. M. Batanov, M. S. Berezhetskij, M. A. Blokh, G. S. Vorosov *et al.*: Plasma Physics and Reseach Controlled Nuclear Fusion **2**, 409 (1985) (Conference Proceedings, London in 1984) IAEA Vienna
[31] K. Uo, A. Iiyoshi, T. Obiki, O. Motojima, S. Morimoto, M. Wakatani *et al.*: Plasma Physics and Controlled Nuclear Fusion Research **2**, 383 (1985) (Conference Proceedings, London in 1984) IAEA Vienna
[32] L. Garcia, B. A. Carreras, J. H. Harris, H. R. Hicks and V. E. Lynch: Nucl. Fusion **24**, 115 (1984)
[33] C. Gourdon, D. Marty, E. K. Maschke and J. P. Dumont: Plasma Physics and Controlled Nuclear Fusion Research **1**, 847 (1969) (Conference Proceedings, Novosibirsk in 1968) IAEA Vienna
[34] K. Uo: Plasma Phys. **13**, 243 (1971)
[35] A. Mohri: J. Phys. Soc. Japan **28**, 1549 (1970)
[36] C. Gourdon, D. Marty, E. K. Maschke and J. Touche: Nucl. Fusion **11**, 161 (1971)
[37] Yu. N. Petrenko and A. P. Popryadukhin: The 3rd International Symposium on Toroidal Plasma Confinements, D 8 March 1973 Garching

[38] H. Wobig and S. Rehker: Proceedings of the 7th Symposium on Fusion Technology, Grenoble 345 (1972)
Rehker and H. Wobig: Proceedings of the 6th European Conference on Controlled Fusion and Plasma Physics p.117 in Moscow (1973),
Rehker and H. Wobig: IPP 2/215 Max Planck Inst. of Plasma Phys. (1973)
[39] B. B. Kadomtsev and O. P. Pogutse: Nucl. Fusion **11**, 67 (1971)
[40] J. A. Derr and J. L. Shohet: Phys. Rev. Lett. **44**, 1730 (1979)
[41] M. Wakatani, S. Kodama, M. Nakasuga and K. Hanatani: Nucl. Fusion **21**,175 (1981)
[42] J. W. Connor and R. J. Hastie: Phys. Fluids **17**, 114 (1974)
[43] L. M. Kovrizhnykh: Nucl. Fusion **24**, 851 (1984)
[44] D. E. Hastings, W. A. Houlberg and K.C.Shaing: Nucl. Fusion **25**, 445 (1985)
[45] K. M. Young: Plasma Phys. **16**, 119 (1974)
[46] K. Miyamoto: Nucl. Fusion **18**, 243 (1978)
[47] B. A. Carreras, G. Griegen, J. H. Harris, J. L. Johnson, J. F. Lyon, O. Motojima, F. Rau, H. Renner, J. A. Rome, K. Uo, M. Wakatani and H. Wobig: Nucl. Fusion **28**, 1613 (1988)
[48] S. Sudo, Y. Takeiri, Z. Zushi, F. Sano, K. Itoh, K. Kondo and A. Iiyoshi: Nucl. Fusion **30**, 11 (1990)
[49] U. Stroth, M. Murakami, R. A. Dory, H. Yamada, S. Okamura, F. Sano, T. Obiki: Nucl. Fusion **36**, 1063, (1996)
[50] A. Fujisawa, H. Iguchi, T. Minami, Y. Yoshimura, H. Sanuki, K. Itoh et al.: Phys. Rev. Lett. **82**, 2669 (1999).
[51] H. Massberg, C. D. Beidler, U. Gasparino, M. Rome, K. S. Dyailin et al.: Phys. Plasmas **7**, 295 (2000).
[52] O. Motojima, N. Ohyabu, A. Komori, O. Kaneko, H. Yamada et al.: 19th Fusion Energy Conf. (Lyon 2002), OV/1-6.
[53] K. Ida, S. Inagaki, T. Shimozuka, T. Tamura, H. Funaba et al.: Phys. Plasmas **11**, 2551 (2004).
[54] A. Fujisawa, K. Itoh, H. Iguchi, K. Matsuoka, S. Okamomura et al.: Phys. Rev. Lett. **93**, 165002 (2004).
[55] U. Stroth, J. Baldzuhm, J. Geiger, T. Geist, L. Giannone et al.: Plasma Phys. Contr. Fusion **40**, 1551 (1998).
[56] K. McCormick, P. Grigull, R. Burhenn, R. Brakel, H. Ehmler et al.: Phys. Rev. Lett. **89**, 015001 (2002).
[57] F. Wagner, R. Burhenn, F. Gadelmeier, J. Geiger, M. Hirsch, et al.: 19th Fusion Energy Conf. (Lyon 2002), OV/2-4.
[58] K. Kawahata, N. Ohyabu, O. Kaneko, A. Komori, H. Yamada et al.: Plasma Phys. Contr. Fusion **42**, B51 (2000).
[59] O. Motojima, K. Ida, K. Y. Watababe, Y. Nagayama, A. Komori et al.: 20th Fusion Energy Conf. (Vilamoura 2004), OV/1-4.
[60] P. J. Heitzenroeder, T. G. Brown, J. H. Chrzanowski, M. J. Cole, P. L. Goranson et al.: 20th Fusion Energy Conf. (Vilamoura 2004), FT/P7-22.
M. C. Zarnstorff, L. A. Berry, A. Brooks, F. Fredrickson, G-Y. Fu et al: Plasma Phys. Contr. Fusion **43**, A237 (2001).
[61] F. S. B. Anderson, A. F. Almagri, D. T. Anderson, P. G. Mathews, J. N. Talmadge, and J. L. Shohet: Fusion Technol. **27**, 273 (1995).
S. P. Gerhardt, A. F. Almagri, D. T. Anderson, F. S. B. Anderson, D. Brower et al.: 20th Fusion Energy Conf. (Vilamoura 2004), EX/8-3.
[62] D. A. Spong, S. P. Hirshman, J. F. Lyon, L. A. Berry, D. J. Strickler et al.: 20th Fusion Energy Conf. (Vilamoura 2004), IC/P6-51.
B. E. Nelson, A. Brooks, R. D. Benson, L. A. Berry, T. G. Brown et al.: 19th Fusion Energy Conf. (Lyon 2002), FT/2-4.
[63] F. Wagner, T. Andreeva, J. Baldzuhn, A. Benndorf, H. Bolt et al.: 20th Fusion Energy Conf. (Vilamoura 2004), FT/3-5.
J. Nührenbberg et. al.: Fusion Technology **27**, 71 (1995)
W. Lotz, P. Merkl, J. Nührenbberg, and E. Strumberger: Plasma Phys. Contr. Fusion **34**, 1037 (1992).
[64] D. A. Spong, S. P. Hirshman, J. C. Whitson, D. B. Batchelor, R. Sanchez, B. A. Carreras et al.: Nucl. Fusion **40**, 563 (2000).
J. R. Cary and S. G. Shasharina: Stellarator. Plasma Phys. Reports **23**, 509 (1997).
[65] M Okamoto, M. Yokoyama, and N. Nakajima: J. Plasma Fusion Res. **74**, 1107 (1998)
[66] C. D. Beidler, E. Harmeyer, F. Herrngger, Yu. Igitkhanov, A. Kendl et al.: Nucl. Fusion **41**, 1759 (2001).
H. Wobig, C. D. Beider, J. Kisslinger, E. Harmeyer, F. Herrnegger et al.: 17th Fusion Energy Conf. (Yokohama 1998), FTP/01.
[67] A. Sagara, S. Imagawa, O. Mitarai, T. Dolan, T. Tanaka et al.: Nucl. Fusion **45**, 258 (2005).

17.3 Open End Systems

[68] D. V. Sivukhin: Reviews of Plasma Physics **4**, 93 (ed. by M. A. Leontovich) Consultants Bureau, New York 1966

[69] I. J. Spalding: Nucl. Fusion **8**, 161 (1968)
I. J. Spalding: *Advances in Plasma Physics* **4**, 79 (ed. by A. Simon and W. B. Thompson), Interscience, New York (1971)
[70] Yu. V. Gott, M. S. Ioffe and V. G. Tel'kovskii: Nucl. Fusion Suppl. Pt.3, 1045 (1962) (Conference Proceedings, Salzburg in 1961) IAEA Vienna
Yu. T. Baiborodov, M. S. Ioffe, V. M. Petrov and R. I. Sobolev: Sov. Atomic Energy **14**, 459 (1963)
[71] Yu. T. Baiborodov, M. S. Ioffe, B. I. Kanaev, R. I. Sobolev and E. E. Yushmanov: Plasma Physics and Controlled Nuclear Fusion Research **2**, 647 (1971) (Conference Proceedings, Madison in 1971) IAEA Vienna
[72] F. H. Coensgen, W. F. Cummins, V. A. Finlayson, W. E. Nexsen, Jr. and T. C. Simonen: ibid. **2**, 721 (1971)
[73] F. H. Coensgen, W. F. Cummins, B. G. Logan, A. W. Halvik, W. E. Nexsen, T. C. Simonen, B. W. Stallard and W. C. Turne: Phys. Rev. Lett. **35**, 1501(1975)
[74] ed. by T. K. Fowler: Nucl. Fusion **9**, 3 (1969)
[75] M. S. Ioffe and B. B. Kadomotsev: Sov. Phys. Uspekhi **13**, 225 (1970)
[76] R. F. Post: Nucl. Fusion **27**, 1579 (1987)
[77] E. G. Harris: Phys. Rev. Lett. **2**,34 (1959)
[78] R. A. Dory, G. E. Guest, E. G. Harris: Phys. Rev. Lett. **14**, 131 (1965)
[79] G. E. Guest and R. A. Dory: Phys. Fluids **8**, 1853 (1965)
[80] J. Gordey, G. Kuo-Petravic, E. Murphy, M. Petravie, D. Sweetman and E. Thompson: Plasma Physics and Controlled Nuclear Fusion Research **2**, 267 (1969) (Conference Proceedings, Novosibirsk in 1968) IAEA Vienna
[81] R. F. Post and M. N. Rosenbluth: Phys. Fluids **9**, 730 (1966)
[82] H. Postman, H. Dunlap, R. Dory, G. Haste and R. Young: Phys. Rev. Lett. **16**, 265 (1966)
[83] B. B. Kadomtsev and O. P. Pogutse: Plasma Physics and Controlled Nuclear Fusion Research **2**, 125 (1969) (Conference Proceedings, Novosibirsk in 1968) IAEA Vienna
[84] R. Z. Sagdeev and V. D. Shafranov: Sov. Phys. JETP **12**, 130 (1961)
[85] J. Sharer and A. Trivelpiece: Phys. Fluids **10**, 591 (1967)
[86] H. Ikegami, H. Ikezi, T. Kawamura, H. Momota, K. Takayama and Y. Terashima: Plasma Physics and Controlled Nuclear Fusion Research **2**, 423 (1969) (Conference Proceedings, Novosibirsk in 1968) IAEA Vienna
[87] G. I. Dimov, V. V. Zakaidakov and M. E. Kishinevskii: Sov. J. Plasma Phys. **2**, 326 (1976)
[88] T. K. Fowler and B. G. Logan: Comments Plasma Phys. Contorolled Fusion Res. **2**,167 (1977)
[89] V. P. Pastukhov: Nucl. Fusion **14**, 3 (1974)
[90] D. E. Baldwin and B. G. Logan: Phys. Rev. Lett. **43**, 1318 (1979)
[91] R. H. Cohen, I. B. Bernstein, J. J. Dorning and G. Rowland: Nucl. Fusion **20**, 1421 (1980)
[92] F. H. Coensgen, C. A. Anderson, T. A. Casper, J. F. Clauser, W. C. Condit et al.: Phys. Rev. Lett. **44**, 1132 (1980).
T. C. Simonen, C. A. Anderson, T. A. Casper, J. F. Clauser, F. H. Coesgen et al.: Plasma Phys. Contr. Nucl. Fusion Res. (Conf. Proceedings, Brussel 1980) **1**, 97 (1981) IAEA, Vienna.
[93] T. C. Simonen, S. L. Allen, D. E. Baldwin, T. A. Casper, J. F. Clauser et al.: Plasma Phys. Contr. Nucl. Fusion Res. (Conf. Proceedings, London 1984) **2**, 255 (1985) IAEA, Vienna.
D. P. Grubb, S. L. Allen, T. A. Casper, J. F. Clauser, F. H. Coesgen et al.: Phys. Rev. Lett. **53**, 783 (1984).
[94] T. Cho, M. Ichimura, M. Inutake, K. Ishii, S. Miyoshi et al.: Plasma Phys. Contr. Nucl. Fusion Res. (Conf. Proceedings, London 1984) **2**, 275 (1985) IAEA, Vienna.
[95] K. Yatsu, L. G. Bruskin, T. Cho, M. Hamada, M. Hirata et al.: 17th Fusion Energy Conf. (Yokohama 1998), EX4/6.
[96] T. Cho, H. Higaki, M. Hirata, H. Hojo, M. Ichimura et al.: 20th Fusion Energy Conf. (Vilamoura 2004), EX/9-6Rd.

Ch.18 Inertial Confinement

The characteristic of inertial confinement is that the extremely high-density plasma is produced by means of an intense energy driver, such as a laser or particle beam, within a short period so that the fusion reactions can occur before the plasma starts to expand (ref.[1]). Magnetic confinement play no part in this process, which has come to be called inertial confinement. For fusion conditions to be reached by inertial confinement, a small solid deuterium-tritium pellet must be compressed to a particle density $10^3 \sim 10^4$ times that of the solid pellet particle density $n_s = 5 \times 10^{22}\,\mathrm{cm}^{-3}$. One cannot expect the laser light pressure or the momentum carried by the particle beam to compress the solid pellet: they are too small. A more feasible method of compression involves irradiating the pellet from all side, as shown in fig.18.1. The plasma is produced on the surface of the pellet and is heated instantaneously. The plasma expands immediately. The reaction of the outward plasma jet accelerates and compresses the inner pellet inward like a spherical rocket. This process is called implosion. The study of implosion processes is one of the most important current issues, and theoretical and experimental research is being carried out intensively.

18.1 Pellet Gain

Let the pellet gain G_{pellet} be the ratio of the output nuclear fusion energy E_{NF} to the input driver energy E_{L} delivered to the pellet. The heating efficiency η_{h} of the incident driver is defined by the conversion ratio of the driver energy E_{L} to the internal energy E_{fuel} of the compressed pellet core. Denote the density and the volume of the compressed core plasma by n and V, respectively, and assume that $\langle \varepsilon_{\mathrm{fuel}} \rangle$ is the average energy of a fuel particle. Then we have the following relation:

$$E_{\mathrm{fuel}} = \langle \epsilon_{\mathrm{fuel}} \rangle nV = \eta_{\mathrm{h}} E_{\mathrm{L}}. \tag{18.1}$$

The average energy of a fuel particle is $3/2\kappa T$ in usual cases. However when the electron density is extremely high, we must take account of electron Fermi energy. Later we discuss on this mautter at the end of this section.

The densities $n_{\mathrm{D}}, n_{\mathrm{T}}$ of the duetrium and tritium are decreased by the D-T fusion reaction ($n_{\mathrm{D}} = n_{\mathrm{T}} = n/2$) and

$$\frac{1}{n_{\mathrm{D}}} \frac{\mathrm{d}n_{\mathrm{D}}}{\mathrm{d}t} = -n_{\mathrm{T}} \langle \sigma v \rangle,$$

$$n(t) = n_0 \frac{1}{1 + n_0 \langle \sigma v \rangle t/2}.$$

When the plasma is confined during the time τ, the fuel-burn ratio f_{B} is given by

$$f_{\mathrm{B}} \equiv \frac{n_0 - n(\tau)}{n_0} = \frac{n_0 \langle \sigma v \rangle \tau/2}{1 + n_0 \langle \sigma v \rangle \tau/2} = \frac{n_0 \tau}{2/\langle \sigma v \rangle + n_0 \tau} \tag{18.2}$$

and the fusion output energy E_{NF} is

$$E_{\mathrm{NF}} = f_{\mathrm{B}} nV \frac{Q_{\mathrm{NF}}}{2} \qquad (Q_{\mathrm{NF}} = 17.5\mathrm{MeV}). \tag{18.3}$$

When the core gain G_{core} and pellet gain G_{pellet} are defined by

$$G_{\mathrm{core}} \equiv \frac{E_{\mathrm{NF}}}{E_{\mathrm{fuel}}} \tag{18.4}$$

$$G_{\mathrm{pellet}} \equiv \frac{E_{\mathrm{NF}}}{E_{\mathrm{L}}} = \eta_{\mathrm{h}} G_{\mathrm{core}} \tag{18.5}$$

the pellet gain G_{pellet} is

$$G_{\mathrm{pellet}} = \eta_{\mathrm{h}} \left(\frac{Q_{\mathrm{NF}}}{2\langle \epsilon_{\mathrm{fuel}} \rangle} \right) \frac{n_0 \tau}{2/\langle \sigma v \rangle + n_0 \tau}. \tag{18.6}$$

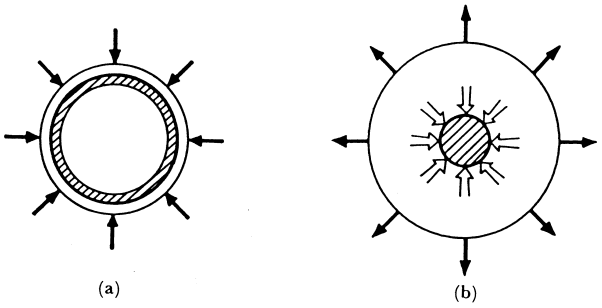

Fig.18.1 Conceptual drawing of implosion. (a) Irradiation by laser or particle beam from all side. (b) Expansion of plasma from the pellet surface and the implosion due to the reaction of the outward plasma jet.

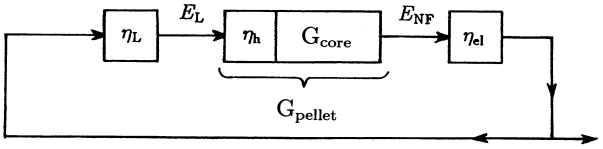

Fig.18.2 Energy flow diagram of an inertial confinement reactor.

Let us consider the energy balance of a possible inertial fusion reactor. The conversion efficiency of the thermal-to-electric energy is $\eta_{\rm el}$, and the conversion efficiency of the electric energy to output energy of the driver is denoted by $\eta_{\rm L}$. Then

$$\eta_{\rm el}\eta_{\rm L}G_{\rm pellet} > 1 \tag{18.7}$$

is at least necessary to obtain usable net energy from the reactor (see fig.18.2) (When $\eta_{\rm L} \sim 0.1$, $\eta_{\rm el} \sim 0.4$ are assumed, $G_{\rm pellet} > 25$ is necessary). Therefore we find from (18.6) and (18.7)

$$n\tau > \frac{4\langle\epsilon_{\rm fuel}\rangle}{\eta_{\rm el}\eta_{\rm L}\eta_{\rm h}Q_{\rm NF}\langle\sigma v\rangle}\frac{1}{[1-2\langle\epsilon_{\rm fuel}\rangle/(\eta_{\rm el}\eta_{\rm L}\eta_{\rm h}Q_{\rm NF})]}. \tag{18.8}$$

The confinement time τ is the characteristic expansion time and is expressed by (ref.[2])

$$\tau \approx \frac{r}{3c_{\rm s}}, \qquad c_{\rm s}^2 = \frac{5}{3}\frac{p}{\rho_{\rm m}} = \frac{10}{3}\frac{\kappa T}{m_{\rm i}} \tag{18.9}$$

where $c_{\rm s}$ is the sound velocity. Since the volume V of the core is

$$V = \frac{4\pi r^3}{3}$$

(18.1) reduces to

$$E_{\rm L} = \frac{4\pi}{3\eta_{\rm h}}nr^3\langle\epsilon_{\rm fuel}\rangle.$$

Equations (18.2) and (18.9) yield

$$\tau = \frac{f_{\rm B}}{(1-f_{\rm B})}\frac{2}{n\langle\sigma v\rangle}, \tag{18.10}$$

$$r = 3c_{\rm s}\tau = 5.48\left(\frac{\kappa T}{m_{\rm i}}\right)^{1/2}\tau. \tag{18.11}$$

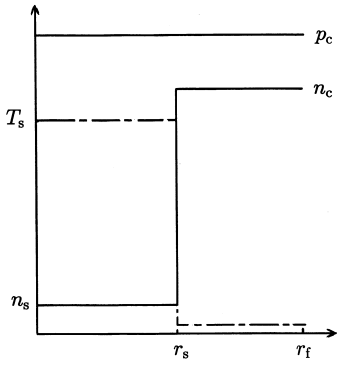

Fig.18.3 Profiles for pressure, temperature and density of isobar model ignition configuration.

The fuel-burn ratio f_B is rewritten by

$$f_B = \frac{r\rho_m}{6c_s m_i/\langle\sigma v\rangle + r\rho_m}, \tag{18.12}$$

where m_i is the average mass of D,T particles ($m_i = 2.5m_p$, m_p is proton mass). When $\beta(T)$ is defined by

$$\beta(T) \equiv \frac{6c_s m_i}{\langle\sigma v\rangle}, \tag{18.13}$$

we have

$$f_B = \frac{r\rho_m}{r\rho_m + \beta(T)}, \qquad f'_B \equiv \frac{f_B}{1-f_B} = \frac{r\rho_m}{\beta(T)}. \tag{18.14}$$

that is

$$r\rho_m = f'_B\beta(T). \tag{18.15}$$

Equation (18.15) with (18.13) is equivalent to (18.11) with (18.10). When $\kappa T = 10\,\mathrm{keV}$, then $\langle\sigma v\rangle \simeq 1.1\times10^{-16}\,\mathrm{cm^3 s^{-1}}$ and $\beta(T) \approx 25.8\mathrm{g/cm^2}$. When the plasma density is expressed by the ratio to the solid density $n_{\mathrm{solid}} = 5\times10^{22}\,\mathrm{cm^{-3}}$ or the mass density $\rho_{m\,\mathrm{solid}} = m_i n_{\mathrm{solid}} = 0.21\mathrm{g/cm^3}$, (18.10),(18.11),(18.6) yield

$$\tau = 0.36\times10^{-6} f'_B \left(\frac{n_{\mathrm{solid}}}{n}\right)\frac{\langle\sigma v\rangle_{10\mathrm{keV}}}{\langle\sigma v\rangle} \quad \mathrm{(s)}$$

$$r = 1.2\times10^{2} f'_B \left(\frac{n_{\mathrm{solid}}}{n}\right)\frac{\langle\sigma v\rangle_{10\mathrm{keV}}}{\langle\sigma v\rangle}\left(\frac{(\kappa T)_{\mathrm{keV}}}{10}\right)^{1/2} \quad \mathrm{(cm)}$$

$$G_{\mathrm{pellet}} = \eta_h f_B \frac{Q_{\mathrm{NF}}/2}{\langle\epsilon_{\mathrm{fuel}}\rangle} = 8.8\times10^{6}\left(\frac{\eta_h f_B}{\langle\epsilon_{\mathrm{fuel}}\rangle_{\mathrm{eV}}}\right)$$

$$E_L = \frac{1}{\eta_h}\langle\epsilon_{\mathrm{fuel}}\rangle\frac{4\pi}{3}nr^3 \propto \frac{\langle\epsilon_{\mathrm{fuel}}\rangle}{\eta_h}\left(\frac{n_{\mathrm{solid}}}{n}\right)^2 {f'_B}^3.$$

Let us estimate the internal energy of the fuel E_{fuel}. At the time of compression, almost all the inward going energy has been converted into internal energy and the pressure is nearly uniform over the total (hot and cold) fuel region at ignition (isobar model) (ref.[3]). But the central spark region becomes hot and is surrounded by the cold compressed fuel (see Fig.18.3). The internal energy of solid cold DT fuel per unit volume is given by the product of Fermi energy

$$\epsilon_F = (\hbar^2/2m_e)\times(3\pi^2 n)^{2/3}$$

($\hbar = h/2\pi$ is Planck's constant, m_e is the electron mass) and the density with a factor of 3/5 (ref.[4]). The Fermi energy of electron with solid density $n_s = 5\times10^{22}\mathrm{cm^{-3}}$ (mass density $\rho_s = 0.21\mathrm{g/cm^3}$)

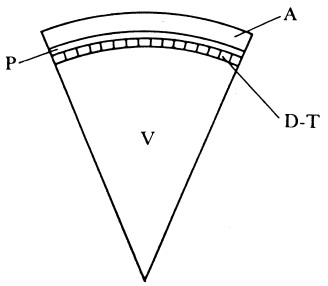

Fig.18.4 Pellet structure. A:ablator, P:pusher, D-T:solid D–T fuel, V:vacuum.

is $\epsilon_{\mathrm{F,s}} = 4.95\mathrm{eV}$. If the preheating occurs before the compression starts, the energy density of the cold fuel is

$$n\langle\epsilon_{\mathrm{fuel}}\rangle = \frac{3}{5}\alpha n\epsilon_{\mathrm{F}} = \frac{3}{5}\alpha n\left(\frac{\hbar^2}{2m_{\mathrm{e}}}\right)(3\pi^2 n)^{2/3}. \tag{18.16}$$

$\alpha = 2 \sim 3$ is called preheating factor. Then the fuel energy is

$$E_{\mathrm{fuel}} = 3n_{\mathrm{s}}\kappa T_{\mathrm{s}}V_{\mathrm{s}} + \frac{3}{5}\alpha\epsilon_{\mathrm{F}}n_{\mathrm{c}}V_{\mathrm{c}} = \frac{3}{5}\alpha\epsilon_{\mathrm{F}}n_{\mathrm{c}}V_{\mathrm{f}} \tag{18.17}$$

because of pressure balance $2n_{\mathrm{s}}\kappa T_{\mathrm{s}} = (2/5)\alpha\epsilon_{\mathrm{F}}$. $V_{\mathrm{s}}, r_{\mathrm{s}}$ and $V_{\mathrm{f}}, r_{\mathrm{f}}$ are the volumes and radii of the spark region and the total region of the fuel respectively. V_{c} is the volume of the cold compressed region $V_{\mathrm{c}} = V_{\mathrm{f}} - V_{\mathrm{s}}$. T_{s} and n_{s} are the temperature and the density of spark region and n_{c} is the density of the cold compressed region. Then the fusion output is

$$E_{\mathrm{NF}} \sim \frac{f_{\mathrm{B}}}{2}n_{\mathrm{c}}V_{\mathrm{c}}Q_{\mathrm{NF}} \qquad f_{\mathrm{B}} \sim \frac{\rho_{\mathrm{c}}(r_{\mathrm{f}} - r_{\mathrm{s}})}{\beta(T) + \rho_{\mathrm{c}}(r_{\mathrm{f}} - r_{\mathrm{s}})}. \tag{18.18}$$

Here the contribution from the spark region is neglected ($n_{\mathrm{s}}V_{\mathrm{s}} \ll n_{\mathrm{c}}V_{\mathrm{c}}$). The core gain G_{core} is

$$G_{\mathrm{core}} \sim \left(\frac{\rho_{\mathrm{c}}(r_{\mathrm{f}} - r_{\mathrm{s}})}{\beta(T) + \rho_{\mathrm{c}}(r_{\mathrm{f}} - r_{\mathrm{s}})}\right)\frac{Q_{\mathrm{NF}}/2}{(3/5)\alpha\epsilon_{\mathrm{F}}}\frac{V_{\mathrm{c}}}{V_{\mathrm{f}}}. \tag{18.19}$$

The ignition condition is given by (ref.[5],[6])

$$\rho_{\mathrm{s}}r_{\mathrm{s}} > 0.3 \sim 0.4\mathrm{g/cm}^2, \tag{18.20}$$

and the slowing down length of alpha particle λ_α is given by $\rho\lambda_\alpha = 0.015\,T_{\mathrm{keV}}^{5/4}\ \mathrm{g/cm}^2$ and $\rho_{\mathrm{s}}r_{\mathrm{s}} > \rho\lambda_\alpha$ is required (ref.[7],[8]).

Let us take an example of $n_{\mathrm{c}} = 2000n_{\mathrm{solid}}$. In this case $\rho_{\mathrm{c}} = 420\mathrm{g/cm}^3$ and $\epsilon_{\mathrm{F}} = 786\mathrm{eV}$. The mass density of the spark region is $\rho_{\mathrm{s}} = \alpha\epsilon_{\mathrm{F}}\rho_{\mathrm{c}}/5\kappa T_{\mathrm{s}} = 26.4\mathrm{g/cm}^3$ ($\kappa T_{\mathrm{s}} = 5\mathrm{keV}, \alpha = 2$). From the ignition condition we choose $r_{\mathrm{s}} = 0.015\mathrm{cm}$. The value of the fuel radius is chosen as $r_{\mathrm{f}} = 0.03\mathrm{cm}$. Then we have $\langle\epsilon_{\mathrm{fuel}}\rangle = 0.6\alpha\epsilon_{\mathrm{F}} = 943\mathrm{eV}$ assuming $\alpha = 2$ and $E_{\mathrm{fuel}} = 1.7\mathrm{MJ}$. The driver energy becomes $E_{\mathrm{L}} = 17\mathrm{MJ}$ under the assumption of $\eta_{\mathrm{h}} = 0.1$ and then the pellet gain is $G_{\mathrm{pellet}} = 3.2\times10^2$ for $f_{\mathrm{B}} \sim 0.34$.

The critical issue for an inertial fusion reactor are how extremely high-density plasmas can be produced by implosion and the optimum design of fuel pellet structures and materials are important.

Technological issues of energy drivers are increase of the efficiency of laser drivers and improvement of the focusing of light ions or heavy ion beams.

18.2 Implosion

A typical structure of a pellet is shown in fig.18.4. Outside the spherical shell of deuterium-tritium fuel, there is a pusher cell, which plays the role of a piston during the compression; an

ablator cell with low-Z material surrounds the pusher cell and the fuel. The heating efficiency $\eta_{\rm h}$ is the conversion ratio of the driver energy to the thermal energy of the compressed core fuel. The heating efficiency depends on the interaction of the driver energy with the ablator, the transport process of the particles and the energy, and motion of the plasma fluid. The driver energy is absorbed on the surface of the ablator, and the plasma is produced and heated.

Then the plasma expands and the inner deuterium-tritium fuel shell is accelerated inward by the reaction of the outward plasma jet. The implosion takes place at the center. Therefore the heating efficiency $\eta_{\rm h}$ is the product of three terms, that is, the absorption ratio $\eta_{\rm ab}$ of the driver energy by the ablator, the conversion ratio $\eta_{\rm hydro}$ of the absorbed driver energy to the kinetic energy of the hydrodynamic fluid motion, and the conversion ratio $\eta_{\rm T}$ of the kinetic energy of the hydrodynamic motion to the internal energy of compressed core:

$$\eta_{\rm h} = \eta_{\rm ab}\eta_{\rm hydro}\eta_{\rm T}.$$

The internal energy of the solid deuterium-tritium fuel per unit volume is given by $(3/5)n\epsilon_{\rm F}$. The internal energy of solid deuterium-tritium per unit mass w_0 can be estimated to be $w_0 = 1.1 \times 10^8$ J/Kg. If the preheating occurs before the compression starts, the initial internal energy is increased to $\alpha_{\rm p}w_0$, and then the solid deuterium-tritium fuel is compressed adiabatically. By use of the equation of state for an ideal gas, the internal energy w after the compression is

$$w = \alpha_{\rm p}w_0\left(\frac{\rho}{\rho_0}\right)^{2/3}$$

where ρ_0 and ρ are the mass densities before and after the compression. If the preheating is well suppressed and $\alpha_{\rm p}$ is of the order of 2 - 3, the internal energy per unit mass after $2000\times$ compression is $w \sim 4.5 \times 10^{10}$ J/Kg. This value w corresponds to the kinetic energy of unit mass with velocity $v \sim 3 \times 10^5$m/s $(w = v^2/2)$. Therefore, if the spherical fuel shell is accelerated to this velocity and if the kinetic energy is converted with good efficiency $\eta_{\rm T}$ into the internal energy of the fuel core at the center, then compression with 2000 times mass density of the solid deuterium-tritium is possible.

When the pellet is irradiated from all sides by the energy driver, the plasma expands with velocity u from the surface of the ablator. Then the spherical shell with mass M is accelerated inward by the reaction with the ablation pressure $P_{\rm a}$. The inward velocity v of the spherical shell can be analyzed by the rocket model with an outward plasma jet (ref.[9],[10]) that is,

$$\frac{{\rm d}(Mv)}{{\rm d}t} = -\frac{{\rm d}M}{{\rm d}t}\cdot u = SP_{\rm a} \tag{18.21}$$

where S is the surface area of the shell. When the average mass density and the thickness of the spherical shell are denoted by ρ and Δ, respectively, the mass M is $M = \rho S\Delta$. Usually the outward velocity of the expanding plasma u is much larger than the inward velocity of the spherical shell v, and u is almost constant. The change of sum of the kinetic energies of the plasma jet and the spherical shell is equal to the absorbed power of the energy driver as follows:

$$\eta_{\rm ab}I_{\rm L}S = \frac{\rm d}{{\rm d}t}\left(\frac{1}{2}Mv^2\right) + \frac{1}{2}\left(-\frac{{\rm d}M}{{\rm d}t}\right)u^2 \tag{18.22}$$

where $I_{\rm L}$ is the input power per unit area of the energy driver. From (18.21) and (18.22), the absorbed energy $E_{\rm a}$ is reduced to

$$E_{\rm a} = \int \eta_{\rm ab}I_{\rm L}S\,{\rm d}t \approx \frac{1}{2}(\Delta M)u^2 \tag{18.23}$$

where the approximations $u \gg v$, and u=const. are used. The quantity ΔM is the absolute value of the change of mass of the spherical shell. The pressure $P_{\rm a}$ is estimated from (18.21) and (18.22) as follows:

$$P_{\rm a} = \frac{u}{S}\left(-\frac{dM}{{\rm d}t}\right) \approx 2\eta_{\rm ab}I_{\rm L}\frac{1}{u}. \tag{18.24}$$

Then the conversion ratio $\eta_{\rm hydro}$ of the absorbed energy to the kinetic energy of the spherical shell is

$$\eta_{\rm hydro} = \frac{1}{2E_{\rm a}}(M_0 - \Delta M)v^2 = \frac{M_0 - \Delta M}{\Delta M}\left(\frac{v}{u}\right)^2 .$$

Since the rocket equation (18.21) implies $v/u = -\ln((M_0 - \Delta M)\,/M_0)$, the conversion ratio $\eta_{\rm hydro}$ is

$$\eta_{\rm hydro} = \left(\frac{M_0}{\Delta M} - 1\right)\left(\ln\left(1 - \frac{\Delta M}{M_0}\right)\right)^2 \approx \frac{\Delta M}{M_0} \tag{18.25}$$

where $\Delta M/M_0 \ll 1$ is a assumed.

The final inward velocity of the accelerated spherical shell must still be larger than $v \sim 3 \times 10^5\,\mathrm{m/s}$. The necessary ablation pressure $P_{\rm a}$ can be obtained from (18.21) with relation $S = 4\pi r^2$, and the approximation $M \approx M_0$, $P_{\rm a} \approx$ const. as follows:

$$\frac{{\rm d}v}{{\rm d}t} = \frac{4\pi P_{\rm a}}{M_0}r^2 = \frac{P_{\rm a}}{\rho_0 r_0^2 \Delta_0}r^2, \qquad v = -\frac{{\rm d}r}{{\rm d}t}.$$

Integration of $v \cdot {\rm d}v/{\rm d}t$ gives

$$P_{\rm a} = \frac{3}{2}\rho_0 v^2 \frac{\Delta_0}{r_0} \tag{18.26}$$

where ρ_0, r_0, and Δ_0 are the mass density, the radius, and the thickness of the spherical shell at the initial condition, respectively. When $r_0/\Delta_0 = 20$ and $\rho_0 = 0.21\mathrm{g/cm^3}$, the necessary ablation pressure is $P_{\rm a} = 1.4 \times 10^{12}\,\mathrm{Newton/m^2} = 14\,\mathrm{Mbar}$ (1 atm = 1.013 bar) in order to achieve the velocity $v = 3 \times 10^5\,\mathrm{m/s}$. Therefore the necessary energy flux intensity of driver $I_{\rm L}$ is

$$\eta_{\rm ab} I_{\rm L} = \frac{P_{\rm a} u}{2}. \tag{18.27}$$

For the evaluation of the velocity u of the expanding plasma, the interaction of the driver energy and the ablator cell must be taken into account. In this section the case of the laser driver is described. Let the sound velocity of the plasma at the ablator surface be $c_{\rm s}$ and the mass density be $\rho_{\rm c}$. The energy extracted by the plasma jet from the ablator surface per unit time is $4\rho_{\rm c}c_{\rm s}^3$ and this must be equal to the absorbed energy power $\eta_{\rm ab}I_{\rm L}$. The plasma density is around the cut off density corresponding to the laser light frequency (wavelength), that is

$$u \sim 4c_{\rm s},$$

$$\eta_{\rm ab} I_{\rm L} \sim 4 m_{\rm DT} n_{\rm c} c_{\rm s}^3$$

where $m_{\rm DT} = 2.5 \times 1.67 \times 10^{-27}\,\mathrm{kg}$ is the average mass of deuterium and tritium and the cutoff density is $n_{\rm c} = 1.1 \times 10^{27}/\lambda^2(\mu\mathrm{m})\,\mathrm{m^{-3}}$ (λ is the wavelength of laser in units of μm). From (18.27) we have

$$P_{\rm a} = 13\left(\frac{(\eta_{\rm ab}I_{\rm L})_{14}}{\lambda(\mu\mathrm{m})}\right)^{2/3} \quad (\mathrm{Mbar}) \tag{18.28}$$

where $(\eta_{\rm ab}I_{\rm L})_{14}$ is the value in $10^{14}\,\mathrm{W/cm^2}$. This scaling is consistent with the experimental results in the range $1 < (\eta_{\rm ab}I_{\rm L})_{14} < 10$.

Most implosion research is carried out by the laser driver. The observed absorption rate $\eta_{\rm ab}$ tends to decrease according to the increase of laser light intensity $I_{\rm L}$.

The absorption rate is measured for a Nd glass laser with wavelength $1.06\,\mu$m (red), second harmonic $0.53\,\mu$m (green), and third harmonic $0.35\,\mu$m (blue). The absorption is better for shorter wavelengths, and it is $\eta_{\rm ab} \approx 0.9 \sim 0.8$ in the case of $\lambda = 0.35\,\mu$m in the range of $I_{\rm L} = 10^{14} \sim 10^{15}\,\mathrm{W/cm^2}$. The conversion ratio $\eta_{\rm hydro}$ determined by the experiments is 0.1∼0.15. The conversion ratio $\eta_{\rm T}$ is expected to be $\eta_{\rm T} > 0.5$. In order to compress the fuel to extremely high density, it is necesary to avoid the preheating of the inner pellet during the implosion process, since the pressure of the inner part of pellet must be kept as low as possible before the compression. When laser light with a long wavelength (CO_2 laser $\lambda = 10.6\,\mu$m) is used, the high-energy electrons are produced by the laser-plasma interaction, and the high-energy electrons penetrate into the inner

part of the pellet and preheat it. However, the production of high-energy electrons is much lower in short-wavelength experiments.

18.3 MHD Instabilities

In the accellerating phase of implosion process, the low density plasma ablating from the surface of ablator accellerates the high density fuel, so that Rayleigh-Taylor (RT) instability likely occurs at the ablation front. Furthermore the boundary of central spark region (low density) and main pusher fuel (high density) can be unstable in the decellerating phase near stagnation time of implosion process. The resultant RT instability may cause the mixing of fuel and ablator material in the accellerating phase, and the mixing of central spark region and pusher fuel in the decellerating phase and may severely degrade the pellet performance.

Let us consider the case that a fluid with mass density of $\rho_{\rm h}$ is supported against accelleration g by a fluid with less density of $\rho_{\rm l}$. In this case the growth rate of Rayleigh-Taylor instability is given by (ref.[11])

$$\gamma = (\alpha_{\rm A} g k)^{1/2}, \quad \alpha_{\rm A} = \frac{\rho_{\rm h} - \rho_{\rm l}}{\rho_{\rm h} + \rho_{\rm l}} \tag{18.29}$$

where k is the wave number of the perturbation in the direction perpendicular to the accelleration. In the case of $\rho_{\rm h} \gg \rho_{\rm l}$, the growth rate is $\gamma = (gk)^{1/2}$. When the density gradient is finite with the scale length of L, the growth rate becomes $\gamma \sim (\alpha_{\rm A} g/L)^{1/2}$ when $kL \gg 1$.

Dispersion relations of RT perturbation near ablation front that are widely used are still analytical fit to numerical simulation and is given by (ref.[12],[13])

$$\gamma = \left(\frac{kg}{1+kL}\right)^{1/2} - \hat{\beta} k V_{\rm a} \tag{18.30}$$

where $\hat{\beta}$ is constant of $\hat{\beta} = 1 \sim 3$ and $V_{\rm a}$ is the flow velocity across the ablation front in the frame moving with the ablation front. The first term in (18.30) is the usual one with the correction of finite density gradient, and the second one is a stabilizing term due to convective effect as is seen in the following.

Let us consider the case that the region of high density is $x < 0$ and the accelleration g is toward positive direction of x. The wave number in the direction of y is k. The irrotational incompressible flow velocity $(v_x.v_y)$ is given by

$$v_x = \frac{\partial \phi}{\partial y}, \quad v_y = -\frac{\partial \phi}{\partial x}$$

$$\Delta \phi = 0$$

so that the stream function ϕ is

$$\phi = \phi_0 \exp(-k|x| + iky) \exp \gamma_0 t$$

in the frame moving with the ablation front. When the fluid flows with the velocity of $V_{\rm a}$ (positive direction of x), the coordinate of the fluid element is $x = x_0 + V_{\rm a} t$ and ϕ is exressed by $(x > 0)$

$$\begin{aligned} \phi &= \phi_0 \exp(-k(x_0 + V_{\rm a} t) + iky) \exp \gamma_0 t \\ &= \phi_0 \exp(-kx_0 + iky) \exp(\gamma_0 - kV_{\rm a}) t. \end{aligned} \tag{18.31}$$

This equation shows the stabilizing effect of convective fluid.

Fig.18.5 shows the result of numerical simulation (ref.[2],[14]), which are in good agreement with the experimental ones.

When a shock encounters a fluid discontinuity, transmitted and reflected shocks are generated, which are refracted by any perturbations at the fluid interface. The modulated shocks produce pressure variations in the upstream and downstream fluids that reinforce the intial interfacial perturbations and cause them grow. This type of instability is called *Richtmyer-Meshkov instability* (ref.[15]-[17]).

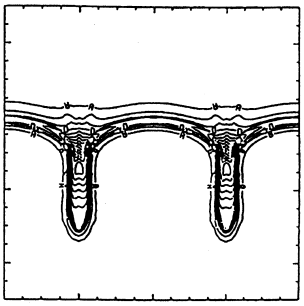

Fig.18.5 The result of numerical simulation of side-on image of the spacial distirbution of perturbed sample of planar target (ref.[2]). The ablated low density plasma is in the upper region and the accelleration is toward upward.

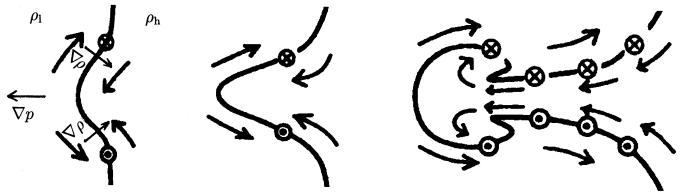

Fig.18.6 The growth of perturbation due to Rayleigh-Talor instability and Richtmyer-Meshkov instability (ref.[18]).

When a shock encounters the perturbed fluid discontinuity, the pressure gradient ∇p and density gradient $\nabla \rho$ are not necessarily parallel and the vortex of flow can be induced. The equation of an ideal fluid is given by

$$\frac{\mathrm{d}\boldsymbol{u}}{\mathrm{d}t} = -\frac{1}{\rho}\nabla p. \tag{18.32}$$

Noting the vortex $\boldsymbol{\omega} = \nabla \times \boldsymbol{u}$, the rotation of (18.32) is reduced to

$$\frac{\mathrm{d}\boldsymbol{\omega}}{\mathrm{d}t} = (\boldsymbol{\omega} \cdot \nabla)\boldsymbol{u} - \boldsymbol{\omega}(\nabla \cdot \boldsymbol{u}) + \frac{1}{\rho^2}\nabla\rho \times \nabla p. \tag{18.33}$$

The third term in the left-hand side of (18.33) induces the vortex and helps the growth of the perturbation of RT instability (ref.[18]) as is shown in Fig.18.6.

In conclusion high quality of spherical symmetry of irradiated laser light intensity and target structures are required for the effective implosion and how small is the RT mixing minimized determines the limit of radius and the density of the compressed fuel core and the required laser input energy.

18.4 Fast Ignition

Ultra high intense lasers with Peta Watt (10^{15}W) have been developed by the technology of chirp pulse amplification (ref.[19]) and new approach called fast ignition (ref.[20]) is being actively studied. A senario of the hot ignition is with three phases. First a fuel capsule is imploded as in the usual approach to assemble a high density fuel configuration. Second, a hole is bored through the capsule corona composed of ablated material, as the critical density is pushed close to the high density core of the capsule by the ponderomotive force associated with high intense laser light. Finally, the fuel is ignited by suprathermal electrons, produced in the high-intensity laser-plasma interactions, which then propagate from critical density to this high density core (see Fig.18.7). This new scheme, if realized, can separat e the process of the implosion and self-spark of central spot and also drastically reduces the difficulty of the implosion and allows lower quality fabrication and less stringent beam quality and symmetry requirement from the implosion driver.

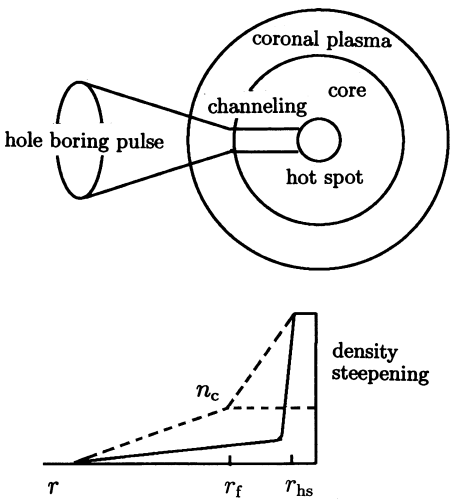

Fig.18.7 A configuration for efficient heating of the imploded core plasma by use of ultra high intense laser as fast ignitor

Fuel ignition requires that the hot spot reaches an average temperture of 5 keV within a fuel areal density of $(\rho r)_{\rm hs} = 0.3 \sim 0.4{\rm g/cm}^2$(refer sec.18.1). The mass of the hot spot region is ($\rho_{\rm hs}, r_{\rm hs}$ are the mass density and the radius of the hot spot region respectively)

$$M_{\rm hs} = \frac{4\pi\rho_{\rm hs}r_{\rm hs}^3}{3} = 4\pi\frac{(\rho r)_{\rm hs}^3}{3\rho_{\rm hs}^2} \sim 4.2(0.4)^3/\rho_{\rm hs}^2 = \frac{0.27}{\rho_{\rm hs}^2} \quad ({\rm g}).$$

The thermal energy of the heated fuel is

$$E_{\rm hs} = \frac{M_{\rm hs}}{m_{\rm i}}3T = 31\frac{T_{\rm keV}}{\rho_{\rm hs}^2} \quad ({\rm MJ}).$$

The energy $E_{\rm f}$ of the cold imploded fuel before fast ignition is

$$E_{\rm f} = \frac{3}{5}\alpha\epsilon_{\rm F}\frac{M_{\rm f}}{m_{\rm i}} = 0.32\alpha\rho_{\rm f}^{2/3}M_{\rm f} \quad ({\rm MJ})$$

where $M_{\rm f}$ is the mass of the main fuel in the unit of g and the mass density $\rho_{\rm f}$, $\rho_{\rm hs}$ is in the unit of ${\rm g/cm}^3$.

When the ignition energy is injected sufficiently rapidly, the hot spot and main fuel are not in pressure equilibrium and uniform density model can be used. Then the total energy of the fuel $E_{\rm fuel}$ is given by

$$E_{\rm fuel} = 31\frac{(T_{\rm hs})_{\rm keV}}{\rho^2} + 0.32\alpha\rho^{2/3}M_{\rm f} \quad ({\rm MJ}) \tag{18.34}$$

and the fusion output energy $E_{\rm NF}$ is

$$E_{\rm NF} = f_{\rm B}\frac{M_{\rm f}}{m_{\rm i}}\frac{Q_{\rm NF}}{2} = 3.36\times10^5 f_{\rm B}M_{\rm f} \quad ({\rm MJ}). \tag{18.35}$$

Therefore the core gain $G_{\rm core}$ is reduced to

$$G_{\rm core} \equiv= \frac{E_{\rm NF}}{E_{\rm fuel}} = \frac{3.36\times10^5 f_{\rm B}M_{\rm f}}{31T_{\rm hs}/\rho^2 + 0.32\alpha\rho^{2/3}M_{\rm f}}. \tag{18.36}$$

Let us take an example of $\rho = 1000\rho_{\rm solid} = 210{\rm g/cm}^3$. We choose $r_{\rm hs} = 0.002$cm and $r_{\rm f} = 0.01$cm. Then we have $M_{\rm f} = 0.88\times10^{-3}$g, $E_{\rm fuel} = (3.5 + 19.9) = 23.4$kJ, $E_{\rm NF} = 65$MJ, $G_{\rm core} = 2.8\times10^3$ assuming $\alpha = 2$, $\kappa T_{\rm hs} = 5$keV, $f_{\rm B} = 0.22$, ($\beta(T)$ is about $7{\rm g/cm}^2$ for $\kappa T = 30 \sim 40$keV) and then $E_{\rm L}$=240kJ, $G_{\rm pellet} = 2.8\times10^2$ under the assumption of $\eta_{\rm h} = 0.1$.

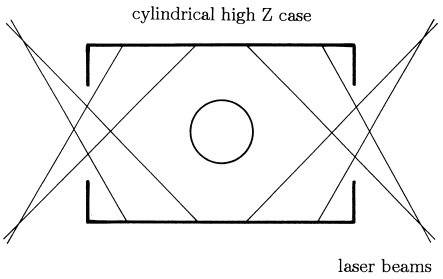

Fig.18.8 Configuration of hohlraum target

Let us estimate the necessary power of the laser for the fast ignition. The required energy to ignite the hot spot region ($\rho_{\rm m} r > 0.4{\rm g/cm}^2$, $\rho_{\rm m} \sim 10^3 \rho_{\rm solid}$, $\kappa T \sim 5{\rm keV}$) is at least 7∼8kJ taking account of heating efficiency. The confinement time $\tau = r/(3c_{\rm s})$ is the order of 8ps. Therefore the power of 10^{15}W=1Peta Watt is necessary. When the radius of the hot spot is 0.02mm, the intensity of laser beam becomes $10^{20}{\rm W/cm}^2$.

The ponderomotive force $\boldsymbol{F}_{\rm p}$ of laser beam is given by (refer (3.63) in ch.3)

$$\boldsymbol{F}_{\rm p} = -\frac{\omega_{\rm p}^2}{\omega^2} \nabla \frac{\epsilon_0 \langle \boldsymbol{E}^2 \rangle}{2}. \tag{18.37}$$

A laser beam of finite diameter causes a radially directed ponderomotive force in a plasma. This force moves plasma out of the beam, so that the plasma frequency $\omega_{\rm p}$ is lower and the dielectric constant ϵ is higher inside the beam than outside. The plasma acts as a convex lens resulting in the self-focus of laser beam. The ponderomotive force will also push the critical surface forward, resulting in the laser channel formation into over dense plasma (ref.[21]). The pressure of the cold imploded fuel with the density of $n = 10^3 n_{\rm solid}$ is $2/5\alpha\epsilon_{\rm F} n \sim 3.2 \times 10^{15}$Pa (Pascal) (1bar = 10^5Pa ∼ 1atm.) and the pressure due to the ponderomotive force of laser beam with the intensity of $I_{\rm L} = 10^{24}{\rm W/m}^2$ is $\epsilon_0 \langle \boldsymbol{E}^2 \rangle /2 = I_{\rm L}/c \sim 3 \times 10^{15}$Pa. Therefore it is possible to push the critical surface into the core plasma. Once the channel is created in the plasma with a critical (cut-off) density, the laser light heats the plasma by $\boldsymbol{J} \times \boldsymbol{B}$ heating (ref.[22]), in which the oscillating component of ponderomotive force (refer to (3.62)) can lead to heating. The interaction of dense plasma and untra high intense laser light are being actively studied in experiments (ref.[23]) and computer simulations.

Hohlraum Target

The implosion process just described is for directly irradiated pellets. The other case is indirectly irradiated pellets. The outer cylindrical case surrounds the fuel pellet, as shown in fig.18.8. The inner surface of the outer cylindrical case is irradiated by the laser light, and the laser energy is converted to X-ray energy and plasma energy. The converted X-rays and the plasma particles irradiate the inner fuel pellet and implosion occurs. The X-ray and plasma energy are confined between the outer cylindrical case and the inner fuel pellet and are used for the implosion effectively. This type of pellet is called a hohlraum target (ref.[2]). In this configuration, possible use of heavy ion beam (ref.[24]) is examined as a energy driver.

Recent activities in inertial confinement fusion including NIF (National Ignition Facility) are well described in (ref.[25]).

Reference

[1] J. Nuckolls, L. Wood, A. Thiessen and G. Zimmerman: Nature **239**, 139 Sept. (1972).
[2] J. Lindl: Phys. Plasmas **2**, 3933 (1995).
[3] J. Meyer-Ter-Vehn: Nucl. Fusion **22**, 561 (1982).
[4] C. Kittel: *Introduction to Solid State Physics, 8th ed.* John Willey & Sons, Inc. 2005.
[5] R. E. Kidder: Nucl. Fusion **19**, 223 (1979).

[6] S. Atzeni: Jpn J. Appl. Phys. **34**, 1980 (1995).
[7] G. S. Fraley, E. J. Linnebur, R. J. Mason and R. L. Morse: Phys. Fluids **17**, 474 (1974).
[8] S. Yu. Guskov, O. N. Krokhin, V. B. Rozanov: *Nucl. Fusion* **16**, 957 (1976).
[9] R. Decoste, S. E. Bodner, B. H. Ripin, E. A. McLean, S. P. Obenshain and C. M. Armstrong: Phys. Rev. Lett. **42**, 1673 (1979).
[10] K. Mima: J. Plasma Fusion Res. (Kakuyugo Kenkyu) **51**, 400 (1984) (in Japanese).
[11] G. Bateman: *MHD Instabilities* The MIT Press, Cambridge, Mass. (1978).
[12] H. Takabe, K. Mima, L. Montierth, R. L. Morse: Phys. Fluids **28**, 3676 (1985).
[13] K. S. Budil, B. A. Remington, T. A. Peyser, K. O. Mikaelian, P. L. Miller et al: Phys. Rev. Lett. **76**, 4536 (1996).
[14] B. A. Remington, S. V. Weber, S. W. Haan, J. D. Kilkenny, S. G. Glendinning, R. J. Wallace, W. H. Goldstein, B. G. Willson, J. K. Nash: Phys. Fluids **B5**, 2589 (1993).
[15] R. D. Richtmyer: Commun. Pure Appl. Math. **13**, 297 (1960).
[16] E. E. Meshkov: Izv. Akad. Sci. USSR Fluid Dynamics: **4**, 101 (1969).
[17] G. Dimonte, C. E. Frerking and M. Schnider: Phys. Rev. Lett. **74**, 4855 (1995).
[18] H. Takabe: J. Plasma Fusion Res. **69**, 1285 (1993) (in Japanese).
[19] D. Strickland and G.Mourou: Optics Comm. **56**, 219 (1985).
G. A. Mourou, C. P. J. Barty and M. D. Perry: Physics Today 22 Jan. (1998).
[20] M. Tabak, J. Hammer, M. E. Glinsky, W. L. Kruer, S. C. Wilks, J. Woodworth, E. M. Campbell and M. D.Perry: Phys. Plasmas **1**, 1626 (1994).
[21] S. C. Wilks, W. L. Kruer, M. Tabak and A. B. Landon: Phys. Rev. Lett. **69**, 1383 (1992).
[22] W. L. Kruer and K. Estabrook: Phys. Fluids 28, 430 (1985).
[23] R. Kodama, P. A. Norreys, K. Mima, A. E. Dangor, R.G. Evans et al: Nature **412**, 798 Aug. (2001).
R. Kodama and the Fast Ignitor Consortium: Nature **418**, 933 Aug. (2002).
[24] R. G. Logan et al: *19th IAEA Fusion Energy Conference* (Lyon in 2002) OV/3-4.
[25] J. Lindl: *Inertial Confinement Fusion* Springer/AIP Press, NewYork (1998).

App.A Derivation of MHD Equations of Motion

When the distribution function is obtained from Boltzmann's equation introduced in ch.4

$$\frac{\partial f}{\partial t} + \boldsymbol{v} \cdot \nabla_{\mathrm{r}} f + \frac{\boldsymbol{F}}{m} \nabla_{\mathrm{v}} f = \left(\frac{\delta f}{\delta t} \right)_{\mathrm{coll}} \tag{A.1}$$

average quantities by velocity space $\boldsymbol{v}$ such as mass density, current density, charge density, flow velocity and pressure can be estimated as the functions of space coordinates $\boldsymbol{r}$ and time t. The relations between these average variables can be reduced by multiplication of a function $g(\boldsymbol{r}, \boldsymbol{v}, t)$ by Boltzmann's equation and integration over the velocity space. When $g = 1$, $\boldsymbol{g} = m\boldsymbol{v}$, $g = \frac{m}{2} v^2$, equations in terms of the density, the momentum, and energy, respectively, can be obtained. Averages of g weighted by the distribution function are denoted by $\langle g \rangle$, i.e.,

$$\langle g(\boldsymbol{r}, t) \rangle = \frac{\int g(\boldsymbol{r}, \boldsymbol{v}, t)\, f(\boldsymbol{r}, \boldsymbol{v}, t)\, \mathrm{d}\boldsymbol{v}}{\int f(\boldsymbol{r}, \boldsymbol{v}, t)\, \mathrm{d}\boldsymbol{v}}. \tag{A.2}$$

Since density is expressed by

$$n(\boldsymbol{r}, t) = \int f(\boldsymbol{r}, \boldsymbol{v}, t)\, \mathrm{d}\boldsymbol{v} \tag{A.3}$$

we find that

$$n(\boldsymbol{r}, t) \langle g(\boldsymbol{r}, t) \rangle = \int g(\boldsymbol{r}, \boldsymbol{v}, t)\, f(\boldsymbol{r}, \boldsymbol{v}, t)\, \mathrm{d}\boldsymbol{v}. \tag{A.4}$$

By integrating by parts, we obtained

$$\begin{aligned}
&\int g \frac{\partial f}{\partial t}\, \mathrm{d}\boldsymbol{v} = \frac{\partial}{\partial t}(n\langle g \rangle) - n \left\langle \frac{\partial}{\partial t} g \right\rangle, \\
&\int g v_i \frac{\partial f}{\partial x_i}\, \mathrm{d}\boldsymbol{v} = \frac{\partial (n\langle v_i g \rangle)}{\partial x_i} - n \left\langle \frac{\partial}{\partial x_i}(v_i g) \right\rangle, \\
&\int g \frac{F_i}{m} \frac{\partial f}{\partial v_i}\, \mathrm{d}\boldsymbol{v} = -\frac{n}{m} \left\langle \frac{\partial}{\partial v_i} g F_i \right\rangle.
\end{aligned}$$

For the force $\boldsymbol{F} = q\boldsymbol{E} + q(\boldsymbol{v} \times \boldsymbol{B})$, the relation

$$\frac{\partial F_i}{\partial v_i} = 0$$

holds, and

$$\int g \frac{F_i}{m} \frac{\partial f}{\partial v_i}\, \mathrm{d}\boldsymbol{v} = -\frac{n}{m} \left\langle F_i \frac{\partial g}{\partial v_i} \right\rangle.$$

Consequently we find, in terms of averages, that

$$\begin{aligned}
&\frac{\partial}{\partial t}(n\langle g \rangle) - n \left\langle \frac{\partial g}{\partial t} \right\rangle + \nabla_{\mathrm{r}} \cdot (n\langle g\boldsymbol{v} \rangle) - n\langle \nabla_{\mathrm{r}} \cdot (g\boldsymbol{v}) \rangle - \frac{n}{m} \langle \boldsymbol{F} \cdot \nabla_{\mathrm{v}} g \rangle \\
&= \int g \left(\frac{\delta f}{\delta t} \right)_{\mathrm{coll}} \mathrm{d}\boldsymbol{v}.
\end{aligned} \tag{A.5}$$

Equation (A.5), with $g = 1$, is

$$\frac{\partial n}{\partial t} + \nabla_{\mathrm{r}} \cdot (n\langle \boldsymbol{v} \rangle) = \int \left(\frac{\delta f}{\delta t} \right)_{\mathrm{coll}} \mathrm{d}\boldsymbol{v}. \tag{A.6}$$

This is the equation of continuity. When the effects of ionization and recombination are neglected, collision term is zero.

Equation (A.5), with $\boldsymbol{g} = m\boldsymbol{v}$, yields the equation of motion:

$$\frac{\partial}{\partial t}\left(mn\langle \boldsymbol{v}\rangle\right) - \sum_j \frac{\partial}{\partial x_j}\left(nm\langle v_j \boldsymbol{v}\rangle\right) - n\langle \boldsymbol{F}\rangle = \int m\boldsymbol{v}\left(\frac{\delta f}{\delta t}\right)_{\rm coll} \mathrm{d}\boldsymbol{v}. \tag{A.7}$$

Let us define the velocity of random motion $\boldsymbol{v}_{\rm r}$ by

$$\boldsymbol{v} \equiv \langle \boldsymbol{v}\rangle + \boldsymbol{v}_{\rm r}$$

By definition of $\boldsymbol{v}_{\rm r}$, its average is zero:

$$\langle \boldsymbol{v}_{\rm r}\rangle = 0.$$

Since

$$\langle v_i v_j\rangle = \langle v_i\rangle\langle v_j\rangle + \langle v_{{\rm r}i} v_{{\rm r}j}\rangle,$$

$$\begin{aligned}\sum_j \frac{\partial}{\partial x_j}\left(n\langle v_i v_j\rangle\right) &= \sum_j \frac{\partial}{\partial x_j}\left(n\langle v_i\rangle\langle v_j\rangle\right) + \sum_j \frac{\partial}{\partial x_j}\left(n\langle v_{{\rm r}i} v_{{\rm r}j}\rangle\right) \\ &= n\sum_j \langle v_j\rangle \frac{\partial}{\partial x_j}\langle v_i\rangle + \langle v_i\rangle \sum_j \frac{\partial}{\partial x_j}\left(n\langle v_j\rangle\right) + \sum_j \frac{\partial}{\partial x_j}\left(n\langle v_{{\rm r}i} v_{{\rm r}j}\rangle\right). \end{aligned} \tag{A.8}$$

Multiplication of the equation of continuity (A.6) by $m\langle \boldsymbol{v}\rangle$ gives

$$m\frac{\partial}{\partial t}\left(n\langle \boldsymbol{v}\rangle\right) = mn\frac{\partial}{\partial t}\langle \boldsymbol{v}\rangle - m\langle \boldsymbol{v}\rangle \sum_j \frac{\partial}{\partial x_j}\left(n\langle v_j\rangle\right) + m\langle \boldsymbol{v}\rangle \int \left(\frac{\delta f}{\delta t}\right)_{\rm coll} \mathrm{d}\boldsymbol{v}. \tag{A.9}$$

Define the *pressure tensor* by

$$mn\langle v_{{\rm r}i} v_{{\rm r}j}\rangle \equiv P_{ij} \tag{A.10}$$

then the equation of motion is reduced from (A.7),(A.8),(A.9) as follows:

$$mn\left(\frac{\partial}{\partial t} + \langle \boldsymbol{v}\rangle\nabla\right)\langle \boldsymbol{v}\rangle = n\langle \boldsymbol{F}\rangle - \sum_j \frac{\partial}{\partial x_j} P_{ij} + \int m\boldsymbol{v}_{\rm r}\left(\frac{\delta f}{\delta t}\right)_{\rm coll} \mathrm{d}\boldsymbol{v}. \tag{A.11}$$

When the distribution function is isotropic, the pressure tensor is

$$P_{ij} = nm\langle v_{{\rm r}i}^2\rangle\delta_{ij} = nm\frac{\langle v_{\rm r}^2\rangle}{3}\delta_{ij} = p\delta_{ij},$$

and $p = n\kappa T$ for a Maxwell distribution. (For an anisotropic plasma, the pressure tensor is given by $P_{ij} = P_\perp\delta_{ij} + (P_\parallel - P_\perp)\boldsymbol{bb}$, where $\boldsymbol{b}$ is the unit vector of magnetic field $\boldsymbol{B}$.)

We introduce the tensor

$$\Pi_{ij} = nm\langle v_{{\rm r}i} v_{{\rm r}j} - (\langle v_{\rm r}^2\rangle/3)\delta_{ij}\rangle,$$

then the pressure tensor may be expressed by

$$P_{ij} = p\delta_{ij} + \Pi_{ij}. \tag{A.12}$$

A nonzero Π_{ij} indicates anisotropic inhomogeneous properties of the distribution function. When the collision term is introduced by

$$\boldsymbol{R} = \int m\boldsymbol{v}_{\rm r}\left(\frac{\delta f}{\delta t}\right)_{\rm coll} \mathrm{d}\boldsymbol{v} \tag{A.13}$$

the equation of motion is expressed by

$$mn\left(\frac{\partial}{\partial t}+\langle\boldsymbol{v}\rangle\nabla\right)\langle\boldsymbol{v}\rangle=n\langle\boldsymbol{F}\rangle-\nabla p-\sum_j\frac{\partial\Pi_{ij}}{\partial x_j}+\boldsymbol{R}. \tag{A.14}$$

Here $\boldsymbol{R}$ measures the change of momentum due to collisions with particles of other kind.

When $g=mv^2/2$, then $(\boldsymbol{v}\times\boldsymbol{B})\cdot\nabla_{\rm v}v^2=0$. The energy- transport equation is reduced to

$$\frac{\partial}{\partial t}\left(\frac{nm}{2}\langle v^2\rangle\right)+\nabla_{\rm r}\left(\frac{n}{2}m\langle v^2\boldsymbol{v}\rangle\right)=qn\boldsymbol{E}\cdot\langle\boldsymbol{v}\rangle+\int\frac{mv^2}{2}\left(\frac{\delta f}{\delta t}\right)_{\rm coll}{\rm d}\boldsymbol{v}. \tag{A.15}$$

The 2nd term in left-hand side of (A.15) is modified to

$$\begin{aligned}\frac{nm}{2}\langle\boldsymbol{v}^2\rangle=&\frac{nm}{2}(\langle\boldsymbol{v}\rangle)^2+\frac{3}{2}p\\ \langle v^2\boldsymbol{v}\rangle=&(\langle\boldsymbol{v}\rangle)^2\langle\boldsymbol{v}\rangle+2\langle(\langle\boldsymbol{v}\rangle\cdot\boldsymbol{v}_{\rm r})\rangle\langle\boldsymbol{v}\rangle+\langle v_{\rm r}^2\rangle\langle\boldsymbol{v}\rangle\\ &+\langle\boldsymbol{v}\rangle^2\langle\boldsymbol{v}_{\rm r}\rangle+2\langle(\langle\boldsymbol{v}\rangle\cdot\boldsymbol{v}_{\rm r})\boldsymbol{v}_{\rm r}\rangle+\langle v_{\rm r}^2\boldsymbol{v}_{\rm r}\rangle.\end{aligned}$$

The 2nd and 4th terms are zero, and the 5th term is

$$\begin{aligned}\sum_i\langle v_i\rangle\langle v_{{\rm r}i}v_{{\rm r}j}\rangle=\sum_i\langle v_i\rangle\frac{P_{ij}}{nm}&=\frac{1}{nm}\sum_i\langle v_i\rangle(p\delta_{ij}+\Pi_{ij})\\ &=\frac{1}{nm}p\langle\boldsymbol{v}\rangle+\frac{1}{nm}\sum_i\langle v_i\rangle\Pi_{ij}\end{aligned}$$

and

$$\langle v^2\boldsymbol{v}\rangle=\left(\langle\boldsymbol{v}\rangle^2+5\frac{p}{nm}\right)\langle\boldsymbol{v}\rangle+2\sum_i\langle v_i\rangle\frac{\Pi_{ij}}{nm}+\langle v_{\rm r}^2\boldsymbol{v}_{\rm r}\rangle.$$

Consequently (A15) is reduced to

$$\frac{\partial}{\partial t}\left(\frac{nm}{2}\langle\boldsymbol{v}\rangle^2+\frac{3}{2}p\right)+\nabla\cdot\left(\frac{nm}{2}\langle\boldsymbol{v}\rangle^2+\frac{5}{2}p\right)\boldsymbol{v}+\nabla\cdot\left(\sum_i\Pi_{ij}\langle v_i\rangle\right)+\nabla\cdot\boldsymbol{q}=qn\boldsymbol{E}\cdot\langle\boldsymbol{v}\rangle+\boldsymbol{R}\cdot\langle\boldsymbol{v}\rangle+Q, \tag{A.16}$$

$$\boldsymbol{q}(\boldsymbol{r},t)=\int\frac{m}{2}v_{\rm r}^2\boldsymbol{v}_{\rm r}f\,{\rm d}\boldsymbol{v}, \tag{A.17}$$

$$Q(\boldsymbol{r},t)=\int\frac{mv_{\rm r}^2}{2}\left(\frac{\delta f}{\delta t}\right)_{\rm coll}{\rm d}\boldsymbol{v}. \tag{A.18}$$

Q is the heat generation by collision and $\boldsymbol{q}$ is the energy-flux density due to random motion. The scalar product of (A.14) and $\langle\boldsymbol{v}\rangle$ is

$$mn\left(\frac{\partial}{\partial t}+\langle\boldsymbol{v}\rangle\cdot\nabla\right)\frac{\langle\boldsymbol{v}\rangle^2}{2}+\langle\boldsymbol{v}\rangle\cdot\nabla p+\sum_{i,j}\frac{\partial\Pi_{ij}}{\partial x_j}\langle v_i\rangle=qn\boldsymbol{E}\cdot\langle\boldsymbol{v}\rangle+\boldsymbol{R}\cdot\langle\boldsymbol{v}\rangle$$

and the equation of continuity (A.6) gives

$$\frac{m}{2}\langle\boldsymbol{v}\rangle^2\left(\frac{\partial n}{\partial t}+\nabla\cdot(n\langle\boldsymbol{v}\rangle)\right)=0$$

then (A.16) is reduced to

$$\frac{\partial}{\partial t}\left(\frac{nm}{2}\langle\boldsymbol{v}\rangle^2\right)+\nabla\cdot\left(\frac{nm}{2}\langle\boldsymbol{v}\rangle^2\langle\boldsymbol{v}\rangle\right)+\langle\boldsymbol{v}\rangle\cdot\nabla p+\sum_{i,j}\frac{\partial\Pi_{ij}}{\partial x_j}\langle v_i\rangle=qn\boldsymbol{E}\cdot\langle\boldsymbol{v}\rangle+\boldsymbol{R}\cdot\langle\boldsymbol{v}\rangle.$$

Subtraction of this equation and (A.16) gives

$$\frac{3}{2}\frac{\partial p}{\partial t} + \nabla\cdot\left(\frac{3}{2}p\langle\boldsymbol{v}\rangle\right) + p\nabla\cdot\langle\boldsymbol{v}\rangle + \sum_{i,j}\Pi_{ij}\frac{\partial}{\partial x_j}\langle v_i\rangle + \nabla\cdot\boldsymbol{q} = Q. \tag{A.19}$$

The relation $p = n\kappa T$ and the equation of continuity (A.6) yield

$$\frac{3}{2}\frac{\partial(n\kappa T)}{\partial t} + \nabla\cdot\left(\frac{3}{2}n\kappa T\langle\boldsymbol{v}\rangle\right) = \frac{3}{2}n\frac{\mathrm{d}\kappa T}{\mathrm{d}t}.$$

By setting $s \equiv \ln\left((\kappa T)^{3/2}/n\right) = \ln\left(p^{3/2}/n^{5/2}\right)$, we may write (A.19) as

$$\kappa T n\frac{\mathrm{d}s}{\mathrm{d}t} = \kappa T\left(\frac{\partial(ns)}{\partial t} + \nabla\cdot(ns\langle\boldsymbol{v}3\rangle)\right) = -\nabla\cdot\boldsymbol{q} - \sum_{i,j}\Pi_{ij}\frac{\partial\langle v_i\rangle}{\partial x_j} + Q. \tag{A.20}$$

App.B Energy Integral of Axisymmetric Toroidal System

B.1 Energy Integral in Illuminating Form

The energy integral

$$W = \frac{1}{2}\int_V \Big(\gamma p(\nabla\cdot\boldsymbol{\xi})^2 + \frac{1}{\mu_0}(\nabla\times(\boldsymbol{\xi}\times\boldsymbol{B}))^2 + (\nabla\cdot\boldsymbol{\xi})(\boldsymbol{\xi}\cdot\nabla p) - \frac{1}{\mu_0}(\boldsymbol{\xi}\times(\nabla\times\boldsymbol{B}))\cdot\nabla\times(\boldsymbol{\xi}\times\boldsymbol{B})\Big)\mathrm{d}\boldsymbol{r}$$

$$= \frac{1}{2}\int_V \Big(\frac{\boldsymbol{B}_1^2}{\mu_0} + \gamma p(\nabla\cdot\boldsymbol{\xi})^2 + (\nabla\cdot\boldsymbol{\xi})(\boldsymbol{\xi}\cdot\nabla p) - \boldsymbol{\xi}\cdot(\boldsymbol{j}\times\boldsymbol{B}_1)\Big)\mathrm{d}\boldsymbol{r} \tag{B.1}$$

was derived in (8.46) of ch.8. This expression can be further rearranged to the more illuminating form of (ref.[1],[2])

$$W = \frac{1}{2}\int \Big(\gamma p(\nabla\cdot\boldsymbol{\xi})^2 + \frac{1}{\mu_0}|\boldsymbol{B}_{1\perp}|^2 + \frac{1}{\mu_0}|\boldsymbol{B}_{1\parallel} - \boldsymbol{B}\frac{\mu_0(\boldsymbol{\xi}\cdot\nabla p)}{B^2}|^2 - \frac{(\boldsymbol{j}\cdot\boldsymbol{B})}{B^2}(\boldsymbol{\xi}\times\boldsymbol{B})\cdot\boldsymbol{B}_1 - 2(\boldsymbol{\xi}\cdot\nabla p)(\boldsymbol{\xi}\cdot\boldsymbol{\kappa})\Big)\,\mathrm{d}\boldsymbol{r}. \tag{B.2}$$

The first term of the integrand of (B.2) is the term of sonic wave. The second and the third terms are of Alfv́en wave. The fourth term is of kink mode. The last one is the term of ballooning mode. $\boldsymbol{\kappa}$ is the vector of curvature of field line. The rearrangement from (B.1) to (B.2) is described in the followings. When $\boldsymbol{\xi}$ is expressed by the sum of the parallel component $\xi_\parallel\boldsymbol{b}$ and the perpendicular component $\boldsymbol{\xi}_\perp$ to the magnetic field $\boldsymbol{B} = B\boldsymbol{b}$

$$\boldsymbol{\xi} = \xi_\parallel\boldsymbol{b} + \boldsymbol{\xi}_\perp$$

the last two terms of (B.1) are reduced to

$$(\nabla\cdot\boldsymbol{\xi})(\boldsymbol{\xi}\cdot\nabla p) + (\boldsymbol{j}\times\boldsymbol{\xi})\cdot\boldsymbol{B}_1$$

$$= (\boldsymbol{\xi}\cdot\nabla p)\nabla\cdot(\xi_\parallel\boldsymbol{b}) + (\boldsymbol{\xi}\cdot\nabla p)\nabla\cdot\boldsymbol{\xi}_\perp + \xi_\parallel(\boldsymbol{j}\times\boldsymbol{b})\cdot\nabla\times(\boldsymbol{\xi}\times\boldsymbol{B}) + (\boldsymbol{j}\times\boldsymbol{\xi}_\perp)\cdot\boldsymbol{B}_1$$

$$= (\boldsymbol{\xi}\cdot\nabla p)\nabla\cdot(\xi_\parallel\boldsymbol{b}) + \frac{\xi_\parallel}{B}\nabla p\cdot\nabla\times(\boldsymbol{\xi}\times\boldsymbol{B}) + (\boldsymbol{\xi}\cdot\nabla p)\nabla\cdot\boldsymbol{\xi}_\perp + (\boldsymbol{j}\times\boldsymbol{\xi}_\perp)\cdot\boldsymbol{B}_1$$

$$= (\boldsymbol{\xi}\cdot\nabla p)(\boldsymbol{B}\cdot\nabla)(\frac{\xi_\parallel}{B}) + \frac{\xi_\parallel}{B}\nabla\cdot((\boldsymbol{\xi}\times\boldsymbol{B})\times\nabla p) + (\boldsymbol{\xi}\cdot\nabla p)\nabla\cdot\boldsymbol{\xi}_\perp + (\boldsymbol{j}\times\boldsymbol{\xi}_\perp)\cdot\boldsymbol{B}_1$$

$$= (\boldsymbol{\xi}\cdot\nabla p)(\boldsymbol{B}\cdot\nabla)(\frac{\xi_\parallel}{B}) + \frac{\xi_\parallel}{B}\nabla\cdot((\boldsymbol{\xi}\cdot\nabla p)\boldsymbol{B}) + (\boldsymbol{\xi}\cdot\nabla p)\nabla\cdot\boldsymbol{\xi}_\perp + (\boldsymbol{j}\times\boldsymbol{\xi}_\perp)\cdot\boldsymbol{B}_1$$

$$= \nabla\cdot\Big(\frac{\xi_\parallel}{B}(\boldsymbol{\xi}\cdot\nabla p)\boldsymbol{B}\Big) + (\boldsymbol{\xi}\cdot\nabla p)\nabla\cdot\boldsymbol{\xi}_\perp + (\boldsymbol{j}\times\boldsymbol{\xi}_\perp)\cdot\boldsymbol{B}_1. \tag{B.3}$$

The current density $\boldsymbol{j}$ can be expressed by the sum of parallel and perpendicular components to the magnetic field as follows:

$$\boldsymbol{j} = \sigma \boldsymbol{B} + \frac{\boldsymbol{B} \times \nabla p}{B^2}$$

where

$$\sigma = \frac{\boldsymbol{j} \cdot \boldsymbol{B}}{B^2}.$$

The last term of (B.3) is

$$(\boldsymbol{j} \times \boldsymbol{\xi}_\perp) \cdot \boldsymbol{B}_1 = \sigma(\boldsymbol{B} \times \boldsymbol{\xi}_\perp) \cdot \boldsymbol{B}_1 - \frac{(\boldsymbol{\xi}_\perp \cdot \nabla p)}{B^2} \boldsymbol{B} \cdot \boldsymbol{B}_1$$

and $\nabla \cdot \boldsymbol{\xi}_\perp$ in the second term of (B.3) is

$$\nabla \cdot \boldsymbol{\xi}_\perp = \nabla \cdot \left(\frac{\boldsymbol{B}}{B^2} \times (\boldsymbol{\xi} \times \boldsymbol{B}) \right) = (\boldsymbol{\xi} \times \boldsymbol{B}) \cdot \nabla \times \frac{\boldsymbol{B}}{B^2} - \frac{\boldsymbol{B}}{B^2} \cdot \nabla \times (\boldsymbol{\xi} \times \boldsymbol{B})$$

$$= (\boldsymbol{\xi} \times \boldsymbol{B}) \cdot \frac{\nabla \times \boldsymbol{B}}{B^2} - 2(\boldsymbol{\xi} \times \boldsymbol{B}) \cdot \frac{\nabla B}{B^3} \times \boldsymbol{B} - \frac{\boldsymbol{B}}{B^2} \nabla \times (\boldsymbol{\xi} \times \boldsymbol{B})$$

$$= -\frac{(\boldsymbol{\xi} \cdot \mu_0 \nabla p)}{B^2} + 2(\boldsymbol{\xi} \times \boldsymbol{B}) \cdot \frac{\boldsymbol{B} \times \nabla B}{B^3} - \frac{\boldsymbol{B}}{B^2} \cdot \boldsymbol{B}_1. \tag{B.4}$$

Then the energy integral (B.1) is reduced to

$$W = \frac{1}{2} \int_V \Big(\gamma p (\nabla \cdot \boldsymbol{\xi}) + \frac{\boldsymbol{B}_1^2}{\mu_0} - \frac{\mu_0 (\boldsymbol{\xi} \cdot \nabla p)^2}{B^2} - (\boldsymbol{\xi} \cdot \nabla p) \frac{\boldsymbol{B} \cdot \boldsymbol{B}_1}{B^2}$$

$$- (\boldsymbol{\xi}_\perp \cdot \nabla p) \frac{\boldsymbol{B} \cdot \boldsymbol{B}_1}{B^2} + \sigma (\boldsymbol{B} \times \boldsymbol{\xi}_\perp) \cdot \boldsymbol{B}_1 + 2(\boldsymbol{\xi} \cdot \nabla p)(\boldsymbol{\xi} \times \boldsymbol{B}) \cdot \frac{\boldsymbol{B} \times \nabla B}{B^3} \Big) \mathrm{d}\boldsymbol{r}$$

$$= \frac{1}{2} \int_V \Big(\gamma p (\nabla \cdot \boldsymbol{\xi}) + \frac{1}{\mu_0} \left| \boldsymbol{B}_1 - \frac{\mu_0 (\boldsymbol{\xi} \cdot \nabla p)}{B^2} \boldsymbol{B} \right|^2 - \frac{(\boldsymbol{j} \cdot \boldsymbol{B})}{B^2} (\boldsymbol{\xi}_\perp \times \boldsymbol{B}) \cdot \boldsymbol{B}_1$$

$$- 2(\boldsymbol{\xi} \cdot \nabla p) \left(\frac{\mu_0 (\boldsymbol{\xi} \cdot \nabla p)}{B^2} - (\boldsymbol{\xi} \times \boldsymbol{B}) \cdot \frac{\boldsymbol{B} \times \nabla B}{B^3} \right) \Big) \mathrm{d}\boldsymbol{r}.$$

The last ballooning term can be expressed as

$$-2(\boldsymbol{\xi} \cdot \nabla p)(\boldsymbol{\xi} \cdot \boldsymbol{\kappa})$$

by introducing a vector $\boldsymbol{\kappa}$

$$\boldsymbol{\kappa} \equiv \frac{1}{2B^4} \Big(\boldsymbol{B} \times \nabla (B^2 + 2\mu_0 p) \Big) \times \boldsymbol{B} = \frac{\mu_0 \nabla p}{B^2} + \frac{(\boldsymbol{B} \times \nabla B) \times \boldsymbol{B}}{B^3}, \tag{B.5}$$

since

$$(\boldsymbol{\xi} \cdot \boldsymbol{\kappa}) = \frac{\mu_0 (\boldsymbol{\xi} \cdot \nabla p)}{B^2} + \frac{\boldsymbol{\xi} \cdot (\boldsymbol{B} \times \nabla B) \times \boldsymbol{B}}{B^3} = \frac{\mu_0 (\boldsymbol{\xi} \cdot \nabla p)}{B^2} - \frac{(\boldsymbol{\xi} \times \boldsymbol{B}) \cdot (\boldsymbol{B} \times \nabla B)}{B^3}. \tag{B.6}$$

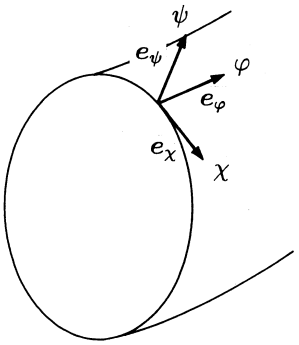

Fig.B.1 Orthogonal coordinate system (ψ, χ, φ) and $\boldsymbol{e}_\psi, \boldsymbol{e}_\chi, \boldsymbol{e}_\varphi$ are unit vectors of ψ, χ, φ directions respectively.

(B.4) and (B.5) reduce

$$\nabla \cdot \boldsymbol{\xi}_\perp + 2(\boldsymbol{\xi}_\perp \cdot \kappa) = \frac{\mu_0(\boldsymbol{\xi}_\perp \cdot \nabla p)}{B^2} - \frac{\boldsymbol{B} \cdot \boldsymbol{B}_1}{B^2} \tag{B.7}$$

From (6.7) of ch.6 we have

$$\nabla(2\mu_0 p + B^2) = 2(\boldsymbol{B} \cdot \nabla)\boldsymbol{B}.$$

Then it becomes clear that $\boldsymbol{\kappa}$ is equal to the vector of curvature as follows:

$$\boldsymbol{\kappa} = \frac{1}{B}(\boldsymbol{b} \times (\boldsymbol{b} \cdot \nabla)(B\boldsymbol{b})) \times \boldsymbol{b} = \left(\boldsymbol{b} \times ((\boldsymbol{b} \cdot \nabla)\boldsymbol{b} + \boldsymbol{b}\frac{1}{B}(\boldsymbol{b} \cdot \nabla)B)\right) \times \boldsymbol{b}$$
$$= ((\boldsymbol{b} \cdot \nabla)\boldsymbol{b})_\perp = -\frac{\boldsymbol{n}}{R}$$

where R is the radius of curvature and $\boldsymbol{n}$ is the unit vector from the center of curvature to the point on the line of magnetic force (see fig.2.4 of ch.2).

B.2 Energy Integral of Axisymmetric Toroidal System

In any axisymmetric toroidal system, the energy integral may be reduced to more convenient form. The axisymmetric magnetic field is expressed as

$$\boldsymbol{B} = \frac{\hat{I}(\psi)}{R}\boldsymbol{e}_\varphi + B_\chi \boldsymbol{e}_\chi \qquad \hat{I}(\psi) \equiv \frac{\mu_0 I(\psi)}{2\pi} \tag{B.8}$$

where φ is the angle around the axis of torus and ψ is the flux function defined by

$$\psi = -RA_\varphi \tag{B.9}$$

where R is the distance from the axis of symmetry and A_φ is the φ component of the vector potential of the magnetic field. B_χ is the poloidal component of the magnetic field. $\boldsymbol{e}_\varphi$ and $\boldsymbol{e}_\chi$ are the unit vectors with the directions of toroidal angle and poloidal angle respectively (see fig.B.1). The R and Z components of the magnetic field are given by

$$RB_R = \frac{\partial \psi}{\partial Z} \qquad RB_Z = -\frac{\partial \psi}{\partial R}.$$

We can introduce an orthogonal coordinate system (ψ, χ, φ), where ψ=const. are the magnetic surfaces and χ, φ are poloidal and toroidal angles respectively. The metric for these coordinates is

$$\mathrm{d}s^2 = \left(\frac{\mathrm{d}\psi}{RB_\chi}\right)^2 + (JB_\chi \mathrm{d}\chi)^2 + (R\mathrm{d}\varphi)^2 \tag{B.10}$$

where the volume element is $\mathrm{d}V = J(\psi)\mathrm{d}\psi\mathrm{d}\chi\mathrm{d}\varphi$. A field line is defined by ψ=const. and by

$$\frac{R\mathrm{d}\varphi}{JB_\chi \mathrm{d}\chi} = \frac{B_\varphi}{B_\chi} = \frac{\hat{I}(\psi)}{RB_\chi}$$

that is

$$\frac{\mathrm{d}\varphi}{\mathrm{d}\chi} = \frac{J(\psi)\hat{I}(\psi)}{R^2} \equiv \hat{q}(\psi,\chi)$$

and the toroidal safety factor is given by

$$q(\psi) = \frac{1}{2\pi}\oint \frac{J(\psi)\hat{I}(\psi)}{R^2}\mathrm{d}\chi.$$

The energy integral of axisymmetric toroidal system is given by (ref.[3])

$$W = \frac{1}{2}\int_V \Big(\frac{|\boldsymbol{B}_1|^2}{\mu_0} + \gamma p|(\nabla\cdot\boldsymbol{\xi})|^2 + (\nabla\cdot\boldsymbol{\xi}^*)(\boldsymbol{\xi}\cdot\nabla p) - \boldsymbol{\xi}^*\cdot(\boldsymbol{j}\times\boldsymbol{B}_1)\Big)\mathrm{d}\boldsymbol{r}$$

$$= \int_V \Big(\frac{1}{2\mu_0}\frac{B^2k_\parallel^2}{B_\chi^2R^2}|X|^2 + \frac{1}{2\mu_0}\frac{R^2}{J^2}\left|\frac{\partial U}{\partial\chi} - I\left(\frac{JX}{R^2}\right)'\right|^2$$

$$+\frac{B_\chi^2}{2\mu_0}\left|inU + X' - \frac{\mu_0 j_\varphi}{RB_\chi^2}X\right|^2 + \frac{1}{2}\gamma p\left|\frac{1}{J}(JX)' + iBk_\parallel Y + inU\right|^2$$

$$-KXX^*\Big) J\mathrm{d}\psi\mathrm{d}\chi\mathrm{d}\varphi \tag{B.11}$$

The derivation of (B.11) is described in the followings. The notations in (B.11) are explained successively.

In a general orthogonal coordinate system (u^1,u^2,u^3) with the metric of

$$\mathrm{d}s^2 = h_1^2(\mathrm{d}u^1)^2 + h_2^2(\mathrm{d}u^2)^2 + h_3^2(\mathrm{d}u^3)^2$$

$$g^{1/2} = h_1h_2h_3$$

operators of gradient, divergence and rotation of a vector
$\boldsymbol{F} = F_1\boldsymbol{e}_1 + F_2\boldsymbol{e}_2 + F_3\boldsymbol{e}_3$ ($\boldsymbol{e}_j$ are unit vectors) are expressed by

$$\nabla\phi = \sum\frac{1}{h_j}\frac{\partial\phi}{\partial u^j}\boldsymbol{e}_j$$

$$\nabla\cdot\boldsymbol{F} = \frac{1}{g^{1/2}}\left(\frac{\partial}{\partial u^1}(h_2h_3F_1) + \frac{\partial}{\partial u^2}(h_3h_1F_1) + \frac{\partial}{\partial u^3}(h_1h_2F_3)\right)$$

$$\nabla\times\boldsymbol{F} = \frac{1}{h_2h_3}\left(\frac{\partial}{\partial u^2}(h_3F_3) - \frac{\partial}{\partial u^3}(h_2F_2)\right)\boldsymbol{e}_1$$

$$+\frac{1}{h_3h_1}\left(\frac{\partial}{\partial u^3}(h_1F_1) - \frac{\partial}{\partial u^1}(h_3F_3)\right)\boldsymbol{e}_2$$

$$+\frac{1}{h_1h_2}\left(\frac{\partial}{\partial u^1}(h_2F_2) - \frac{\partial}{\partial u^2}(h_1F_1)\right)\boldsymbol{e}_3.$$

In the coordinate system (ψ, χ, φ), $(\boldsymbol{\xi} \cdot \nabla p)$ is reduced to

$$(\boldsymbol{\xi} \cdot \nabla p) = \xi_\psi R B_\chi \frac{\partial p}{\partial \psi} = \xi_\psi R B_\chi p'$$

The prime on p means the differentiation by ψ. From (6.15),(6.16) in ch.6, we have

$$-j_\varphi = Rp' + \frac{\hat{I}\hat{I}'}{\mu_0 R} \tag{B.12}$$

$$p' = -\frac{j_\varphi}{R} - \frac{\hat{I}\hat{I}'}{\mu_0 R^2}$$

Note that ψ defined by (B.9) in this appendix is $-RA_\varphi$, while ψ in (6.15),(6.16) of ch.6 is RA_φ. $\nabla \cdot \boldsymbol{\xi}$ is expressed as

$$\nabla \cdot \xi = \frac{1}{J}\left(\frac{\partial}{\partial \psi}(JB_\chi R\xi_\psi) + \frac{\partial}{\partial \chi}\left(\frac{\xi_\chi}{B_\chi}\right) + \frac{\partial}{\partial \varphi}\left(\frac{J\xi_\varphi}{R}\right)\right).$$

It is convenient to introduce

$$X \equiv RB_\chi \xi_\psi$$

$$Y \equiv \frac{\xi_\chi}{B_\chi}$$

$$U \equiv \frac{1}{RB_\chi}(B_\chi \xi_\varphi - B_\varphi \xi_\chi) = \frac{\xi_\varphi}{R} - \frac{\hat{I}}{R^2 B_\chi}\xi_\chi.$$

Then

$$\xi_\psi = \frac{X}{RB_\chi}$$

$$\xi_\chi = B_\chi Y$$

$$\xi_\varphi = RU + \frac{\hat{I}}{R}Y$$

and

$$\boldsymbol{\xi} \cdot \nabla p = Xp' = X\left(-\frac{j_\varphi}{R} - \frac{\hat{I}\hat{I}'}{\mu_0 R^2}\right). \tag{B.13}$$

We analyze an individual Fourier mode $\boldsymbol{\xi} = \boldsymbol{\xi}(\psi, \chi)\exp(in\varphi)$. Then

$$(Bik_\parallel)Y \equiv \left(B_\chi \frac{1}{JB_\chi}\frac{\partial}{\partial \chi} + B_\varphi \frac{1}{R}\frac{\partial}{\partial \varphi}\right)Y = \left(\frac{1}{J}\frac{\partial}{\partial \chi} + \frac{\hat{I}}{R^2}in\right)Y$$

$$\frac{1}{J}\frac{\partial}{\partial \chi}Y = (Bik_\parallel)Y - in\frac{\hat{I}}{R^2}Y.$$

Since

$$\nabla \cdot \boldsymbol{\xi} = \frac{1}{J}(JX)' + iBk_\parallel Y + inU \tag{B.14}$$

$(\xi \cdot \nabla p)(\nabla \cdot \boldsymbol{\xi}^*)$ is

$$(\boldsymbol{\xi} \cdot \nabla p)(\nabla \cdot \boldsymbol{\xi}^*) = X \left(-\frac{j_\varphi}{R} - \frac{\hat{I}\hat{I}'}{\mu_0 R^2} \right) \left(\frac{1}{J}(JX^*)' - iBk_\parallel Y^* - inU^* \right). \tag{B.15}$$

Let us derive the expression of $\boldsymbol{B}_1$

$$\boldsymbol{B}_1 = \nabla \times (\boldsymbol{\xi} \times \boldsymbol{B})$$

$$(\boldsymbol{\xi} \times \boldsymbol{B})_\psi = \xi_\chi B_\varphi - \xi_\varphi B_\chi$$

$$(\boldsymbol{\xi} \times \boldsymbol{B})_\chi = -\xi_\psi B_\varphi$$

$$(\boldsymbol{\xi} \times \boldsymbol{B})_\varphi = \xi_\psi B_\chi$$

$$B_{1\psi} = \frac{1}{JB_\chi R} \left(\frac{\partial X}{\partial \chi} + \frac{\partial}{\partial \varphi} \left(\frac{JB_\varphi}{R} X \right) \right) = \frac{1}{B_\chi R} iBk_\parallel X$$

$$B_{1\chi} = -B_\chi \left(inU + \frac{\partial X}{\partial \psi} \right)$$

$$B_{1\varphi} = \frac{R}{J} \left(-\frac{\partial}{\partial \psi} \left(\frac{J\hat{I}}{R^2} X \right) + \frac{\partial U}{\partial \chi} \right).$$

Each component of the current density is

$$\mu_0 j_\psi = 0$$

$$\mu_0 j_\chi = -B_\chi \frac{\partial}{\partial \psi}(RB_\varphi) = -B_\chi \hat{I}'$$

$$\mu_0 j_\varphi = \frac{R}{J} \frac{\partial}{\partial \psi}(JB_\chi^2) \tag{B.16}$$

and

$$(\boldsymbol{B}_1 \times \boldsymbol{\xi}^*)_\chi = \frac{R}{J} \frac{\partial U}{\partial \chi} \xi_\psi^* - \frac{R}{J} \left(\frac{IJ}{R^2} X \right)' \xi_\psi^* - \frac{iBk_\parallel}{B_\chi R} X \xi_\varphi^*$$

$$(\boldsymbol{B}_1 \times \boldsymbol{\xi}^*)_\varphi = \frac{iBk_\parallel}{B_\chi R} X \xi_\chi^* + (inU + X') B_\chi \xi_\psi^*.$$

Then $\boldsymbol{\xi}^* \cdot (\boldsymbol{j} \times \boldsymbol{B}_1)$ is

$$\boldsymbol{\xi}^* \cdot (\boldsymbol{j} \times \boldsymbol{B}_1) = \boldsymbol{j} \cdot (\boldsymbol{B}_1 \times \boldsymbol{\xi}^*)$$

$$= -B_\chi \frac{\hat{I}'}{\mu_0} \left(\frac{R}{J} \frac{\partial U}{\partial \chi} \xi_\psi^* - \frac{R}{J} \left(\frac{IJ}{R^2} X \right)' \xi_\psi^* - \frac{iBk_\parallel}{B_\chi R} X \xi_\varphi^* \right) + j_\varphi \left(\frac{iBk_\parallel}{B_\chi R} X \xi_\chi^* + (inU + X') B_\chi \xi_\psi^* \right)$$

$$= \frac{iBk_\parallel}{R} X \left(Y^* j_\varphi + \frac{\hat{I}'}{\mu_0} (RU^* + \frac{\hat{I}}{R} Y^*) \right) + \frac{\hat{I}'}{\mu_0 J} \left(\frac{IJ}{R^2} X \right)' X^* - \frac{\hat{I}'}{\mu_0 J} \frac{\partial U}{\partial \chi} X^* + inUX^* \frac{1}{R} j_\varphi + X' X^* \frac{1}{R} j_\varphi$$

and

$$
\begin{aligned}
&(\nabla\cdot\boldsymbol{\xi}^*)(\boldsymbol{\xi}\cdot\nabla p)-(\boldsymbol{\xi}^*\times\boldsymbol{j})\cdot\boldsymbol{B}_1\\
&=\left(-\frac{j_\varphi}{R}-\frac{\hat{I}\hat{I}'}{\mu_0R^2}\right)(XX^{*\prime}+X'X^*)+\frac{j_\varphi}{R}(inXU^*-inX^*U)\\
&\quad+in\frac{\hat{I}}{R^2}XU^*\frac{\hat{I}'}{\mu_0}+iBk_\parallel XU^*\frac{\hat{I}'}{\mu_0}+\frac{1}{J}\frac{\partial U}{\partial\chi}X^*\frac{\hat{I}'}{\mu_0}\\
&\quad+XX^*\left(-\frac{J'}{J}\frac{j_\varphi}{R}-\frac{\hat{I}'^2}{\mu_0R^2}+\frac{\hat{I}\hat{I}'}{\mu_0R^2}2\frac{R'}{R}-2\frac{\hat{I}\hat{I}'}{\mu_0R^2}\frac{J'}{J}\right)
\end{aligned}
\tag{B.17}
$$

$$
\begin{aligned}
\frac{|B_{1\varphi}|^2}{\mu_0}&=\frac{R^2}{\mu_0J^2}\left|\frac{\partial U}{\partial\chi}-I\left(\frac{JX}{R^2}\right)'-\frac{JX}{R^2}\hat{I}'\right|^2\\
&=\frac{R^2}{\mu_0J^2}\left|\frac{\partial U}{\partial\chi}-I\left(\frac{JX}{R^2}\right)'\right|^2-\frac{\hat{I}'}{\mu_0J}\left(\frac{\partial U}{\partial\chi}X^*+\frac{\partial U^*}{\partial\chi}X\right)\\
&\quad+\frac{\hat{I}\hat{I}'}{\mu_0R^2}(X'X^*+X^{*\prime}X)+2\frac{\hat{I}\hat{I}'}{\mu_0J}\left(\frac{J'}{R^2}-\frac{2R'}{R^3}J\right)XX^*+\frac{\hat{I}'^2}{\mu_0R^2}XX^*\\
\frac{|B_{1\chi}|^2}{\mu_0}&=\frac{B\chi^2}{\mu_0}|inU+X'|^2\\
&=\frac{B\chi^2}{\mu_0}\left|inU+X'-\frac{\mu_0j_\varphi}{RB_\chi^2}X\right|^2+(inUX^*-inU^*X)\frac{j_\varphi}{R}+(X'X^*+X^{*\prime})\frac{j_\varphi}{R}-\frac{\mu_0j_\varphi^2}{R^2B_\chi^2}XX^*.
\end{aligned}
$$

Finally the energy integral of axisymmetric toroidal system becomes

$$
\begin{aligned}
W&=\frac{1}{2}\int_V\left(\frac{|\boldsymbol{B}_1|^2}{\mu_0}+\gamma p|(\nabla\cdot\boldsymbol{\xi})|^2+(\nabla\cdot\boldsymbol{\xi}^*)(\boldsymbol{\xi}\cdot\nabla p)-\boldsymbol{\xi}^*\cdot(\boldsymbol{j}\times\boldsymbol{B}_1)\right)\mathrm{d}\boldsymbol{r}\\
&=\int_V\left(\frac{1}{2\mu_0}\frac{B^2k_\parallel^2}{B_\chi^2R^2}|X|^2+\frac{1}{2\mu_0}\frac{R^2}{J^2}\left|\frac{\partial U}{\partial\chi}-I\left(\frac{JX}{R^2}\right)'\right|^2\right.\\
&\quad\left.+\frac{B_\chi^2}{2\mu_0}\left|inU+X'-\frac{\mu_0j_\varphi}{RB_\chi^2}X\right|^2+\frac{1}{2}\gamma p\left|\frac{1}{J}(JX)'+iBk_\parallel Y+inU\right|^2-KXX^*\right)J\mathrm{d}\psi\mathrm{d}\chi\mathrm{d}\varphi
\end{aligned}
\tag{B.18}
$$

where

$$
\begin{aligned}
K&\equiv\frac{\hat{I}\hat{I}'}{\mu_0R^2}\frac{R'}{R}+\frac{j_\varphi}{2R}\left(\frac{J'}{J}+\frac{\mu_0j_\varphi}{RB_\chi^2}\right)\\
&=\frac{\hat{I}\hat{I}'}{\mu_0R^2}\frac{R'}{R}+\frac{j_\varphi}{R}\left(\frac{J'}{J}+\frac{B_\chi'}{B_\chi}\right),
\end{aligned}
$$

since (refer (B.16))

$$\mu_0 j_\varphi = \frac{R}{J}(J' B_\chi^2 + J 2 B_\chi B_\chi').$$

B.3 Energy Integral of High n Ballooning Modes

The energy integral (B.18) was used for stability analysis of high n modes and ballooning mode[3,4].

The first step in minimization of δW is to select Y so that the last second positive term in (B.18) vanishes ($\nabla \cdot \boldsymbol{\xi} = 0$). The second step is minimization with respect to U. When we concern ballooning modes, the perturbations with large toroidal mode number n and $|m - \hat{q}n| \ll n$ are important (see sec.8.5). After long mathematical calculation, the energy integral with $O(1/n)$ accuracy is derived as follows (ref.[3]);

$$W = \frac{\pi}{\mu_0} \int \mathrm{d}\psi \mathrm{d}\chi \left(\frac{JB^2}{R^2 B_\chi^2} \left| k_\parallel X \right|^2 + \frac{R^2 B_\chi^2}{JB^2} \left| \frac{1}{n} \frac{\partial}{\partial \psi} (JBk_\parallel X) \right|^2 \right.$$

$$- \frac{2J\mu_0 p'}{B^2} \left(|X|^2 \frac{\partial}{\partial \psi}(\mu_0 p + \frac{B^2}{2}) - \frac{i\hat{I}}{JB^2} \frac{\partial}{\partial \chi} \left(\frac{B^2}{2} \right) \frac{X^*}{n} \frac{\partial X}{\partial \psi} \right)$$

$$\left. + \frac{X^*}{n} JBk_\parallel (X\sigma') - \frac{1}{n}(P^* JBk_\parallel Q + \text{c.c.}) \right) \tag{B.19}$$

where

$$P = X\sigma - \frac{B_\chi^2}{\hat{q}B^2} \frac{I}{n} \frac{\partial}{\partial \psi}(JBk_\parallel X)$$

$$Q = \frac{X\mu_0 p'}{B^2} + \frac{\hat{I}^2}{\hat{q}^2 R^2 B^2} \frac{1}{n} \frac{\partial}{\partial \psi}(JBk_\parallel X)$$

$$\sigma = \frac{\hat{I}\mu_0 p'}{B^2} + \hat{I}'$$

$$iJk_\parallel B = \frac{\partial}{\partial \chi} + in\hat{q}, \qquad \hat{q}(\psi, \chi) = \frac{\hat{I}J}{R^2}.$$

δW must be minimized with respect to all periodic functions X subject to an appropriate normalization

$$\pi \int J \mathrm{d}\psi \mathrm{d}\chi \rho_m \left(\frac{|X|^2}{R^2 B_\chi^2} + \left(\frac{RB_\chi}{B} \right)^2 \left| \frac{1}{n} \frac{\partial X}{\partial \psi} \right|^2 \right) = \text{const.} \tag{B.20}$$

where ρ_m is mass density and (B.20) corresponds to the total kinetic energy of perpendicular component to field line.

The Euler equation for the minimizing function $X(\psi, \chi)$ can be deduced form (B.19) and (B.20). As $X(\psi, \chi)$ is periodic in χ, it can be expanded in Fourier series

$$X(\psi, \chi) = \sum_m X_m(\psi) \exp(im\chi)$$

A continuous function $X_s(\psi)$ of s, which is equal to $X_m(\psi)$ at s equal to integer m, can be constructed and can be expressed by Fourier integral

$$X_s(\psi) = \frac{1}{2\pi}\int_{-\infty}^{\infty} \hat{X}(\psi, y)\exp(isy)\mathrm{d}y, \qquad \hat{X}(\psi, y) = \int_{-\infty}^{\infty} X_s(\psi)\exp(-isy)\mathrm{d}s$$

$\hat{X}(\psi, y)$ is called by ballooning representation of $X(\psi, \chi)$. Then $X(\psi, \chi)$ is reduced to

$$X(\psi, \chi) = \sum_m \exp(-im\chi)\int_{-\infty}^{\infty} \hat{X}(\psi, y)\exp(imy)\mathrm{d}y. \tag{B.21}$$

Since

$$\frac{1}{2\pi}\sum_m \exp(-im(\chi - y)) = \sum_N \delta(y - \chi + 2\pi N)$$

($\delta(x)$ is δ function), the relation of $X(\psi, \chi)$ and $\hat{X}(\psi, y)$ is

$$X(\psi, \chi) = \sum_N \hat{X}(\psi, \chi - 2\pi N). \tag{B.22}$$

$X(\psi, \chi)$ is expressed by an infinite sum of quasi-modes.

The Euler equation for $X(\psi, \chi)$ is converted into an identical equation for $\hat{X}(\psi, y)$ but with $\hat{X}$ in the infinite domain of y and free of periodicity requirement. Let us consider $\hat{X}(\psi, y)$ with the form of

$$\hat{X}(\psi, y) = F(\psi, y)\exp(-in\int_{y_0}^{y} \hat{q}\mathrm{d}y) \tag{B.23}$$

in which the amplitude $F(\psi, y)$ reminds a more slowly varying function as $n \to \infty$. Then

$$iJk_{\parallel}B\hat{X}(\psi, y) = \left(\frac{\partial}{\partial y} + in\hat{q}\right)\hat{X}(\psi, y)$$

$$= \frac{\partial F(\psi, y)}{\partial y}\exp(-in\int_{y_0}^{y} \hat{q}\mathrm{d}y).$$

The leading term of the Euler equation for $\hat{X}(\psi, y)$ is reduced to (ref.[3])

$$\frac{1}{J}\frac{\partial}{\partial y}\left(\frac{1}{JR^2B_\chi^2}\left(1 + \left(\frac{R^2B_\chi^2}{B}\int_{y_0}^{y} \hat{q}'\mathrm{d}y\right)^2\right)\frac{\partial F_0}{\partial y}\right)$$

$$+\left(\frac{2\mu_0 p'}{B^2}\frac{\partial}{\partial \psi}\left(\mu_0 p + \frac{B^2}{2}\right) - \frac{\hat{I}\mu_0 p'}{B^4}\left(\int_{y_0}^{y} \hat{q}'\mathrm{d}y\right)\frac{1}{J}\frac{\partial B^2}{\partial y}\right)F_0$$

$$+\frac{\omega^2(\psi, y_0)}{R^2B_\chi^2}\left(1 + \left(\frac{R^2B_\chi^2}{B}\int_{y_0}^{y} \hat{q}'\mathrm{d}y\right)^2\right)F_0 = 0. \tag{B.24}$$

By use of this Euler equation, stability of ballooning mode is analyzed (ref.[4]) (see sec.8.5).

References

[1] J. M. Greene and J. L. Johnson: Plasma Phys. **10**, 729 (1968)
[2] G. Bateman: *MHD Instabilities*, The MIT Press, 1978
[3] J. W. Connor, R. J. Hastie and J. B. Taylor: Proc. Roy. Soc. **A365** 1, (1979)
[4] J. W. Connor, R. J. Hastie and J. B. Taylor: Phys. Rev.Lett. **40**, 396 (1978)

App.C Derivation of Dielectric Tensor in Hot Plasma

C.1 Formulation of Dispersion Relation in Hot Plasma

In ch.10 dispersion relation of cold plasma was derived. In the unperturbed state, both the electrons and ions are motionless in cold plasma. However, in hot plasma, the electron and ions move along spiral trajectories even in the unperturbed state. The motion of charged particles in a uniform magnetic field $\boldsymbol{B}_0 = B_0\hat{\mathbf{z}}$ may be described by

$$\frac{\mathrm{d}\boldsymbol{r}'}{\mathrm{d}t'} = \boldsymbol{v}', \qquad \frac{\mathrm{d}\boldsymbol{v}'}{\mathrm{d}t'} = \frac{q}{m}\boldsymbol{v}' \times \boldsymbol{B}_0. \tag{C.1}$$

Assuming that $\boldsymbol{r}' = \boldsymbol{r}$, $\boldsymbol{v}' = \boldsymbol{v} = (v_\perp \cos\theta, v_\perp \sin\theta, v_z)$ at $t' = t$, the solution of eqs.(C.1) is obtained as follows:

$$\begin{aligned} v'_x(t') &= v_\perp \cos(\theta + \Omega(t'-t)), \\ v'_y(t') &= v_\perp \sin(\theta + \Omega(t'-t)), \\ v'_z(t') &= v_z, \end{aligned} \tag{C.2}$$

$$\begin{aligned} x'(t') &= x + \frac{v_\perp}{\Omega}(\sin(\theta + \Omega(t'-t)) - \sin\theta), \\ y'(t') &= y - \frac{v_\perp}{\Omega}(\cos(\theta + \Omega(t'-t)) - \cos\theta), \\ z'(t') &= z + v_z(t'-t) \end{aligned} \tag{C.3}$$

where $\Omega = -qB_0/m$ and $v_x = v_\perp \cos\theta, v_y = v_\perp \sin\theta$. The analysis of the behavior due to a perturbation of this system must be based on Boltzmann's equation. The distribution function $f_k(\boldsymbol{r}, \boldsymbol{v}, t)$ of kth kind of particles is given by

$$\frac{\partial f_k}{\partial t} + \boldsymbol{v} \cdot \nabla_{\mathrm{r}} f_k + \frac{q_k}{m_k}(\boldsymbol{E} + \boldsymbol{v} \times \boldsymbol{B}) \cdot \nabla_{\mathrm{v}} f_k = 0, \tag{C.4}$$

$$\nabla \cdot \boldsymbol{E} = \frac{1}{\epsilon_0}\sum_k q_k \int \boldsymbol{v} f_k \mathrm{d}\boldsymbol{v}, \tag{C.5}$$

$$\frac{1}{\mu_0}\nabla \times \boldsymbol{B} = \epsilon_0 \frac{\partial \boldsymbol{E}}{\partial t} + \sum_k q_k \int \boldsymbol{v} f_k \mathrm{d}\boldsymbol{v}, \tag{C.6}$$

$$\nabla \times \boldsymbol{E} = -\frac{\partial \boldsymbol{B}}{\partial t}, \tag{C.7}$$

$$\nabla \cdot \boldsymbol{B} = 0. \tag{C.8}$$

As usual, we indicate zeroth order quantities (the unperturbed state) by a subscript 0 and the 1st order perturbation terms by a subscript 1. The 1st order terms are expressed in the form of $\exp i(\boldsymbol{k} \cdot \boldsymbol{r} - \omega t)$. Using

$$f_k = f_{k0}(\boldsymbol{r}, \boldsymbol{v}) + f_{k1}, \tag{C.9}$$

$$\boldsymbol{B} = \boldsymbol{B}_0 + \boldsymbol{B}_1, \tag{C.10}$$

$$\boldsymbol{E} = 0 + \boldsymbol{E}_1 \tag{C.11}$$

we can linearize eqs.(C.4)∼(C.8) as follows:

$$\boldsymbol{v}\cdot\nabla_{\mathrm{r}} f_{k0} + \frac{q_k}{m_k}(\boldsymbol{v}\times\boldsymbol{B}_0)\cdot\nabla_{\mathrm{v}} f_{k0} = 0, \tag{C.12}$$

$$\sum_k q_k \int f_{k0}\mathrm{d}\boldsymbol{v} = 0, \tag{C.13}$$

$$\frac{1}{\mu_0}\nabla\times\boldsymbol{B}_0 = \sum_k q_k \int \boldsymbol{v} f_{k0}\mathrm{d}\boldsymbol{v} = \boldsymbol{j}_0, \tag{C.14}$$

$$\frac{\partial f_{k1}}{\partial t} + \boldsymbol{v}\cdot\nabla_{\mathrm{r}} f_{k1} + \frac{q_k}{m_k}(\boldsymbol{v}\times\boldsymbol{B}_0)\cdot\nabla_{\mathrm{v}} f_{k1} = -\frac{q_k}{m_k}(\boldsymbol{E}_1 + \boldsymbol{v}\times\boldsymbol{B}_1)\cdot\nabla_{\mathrm{v}} f_{k0}, \tag{C.15}$$

$$i\boldsymbol{k}\cdot\boldsymbol{E}_1 = \frac{1}{\epsilon_0}\sum_k q_k \int f_{k1}\mathrm{d}\boldsymbol{v}, \tag{C.16}$$

$$\frac{1}{\mu_0}\boldsymbol{k}\times\boldsymbol{B}_1 = -\omega\left(\epsilon_0\boldsymbol{E}_1 + \frac{i}{\omega}\sum_k q_k\int \boldsymbol{v} f_{k1}\mathrm{d}\boldsymbol{v}\right), \tag{C.17}$$

$$\boldsymbol{B}_1 = \frac{1}{\omega}(\boldsymbol{k}\times\boldsymbol{E}_1). \tag{C.18}$$

The right-hand side of (C.15) is a linear equation in $\boldsymbol{E}_1$ as is clear from (C.18), so that f_{k1} is given as a linear function in $\boldsymbol{E}_1$. The electric tensor of the hot plasma is defined by $\boldsymbol{K}(\boldsymbol{D} = \epsilon_0\boldsymbol{K}\cdot\boldsymbol{E})$ is given by

$$\boldsymbol{E}_1 + \frac{i}{\epsilon\omega}\boldsymbol{j} = \boldsymbol{E}_1 + \frac{i}{\epsilon_0\omega}\sum_k q_k\int \boldsymbol{v} f_{k1}\mathrm{d}\boldsymbol{v} \equiv \boldsymbol{K}\cdot\boldsymbol{E}_1. \tag{C.19}$$

The linear relation of $\boldsymbol{E}_1$ is derived from (C.17) (C.18):

$$\boldsymbol{k}\times(\boldsymbol{k}\times\boldsymbol{E}_1) + \frac{\omega^2}{c^2}\boldsymbol{K}\cdot\boldsymbol{E}_1 = 0 \tag{C.20}$$

and the dispersion relation is obtained by equating the determinant of the coefficient matrix of the linear equation to zero as is (10.19),(10.20). Consequently if f_{k1} can be solved from (C.15), then, $\boldsymbol{K}$ can be obtained. As for cold plasmas, the properties of waves in hot plasmas can be studied by the dispersion relation of hot plasma.

C.2 Solution of Linearized Vlasov Equation

When the right-hand side of (C.15) is time-integrated along the particle orbit (C.2),(C.3) in the unperturbed state, we find

$$f_{k1}(\boldsymbol{r},\boldsymbol{v},t) = -\frac{q_k}{m_k}\int_{-\infty}^{t}\left(\boldsymbol{E}_1(\boldsymbol{r}'(t'),t') + \frac{1}{\omega}\boldsymbol{v}'(t')\times(\boldsymbol{k}\times\boldsymbol{E}_1(\boldsymbol{r}'(t'),t'))\right)\cdot\nabla'_{\mathrm{v}} f_{k0}(\boldsymbol{r}'(t'),\boldsymbol{v}'(t'))\mathrm{d}t' \tag{C.21}$$

Substitution of (C.21) into (C.15) yields

$$\begin{aligned}
&-\frac{q_k}{m_k}\left(\boldsymbol{E}_1 + \frac{1}{\omega}\boldsymbol{v}\times(\boldsymbol{k}\times\boldsymbol{E}_1)\right)\cdot\nabla_{\mathrm{v}} f_{k0} \\
&-\frac{q_k}{m_k}\int_{-\infty}^{t}\left(\frac{\partial}{\partial t} + \boldsymbol{v}\cdot\nabla_{\mathrm{r}} + \frac{q_k}{m_k}(\boldsymbol{v}\times\boldsymbol{B}_0)\cdot\nabla_{\mathrm{v}}\right)[\text{integrand}]\mathrm{d}t' \\
&\quad = -\frac{q_k}{m_k}(\boldsymbol{E}_1 + \boldsymbol{v}\times\boldsymbol{B}_1)\cdot\nabla_{\mathrm{v}} f_{k0}.
\end{aligned} \tag{C.22}$$

Therefore if it is proven that the 2nd term of the left-hand side of (C.22) is zero, (C.21) is confirmed to be the solution of (C.15). When the variables $(\boldsymbol{r}, \boldsymbol{v}, t)$ are changed to $(\boldsymbol{r}', \boldsymbol{v}', t')$ by use of (C.2),(C.3), the differential operators in the 2nd term of left-hand side of (C.22) are reduced to

$$\begin{aligned}
\frac{\partial}{\partial t} &= \frac{\partial t'}{\partial t}\frac{\partial}{\partial t'} + \frac{\partial \boldsymbol{r}'}{\partial t}\cdot\nabla'_{\mathrm{r}} + \frac{\partial \boldsymbol{v}'}{\partial t}\cdot\nabla'_{\mathrm{v}} \\
&= \frac{\partial(t'-t)}{\partial t}\left(\frac{\partial \boldsymbol{r}'}{\partial(t'-t)}\cdot\nabla'_{\mathrm{r}} + \frac{\partial \boldsymbol{v}'}{\partial(t'-t)}\cdot\nabla'_{\mathrm{v}}\right) \\
&= -\boldsymbol{v}'\cdot\nabla'_{\mathrm{r}} - \frac{q_k}{m_k}(\boldsymbol{v}'\times\boldsymbol{B}_0)\cdot\nabla'_{\mathrm{v}},
\end{aligned}$$

$$\boldsymbol{v}\cdot\nabla_{\mathrm{r}} = \boldsymbol{v}\cdot\nabla'_{\mathrm{r}},$$

$$\begin{aligned}
\frac{\partial}{\partial v_x} &= \frac{\partial \boldsymbol{r}'}{\partial v_x}\cdot\nabla'_{\mathrm{r}} + \frac{\partial \boldsymbol{v}'}{\partial v_x}\cdot\nabla'_{\mathrm{v}} \\
&= \frac{1}{\Omega}\left(\sin\Omega(t'-t)\frac{\partial}{\partial x'} + [-\cos\Omega(t'-t)+1]\frac{\partial}{\partial y'}\right) \\
&\quad + \left(\cos\Omega(t'-t)\frac{\partial}{\partial v'_x} + \sin\Omega(t'-t)\frac{\partial}{\partial v'_y}\right), \\
\frac{\partial}{\partial v_y} &= \frac{1}{\Omega}\left((\cos\Omega(t'-t)-1)\frac{\partial}{\partial x'} + \sin\Omega(t'-t)\frac{\partial}{\partial y'}\right) \\
&\quad + \left(-\sin\Omega(t'-t)\frac{\partial}{\partial v'_x} + \cos\Omega(t'-t)\frac{\partial}{\partial v'_y}\right), \\
\frac{q}{m}(\boldsymbol{v}\times\boldsymbol{B}_0)\cdot\nabla_{\mathrm{v}} &= -\Omega\left(v_y\frac{\partial}{\partial v_x} - v_x\frac{\partial}{\partial v_y}\right) \\
&= v'_x\frac{\partial}{\partial x'} + v'_y\frac{\partial}{\partial y'} - \left(v_x\frac{\partial}{\partial x'} + v_y\frac{\partial}{\partial y'}\right) - \Omega\left(v'_y\frac{\partial}{\partial v'_x} - v'_x\frac{\partial}{\partial v'_y}\right) \\
&= (\boldsymbol{v}'-\boldsymbol{v})\cdot\nabla'_{\mathrm{r}} + \frac{q}{m}(\boldsymbol{v}'\times\boldsymbol{B}_0)\cdot\nabla'_{\mathrm{v}}.
\end{aligned}$$

Therefore the 2nd term of left-hand side of (C.22) is zero.

Since the 1st order terms vary as $\exp(-i\omega t)$, the integral (C.21) converges when the imaginary part of ω is positive. When the imaginary part of ω is negative, the solution can be given by analytic continuation from the region of the positive imaginary part.

C.3 Dielectric Tensor of Hot Plasma

The zeroth-order distribution function f_0 must satisfiy (C.12) and

$$f_0(\boldsymbol{r}, \boldsymbol{v}) = f(v_\perp, v_z), \quad v_\perp^2 = v_x^2 + v_y^2.$$

Let us consider

$$\boldsymbol{E}_1(\boldsymbol{r}', t') = \boldsymbol{E}\exp i(\boldsymbol{k}\cdot\boldsymbol{r}' - \omega t').$$

The z axis is taken along $\boldsymbol{B}_0$ direction and x axis is taken in the plane spanned by $\boldsymbol{B}_0$ and the propagation vector $\boldsymbol{k}$, so that y component of the propagation vector is zero ($k_y = 0$), that is:

$$\boldsymbol{k} = k_x\hat{\mathbf{x}} + k_z\hat{\mathbf{z}}.$$

Then (C.21) is reduced to

$$f_1(\boldsymbol{r},\boldsymbol{v},t) = -\frac{q}{m}\exp i(k_x x + k_z z - \omega t)\int_\infty^t \left(\Big(1-\frac{\boldsymbol{k}\cdot\boldsymbol{v}'}{\omega}\Big)\boldsymbol{E} + (\boldsymbol{v}'\cdot\boldsymbol{E})\frac{\boldsymbol{k}}{\omega}\right)\cdot\nabla'_v f_0$$
$$\times\exp\left(i\frac{k_x v_\perp}{\omega}\sin(\theta+\Omega(t'-t)) - i\frac{k_x v_\perp}{\Omega}\sin\theta + i(k_z v_z-\omega)(t'-t)\right)\mathrm{d}t'.$$

We introduce $\tau = t'-t$ and use following formulas of Bessel function:

$$\exp(ia\sin\theta) = \sum_{\mathrm{m}=-\infty}^{\infty} J_{\mathrm{m}}(a)\exp i\mathrm{m}\theta,$$

$$J_{-\mathrm{m}}(a) = (-1)^{\mathrm{m}}J_{\mathrm{m}}(a),$$

$$\exp\Big(\quad\Big) = \sum_{\mathrm{m}=-\infty}^{\infty}\sum_{\mathrm{n}=-\infty}^{\infty} J_{\mathrm{m}}\exp(-i\mathrm{m}\theta)J_{\mathrm{n}}\exp\left(i\mathrm{n}(\theta+\Omega\tau)\right)\exp i(k_z v_z-\omega)\tau.$$

Since

$$\left(\Big(1-\frac{\boldsymbol{k}\cdot\boldsymbol{v}'}{\omega}\Big)\boldsymbol{E} + (\boldsymbol{v}'\cdot\boldsymbol{E})\frac{\boldsymbol{k}}{\omega}\right)\cdot\nabla'_{\mathrm{v}} f_0$$
$$= \frac{\partial f_0}{\partial v_z}\left(\Big(1-\frac{k_x v'_x}{\omega}\Big)E_z + (v'_x E_x + v'_y E_y)\frac{k_z}{\omega}\right) + \frac{\partial f_0}{\partial v_\perp}\left(\Big(1-\frac{k_z v'_z}{\omega}\Big)\Big(E_x\frac{v'_x}{v_\perp}+E_y\frac{v'_y}{v_\perp}\Big) + v_z E_z\frac{k_x}{\omega}\frac{v'_x}{v_\perp}\right)$$
$$= \left(\frac{\partial f_0}{\partial v_\perp}\Big(1-\frac{k_z v_z}{\omega}\Big) + \frac{\partial f_0}{\partial v_z}\frac{k_z v_\perp}{\omega}\right)\left(\frac{E_x}{2}(e^{i(\theta+\Omega\tau)}+e^{-i(\theta+\Omega\tau)}) + \frac{E_y}{2i}(e^{i(\theta+\Omega\tau)}-e^{-i(\theta+\Omega\tau)})\right)$$
$$+\Big(\frac{\partial f_0}{\partial v_\perp}\frac{k_x v_z}{\omega} - \frac{\partial f_0}{\partial v_z}\frac{k_x v_\perp}{\omega}\Big)\frac{E_z}{2}(e^{i(\theta+\Omega\tau)}+e^{-i(\theta+\Omega\tau)}) + \frac{\partial f_0}{\partial v_z}E_z$$

we find

$$f_1(\boldsymbol{r},\boldsymbol{v},t) = -\frac{q}{m}\exp i(k_x x + k_z z - \omega t)\sum_{\mathrm{mn}}\left(U\Big(\frac{J_{\mathrm{n}-1}+J_{\mathrm{n}+1}}{2}\Big)E_x - iU\Big(\frac{J_{\mathrm{n}-1}-J_{\mathrm{n}+1}}{2}\Big)E_y\right.$$
$$\left.+\Big(W\frac{J_{\mathrm{n}-1}+J_{\mathrm{n}+1}}{2} + \frac{\partial f_0}{\partial v_z}J_{\mathrm{n}}\Big)E_z\right)\cdot\frac{J_{\mathrm{m}}(a)\exp(-i(\mathrm{m}-\mathrm{n})\theta)}{i(k_z v_z-\omega+\mathrm{n}\Omega)}$$

where

$$U = \left(1-\frac{k_z v_z}{\omega}\right)\frac{\partial f_0}{\partial v_\perp} + \frac{k_z v_\perp}{\omega}\frac{\partial f_0}{\partial v_z}, \tag{C.23}$$

$$W = \frac{k_x v_z}{\omega}\frac{\partial f_0}{\partial v_\perp} - \frac{k_x v_\perp}{\omega}\frac{\partial f_0}{\partial v_z}, \tag{C.24}$$

$$a = \frac{k_x v_\perp}{\Omega}, \qquad \Omega = \frac{-qB}{m}, \tag{C.25}$$

and

$$\frac{J_{\mathrm{n}-1}(a)+J_{\mathrm{n}+1}(a)}{2} = \frac{\mathrm{n}J_{\mathrm{n}}(a)}{a}, \quad \frac{J_{\mathrm{n}-1}(a)-J_{\mathrm{n}+1}(a)}{2} = \frac{\mathrm{d}}{\mathrm{d}a}J_{\mathrm{n}}(a).$$

Since f_1 is obtained, the dielectric tensor $\boldsymbol{K}$ of hot plasma is reduced from (C.19) to

$$(\boldsymbol{K}-\boldsymbol{I})\cdot\boldsymbol{E} = \frac{i}{\epsilon_0\omega}\sum_j q_j\int \boldsymbol{v}f_{j1}\mathrm{d}\boldsymbol{v}. \tag{C.26}$$

Since $v_x = v_\perp \cos\theta$, $v_y = v_\perp \sin\theta$, $v_z = v_z$, only the terms of $e^{i(\mathrm{m}-\mathrm{n})\theta} = e^{\pm i\theta}$ in f_{j1} can contribute to x, y components of the integral (C.26) and only the term of $e^{i(\mathrm{m}-\mathrm{n})\theta} = 1$ in f_{j1} can contribute to z component of the integral (C.26) and we find:

$$\boldsymbol{K} = \boldsymbol{I} - \sum_j \frac{\Pi_j^2}{\omega n_{j0}} \sum_{\mathrm{n}=-\infty}^{\infty} \int \mathrm{d}\boldsymbol{v} \frac{S_{j\mathrm{n}}}{k_z v_z - \omega + \mathrm{n}\Omega_j}, \tag{C.27}$$

$$S_{j\mathrm{n}} = \begin{bmatrix} v_\perp (\mathrm{n}\frac{J_\mathrm{n}}{a})^2 U & -iv_\perp (\mathrm{n}\frac{J_\mathrm{n}}{a}) J'_\mathrm{n} U & v_\perp (\mathrm{n}\frac{J_\mathrm{n}}{a}) J_\mathrm{n} (\frac{\partial f_0}{\partial v_z} + \frac{\mathrm{n}}{a} W) \\ iv_\perp J'_\mathrm{n} (\mathrm{n}\frac{J_\mathrm{n}}{a}) U & v_\perp (J'_\mathrm{n})^2 U & iv_\perp J'_\mathrm{n} J_\mathrm{n} (\frac{\partial f_0}{\partial v_z} + \frac{\mathrm{n}}{a} W) \\ v_z J_\mathrm{n} (\mathrm{n}\frac{J_\mathrm{n}}{a}) U & -iv_\perp J_\mathrm{n} J'_\mathrm{n} U & v_z J_\mathrm{n}^2 (\frac{\partial f_0}{\partial v_z} + \frac{\mathrm{n}}{a} W) \end{bmatrix}$$

where

$$\Pi_j^2 = \frac{n_j q_j^2}{\epsilon_0 m_j}.$$

When we use the relations

$$\frac{v_z U - v_\perp (\frac{\partial f_0}{\partial v_z} + \frac{\mathrm{n}\Omega}{k_x v_\perp} W)}{k_z v_z - \omega + \mathrm{n}\Omega} = -\frac{v_z}{\omega} \frac{\partial f_0}{\partial v_\perp} + \frac{v_\perp}{\omega} \frac{\partial f_0}{\partial v_z},$$

$$\sum_{\mathrm{n}=-\infty}^{\infty} J_\mathrm{n}^2 = 1, \qquad \sum_{\mathrm{n}=-\infty}^{\infty} J_\mathrm{n} J'_\mathrm{n} = 0, \qquad \sum_{\mathrm{n}=-\infty}^{\infty} \mathrm{n} J_\mathrm{n}^2 = 0 \quad (J_{-\mathrm{n}} = (-1)^\mathrm{n} J_\mathrm{n})$$

and replace n by $-$n, then (C.27) is reduced to

$$\boldsymbol{K} = \boldsymbol{I} - \sum_j \frac{\Pi_j^2}{\omega} \sum_{\mathrm{n}=-\infty}^{\infty} \int T_{j\mathrm{n}} \frac{v_\perp^{-1} U_j n_{j0}^{-1}}{k_z v_z - \omega - \mathrm{n}\Omega_j} \mathrm{d}\boldsymbol{v} - \boldsymbol{L} \sum_j \frac{\Pi_j^2}{\omega^2} \left(1 + \frac{1}{n_{j0}} \int \frac{v_z^2}{v_\perp} \frac{\partial f_{j0}}{\partial v_\perp} \mathrm{d}\boldsymbol{v} \right),$$

$$T_{j\mathrm{n}} = \begin{bmatrix} v_\perp^2 (\mathrm{n}\frac{J_\mathrm{n}}{a})(\mathrm{n}\frac{J_\mathrm{n}}{a}) & iv_\perp^2 (\mathrm{n}\frac{J_\mathrm{n}}{a}) J'_\mathrm{n} & -v_\perp v_z (\mathrm{n}\frac{J_\mathrm{n}}{a}) J_\mathrm{n} \\ -iv_\perp^2 J'_\mathrm{n} (\mathrm{n}\frac{J_\mathrm{n}}{a}) & v_\perp^2 J'_\mathrm{n} J'_\mathrm{n} & iv_\perp v_z J'_\mathrm{n} J_\mathrm{n} \\ -v_\perp v_z J_\mathrm{n} (\mathrm{n}\frac{J_\mathrm{n}}{a}) & -iv_\perp v_z J_\mathrm{n} J'_\mathrm{n} & v_z^2 J_\mathrm{n} J_\mathrm{n} \end{bmatrix}$$

where all the components of matrix $\boldsymbol{L}$ are zero except $L_{zz} = 1$. From the relations

$$\frac{U_j}{k_z v_z - \omega - \mathrm{n}\Omega_j} = -\frac{1}{\omega} \frac{\partial f_{j0}}{\partial v_\perp} + \frac{1}{\omega (k_z v_z - \omega - \mathrm{n}\Omega_j)} \left(-\mathrm{n}\Omega_j \frac{\partial f_{j0}}{\partial v_\perp} + k_z v_\perp \frac{\partial f_{j0}}{\partial v_z} \right),$$

$$\sum_{\mathrm{n}=-\infty}^{\infty} (J'_\mathrm{n})^2 = \frac{1}{2}, \qquad \sum_{\mathrm{n}=-\infty}^{\infty} \frac{\mathrm{n}^2 J_\mathrm{n}^2(a)}{a^2} = \frac{1}{2}$$

another expression of the dielectric tensor is obtained: (ref.[1])

$$\boldsymbol{K} = \left(1 - \frac{\Pi_j^2}{\omega^2} \right) \boldsymbol{I} - \sum_{j,\mathrm{n}} \frac{\Pi_j^2}{\omega^2} \int \frac{T_{j\mathrm{n}}}{k_z v_z - \omega - \mathrm{n}\Omega_j} \left(\frac{-\mathrm{n}\Omega_j}{v_\perp} \frac{\partial f_{j0}}{\partial v_\perp} + k_z \frac{\partial f_{j0}}{\partial v_z} \right) \frac{1}{n_{j0}} \mathrm{d}\boldsymbol{v}. \tag{C.28}$$

Using

$$\boldsymbol{N} \equiv \frac{\boldsymbol{k}}{\omega} c$$

the dispersion relation (C.20) is given by

$$(K_{xx} - N_\parallel^2) E_x + K_{xy} E_y + (K_{xz} + N_\perp N_\parallel) E_z = 0,$$

$$K_{yx} E_x + (K_{yy} - N^2) E_y + K_{yz} E_z = 0,$$

$$(K_{zx} + N_\perp N_\parallel)E_x + K_{zy}E_y + (K_{zz} - N_\perp^2)E_z = 0$$

where $N_\parallel$ is z component of $\boldsymbol{N}$ (parallel to $\boldsymbol{B}$) and $N_\perp$ is x component of $\boldsymbol{N}$ (perpendicular to $\boldsymbol{B}$). The dispersion relation is given by equating the determinent of the coefficient matrix to zero.

C.4 Dielectric Tensor of bi-Maxwellian Plasma

When the zeroth-order distribution function is bi-Maxwellian,

$$f_0(v_\perp, v_z) = n_0 F_\perp(v_\perp) F_z(v_z), \tag{C.29}$$

$$F_\perp(v_\perp) = \frac{m}{2\pi\kappa T_\perp} \exp\left(-\frac{m v_\perp^2}{2\kappa T_\perp}\right), \tag{C.30}$$

$$F_z(v_z) = \left(\frac{m}{2\pi\kappa T_z}\right)^{1/2} \exp\left(-\frac{m(v_z - V)^2}{2\kappa T_z}\right) \tag{C.31}$$

we find

$$\left(-\frac{\mathrm{n}\Omega_j}{v_\perp}\frac{\partial f_0}{\partial v_\perp} + k_z \frac{\partial f_0}{\partial v_z}\right)\frac{1}{n_0} = m\left(\frac{\mathrm{n}\Omega_j}{\kappa T_\perp} - \frac{k_z(v_z - V)}{\kappa T_z}\right) F_\perp(v_\perp) F_z(v_z).$$

Integration over v_z can be done by use of *plasma dispersion function* $Z(\zeta)$. Plasma dispersion function $Z(\zeta)$ is defined by:

$$Z(\zeta) \equiv \frac{1}{\pi^{1/2}} \int_{-\infty}^{\infty} \frac{\exp(-\beta^2)}{\beta - \zeta} \mathrm{d}\beta. \tag{C.32}$$

Using following relations

$$\int_{-\infty}^{\infty} \frac{F_z}{k_z(v_z - V) - \omega_\mathrm{n}} \mathrm{d}v_z = \frac{1}{\omega_\mathrm{n}} \zeta_\mathrm{n} Z(\zeta_\mathrm{n}),$$

$$\int_{-\infty}^{\infty} \frac{k_z(v_z - V) F_z}{k_z(v_z - V) - \omega_\mathrm{n}} \mathrm{d}v_z = 1 + \zeta_\mathrm{n} Z(\zeta_\mathrm{n}),$$

$$\int_{-\infty}^{\infty} \frac{(k_z(v_z - V))^2 F_z}{k_z(v_z - V) - \omega_\mathrm{n}} \mathrm{d}v_z = \omega_\mathrm{n}(1 + \zeta_\mathrm{n} Z(\zeta_\mathrm{n})),$$

$$\int_{-\infty}^{\infty} \frac{(k_z(v_z - V))^3 F_z}{k_z(v_z - V) - \omega_\mathrm{n}} \mathrm{d}v_z = \frac{k_z^2(\kappa T_z)}{m} + \omega_\mathrm{n}^2(1 + \zeta_\mathrm{n} Z(\zeta_\mathrm{n})),$$

$$\omega_\mathrm{n} \equiv \omega - k_z V + \mathrm{n}\Omega,$$

$$\zeta_\mathrm{n} \equiv \frac{\omega - k_z V + \mathrm{n}\Omega}{k_z(2\kappa T_z/m)^{1/2}},$$

$$\int_0^\infty J_\mathrm{n}^2(b^{1/2}x) \exp\left(-\frac{x^2}{2\alpha}\right) x \mathrm{d}x = \alpha I_\mathrm{n}(\alpha b) e^{-b\alpha},$$

$$\sum_{\mathrm{n}=-\infty}^{\infty} I_\mathrm{n}(b) = e^b, \qquad \sum_{\mathrm{n}=-\infty}^{\infty} \mathrm{n} I_\mathrm{n}(b) = 0, \qquad \sum_{\mathrm{n}=-\infty}^{\infty} \mathrm{n}^2 I_\mathrm{n}(b) = b e^b$$

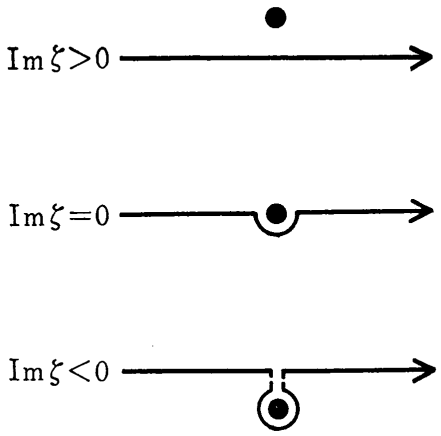

Fig.C.1 Integral paths of (9.62) for $\mathrm{Im}\zeta > 0$, $\mathrm{Im}\zeta = 0$, and $\mathrm{Im}\zeta < 0$ in the case of $k_z > 0$.

(where $I_\mathrm{n}(x)$ is nth modified Bessel function) the formula for the dielectric tensor of a bi-Maxwellian plasma is obtained as follows: (ref.[2])

$$\boldsymbol{K} = \boldsymbol{I} + \sum_{\mathrm{i,e}} \frac{\Pi^2}{\omega^2} \left(\sum_{\mathrm{n}} \left(\zeta_0 Z(\zeta_\mathrm{n}) - \left(1 - \frac{1}{\lambda_\mathrm{T}}\right)(1 + \zeta_\mathrm{n} Z(\zeta_\mathrm{n})) \right) e^{-b} \boldsymbol{X}_\mathrm{n} + 2\eta_0^2 \lambda_\mathrm{T} \boldsymbol{L} \right), \tag{C.33}$$

$$\boldsymbol{X}_\mathrm{n} = \begin{bmatrix} \mathrm{n}^2 I_\mathrm{n}/b & i\mathrm{n}(I'_\mathrm{n} - I_\mathrm{n}) & -(2\lambda_\mathrm{T})^{1/2}\eta_\mathrm{n}\frac{\mathrm{n}}{\alpha} I_\mathrm{n} \\ -i\mathrm{n}(I'_\mathrm{n} - I_\mathrm{n}) & (\mathrm{n}^2/b + 2b)I_\mathrm{n} - 2bI'_\mathrm{n} & i(2\lambda_\mathrm{T})^{1/2}\eta_\mathrm{n}\alpha(I'_\mathrm{n} - I_\mathrm{n}) \\ -(2\lambda_\mathrm{T})^{1/2}\eta_\mathrm{n}\frac{\mathrm{n}}{\alpha} I_\mathrm{n} & -i(2\lambda_\mathrm{T})^{1/2}\eta_\mathrm{n}\alpha(I'_\mathrm{n} - I_\mathrm{n}) & 2\lambda_\mathrm{T}\eta_\mathrm{n}^2 I_\mathrm{n} \end{bmatrix} \tag{C.34}$$

$$\eta_\mathrm{n} \equiv \frac{\omega + \mathrm{n}\Omega}{2^{1/2} k_z v_{Tz}}, \quad \lambda_\mathrm{T} \equiv \frac{T_z}{T_\perp}, \quad b \equiv \left(\frac{k_x v_{\mathrm{T}\perp}}{\Omega} \right)^2,$$

$$\alpha \equiv \frac{k_x v_{T\perp}}{\Omega}, \quad v_{\mathrm{T}z}^2 \equiv \frac{\kappa T_z}{m}, \quad v_{\mathrm{T}\perp}^2 \equiv \frac{\kappa T_\perp}{m},$$

$\boldsymbol{L}$ matrix components are $L_{zz} = 1$ and all others are 0.

C.5 Plasma Dispersion Function

Let us examine the property of *plasma dispersion function* $Z_\mathrm{p}(\zeta)$ defined by

$$Z_\mathrm{p}(\zeta) \equiv \frac{1}{\pi^{1/2}} \int_{-\infty}^{\infty} \frac{\exp(-\beta^2)}{\beta - \zeta} \mathrm{d}\beta, \tag{C.35}$$

in the case of $\mathrm{Im}\zeta > 0$. The solution (C.21) of the first order Vlasov equation is obtained by time integration of $\exp(-i\omega t)$ along the particle orbit from $-\infty$ to t. Therefore, the imaginary part ω_i must be positive. First, let us consider the case $k_z > 0$, so that $\mathrm{Im}\zeta > 0$. For $Z_\mathrm{p}(\zeta)$ in the case of $\mathrm{Im}\zeta < 0$, analytic continuation must be used. The integral paths for $\mathrm{Im}\zeta > 0$, $\mathrm{Im}\zeta = 0$, and $\mathrm{Im}\zeta < 0$ are shown in fig.C.1.

Setting $\beta - \zeta = \gamma$ in (C.35) and using the relation

$$\int_{-\infty}^{\infty} \frac{\exp(-\gamma^2 - 2\zeta\gamma)}{\gamma} \mathrm{d}\gamma = -2\pi^{1/2} \int_{+i\infty}^{\zeta} \exp(t^2) \mathrm{d}t$$

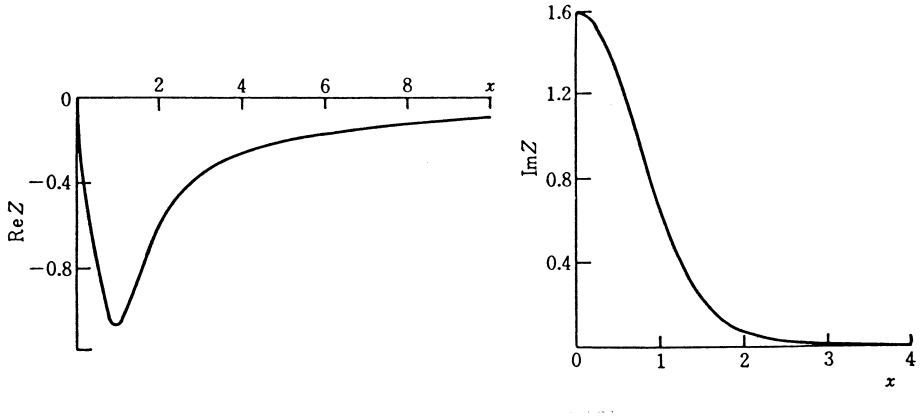

Fig.C.2 Real part $\mathrm{Re}\,Z(x)$ and imaginary part $\mathrm{Im}\,Z(x)$ of $Z(x)$ in the case of real x.

(if both sides are differentiated by ζ, it is clear that they are equal), we find (ref.[1],[3])

$$Z_{\mathrm{p}}(\zeta) = -2\exp(-\zeta^2)\int_{+i\infty}^{\zeta} \exp(t^2)\mathrm{d}t = -i\exp(-\zeta^2) - 2S(\zeta)$$

$$Z_{\mathrm{p}}(\zeta) = 2i\exp(-\zeta^2)\int_{-\infty}^{i\zeta} \exp(-s^2)\mathrm{d}s = i2\pi^{1/2}\exp(-\zeta^2)\Phi(2^{1/2}i\zeta),$$

where

$$S(\zeta) = \exp(-\zeta^2)\int_0^{\zeta} \exp(t^2)\mathrm{d}t \qquad \Phi(x) \equiv \frac{1}{(2\pi)^{1/2}}\int_{-\infty}^{x} \exp\left(-\frac{t^2}{2}\right)\mathrm{d}t.$$

The series expansion of $Z_{\mathrm{p}}(\zeta)$ is

$$Z_{\mathrm{p}}(\zeta) = i\pi^{1/2}\exp(-\zeta^2) - \zeta\sum_{n=0}^{\infty}\frac{(-\zeta^2)^n\pi^{1/2}}{\Gamma(n+3/2)}$$

$$= i\pi^{1/2}\exp(-\zeta^2) - 2\zeta\left(1 - \frac{2\zeta^2}{3} + \frac{4\zeta^4}{15} - \cdots\right),$$

in the case of hot plasma ($|\zeta| \ll 1$) by using partial integral of $\int_0^z 1 \times \exp(t^2)\mathrm{d}t$ (ref.[1]). The asymptotic expansion of $Z_{\mathrm{p}}(\zeta)$ is given by

$$Z_{\mathrm{p}}(\zeta) = i\sigma\pi^{1/2}\exp(-\zeta^2) - \sum_{n=0}^{\infty}\zeta^{-(2n+1)}\frac{\Gamma(n+1/2)}{\pi^{1/2}}$$

$$= i\sigma\pi^{1/2}\exp(-\zeta^2) - \frac{1}{\zeta}\left(1 + \frac{1}{2\zeta^2} + \frac{3}{4\zeta^4} + \cdots\right),$$

$$\sigma = 0 \quad \text{for } \mathrm{Im}\,\zeta > 0,$$

$$\sigma = 2 \quad \text{for } \mathrm{Im}\,\zeta < 0,$$

but

$$\sigma = 1 \quad \text{for } |\mathrm{Im}\,\zeta||\mathrm{Re}\,\zeta| \lesssim \pi/4, \quad |\zeta| \gg 1,$$

in the case of cold plasma ($|\zeta| \gg 1$) (ref.[1]). The curves for real and imaginary parts of $Z_{\mathrm{p}}(x)$ (x is real) are shown in fig.C.2.

The function $Z(\zeta)$ of dielectric tensor (C.33) is defined for $\mathrm{Im}\omega > 0$ because we solved the linear Vlasov equation by time integral along the particle path from $-\infty$ to t ($|\exp(-i\omega t)| = \exp \mathrm{Im}\omega t$). Accordingly, in the case of $k > 0$, the function $Z(\zeta)$ of dielectric tensor (C.33) is the same as the plasma dispersion function $Z_{\mathrm{p}}(\zeta)$ defined by (C.35); that is

$$Z(\zeta) = Z_{\mathrm{p}}(\zeta) \quad \text{when } k > 0.$$

Let us consider the case for $k < 0$. Since the function $Z(\zeta)$ of dielectric tensor (C.33) was defined for $\mathrm{Im}\omega > 0$, this function $Z(\zeta)$ was defined when $\mathrm{Im}\zeta = \mathrm{Im}\omega/(2^{1/2}k_z v_{\mathrm{Tz}}) < 0$. Analytic continuation must be used for $\mathrm{Im}\zeta = \mathrm{Im}\omega/(2^{1/2}k_z v_{\mathrm{Tz}}) > 0$. The relation of $Z(\zeta)$ and $Z_{\mathrm{p}}(\zeta)$ is

$$Z(\zeta) = Z_{\mathrm{p}}(\zeta) - 2\pi^{1/2} i \exp(-\zeta^2) \quad \text{when } k < 0.$$

When ζ is real and equal to x, Cauchy's principal value is $\lim_{\varepsilon\to 0}\left(\int_{-\infty}^{x-\varepsilon} + \int_{x+\varepsilon}^{\infty}\right)$. When ζ is complex, Cauchy's principal value is the average of the two integral which pass just above and just below the singular point (ref.[1]). We can then write ζ in the form valid for all ζ as follow:

$$Z(\zeta) \equiv \frac{1}{\pi^{1/2}} \mathrm{P} \int_{-\infty}^{\infty} \frac{\exp(-\beta^2)}{\beta - \zeta} \mathrm{d}\beta + i\pi^{1/2} \frac{k_z}{|k_z|} \exp(-\zeta^2),$$

where P means Cauchy's principal value.

The series expansion of $Z(\zeta)$ is ($|\zeta| \ll 1$, hot plasma)

$$Z(\zeta) = i\pi^{1/2} \frac{k_z}{|k_z|} \exp(-\zeta^2) - 2\zeta \left(1 - \frac{2\zeta^2}{3} + \frac{4\zeta^4}{15} - \cdots\right), \tag{C.36}$$

and the asymptotic expansion of $Z(\zeta)$ is ($|\zeta| \gg 1$, cold plasma) (ref.1))

$$Z(\zeta) = i\sigma\pi^{1/2} \frac{k_z}{|k_z|} \exp(-\zeta^2) - \frac{1}{\zeta}\left(1 + \frac{1}{2\zeta^2} + \frac{3}{4\zeta^4} + \cdots\right), \tag{C.37}$$

$$\sigma = 0, \quad \text{when and } (k_z/|k_z|)\mathrm{Im}\,\zeta > 0, \text{ that is, } \mathrm{Im}\,\omega > 0$$

$$\sigma = 2, \quad \text{when and } (k_z/|k_z|)\mathrm{Im}\,\zeta < 0, \text{ that is, } \mathrm{Im}\,\omega < 0$$

but $$\sigma = 1 \quad \text{for } |\mathrm{Im}\,\zeta||\mathrm{Re}\,\zeta| \lesssim \pi/4, \quad |\zeta| \gg 1,,$$

The term $i\pi^{1/2}\exp(-\zeta^2)$ of $Z(\zeta)$ represents the terms of Landau damping and cyclotron damping.

When $T \to 0$, that is, $\zeta_{\mathrm{n}} \to \pm\infty$, $b \to 0$, the dielectric tensor of hot plasma is reduced to the dielectric tensor (8.9) of cold plasma.

C.6 Dispersion Relation of Electrostatic Wave

When the electric field $\boldsymbol{E}$ of waves is expressed by electrostatic potential ϕ:

$$\boldsymbol{E} = -\nabla\phi$$

the waves is called electrostatic wave. In this section the dispersion relation of electrostatic wave in hot plasma is described. Since $\partial \boldsymbol{B}_1/\partial t = \nabla \times \boldsymbol{E}$ and

$$\boldsymbol{B}_1 = \boldsymbol{k} \times \boldsymbol{E}/\omega = 0$$

the dispersion relation is reduced from (10.92) to

$$k_x^2 K_{xx} + 2k_x k_z K_{xz} + k_z^2 K_{zz} = 0. \tag{C.38}$$

When $\boldsymbol{K}$ given by (C.33) is substituted in (C.38), we find:

$$k_x^2 + k_z^2 + \sum_{\mathrm{i,e}} \frac{\mathit{\Pi}^2}{\omega^2}\left[k_z^2 2\eta_0^2\lambda_{\mathrm{T}} + \sum_{\mathrm{n}=-\infty}^{\infty}\left(\frac{\mathrm{n}^2 I_{\mathrm{n}}}{b}k_x^2 - (2\lambda_{\mathrm{T}})^{1/2}\eta_{\mathrm{n}}\frac{\mathrm{n}}{b^{1/2}} I_{\mathrm{n}} 2k_x k_z + 2\lambda_{\mathrm{T}}\eta_{\mathrm{n}}^2 I_{\mathrm{n}} k_z^2\right)\right.$$
$$\left.\times\left(\eta_0 Z(\zeta_{\mathrm{n}}) - \left(1 - \frac{1}{\lambda_{\mathrm{T}}}\right)(1 + \zeta_{\mathrm{n}} Z(\zeta_{\mathrm{n}}))\right) e^{-b}\right] = 0$$

where

$$\omega_{\rm n} \equiv \omega - k_z V + {\rm n}\Omega, \qquad \sum_{\rm n=-\infty}^{\infty} I_{\rm n}(b) = e^b,$$

$$\zeta_{\rm n} = \frac{\omega_{\rm n}}{2^{1/2} k_z v_{{\rm T}z}}, \qquad \lambda_{\rm T} = \frac{T_z}{T_\perp},$$

$$\eta_{\rm n} = \frac{\omega + {\rm n}\Omega}{2^{1/2} k_z v_{{\rm T}z}},$$

$$b = \Big(\frac{k_x v_{{\rm T}\perp}}{\Omega}\Big)^2$$

and

$$k_x^2 + k_z^2 + \sum_{\rm i,e} \frac{\Pi^2}{\omega^2}\Big(\frac{m\omega^2}{\kappa T_\perp} + \sum_{\rm n=-\infty}^{\infty} \frac{m\omega^2}{\kappa T_\perp} I_{\rm n}\Big(\zeta_0 Z(\zeta_{\rm n}) - \Big(1 - \frac{1}{\lambda_{\rm T}}\Big)(1 + \zeta_{\rm n} Z(\zeta_{\rm n}))\Big) e^{-b}\Big) = 0,$$

$$k_x^2 + k_z^2 + \sum_{\rm i,e} \Pi^2 \frac{m}{\kappa T_z}\Big(1 + \sum_{\rm n=-\infty}^{\infty} \Big(1 + \frac{T_z}{T_\perp}\Big(\frac{-{\rm n}\Omega}{\omega_{\rm n}}\Big)\Big) \zeta_{\rm n} Z(\zeta_{\rm n}) I_{\rm n} e^{-b}\Big) = 0. \tag{C.39}$$

C.7 Dispersion Relation of Electrostatic Wave in Inhomogenous Plasma

Equation (C.39) is the dispersion relation of electrostatic wave in a homogenenous bi-Mawellian plasma. When the density and temperature of the zeroth-order state change in the direction of y, we must resort to (C.5),(C.21) and

$$\boldsymbol{E}_1 = -\nabla\phi_1, \qquad \frac{\partial \boldsymbol{B}_1}{\partial t} = -\nabla \times \boldsymbol{E}_1 = 0,$$

$$-\nabla^2 \phi_1 = \frac{1}{\epsilon_0} \sum_k q_k \int f_{k1} {\rm d}\boldsymbol{v}, \tag{C.40}$$

$$f_{k1} = \frac{q_k}{m_k} \int_{-\infty}^{t} \nabla'_{\rm r}\phi_1(\boldsymbol{r}', t') \cdot \nabla'_{\rm v} f_{k0}(\boldsymbol{r}', \boldsymbol{v}') {\rm d}t'. \tag{C.41}$$

The zeroth-order distribution function f_{k0} must satisfy (C.12) and

$$v_y \frac{\partial f_0}{\partial y} - \Omega(v_y \frac{\partial}{\partial v_x} - v_x \frac{\partial}{\partial v_y}) f_0 = 0.$$

$\alpha = v_\perp^2$, $\beta = (v_z - V)^2$, $\gamma = y + v_x/\Omega$ are the constant of motion. Consequently $f_0(\alpha, \beta, \gamma)$ satisfies (C.12) and we adopt the following zeroth order distribution function

$$f_0\left(v_\perp^2, (v_z - V)^2, y + \frac{v_x}{\Omega}\right) = n_0 \left(1 + \left(-\epsilon + \delta_\perp \frac{v_\perp^2}{2v_{{\rm T}\perp}^2} + \delta_z \frac{(v_z - V)^2}{2v_{\perp z}^2}\right)\left(y + \frac{v_x}{\Omega}\right)\right)$$
$$\times \left(\frac{1}{2\pi v_{{\rm T}\perp}^2}\right)\left(\frac{1}{2\pi v_{{\rm T}z}^2}\right)^{1/2} \exp\left(-\frac{v_\perp^2}{2v_{{\rm T}\perp}^2} - \frac{(v_z - V)^2}{2v_{{\rm T}z}^2}\right). \tag{C.42}$$

The density gradient and temperature gradient of this distribution function are

$$\frac{1}{n_0}\frac{{\rm d}n_0}{{\rm d}y} = -\epsilon + \delta_\perp + \frac{\delta_z}{2},$$

$$\frac{1}{T_\perp}\frac{\mathrm{d}T_\perp}{\mathrm{d}y} = \delta_\perp,$$

$$\frac{1}{T_z}\frac{\mathrm{d}T_z}{\mathrm{d}y} = \delta_z.$$

Let us consider the following perturbation:

$$\phi_1(\boldsymbol{r},t) = \phi_1(y)\exp(ik_x x + ik_z z - i\omega t).$$

Then the integrand becomes

$$\nabla'_{\mathrm{r}}\phi_1 \cdot \nabla'_{\mathrm{v}} f_0 = (\boldsymbol{v}'\cdot\nabla'_{\mathrm{r}}\phi_1)2\frac{\partial f_0}{\partial \alpha'} + \left(2ik_z(v'_z - V)\frac{\partial f_0}{\partial \beta'} - 2ik_z v'_z\frac{\partial f_0}{\partial \alpha'} + \frac{ik_x}{\Omega}\frac{\partial f_0}{\partial \gamma'}\right)\phi_1.$$

Using

$$\frac{\mathrm{d}\phi_1}{\mathrm{d}t'} = \frac{\partial\phi_1}{\partial t'} + (\boldsymbol{v}'\cdot\nabla'_{\mathrm{r}}\phi_1) = -i\omega\phi_1 + \boldsymbol{v}'\cdot\nabla'_{\mathrm{r}}\phi_1,$$

$$\int^t \boldsymbol{v}'\cdot\nabla'_{\mathrm{r}}\phi_1\mathrm{d}t' = \phi_1 + i\omega\int^t \phi_1\mathrm{d}t',$$

$$\alpha' = \alpha, \qquad \beta' = \beta, \qquad \gamma' = \gamma$$

we find that

$$f_1 = \frac{q}{m}\left(2\frac{\partial f_0}{\partial\alpha}\phi_1 + \left(2i\omega\frac{\partial f_0}{\partial\alpha} + 2ik_z(v_z - V)\frac{\partial f_0}{\partial\beta} - 2ik_z v_z\frac{\partial f_0}{\partial\alpha} + \frac{ik_x}{\Omega}\frac{\partial f_0}{\partial\gamma}\right)\right.$$
$$\left.\times\int_{-\infty}^t \phi_1(y')\exp(ik_x x' + ik_z z' - i\omega t')\mathrm{d}t'\right) \tag{C.43}$$

and

$$\int_{-\infty}^t \phi(\boldsymbol{r}',t')\mathrm{d}t' = \int_{-\infty}^t \phi_1(y')\exp(ik_x x' + ik_z z' - i\omega t')\mathrm{d}t'$$
$$= \phi_1(y)\exp(ik_x x + ik_z z - i\omega t)\exp\left(-i\frac{k_x v_\perp}{\Omega}\sin\theta\right)$$
$$\times\int_{-\infty}^t \exp\left(\frac{ik_x v_\perp}{\Omega}\sin(\theta+\Omega\tau) + i(k_z v_z - \omega)\tau\right)\mathrm{d}\tau. \tag{C.44}$$

Using the expansion

$$\exp(ia\sin\theta) = \sum_{\mathrm{m}=-\infty}^{\infty} J_{\mathrm{m}}(a)\exp i\mathrm{m}\theta,$$

$$J_{-\mathrm{m}}(a) = (-1)^{\mathrm{m}}J_{\mathrm{m}}(a)$$

we write the integral as

$$\int_{-\infty}^t \phi_1(\boldsymbol{r}',t')\mathrm{d}t'$$
$$= \phi_1(\boldsymbol{r},t)\sum_{\mathrm{n}=-\infty}^{\infty}\frac{i}{\omega - k_z v_z - \mathrm{n}\Omega}(J_{\mathrm{n}}^2(a) + J_{\mathrm{n}}(a)J_{\mathrm{n}-1}(a)\exp i\theta + J_{\mathrm{n}}(a)J_{\mathrm{n}+1}(a)\exp(-i\theta) + \cdots)$$

(C.45)

where $a = k_x v_\perp/\Omega$. Substitution of the foregoing equation into (C.43) gives

$$f_1 = \frac{q}{m}\phi_1\left[2\frac{\partial f_0}{\partial \alpha} - \left(2(\omega - k_z v_z)\frac{\partial f_0}{\partial \alpha} + 2k_z(v_z - V)\frac{\partial f_0}{\partial \beta} + \frac{k_x}{\Omega}\frac{\partial f_0}{\partial \gamma}\right)\sum \frac{(J_{\rm n}^2(a) + \cdots)}{\omega - k_z v_z - {\rm n}\Omega}\right]. \tag{C.46}$$

When this expression for f_1 is substituted into (C.40), we find the dispersion relation of electrostatic wave in more general inhomogenous plasma as follows:

$$\left(k_x^2 + k_z^2 - \frac{\partial^2}{\partial y^2}\right)\phi_1 = \phi_1 \sum_j \frac{q_j^2}{\epsilon_0 m_j}\int\int\int\left[2\frac{\partial f_0}{\partial \alpha}\right.$$
$$- \left(2(\omega - k_z v_z)\frac{\partial f_0}{\partial \alpha} + 2k_z(v_z - V)\frac{\partial f_0}{\partial \beta} + \frac{k_x}{\Omega}\frac{\partial f_0}{\partial \gamma}\right)$$
$$\left.\times \sum_{{\rm n}=-\infty}^{\infty} \frac{J_{\rm n}^2 + J_{\rm n}J_{\rm n-1}\exp i\theta + J_{\rm n}J_{\rm n+1}\exp(-i\theta)}{\omega - k_z v_z - {\rm n}\Omega} + \cdots\right]_j {\rm d}\theta {\rm d}v_\perp {\rm d}v_\perp {\rm d}v_z. \tag{C.47}$$

For $|(k_x^2 + k_z^2)\phi_1| \gg |\partial^2\phi_1/\partial y^2|$, (C.47) is reduced to

$$(k_x^2 + k_z^2) - \sum_j \mathit{\Pi}_j^2 \frac{1}{n_{0j}}\int\int\int[\quad]_j {\rm d}\theta {\rm d}v_\perp {\rm d}v_\perp {\rm d}v_z = 0.$$

By the same way as sec.C.3, this dispersion relation is reduced to

$$k_x^2 + k_z^2 + \sum_j \mathit{\Pi}_j^2\left[\frac{1}{v_{{\rm T}z}^2}\right.$$
$$+ \sum_{{\rm n}=-\infty}^{\infty} I_{\rm n}(b)e^{-b}\left(\left(\frac{1}{v_{{\rm T}z}^2} - \frac{1}{v_{{\rm T}\perp}^2}\frac{{\rm n}\Omega}{\omega_{\rm n}}\right)\zeta_{\rm n}Z(\zeta_{\rm n}) - \frac{1}{v_{{\rm T}\perp}^2}\frac{\rm n}{k_x}\left[(\epsilon + \delta_\perp - f_{\rm n}(b)\delta_\perp)\left(1 + \frac{{\rm n}\Omega}{\omega_{\rm n}}\zeta_{\rm n}Z(\zeta_{\rm n})\right)\right.\right.$$
$$\left.\left. - \frac{\delta_z}{2}\left(1 + \frac{{\rm n}\Omega\omega_{\rm n}}{k_z^2 v_{{\rm T}z}^2}(1 + \zeta_{\rm n}Z(\zeta_{\rm n}))\right)\right]\right.$$
$$+ \frac{1}{v_{{\rm T}z}^2}\frac{\rm n}{k_x}\left[(\epsilon + \delta_z - f_{\rm n}(b)\delta_\perp)(1 + \zeta_{\rm n}Z(\zeta_{\rm n})) - \frac{\delta_z}{2}\left(1 + \frac{\omega_{\rm n}^2}{k_z^2 v_{{\rm T}z}^2}(1 + \zeta_{\rm n}Z(\zeta_{\rm n}))\right)\right]$$
$$\left.\left. + \frac{k_x}{\Omega}\left[(\epsilon - f_{\rm n}(b)\delta_\perp)\frac{\zeta_n}{\omega_{\rm n}}Z(\zeta_{\rm n}) - \frac{\delta_z}{2}\frac{\omega_{\rm n}}{k_z^2 v_{{\rm T}z}^2}(1 + \zeta_{\rm n}Z(\zeta_{\rm n}))\right]\right)\right]_j = 0. \tag{C.48}$$

Here we set $y = 0$ and used the following relations:

$$\omega_{\rm n} = \omega - k_z V + {\rm n}\Omega,$$

$$\int_{-\infty}^{\infty} J_{\rm n}^2(b^{1/2}x)\exp\left(-\frac{x^2}{2}\right)\cdot\frac{x^2}{2}x{\rm d}x = f_{\rm n}(b)I_{\rm n}(b)e^{-b},$$

$$f_{\rm n}(b) \equiv (1 - b) + bI_{\rm n}'(b)/I_{\rm n}(b).$$

When $\epsilon = \delta_\perp = \delta_z = 0$, this dispersion relation becomes (C.39).

In the case of low frequency $\omega \ll |\Omega|$, we have $\zeta_n \gg 1$ $(n \neq 0)$, $\zeta_n Z(\zeta_n) \to -1$ $(n \neq 0)$ and $1 + \zeta_n Z(\zeta_n) \to -(1/2)\zeta_n^{-2}$ $(n \neq 0)$. Then (C.48) reduces to

$$k_x^2 + k_z^2 + \sum_j \mathit{\Pi}_j^2\left(\frac{1}{v_{{\rm T}z}^2} + I_0(b)e^{-b}\left(\frac{1}{v_{{\rm T}z}^2}(1 + \zeta_0 Z(\zeta_0)) - \frac{1}{v_{{\rm T}\perp}^2}\right.\right.$$

$$+\frac{k_x}{\Omega\omega_0}(\epsilon - f_0(b)\delta_\perp)\zeta_0 Z(\zeta_0) - \frac{k_x}{\Omega\omega_0}\delta_z\zeta_0^2(1+\zeta_0 Z(\zeta_0))\Bigg)\Bigg)_j = 0. \tag{C.49}$$

The relation

$$\sum_{-\infty}^{\infty} I_n(b)e^{-b} = 1$$

was used. When $v_{\mathrm{T}\perp} = v_{\mathrm{T}z} = v_{\mathrm{T}}$, $\delta_\perp = \delta_z = 0$, $V = 0$, we have familiar dispersion relation of drift wave due to the density gradient as follows,

$$k_x^2 + k_z^2 + \sum_j \Pi_j^2 \left(\frac{1}{v_{\mathrm{T}}^2} + I_0(b)e^{-b}\left(\frac{1}{v_{\mathrm{T}}^2}\zeta_0 Z(\zeta_0) + \frac{k_x}{\Omega\omega_0}\epsilon\zeta_0 Z(\zeta_0)\right)\right)_j = 0. \tag{C.50}$$

We can usually assume $b_{\mathrm{e}} = 0$ for electrons. (C.50) reduces to

$$0 = (k_x^2 + k_z^2)\frac{v_{\mathrm{Te}}^2}{\Pi_{\mathrm{e}}^2} + 1 + \zeta_{\mathrm{e}} Z(\zeta_{\mathrm{e}})\left(1 - \frac{\omega_{\mathrm{e}}^*}{\omega}\right) + \frac{ZT_{\mathrm{e}}}{T_{\mathrm{i}}}\left(1 + I_0(b)e^{-b}\zeta_0 Z(\zeta_0)\left(1 - \frac{\omega_{\mathrm{i}}^*}{\omega}\right)\right), \tag{C.51}$$

where

$$\omega_{\mathrm{e}}^* = \frac{-k_x\epsilon v_{\mathrm{Te}}^2}{\Omega_{\mathrm{e}}} = \frac{-k_x\epsilon T_{\mathrm{e}}}{eB}$$

$$\omega_{\mathrm{i}}^* = \frac{-k_x\epsilon v_{\mathrm{Ti}}^2}{\Omega_{\mathrm{i}}} = \frac{k_x\epsilon T_{\mathrm{i}}}{ZeB}.$$

Note that the x direction is opposite to the electron drift velocity $\boldsymbol{v}_{\mathrm{de}}$, y is the direction of negative density gradient and z is the direction of the magnetic field.

References

[1] . H. Stix: *The Theory of Plasma Waves*, McGraw-Hill, New York 1962.
T. H. Stix: *Waves in Plasmas*, American Institute of Physics, New York, 1992.

[2] K. Miyamoto: *Plasma Physics for Nuclear Fusion*, The MIT Press, Cambridge, Mass. (1980).

[3] B. D. Fried and S. D. Conte: *The Plasma Dispersion Function*, Academic Press, New York (1961).

App.D Quasi-Symmetric Stellarators

D.1 Magnetic Coordinates (Boozer Coordinates) and Natural Coordinates (Hamada Coordinates)

A suitable choice of the coordinates system is very important to analyze particle orbits and MHD stabilities, especially in non-axisymmetric toroidal sytems. The natural (Hamada) coordinates (ref.[1]) and magnetic (Boozer) coordinates (ref.[2]) are often used on particle orbits analysis and MHD stabilities study. In this subsection, the relation between them is described according to (ref.[3]). The equiliblium equations are as follows:

$$\nabla p = \boldsymbol{j} \times \boldsymbol{B}, \tag{D.1}$$

$$\mu_0 \boldsymbol{j} = \nabla \times \boldsymbol{B}, \tag{D.2}$$

$$\nabla \cdot \boldsymbol{B} = 0, \tag{D.3}$$

$$\nabla \cdot \boldsymbol{j} = 0, \tag{D.4}$$

$$\boldsymbol{B} \cdot \nabla p = 0, \tag{D.5}$$

$$\boldsymbol{j} \cdot \nabla p = 0. \tag{D.6}$$

We assume that the toroidal MHD equilibrium given by (D.1)$\sim$(D.6) has nested magnetic flux surface having a single magnetic axis, each of which is specified by ρ.

$$p = p(\rho). \tag{D.7}$$

From (D.3), (D.5), and (D.7), we have

$$\boldsymbol{B} = \nabla\rho \times \nabla v. \tag{D.8}$$

The vector potential $\boldsymbol{A}$ is given by

$$\boldsymbol{A} = \rho \nabla v.$$

From (D.4), (D.6), and (D.7), we have

$$\mu_0 \boldsymbol{j} = \nabla w \times \nabla \rho. \tag{D.9}$$

Since there is the relation of

$$\nabla \times (\boldsymbol{B} - w\nabla\rho) = 0$$

due to (D.2) and (D.9), we have

$$\boldsymbol{B} = \nabla u + w\nabla\rho. \tag{D.10}$$

Equations (D.1), (D.7), (D.8), and (D.9) reduce to

$$\mu_0 \frac{\mathrm{d}p}{\mathrm{d}\rho} \nabla\rho = \mu_0 \nabla p = (\nabla w \times \nabla\rho) \times (\nabla\rho \times \nabla v)$$

$$= [(\nabla w \times \nabla\rho) \cdot \nabla v]\nabla\rho = (\boldsymbol{B} \cdot \nabla w)\nabla\rho = \mu_0(\boldsymbol{j} \cdot \nabla v)\nabla\rho;$$

that is,

$$\mu_0 \frac{\mathrm{d}p}{\mathrm{d}\rho} = \boldsymbol{B} \cdot \nabla w = \mu_0 \boldsymbol{j} \cdot \nabla v. \tag{D.11}$$

Equations (D.8),(D.10) and (D.9),(D.10) reduce to

$$\boldsymbol{B} \cdot \boldsymbol{B} = \boldsymbol{B} \cdot \nabla u, \tag{D.12}$$

$$\boldsymbol{j}\cdot\boldsymbol{B}=\boldsymbol{j}\cdot\nabla u. \tag{D.13}$$

Let θ and ζ be the poloidal and toroidal angle variables in cordinates system ρ,θ,ζ, respectively, and they have a period of 2π. The functions $u,\ v,\ w$ must give single-valued $\boldsymbol{B}$ and $\boldsymbol{j}$ for the angle variables θ and ζ. Therefore, we can put them as follows:

$$v=\frac{\mathrm{d}\psi_\mathrm{t}}{\mathrm{d}\rho}\theta-\frac{\mathrm{d}\psi_\mathrm{p}}{\mathrm{d}\rho}\zeta+\tilde{v}(\rho,\theta,\zeta), \tag{D.14}$$

$$w=-\mu_0\frac{\mathrm{d}I_\mathrm{t}}{\mathrm{d}\rho}\theta-\mu_0\frac{\mathrm{d}I_\mathrm{p}}{\mathrm{d}\rho}\zeta+\tilde{w}(\rho,\theta,\zeta), \tag{D.15}$$

$$u=\mu_0 I_\mathrm{t}\theta+\mu_0 I_\mathrm{p}\zeta+\tilde{u}(\rho,\theta,\zeta). \tag{D.16}$$

$2\pi\psi_\mathrm{t}$ and $2\pi\psi_\mathrm{p}$ are toroidal and poloidal flux inside a flux surface ρ and $2\pi I_\mathrm{t}$ is toroidal current inside a flux surface ρ and $2\pi I_\mathrm{p}$ is poloidal current outside a flux surface ρ.

Equations (D.11) and (D.15) reduce to

$$\boldsymbol{B}\cdot\nabla\tilde{w}=\mu_0\frac{\mathrm{d}p}{\mathrm{d}\rho}+\mu_0\frac{\mathrm{d}I_\mathrm{t}}{\mathrm{d}\rho}\boldsymbol{B}\cdot\nabla\theta+\mu_0\frac{\mathrm{d}I_\mathrm{p}}{\mathrm{d}\rho}\boldsymbol{B}\cdot\nabla\zeta, \tag{D.17}$$

and Equations (D.12) and (D.13) reduce to

$$\boldsymbol{B}\cdot\nabla\tilde{u}=|\boldsymbol{B}|^2-\mu_0 I_\mathrm{t}\boldsymbol{B}\cdot\nabla\theta-\mu_0 I_\mathrm{p}\boldsymbol{B}\cdot\nabla\zeta. \tag{D.18}$$

These equations are magnetic differential equations. Solvability condtion of

$$\boldsymbol{B}\cdot\nabla F=S,\qquad \boldsymbol{b}\cdot\nabla F=\frac{S}{B}, \tag{D.19}$$

are

$$\oint S\frac{\mathrm{d}l}{B}=0, \tag{D.20}$$

for a closed field line and

$$\int S\mathrm{d}V=0 \tag{D.21}$$

for the integral region inside a magnetic surface $\rho=$const. (D.17) and (D.21) reduce to

$$\frac{\mathrm{d}p}{\mathrm{d}V}=-(2\pi)^2\left(\frac{\mathrm{d}I_\mathrm{p}}{\mathrm{d}V}\frac{\mathrm{d}\psi_\mathrm{t}}{\mathrm{d}V}+\frac{\mathrm{d}I_\mathrm{t}}{\mathrm{d}V}\frac{\mathrm{d}\psi_\mathrm{p}}{\mathrm{d}V}\right). \tag{D.22}$$

In the reduction process of (D.22), we used the following relation:

$$\boldsymbol{B}\cdot\nabla\theta=(\nabla\theta\times\nabla\rho)\cdot\nabla v=(\nabla\theta\times\nabla\rho)\cdot\nabla\zeta\frac{\partial v}{\partial\zeta}=g^{-1/2}\left(\frac{\mathrm{d}\psi_\mathrm{p}}{\mathrm{d}\rho}-\frac{\partial\tilde{v}}{\partial\zeta}\right).$$

As is shown in ch.8, (8.18) yield

$$\frac{1}{N}\oint\frac{\mathrm{d}l}{B}=\frac{1}{2\pi}\frac{\mathrm{d}V}{\mathrm{d}\psi_\mathrm{t}}. \tag{D.23).}$$

Equations (D.18) and (D.21) reduce to

$$\langle|\boldsymbol{B}|^2\rangle=(2\pi)^2\frac{\mathrm{d}\psi_\mathrm{t}}{\mathrm{d}V}(I_\mathrm{p}+q^{-1}I_\mathrm{t}), \tag{D.24}$$

where $q(\psi_\mathrm{t})$ is safety factor $q\equiv\mathrm{d}\psi_\mathrm{t}/\mathrm{d}\psi_\mathrm{p}$ and $\langle A\rangle$ is volume average of A. (D.18) reduces to

$$\frac{1}{N}\oint\boldsymbol{B}\cdot\mathrm{d}\boldsymbol{l}=2\pi\mu_0(I_\mathrm{p}+q^{-1}I_\mathrm{t}). \tag{D.25}$$

Equation (D.8) indicates that a magnetic field line is determined as the intersection of a flux surface $\rho = \text{const.}$ with a surface $v = \text{const.}$ Then as is clear from (D.14) in a coordinates system where $\tilde{v} = 0$, magnetic field lines are expressed as straight lines. An adequate coordinates transformation with respect to periodic coordinates makes two of $\tilde{u}, \tilde{v},$ and $\tilde{w}$ to zero.

Natural (Hamada) Coordinates System is the system with $\tilde{u} = 0,\ \tilde{w} = 0$. Both magnetic field line and current line are straight in Hamada coordinates and we have

$$v = \frac{\mathrm{d}\psi_\mathrm{t}}{\mathrm{d}\rho}\theta_\mathrm{H} - \frac{\mathrm{d}\psi_\mathrm{p}}{\mathrm{d}\rho}\zeta_\mathrm{H}, \tag{D.26}$$

$$w = -\mu_0\frac{\mathrm{d}I_\mathrm{t}}{\mathrm{d}\rho}\theta_\mathrm{H} - \mu_0\frac{\mathrm{d}I_\mathrm{p}}{\mathrm{d}\rho}\zeta_\mathrm{H}, \tag{D.27}$$

$$u = \mu_0 I_\mathrm{t}\theta_\mathrm{H} + \mu_0 I_\mathrm{p}\zeta_\mathrm{H} + \tilde{u}_\mathrm{H}. \tag{D.28}$$

The magnetic field is expressed by

$$\boldsymbol{B} = \frac{\mathrm{d}\psi_\mathrm{t}}{\mathrm{d}\rho}\nabla\rho\times\nabla\theta_\mathrm{H} - \frac{\mathrm{d}\psi_\mathrm{p}}{\mathrm{d}\rho}\nabla\rho\times\nabla\zeta_\mathrm{H}, \tag{D.29}$$

$$\boldsymbol{B} = \mu_0 I_\mathrm{t}\nabla\theta_\mathrm{H} + \mu_0 I_\mathrm{p}\nabla\zeta + \nabla\tilde{u}_\mathrm{H}. \tag{D.30}$$

The current density is expressed by

$$\boldsymbol{j} = \mu_0\frac{\mathrm{d}I_\mathrm{t}}{\mathrm{d}\rho}\nabla\rho\times\nabla\theta_\mathrm{H} + \mu_0\frac{\mathrm{d}I_\mathrm{p}}{\mathrm{d}\rho}\nabla\rho\times\nabla\zeta_\mathrm{H}. \tag{D.31}$$

The Jacobian $g^{1/2}$ ($\mathrm{d}x\mathrm{d}y\mathrm{d}z = g^{1/2}\mathrm{d}\rho\mathrm{d}\theta\mathrm{d}\zeta$) is given by the substitution of (D.26) and (D.31) into (D.11) with use of (D.22) (refer to Table D.1)

$$g_\mathrm{H}^{1/2} = [\nabla\rho\cdot(\nabla\theta\times\nabla\zeta)]^{-1} = \frac{1}{(2\pi)^2}\frac{\mathrm{d}V}{\mathrm{d}\rho}. \tag{D.32}$$

Magnetic (Boozer) Coordinates System is the system with $\tilde{u} = 0,\ \tilde{v} = 0$. The magnetic field line is straight in Boozer coordinates and we have

$$v = \frac{\mathrm{d}\psi_\mathrm{t}}{\mathrm{d}\rho}\theta_\mathrm{B} - \frac{\mathrm{d}\psi_\mathrm{p}}{\mathrm{d}\rho}\zeta_\mathrm{B}, \tag{D.33}$$

$$w = -\mu_0\frac{\mathrm{d}I_\mathrm{t}}{\mathrm{d}\rho}\theta_\mathrm{B} - \mu_0\frac{\mathrm{d}I_\mathrm{p}}{\mathrm{d}\rho}\zeta_\mathrm{B} + \tilde{w}_\mathrm{B}, \tag{D.34}$$

$$u = \mu_0 I_\mathrm{t}\theta_\mathrm{B} + \mu_0 I_\mathrm{p}\zeta_\mathrm{B}. \tag{D.35}$$

The magnetic field is expressed by

$$\boldsymbol{B} = \frac{\mathrm{d}\psi_\mathrm{t}}{\mathrm{d}\rho}\nabla\rho\times\nabla\theta_\mathrm{B} - \frac{\mathrm{d}\psi_\mathrm{p}}{\mathrm{d}\rho}\nabla\rho\times\nabla\zeta_\mathrm{B}, \tag{D.36}$$

$$\boldsymbol{B} = \mu_0 I_\mathrm{t}\nabla\theta_\mathrm{B} + \mu_0 I_\mathrm{p}\nabla\zeta + \tilde{w}_\mathrm{B}\nabla\rho. \tag{D.37}$$

The current density is expressed by

$$\mu_0\boldsymbol{j} = \mu_0\frac{\mathrm{d}I_\mathrm{t}}{\mathrm{d}\rho}\nabla\rho\times\nabla\theta_\mathrm{B} + \mu_0\frac{\mathrm{d}I_\mathrm{p}}{\mathrm{d}\rho}\nabla\rho\times\nabla\zeta_\mathrm{B} + \nabla\tilde{w}_\mathrm{B}\times\nabla\rho. \tag{D.38}$$

Jacobian is given by substitution of (D.35) and (D.36) into (D.12) with use of (D.24) as follows:

$$g_\mathrm{B}^{1/2} = \mu_0\frac{I_\mathrm{p} + q^{-1}I_\mathrm{t}}{|B|^2}\frac{\mathrm{d}\psi_\mathrm{t}}{\mathrm{d}\rho}. \tag{D.39}$$

Table D.1 Vector calculus in general coordinates.

$$\boldsymbol{a}_j \equiv \frac{\partial \boldsymbol{r}}{\partial u^j}, \qquad \boldsymbol{a}^i \equiv \nabla u^i, \qquad V \equiv \boldsymbol{a}_1 \cdot (\boldsymbol{a}_2 \times \boldsymbol{a}_3), \tag{1}$$

$$\mathrm{d}\boldsymbol{r} = \textstyle\sum_j \frac{\partial \boldsymbol{r}}{\partial u^j}\mathrm{d}u^j, \qquad \boldsymbol{a}^i \cdot \boldsymbol{a}_j = \delta^i_j, \tag{2}$$

$$\boldsymbol{a}^1 = V^{-1}(\boldsymbol{a}_2 \times \boldsymbol{a}_3), \quad \boldsymbol{a}^2 = V^{-1}(\boldsymbol{a}_3 \times \boldsymbol{a}_1), \quad \boldsymbol{a}^3 = V^{-1}(\boldsymbol{a}_1 \times \boldsymbol{a}_2), \tag{3}$$

$$\boldsymbol{a}_1 = V(\boldsymbol{a}^2 \times \boldsymbol{a}^3), \quad \boldsymbol{a}_2 = V(\boldsymbol{a}^3 \times \boldsymbol{a}^1), \quad \boldsymbol{a}_3 = V(\boldsymbol{a}^1 \times \boldsymbol{a}^2), \tag{4}$$

$$\boldsymbol{a}^1 \cdot (\boldsymbol{a}^2 \times \boldsymbol{a}^3) = V^{-1}, \tag{5}$$

$$g_{i\,j} \equiv \boldsymbol{a}_i \cdot \boldsymbol{a}_j = g_{j\,i}, \qquad g^{i\,j} \equiv \boldsymbol{a}^i \cdot \boldsymbol{a}^j = g^{j\,i}, \tag{6}$$

$$\boldsymbol{F} = \textstyle\sum_i f^i \boldsymbol{a}_i, \qquad f^i \equiv \boldsymbol{F} \cdot \boldsymbol{a}^i \quad \text{(contravariant)}, \tag{7}$$

$$\boldsymbol{F} = \textstyle\sum_i f_i \boldsymbol{a}^i, \qquad f_i \equiv \boldsymbol{F} \cdot \boldsymbol{a}_i \quad \text{(covariant)}, \tag{8}$$

$$f_j = \textstyle\sum_i g_{j\,i} f^i, \qquad f^i = \sum_j g^{i\,j} f_j, \tag{9}$$

$$g \equiv |g_{i\,j}| = V^2, \quad \mathrm{d}x\mathrm{d}y\mathrm{d}z = g^{1/2}\mathrm{d}u^1\mathrm{d}u^2\mathrm{d}u^3, \quad g^{1/2} = [\nabla u^1 \cdot (\nabla u^2 \times \nabla u^3)]^{-1}, \tag{10}$$

$$(\mathrm{d}s)^2 = (\mathrm{d}\boldsymbol{r})^2 = \textstyle\sum_{i\,j} g_{i\,j}\mathrm{d}u^i\mathrm{d}u^j = \sum_{i\,j} g^{i\,j}\mathrm{d}u_i\mathrm{d}u_j, \tag{11}$$

$$(\boldsymbol{a} \times \boldsymbol{b})^1 = g^{-1/2}(a_2 b_3 - a_3 b_2), \qquad (\boldsymbol{a} \times \boldsymbol{b})_1 = g^{1/2}(a^2 b^3 - a^3 b^2), \tag{12}$$

$$\nabla\phi = \textstyle\sum_i \frac{\partial \phi}{\partial u^i}\boldsymbol{a}^i, \qquad \nabla \cdot \boldsymbol{F} = \frac{1}{g^{1/2}} \sum_i \frac{\partial}{\partial u^i}(g^{1/2} f^i), \tag{13}$$

$$\nabla \times \boldsymbol{F} = \frac{1}{g^{1/2}}\left(\left(\frac{\partial f_3}{\partial u^2} - \frac{\partial f_2}{\partial u^3}\right)\boldsymbol{a}_1 + \left(\frac{\partial f_1}{\partial u^3} - \frac{\partial f_3}{\partial u^1}\right)\boldsymbol{a}_2 + \left(\frac{\partial f_2}{\partial u^1} - \frac{\partial f_1}{\partial u^2}\right)\boldsymbol{a}_3\right), \tag{14}$$

$$\nabla^2\phi = \nabla \cdot (\nabla\phi) = \frac{1}{g^{1/2}} \sum_{i\,j} \frac{\partial}{\partial u^i}\left(g^{1/2} g^{i\,j} \frac{\partial \phi}{\partial u^j}\right), \tag{15}$$

D.2 Boozer Equation of Drift Motion

The velocity of drift motion of guiding center was given in (3.47) as follows:

$$\boldsymbol{v} = \frac{v_\parallel}{B}\frac{1}{1+\rho_\parallel \boldsymbol{b}\cdot\nabla\times\boldsymbol{b}}(\boldsymbol{B}+\nabla\times(\rho_\parallel\boldsymbol{B})), \tag{D.40}$$

where

$$\rho_\parallel = \frac{mv_\parallel}{eB}. \tag{D.41}$$

The magnetic field in Boozer coordinates (ρ,θ,ζ) is given by (D.36) and (D.37) as follows ($v \leftrightarrow \theta_0,\ u \leftrightarrow \chi$):

$$\boldsymbol{B} = \nabla\psi\times\nabla\theta_0, \qquad \theta_0 = \theta - q^{-1}\zeta, \qquad q^{-1} = \frac{\mathrm{d}\psi_\mathrm{p}}{\mathrm{d}\psi}, \tag{D.42}$$

$$\boldsymbol{B} = \nabla\chi + \beta\nabla\psi, \quad \psi\equiv\psi_\mathrm{t}, \quad \chi = \mu_0 I_\mathrm{t}\theta + \mu_0 I_\mathrm{p}\zeta, \quad \beta \equiv \mu_0 I_\mathrm{t}'\theta + \mu_0 I_\mathrm{p}' + \tilde{w}. \tag{D.58}$$

The term $\boldsymbol{b}\cdot\nabla\times\boldsymbol{b}$ in (D.40) is expressed by

$$\boldsymbol{b}\cdot\nabla\times\boldsymbol{b} = \frac{1}{B^2}\boldsymbol{B}\cdot\nabla\times\boldsymbol{B} = \frac{1}{B^2}\nabla\chi\cdot(\nabla\beta\times\nabla\psi) = \frac{1}{B^2}(\nabla\psi\times\nabla\chi)\cdot\nabla\beta.$$

(D.42), (D.43) reduce to $(\nabla\psi\times\nabla\theta_0)\cdot\nabla\chi = B^2$. The substitution of $u^1=\psi$, $u^2=\theta_0$, and $u^3=\chi$ into Equations (1), (4), and (5) in Table D.1 reduces $(\nabla\psi\times\nabla\chi) = -B^2(\mathrm{d}\boldsymbol{r}/\mathrm{d}\theta_0)$. Therefore, we obtain

$$\begin{aligned}\nabla\times(\rho_\parallel\boldsymbol{B})\cdot\nabla\chi &= \rho_\parallel(\nabla\beta\times\nabla\psi)\cdot\nabla\chi + (\nabla\rho_\parallel\times\boldsymbol{B})\cdot\nabla\chi \\ &= \rho_\parallel(\nabla\psi\times\nabla\chi)\cdot\nabla\beta + \beta(\nabla\psi\times\nabla\chi)\cdot\nabla\rho_\parallel = -B^2\rho_\parallel\frac{\partial\beta}{\partial\theta_0} - B^2\beta\frac{\partial\rho_\parallel}{\partial\theta_0}.\end{aligned}$$

and

$$\begin{aligned}\dot{\chi} = \boldsymbol{v}\cdot\nabla\chi &= \frac{v_\parallel}{B}\left(\frac{1}{1-\rho_\parallel(\partial\beta/\partial\theta_0)}\right)(\boldsymbol{B}+\nabla\times(\rho_\parallel\boldsymbol{B}))\cdot\nabla\chi \\ &= v_\parallel B\left(1-\frac{\beta(\partial\rho_\parallel/\partial\theta_0)}{1-\beta(\partial\rho_\parallel/\partial\theta_0)}\right).\end{aligned} \tag{D.44}$$

$(\partial\rho_\parallel/\partial\theta_0)$ means differentiation by θ_0 while keeping ψ, χ, and Hamiltonian H_0 constant. Hamiltonian is

$$H_0 \equiv \frac{e}{2m}B^2\rho_\parallel^2 + \frac{\mu}{e}B + \Phi, \tag{D.45}$$

where $B = B(\psi,\theta_0,\chi)$ and $\Phi = \Phi(\psi,\theta_0,\chi)$ and $\rho_\parallel = (m/e)(v_\parallel/B)$. We define

$$\theta_{0\mathrm{c}} \equiv \theta_0 - \beta(\psi,\theta_0,\chi)\rho_\parallel. \tag{D.46}$$

There are the following relations:

$$\left.\frac{\partial\theta_0}{\partial\rho_\parallel}\right|_{\theta 0\mathrm{c}} = \beta + \rho_\parallel\frac{\partial\beta}{\partial\theta_0}\left.\frac{\partial\theta_0}{\partial\rho_\parallel}\right|_{\theta 0\mathrm{c}}, \qquad \left.\frac{\partial\theta_0}{\partial\rho_\parallel}\right|_{\theta 0\mathrm{c}} = \frac{\beta}{1-\rho_\parallel(\partial\beta/\partial\theta_0)},$$

$$-\frac{e}{m}B^2\rho_\parallel\left.\frac{\partial\rho_\parallel}{\partial\theta_0}\right|_{H0} = \frac{e}{m}\rho_\parallel^2\frac{\partial B^2}{\partial\theta_0} + \frac{\mu}{e}\frac{\partial B}{\partial\theta_0} + \frac{\partial\Phi}{\partial\theta_0},$$

$$\left.\frac{\partial\theta_0}{\partial\chi}\right|_{\theta 0\mathrm{c}} = \frac{\rho_\parallel\partial\beta/\partial\chi}{1-\rho_\parallel(\partial\beta/\partial\theta_0)}, \qquad \frac{\partial\theta_0}{\partial\theta_{0c}} = \frac{1}{1-\rho_\parallel(\partial\beta/\partial\theta_0)},$$

$$\left.\frac{\partial\theta_0}{\partial\psi}\right|_{\theta 0\mathrm{c}} = \frac{\rho_\parallel\partial\beta/\partial\psi}{1-\rho_\parallel(\partial\beta/\partial\theta_0)}.$$

Let us change the independent variable θ_0 to $\theta_{0c} = \theta_0 - \beta\rho_\parallel$ and $H(\rho_\parallel, \psi, \theta_{0c}, \chi) \equiv H_0(\rho_\parallel, \psi, \theta_{0c} + \beta\rho_\parallel, \chi)$, that is,

$$H(\rho_\parallel, \psi, \theta_{0c}, \chi) = \frac{1}{2}\frac{e}{m}B^2\rho_\parallel^2 + \frac{\mu}{e}B + \Phi, \tag{D.47}$$

$$B = B(\psi, \theta_{0c} + \beta\rho_\parallel, \chi), \qquad \Phi = \Phi(\psi, \theta_{0c} + \beta\rho_\parallel, \chi).$$

Then we have

$$\left.\frac{\partial H}{\partial \rho_\parallel}\right|_{\theta 0c,\psi,\chi} = \frac{\partial H_0}{\partial \rho_\parallel} + \frac{\partial H_0}{\partial \theta_0}\left.\frac{\partial \theta_0}{\partial \rho_\parallel}\right|_{\theta 0c} = \frac{e}{m}B^2\rho_\parallel + \left.\frac{\partial H_0}{\partial \theta_0}\frac{\partial \theta_0}{\partial \rho_\parallel}\right|_{\theta 0c}$$

$$= \frac{e}{m}B^2\rho_\parallel + \left(\frac{e}{2m}\rho_\parallel^2\frac{\partial B^2}{\partial \theta_0} + \frac{\mu}{e}\frac{\partial B}{\partial \theta_0} + \frac{\partial \Phi}{\partial \theta_0}\right) \times \left(\frac{\beta}{1 - \rho_\parallel(\partial\beta/\partial\theta_0)}\right)$$

$$= v_\parallel B - \left(\frac{\partial \rho_\parallel}{\partial \theta_0}v_\parallel B\right)\frac{\beta}{1 - \rho_\parallel(\partial\beta/\partial\theta_0)} = v_\parallel B\left(1 - \frac{\beta(\partial\rho_\parallel/\theta_0)}{1 - \rho_\parallel(\partial\beta/\partial\theta_0)}\right).$$

Finally we reduce desirous result $\dot{\chi} = \partial H/\partial\rho_\parallel|_{\theta 0\,c}$. Then the equation of drift motion is expressed in Hamilton's canonical form similar to $\dot{\chi}$ (ref.[4])

$$\dot{\chi} = \frac{\partial H}{\partial \rho_\parallel}, \qquad \dot{\rho}_\parallel = -\frac{\partial H}{\partial \chi}, \tag{D.48}$$

$$\dot{\theta}_{0c} = \frac{\partial H}{\partial \psi}, \qquad \dot{\psi} = -\frac{\partial H}{\partial \theta_{0c}}. \tag{D.49}$$

The canonical transformation to new coordinates

$$(\theta_{0c}, \chi, \psi, \rho_\parallel) \to (\theta_c, \zeta, P_\theta, P_\zeta)$$

is given by the following generating function:

$$F(\psi, \rho_\parallel, \theta_c, \zeta) = \mu_0\rho_\parallel(g(\psi)\zeta + I(\psi)\theta_c) + \psi\theta_c - \zeta\psi/q, \tag{D.50}$$

that is,

$$\theta_{0c} = \frac{\partial F}{\partial \psi} = \left(\theta_c - \frac{\zeta}{q}\right) + \mu_0\rho_\parallel(\zeta g' + \theta_c I'), \tag{D.51}$$

$$\chi = \frac{\partial F}{\partial \rho_\parallel} = \mu_0(g\zeta + I\theta_c), \tag{D.52}$$

$$P_\theta = \frac{\partial F}{\partial \theta_c} = \mu_0\rho_\parallel I + \psi, \tag{D.53}$$

$$P_\zeta = \frac{\partial F}{\partial \zeta} = \mu_0\rho_\parallel g + \psi/q. \tag{D.54}$$

New Hamilton is (ref.[5])

$$H(\theta_c, \zeta, P_\theta, P_\zeta) = \frac{1}{2}\frac{e}{m}B^2\rho_\parallel^2(P_\theta, P_\zeta, \psi) + \frac{\mu}{e}B + \Phi, \tag{D.55}$$

where

$$\rho_\parallel = \frac{P_\theta/q - P_\zeta}{\mu_0(I/q - g)}, \qquad \psi = \frac{P_\theta g - P_\zeta I}{I/q - g}, \tag{D.56}$$

$$\theta_0 = \theta_c - \zeta/q + \rho_\parallel\delta, \qquad \delta = \mu_0(\zeta g' + \theta I') + \beta. \tag{D.57}$$

$$(B,\ \Phi) = (B,\ \Phi)(\psi, \theta_0, \chi) = (B,\ \Phi)(\psi, \theta_c - \zeta/q + \delta\rho_\parallel, \chi). \tag{D.58}$$

Then Hamilton's equation in new coordinates is

$$\dot{\theta}_{\rm c} = \frac{\partial H}{\partial P_\theta}, \qquad \dot{P}_\theta = -\frac{\partial H}{\partial \theta_{\rm c}}, \tag{D.59}$$

$$\dot{\zeta} = \frac{\partial H}{\partial P_\zeta}, \qquad \dot{P}_\zeta = -\frac{\partial H}{\partial \zeta}. \tag{D.60}$$

The substitution of $\theta_{\rm c}$ by θ gives formally

$$H(\theta, \zeta, P_\theta, P_\zeta) = \frac{1}{2}\frac{e}{m}B^2\rho_\parallel^2(P_\theta, P_\zeta, \psi) + \frac{\mu}{e}B + \Phi \tag{D.61}$$

$$\dot{\theta} = \frac{\partial H}{\partial P_\theta}, \qquad \dot{P}_\theta = -\frac{\partial H}{\partial \theta}. \tag{D.62}$$

$$\dot{\zeta} = \frac{\partial H}{\partial P_\zeta}, \qquad \dot{P}_\zeta = -\frac{\partial H}{\partial \zeta}. \tag{D.63}$$

The distinction between the solutions of (D.59), (D.60) and (D.62), (D.63) is the order of gyroradius ($\theta = \theta_{\rm c} + \rho_\parallel \delta$). Therefore, the nonresonant difference between them is negligible (ref.[6]). In the currentless case ($\beta = \delta = 0$), they are identical.

References

[1] S. Hamada: Hydromagnetic Equilibria and Their Proper Coordinates. Nucl. Fusion **2**, 23 (1962).

[2] A. H. Boozer: Guiding Center Drift Equations. *Phys. Fluids* **23**, 904 (1980).

[3] N. Nakajima, J. Todoroki, and M. Okamoto: On Relation between Hamada and Boozer Magnetic Coordinates Systems. J. Plasma Fusion Res. **68**, 395 (1992).

[4] R. B. White, A. H. Boozer, and R. Hay: Drift Hamiltonian in Magnetic Coordinates. Phys. Fluids **25**, 575 (1982).

[5] R. B. White and M. S. Chance: Hamiltonian Guiding Center Drift Orbit Calculation for Plasmas of Arbitrary Cross Section. Phys. Fluids **27**, 2455 (1984).

[6] A. H. Boozer: Time-Dependent Drift Hamiltonian. Phys. Fluids **27**, 2441 (1984).

App.E Zonal Flow

E.1 Hasegawa-Mima Equation for Drift Turbulence

A model equation is the equation of continuity for ions, in which the parallel ion inertia is neglected. Ions are assumed to be cold:

$$\frac{\partial n}{\partial t} + \nabla \cdot (n\boldsymbol{v}_\perp) = \frac{\partial n}{\partial t} + (\boldsymbol{v}_\perp \cdot \nabla)n + n\nabla \cdot \boldsymbol{v}_\perp = 0. \tag{E.1}$$

The ion motion consists of $\boldsymbol{E} \times \boldsymbol{B}$ drift and polarization drift (refer to sec.3.9):

$$\boldsymbol{v}_\perp = -\frac{1}{B}\nabla\phi \times \hat{z} - \frac{1}{\Omega_\mathrm{i} B}\frac{\mathrm{d}}{\mathrm{d}t}\nabla\phi, \qquad \frac{\mathrm{d}}{\mathrm{d}t} = \frac{\partial}{\partial t} - \frac{1}{B}(\nabla\phi \times \hat{z}) \cdot \nabla. \tag{E.2}$$

A slow variation of the potential ϕ in the parallel direction along the magnetic field line allows the electrons to obey the Boltzmann distribution, that is,

$$n = n_0 + \delta n, \qquad \frac{\delta n}{n_0} = \frac{e\phi}{\kappa T_\mathrm{e}} \equiv \tilde{\phi}. \tag{E.3}$$

We assume the following ordering:

$$\frac{1}{\Omega_\mathrm{i}}\frac{\mathrm{d}}{\mathrm{d}t} \sim \delta, \quad \tilde{\phi} \sim \delta, \quad L_n\nabla \sim \delta^{-1}.$$

Denoting $c_\mathrm{s}^2 \equiv \kappa T_\mathrm{e}/m_\mathrm{i}$, $\rho_\mathrm{s} \equiv c_\mathrm{s}/\Omega_\mathrm{i}$ and $\Omega_\mathrm{i} = eB/m_\mathrm{i}$, (E.1), (E.2), and (E.3) reduce to

$$\boldsymbol{v}_\perp = -\rho_\mathrm{s}c_\mathrm{s}(\nabla\tilde{\phi} \times \hat{\boldsymbol{z}}) - \rho_\mathrm{s}^2\left(\frac{\partial}{\partial t} - \rho_\mathrm{s}c_\mathrm{s}(\nabla\tilde{\phi} \times \hat{z}) \cdot \nabla\right)\nabla\tilde{\phi}, \tag{E.4}$$

$$\begin{aligned}
&\frac{\partial\tilde{\phi}}{\partial t} - \rho_\mathrm{s}c_\mathrm{s}(\nabla\tilde{\phi} \times \hat{\boldsymbol{z}})\left(\nabla\tilde{\phi} + \frac{\nabla n_0}{n_0}\right) \\
&\quad +(1+\tilde{\phi})\nabla \cdot \left(-\rho_\mathrm{s}c_\mathrm{s}(\nabla\tilde{\phi} \times \hat{\boldsymbol{z}}) - \rho_\mathrm{s}^2\left(\frac{\partial}{\partial t} - \rho_\mathrm{s}c_\mathrm{s}(\nabla\tilde{\phi} \times \hat{z}) \cdot \nabla\right)\nabla\tilde{\phi}\right) = 0, \\
&\quad \frac{\partial\tilde{\phi}}{\partial t} - \rho_\mathrm{s}c_\mathrm{s}\left(\frac{\partial\tilde{\phi}}{\partial y}\frac{\mathrm{d}n_0}{\mathrm{d}x}\frac{1}{n_0}\right) - \rho_\mathrm{s}^2\frac{\partial\nabla^2\tilde{\phi}}{\partial t} + \rho_\mathrm{s}^3c_\mathrm{s}\nabla \cdot ((\nabla\tilde{\phi} \times \hat{z}) \cdot \nabla)\nabla\tilde{\phi} = 0, \\
&\qquad (1-\rho_\mathrm{s}^2\nabla^2)\frac{\partial\tilde{\phi}}{\partial t} + \rho_\mathrm{s}^3c_\mathrm{s}\left(\frac{\partial\nabla^2\tilde{\phi}}{\partial x}\frac{\partial\tilde{\phi}}{\partial y} - \frac{\partial\nabla^2\tilde{\phi}}{\partial y}\frac{\partial\tilde{\phi}}{\partial x}\right) + v_\mathrm{d}^*\frac{\partial\tilde{\phi}}{\partial y} = 0,
\end{aligned} \tag{E.5}$$

where v_d^* is the drift velocity of the electron and

$$v_\mathrm{d}^* = \frac{\kappa_n\kappa T_\mathrm{e}}{eB} = c_\mathrm{s}(\kappa_n\rho_\mathrm{s}).$$

(E.5) is called the *Hasegawa-Mima-Charney equation* (ref.[1]). Here we used the following relation:

$$((\nabla\tilde{\phi} \times \hat{z}) \cdot \nabla)\nabla^2\tilde{\phi} = \left(\frac{\partial\nabla^2\tilde{\phi}}{\partial x}\frac{\partial\tilde{\phi}}{\partial y} - \frac{\partial\nabla^2\tilde{\phi}}{\partial y}\frac{\partial\tilde{\phi}}{\partial x}\right).$$

When the density gradient is negligible, (E.5) becomes

$$(1-\rho_\mathrm{s}^2\nabla^2)\frac{\partial\tilde{\phi}}{\partial t} + \rho_\mathrm{s}^4\Omega_\mathrm{i}\left(\frac{\partial\nabla^2\tilde{\phi}}{\partial x}\frac{\partial\tilde{\phi}}{\partial y} - \frac{\partial\nabla^2\tilde{\phi}}{\partial y}\frac{\partial\tilde{\phi}}{\partial x}\right) = 0. \tag{E.6}$$

(E.6) is called the *Hasegawa-Mima equation* (ref.[2]).
A solution of (E.5) is

$$\tilde{\phi} = A \exp i(k_x x + k_y y) \exp(-i\omega_k^{\mathrm{l}} t), \qquad \omega_k^{\mathrm{l}} = \frac{1}{1+\rho_{\mathrm{s}}^2 k^2} k_y v_{\mathrm{d}}^*. \tag{E.7}$$

There are two constants of motion:

$$\frac{\partial}{\partial t}\int (\tilde{\phi}^2 + \rho_{\mathrm{s}}^2 (\nabla\tilde{\phi})^2) \mathrm{d}V = 0, \tag{E.8}$$

$$\frac{1}{2}\frac{\partial}{\partial t}\int \left((\nabla\tilde{\phi})^2 + \rho_{\mathrm{s}}^2 (\nabla^2\tilde{\phi})^2 \right) \mathrm{d}V - \int v_{\mathrm{d}}^* \nabla^2\tilde{\phi}\frac{\partial\tilde{\phi}}{\partial y}\mathrm{d}V = 0. \tag{E.9}$$

If (E.5) is multiplied by ϕ and integrated over the entire volume, the nonlinear equation becomes

$$\int \tilde{\phi}((\nabla\tilde{\phi}\times\hat{z})\cdot\nabla)\nabla^2\tilde{\phi}\mathrm{d}V = \int \tilde{\phi}\nabla\cdot((\nabla\tilde{\phi}\times\hat{z})\nabla^2\tilde{\phi})\mathrm{d}V = \int \nabla\cdot(\tilde{\phi}\nabla^2\tilde{\phi}(\nabla\tilde{\phi}\times\hat{z}))\mathrm{d}V$$

$$= \int \boldsymbol{J}_1\cdot\boldsymbol{n}\mathrm{d}S, \qquad\qquad \boldsymbol{J}_1 \equiv \tilde{\phi}\nabla^2\tilde{\phi}(\nabla\tilde{\phi}\times\hat{z}),$$

$$\frac{1}{2}\frac{\partial}{\partial t}\int (\tilde{\phi}^2 + \rho_{\mathrm{s}}^2(\nabla\tilde{\phi})^2)\mathrm{d}V = -\rho_{\mathrm{s}}^3 c_{\mathrm{s}} \int \boldsymbol{J}_1\cdot\boldsymbol{n}\mathrm{d}S - \frac{1}{2}\int v_{\mathrm{d}}^* \frac{\partial\tilde{\phi}^2}{\partial y}\mathrm{d}V \to 0.$$

Similarly, if we multiply (E.5) by $\nabla^2\tilde{\phi}$, we have

$$\int \left(\nabla^2\tilde{\phi}((\nabla\tilde{\phi}\times\hat{\boldsymbol{z}})\cdot)\nabla^2\tilde{\phi} + \nabla^2\tilde{\phi}\left(\frac{\partial\tilde{\phi}}{\partial t} - \rho_{\mathrm{s}}\nabla^2\frac{\partial\tilde{\phi}}{\partial t}\right) + v_{\mathrm{d}}^*\nabla^2\tilde{\phi}\frac{\partial\tilde{\phi}}{\partial y}\right)\mathrm{d}V = 0,$$

$$-\nabla\cdot\boldsymbol{J}_2 \equiv \nabla\cdot\left(\frac{\partial\tilde{\phi}}{\partial t}\nabla\tilde{\phi} + \frac{1}{2}(\nabla^2\tilde{\phi})^2(\nabla\tilde{\phi}\times\hat{\boldsymbol{z}})\right)$$

$$= \frac{1}{2}\frac{\partial}{\partial t}(\nabla\tilde{\phi})^2 + \frac{\partial\tilde{\phi}}{\partial t}\nabla^2\tilde{\phi} + \frac{1}{2}((\nabla\tilde{\phi}\times\hat{\boldsymbol{z}})\cdot\nabla)(\nabla^2\tilde{\phi})^2,$$

$$-\nabla\cdot\boldsymbol{J}_2 - \frac{1}{2}\frac{\partial}{\partial t}\left((\nabla\tilde{\phi})^2 + \rho_{\mathrm{s}}^2(\nabla^2\tilde{\phi})^2\right) + v_{\mathrm{d}}^*\nabla^2\tilde{\phi}\frac{\partial\tilde{\phi}}{\partial y} = 0,$$

$$\frac{1}{2}\frac{\partial}{\partial t}\int \left((\nabla\tilde{\phi})^2 + \rho_{\mathrm{s}}^2(\nabla^2\tilde{\phi})^2\right)\mathrm{d}V - \int v_{\mathrm{d}}^*\nabla^2\tilde{\phi}\frac{\partial\tilde{\phi}}{\partial y}\mathrm{d}V = -\nabla\cdot\boldsymbol{J}_2 \to 0.$$

When $\boldsymbol{E}\times\boldsymbol{B}$ drift velocity is denoted by $\boldsymbol{v}_E$, we have $v_E = c_{\mathrm{s}}\rho_{\mathrm{s}}|\nabla\tilde{\phi}|$ and $\nabla\times\boldsymbol{v}_E|_z = c_{\mathrm{s}}\rho_{\mathrm{s}}\nabla^2\tilde{\phi}$. Equations (E.8) and (E.9) reduce to

$$\int \left(\left(\frac{\delta n}{n_0}\right)^2 + \frac{m_{\mathrm{i}} v_E^2}{\kappa T_{\mathrm{e}}} \right)\mathrm{d}V = \text{const.}$$

$$\frac{1}{2}\frac{\partial}{\partial t}\int \left(\frac{1}{\rho_{\mathrm{s}}^2}\frac{v_E^2}{c_{\mathrm{s}}^2} + \frac{1}{c_{\mathrm{s}}^2}(\nabla\times v_E)^2 \right)\mathrm{d}V + \Omega_{\mathrm{i}}\frac{1}{c_{\mathrm{s}}^2}(\nabla\times v_E)_z\kappa_n v_{Ex}\mathrm{d}V = 0.$$

Let us normalize the coordinates (x, y) and time t as follows:

$$x = \rho_{\mathrm{s}}\hat{x}, \quad y = \rho_{\mathrm{s}}\hat{y}, \quad t = \Omega^{-1}\hat{t}, \quad \boldsymbol{k} = \rho_{\mathrm{s}}^{-1}\hat{\boldsymbol{k}}, \quad \omega = \Omega_{\mathrm{i}}\hat{\omega}.$$

Then (E.5) and (E.7) reduce to

$$\partial_{\hat{t}}(\hat{\nabla}^2\tilde{\phi} - \tilde{\phi}) - (\kappa_n\rho_{\mathrm{s}})\partial_{\hat{y}}\tilde{\phi} + (\partial_{\hat{y}}\hat{\nabla}^2\tilde{\phi})\partial_{\hat{x}}\tilde{\phi} - (\partial_{\hat{x}}\hat{\nabla}^2\tilde{\phi})\partial_{\hat{y}}\tilde{\phi} = 0, \tag{E.10}$$

$$\hat{\omega}_k^1 = \frac{(\kappa_n \rho_s)\hat{k}_{\hat{y}}}{1+\hat{k}^2}.$$

From now on the notation $\hat{}$ is omitted. When we expand $\tilde{\phi}(x,t)$ in a spatial Fourier series

$$\tilde{\phi}(\boldsymbol{\xi},t) = \sum \tilde{\phi}_k(t)\exp(i\boldsymbol{k}\cdot\boldsymbol{\xi}), \qquad \tilde{\phi}_k^* = \tilde{\phi}_{-k}, \tag{E.11}$$

where the asterisk means conjugate complex.

Let us consider three waves with wavenumbers $\boldsymbol{k}_1$, $\boldsymbol{k}_2$, and $\boldsymbol{k}_3$ such that $\boldsymbol{k}_1+\boldsymbol{k}_2+\boldsymbol{k}_3=0$. Let us suppose that these waves have amplitudes larger than other waves in the summation of (E.11) and study the energy flow among these three waves. Equations (E.5) and (E.11) are reduced to

$$\frac{\mathrm{d}\tilde{\phi}_{k1}}{\mathrm{d}t} + i\omega_{k1}\tilde{\phi}_{k1} = \sum_{\boldsymbol{k}1+\boldsymbol{k}2+\boldsymbol{k}3=0} \Lambda^{k1}_{k2,k3}\tilde{\phi}^*_{k2}\tilde{\phi}^*_{k3}, \tag{E.12}$$

$$\Lambda^{k1}_{k2,k3} = \frac{1}{2}\frac{1}{1+k_1^2}((\boldsymbol{k}_2\times\boldsymbol{k}_3)\cdot\hat{\boldsymbol{z}})(k_3^2-k_2^2). \tag{E.13}$$

Denoting $\tilde{\phi}_j = \tilde{\phi}_{kj}$, (E.12) is

$$\frac{\mathrm{d}\tilde{\phi}_1}{\mathrm{d}t} + i\omega_1\tilde{\phi}_1 = \Lambda^1_{2,3}\tilde{\phi}^*_2\tilde{\phi}^*_3, \tag{E.14}$$

$$\frac{\mathrm{d}\tilde{\phi}_2}{\mathrm{d}t} + i\omega_2\tilde{\phi}_2 = \Lambda^2_{3,1}\tilde{\phi}^*_3\tilde{\phi}^*_1, \tag{E.15}$$

$$\frac{\mathrm{d}\tilde{\phi}_3}{\mathrm{d}t} + i\omega_3\tilde{\phi}_3 = \Lambda^3_{1,2}\tilde{\phi}^*_1\tilde{\phi}^*_2. \tag{E.16}$$

Without loss of generality, we can assume that

$$k_1 < k_2 < k_3.$$

First we consider a case in which the k_2 mode is highly populated, so that $|\tilde{\phi}_2| \gg |\tilde{\phi}_1|, |\tilde{\phi}_3|$. Then (E.14)$\sim$(E.16) are reduced to

$$\tilde{\phi}_i = A_i\exp(-i\omega_i t),$$

$$A_2 = \text{const.} \qquad \frac{\mathrm{d}A_1}{\mathrm{d}t} = \Lambda^1_{2,3}A^*_2A^*_3\exp(i\theta t), \qquad \frac{\mathrm{d}A_3}{\mathrm{d}t} = \Lambda^3_{1,2}A^*_1A^*_2\exp(i\theta t), \tag{E.17}$$

where $\theta \equiv (\omega_1+\omega_2+\omega_3)$ is frequency mismatch. From (E.17), we have

$$\frac{\mathrm{d}^2A_1}{\mathrm{d}t^2} - i\theta\frac{\mathrm{d}A_1}{\mathrm{d}t} - \Lambda^1_{2,3}\Lambda^3_{1,2}|A_2|^2A_1 = 0. \tag{E.18}$$

Hence, instability occurs when

$$\theta^2 - 4\Lambda^1_{2,3}\Lambda^3_{1,2}|A_2|^2 < 0.$$

and the growth rate is

$$\gamma = \left(\Lambda^1_{2,3}\Lambda^3_{1,2}|A_2|^2 - \frac{1}{4}\theta^2\right)^{1/2}. \tag{E.19}$$

Because of the assumption $k_1 < k_2 < k_3$, then $\Lambda^1_{2,3}\Lambda^3_{1,2} > 0$ and the system can be unstable. The cascade in $\boldsymbol{k}$ space occurs from the wave with wave number k_2 such that $k_1 < k_2 < k_3$ to the waves with wavenumbers k_1 k_3. If the frequency mismatch $\theta = (\omega_1+\omega_2+\omega_3)$ is zero, the case occurs from the wave with the highest frequency $\omega_2 = -(\omega_1+\omega_3)$ to the waves with lower frequencies ω_1 and ω_3.

On the other hand, if modes 1 or 3 are highly populated, the system is stable, since $\Lambda^2_{3,1}, \Lambda^3_{1,2}$ are always negative.

When we introduce a number

Fig.E.1 Dependence of energy density $W_k = (1+k^2)|\tilde{\phi}_k|^2$ of N_k mode on k_x (left-hand side) and dependence of $W_k = (1+k^2)|\tilde{\phi}_k|^2$ on k_y (right-hand side). x is the coordinate parallel to density gradient. The spectrum cascade in k_x plane tends to stop at a critical value of $k_x = k_{\rm c}$, while the spectrum cascade in k_y plane tends to condence at $k_y \approx 0$. After (ref.[1])

$$N_p \equiv \frac{(1+k_p^2)|\tilde{\phi}_p|^2}{|k_q^2 - k_r^2|}, \tag{E.20}$$

we have the following relations from (E.14)∼(E.16),

$$N_3 - N_1 = \text{const.}, \qquad N_2 + N_3 = \text{const.} \qquad N_1 + N_2 = \text{const.}. \tag{E.21}$$

These equations mean that a loss of 1 in N_2 appears as a gain of 1 in N_1, N_3. N_k mode has the energy $W_k = (1+k^2)|\tilde{\phi}_k|$ as is seen in (E.8). Hence, from (E.20) and (E.21) the partition of energy of mode N_1 and N_3 is

$$\frac{\Delta W_1}{\Delta W_2} = \frac{k_3^2 - k_2^2}{k_3^2 - k_1^2}, \qquad \frac{\Delta W_3}{\Delta W_2} = \frac{k_2^2 - k_1^2}{k_3^2 - k_1^2}.$$

Computer experiments of $\boldsymbol{k}$ spectrum cascade yield (ref.[1]) that the cascade in k_x plane tends to stop at a critical value of $k_x = k_{\rm c}$ where the nonlinear term and the linear term in (E.5) are comparable, that is, $(k_x\rho_{\rm s})^3\tilde{\phi} = \kappa_n\rho_{\rm s}$, $k_{\rm c}\rho_{\rm s} \equiv (\kappa_n\rho_s/\tilde{\phi})^{1/3}$ and the energy spectrum tends to condense near $k_x \approx k_{\rm c}$. With respect to the k_y dependence of the spectrum, energy spectrum tends to condense at $k_y \approx 0$ (refer to fig.E.1). These results suggest the appearance of zonal flows in drift turbulence.

Evolution of k Spectrum Power Density for $\tilde{\phi}$

Let $\langle\tilde{\phi}\rangle_{pi}$ and $\tilde{\phi}_{ki}$ be the functions of 2D wave vectors $\boldsymbol{p}_i = (p_{ix}, p_{iy})$, $\boldsymbol{k}_i = (k_{ix}, k_{iy})$ corresponding to the large spatial scales with low freqencies and small spatial scales with high frequencies of $\tilde{\phi}$ and $|\boldsymbol{p}_i| \ll |\boldsymbol{k}_i|$ Then we have

$$\tilde{\phi} = \langle\tilde{\phi}_p\rangle + \tilde{\phi}_k.$$

The bracket means average over the fast time scales. Then an average of $\tilde{\phi}_1\tilde{\phi}_2$ over the fast time scales is given by

$$\langle\tilde{\phi}_1\tilde{\phi}_2\rangle = \langle\tilde{\phi}_{1p}\rangle\langle\tilde{\phi}_{2p}\rangle + \langle\tilde{\phi}_{1k}\tilde{\phi}_{2k}\rangle.$$

To obtain the equation for the evolution of large scale components, let us Fourier transform (E.10) and average over the characteristic times of small scale (ref.[3]):

$$\partial_t(p^2+1)\langle\tilde{\phi}_p\rangle - i(\kappa_n\rho_{\rm s})\partial_y\langle\tilde{\phi}_p\rangle - \int [\boldsymbol{p}_2, \boldsymbol{p}_1]p_2^2\langle\tilde{\phi}_{p1}\rangle\langle\tilde{\phi}_{p2}\rangle\delta(\boldsymbol{p}_1 + \boldsymbol{p}_2 - \boldsymbol{p})\mathrm{d}\boldsymbol{p}_1\mathrm{d}\boldsymbol{p}_2$$

$$- \int [\boldsymbol{k}_2, \boldsymbol{k}_1]k_2^2\langle\tilde{\phi}_{k1}\tilde{\phi}_{k2}\rangle\delta(\boldsymbol{k}_1 + \boldsymbol{k}_2 - \boldsymbol{p})\mathrm{d}\boldsymbol{k}_1\mathrm{d}\boldsymbol{k}_2 = 0, \tag{E.22}$$

where [ ] means the z component of vector multiplication $[\boldsymbol{a},\boldsymbol{b}] = a_x b_y - a_y b_x$ and $\partial_t = \partial/\partial t$. By introducing $\boldsymbol{k}$ and $\boldsymbol{p}$ as follows

$$\boldsymbol{k}_1 = -\boldsymbol{k} + \frac{1}{2}\boldsymbol{p}, \qquad \boldsymbol{k}_2 = \boldsymbol{k} + \frac{1}{2}\boldsymbol{p},$$

$$\begin{aligned}[\boldsymbol{k}_2,\boldsymbol{k}_1]k_2^2 &= ((k_x + p_x/2)(-k_y + p_y/2) - (k_y + p_y/2)(-k_x + p_x/2))(\boldsymbol{k} + \boldsymbol{p}/2)^2 \\ &= [\boldsymbol{k},\boldsymbol{p}](\boldsymbol{k}\cdot\boldsymbol{p} + k^2 + p^2/4),\end{aligned}$$

the second integral in (E.22) can be rewritten in the form of

$$\begin{aligned}\int [\boldsymbol{k},\boldsymbol{p}](\boldsymbol{k}+\boldsymbol{p}/2)^2\langle\tilde{\phi}_{p/2-k}\tilde{\phi}_{p/2+k}\rangle \mathrm{d}\boldsymbol{k} &= \int [\boldsymbol{k},\boldsymbol{p}](\boldsymbol{k}\cdot\boldsymbol{p})\langle\tilde{\phi}_{p/2-k}\tilde{\phi}_{p/2+k}\rangle \mathrm{d}\boldsymbol{k} \\ &= \int (-k_x k_y(p_x^2 - p_y^2) - (k_y^2 - k_x^2)p_x p_y)\langle\tilde{\phi}_{p/2-k}\tilde{\phi}_{p/2+k}\rangle \mathrm{d}\boldsymbol{k},\end{aligned}$$

where $[\boldsymbol{k},\boldsymbol{p}](k^2 + p^2/4) = -[\boldsymbol{k}_1,\boldsymbol{k}_2](k_1^2 + k_2^2)/2$. Performing an inverse Fourier transform on (E.22), we get the following equation for the evolution of large scales:

$$\begin{aligned}&\partial_t(\nabla^2\tilde{\phi}_{\mathrm{L}} - \tilde{\phi}_{\mathrm{L}}) - (\kappa_n\rho_{\mathrm{s}})\partial_y\tilde{\phi}_{\mathrm{L}} + (\partial_y\nabla^2\tilde{\phi}_{\mathrm{L}})\partial_x\tilde{\phi}_{\mathrm{L}} - (\partial_x\nabla^2\tilde{\phi}_{\mathrm{L}})\partial_y\tilde{\phi}_{\mathrm{L}} \\ &\quad = -\partial_{xx}A - \partial_x\partial_y B + \partial_{yy}A, \qquad \text{(E.23)}\end{aligned}$$

where

$$\begin{aligned}A(\boldsymbol{\xi},t) &= 2\int \frac{k_x k_y}{k^2(1+k^2)} n_k \mathrm{d}\boldsymbol{k}, \\ B(\boldsymbol{\xi},t) &= 2\int \frac{k_y^2 - k_x^2}{k^2(1+k^2)} n_k \mathrm{d}\boldsymbol{k}, \\ n_k(\boldsymbol{k},\boldsymbol{\xi},t) &\equiv \frac{1}{2}k^2(1+k^2)\int \langle\tilde{\phi}_{p/2-k}\tilde{\phi}_{p/2+k}\rangle \exp(i\boldsymbol{p}\cdot\boldsymbol{\xi})\frac{\mathrm{d}\boldsymbol{p}}{(2\pi)^2}. \qquad \text{(E.24)}\end{aligned}$$

n_k is the power density of high-frequency spectrum of $\tilde{\phi}$.

To derive the evolution equation for the density of high-frequency n_k, the evolution equation for the Fourier component $\tilde{\phi}_k$ is described as follows:

$$\begin{aligned}&-\partial_t(1+k^2)\tilde{\phi}_k - (\kappa_n\rho_{\mathrm{s}})ik_y\tilde{\phi}_k \\ &\quad - \int (-k'_y k'^2\tilde{\phi}_{k'}q_x\tilde{\phi}_q) + k'_x k'^2\tilde{\phi}_{k'}q_y\tilde{\phi}_q)\delta(\boldsymbol{q}+\boldsymbol{k}'-\boldsymbol{k})\mathrm{d}\boldsymbol{k}'\mathrm{d}\boldsymbol{q} = 0.\end{aligned}$$

Integrating by $\boldsymbol{k}'$ and taking account of

$$k'^2(k'_x q_y - k'_y q_x) = [\boldsymbol{k},\boldsymbol{q}](\boldsymbol{k}-\boldsymbol{q})^2, \qquad (\boldsymbol{k}' = \boldsymbol{k} - \boldsymbol{q}),$$

we have

$$\partial_t\tilde{\phi}_k + \frac{i(\kappa_n\rho_{\mathrm{s}})k_y}{1+k^2}\tilde{\phi}_k + \int \frac{[\boldsymbol{k},\boldsymbol{q}](\boldsymbol{k}-\boldsymbol{q})^2}{1+k^2}\tilde{\phi}_{k-q}\tilde{\phi}_q \mathrm{d}\boldsymbol{q} = 0.$$

Let us take the sum of the evolution equation for $\tilde{\phi}_k$ muliplied by $\tilde{\phi}_{k'}$ and the similar equation for $\tilde{\phi}_{k'}$ muliplied by $\tilde{\phi}_k$; as a result we get

$$\partial_t(\tilde{\phi}_k\tilde{\phi}_{k'}) + i(\omega_k^{\mathrm{l}} + \omega_{k'}^{\mathrm{l}})(\tilde{\phi}_k\tilde{\phi}_{k'}) + R_{k\,k'} = 0, \qquad \text{(E.25)}$$

where

$$R_{k\,k'} \equiv \int \left(\frac{[\boldsymbol{k},\boldsymbol{q}](\boldsymbol{k}-\boldsymbol{q})^2}{1+k^2}\tilde{\phi}_{k-q}\tilde{\phi}_{k'} + \frac{[\boldsymbol{k}',\boldsymbol{q}](\boldsymbol{k}'-\boldsymbol{q})^2}{1+k^2}\tilde{\phi}_{k'-q}\tilde{\phi}_k\right)\tilde{\phi}_q \mathrm{d}\boldsymbol{q}.$$

and $\omega_k^{\rm l} = (\kappa_n \rho_{\rm s}) k_y/(1+k^2)$.

Let us suppose that the concentration of turbulence spectrum at large scales is high enough to neglect the interaction of small scales among themselves in comparison with their interaction with large scales. The correlator of the small-scale field $\langle \tilde{\phi}_k \tilde{\phi}_{k'} \rangle$ is of an appreciable value only for the small values of $\boldsymbol{k}+\boldsymbol{k}'$, which are comparable to the characteristic wave number of large-scale motions. Taking account of these arguments, $\boldsymbol{k}$ and $\boldsymbol{k}'$ are replaced by $-\boldsymbol{k}+\boldsymbol{p}/2$ and $\boldsymbol{k}+\boldsymbol{p}/2$ as follows:

$$\boldsymbol{k} \to -\boldsymbol{k}+\boldsymbol{p}/2, \qquad \boldsymbol{k}' \to \boldsymbol{k}+\boldsymbol{p}/2, \qquad \tilde{\phi}_k \tilde{\phi}_{k'} \to \tilde{\phi}_{p/2-k} \tilde{\phi}_{p/2+k}.$$

Then we have

$$(\kappa_n \rho_{\rm s})^{-1} i(\omega_k^{\rm l} + \omega_{k'}^{\rm l}) = i\frac{-(k_y - p_y/2)}{1+(\boldsymbol{k}-\boldsymbol{p}/2)^2} + \frac{(k_y+p_y/2)}{1+(\boldsymbol{k}+\boldsymbol{p}/2)^2} = \frac{\partial}{\partial \boldsymbol{k}} \left(\frac{k_y}{1+k^2} \right) \cdot i\boldsymbol{p},$$

as $|\boldsymbol{p}| \ll |\boldsymbol{k}|$, and the first two terms of (E.25) reduce to

$$\partial_t n_k + (\kappa_n \rho_{\rm s}) \frac{\partial}{\partial \boldsymbol{k}} \left(\frac{k_y}{1+k^2} \right) \cdot \frac{\partial n_k}{\partial \boldsymbol{\xi}}.$$

The first integral of $R_{kk'}$ reduces to

$$\begin{aligned}
&\text{first term of } R_{p/2-k,p/2+k} = \\
&\qquad \int \left(\frac{-[\boldsymbol{k}-\boldsymbol{p}/2, \boldsymbol{q}](\boldsymbol{k}-\boldsymbol{p}/2+\boldsymbol{q})^2}{1+(\boldsymbol{k}-\boldsymbol{p}/2)^2} \tilde{\phi}_{-k+p/2-q} \tilde{\phi}_{k+p/2} \right) \tilde{\phi}_q {\rm d}\boldsymbol{q} \\
&= \int \frac{-[\boldsymbol{k}-\boldsymbol{p}'/2, \boldsymbol{q}](\boldsymbol{k}-\boldsymbol{p}'/2+\boldsymbol{q}/2)^2}{1+(\boldsymbol{k}-\boldsymbol{p}'/2-\boldsymbol{q}/2)^2} \frac{2}{(\boldsymbol{k}+\boldsymbol{q}/2)^2(1+(\boldsymbol{k}+\boldsymbol{q}/2)^2)^2)} \\
&\qquad \times \left(\tilde{\phi}_{p'/2-(k+q/2)} \tilde{\phi}_{p'/2+(k+q/2)} \frac{(\boldsymbol{k}+\boldsymbol{q}/2)^2(1+(\boldsymbol{k}+\boldsymbol{q}/2)^2)^2)}{2} \right) \tilde{\phi}_q {\rm d}\boldsymbol{q},
\end{aligned}$$

where $\boldsymbol{p} = \boldsymbol{p}' + \boldsymbol{q}$. Finally we have

$$\begin{aligned}
&\frac{1}{2}k^2(1+k^2) \int R_{p/2-k,p/2+k} \exp(i\boldsymbol{p}\cdot\boldsymbol{\xi}) \frac{{\rm d}\boldsymbol{p}}{(2\pi)^2} \\
&\qquad = \frac{1}{2}k^2(1+k^2) \int R_{p/2-k,p/2+k} \exp((i\boldsymbol{p}'\cdot\boldsymbol{\xi}) + i\boldsymbol{q}\cdot\boldsymbol{\xi})) \frac{{\rm d}\boldsymbol{p}'}{(2\pi)^2} \\
&= \frac{-k^2}{1+k^2}[\boldsymbol{k},\boldsymbol{q}](n_{k+q/2} - n_{k-q/2}) \tilde{\phi}_{\rm L} + \frac{2[\boldsymbol{k},\boldsymbol{q}]}{(1+k^2)^2}(\boldsymbol{k}\cdot\boldsymbol{p}') n_k \tilde{\phi}_{\rm L} + \frac{k^2}{(1+k^2)}[\boldsymbol{p}',\boldsymbol{q}] n_k \tilde{\phi}_{\rm L} \\
&\qquad = \frac{-k^2}{1+k^2}[\boldsymbol{k},\boldsymbol{q}] \frac{\partial n_k}{\partial \boldsymbol{k}} \cdot \boldsymbol{q} \tilde{\phi}_{\rm L} + \frac{2[\boldsymbol{k},\boldsymbol{q}]}{(1+k^2)^2}(\boldsymbol{k}\cdot\boldsymbol{p}') n_k \tilde{\phi}_{\rm L} + \frac{k^2}{(1+k^2)}[\boldsymbol{p}',\boldsymbol{q}] n_k \tilde{\phi}_{\rm L}.
\end{aligned}$$

Here $|\boldsymbol{q}|, |\boldsymbol{p}'| \ll |\boldsymbol{k}|$ is assumed and the integrand of $R_{kk'}$ was expanded. Equation (E.25) is reduced to

$$\begin{aligned}
\partial_t n_k + (\kappa_n \rho_{\rm s}) \frac{\partial}{\partial \boldsymbol{k}} \left(\frac{k_y}{1+k^2} \right) \cdot \nabla_x n_k - \frac{k^2}{1+k^2}[\boldsymbol{k},\boldsymbol{q}] \frac{\partial n_k}{\partial \boldsymbol{k}} \cdot \boldsymbol{q} \tilde{\phi}_{\rm L} + \frac{2[\boldsymbol{k},\boldsymbol{q}]}{(1+k^2)^2}(\boldsymbol{k}\cdot\boldsymbol{p}') n_k \tilde{\phi}_{\rm L} \\
+ \frac{k^2}{(1+k^2)}[\boldsymbol{p}',\boldsymbol{q}] n_k \tilde{\phi}_{\rm L} = 0. \qquad \text{(E.26)}
\end{aligned}$$

If ω_k is newly introduced,

$$\omega_k = \omega_k^{\rm l} + \omega_k^{\rm nl} \equiv \frac{(\kappa_n \rho_{\rm s}) k_y + (\hat{\boldsymbol{v}}_E \cdot \boldsymbol{k}) k^2}{1+k^2}, \qquad \hat{\boldsymbol{v}}_E \equiv \frac{\boldsymbol{v}_E}{c_{\rm s}} = \left(-\frac{\partial \tilde{\phi}}{\partial \hat{y}}, \frac{\partial \tilde{\phi}}{\partial \hat{x}} \right),$$

(E.26) is reduced to (ref.[3])

$$\left(\partial_t + \frac{\partial\omega_k}{\partial \boldsymbol{k}}\partial_x - \frac{\partial\omega_k}{\partial \boldsymbol{\xi}}\partial_k\right) n_k = 0. \tag{E.27}$$

When the ordinary coordinates and time are used instead of normalized dimensionless coordinates and time, (E.27) becomes

$$\left(\frac{\partial}{\partial t} + \frac{\partial\omega_k}{\partial \boldsymbol{k}}\frac{\partial}{\partial x} - \frac{\partial\omega_k}{\partial \boldsymbol{\xi}}\frac{\partial}{\partial \boldsymbol{k}}\right) n_k = 0, \qquad \omega_k = \frac{k_y v_{\rm d}^* + (\boldsymbol{v}_E\cdot\boldsymbol{k})\rho_{\rm s}^2 k^2}{1+\rho_{\rm s}^2 k^2}. \tag{E.28}$$

E.2 Generation of Zonal Flow

The scale of sheared mean flow is macroscopic and the stabilizing effect of sheared mean flow on drift turbulence was discussed in sec.16.7. On the other hand, the scale of zonal flow is mesoscopic scale. The difference of sheared mean flow and zonal flow is illustrated in fig.E.2.

Numerical simulation studies of drift turbulence have played a crucial role in the developement of research on zonal flow. The synergy between the theory and numerical simulation has been the key promotor of interest in the physics of zonal flow. A result of numerical simulation based on the gyrokinetic particle model is shown in fig.E.3 (ref.[4]). It is clearly seen in this figure that radial size of turbulent eddies is greatly reduced by the shearing of zonal flows.

The potential ϕ_z of zonal field has the structure of $k_y = k_z = 0$ on the magnetic surface with finite k_x (radial direction), so that the phase velocity of ϕ_z along the magnetic field line is infinity. Therefore, adiabatic response of the potential is modified to

$$\frac{\delta n}{n_0} = \frac{e}{\kappa T_{\rm e}}(\phi - \bar{\phi}), \qquad \phi = \bar{\phi} + \delta\phi_{\rm d},$$

where $\bar{\phi}$ is a spatial average of ϕ on a magnetic surface. Therefore, adiabatic response is

$$\frac{\delta n}{n_0} = \frac{e\delta\phi_{\rm d}}{\kappa T_{\rm e}} \equiv \tilde{\phi}_{\rm d}.$$

We assume the following ordering:

$$\frac{e\bar{\phi}}{\kappa T_{\rm e}} \equiv \bar{\phi}_{\rm z}, \qquad \tilde{\phi}_{\rm d} \sim \delta, \quad \bar{\phi}_{\rm z} \sim \delta, \quad \nabla\tilde{\phi}_{\rm d} \sim O(1), \quad \nabla\bar{\phi}_{\rm z} \sim O(1).$$

The equation of continuity for ions is derived (ref.[5]) by modifying (E.5) to

$$(1-\rho_{\rm s}^2\nabla^2)\frac{\partial\tilde{\phi}_{\rm d}}{\partial t} - \rho_{\rm s}c_{\rm s}(\nabla\tilde{\phi}_{\rm d}\times\hat{\boldsymbol{z}})\cdot\frac{\nabla n_0}{n_0} - \rho_{\rm s}c_{\rm s}(\nabla\bar{\phi}_{\rm z}\times\hat{\boldsymbol{z}})\cdot\nabla\tilde{\phi}_{\rm d}$$
$$+\rho_{\rm s}^3 c_{\rm s}\nabla\cdot\Big(((\nabla\bar{\phi}_{\rm z}\times\hat{\boldsymbol{z}})\cdot\nabla)\nabla\tilde{\phi}_{\rm d} + ((\nabla\tilde{\phi}_{\rm d}\times\hat{\boldsymbol{z}})\cdot\nabla)\nabla\bar{\phi}_{\rm z}\Big) = 0, \tag{E.29}$$

$$-\frac{\partial}{\partial t}\rho_{\rm s}^2\nabla^2\bar{\phi}_{\rm z} + \rho_{\rm s}^3 c_{\rm s}\nabla\cdot\Big((\nabla\tilde{\phi}_{\rm d}\times\hat{\boldsymbol{z}}\cdot\nabla)\nabla\tilde{\phi}_{\rm d}\Big) = 0. \tag{E.30}$$

A low-dimensional model for generation of zonal flow is developed under the assumption of

$$\tilde{\phi}_{\rm d} = \tilde{\phi}_{\rm d0}(t)\cos(k_y y - \omega_0 t) + \tilde{\phi}_{\rm d\,c}(t)\sin(k_x x - \omega_{\rm z} t)\cos(k_y y - \omega_0 t)$$
$$+\tilde{\phi}_{\rm d\,s}(t)\sin(k_x x - \omega_{\rm z} t)\sin(k_y - \omega_0 t), \tag{E.31}$$

$$\bar{\phi}_{\rm z} = \bar{\phi}_{\rm z}(t)\cos(k_x x - \omega_{\rm z} t), \tag{E.32}$$

with

$$\omega_0 = \frac{k_y v_{\rm d}^*}{1+\rho_{\rm s}^2 k^2}.$$

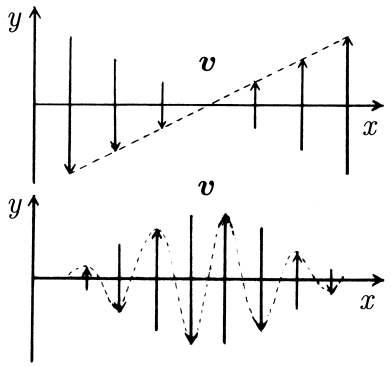

Fig.E.2 Upper figure: Sheared mean flow. Lower figure: Zonal flow.

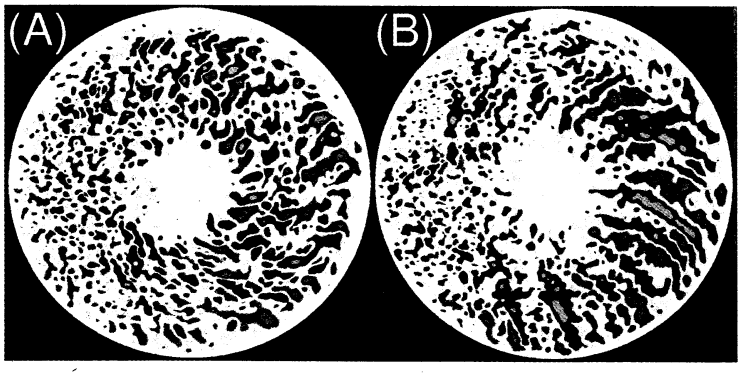

Fig.E.3 Radial size of turbulent eddies shown in poloidal contour plots of ambient potential fluctuation $e\phi/\kappa T_{\rm e}$ gets reduced due to random shearing by self-regulated $\boldsymbol{E} \times \boldsymbol{B}$ zonal flow from gyrokinetic particle simulation with zonal flow (A) and with zonal flow suppressed (B). After (ref.[4]).

When (E.31) and (E.32) are substituted in (E.29) and (E.30), components of $\cos(k_y y - \omega_0 t)$, $\sin(k_x x - \omega_z t)\cos(k_y y - \omega_0 t)$, $\sin(k_x x - \omega_z t)\sin(k_y - \omega_0 t)$ and $\cos(k_x x - \omega_z t)$ reduce to

$$(1+\rho_{\rm s}^2 k^2)\frac{{\rm d}\tilde{\phi}_{{\rm d}\,0}}{{\rm d}t} - \frac{\rho_{\rm s} c_{\rm s}}{2} k_x k_y \bar{\phi}_{\rm z}\tilde{\phi}_{{\rm d}\,{\rm s}} = 0,$$

$$(1+\rho_{\rm s}^2 k^2)\frac{{\rm d}\tilde{\phi}_{{\rm d}\,{\rm c}}}{{\rm d}t} - \frac{k_y k_x^2 \rho_{\rm s}^2 v_{\rm d}^*}{1+k_y^2\rho_{\rm s}^2}\tilde{\phi}_{{\rm d}\,{\rm s}} = 0,$$

$$(1+\rho_{\rm s}^2 k^2)\frac{{\rm d}\tilde{\phi}_{{\rm d}\,{\rm s}}}{{\rm d}t} + \frac{k_y k_x^2 \rho_{\rm s}^2 v_{\rm d}^*}{1+k_y^2\rho_{\rm s}^2}\tilde{\phi}_{{\rm d}\,{\rm c}} + \rho_{\rm s} c_{\rm s} k_x k_y (1+k_y^2\rho_{\rm s}^2 - k_x^2\rho_{\rm s}^2)\bar{\phi}_{\rm z}\tilde{\phi}_{{\rm d}\,0} = 0,$$

$$\frac{{\rm d}\bar{\phi}_{\rm z}}{{\rm d}t} + \frac{\rho_{\rm s} c_{\rm s}}{2} k_x k_y \tilde{\phi}_{{\rm d}\,0}\tilde{\phi}_{{\rm d}\,{\rm s}} = 0.$$

If we assume that the drift wave $\tilde{\phi}_{{\rm d}\,0}$ is pumped and the following conditions are satisfied,

$$|\tilde{\phi}_{{\rm d}\,{\rm c}}|, |\tilde{\phi}_{{\rm d}\,{\rm s}}|, |\bar{\phi}_{\rm z}| \ll |\tilde{\phi}_{{\rm d}\,0}|,$$

and that the perturbed state variables have a time dependence given as $\exp(\gamma t)$, then the linearized system of equations under the assumption $\tilde{\phi}_{{\rm d}\,0} = $ const. yields the following dispersion relation:

$$\gamma^2 = \frac{c_{\rm s}^4 k_x^2 k_y^2}{\Omega_{\rm i}^2 (1+k^2\rho_{\rm s}^2)^2}\left(\frac{(1+k_y^2\rho_{\rm s} - k_x^2\rho_{\rm s}^2)(1+k^2\rho_{\rm s}^2)}{2}\tilde{\phi}_{{\rm d}\,0}^2 - \frac{k_x^2\rho_s^2 v_{\rm d}^{*2}}{c_{\rm s}^2(1+k^2\rho_{\rm s}^2)^2}\right). \tag{E.33}$$

The unstable condition for the modulational instability of four waves is

$$k_{xc}^2\rho_{\rm s}^2 < \frac{(1+k^2\rho_{\rm s}^2)^3((1+k_y^2\rho_{\rm s} - k_x^2\rho_{\rm s}^2))}{2}\left(\frac{c_{\rm s}\tilde{\phi}_{\rm d0}}{v_{\rm d}^*}\right)^2 \approx \frac{(1+k_y^2\rho_{\rm s})^4}{2}\left(\frac{c_{\rm s}\tilde{\phi}_{\rm d0}}{v_{\rm d}^*}\right)^2. \tag{E.34}$$

This condition shows the critical wave number k_{xc} below which the drift wave is unstable to the generation of zonal flow in the slab case.

There is the other intuitive way to analyze the driving mechanism of zonal flow (ref.[6]). Let us assume that $\boldsymbol{v} = \bar{\boldsymbol{v}} + \tilde{\boldsymbol{v}}$, where $\bar{\boldsymbol{v}}$ is the component of large spatial scale with low frequency and $\tilde{\boldsymbol{v}}$ is the component of small spatial scale with high frequency. Since the potential of zonal flow has $k_\theta = k_z = 0$ and $k_r \neq 0$, a component of poloidal zonal flow can be extracted by average mean of Reynold stress over a magnetic surface. The second order of

$$\frac{\partial \boldsymbol{v}}{\partial t} = -(\boldsymbol{v}\cdot\nabla)\boldsymbol{v} + \cdots$$

becomes

$$\frac{\partial \bar{v}_\theta^{\rm z}}{\partial t} = -\langle(\tilde{\boldsymbol{v}}\cdot\nabla)\tilde{\boldsymbol{v}})_\theta\rangle + \cdots = -\frac{1}{r^2}\frac{\partial}{\partial r}\langle(r^2\tilde{v}_r\tilde{v}_\theta)\rangle + \cdots \approx \frac{\partial}{\partial r}\langle(\tilde{v}_r\tilde{v}_\theta)\rangle + \cdots. \tag{E.35}$$

with use of the following relation:

$$((\tilde{\boldsymbol{v}}\cdot\nabla)\tilde{\boldsymbol{v}})_\theta = (\tilde{\boldsymbol{v}}\cdot\nabla)\tilde{v}_\theta + \frac{\tilde{v}_r\tilde{v}_\theta}{r} = \frac{1}{r^2}\frac{\partial}{\partial r}(r^2\tilde{v}_r\tilde{v}_\theta) + \frac{1}{r}\frac{\partial\tilde{v}_\theta^2}{\partial\theta} + \frac{\partial}{\partial z}(\tilde{v}_\theta\tilde{v}_z).$$

The notation $\langle\ \rangle$ means the average over a magnetic surface (θ, z). Since

$$\langle(\tilde{v}_r\tilde{v}_\theta)\rangle = \frac{k_r k_\theta}{B^2}\langle\phi^2\rangle = c_{\rm s}^2(k_r k_\theta\rho_{\rm s}^2)\tilde{\phi}^2,$$

$$\tilde{\phi}^2 = \int\int(\tilde{\phi}_{k'}\tilde{\phi}_{p-k'}){\rm d}\boldsymbol{k}'\exp(i\boldsymbol{p}\cdot\boldsymbol{\xi}){\rm d}\boldsymbol{p} = \int\int(\tilde{\phi}_{p/2+k}\tilde{\phi}_{p/2-k})\exp(i\boldsymbol{p}\cdot\boldsymbol{\xi}){\rm d}\boldsymbol{p}{\rm d}\boldsymbol{k}$$

$$= \int \frac{2n_k}{\rho_{\rm s}^2 k^2 (1+\rho_{\rm s}^2 k^2)} {\rm d}\boldsymbol{k} \rho_{\rm s}^2,$$

(E.35) becomes (ref.[6])

$$\frac{\partial \bar{v}_\theta^{\rm z}}{\partial t} = -\frac{\partial}{\partial r} \int c_{\rm s}^2 \frac{(k_r k_\theta \rho_{\rm s}^2) 2 n_k}{\rho_{\rm s}^2 k^2 (1+\rho_s^2 k^2)} {\rm d}k_r {\rm d}k_\theta \rho_{\rm s}^2 - \gamma_{\rm damp} \bar{v}_\theta^{\rm z}, \tag{E.36}$$

where n_k is the power density of high-frequency spectrum of $\tilde{\phi}$ and the equation of n_k was described by (E.28). n_k can be obtained by linearizing (E.28) for small perturbations $n_k^{(1)}$ with the frequency Ω and the radial wave number K,

$$n_k^{(1)} \propto \exp(iKr - i\Omega t),$$

and

$$i\left(-\Omega + \frac{\partial \omega_k}{\partial k_r} K + i\gamma\right) n_k^{(1)} - \frac{\partial \omega_k}{\partial r} \frac{\partial n_k^{(0)}}{\partial k_r} = 0,$$

and

$$n_k^{(1)} = \frac{\frac{\partial \omega_k}{\partial r} \frac{\partial n_k^{(0)}}{\partial k_r}}{-i\left(\Omega - \frac{\partial \omega_k}{\partial k_r} K - i\gamma\right)} = R(K,\Omega) \frac{\partial}{\partial r} (k_\theta \bar{v}_\theta^{\rm z}) \frac{\partial n_k^{(0)}}{\partial k_r},$$

$$R(K,\Omega) = \frac{i}{\Omega - \frac{\partial \omega_k}{\partial k_r} K - i\gamma} = \frac{-\gamma + i(\Omega - (\partial \omega_k / \partial k_r) K)}{(\Omega - (\partial \omega_k / \partial k_r) K)^2 + \gamma^2}.$$

Finally, we obtain

$$\frac{\partial \bar{v}_\theta^{\rm z}}{\partial t} = -\frac{\partial}{\partial r} \int c_{\rm s}^2 \frac{(k_r k_\theta \rho_{\rm s}^2) 2}{(1+\rho_s^2 k^2)} R k_\theta \frac{\partial \bar{v}_\theta^{\rm z}}{\partial r} \frac{\partial n_k^{(0)}}{\partial k_r} {\rm d}k_r {\rm d}k_\theta \rho_{\rm s}^2 - \gamma_{\rm damp} \bar{v}_\theta^{\rm z}, \tag{E.37}$$

(E.37) is the equation of diffusion

$$\frac{\partial \bar{v}_\theta^{\rm z}}{\partial t} = \frac{\partial}{\partial r} D_{rr} \frac{\partial \bar{v}_\theta^{\rm z}}{\partial r} - \gamma_{\rm damp} \bar{v}_\theta^{\rm z}, \tag{E.38}$$

if the following diffusion coefficient is introduced:

$$D_{rr} = -c_{\rm s}^2 \int \frac{2(k_\theta \rho_{\rm s})^2}{(1+\rho_{\rm s}^2 k^2)} R(K,\Omega) k_r \frac{\partial n_k^{(0)}}{\partial k_r} \rho_{\rm s}^2 {\rm d}k_r {\rm d}k_\theta. \tag{E.39}$$

The growth rate $\gamma_{\rm z}$ of zonal flow due to the first term of (E.38) is

$$\gamma_{\rm z} = -K^2 {\rm Re}({\rm D_{rr}}) = -K^2 c_{\rm s}^2 \int \frac{2(k_\theta \rho_{\rm s})^2}{(1+\rho_{\rm s}^2 k^2)} \frac{\gamma k_r (\partial n_k^{(0)} / \partial k_r)}{(\Omega - (\partial \omega_k / \partial k_r) K)^2 + \gamma^2} \rho_{\rm s}^2 {\rm d}k_r {\rm d}k_\theta. \tag{E.40}$$

$k_r (\partial n_k / \partial r)$ is negative in typical drift turbulence, so that $\gamma_{\rm z}$ is positive and zonal flows are driven, if the growth rate is larger than damping rate $\gamma_{\rm damp}$ of zonal flow, that is,

$$k_r \frac{\partial n_{(0)}}{\partial k_r} < 0, \qquad \gamma_{\rm z} - \gamma_{\rm damp} > 0. \tag{E.41}$$

In other words, when the diffusion coefficient is negative, the system can be unstale.

E.3 Geodesic Acoustic Mode (GAM)

When one constructs an eigenmode in the regime of time scale of $|\partial/\partial t| \sim \omega_{\rm t} = v_{T_{\rm i}}/qR$, one finds the geodesic acoustic mode (GAM) (ref.[7]). GAM is a perturbation for which $m = n = 0$

electrostatic potential is linearly couped by toroidal effect to $m = 1/n = 0$ side band density perturation. The equation of continuity and the equation of motion are

$$\frac{\partial n}{\partial t} + \nabla \cdot (n\boldsymbol{v}_\perp) + \nabla_\parallel (nv_\parallel) = 0, \tag{E.42}$$

$$nm_\mathrm{i}\left(\frac{\partial}{\partial t}\boldsymbol{v} + (\boldsymbol{v}\cdot\nabla)\boldsymbol{v}\right) = -\nabla p + \boldsymbol{j}\times\boldsymbol{B}, \tag{E.43}$$

$$\nabla\cdot\boldsymbol{j} = 0, \qquad \boldsymbol{E} + \boldsymbol{v}\times\boldsymbol{B} = 0.$$

Since $\nabla\cdot(\boldsymbol{E}\times\boldsymbol{B}/B^2) = -\boldsymbol{E}\cdot\nabla\times(\boldsymbol{B}/B^2) = 2\boldsymbol{E}\cdot(\nabla B\times\boldsymbol{b})/B^2$
$= 2(E_r/B)\sin\theta/R$ due to the geodesic curvature of magnetic field line on the magnetic surface, a density accumulation is caused due to the equation of continuity ($\tilde{n}$ is normalized density fluctuation):

$$\frac{\partial\tilde{n}}{\partial t} - \frac{2}{R}\sin\theta\tilde{v}_{E\times B} + \nabla_\parallel\tilde{v}_\parallel = 0. \tag{E.44}$$

Since the axisymmetric toroidal field is given by (refer to sec.6.2)

$$\boldsymbol{B} = B_\mathrm{t}\boldsymbol{i}_\varphi + \frac{1}{R}\nabla\psi\times\boldsymbol{i}_\varphi,$$

the poloidal component of the equation of motion is given by

$$\boldsymbol{B}_\mathrm{p}\cdot\left(nm_\mathrm{i}\frac{\mathrm{d}}{\mathrm{d}t}\boldsymbol{v} + \kappa(T_\mathrm{i}+T_\mathrm{e})\nabla n\right) = B_\mathrm{t}R^{-1}\boldsymbol{j}\cdot\nabla\psi.$$

The density accumulation generates radial current across the magnetic surface and acts to reverse $\boldsymbol{E}$. Since $\int\boldsymbol{j}\cdot\boldsymbol{n}\mathrm{d}S = 0$ and RB_t =const, we have

$$\int\frac{R^2}{|\nabla\psi|}\frac{B_\mathrm{t}(\boldsymbol{j}\cdot\nabla\psi)}{R}\mathrm{d}S = \int\frac{R^2}{|\nabla\psi|}\boldsymbol{B}_\mathrm{p}\cdot\left(nm_\mathrm{i}\frac{\mathrm{d}}{\mathrm{d}t}\boldsymbol{v} + \kappa(T_\mathrm{i}+T_\mathrm{e})\nabla n\right)\mathrm{d}S = 0,$$

and the poloidal components of the equation of motion is reduced to (ref.[7][8]) ($\mathrm{d}S = 2\pi(R_0 + r\cos\theta)r\mathrm{d}\theta$, $c_\mathrm{s}^2 \equiv \kappa(T_\mathrm{i}+T_\mathrm{e})/m_\mathrm{i}$)

$$\frac{\partial\tilde{v}_{E\times B}}{\partial t} + \frac{2c_\mathrm{s}^2}{2\pi R}\oint\tilde{n}\sin\theta\mathrm{d}\theta = 0. \tag{E.45}$$

The parallel components of equation of motion are

$$\frac{\partial\tilde{v}_\parallel}{\partial t} + c_\mathrm{s}^2\nabla_\parallel\tilde{n} = 0. \tag{E.46}$$

In the case in which density perturbaton is in the form of $\tilde{n} = \tilde{n}_1\sin\theta$, we have

$$\frac{\partial\tilde{v}_{E\times B}}{\partial t} = -\frac{c_\mathrm{s}^2}{R}\tilde{n}_1, \tag{E.47}$$

$$\frac{\partial^2\tilde{n}}{\partial t^2} + \frac{2}{R^2}\sin\theta\frac{c_\mathrm{s}^2}{R}\tilde{n_1} - c_\mathrm{s}^2\nabla_\parallel^2\tilde{n} = 0$$

and the dispersion relation is ($\tilde{n}\propto\exp(ik_r r + ik_\parallel l - i\Omega t)\sin\theta$)

$$-\Omega^2 + \frac{2c_\mathrm{s}^2}{R^2} + k_\parallel^2 c_\mathrm{s}^2 = 0.$$

The frequency of GAM is given by ($k_\parallel = 1/q_\mathrm{s}R$)

$$\omega_\mathrm{GAM}^2 = 2c_\mathrm{s}^2R^{-2}\left(1 + \frac{k_\parallel^2R^2}{2}\right) = c_\mathrm{s}^2\left(k_\parallel^2 + \frac{2}{R^2}\right) = 2c_\mathrm{s}^2R^{-2}(1 + q_\mathrm{s}^{-2}/2) \approx 2c_\mathrm{s}^2R^{-2}, \tag{E.48}$$

$$v_{\mathrm{ph}\parallel} = \omega_{\mathrm{GAM}}/k_\parallel \approx 2^{1/2} q_{\mathrm{s}} c_{\mathrm{s}}.$$

When $q_{\mathrm{s}} \gg 1$ or $T_{\mathrm{e}} \gg T_{\mathrm{i}}$, GAM is not damped by ion Landau damping. $\tilde{n}$ of GAM is $k_r\rho_{\mathrm{s}}$ times smaller than normalized electrostatic potential as is reduced from (E.47) and (E.48) ($E_r = -ik_r\phi$),

$$\tilde{n} = 2^{1/2} k_r \rho_{\mathrm{s}} (1 + q_{\mathrm{s}}^{-2}/2)^{1/2} \frac{e\phi}{\kappa T_{\mathrm{e}}}.$$

In the case in which density perturbation has dependence other than $\sin\theta$, we have

$$-\Omega i\tilde{n} - \frac{2}{R}\sin\theta \tilde{v}_{E\times B} + \nabla\tilde{v}_\parallel = 0, \qquad ik_\parallel c_{\mathrm{s}}^2 \tilde{n} - i\Omega\tilde{v}_\parallel = 0, \qquad -i\Omega\tilde{v}_{E\times B} = 0.$$

One solution is zonal flow branch ($\nabla_\parallel = (\partial\theta/\partial l)\partial\partial\theta = (1/q_{\mathrm{s}}R)\partial/\partial\theta$);

$$\Omega = 0, \qquad \tilde{v}_\parallel = -2q_{\mathrm{s}}\cos\theta\tilde{v}_{E\times B},$$

where $\tilde{v}_\parallel$ is return flow along the magnetic field line. The other one is ion sound wave ($\nabla_\parallel = ik_\parallel$);

$$\Omega^2 = k_\parallel^2 c_{\mathrm{s}}^2.$$

E.4 Zonal Flow in ETG Turbulence

The electron temperature gradient driven (ETG) turbulence is considered to be one candidate for causing anomalous electron thermal transport. ETG is almost isomorphic to ITG in electrostatic limit, with the role of electrons and ions reversed. If the isomorphism could be assumed, ETG turbulence at electron gyroradius scale would produce electron thermal diffusion coefficient $\chi_{\mathrm{e}}^{\mathrm{ETG}} \sim \rho_{\mathrm{e}}^2 v_{T\,\mathrm{e}}/L_T$ and $\chi_{\mathrm{e}}^{\mathrm{ETG}} \sim (m_{\mathrm{e}}/m_{\mathrm{i}})^{1/2}\chi_{\mathrm{i}}^{\mathrm{ITG}}$, which is too small to be relevant to tokamak experimental results. This isomorphism is broken if one considers zonal flow in the scale of Debye shielding length. As stated in sec.E.2 for ITG turbulence, the proper electron response with $\mathrm{n_e}/n = e(\phi - \bar{\phi})/\kappa T_{\mathrm{e}}$ was essential to obtaining an enhanced zonal flow amplitude (ref.[5]). On the other hand, for ETG turbulence, the ion dynamics asympttes to $\mathrm{n_i}/n = -e\phi/\kappa T_{\mathrm{i}}$, as it is unmagnetized for $k_\perp\rho_{\mathrm{i}} \gg 1$. Because of this, ETG-driven zonal flows are expected to be weaker than that for ITG-driven zonal flows in regulating turbulence.

Recently several gyrokinetic particle simulations have provided substantial progress in understanding ETG turbulence. However, results from different simulation models provided different estimations of electron heat conductivity χ_{e} and streamers at the present time. Nevertheless, because of important and interesting topics, results of ETG turbulence by toroidal particle code GT3D (ref.[9]) based on the gyrokinetic particle model (electrostatic) are shown in fig.E.4 in the cases of positive magnetic shear and reversed shear configurations of tokamak (ref.[10]). The minor radius a is $200 \sim 10^5$ times the electron Larmor radius ρ_{e}. Figures in the left-hand side are the case of positive shear configuration. At quasi-steady state (lower figure), large quasi-linear streamers are seen and provide $\chi_{\mathrm{e}} \sim 10\chi_{\mathrm{GB}}$, $\chi_{\mathrm{GB}} = \rho_{\mathrm{e}}^2 v_{T\mathrm{e}}/L_T$. Figures in the right-hand side are the case of reversed shear configuration. ETG mode with $k_\theta\rho_{T\mathrm{e}} \approx 1.3$ is excited around the $q_{\min}$ surface at linear phase (upper figure). At quasi-steady state $t = 380L_n/v_{T\mathrm{e}}$ (lower figure), at which quasi-steady zonal flows are sustained and ETG turbulence is suppressed. As a possible cause to drive zonal flow of ETG turbulence, self-organization process (inverse cascade of $\boldsymbol{k}$ spectrum) is examined.

Remarks

Zonal flows are universal phenomena in microturbulence. Zonal flows have been observed in the experiments of CHS (ref.[11]) and ASDEX-U (ref.[12]). There are extensive reviews on zonal flows (ref.[13]). The summary of Appendix E is as follows:

Zonal flows in ITG are pumped by modulational instability of the drift waves.

Magnetic field structures with $m = 0$, $n = 0$ and finite k_r, called zonal field, can be generated by drift wave turbulence. Zonal flows can modify the onset criterion for turbulence and turbulent transport.

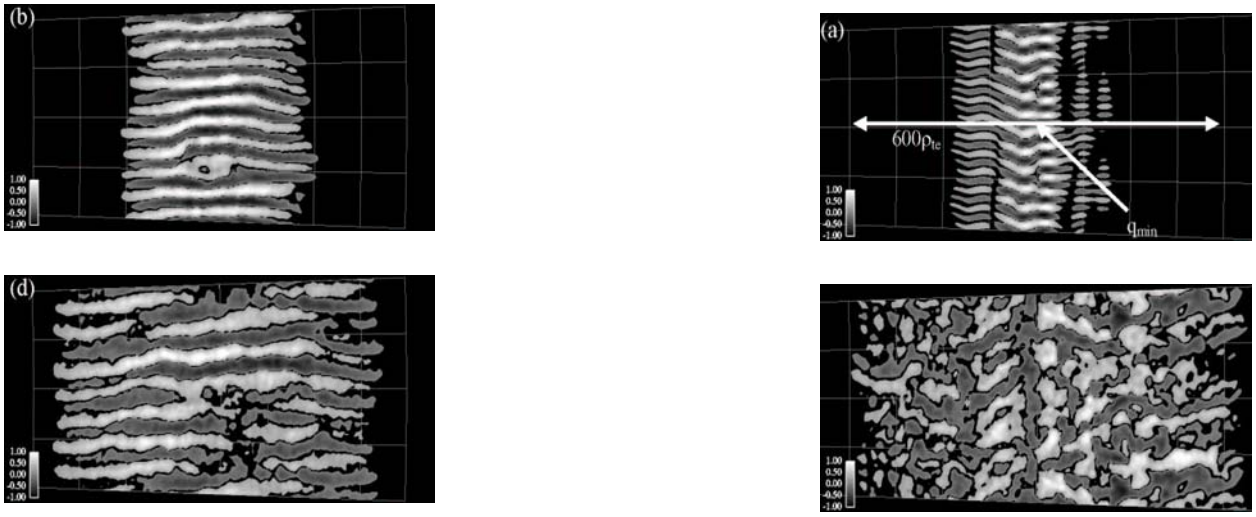

Fig.E.4 Electrostatic potential contours of ETG turbulence. Figures in the left-hand side are the case of positive shear configuration of tokamak. The upper one is the eletrostatic potential at initial saturation phase $t = 172L_n/v_{Te}$ and the lower one is at quasi-steady state $t = 250L_n/v_{Te}$. At quasi-steady state positive shear configuration, large quasi-linear streamers are seen. Figures in the right-hand side are the case of reversed shear configuration. The upper one is the potential contour at linear phase $t = 110L_n/v_{Te}$. The lower one is at quasi-steady state $t = 380L_n/v_{Te}$, at which quasi-steady zonal flows are sustained. The length of the arrow is $600\rho_{Te}$. After (ref.[10]).

A variant of zonal flows, refered to as GAM, is likely important in regulating turbulence.

In low collisonality regimes, zonal flows damp by scale-independent friction between trapped and circulating ions in ITG induced turbulence (ref.[13]).

Understanding of the zonal flow drive and damping has suggested several routes to improving confinement via externally driven flow shear amplification or by tuning the configuration design to lower the zonal flow damping.

Further studies of zonal flows driven by ETG are required.

References

[1] A. Hasegawa, C. G. Maclennan, and Y. Kodama: Nonlinear Behavior and Turbulence Spectra of Drift Waves and Rossy Waves. Phys. Fluids **22**, 2122 (1979).

[2] A. Hasegawa, and K. Mima: Pseudo-Three-Dimensional Turbulence in Magnetized Nonuniform Plasma. Phys. Fluids **21**, 87 (1978).

[3] A. I. Dyachenko, S. V. Nazarenko, and V. E. Zakharov: Wave-Vortex Dynamics in Drift and β-Plane Turbulence. Phys. Lett. **A165**, 330 (1992).

[4] Z. Lin, T. S. Hahm, W. W. Lee, W. M. Tang, and R. B. White: Turbulent Transport Reduction by Zonal Flows: Massively Parallel Simulations. Science **281**, 1835 (1998).

[5] P. N. Guzdar, R. G. Kleva, and Liu Chen: Shear Flow Generation by Drift Waves Revisited. Phys. Plasmas **87**, 459 (2001).

[6] A. I. Smolyakov, P. H. Diamond, and M. Malkov: Coherent Structure Phenomenoa in Drift Wave-Zonal Flow Turbulence. Phys. Rev. Lett. **84**, 491 (2000).

[7] N. Winsor, J. L. Johnson, and J. M. Dawson: Geodesic Acoustic Waves in Hydromagnetic System. Phys. Fluids **11**, 2448 (1968).

[8] K. Itoh, K. Hallatschek, and S.-I. Itoh: Excitation of Geodesic Acoustic Mode in Toroidal Plasmas. Plasma Phys. Contr. Fusion **47**, 451 (2005).

[9] Y. Idomura, S. Tokuda, and Y. Kishimoto: Global Gyrokinetic Simulation of Ion Temperature Gradient Driven Turbulence in Plasmas Using a Canonical Maxwellian Distribution. Nucl. Fusion **43**, 234 (2003).

[10] Y.Idomura, S. Totsuka, and Y. Kishimoto: Global Gyrokinetic Simulation of Toroidal Electron Temperature Gradient Driven Mode in Reversed Shear Tokamaks. 20th Fusion Energy Conf. (Vilamoura in 2004) TH/8-1.

Y. Idomura, M. Wakatani, and S. Tokuda: Stability of $E \times B$ Zonal Flow in Electron Temperature Gradient Driven Turbulence. Phys. Plasmas **7**, 3551 (2000).

[11] A. Fujisawa, K. Itoh, H. Iguchi, K. Matsuoka, S. Okamomura et al.: Identification of Zonal Flows in a Toroidal Plasma. Phys. Rev. Lett. **93**, 165002 (2004).

[12] G. D. Conway, B. Scott, J. Schirmer, M. Reich, A. Kendl and ASDEX-U Team: Direct Measurement of Zonal Flows and Geodesic Acoustic Mode Oscillations in ASDEX Upgrade Using Doppler Reflectometry. Plasma Phys. Contr. Fusion **47**, 1165 (2005).

[13] P. H. Diamond, S.-L. Itoh, K. Itoh, and T. S. Hahm: Zonal Flows in Plasma - A Review. Plasma Phys. Contr. Fusion **47**, R35 (2005).P. H. Diamond, K. Itoh, S.-L. Itoh, and T. S. Hahm: Overview of Zonal Flow Physics. 20th Fusion Energy Conf. (Vilamoura 2004) OV/2-1.

Physical Constants, Plasma Parameters and Mathematical Formula

c (speed of light in vacuum)	2.99792458×10^8 m/s (definition)
ϵ_0 (dielectric constant of vacuum)	$8.8541878 \times 10^{-12}$ F/m
μ_0 (permeability of vacuum)	$1.25663706 \times 10^{-6}$ H/m $(= 4\pi \times 10^{-7})$
h (Planck's constant)	$6.6260755(40) \times 10^{-34}$ Js
κ (Boltzmann's constant)	$1.380658(12) \times 10^{-23}$ J/K
A (Avogadro's number)	$6.0221367(36) \times 10^{23}$/mol(760 torr,0°C, 22.4l)
e (charge of electron)	$1.60217733(49) \times 10^{-19}$ C
1 electron volt (eV)	$1.60217733(49) \times 10^{-19}$ J
m_p (mass of proton)	$1.6726231(10) \times 10^{-27}$ kg
m_e (mass of electron)	$9.1093897(54) \times 10^{-31}$ kg
e/κ	11, 604 K/V
$m_\mathrm{p}/m_\mathrm{e}$	1836
$(m_\mathrm{p}/m_\mathrm{e})^{1/2}$	42.9
$m_\mathrm{e}c^2$	0.5110 MeV

Units are MKS, $\kappa T/e$ in eV, $\ln \Lambda = 20$, $10^{1/2} = 3.16$

$$\Pi_\mathrm{e} = \left(\frac{n_\mathrm{e}e^2}{m_\mathrm{e}\epsilon_0}\right)^{1/2} = 5.64 \times 10^{11}\left(\frac{n_\mathrm{e}}{10^{20}}\right)^{1/2}, \quad \frac{\Pi_\mathrm{e}}{2\pi} = 8.98 \times 10^{10}\left(\frac{n_\mathrm{e}}{10^{20}}\right)^{1/2},$$

$$\Omega_\mathrm{e} = \frac{eB}{m_\mathrm{e}} = 1.76 \times 10^{11}B, \qquad \frac{\Omega_\mathrm{e}}{2\pi} = 2.80 \times 10^{10}B,$$

$$-\Omega_\mathrm{i} = \frac{ZeB}{m_\mathrm{i}} = 9.58 \times 10^{7}\frac{Z}{A}B, \qquad \frac{-\Omega_\mathrm{i}}{2\pi} = 1.52 \times 10^{7}\frac{Z}{A}B,$$

$$\nu_{\mathrm{ei}\|} = \frac{1}{\tau_{\mathrm{ei}\|}} = \frac{n_\mathrm{i}Z^2e^4\ln\Lambda}{51.6\pi^{1/2}\epsilon_0^2 m_\mathrm{e}^{1/2}(\kappa T_\mathrm{e})^{3/2}} = 2.9 \times 10^9 Z^2\left(\frac{\kappa T_\mathrm{e}}{e}\right)^{-3/2}\frac{n_\mathrm{i}}{10^{20}},$$

$$\nu_{\mathrm{ii}\|} = \frac{1}{\tau_{\mathrm{ii}\|}} = \frac{n_\mathrm{i}Z^4e^4\ln\Lambda}{3^{1/2}6\pi\epsilon_0^2 m_\mathrm{i}^{1/2}(\kappa T_\mathrm{i})^{3/2}} = 0.18 \times 10^9\frac{Z^4}{A^{1/2}}\left(\frac{\kappa T_\mathrm{i}}{e}\right)^{-3/2}\frac{n_\mathrm{i}}{10^{20}},$$

$$\nu_\mathrm{ie}^{\epsilon} = \frac{Z^2 n_\mathrm{e}e^4\ln\Lambda}{(2\pi)^{1/2}3\pi\epsilon_0^2 m_\mathrm{e}{}^{1/2}(\kappa T_\mathrm{e})^{3/2}}\frac{m_\mathrm{e}}{m_\mathrm{i}} = 6.35 \times 10^6\frac{Z^2}{A}\left(\frac{\kappa T_\mathrm{e}}{e}\right)^{-3/2}\frac{n_\mathrm{e}}{10^{20}},$$

$$\lambda_\mathrm{D} = \left(\frac{\epsilon_0\kappa T}{n_\mathrm{e}e^2}\right)^{1/2} = 7.45 \times 10^{-7}\left(\frac{\kappa T_\mathrm{e}}{e}\right)^{1/2}\left(\frac{n_\mathrm{e}}{10^{20}}\right)^{-1/2},$$

$$\rho_{\Omega\mathrm{e}} = 2.38 \times 10^{-6}\left(\frac{\kappa T_\mathrm{e}}{e}\right)^{1/2}\frac{1}{B},$$

$$\rho_{\Omega\mathrm{i}} = 1.02 \times 10^{-4}\frac{1}{Z}\left(\frac{A\kappa T_\mathrm{i}}{e}\right)^{1/2}\frac{1}{B}$$

$$\lambda_\mathrm{ei} = \left(\frac{3\kappa T_\mathrm{e}}{m_\mathrm{e}}\right)^{1/2}\frac{1}{\nu_{\mathrm{ei}\|}} = 2.5 \times 10^{-4}\left(\frac{\kappa T_\mathrm{e}}{e}\right)^2\left(\frac{n_\mathrm{e}}{10^{20}}\right)^{-1},$$

$$\lambda_\mathrm{ii} = \left(\frac{3\kappa T_\mathrm{i}}{m_\mathrm{i}}\right)^{1/2}\frac{1}{\nu_{\mathrm{ii}\|}} = 0.94 \times 10^{-4}\frac{1}{Z^4}\left(\frac{\kappa T_\mathrm{i}}{e}\right)^2\left(\frac{n_\mathrm{i}}{10^{20}}\right)^{-1},$$

$$v_{\rm A} = \left(\frac{B^2}{\mu_0 n_{\rm i} m_{\rm i}}\right)^{1/2} = 2.18 \times 10^6 \frac{B}{(A n_{\rm i}/10^{20})^{1/2}},$$
$$v_{\rm Te} = \left(\frac{\kappa T_{\rm e}}{m_{\rm e}}\right)^{1/2} = 4.19 \times 10^5 \left(\frac{\kappa T_{\rm e}}{e}\right)^{1/2},$$
$$v_{\rm Ti} = \left(\frac{\kappa T_{\rm i}}{m_{\rm i}}\right)^{1/2} = 9.79 \times 10^3 \left(\frac{\kappa T_{\rm i}}{Ae}\right)^{1/2},$$

$$\eta_{\parallel} = \frac{Z e^2 m_{\rm e}^{1/2} \ln \Lambda}{51.6 \pi^{1/2} \epsilon_0^2 (\kappa T_{\rm e})^{3/2}} = 5.2 \times 10^{-5} Z \ln \Lambda \left(\frac{\kappa T_{\rm e}}{e}\right)^{-3/2},$$
$$D_{\rm cl} = \frac{m_{\rm e} \kappa T_{\rm e}}{e^2 B^2} \nu_{{\rm ei}\perp} = 3.3 \times 10^{-2} \frac{Z}{B} \left(\frac{n}{10^{20}}\right) \left(\frac{\kappa T_{\rm e}}{e}\right)^{-1/2},$$
$$D_{\rm B} = \frac{1}{16} \frac{\kappa T_{\rm e}}{eB},$$

$$\left(\frac{\Omega_{\rm e}}{\Pi_{\rm e}}\right)^2 = \frac{\epsilon_0 B^2}{m_{\rm e} n_{\rm e}} = \left(\frac{v_{\rm A}}{c}\right)^2 \frac{m_{\rm i}}{m_{\rm e}} = \frac{\kappa T_{\rm e}}{m_{\rm e} c^2} \frac{2}{\beta_{\rm e}} = 0.097 B^2 \left(\frac{n_{\rm e}}{10^{20}}\right)^{-1},$$
$$N_\lambda \equiv \frac{4\pi}{3} n_{\rm e} \lambda_{\rm D}^3 = 1.73 \times 10^2 \left(\frac{\kappa T_{\rm e}}{e}\right)^{3/2} \left(\frac{n_{\rm e}}{10^{20}}\right)^{-1/2},$$
$$\beta = \frac{n \kappa T}{(B^2/2\mu_0)} = 4.03 \times 10^{-5} \frac{1}{B^2} \left(\frac{\kappa T}{e}\right) \left(\frac{n}{10^{20}}\right),$$
$$\left(\frac{v_{\rm Te}}{v_{\rm A}}\right)^2 = \frac{m_{\rm i}}{2 m_{\rm e}} \beta_{\rm e}, \qquad \left(\frac{v_{\rm Ti}}{v_{\rm A}}\right)^2 = \frac{1}{2} \beta_{\rm i}, \qquad \left(\frac{v_{\rm A}}{c}\right)^2 = \left(\frac{\lambda_{\rm D}}{\rho_{\Omega {\rm e}}}\right)^2 \frac{m_{\rm e} n_{\rm e}}{m_{\rm i} n_{\rm i}},$$
$$S \text{ number} \equiv \frac{\tau_{\rm R}}{\tau_{\rm H}} = \left(\frac{\mu_0 a^2}{\eta}\right) \left(\frac{B}{\mu_0 (n_{\rm i} m_{\rm i})^{1/2} a}\right) = 2.6 \times 10^3 \frac{a B (\kappa T_{\rm e}/e)^{3/2}}{Z A^{1/2} (n/10^{20})^{1/2}},$$
$$\frac{D_{\rm B}}{D_{\rm cl}} = \frac{1}{16} \frac{\Omega_{\rm e}}{\nu_{{\rm ei}\perp}}, \qquad \frac{\Pi_{\rm e}}{\nu_{{\rm ei}\parallel}} = \frac{51.6 \pi^{1/2}}{\ln \Lambda Z} n_{\rm e} \lambda_{\rm D}^3.$$

$$\boldsymbol{a}\cdot(\boldsymbol{b}\times\boldsymbol{c})=\boldsymbol{b}\cdot(\boldsymbol{c}\times\boldsymbol{a})=\boldsymbol{c}\cdot(\boldsymbol{a}\times\boldsymbol{b}),$$

$$\boldsymbol{a}\times(\boldsymbol{b}\times\boldsymbol{c})=(\boldsymbol{a}\cdot\boldsymbol{c})\boldsymbol{b}-(\boldsymbol{a}\cdot\boldsymbol{b})\boldsymbol{c},$$

$$\begin{aligned}(\boldsymbol{a}\times\boldsymbol{b})\cdot(\boldsymbol{c}\times\boldsymbol{d})&=\boldsymbol{a}\cdot\boldsymbol{b}\times(\boldsymbol{c}\times\boldsymbol{d})\\&=\boldsymbol{a}\cdot((\boldsymbol{b}\cdot\boldsymbol{d})\boldsymbol{c}-(\boldsymbol{b}\cdot\boldsymbol{c})\boldsymbol{d})\\&=(\boldsymbol{a}\cdot\boldsymbol{c})(\boldsymbol{b}\cdot\boldsymbol{d})-(\boldsymbol{a}\cdot\boldsymbol{d})(\boldsymbol{b}\cdot\boldsymbol{c}),\end{aligned}$$

$$\nabla\cdot(\phi\boldsymbol{a})=\phi\nabla\cdot\boldsymbol{a}+(\boldsymbol{a}\cdot\nabla)\phi,$$

$$\nabla\times(\phi\boldsymbol{a})=\nabla\phi\times\boldsymbol{a}+\phi\nabla\times\boldsymbol{a},$$

$$\begin{aligned}\nabla(\boldsymbol{a}\cdot\boldsymbol{b})&=(\boldsymbol{a}\cdot\nabla)\boldsymbol{b}+(\boldsymbol{b}\cdot\nabla)\boldsymbol{a}\\&\quad+\boldsymbol{a}\times(\nabla\times\boldsymbol{b})+\boldsymbol{b}\times(\nabla\times\boldsymbol{a}),\end{aligned}$$

$$\nabla\cdot(\boldsymbol{a}\times\boldsymbol{b})=\boldsymbol{b}\cdot\nabla\times\boldsymbol{a}-\boldsymbol{a}\cdot\nabla\times\boldsymbol{b},$$

$$\begin{aligned}\nabla\times(\boldsymbol{a}\times\boldsymbol{b})&=\boldsymbol{a}(\nabla\cdot\boldsymbol{b})-\boldsymbol{b}(\nabla\cdot\boldsymbol{a})\\&\quad+(\boldsymbol{b}\cdot\nabla)\boldsymbol{a}-(\boldsymbol{a}\cdot\nabla)\boldsymbol{b},\end{aligned}$$

$$\nabla\times\nabla\times\boldsymbol{a}=\nabla(\nabla\cdot\boldsymbol{a})-\nabla^2\boldsymbol{a}$$
$(x,y,z$ coordinates only),

$$\nabla\times\nabla\phi=0,$$

$$\nabla\cdot(\nabla\times\boldsymbol{a})=0,$$

$$\boldsymbol{r}=x\boldsymbol{i}+y\boldsymbol{j}+z\boldsymbol{k},$$

$$\nabla\cdot\boldsymbol{r}=3,\qquad\nabla\times\boldsymbol{r}=0,$$

$$\int_{\mathrm{V}}\nabla\phi\cdot\mathrm{d}V=\int_{\mathrm{S}}\phi\boldsymbol{n}\mathrm{d}a,$$

$$\int_{\mathrm{V}}\nabla\cdot\boldsymbol{a}\mathrm{d}V=\int_{\mathrm{S}}\boldsymbol{a}\cdot\boldsymbol{n}\mathrm{d}a,$$

$$\int_{\mathrm{V}}\nabla\times\boldsymbol{a}\mathrm{d}V=\int_{\mathrm{S}}\boldsymbol{n}\times\boldsymbol{a}\mathrm{d}a,$$

$$\int_{\mathrm{S}}\boldsymbol{n}\times\nabla\phi\mathrm{d}a=\oint_{\mathrm{C}}\phi\mathrm{d}\boldsymbol{s},$$

$$\int_{\mathrm{S}}\nabla\times\boldsymbol{a}\cdot\boldsymbol{n}\mathrm{d}a=\oint_{\mathrm{C}}\boldsymbol{a}\cdot\mathrm{d}\boldsymbol{s}.$$

cylindrical coordinates (r,θ,z)

$$\mathrm{d}s^2=\mathrm{d}r^2+r^2\mathrm{d}\theta^2+\mathrm{d}z^2,$$

$$\nabla\psi=\frac{\partial\psi}{\partial r}\boldsymbol{i}_1+\frac{1}{r}\frac{\partial\psi}{\partial\theta}\boldsymbol{i}_2+\frac{\partial\psi}{\partial z}\boldsymbol{i}_3,$$

$$\nabla\cdot\boldsymbol{F}=\frac{1}{r}\frac{\partial}{\partial r}(rF_1)+\frac{1}{r}\frac{\partial F_2}{\partial\theta}+\frac{\partial F_3}{\partial z},$$

$$\begin{aligned}\nabla\times\boldsymbol{F}&=\left(\frac{1}{r}\frac{\partial F_3}{\partial\theta}-\frac{\partial F_2}{\partial z}\right)\boldsymbol{i}_1\\&\quad+\left(\frac{\partial F_1}{\partial z}-\frac{\partial F_3}{\partial r}\right)\boldsymbol{i}_+\left(\frac{1}{r}\frac{\partial}{\partial r}(rF_2)-\frac{1}{r}\frac{\partial F_1}{\partial\theta}\right)\boldsymbol{i}_3,\end{aligned}$$

$$\nabla^2\psi=\frac{1}{r}\frac{\partial}{\partial r}\left(r\frac{\partial\psi}{\partial r}\right)+\frac{1}{r^2}\frac{\partial^2\psi}{\partial\theta^2}+\frac{\partial^2\psi}{\partial z^2},$$

spherical coordinates (r,θ,ϕ)

$$\mathrm{d}s^2=\mathrm{d}r^2+r^2\mathrm{d}\theta^2+r^2\sin^2\theta\mathrm{d}\phi^2,$$

$$\nabla\psi=\frac{\partial\psi}{\partial r}\boldsymbol{i}_1+\frac{1}{r}\frac{\partial\psi}{\partial\theta}\boldsymbol{i}_2+\frac{1}{r\sin\theta}\frac{\partial\psi}{\partial\phi}\boldsymbol{i}_3,$$

$$\begin{aligned}\nabla\cdot\boldsymbol{F}&=\frac{1}{r^2}\frac{\partial}{\partial r}(r^2F_1)\\&\quad+\frac{1}{r\sin\theta}\frac{\partial}{\partial\theta}(\sin\theta F_2)+\frac{1}{r\sin\theta}\frac{\partial F_3}{\partial\phi},\end{aligned}$$

$$\begin{aligned}\nabla\times\boldsymbol{F}&=\frac{1}{r\sin\theta}\left(\frac{\partial}{\partial\theta}(\sin\theta F_3)-\frac{\partial F_2}{\partial\phi}\right)\boldsymbol{i}_1\\&\quad+\frac{1}{r}\left(\frac{1}{\sin\theta}\frac{\partial F_1}{\partial\phi}-\frac{\partial}{\partial r}(rF_3)\right)\boldsymbol{i}_2\\&\quad+\frac{1}{r}\left(\frac{\partial}{\partial r}(rF_2)-\frac{\partial F_1}{\partial\theta}\right)\boldsymbol{i}_3,\end{aligned}$$

$$\begin{aligned}\nabla^2\psi&=\frac{1}{r^2}\frac{\partial}{\partial r}\left(r^2\frac{\partial\psi}{\partial r}\right)+\frac{1}{r^2\sin\theta}\frac{\partial}{\partial\theta}\left(\sin\theta\frac{\partial\psi}{\partial\theta}\right)\\&\quad+\frac{1}{r^2\sin^2\theta}\frac{\partial^2\psi}{\partial\phi^2}.\end{aligned}$$

Index

(Numbers are of chapters, sections and subsections)